SINGLE-PHASE INDUCTION GENERATORS

AND

SWITCHED RELUCTANCE MOTORS

Thesis submitted for the degree
of Doctor of Philosophy of the
University of London

by

SOMCHAI CHATRATANA M.Sc.(Eng),D.I.C.

September 1982

Department of Electrical Engineering
Imperial College of Science and Technology
London SW7 2AZ

ABSTRACT

Part A: Single-phase Induction Generators

An assessment is made of the plain single-phase mains-connected induction generator (i.e. without auxil-iary winding and capacitor). The analysis is based on the steady-state circuit and enables approximate relations to be found for slip at maximum and at zero airgap power.

Comparisons between predicted slips and powers calculated from the approximate formula and the values calculated from the equivalent circuit are presented with the test results.

Design considerations and selection factors for optimum efficiency are discussed in the light of the results.

Part B: Single-phase Switched Reluctance Motor Drive Systems

The second part of the thesis describes an investigation into the single phase switched reluctance motor drive system. Four configurations of motor structure have been studied, built and tested for both high-and low-speed applications. The configurations can be divided

into two categories: (1) Radial/circumferential flux motor and (2) Radial/axial flux motor.

Motor operation with two feed configurations were investigated. In one the motor winding is connected to the a.c.mains via a shaft-position controlled triac and in the other the winding is fed from a d.c. link inverter of the half or the quarter bridge type.

The a.c. triac feed provides an extremely low cost system suitable for certain limited range applications. The d.c. link scheme though somewhat more expensive, greatly extends the speed range and power output, and with PWM-driven output transistors improves control flexibility.

A time stepping method has been used for analysis of all the scheme tested. Comparisons between predicted and test results are presented.

ACKNOWLEDGEMENTS

The author would like to express his sincere gratitude to his supervisor Dr. H.R. Bolton, Reader in Electrical Machines, of the Department of Electrical Engineering, Imperial College for providing inspiration and for his invaluable encouragement, enthusiasm and guidance during the course of this work.

The author also wishes to acknowledge a large debt of gratitude to Dr. D.A.G. Pedder of Kingston Polytechnic for considerable help in the design and advice during the construction of the drive circuits.

The construction of the prototypes and test rigs was carried out in the Electrical Engineering Workshop at Imperial College, under the supervision of Mr. R. Moore, to whom and his staff the author is grateful. Acknowledgement must also be made of the practical assistance and advice recieved from Mr. R.B. Owen.

Thanks are due to many colleagues in the Electrical Machines Section at Imperial College for useful discussions which have taken place throughout the work. Particular thanks are due to Mr. N. Mallinson for his considerable assistance on problems associated with the electronic portions of the work.

The author also wishes to acknowledge Mr. N. Capaldi of Smiths Industries Aerospace and Defence Systems Company for practical suggestions and permission to use the material described in Section 7.2.

Thanks are finally due to Thai Government for generous financial support during the course of the work.

To my family

and TAS

CONTENTS

	Page
Title	1
Abstract	2
Acknowledgements	4
Contents	6
List of principal symbols	11
Part A: SINGLE-PHASE INDUCTION GENERATORS	16
CHAPTER 1: THEORY OF OPERATION	17
1.1 General introduction	17
1.2 Analysis	20
1.2.1 Introduction	20
1.2.2 Equivalent circuit	23
1.2.3 Steady-state performance	26
1.2.4 Analysis of machine performance in generating mode	30
1.2.5 Range of operating slips	33
1.2.6 Maximum airgap power condition	35
1.2.7 Performance of single-phase induction machine running on main winding only	37
1.3 Conclusions	40
CHAPTER 2: EXPERIMENTAL RESULTS AND OPTIMISATION	41
2.1 Introduction	41
2.2 Experimental systems and measurements	42
2.3 Effect on performance of design parameters	46
2.4 Design consideration	53
2.5 Conclusions and further works	55

		Page
Part B:	SINGLE-PHASE SWITCHED RELUCTANCE MOTOR DRIVE SYSTEMS	59
CHAPTER 1:	GENERAL INTRODUCTION	60
1.1	Principle of the switched reluctance motor drive system	60
1.1.1	Basic system operation	67
1.1.2	Magnetising characteristic	67
1.2	Brief survey of SRM literature	72
1.3	Introduction to the work described in the thesis	76
CHAPTER 2:	SINGLE-PHASE SWITCHED RELUCTANCE MOTOR DRIVE SYSTEM	79
2.1	Introduction	79
2.2	The SPSRM drive system configuration	80
2.3	Motor types	81
2.3.1	Low-speed SPSR motor	82
2.3.2	High-speed SPSR motors	83
2.4	Power circuit configurations	88
2.4.1	The 'a.c.' feed system	88
2.4.2	The 'd.c.' feed system	92
2.5	Position-sensor systems	98
2.6	Speed-control methods	101
2.7	Protection circuits	104
2.7.1	Protection circuits for thyristor or triac	104
2.7.2	Protection circuits for transistors	108
2.8	Merits of SPSRM drive system	110
2.9	Concluding remarks	119
CHAPTER 3:	THEORY OF OPERATION OF SPSR MOTOR	120
3.1	Introduction	120
3.2	Steady-state analysis for 'd.c.' operation of SPSR motor	127
3.2.1	Simplified analytic method	129
3.2.2	Step by step method	141
3.3	Steady-state analysis for 'a.c.' operation of SPSR motor	149

Page

3.4 Discussion of phenomena adversely affecting the accuracy of the analysis and predictions 164

3.5 Concluding remarks 169

CHAPTER 4: PERFORMANCE OF A LOW-SPEED SIX-SALIENCY MOTOR 171

4.1 Introduction 171

4.2 Measurement of equivalent circuit parameters 178

4.3 Motor performance with 'd.c.'link PWM transistor-fed circuit 185

4.3.1 The 'd.c.'link PWM transistor-fed system 185

4.3.2 Load tests of low-speed six-saliency motor with different switching angles 191

4.3.3 Results and discussion 195

4.4 Motor performance with 'a.c.' triac-fed circuit 205

4.4.1 The 'a.c.' triac-fed system 205

4.4.2 Load tests of low-speed six-saliency motor with triac feed- effect of firing angle and switching angle variation 211

4.4.3 Results and discussion 213

4.4.4 Theoretical investigation of the motor performance with d.c. trigger firing circuit 223

4.4.5 Mains harmonics with triac-fed circuit 227

4.5 Conclusions 241

CHAPTER 5: PERFORMANCE OF THE HIGH-SPEED, TWO-POLE MOTORS 244

5.1 Introduction 244

5.1.1 Experimental motors 244

5.1.2 Test on the original form 1 motor 254

5.1.3 Introduction to the experimental work on the small SPSRMs 257

5.2 Performance of the form 1 motor with 'a.c.' triac-fed circuit 258

5.2.1 'A.C.' triac-fed circuit with d.c. trigger 258

		Page
5.2.2	Experimental system	262
5.2.3	Laod test with 'a.c.' triac-fed circuit	271
5.2.4	Results and discussion	275
5.2.4.1	Test results	275
5.2.4.2	Predictions	282
5.3	Performance of the two-pole motors with 'd.c.'link transistor-fed circuit	290
5.3.1	Introduction	290
5.3.2	The PWM circuit and driver circuit of the two-pole motors	295
5.3.3	Performance of the form 1 motor (with original winding)	300
5.3.3.1	Load tests	300
5.3.3.2	Results and discussion	302
5.3.3.3	Predictions	313
5.3.4	Performance of the form 1, form 2 and form 3 motors	319
5.3.4.1	Introduction	319
5.3.4.2	Preliminary test with the form 1 motor with reduced turns	322
5.3.4.3	Preliminary measurements of all test motors	325
5.3.4.4	Modification to drive circuit and test rig	339
5.3.4.5	Retardation tests	346
5.3.4.6	Load tests of the two-pole high-speed motors with 'd.c.' feed circuit	350
5.3.4.7	Predictions	361
5.4	Performance of two-pole motors with 'd.c.' feed circuit	371
5.4.1	Test results	371
5.4.2	Discussion	377
5.5	Conclusions	395
CHAPTER 6:	SOME DESIGN ASPECTS OF SPSRM DRIVE SYSTEMS	398
6.1	Introduction	398
6.2	Magnetic-circuit, excitation-winding and rotor configurations	400

		Page
6.3	Stator number of poles and castellation	404
6.4	Ratio of stator pole number to rotor pole number	406
6.5	Ratio of stator pole width to rotor pole width	406
6.6	Airgap length, slot and gap geometry	409
6.7	Choice of lamination and wire	411
6.8	Number of turns of the excitation coil	411
6.9	Choice of feed circuits, pull-down circuits, sensors and switching devices	412
6.10	Choice of control methods	414
6.11	Conclusions	416
CHAPTER 7:	CONCLUSIONS AND SUGGESTIONS FOR FURTHER WORK	417
7.1	Conclusions	417
7.2	An example of industrial application of SPSRM drive system	420
7.3	Suggestions for further work	422
APPENDIX A1		425
APPENDIX A2		433
APPENDIX B1		442
APPENDIX B2		447
APPENDIX B3		453
APPENDIX B4		455
APPENDIX B5		457
References		460
Publications submitted in support of thesis		470

LIST OF PRINCIPAL SYMBOLS

A_a	airgap area
A_c	winding area
A_i	cross-sectional area of the magnetic circuit
A_{siron}	smallest cross-sectional area of the magnetic circuit
AT_{iron}	m.m.f. drop in iron
AT_{gap}	m.m.f. drop in airgap
$AT_{iron}+AT_{gap}$	total m.m.f. needed to drive magnetic circuit
a	operator $-\frac{1}{2} + j\frac{\sqrt{3}}{2}$
a, a_w	wire cross-section^2
B, B_{ave}	average flux density
B_d	average flux density (homopolar case)
B_s	flux density at the smallest cross-section
B_l	flux density per gap (heteropolar case)
b	$L_{min}/\Delta L$
C	energy density
D	airgap diameter, rotor diameter
d axis	axis of minimum reluctance
E_b	induced e.m.f. for backward field
E_c	change in magnetic stored energy/gap/cycle
E_f	induced e.m.f. for forward field
F	magnetomotive force
f	supply frequency
g, g_a	airgap length
H_n	harmonic content of order n
I	stator current
I	moment of inertia
I	unit current for normalisation
I_L	load current
I_p	transistor peak current
I_n	harmonic current of order n
I_o, I_+, I_-	zero, positive and negative sequence currents
i	instantaneous coil current
$\hat{i}$	peak current
$\mathbf{i}$	normalised current
J	mean surface current density

J	moment of inertia
j	normalised current
j_{Dmean}	normalised diode mean current
j_{Drms}	normalised diode r.m.s.current
j_{Tmean}	normalised transistor mean current
j_{Trms}	normalised transistor r.m.s.current
$j_{\tau rms}$	normalised torque producing r.m.s. current
L	inductance
ΔL	$L_{max} - L_{min}$
L_d, L_{max}	d axis inductance, maximum inductance
L_g	airgap inductance
L_q, L_{min}	q axis inductance , minimum inductance
L_t	mean length per turn
L_s	slot leakage inductance
l_a	active core length
m	mass
N	number of turns
n	turns ratio
P	output power
P_{cu}	copper loss
P_d	gross power output
P_{ein}	electrical power input
P_i	iron loss
P_{in}	power input
P_{mech}	electrical power converted into mechanical power
P_{out}	output power
P_{RC}	power dissipation in R_C
P_{RL}	power dissipation in R_L
P_1, P_2	airgap permeance functions
p	number of pole
p	number of gap
p	number of rotor saliencies
q axis	axis of maximum reluctance
R	rotor radius
R	winding resistance, resistance of stator circuit
R_C	snubber C resistor
R_L	snubber L resistor
R_1, X_1	stator resistance and leakage reactance per phase (three phase machine)

R_2, X_2	referred rotor resistance and leakage reactance per phase (three phase machine)
R_{11}, X_{11}	stator resistance and leakage reactance (single phase machine)
R_{21}, X_{21}	referred rotor resistance and leakage reactance (single phase machine)
$\mathcal{R}$	reluctance of the magnetic circuit
$\mathcal{R}_d$	direct axis reluctance
rpm	rotor speed in rev/min
r	apparent coil resistance
S	slip
S	current integral
SS	current square integral
S_o	slip for zero power
S_{max}	slip for maximum airgap power
s	slot width
T	output torque
T_f	friction torque
T_t	period of torque cycle time
T_e	period of supply frequency
T_m	numerator of the smallest ratio of 60000/(pxrpm)
t	time
t	pole width
t_α , t_β	switching times
t_γ	firing time
t_{hcyc}	zero crossing time of supply voltage
t_p	time required for rotor to move by 1 pole
t_f	fall time
t_{rr}	reverse recovery time
t_{on}	period of on time
t_{off}	period of off time
V_{cc}	rail voltage
V_s	supply voltage
V_s	rail to rail voltage
V/N	volt per turn
v	instanteneous voltage
W'(Q,i)	coenergy

X_m	magnetising reactance per phase (three phase machine)
X_{ml}	magnetising reactance (single phase machine)
X_L	coil apparent leakage reactance
X_o	zero sequence reactance per phase
Z	coil impedance
Z_o, Z_+, Z_-	zero, positive and negative sequence impedances
α	advance switch-on angle
α	temperature coefficient
α'	phase angle
β	advance switch-off angle
γ	phase delay angle
γ	number of voltage changes/minute
δ	current density
η	efficiency
λ	pole pitch
μ_o	permeability of air
ρ	conductivity of copper
σ	percentage of leakage flux
$\tau\ (\theta, i)$	instantaneous gross torque
τ_{mean}	mean torque per cycle
τ	output torque
ψ	flux linkage
$\hat{\psi}$	peak flux linkage
ω	angular speed
ω	angular frequency ($2\pi f$)
ω_m	mechanical angular speed
ω_r	rotor angular speed
θ	phase angle
θ_r	rotor angle, rotor position
θ	voltage phase relationship
θ_s, θ_r	stator,rotor pole arcs
θ_p	angle between two maximum alignment position
θ_o	switch-on angle
θ_p	switch-off angle
θ_q	current extinction angle
$\boldsymbol{\theta}$	normalised rotor angle
θ_{cy}	angular repetition period

$\Delta\theta$	angular duration of rising inductance (unit angle for normalisation)
ϕ	magnetic flux
ϕ	total flux
ϕ	normalised rotor angle
ϕ_o	normalised switch-on angle
ϕ_p	normalised switch-off angle
ϕ_q	normalised current extinction angle

Part A

SINGLE-PHASE INDUCTION GENERATORS

CHAPTER 1

THEORY OF OPERATION

1.1 General introduction

Induction generators find their main applications in remote un-manned hydro power stations[1.1], usually of small or medium size where the absence of a field regulator, of a field supply system and of a field winding and slip rings has considerable merit in reliability and economic terms. However the resurgence of interest in wind power is likely to lead to induction generators' usage for wind energy conversion on an increasing scale and a number of studies of induction generators operation with wind turbines are now available in the literature[1.2, 1.3, 1.4]

Induction generators have also been examined for use with small, high-speed turbines as part of a recent joint SERC/Universities/Industry (TIGER) project into the feasibility of recovering waste (low grade) heat from commercial buildings. The induction generator was selected in this case because of the capacity for fabricating rotors of exceptional strength under high centrifugal force loading. The use of supersynchronous generating action to provide braking has received considerable attention and capacitor braking is used widely in drive systems. The motor is usually disconnected from the mains

and connected to a set of capacitors. These provide excitation VArs and the kinetic energy of the motor and load is dissipated in the motor winding and cage.

Capacitor-excited induction machines used specifically as generators have also recieved considerable attention[1.5,1.6] and capacitor or synchronous machine-excited induction generator schemes for wind power conversion at non-mains-connected sites have been examined recently by two groups.[1.7,1.8]

So far as is known , there has hitherto been no case where a single-phase rather than a three-phase machine has been used in those types of generating schemes and there seems to be no literature dealing with the analysis of the single-phase induction generator. The reason for this is not difficult to discern: the inevitable presence in a single-phase induction generator of a backward field (hopefully of small magnitude) will always affect efficiency and I^2R heating adversely. A three-phase generator is hence generally preferable so long as (for mains connected schemes) three-phase mains are available. What prompted the investigation reported here was the evident need for knowledge of induction generator schemes suitable for direct connection to a single-phase mains feeder. To an extent in the U.K. but particularly in certain countries overseas, official encouragement is being given to the implementation of private, mains-connected generation schemes. Subject to tariff, fuel-cost and

other factors, this is a trend that may intensify. Given the fact that many consumers (including the main relevant groups: farmers and small holders) are connected via a single-phase feeder only, knowledge of the performance levels possible and of the characteristics of single-phase, mains-connected induction generators is important.

This chapter deals with the simplest and most reliable type of single-phase induction generator scheme where the quadrature (capacitor-run) phase is absent and where the machine is connected to a constant-frequency, constant-voltage supply. Other schemes including "capacitor-run" and capacitor-excited, non-mains-connected categories are mentioned along with other suggestions for further work at the end of chapter 2.

The analysis of the single-phase induction generator will be developed by examining the negative slip performance of a three-phase induction motor operating on one phase only. The symmetrical components method used is explained in 1.2.1. An equivalent circuit for this mode of operation is derived in 1.2.2. In 1.2.3, parameters determining the steady-state performance in terms of equivalent circuit parameters are given and the performance in the generating mode is analysed in 1.2.4. The similarity between the derived equivalent circuit and the equivalent circuit for a "genuine" single-phase induction motor running on main winding alone is pointed out in 1.2.5 and the corresponding parameters determining

performance in the generating mode for the single-phase induction motor are also derived.

1.2 Analysis

1.2.1 Introduction

The unbalanced operation of the three-phase induction motor with short-circuited rotor can be analysed by the use of the Symmetrical Components Transformation given in reference 1.9. The sequence components are defined in terms of the phase quantities (Fig. 1.2.1) as:

$$\begin{bmatrix} I_o \\ I_+ \\ I_- \end{bmatrix} = \frac{1}{\sqrt{3}} \begin{bmatrix} 1 & 1 & 1 \\ 1 & a & a^2 \\ 1 & a^2 & a \end{bmatrix} \begin{bmatrix} I_a \\ I_b \\ I_c \end{bmatrix} \quad ; \quad \begin{bmatrix} V_o \\ V_+ \\ V_- \end{bmatrix} = \frac{1}{\sqrt{3}} \begin{bmatrix} 1 & 1 & 1 \\ 1 & a & a^2 \\ 1 & a^2 & a \end{bmatrix} \begin{bmatrix} V_a \\ V_b \\ V_c \end{bmatrix} \tag{1.2.1}$$

and the reverse relationships are

$$\begin{bmatrix} I_a \\ I_b \\ I_c \end{bmatrix} = \frac{1}{\sqrt{3}} \begin{bmatrix} 1 & 1 & 1 \\ 1 & a^2 & a \\ 1 & a & a^2 \end{bmatrix} \begin{bmatrix} I_o \\ I_+ \\ I_- \end{bmatrix} \quad ; \quad \begin{bmatrix} V_a \\ V_b \\ V_c \end{bmatrix} = \frac{1}{\sqrt{3}} \begin{bmatrix} 1 & 1 & 1 \\ 1 & a^2 & a \\ 1 & a & a^2 \end{bmatrix} \begin{bmatrix} V_o \\ V_+ \\ V_- \end{bmatrix} \tag{1.2.2}$$

where subscripts a,b,c denote the phases and ; o,+,- denote zero, positive and negative components respectively, and "a" is equal to $-\frac{1}{2} + j\frac{\sqrt{3}}{2}$ (Fig. 1.2.2)

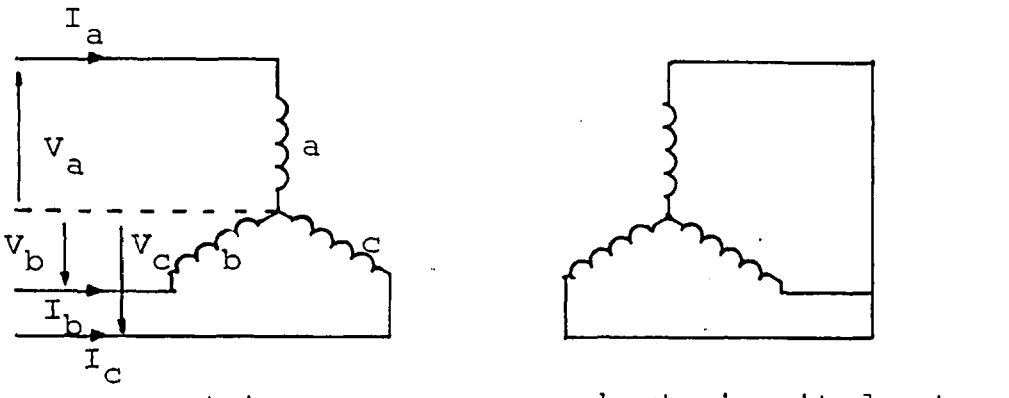

(a)

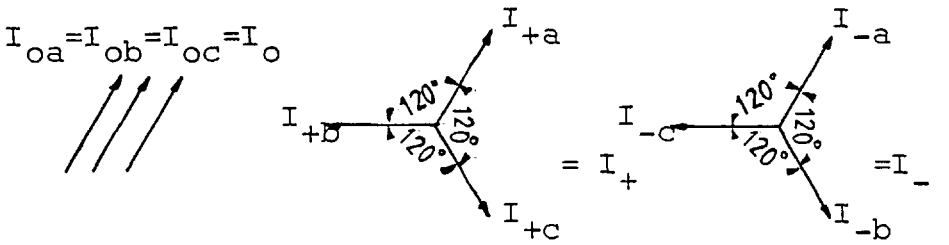

(b) (c) (d)

Fig. 1.2.1 (a) Induction motor configuration and representation of symmetrical components: (b) zero sequence components, (c) positive sequence components, and (d) negative sequence components

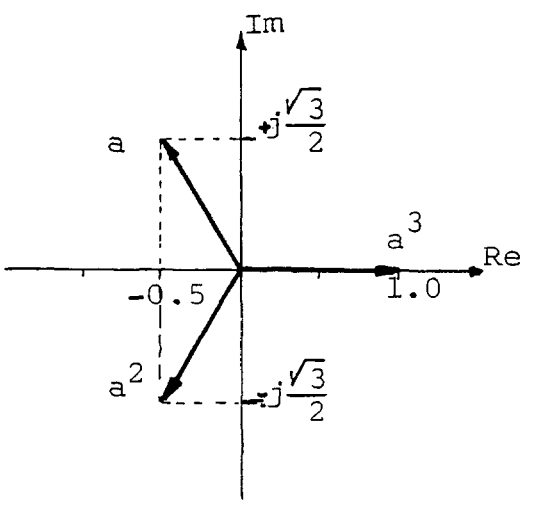

Fig. 1.2.2 Representation of 'a' in complex plane

The steady-state voltage equations of the induction motor after transformation can be written as in eq. (1.2.3), i.e.

$$\begin{bmatrix} V_o \\ V_+ \\ V_- \end{bmatrix} = \begin{bmatrix} Z_o & 0 & 0 \\ 0 & Z_+ & 0 \\ 0 & 0 & Z_- \end{bmatrix} \begin{bmatrix} I_o \\ I_+ \\ I_- \end{bmatrix} \qquad (1.2.3)$$

where Z_o, Z_+, Z_- are zero sequence, positive sequence and negative sequence impedance of the machine respectively. These can be represented by the equivalent circuit as shown in Fig. 1.2.3.

For simplicity the core losses are neglected and the terms in the equivalent circuit are defined as follows :

R_2 and X_2 are the referred rotor resistance and leakage reactance per phase for three-phase operation expressed in terms of stator voltage and frequency.

R_1 and X_1 are the stator resistance and leakage reactance per phase.

X_m is the magnetising reactance per phase for three-phase operation.

X_o is the zero sequence reactance per phase.

S is the slip.

Although the variation of R_2 and L_2 with slip frequency (due to deep bar effect) could be accounted for in this method, it will be assumed for simplicity that R_2 and L_2 are fixed. This assumption unfortunately involves somewhat more error with single-phase cage machines than with three-phase induction generators since the response of the cage to the backward field (at frequency approximately twice that of the mains for normal slips) is important.

1.2.2 Equivalent circuit

The diagram in Fig. 1.2.4 shows the connections of a three-phase induction motor when just a single-phase winding is utilised.

From the diagram, the phase currents are

$$\begin{aligned} I_a &= I \\ I_b &= 0 \\ I_c &= 0 \end{aligned} \qquad (1.2.4)$$

Substituting phase currents in eq. (1.2.4) into eq. (1.2.1), the sequence component currents can be written as

$$\begin{aligned} I_o &= \frac{I}{\sqrt{3}} \\ I_+ &= \frac{I}{\sqrt{3}} \\ I_- &= \frac{I}{\sqrt{3}} \end{aligned} \qquad (1.2.5)$$

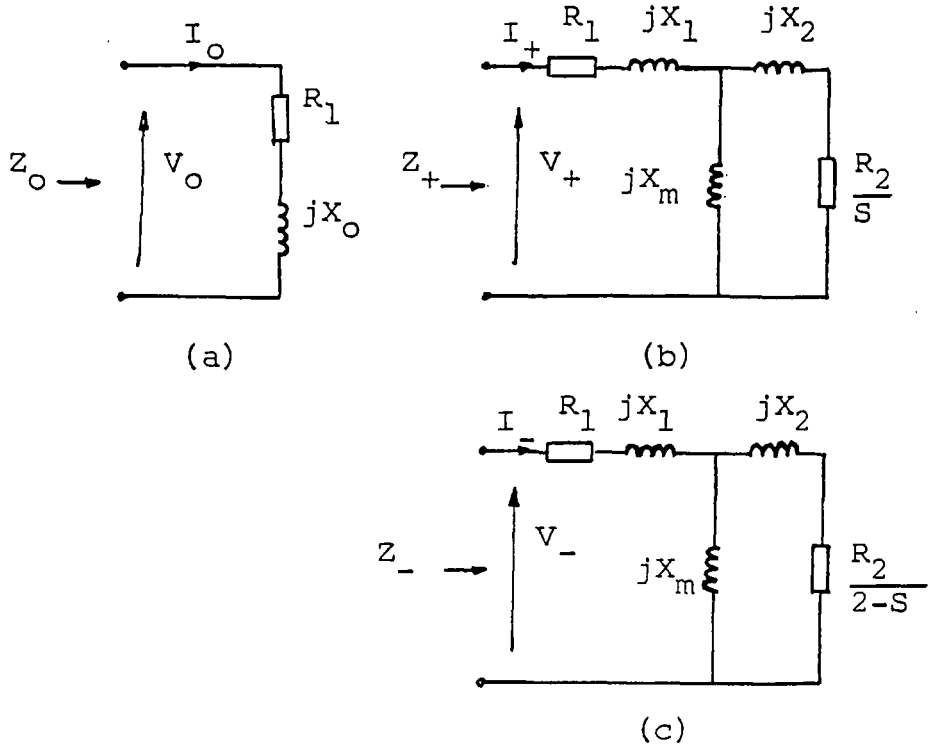

Fig. 1.2.3 Sequence impedances for a three-phase induction motor with short-circuited rotor (iron losses neglected)

(a) Zero sequence impedance (neglecting harmonics effect)

(b) Positive sequence impedance

(c) Negative sequence impedance

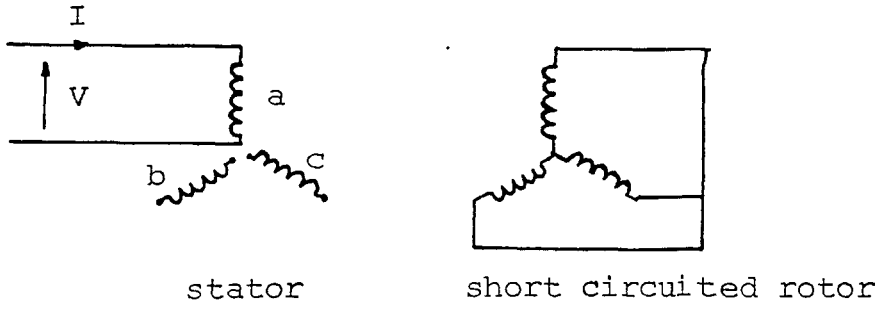

Fig. 1.2.4 Connection diagram for single-phase operation of a three-phase induction motor

and from eq.(1.2.3) the sequence voltages are

$$\begin{aligned} V_o &= Z_o \frac{I}{\sqrt{3}} \\ V_+ &= Z_+ \frac{I}{\sqrt{3}} \\ V_- &= Z_- \frac{I}{\sqrt{3}} \end{aligned} \qquad (1.2.6)$$

With the reverse transformation given in eq.(1.2.2), the supply voltage V which is equal to V_a is

$$V = V_a = \frac{1}{\sqrt{3}} \left(Z_o \frac{I}{\sqrt{3}} + Z_+ \frac{I}{\sqrt{3}} + Z_- \frac{I}{\sqrt{3}} \right)$$

so

$$V = \left(\frac{Z_o}{3} + \frac{Z_+}{3} + \frac{Z_-}{3} \right) I \qquad (1.2.7)$$

Equation (1.2.7) leads to the equivalent circuit of fig. 1.2.5, which is a series connection of zero ,positive and negative sequence impedances with all parameters divided by three.

An examination of the equivalent circuit shows that the portion which represents the effect of airgap flux is split into two parts representing the effect of forward field and backward field. Although the difference in referred rotor resistance ($R_2/3S$ and $R_2/3(2-S)$) is the only apparent difference between two parts, in practice further second-order effects, the most important of which was referred to previously, must be expected.

However the impedance of the equivalent circuit for the backward field will be approximately constant over the normal (fairly small) working range of slips.

1.2.3 Steady-state performance

With the equivalent circuit of Fig. 1.2.5, the stator current, power and other quantities can be computed for any assumed value of slip when applied voltage and motor impedances are known.

With the assumption that R_2 and X_2 in both equivalent circuits representing the forward and backward field do not change with slip , the steady-state performance can be derived as follows :

In order to simplify the derivation let (Fig.1.2.6)

$$Z_1 = R_1 + j\left(\frac{X_0}{3} + \frac{2X_1}{3}\right) = R_1 + jX_s$$

$$Z_f = j\frac{X_m}{3} \,//\, \left(\frac{R_2}{3S} + j\frac{X_2}{3}\right) \qquad (1.2.8)$$

and $$Z_b = j\frac{X_m}{3} \,//\, \left(\frac{R_2}{3(2-S)} + j\frac{X_2}{3}\right)$$

and the rotor resistance be split into two parts representing losses and converted powers,

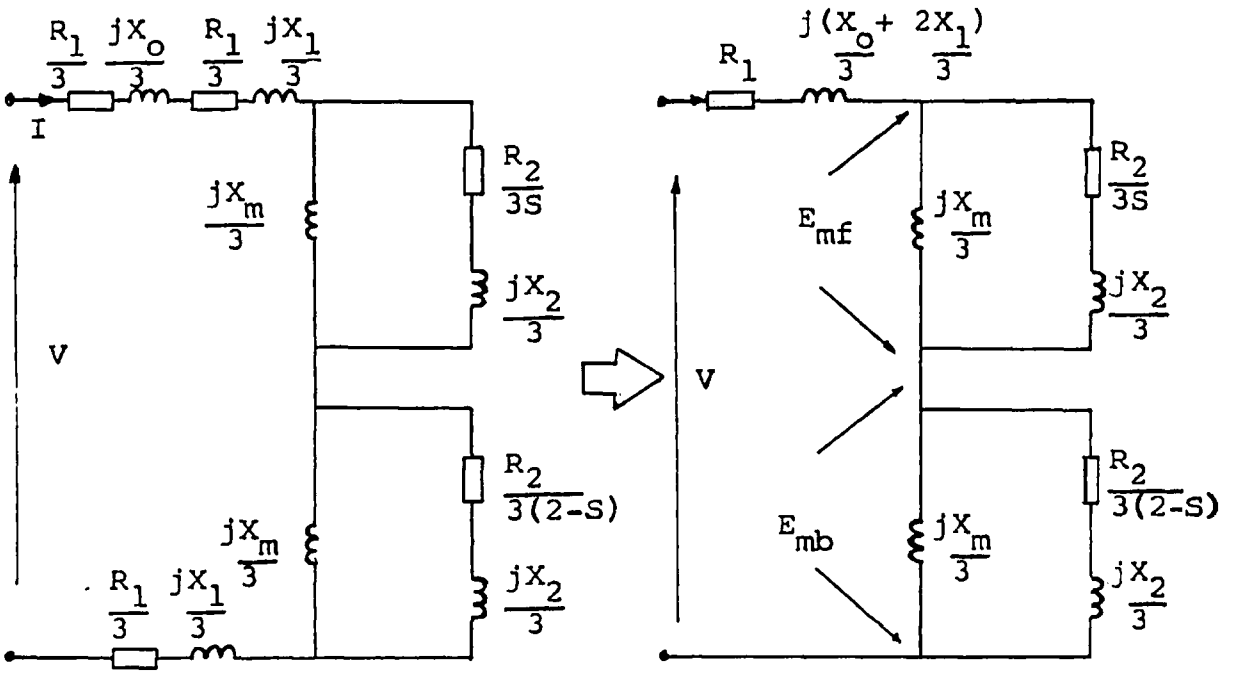

Fig. 1.2.5 The equivalent circuit of a three-phase induction machine when only one phase is connected.

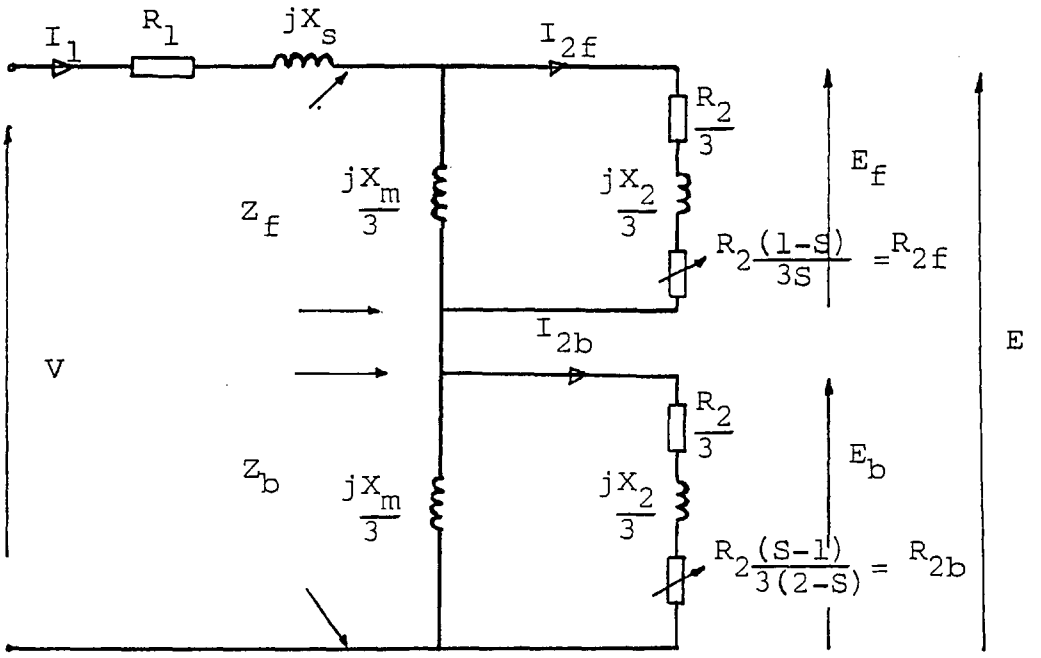

Fig. 1.2.6 Equivalent circuit used in the derivation

$$\frac{R_2}{3S} = \frac{R_2}{3} + \frac{R_2(1-S)}{3S}$$

$$\frac{R_2}{3(2-S)} = \frac{R_2}{3} + \frac{R_2(S-1)}{3(2-S)} \qquad (1.2.9)$$

or $$\frac{R_2}{3S} = \frac{R_2}{3} + R_{2f} \quad \text{where} \quad R_{2f} = \frac{R_2(1-S)}{3S}$$

$$\frac{R_2}{3(2-S)} = \frac{R_2}{3} + R_{2b} \quad \text{where} \quad R_{2b} = \frac{R_2(S-1)}{3(2-S)}$$

therefore the stator current for supply voltage V is

$$I_1 = \frac{V}{Z_1 + Z_f + Z_b} \qquad (1.2.10)$$

and the induced e.m.f. is:

$$E = V - Z_1 I_1 \qquad (1.2.11)$$

which can be divided into the induced e.m.f. for the forward field(E_f) :

$$E_f = \frac{E.Z_f}{Z_f + Z_b} \qquad (1.2.12)$$

and the induced e.m.f. for backward field (E_b):

$$E_b = \frac{E.Z_b}{Z_f + Z_b} \qquad (1.2.13)$$

The forward and backward rotor currents (I_{2f} and I_{2b}) in the rotor branches are

$$I_{2f} = \frac{E_f}{\frac{R_2}{3S} + j\frac{X_2}{3}} \quad ; \quad I_{2b} = \frac{E_b}{\frac{R_2}{3(2-S)} + j\frac{X_2}{3}} \tag{1.2.14}$$

From the rotor currents, the electrical power converted into mechanical power is

$$P_{mech} = \frac{|I_{2f}|^2 R_2(1-S)}{3S} + \frac{|I_{2b}|^2 R_2(S-1)}{3(2-S)} \tag{1.2.15}$$

and the output torque T is

$$T = \frac{P_{mech}}{\omega_m} \tag{1.2.16}$$

where ω_m is the mechanical angular velocity which can be calculated from the rotor speed (n_r) in rev/min from

$$\omega_m = \frac{2\pi n_r}{60} \quad \text{rad/sec.}$$

The electrical power input $P_{e\ in}$ is

$$P_{e\ in} = |V||I_1| \cos\theta \tag{1.2.17}$$

where θ is the phase angle between V and I_1

1.2.4 Analysis of machine performance in the generating mode

The variation of electrical power of a typical three-phase induction motor, when only one phase is utilised, for a range of operating slips is shown in Fig. 1.2.7. The electrical powers are calculated from the equivalent circuit as shown in Fig. 1.2.6 at a constant voltage supply of 50 Hz with neglected iron, friction & windage losses. It can be seen that at slip equal to 1 , corresponding to standstill operation, the rotor resistors (R_{2f} & R_{2b}) which represent converted power in Z_f and Z_b act virtually as short-circuits and the power input to the motor is high with no mechanical power output. At slips lower than one, input power increases with increasing power output and is maximum for the set of parameters considered at a slip of approximately 0.1. Note that with operating slips between 1 and 0, R_{2f} is always positive and R_{2b} is always negative, and the converted output power is the difference between power losses in R_{2f} and R_{2b} .

Since R_{2f} increases with decreasing slips, at very low values of slip ($s < 0.1$) , R_{2f} becomes very big and I_{2f} will be small. The positive power output is very low and negative power output in R_{2b} becomes dominant. At a slip of zero R_{2f} is an open-circuit and the converted power output is equal to zero. The power input

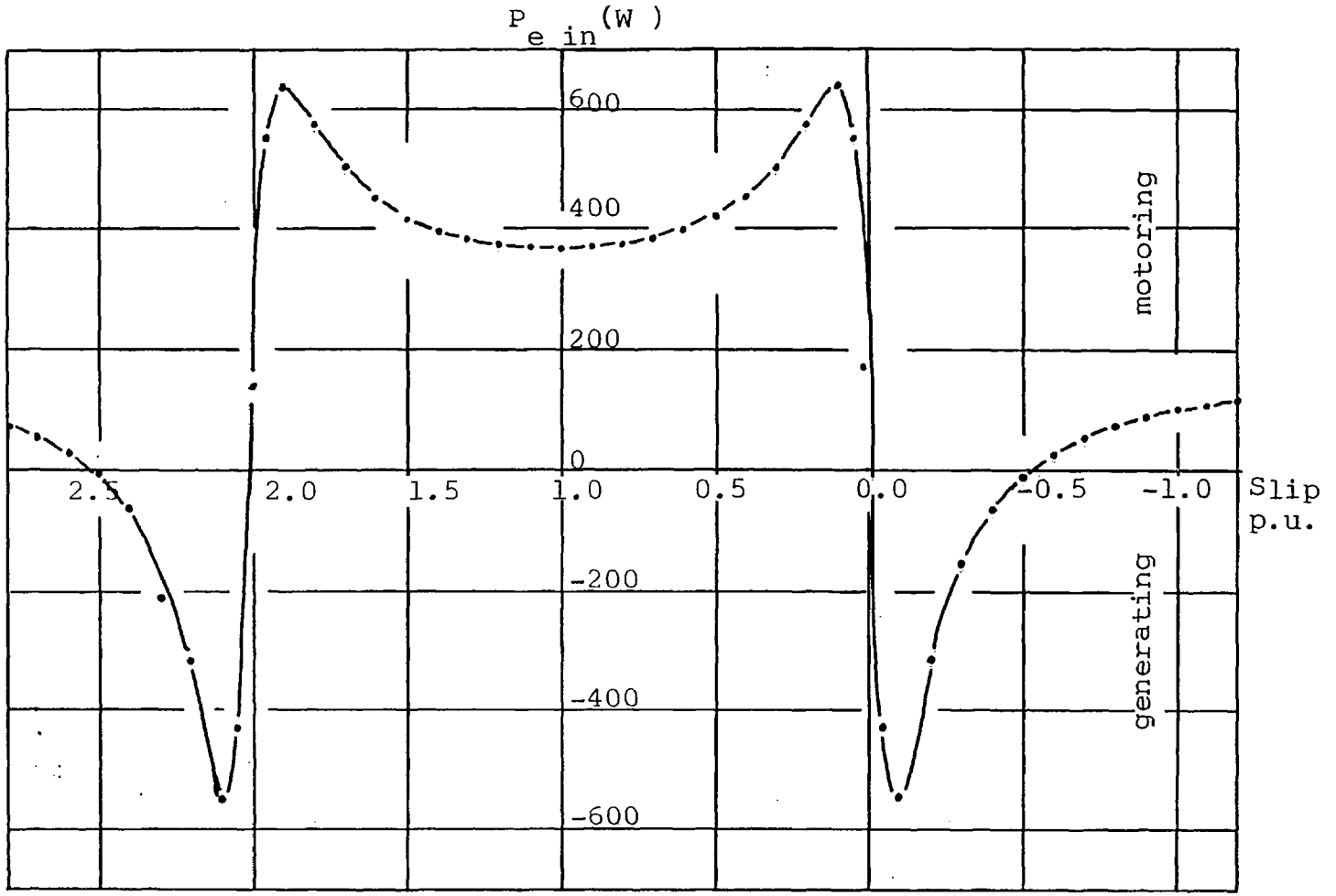

Fig. 1.2.7 Electrical power input-slip characteristic for single phase operation of a typical three-phase induction motor

at this point will be dissipated in R_1 , R_2 with some power input (negative converted power) from R_{2b} .

With negative slips both R_{2f} and R_{2b} become negative and will convert the mechanical power from the shaft to electrical power at the terminal , i.e. the machine operates in the generating mode. The operation is similar to that in the slip range of 1 to 0 but in the reverse sense. With the set of parameters chosen, the maximum electrical power output occurs when the slip is near to -0.1 .

As the slip becomes more negative the currents increase thus increasing the losses in R_1 and R_2 and resulting in a decreasing generated output power.

For this particular case at slip $\leq$ -0.5 the power losses exceed the converted mechanical power and the output power falls to zero.

The power-slip characteristic from S=1 to S =3 is the same as explained above except the machine is driven in the opposite direction ,i.e. the machine can act as a generator (for slips within 0 to -0.5 or 2 to 2.5) whichever way it is driven with no need for reconnection.

The quantitative analysis of the performance in the generating mode, e.g. range of operating slips, slip at maximum airgap power and maximum generating airgap power, related to the machine parameters in the equivalent circuit can be derived from the steady state relations and are detailed in the following two subsections.

1.2.5 Range of operating slips

For negative values of slip, the slip S_o at which the electrical power P_e falls to zero can be found by the equation :

$$P_e = \text{Re}\,(V\, I_1^*) = 0 \qquad (1.2.18)$$

Substituting the expression for I_1 (V is taken as reference), the characteristic equation is (Appendix A1),

$$3R_1\left(\frac{R_2}{X_2+X_m}\right)^4 + 3R_1S^2(2-S)^2 + 3R_1\frac{(S^2-(2-S)^2)}{(X_2+X_m)^2} + \frac{2R_2^3X_m^2}{(X_2+X_m)^4} + 2R_2S(2-S)\left(\frac{X_m}{X_2+X_m}\right)^2 = 0 \qquad (1.2.19)$$

With the assumption that $R_2 \ll X_2 + X_m$ eq. (1.2.19) reduces to

$$S(2-S)\ (3R_1S(2-S) + 2R_2\ (\frac{X_m}{X_2+X_m})^2) = 0$$

So the first and the second roots of this equation are

$$S_o = 0 \qquad \text{and} \qquad S_o = 2 \qquad (1.2.20)$$

The other two roots can be calculated from the characteristic equation

$$3R_1\ S(2-S) + 2R_2\ (\frac{X_m}{X_2+X_m})^2 = 0$$

and the roots of the equation are

$$S_o = 1 \pm \sqrt{1 + \frac{2}{3}\frac{R_2}{R_1}\ (\frac{X_m}{X_2+X_m})^2} \qquad (1.2.21)$$

Hence the operating slip range is

$$S_o = 0$$

and $$S_o = 1 - \sqrt{1 + \frac{2}{3}\frac{R_2}{R_1}\ (\frac{X_m}{X_2+X_m})^2} \qquad (1.2.22)$$

The other two roots define the operating slip range at $S > 2$ for operation in the opposite direction (Fig.1.2.7).

It should be noted that a) the stator reactance X_1 does not have any effect at all on the operating slip range and b) since X_m is usually much greater than X_2 , the slip range depends almost entirely on the ratio of stator to rotor resistance.

1.2.6 Maximum airgap power condition

If the airgap power is defined as

$$P_a = \mathrm{Re}\ (E\, I_1^*) \qquad (1.2.23)$$

where E is the induced e.m.f. due to airgap flux and is regarded as a constant and I_1^* is the conjugate of the stator current with Z_1 neglected , the slip S_{max} for maximum airgap power $P_{a\ max}$ can be found by setting

$$\frac{d}{dS} \left(\mathrm{Re}\ (E\, I_1^*) \right) = 0 \qquad (1.2.24)$$

with the same assumption that $R_2 \ll (X_2 + X_m)$, the roots of the characteristic equation are (Appendix A2)

$$S_m = 1$$

$$S_m = 1 \pm \sqrt{1 + K} \qquad (1.2.25)$$

$$S_m = 1 \pm \sqrt{1 - K}$$

where $K = \frac{R_2}{X_2} \frac{(2X_2 + X_m)}{(X_2 + X_m)}$

$S = 1$ corresponds to the maximum airgap power in the motoring mode. Because R_2 is always less than X_2, and with $X_2 \ll X_m$ the value of K is less than 1. Hence three values of slip given by : $1 \pm \sqrt{1 - K}$ and $1 - \sqrt{1-K}$ are always positive and do not occur in the generating region.

Consequently, the slip for maximum generating airgap power is given by the remaining root :

$$S_{max} = 1 - \sqrt{1 + K} \qquad (1.2.26)$$

where $K = \frac{R_2}{X_2} \frac{(2X_2 + X_m)}{(X_2 + X_m)}$

When this is substituted into the P_a relation, eq. (1.2.23), $P_{a\ max}$ is found to be :

$$P_{a\ max} = -\frac{3}{2} E^2 \frac{(\frac{X_{3m}\ X_{2m}}{X_2} - R_2)}{(R_2^2 + 2R_2\ X_{3m} + 2X_{3m}^2)} \qquad (1.2.27)$$

where $X_{3m} = 2X_2 + X_m$

$X_{2m} = X_2 + X_m$

Assuming again that $R_2 \ll (X_m + X_2)$ gives the approximate maximum airgap power as :

$$P_{a\ max} = - \frac{3}{4} \frac{E^2 (X_2 + X_m)}{X_2 (2X_2 + X_m)} \qquad (1.2.28)$$

1.2.7 Performance of single-phase induction machine running on main winding only

The equivalent circuit for a "genuine" single-phase induction machine when it runs on main winding alone and iron losses are negligible is shown in Fig. 1.2.8[1.10] where R_{11} and X_{11} are the resistance and the leakage reactance of the winding, X_{m1} is the magnetising reactance, R_{21} and X_{21} are the rotor referred resistance and standstill leakage reactance (assumed constant) and S is the per unit slip respectively.

Comparing Fig. 1.2.8 and the equivalent circuit obtained from the transformation in Fig. 1.2.5, the apparent similarity between the two equivalent circuits can be seen very clearly. Table 1 lists the equivalent circuit impedances used in the two equivalent circuits.

With the same circuit configuration as in Fig. 1.2.5, the expressions for the range of operating slips and for the maximum airgap power condition can be easily derived by the same procedure.

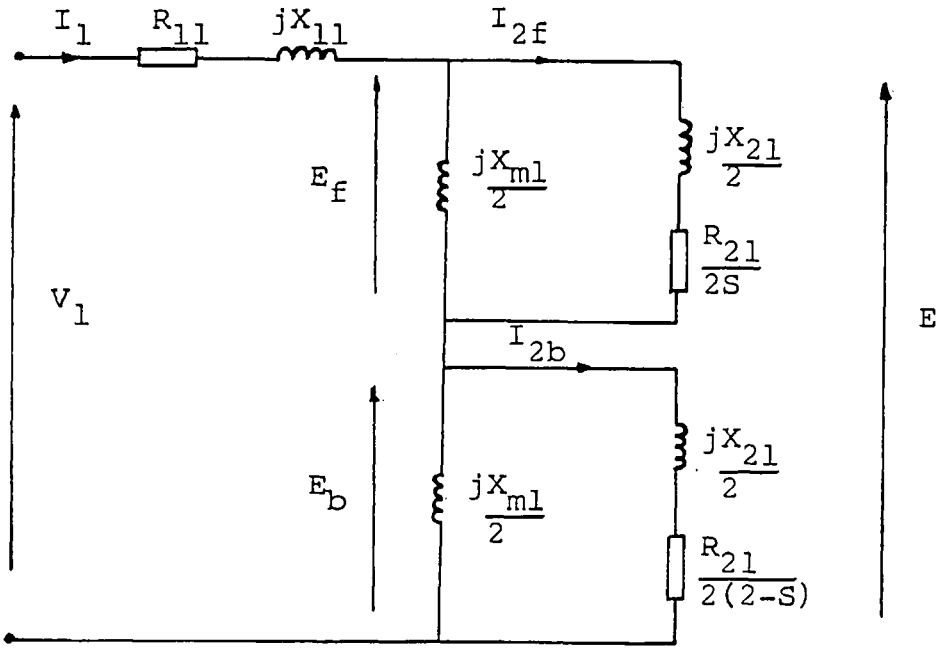

Fig. 1.2.8 Equivalent circuit of a single-phase induction motor in running condition (main winding only)

Table 1 1: Parameters from single-phase operation of the three-phase machine
2: Parameters from the single-phase induction machine (main winding only)

Parameter	1	2
Stator resistance	R_1	R_{11}
Stator reactance	$X_s = \frac{2X_1}{3} + \frac{X_o}{3}$	X_{11}
Forward or backward magnetising reactance	$\frac{X_m}{3}$	$\frac{X_{m1}}{2}$
Forward or backward rotor resistance at standstill	$\frac{R_2}{3}$	$\frac{R_{21}}{2}$
Forward or backward rotor reactance at standstill	$\frac{X_2}{3}$	$\frac{X_{21}}{2}$

The results are as follows:

With the same assumption that $R_{21} \ll X_{21}+X_{m1}$

a) Range of operating slips

For negative slip, the range is between

$$S_o = 0 \quad \text{and} \quad S_o = 1 - \sqrt{1+\frac{R_{21}}{R_{11}}\left(\frac{X_{m1}}{X_{m1}+X_{21}}\right)^2} \qquad (1.2.29)$$

b) Maximum airgap power condition

$$S_{max} = 1 - \sqrt{1+K} \qquad (1.2.30)$$

where $$K = \frac{R_{21}}{X_{21}} \frac{(2X_{21}+X_{m1})}{(X_{21}+X_{m1})}$$

and maximum airgap power

$$P_{a\ max} = \frac{-E^2\left(\frac{X_{3m1}X_{2m1}}{X_{21}} - R_{21}\right)}{R_{21}^2+2R_{21}X_{3m1}+2X_{3m1}^2} \qquad (1.2.31)$$

where $X_{3m1} = 2X_{21}+X_{m1}$ and $X_{2m1} = X_{21}+X_{m1}$

and the approximate airgap power is

$$P_{a\ max} = \frac{-E^2\ (X_{21}+X_{m1})}{2X_{21}(2X_{21}+X_{m1})} \qquad (1.2.32)$$

1.3 Conclusions

An analysis method and some theoretical results have been presented for the steady-state single-phase operation of the three-phase induction motor. It was found that the equivalent circuit obtained from a symmetrical components transformation method is similar to the well known equivalent circuit of the single-phase induction motor running on main winding only.

Expressions determining the characteristics in the generating mode have been derived from the equivalent circuits. These expressions if confirmed by the test results can be very useful in choosing a suitable machine for use as a plain single-phase, mains-connected induction generator.

CHAPTER 2

EXPERIMENTAL RESULTS AND OPTIMISATION

2.1 Introduction

In the first part of this chapter, the tests and measurements for determining equivalent circuit parameters on a wound-rotor three-phase induction motor will be described. The comparisons between the predicted results calculating from the equivalent circuit and results from load test will be made in section 2.2. The numerical values of the performance parameters derived in the last chapter will be calculated from the equivalent circuit parameters and will be compared with the predicted results to check the validity and accuracy of the expressions , at least for wound-rotor machines.

The effect on performance of design parameters will be investigated and discussed in sec. 2.3. The way in which the design of an induction machine should be biassed in order to achieve reasonably good operation as a single-phase induction generator will be discussed in sec. 2.4.

2.2 Experimental systems and measurements

The parameters of the machine were taken from the measurements of a typical three-phase , four-pole, 50 Hz, wound-rotor induction machine rated (under balanced three phase conditions) at : 6.3 KW , 110 Volts (Δ) . The (hot) stator resistance, measured by "Kelvin Bridge" is 0.52 Ω . The results of the no load test are shown in Fig. 2.1.1, and the corresponding calculated machine parameters are as follows :

$R_1 = 0.52\ \Omega$ $\qquad$ $R_2 = 1.05\ \Omega$

$X_1 = 1.49\ \Omega$ $\qquad$ $X_2 = 1.49\ \Omega$

$X_m = 49.06\ \Omega$

voltage ratio (stator:rotor) = 2.0

total friction and windage losses = 420 W at rated speed.

To illustrate the use of the equivalent circuit, a simple computer program was written to calculate the powers and currents as given in eqs. (1.2.10) and (1.2.17). The zero sequence reactance, X_o was also measured and is 3.21 Ω. In making the predictions, iron losses were allowed for by the addition of 40 Ω "iron losses" resistor to the equivalent circuit in parellel with the magnetising reactance branch, and friction and windage losses were allowed for by adding 420(1-S) Watts to the predicted value of the gross mechanical power (i.e. iron losses assumed proportional to airgap flux squared

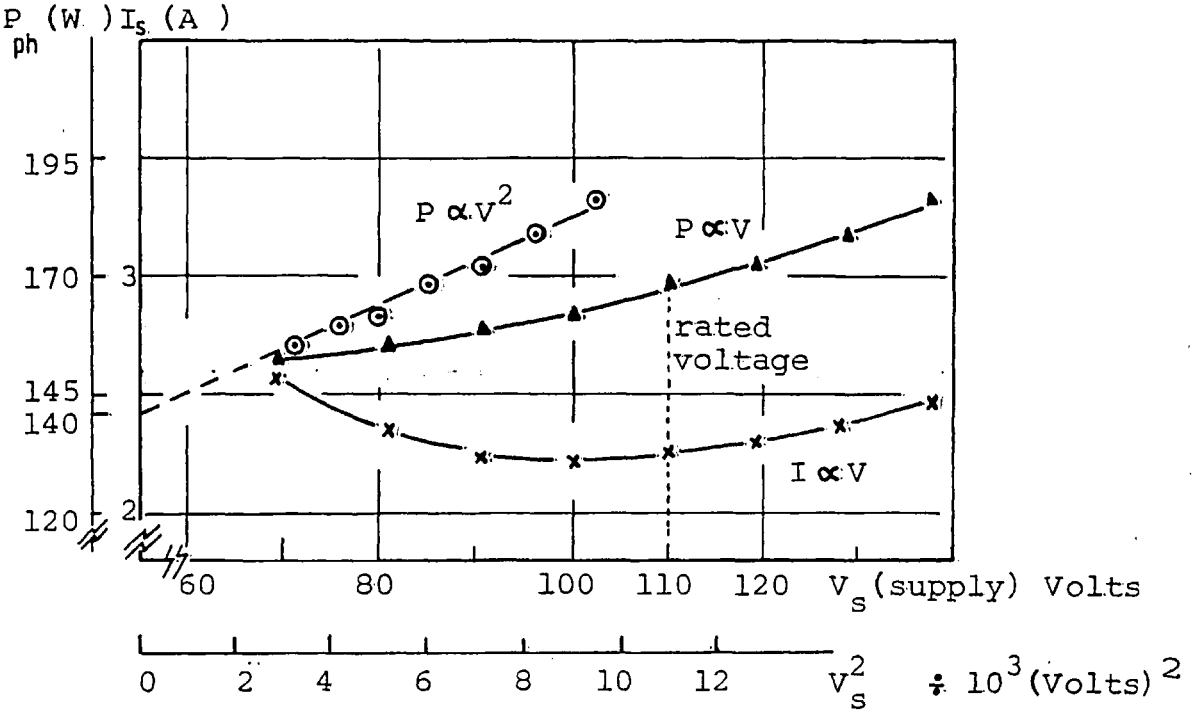

a.) No-load Test

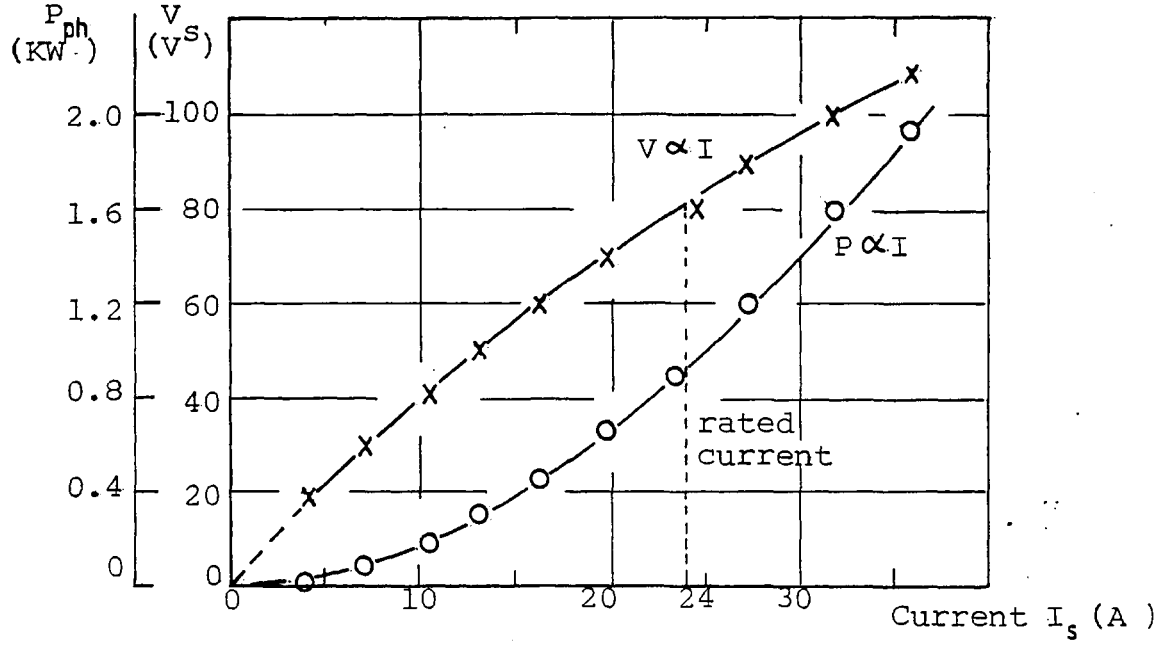

b.) Locked-rotor Test

Fig. 2.1.1 Results from the no-load and locked-rotor test

and friction and windage losses to speed) , both allowances being based on measured loss values.

Fig. 2.1.2 shows current and power versus speed predictions for single-phase operation using the relations of the analysis in sec. (1.2.3) , together with the measured results.

There are some discrepancies between the curves, probably arising from changes in rotor resistance, magnetising reactance and zero sequence impedance due to skin effect in the winding turns, saturation, and from the approximation involved in assuming that iron losses increase simply as E^2 and so on, but the agreement is reasonably good. The good agreement obtained in these comparisons is to some extent due to the fact that the machine tested was of the wound-rotor, slip-ring type. With a squirrel-cage machine, particularly one rated at a power beyond say 1 KW , deep bar effects would be significant and , as stated previously, the analysis would probably not correlate so well with measurements.

The expressions for the operating slip range, the slip for maximum airgap power and the maximum airgap power itself were checked from the calculations and found to be in good agreement with the value obtained from the equations given in section 1.2.5 and 1.2.6. This is shown in Table 2 .

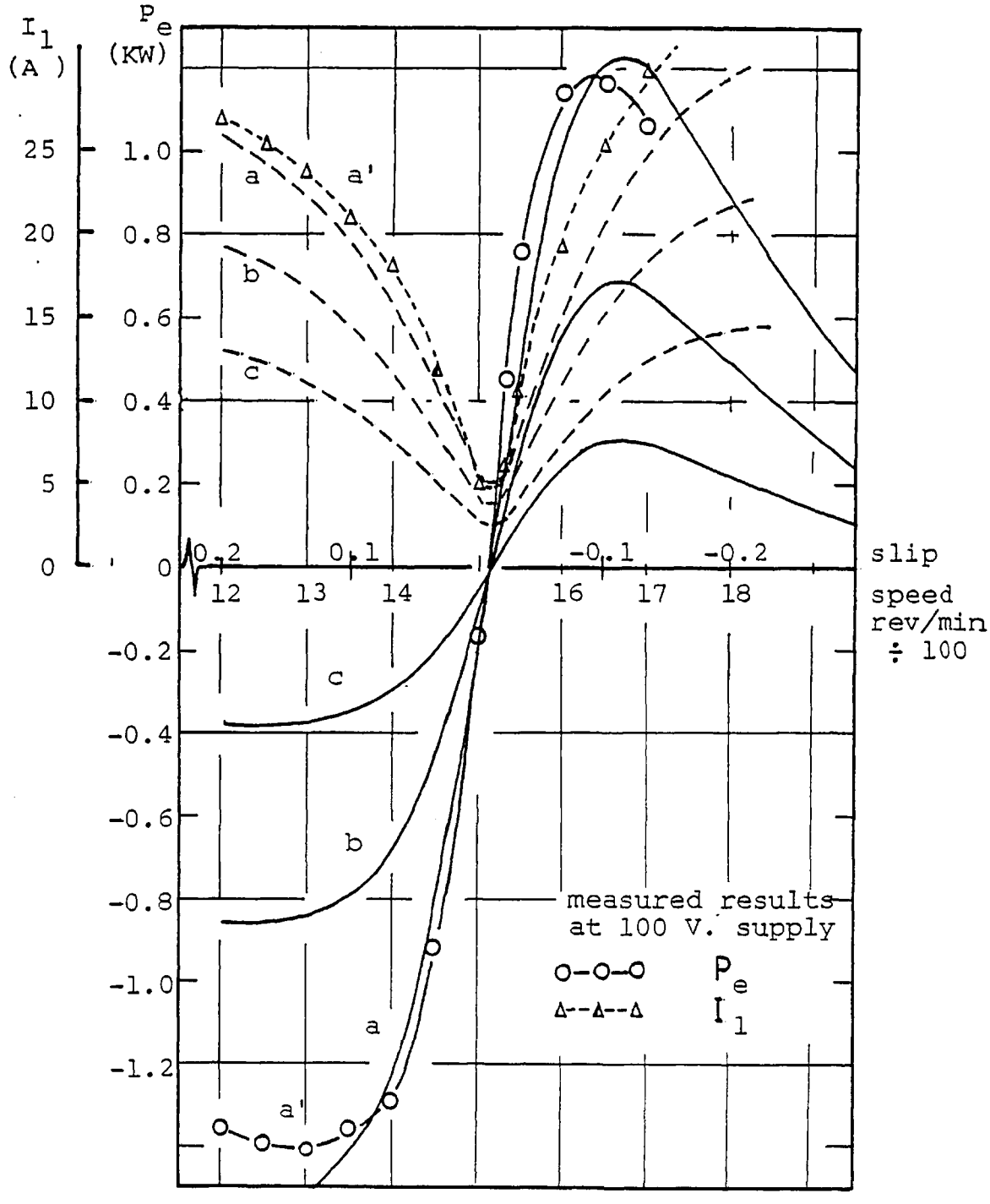

Fig. 2.1.2 Performance curves of the single-phase induction generator

P_e: Power to supply ————

I_1: Supply current ----------

a: at 100 V , b: at 75 V , c: at 50 V

For this particular case the approximate maximum rotor power is different from the exact value by only 2.5 %.

Table 2

Quantity		A	B
Slip at zero output power	(%)	-50.6	-51.5
Slip for maximum airgap power	(%)	-31.6	-32.0
Maximum airgap power	(KW)	4.79	4.75
Approximate max. airgap power	(KW)	4.89	4.75

Comparison made at 100 V supply

A : calculated from approximate relations

B : computed from the equivalent circuit

2.3 Effect on performance of design parameters

In order to investigate the performance in the generating mode of a single-phase induction machine, predictions of output power P_e versus speed for a set of machines having equal magnetising reactances but various combinations of R_1 , R_2 , X_2 and X_m were made. In this computation, iron , friction and windage losses were neglected. The results for output power are shown in Fig. 2.3.1 , 2.3.2 and 2.3.3 . As might be expected, this indicates that :

1) a progressive decrease in useful slip range occurs as R_1 increases ,

2) X_2 determines the peak power

3) The higher the value of R_2 , the less steep is the initial slope of the output power versus slip curve and the bigger is the useful slip range .

4) The maximum power output is unaffected by R_2 but high rotor resistance gives a larger slip range and a larger S_{max} .

Fig. 2.3.4 , 2.3.5 , 2.3.6 and 2.3.7 show corresponding efficiency curves. It can be seen that, even when iron,windage and friction losses are neglected, efficiency levels are generally rather low. If reasonably efficient operation is to be obtained, low R_1, R_2 , X_1 and X_2 values, and high X_m value and low iron, windage and friction losses are desirable.

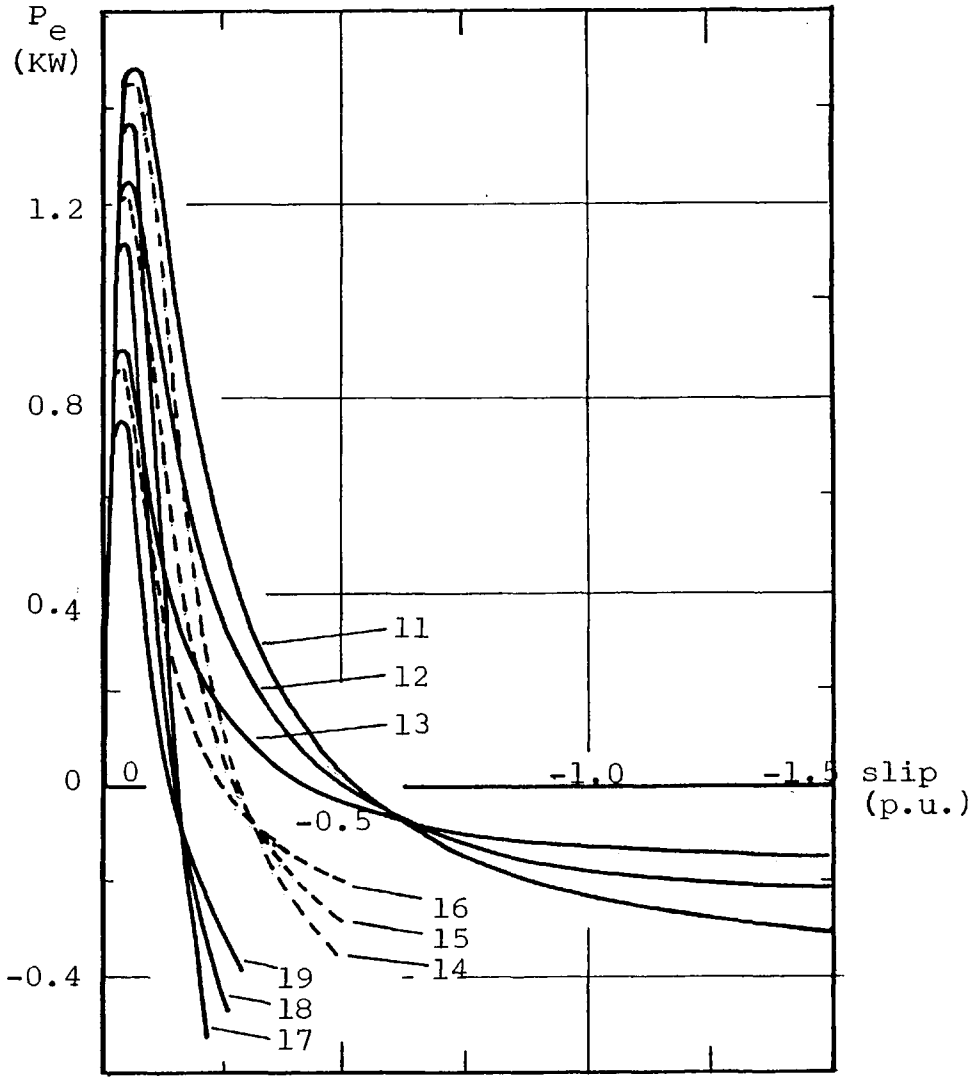

Fig. 2.3.1 Effect of design changes on P_e - slip characteristic

ref no.	R_2/R_{20}	R_1/R_{10}	X_2/X_{20}
11	½	½	½
12	½	½	1
13	½	½	2
14	½	1	½
15	½	1	1
16	½	1	2
17	½	2	½
18	½	2	1
19	½	2	2

R_{20}, R_{10}, X_{20} are the base values of R_2, R_1 and X_2 respectively.

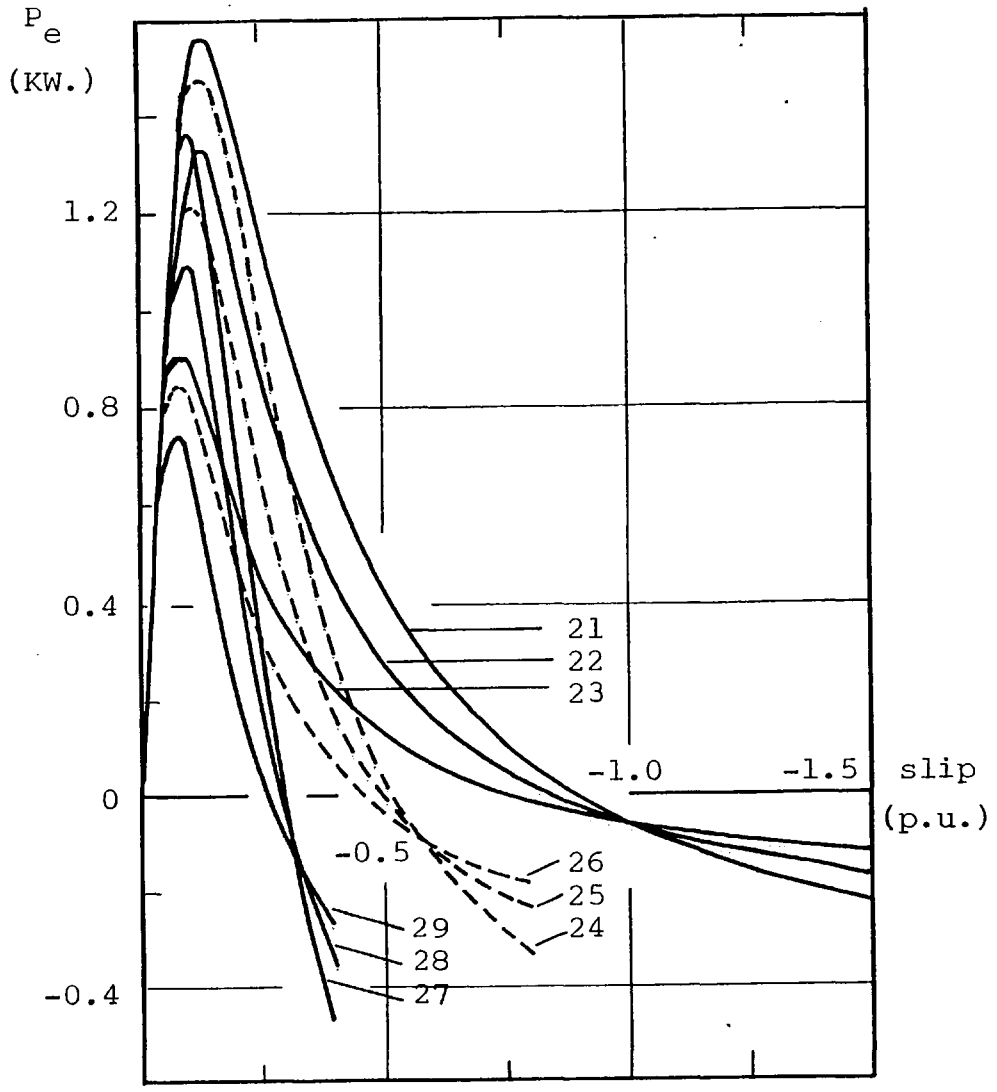

Fig. 2.3.2 Effect of design changes on P_e- slip characteristic

ref no.	R_2/R_{20}	R_1/R_{10}	X_2/X_{20}
21	1	½	½
22	1	½	1
23	1	½	2
24	1	1	½
25	1	1	1
26	1	1	2
27	1	2	½
28	1	2	1
29	1	2	2

R_{20}, R_{10} and X_{20} are the base values of R_2, R_1 and X_2 , respectively.

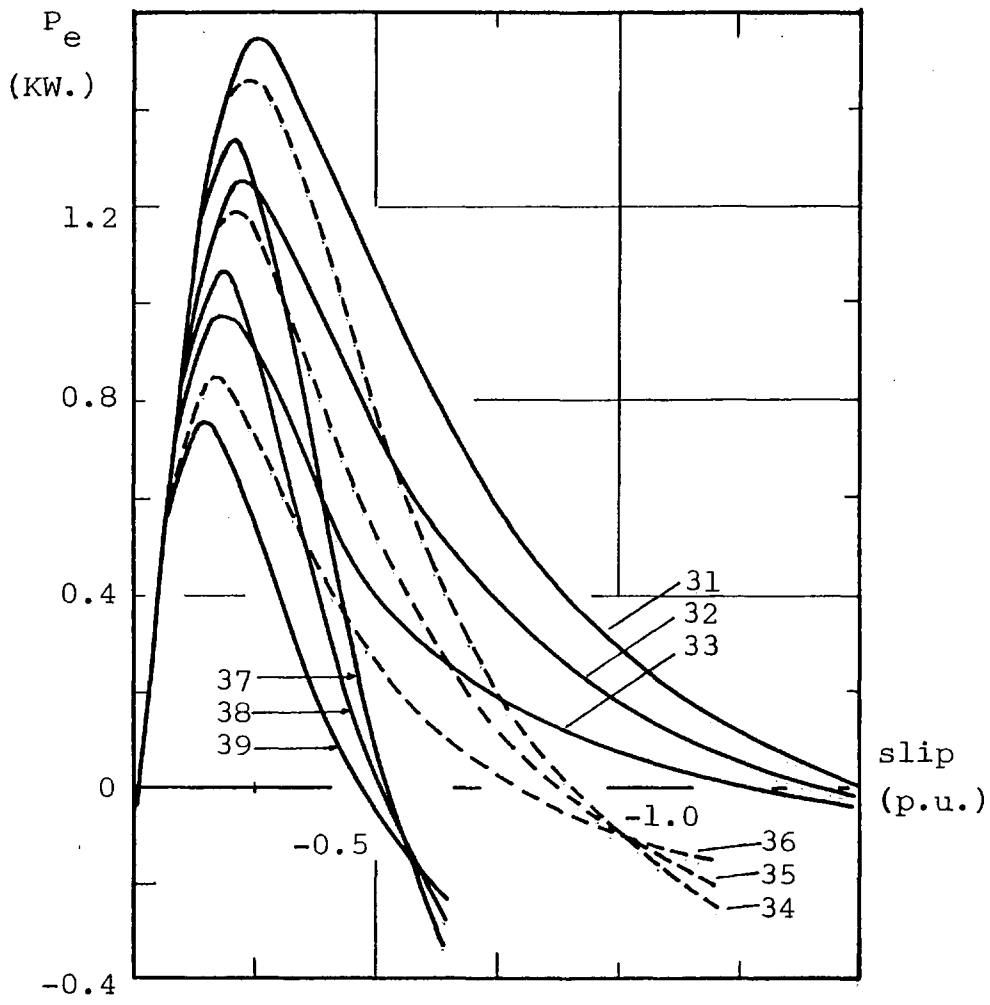

Fig. 2.3.3 Effect of design changes on P_e- slip characteristic

ref no.	R_2/R_{20}	R_1/R_{10}	X_2/X_{20}
31	2	½	½
32	2	½	1
33	2	½	2
34	2	1	½
35	2	1	1
36	2	1	2
37	2	2	½
38	2	2	1
39	2	2	2

R_{20}, R_{10} and X_{20} are the base values of R_2, R_1 and X_2, respectively.

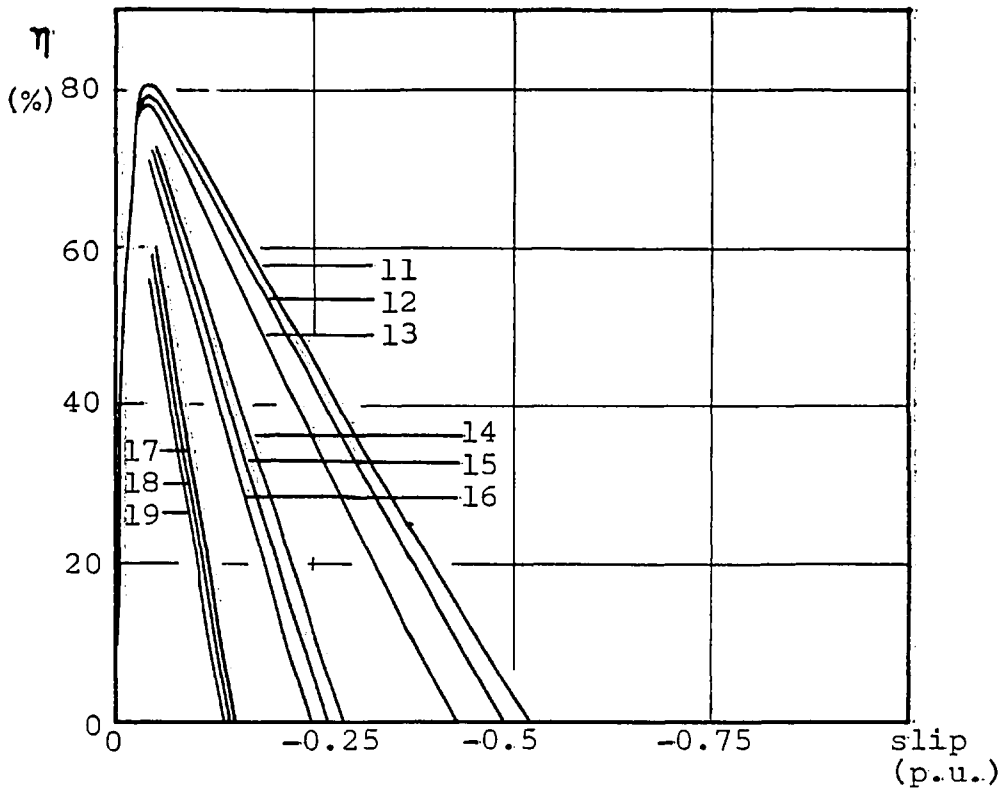

Fig. 2.3.4 Effect of design changes on efficiency-slip characteristic (see Fig.2.3.1 for ref no.)

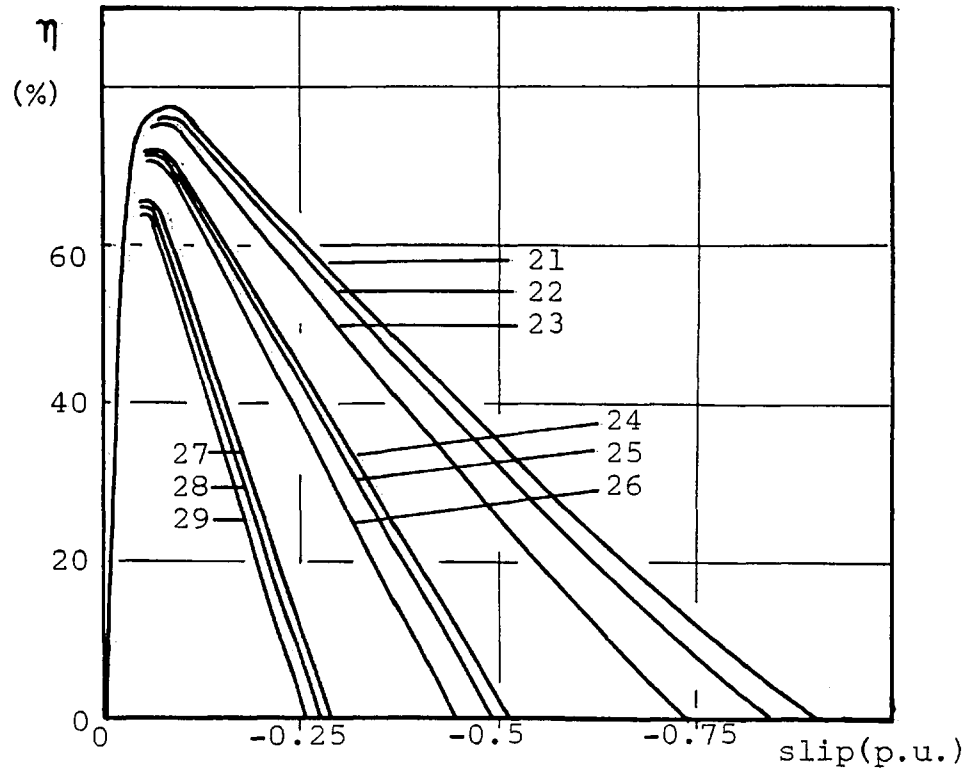

Fig. 2.3.5 Effect of design changes on efficiency-slip characteristic (see Fig. 2.3.2 for ref no.)

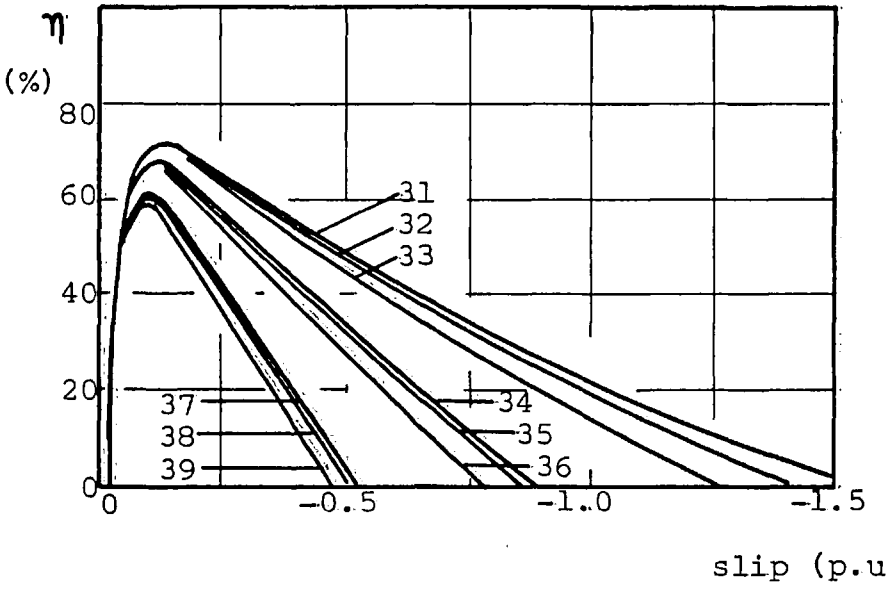

Fig. 2.3.6 Effect of design changes on efficiency-slip characteristic (see Fig. 2.3.3 for ref. no.)

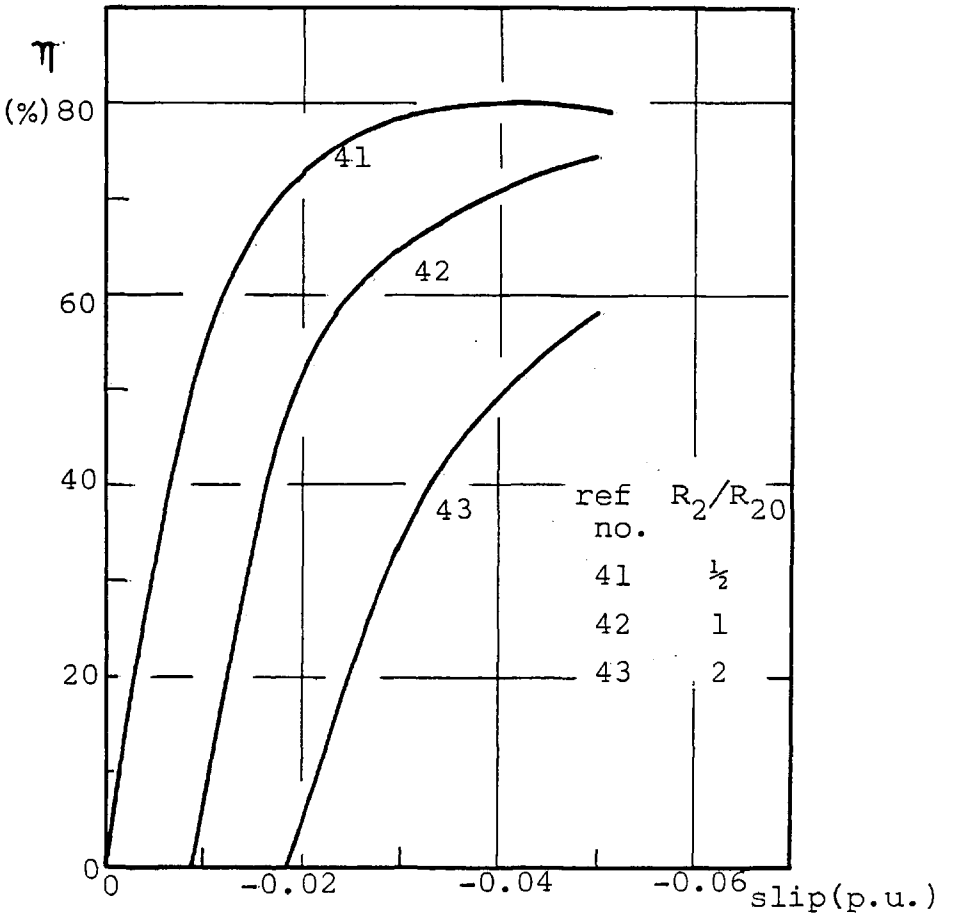

Fig. 2.3.7 Effect of design changes on efficiency-slip characteristic at low negative slips (R_1/R_{10} and X_2/X_{20} are equal to 1 .)

2.4 Design consideration

Given that the efficiencies of single-phase induction generators seem to be a little low, it is obviously particularly important to consider the question of how to design for as good an operating efficiency as possible. A low R_1 , R_2 , X_1 , X_2 and a high X_m are required and the following factors are hence relevant.

1) As X_m varies inversely with both (number of pole)^2 and airgap length$^{2.1}$, a small number of poles and a small airgap length* are preferred.

2) Copper rotor bars are preferred to cast aluminium or fabricated aluminium cage rotor since a lower R_2 will result from the same bar cross-section.

3) The rotor should preferrably not be a deep-bar type or a double-cage type because high rotor frequencies due to the backward field will result in an increase both in resistance and reactance and hence higher backward field losses for the whole operating slip range. Maximum thickness rotor slot bridges are preferred to minimise X_2 , subject to starting current constraints.

4) The number of slots, the number of turns of the stator winding and the magnitude of the stator voltage do not in themselves seriously affect the per unit impedances of the machine.

5) Although wide and shallow slots give low

---

* though increases in surface losses and zig-zag leakage flux would have to be watched.

slot leakage reactance, the conductor areas will be small and/or the number of slot per poles will be small, which results in an increase in resistance and zigzag leakage reactance.[2.2] A good compromise in the slot design (e.g. 50% slot width/slot pitch) is therefore desirable.

6) The stator should be wound specifically for single-phase operation rather than be a reconnected three-phase machine so that the volume of useful copper and iron is maximised.

7) Machines which are large for their rating (or derated machines) will give better efficiencies because operating current densities and flux densities will be low hence giving low losses. Big diameter machines also have a lower slot leakage reactances and lower per unit resistances than the smaller machines.[2.3] Obviously low loss laminations are preferred.

8) Big pole pitches (implying large diameter, few poles) give lower per unit resistances and per unit slot reactances.[2.4] Increases in the coil-end-leakage reactances and end-turn reactances will however limit the maximum desirable pole pitch.

9) Low loss bearings, and high efficiency fans should be used to minimise friction and windage losses.

2.5 Conclusions and further works

An analysis method and results have been presented for the single-phase generation of an induction generator. The generator's torque versus speed characteristics are very similar to those of standard three-phase, mains-connected induction generators and the same considerations are relevant when the design of a complete turbine/gearbox/generator/feeder/protection and control system is undertaken.[2.5,2.6,2.7]

The generator torque will obviously be modulated at twice mains frequency and some mechanical shaft damper may be desirable to avoid resonance phenomena. The results show that, though the efficiency levels are only moderately good, the plain single-phase induction machine is worth considering when single-phase supplies only are available or in locations where there are no supplies at all. The availability of single-phase induction machine, the simplicity and and robustness of the structure (no field winding, cage rotor) and the lower cost of just one exciting capacitor, and just one load bank (instead of three-phase banks of capacitors and loads) suggest that the single-phase self-excited scheme could be well worth considering.

However, there is a clear need for further investigations in the areas such as the followings :

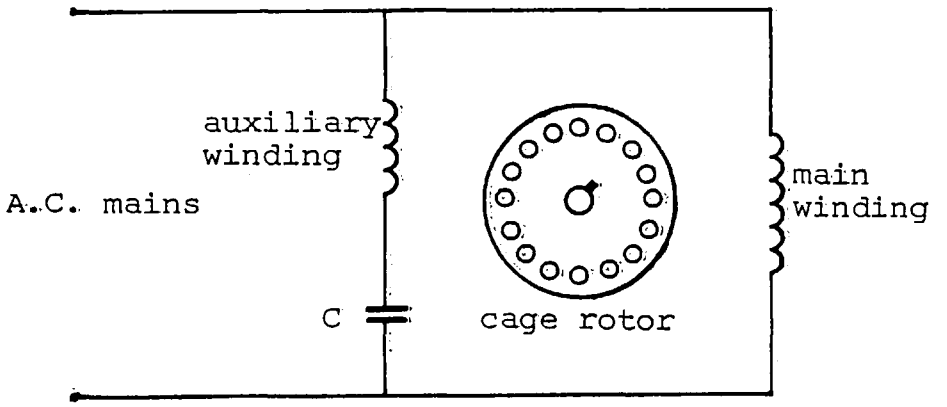

Fig. 2.5.1 Diagram of a single-phase squirrel-cage induction generator with auxiliary - winding and capacitor

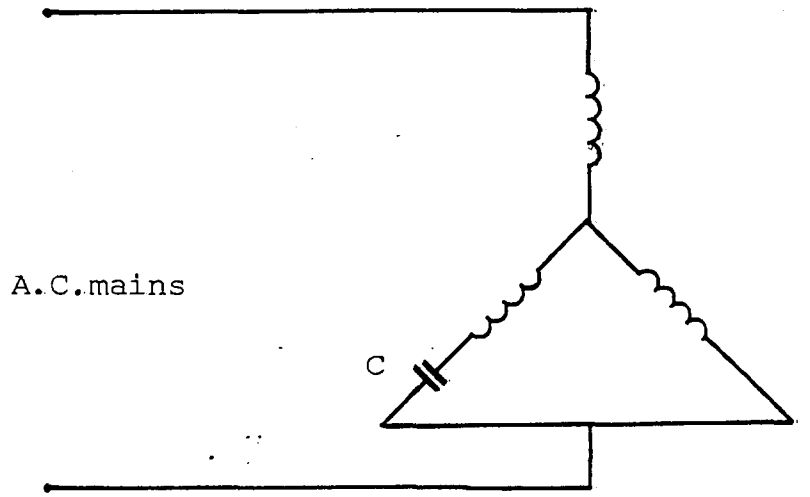

Fig. 2.5.2 Connection diagram of closed 'V' scheme with capacitor and three-phase induction machine.

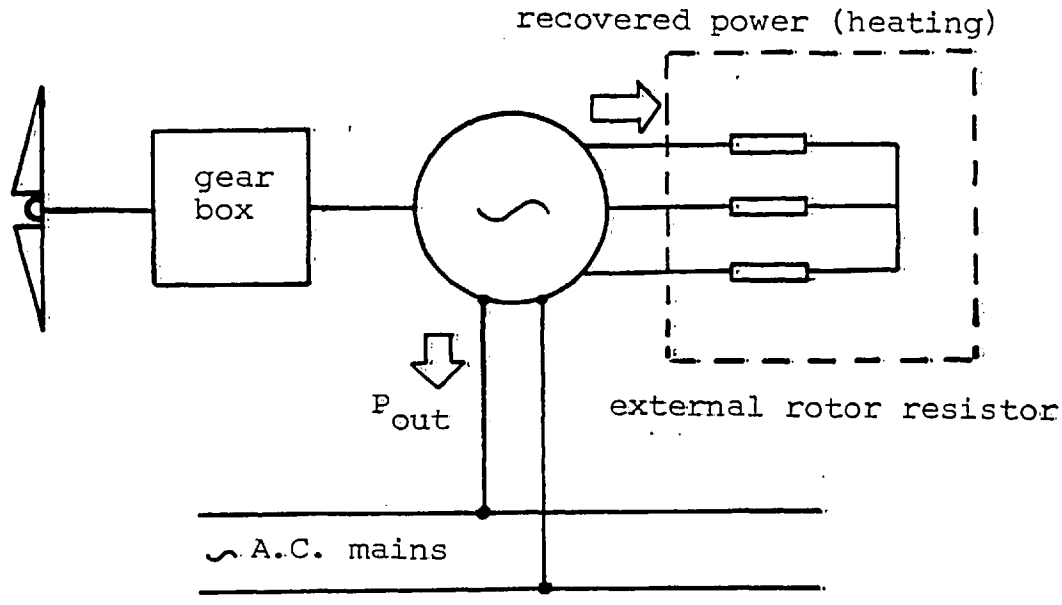

Fig. 2.5.3 Possible single-phase mains-connected system

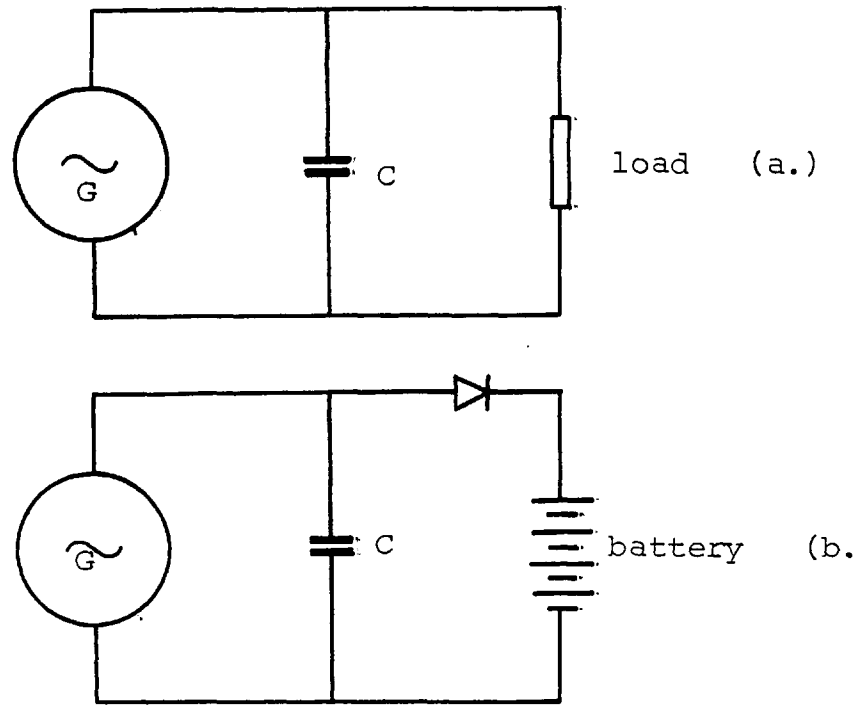

Fig, 2.5.4 Possible self-excited system

a. Resistive load

b. Battery loading

1) Performance of single-phase, squirrel-cage induction generators running on main winding and/or with auxilliary winding and run capacitor (Fig. 2.5.1),

2) Other single-phase connections of three-phase induction generators, i.e. closed 'V' with capacitor in the loop (Fig. 2.5.2),

3) Feasibility of various unusual generator/excitation/load configurations with and without mains connection. Fig. 2.5.3 and Fig. 2.5.4 show some typical possibilities.

Part B

SINGLE-PHASE SWITCHED RELUCTANCE MOTOR DRIVE SYSTEMS

CHAPTER 1

GENERAL INTRODUCTION

1.1 Principle of the switched reluctance motor drive system

Mechanical force development in the vast majority of electrical machines can be ascribed to two types of phenomenon: (a) 'reluctance', 'alignment' or 'magnetic' action and (b) 'interaction' or 'electromagnetic' action. These are shown in Fig. 1.1.1. As is well known, if a piece of ferromagnetic material is placed in a magnetic field, it experiences a force or torque urging it to move to a position in which the energy stored in the magnetic field is maximised. The shaped iron rotor shown in Fig. 1.1.2 for example will experience a torque tending to align its direct axis in the direction of the magnetic field. The magnetic path reluctance is minimised and the airgap-field-stored energy is hence normally maximised. These reluctance or alignment forces can be explained in terms of magnetic poles, so-called 'induced poles' being set up on the rotor saliencies and being attracted to corresponding poles on the stator.

Pure reluctance forces are exploited in limited motion devices (e.g. moving iron instruments, relays, etc.), incremental motion devices such as stepper motors, and

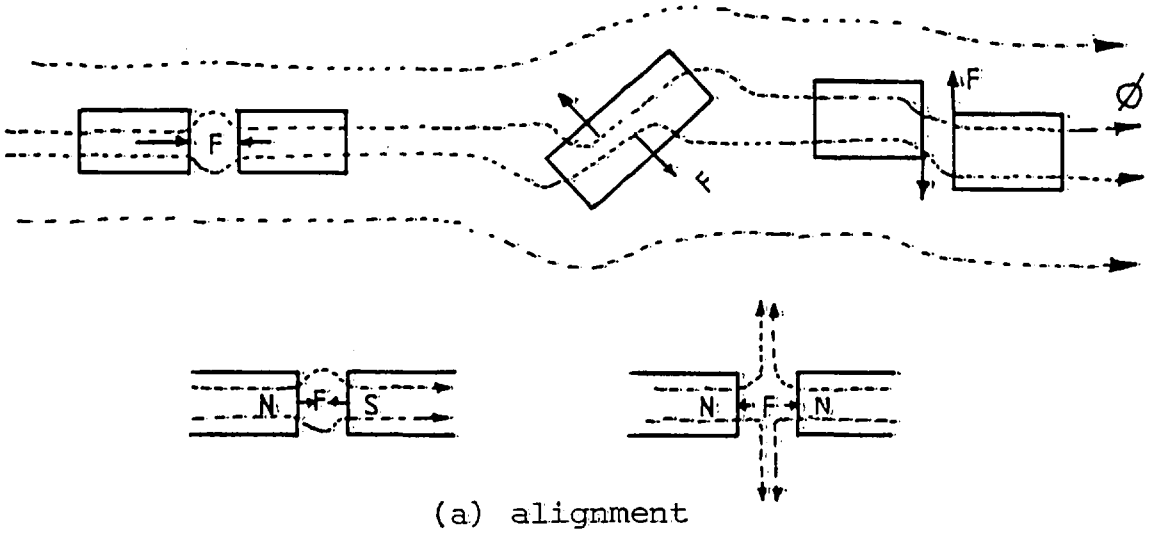

(a) alignment

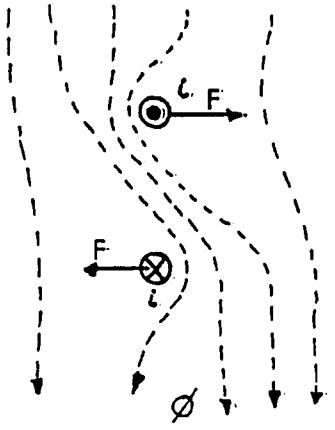

(b) interaction

Fig. 1.1.1 Forces in a magnetic field

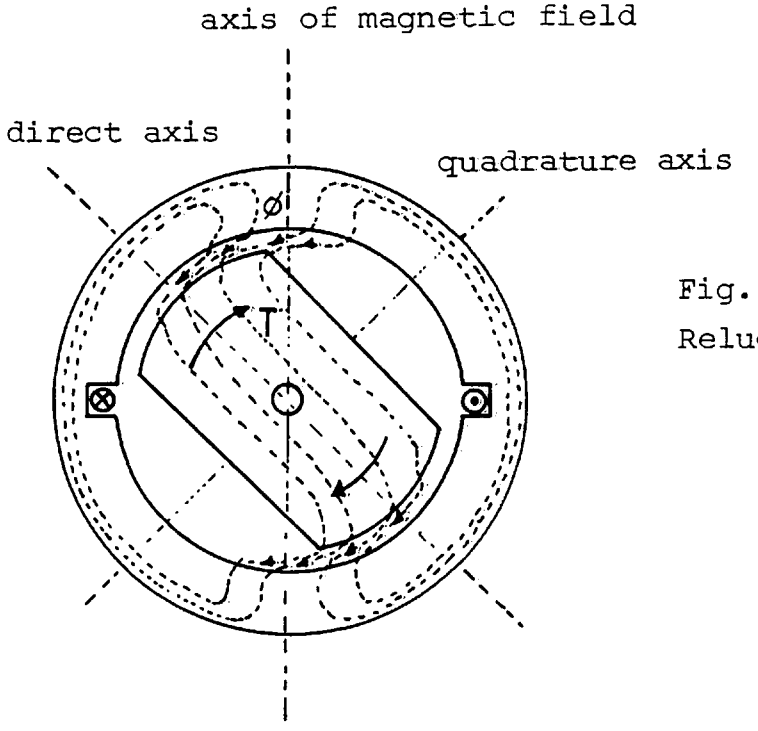

Fig. 1.1.2
Reluctance torque

reluctance forces occur as incidental components of synchronous torque in conventional synchronous machines which have salient poles or which possess magnetic saliency due e.g. to slotting. Another category of motor which uses reluctance forces to provide an essential feature of its operating characteristic is the 'reluctance motor'. In terms of usage and to some extent construction, reluctance motors can be thought of as synchronous motors that operate without d.c. field excitation. Stator constructions are similar to those in synchronous and induction motors, i.e. essentially smooth-bore, uniformly-slotted stators are used. Rotor constructions vary and have been the subject of considerable research and development over the past twenty years but can broadly be categorised into 'conventional salient' and 'segmented' types. The literature dealing with conventional reluctance motors is extensive and since it is easily accessible and of peripheral interest in the present context, it is not summarised or listed here.

Conventional reluctance motors are normally operated on the fixed-frequency mains. With motors of any size, imduction forces have to be used to accelerate the motors to synchronous speed and conductors are hence incorporated in the rotor. With some small (i.e. instrument sized) motors, torque to inertia levels are high enough to enable the acceleration process to occur within half a mains cycle and induction action in the rotor is less vital. Mains-fed reluctance motors are of course used in

applications requiring a fixed-speed, synchronised form of drive and instrument sized motors, which may be single-phase rather than three-phase excited are used for clocks and other timing systems. Conventional reluctance motors are also used in conjunction with variable frequency supplies, and multi-motor installations fed from single inverter are widely used (e.g. in the textile industry) where synchronism must be maintained throughout a complex item of production plant. When the only connection between the motor (in a single motor system) and the variable frequency feed is the system of winding supply conductors, the feed controller knows little of the motor's detailed behaviour and speed instabilities can occur. Some of the literature dealing with the design of conventional reluctance motors examines this problem and shows how changes in design parameters (particular of the rotor conductor work) can influence the range of operating conditions over which instabilities can occur.

Similar remarks apply to the other well-established form of motor employing reluctance principles: the stepper motor. This is also normally operated 'open-loop' in that the feed is controlled solely on the basis of command signals from an external source. Stepper motors are characterised by their doubly-salient construction incorporating stator and rotor slot pitches that differ only moderately, by their operating mode in which ,typically, unidirectional currents are supplied in turn to a

large number (often four or more) of stator phases from a transistorised, d.c.-fed switching feed. The use of small slot pitches, non-integral (stator to rotor) tooth ratios and high phase numbers is general in order to obtain small step angles. This has the great advantage for position control applications that acceptable positional accuracy is achievable without the need for position feedback, but speeds and output powers are in practice limited to a few thousand rev/min and 1 or 2 KW due to high switching frequencies, iron losses and noise that accompany small step-angle working at high loads and speeds.

The 'switched reluctance motor' (SRM) is now recognised as a third category of reluctance motor, though it could be said to share many of the constructional and operational features of the V.R. stepper motor. The features it shares (in most cases) are the use of a doubly-salient stator and rotor construction, the use of a switched, unipolar, multiphase supply, the adoption of non-integral stator to rotor tooth ratios, and the use of non-segmented rotor constructions. However the step angles of the SRM are large (compared to those in most stepper motors) to allow high speed operation, the motor is normally operated in the (essentially constant speed) 'slewing' mode rather than the 'stepping' mode, and the switching instants of the switching unit devices rather than being solely dependent on 'external' signals are largely controlled by signals from a shaft-angle sensor. This last feature eliminates

the possibility of loss of synchronism (missed steps, dynamic instabilities, etc.) though does not exclude the possibilities for speed control.

As a variant on the 'standard' SRM as described above, it is of course possibly to operate a 'smooth-bore'-stator reluctance motor as a SRM and there may be advantage in doing so (a) for high-speed operation since switching frequency will be reduced (b) since segmented-rotor constructions with their higher $L_d(1 - L_q/L_d)$ levels are then feasible. Of course smooth-bore stators require distributed rather than concentrated windings and are therefore not so suitable due to cost factors for low power motors (i.e. sub 100 W at 3000 rev/min), aerospace and servo motors apart. Similar remarks apply to another variant: the doubly-salient ⟷ reluctance motor in which the ratio of stator to rotor saliencies is integral, even 1:1. Again the switching frequency is relatively low (step angle with a 4-tooth stator, 4- or 2-tooth rotor could be 90° for instance) and feasible maximum speeds correspondingly high.

Finally it is of course possible to choose a phase number of unity for the design of the motor, its winding and switching unit. When this is done a drive system results that although sharing many of the features and characteristics of multi-phase SRM systems, has a sufficient numbers of differences to be considered as a distinct variant within the SRM family of drives and also to

be worthy of special study. It is with aspects of single-phase SRM systems that the thesis is concerned.

The basic action and typical construction of a single-phase SRM can be described by reference to the simplified diagram in Fig. 1.1.3. The motor is shown with salient poles on both stator and rotor and the pole surfaces are shown in the uncastellated, smooth form. The rotor has no cage or other conductor work and the stator no shading rings. There is only one winding on the stator and there is an absence of brushes, commutators or slip rings. This form of structure is hence straightforward, robust and can be relatively cheap compared to the other types of motors, though proper comparisons must always include consideration of the switching unit since there is no question of this type of motors operating without it. Currents in the stator circuit are switched 'on' and 'off' in synchronism with the rotor position. For example the current may be switched 'on' when the rotor is at the misalignment position (q axis) and may be switched 'off' when the rotor is at full alignment (d axis), the inertia of the rotor generally carrying the rotor to the next q position from which the cycle repeats. Continuous motion is hence achievable, subject to the drop in speed due to load and friction torque during the 'off' period being less than the speed at the end of the 'on' period. This condition is met for a wide range of conditions found in practice.

1.1.1 Basic system operation

Basic operation is described with reference to a motor of the simple Fig. 1.1.3 type but much of what follows would be equally valid for other types.

Fig. 1.1.4(a) shows a developed view of the motor in which the stator and rotor pole arcs have been arbitrary chosen as equal and the ratio of pole arc to pole pitch is 0.5. Fig. 1.1.4(b) shows the idealised (current-independent) variation of inductance $L(\theta)$ with rotor positon θ, and Fig. 1.1.4(c) shows the corresponding variation of $\tau(\theta)$ for constant current excitation, torque being proportional to $dL(\theta)/d\theta$. With constant current the mean torque is of course zero because negative torque is produced in the negative slope region of the inductance waveform (i.e. $dL(\theta)/d\theta$ is negative).

For a positive mean torque to be produced, the current must be modulated at the inductance-cycle frequency and Fig. 1.1.5 shows the ideal current waveform for the mean torque per r.m.s. or mean current to be maximised.

1.1.2 Magnetising characteristic

The mean torque developed by the motor with the current waveform in Fig, 1.1.5 can be shown to be proportional to the area enclosed by coil flux linkage ψ

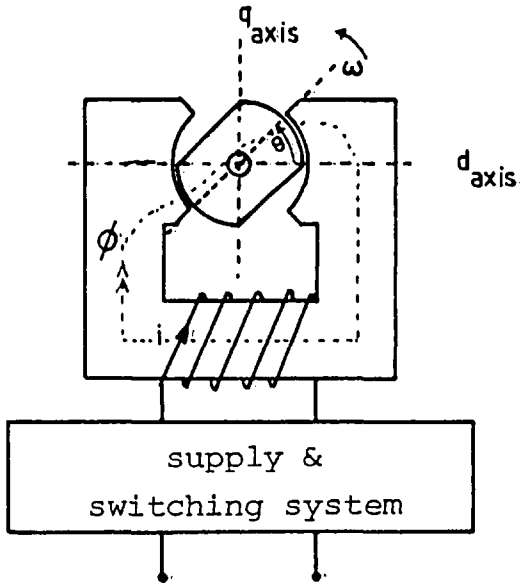

Fig. 1.1.3
Simplified diagram of a single-phase switched reluctance motor drive system

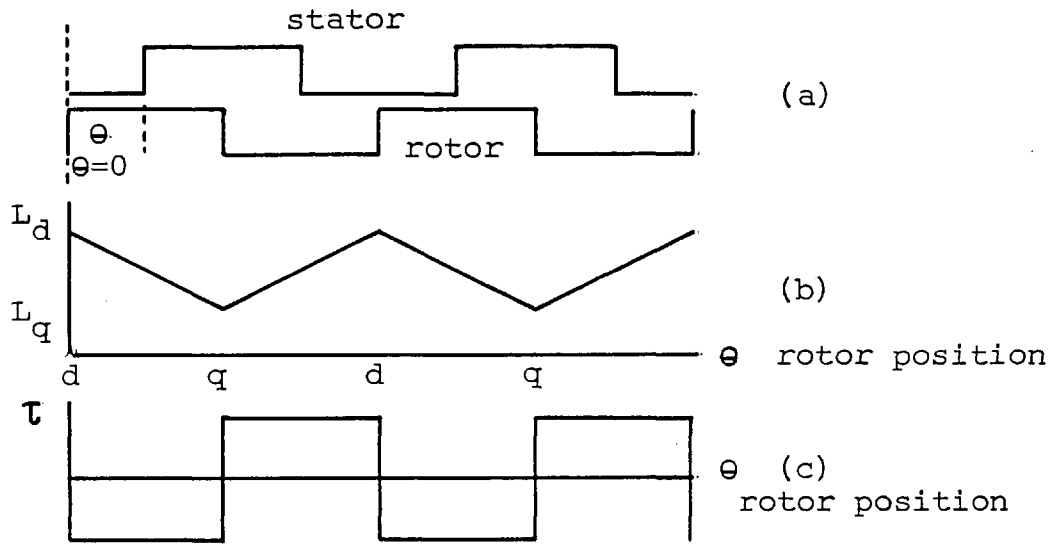

Fig. 1.1.4 (a) Developed view of the motor
(b) Variation of ideal inductance
(c) Variation of developed torque with constant current

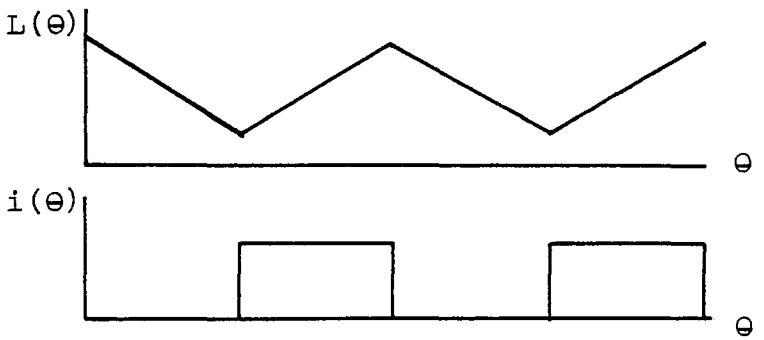

Fig. 1.1.5 Ideal current pulse for maximum mean torque to r.m.s. or mean current ratio

versus current i trajectory on ψ i diagram of the type shown in Fig. 1.1.6, where the ψi lines correspond to unsaturated conditions. In Fig. 1.1.6, the path AB indicates the rise in flux at the rising current edge at the instant when the rotor is at the q position and CD indicates the fall in flux at the falling current edge at the instant when the rotor is at the d position. Along path 2 the current is constant while the rotor moves from the q positon to the d position and ψ increases from ψ_B to ψ_C, while along path 3 the current decreases as the motor is 'de-excitated'.

For the more practical operation with a constant voltage rail, the voltage waveform rather than the current waveform is square as shown in Fig. 1.1.7 (a) and the operating cycle changes to the one typified in Fig. 1.1.7 (d). It is usually desirable to be able to supply negative volt-seconds during stage 3 to hasten de-excitation. As is well known, the torque is proportional to $i^2(dL/d\theta)$ (assuming unsaturated operation) and hence the sense of the torque is sensitive to the sign of $dL/d\theta$ only not to the polarity of the current. Although there is no reason for the motor why alternate pulses of current should not be negative (corresponding to alternating supply voltage pulses) it is more convenient from the switching unit's point of view if in fact the polarity of the successive supply voltage pulses, and hence the polarity of successive current pulses remains unidirectional. As stated

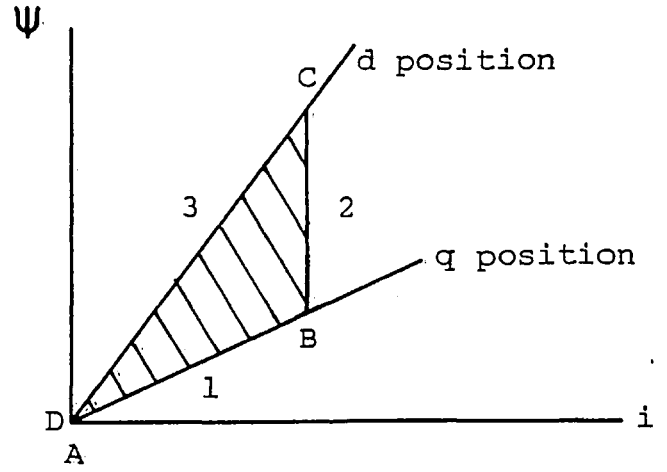

Fig. 1.1.6
Magnetising characteristic for current-force opearation

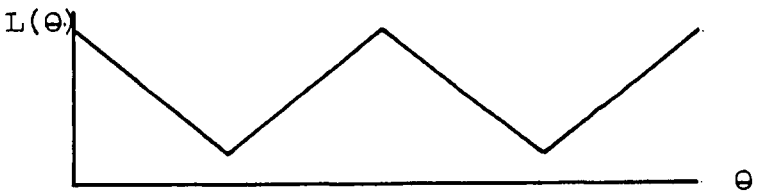

(a) inductance

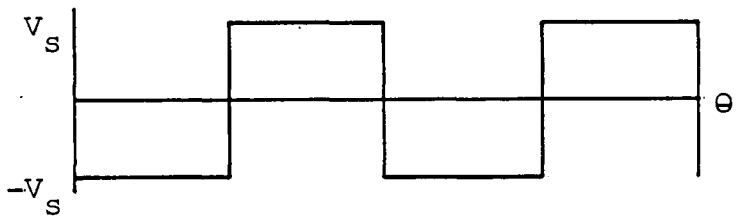

(b) voltage supply

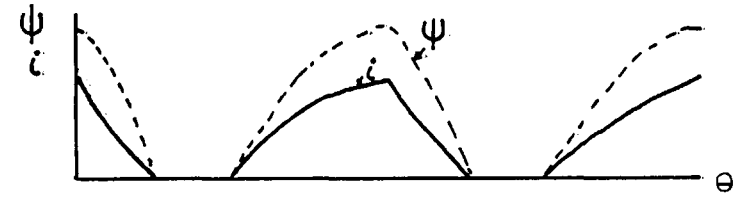

(c) current and flux

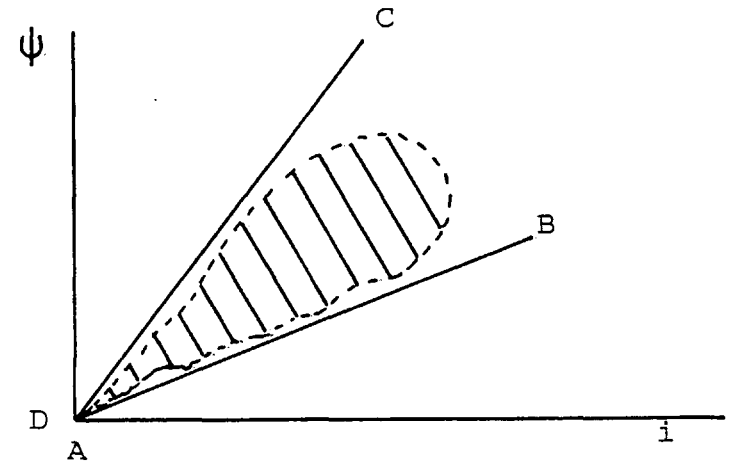

(d) magnetising characteristic for voltage-force operation

Fig. 1.1.7 Operation with a constant-voltage rail

in Ref. 1.14 the trajectory shape on Fig. 1.1.7(d) depends on the shape of the winding inductance L versus rotor position θ curve and its width and extent depend on the magnitude of voltage and speed. With fixed rail volts and a given motor, the loop size decreases with speed (since with $iR \ll d(Li)/dt$, $d(Li)$ is held constant by the rail volts) and hence motors with constant switching angles would be expected to possess d.c. series motor torque characteristics.

The starting point for the analysis of the SPSRM is the flux linkage function $\psi(\theta,i)$ where θ is the rotor position and i the winding current. A simple loop equation can then be written in terms of supply voltage v(t):

$$v(t) = Ri + \frac{d\psi(\theta,i)}{dt} \quad (1.1.1)$$

where R is the winding resistance.

By expressing the flux linkage in terms of winding inductance $\psi(\theta,i) = iL(\theta,i)$, this becomes

$$v(t) = Ri + \left[L(\theta,i) + i\frac{\partial L(\theta,i)}{\partial i}\right]\frac{di}{dt} + i\frac{\partial L(\theta,i)}{\partial \theta}\omega \quad (1.1.2)$$

where $\omega = \frac{d\theta}{dt}$

The instanteneous gross torque produced by the motor is given by

$$\tau(\theta,i) = \frac{\partial W'(\theta,i)}{\partial \theta} \qquad (1.1.3)$$

where $W'(\theta,i)$ is the winding coenergy for a given rotor angle defined by

$$W'(\theta,i) = \int_0^i iL(\theta,i)\,di\Big|_\theta = \text{constant} \qquad (1.1.4)$$

For magnetically non-linear conditions it may often be more convenient not to formulate the relations in terms of L as defined above but to work in terms of $\psi(\theta,i)$ directly. For linear conditions, the relation 1.1.2 in terms of L is most convenient for prediction of currents but the well known $\tau = \frac{1}{2} i^2 (dL/d\theta)$ relation for torque (obtainable from 1.1.3 and 1.1.4) can be used directly. This avoids the need to calculate $W'(\theta,i)$ and $\frac{\partial W'(\theta,i)}{\partial \theta}$ explicitly.

1.2 Brief survey of SRM literature

Synchronous motors in which synchronism is maintained over a wide range of speed by means of rotor-position-controlled, variable frequency feeds have been recieving considerable attention in recent years and a large and growing body of literature exists. The earliest reluctance motors so operated were probably those of

Wheatstone and Davidson in 1840's as described by Bowers[1.1] but the difficulties associated with the mechanical switches, which are required to switch off currents when coil inductances are maximum, brought this early activity to a halt. It is probably true to say that the main factors in the recently re-birth of the switched reluctance motor were:

(a) the availability of solid state switching devices and circuitry know-how

(b) the existence of a large pool of knowledge and experience on the related motor categories, viz V.R. stepper motors and reluctance motors for mains operation

(c) market pull:- the needs for robust, variable speed drives and for a motor type allowing cheaper power electronics conditioning equipment.

It is however difficult to account for the long delay between the development of inverter-fed induction motor systems and the development of switched reluctance motor systems.

The earliest known publication in the 20th century was Ref. 1.2 (1969) in which Nasar reported the test results on small and fairly primitive, experimental 6-blade, 6-coil, switched reluctance motor. A 12 V d.c. supply was used and a maximum test speed of 130 rev/min was recorded. Later in 1971 Nasar[1.3] stated that for maximum power per weight, d axis inductance in a reluctance motor should be twice the q axis inductance.

Unnewehr and Koch in 1974[1.4] described a multiple-stack disc-rotor machine for battery-powered traction applications. Three motors and five controller configurations were tested. One of the motors was a single-phase machine of 8 H.P. with 17 poles and 2 rotor discs which ran at 5000 rev/min and weighed 43 lbs. Efficiency varied between 46-88 % over a speed range up to 5400 rev/min was reported.

Byrne and Lacy in 1976[1.5] described a 6 KW motor with a 4-pole 2-phase stator and a 2-pole rotor. The rotor pole faces were laminated and the pole-face width was specially graded in an axial sense with the object of maintaining pole faces saturation throughout much of the q to d alignment process and hence increasing output torque. The motor was tested at fixed speed, being fed directly from the single phase mains, and at variable speed with the d.c. supply rails being regulated by a chopper. At low speeds the chopper was controlled to give approximately constant current operation.

Koch in 1977[1.6] presented an analysis of a three phase motor with a 6-pole stator and a 4-salient-pole cylindrical rotor. The switching unit was supplied directly from a fixed voltage d.c. power source. The paper indicated how exciting e.m.f. and torque/rotor volume levels were derivable for normalised current from the differential equations. Current waveforms and power levels were

predicted. Low L_d/L_q ratios were recommended for pump loads and high L_d/L_q ratios for traction loads.

Bausch and Rieke in 1978[1.7] described a four-phase reluctance motor supplied from a switched d.c. source. Torque and speed were controlled by a pulse-inverter with variable pulse-width and current control. The outside-rotor motor had 4 phases, 8 stator poles, 32 stator sub-teeth and 38 rotor teeth for low speed running in the manner familiar in small-angle stepper motors. Predictions using a step by step integration method show the effects of an advanced switch-off angle in reducing undesirable negative torque effects. Predicted characteristics of the motor with different control strategies were shown. It was suggested that by varying the switch-off angle according to speed, the negative torques can be reduced to a minimum and mean torque and efficiency improved over the whole speed range.

Major contributions in polyphase switched reluctance motor drive systems for traction applications have been made from the collaboration between Leeds and Nottingham Universities and the Chloride Company. It is not known when this work commenced but three recent papers[1.8,1.9,1.10] have explored the theory, potential and test performance of doubly-salient polyphase switched reluctance motors. The basic mode of operation, analysis design considerations and experimental results are given from a range of prototype

motors with ratings up to 15 KW at 750 rev/min. The continuous rating is claimed to be 1.4 times that of the equivalent induction motor. The drive is analysed using a linear model for the motor. Phase-current waveforms are predicted and it is stated that methods have been developed that enable the switching unit and motor system to be designed for optimum performance/cost ratio. Various thyristor inverter circuit options are considered for 'conventionally-wound' and 'bifilar-wound' motors. The inverter design process is explained briefly, calculation of main and commutation component ratings being included.

A number of related conference papers[1.11, 1.12] have also been published by the group, amplifying the points covered in the Refs. 1.8 to 1.10 and giving some details of further work.

1.3 Introduction to the work described in the thesis

Work on single-phase switched reluctance motor (SPSRM) drive systems at Imperial College started in 1975. An industrial request was recieved from Simplex-Circulume Ltd. manufacturers of ceiling fans and a subsidiary of the Tube Investments group. The company felt that the existing ceiling fan induction motor drive was too expensive and wanted to explore the possibilities for cheaper motors satisfying the very stringent cost and lifetime constraints. Direct drive was considered essential to avoid the penalties

of step down mechanical transmissions. The I.C. project was done in parallel with a company exercise to redesign for the minimum first cost the existing high diameter/length, capacitor-run, single-phase, external-rotor, direct-drive induction motor. Ultimately it turned out that for various reasons the redesigned induction motor represented a better solution than the switched reluctance drive designed, built and tested (within three months) by the Imperial College group. However the project provided a valuable lead into SPSRM systems at a time when the Nasar paper[1.2] was the only published work in the SRM field known to I.C. personnel. (The Unnewehr and Koch paper[1.4] published in 1974 had not been spotted. This is still the only other known pre-1975, 20th century paper on SRMs.)

The company factory cost target for the entire drive was extremely low: £ 8 in 1975 prices. The application required controllable-speed operation over a zero to 150 (later revised to 250) rev/min speed range, load torque varied with $(\text{speed})^2$ up to a rated value of 1.1 N-m and no maintenance over 25 years. Ref. 1.13 presented design of and results from the first experimental unit. These were also presented in Ref. 1.14, published in 1979 together with the results of further tests.

I.C. Work on higher-speed SPSRM systems and on d.c. link-fed systems commenced in 1978 and the results of early experimental work suggested that SPSRM drives

were worthy of further investigation for possible low-power applications in the domestic, industrial and aero-space fields.

This part of the thesis reports the I.C. work done on SPSRM drives during the period 1978 to 1982. The very wide range of motor and feed design features even within the single phase category of system has made some concentration inevitable and the investigations have excluded experimental consideration of motors having cas-tellated saliencies and having unequal numbers of rotor and stator saliencies. All the investigations were done on small motors having power ratings (referred to 3000 rev/min) of less than 100 W. As stated previously, cost factors militate against the use of distributed windings at this size level and so no consideration was given to systems based on smooth-bore, singly-salient type reluc-tance motors. In any further work involving SPSRM drives of higher power, this should certainly be done.

Chapters 2 to 6 deal respectively with the features of different types of SPSRM and feed, with the two analysis and prediction methods developed, with the experimental program and its results (including some com-parisons between the different types of SPSRM system) and with some design aspects. Brief details of a short indus-trial-collaborative program are included with some conclu-sions in the final chapter.

CHAPTER 2

THE SINGLE-PHASE SWITCHED RELUCTANCE MOTOR DRIVE SYSTEM

2.1 Introduction

The switched reluctance motor system of the single-phase type (SPSRM) is felt to be worthy of investigation because of its likely potential, arising from its straightforward construction, for relatively low cost per rated output. The advantages in terms of feed circuit and motor winding simplicity of adopting a single-phase basis are obvious. Almost all domestic appliances use single-phase electric motors of one type or another (with the exception of capacitor-run induction motor and thyristor-fed d.c. motors) and the development of a single-phase brushless, high/variable-speed drive viable for domestic applications would be apposite.

In this chapter, the essential features of a SPSRM drive system are described in section 2.2. The motor configurations used in the present investigation, together with other possibilities will be described in section 2.3. In section 2.4 possible feed circuits, including what are terms 'd.c.' and 'a.c.' feed systems will be described. Sections 2.5,2.6 and 2.7 outline the position-sensor system, speed-control methods and device protection circuits, respectively. The merits of SPSRM

drive systems in comparison with other drive systems will be outlined in section 2.8.

2.2 The SPSRM drive system configuration

The essential parts of a SPSRM system can be shown in the diagram of Fig. 2.2.1. It consists of a power supply unit whose output is fed to the SPSR motor through a power switching circuit. The power supply block can comprise either a 50 Hz, single-phase a.c. mains supply in the case of the 'a.c. feed circuit' option or in the case of the 'd.c. feed circuit' option, a rectified a.c. supply or battery. The switching sequences of the power circuit are synchronised with the rotor position as monitored by a position sensor of some type. Motor performance can be controlled by varying the supply pulse timing or length relative and/or by varying the amplitude of the pulse by voltage or current control. Control is exercised at the switching stage and/or at the power supply (indicated by arrows).

The choices of motor, power circuit and control configuration for a particular SPSRM system, as with other drive systems, have to be chosen according to cost, power level, degree of sophistication in control and performance level required in the application. In the next three sections, a number of alternative motor, power circuit and control circuit options will be discussed. With low power drives, some sacrifice in terms of certain

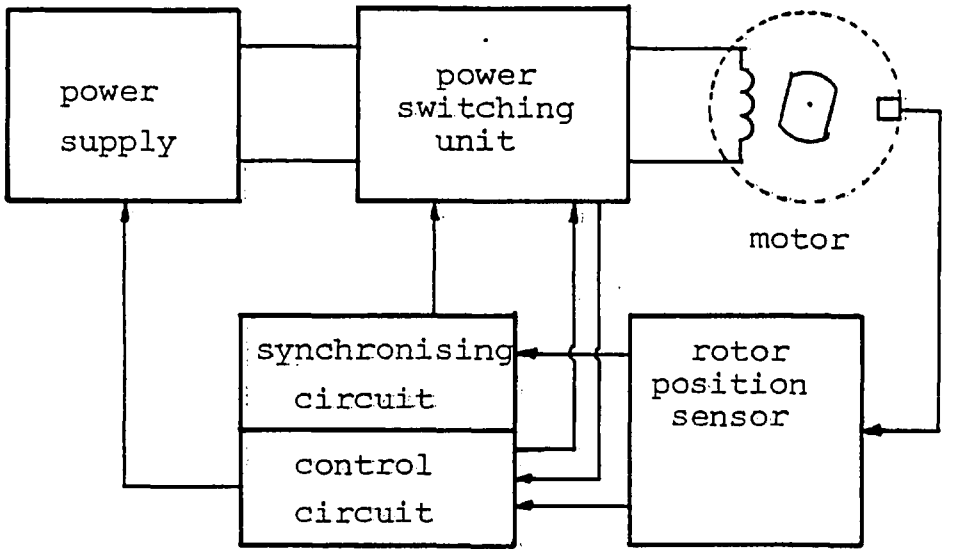

Fig. 2.2.1 The essential parts of a SPSRM system

performance criteria such as efficiency, power to weight and supply harmonic levels can often be worthwhile if this reduces first cost, and options where this is possible or inherent are discussed along with more refined systems with offer the opportunity for high quality operation. (It may be noted that a discussion of the relative merits of various design features is given in chapter 6.)

2.3 Motor types

Single-phase reluctance motors for switched-supply operation can be classified in many ways according to whether the number of poles, the number of saliencies

per pole, the ratio of stator to rotor saliencies, the type of main flux path (standard or non standard), magnetic circuit material, type of feed, rotor D/L ratio, standard or segmented-rotor construction, etc. is adopted as primary basis. Rather than attempt the lengthy task of describing all possible motors or even a comprehensive selection of them it is perhaps more sensible, in order to illustrate what is meant by some of these terms, and to introduce the types of motor that play an important part in the investigations, to describe the main features of four particular types of motor.

2.3.1 Low-speed SPSR motor

The first of these, suitable for low-speed application is shown in Fig. 2.3.1. The main features of the motor may be listed as: (i) homopolar configuration with 6 saliencies per pole, (ii) external rotor/internal stator, (iii) high diameter to length ratio, (iv) equal stator and rotor number of saliencies with smooth pole faces, (v) radial/axial main flux paths, (vi) solid-iron magnetic circuit with slits on the stator poles, (vii) single-concentrated-coil excitation system. As stated in reference 2.1 " A high D/L ratio is common for all low-speed motors and use of an external-rotor construction tends to give lower overall diameter when the radial depth of the rotor can be made small. Torque per size increases in general as the number of saliencies on the stator and rotor increases. However by keeping this number down to six

with no vernier action (i.e. equal saliency number on both stator and rotor), torque per size can still be acceptable while switching frequency can be low enough to be able to consider the use of a low cost, cast, solid iron structure particularly when the design flux density is made reasonably low. The slits on the stator pole help to reduce eddy current losses. The stator and rotor require a minimum of machining. The circular coil excitation means is particularly simple and the entire periphery of the motor (as opposed to the situation in stepper motors and polyphase SRMs) is used for torque production during the switching 'on' periods. The avoidance of an axial airgap or disc layout avoids axial force problems."

2.3.2 High-speed SPSR motors

For high-speed applications the design constraints are inevitably different. A solid-iron structure is ruled out because the iron losses will be too high to be acceptable at high operating frequencies. The number of saliencies is preferably small to minimise operating frequencies and one saliency per pole for homopolar motors (stator) or for heteropolar motors are feasible. Fig. 2.3.2 and 2.3.3 show two examples of high-speed motors. Each employs a 2-pole configuration with 1 saliency/pole and a radial/circumferential main flux path. In Fig. 2.3.2 (which shows what will be called the 'Form 1' motor), the stator configuration is similar to that used in some small

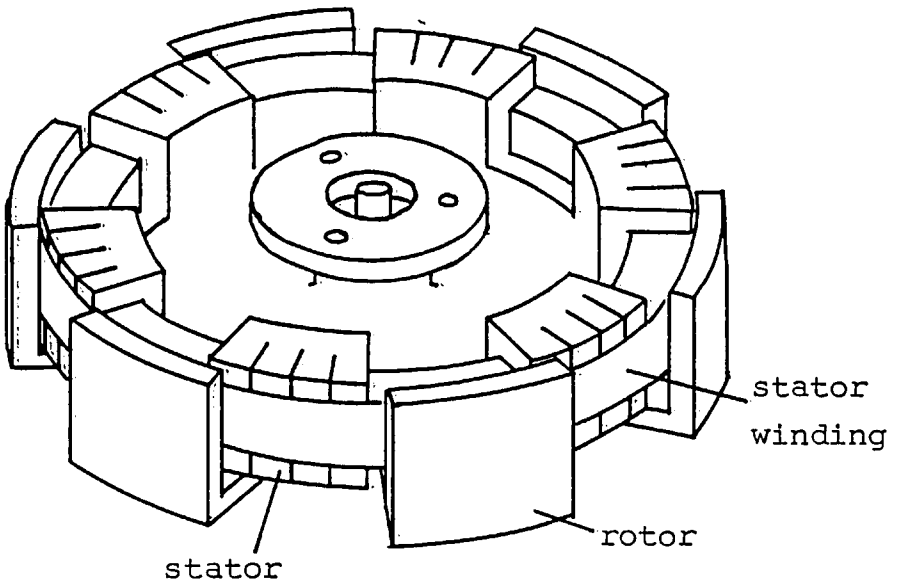

Fig. 2.3.1 The 6-saliency homopolar motor

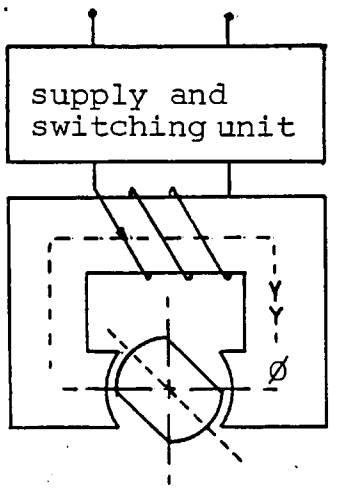

Fig. 2.3.2
The form 1 motor

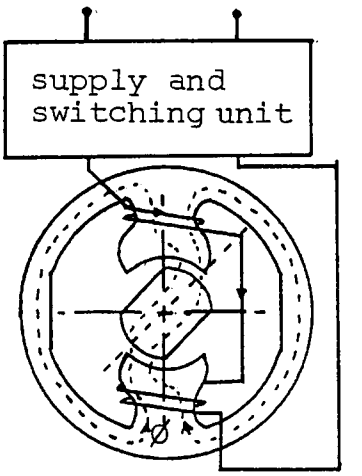

Fig. 2.3.3
The form 2 motor

50 Hz clock motors and in single-phase shaded-pole induction motors. The manufacturing cost can be very low due to the straightforward coil winding and assembly operations. The bobbin coil is wound on the detachable, top core-portion. The stator leakage reactance is likely to be a little high because the excitation coil is relatively remote from the pole face.

For Fig. 2.3.3 (which shows what will be called 'Form 2' motor) stator lamination pattern is similar to that in the two-pole single-phase commutator or shaded-pole induction motor. The stator leakage reactance is likely to be smaller than in the form 1 motor but the winding area tends to be more restricted. Moreover, the winding is likely to be rather more difficult and costly to assemble compared to the bobbin coil in the form 1 motor. A modified version of form 2 motor is shown in Fig. 2.3.4. In this configuration the outer member rotates while the inner member is fixed. The excitation coil is simply wound on the inner member as shown and the leads brought out through the shaft. This configuration would make for very low winding costs but the motor's rotor inertia will be higher than with the rotor-inside layouts.

A homopolar radial/axial flux motor with 2 saliencies per pole is shown in Fig. 2.3.5. This will be called the 'Form 3' motor. The motor's magnetic circuit can be made from 2 strip-wound cores as used in small

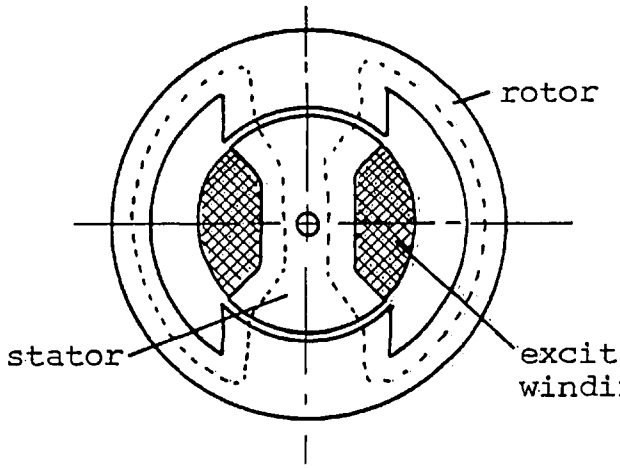

Fig. 2.3.4

The 'inside-out' form 2 motor

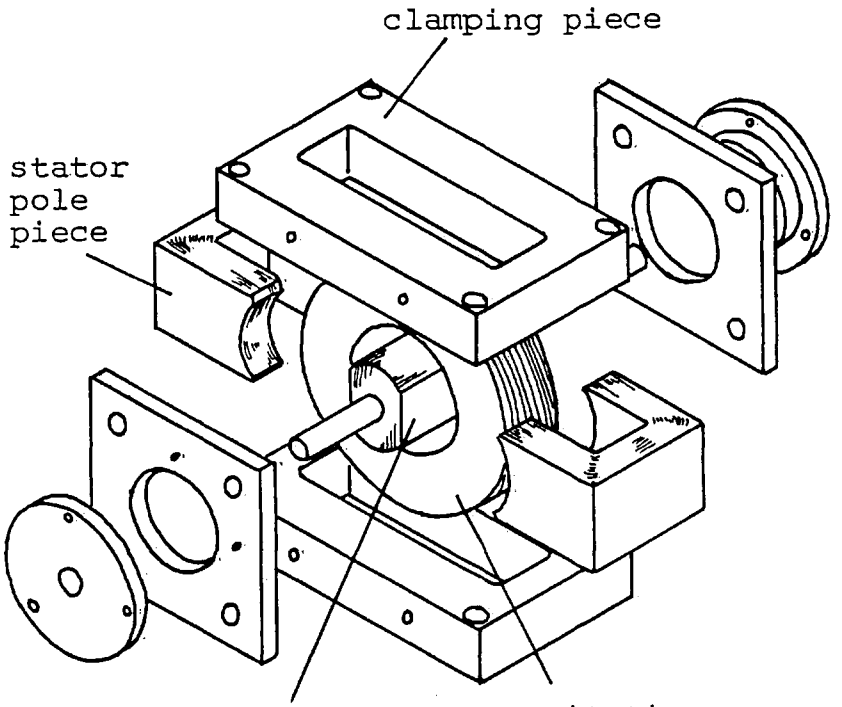

Fig. 2.3.5

The form 3 motor

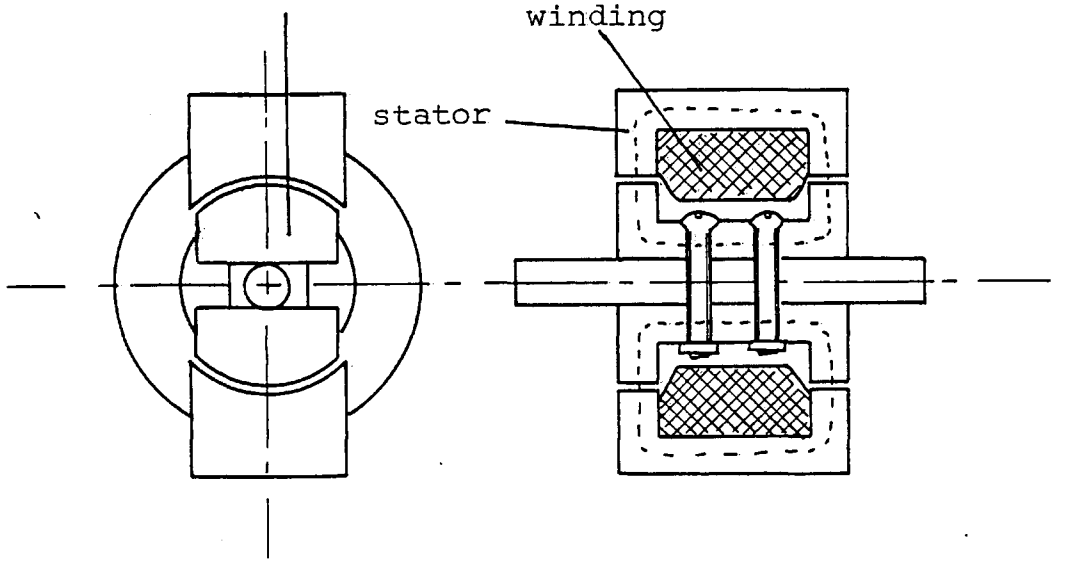

Fig. 2.3.6 Another version of the form 3 motor

transformers. The cores are machined to form 2 stator pole pieces. The stator winding can comprise a single circular coil. Because of the axial flux path in the rotor, the rotor laminations have to be stacked along shaft axis and this may make the rotor more difficult to make. It is also possible to use strip-wound cores for both rotor and stator as shown in Fig. 2.3.6. The rotor strip-cores can be bolted to the shaft and machined in the same way as the stator pole pieces. Potential advantages occurring from this construction are better use of rotor material, stronger rotor, lower inertia and more winding area for the same size of motor.

For all the motors illustrated in Figs. 2.3.2 to 2.3.6, the number of stator and rotor saliencies are identical and fairly low, no vernier action occurs, no pole castellation is employed and hence relatively large step angles and low switching frequencies result. The choice of pole arc to pole pitch ratio is crucial to the achievement of satisfactory d and q inductances and a typical value being 0.5.

Tests have been carried out on a six-saliency homopolar motor for low-speed applications and on experimental form 1, form 2 and form 3 motors high-speed operation.

2.4 Power circuit configurations

The possible power circuits that can be used to feed SPSR motors may be divided into two categories, designated as 'a.c.' and 'd.c.' (See chapter 6 for a tabular comparison between the various feed circuit options). The 'a.c.' feed system operates directly from the mains supply and can be arranged to use only one or two triac or thyristor switches. The 'd.c.' feed system contains a rectifier or battery, a 'd.c.' link and some forms of switching unit, often of the bridge type. The 'd.c.' feed system although more complicated and more expensive provides better control, stability and performance.

2.4.1 The 'a.c.' feed system

The basic configurations of a.c. power control circuit for various types of load with triac or thyristor switches have been well described in many text books.[2.2, 2.3] These include circuits employing natural commutation in which the supply voltage either produces thyristor turn-off at naturally occuring current zero, or enables the firing of one thyristor to turn-off the preceding one, and forced commutation circuit, in which a precharged capacitor performs the turn-off function. Various naturally -commutated circuit configurations including twin or tapped-coil full-wave and single-coil, half-wave and full-wave arrangement were investigated (some of them

before the start of the present project) for possible use of a low-cost motor feed circuit. Forced commutation circuits although provide greater flexibility in control were ruled out at that stage since their costs lay above the target figure set by the customer of the R&D contract concerned, and they have not been examined since due to the pressure of time. Twin-coil or tapped-coil arrangements, although having some desirable features, were also found to be too costly for the application, requiring not only more copper in the machine but also two high voltage power switches. Three possible circuits for single coil winding were chosen for examination and are shown in Figs. 2.4.1(a), (b) and 2.4.2.[2.1]

Fig. 2.4.1 shows two half wave circuits. A controlled freewheel path is used in (a) and an uncontrolled freewheel path in (b). Fig. 2.4.2 shows a full-wave circuit with a bidirectional switch (triac) and having no freewheel path as such. In each circuit the switches are burst fired under the control of the position sensor and a phase-angle delay capability is employed as an open-loop speed-control method.

Two alternative coil-current turn-off mechanisms occur in the Fig. 2.4.1 (a) circuit: natural decay through the freewheel path and forced turn-off via reverse mains polarity during a negative half cycle. The instantaneous mains voltage at the instant of desired turn-off, determined by rotor position, decides which mechanism is

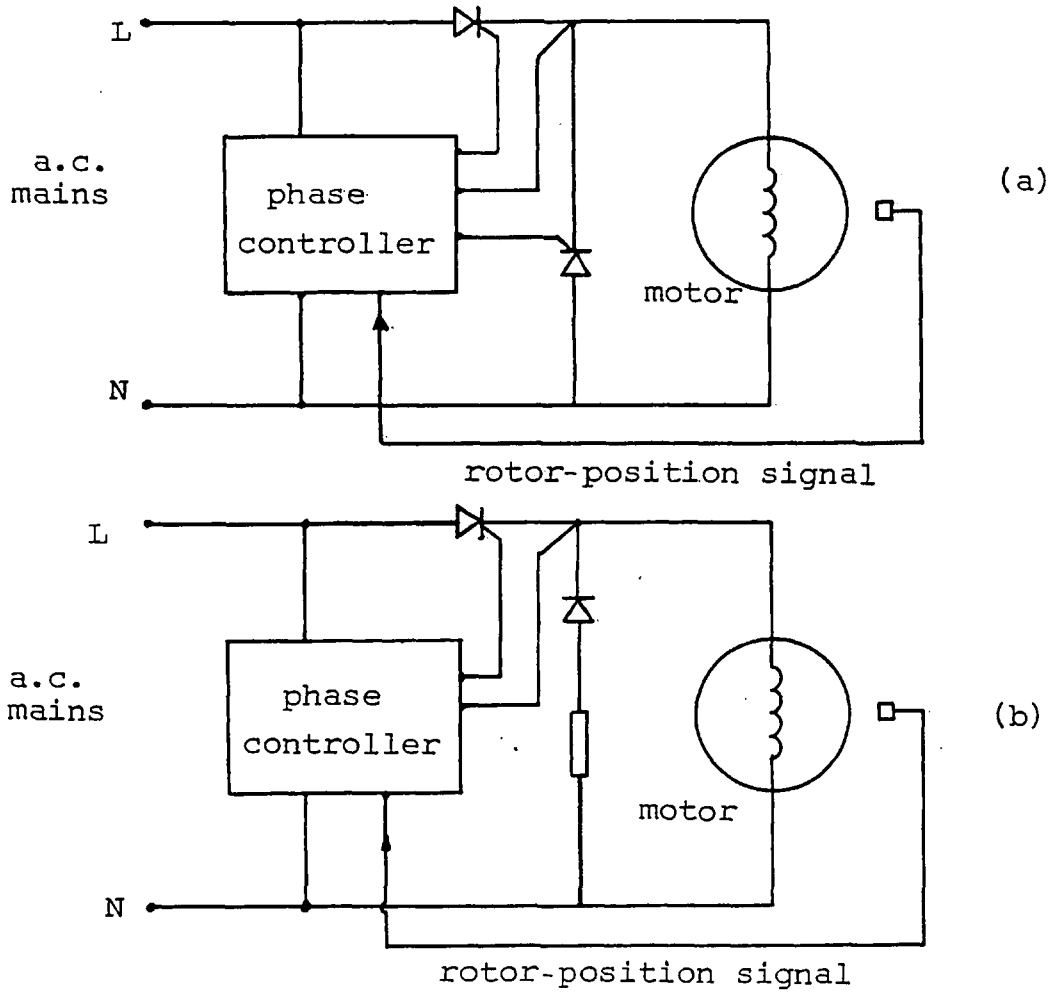

Fig. 2.4.1 Power circuits using thyristors
(a) Controlled freewheel path
(b) Uncontrolled freewheel path

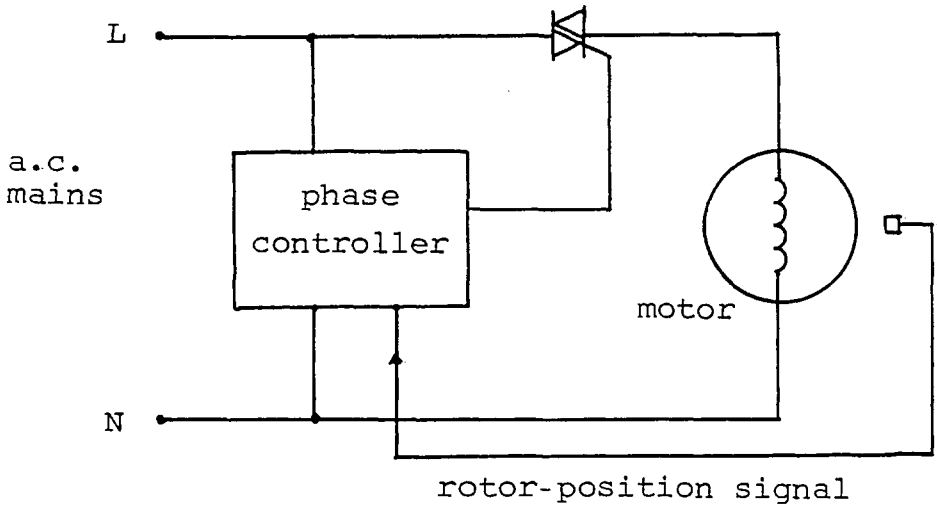

Fig. 2.4.2 Power circuit using triac (no freewheel path)

used. The natural freewheel decay mode can cause negative torque pulses if the current continues into the normal 'off' period. Vibration and a low mean torque can result. The Fig. 2.4.1(b) circuit employs a resistive freewheel path in order to increase decay rates and hence minimise the occurrence of negative torque pulses due to current overlap into periods of negative dL/dt. Tests showed that level of torque pulsation was reduced but mean torque also reduced since the fast mains-driven turn-off mode was now absent.[2.1]

As the freewheel resistance was increased, the situation improved and this suggested that removal of the freewheel path might be beneficial. The Fig. 2.4.2 circuit can be used with triac or thyristor. The full-wave triac circuit has the advantage of utilising both negative and positive half cycles and hence gives higher mean torque. It was also found that the reverse voltage pull down with reverse mains polarity in the triac circuit was more rapid than with the thyristor circuit with freewheel path. The negative torque pulses produced were thus reduced and resulted in a lower percentage of ripple in the output torque and a higher mean torque.[2.1] However, since the triac circuit operates in both half cycles a more complicated phase delay circuit is required.

Of course the unusual feature of this category of SPSRM system is that interactions are inevitable between

the mains frequency and the motor switching frequency. The interactions are bound to be particularly strong for switching frequencies above say ¼ of the mains frequency, and they make the system at once interesting intellectually, complicated in operation and somewhat snag-ridden in application.

2.4.2 The 'd.c.' feed system

The basic configuration of a typical 'd.c.' power switching circuit is shown in Fig. 2.4.3. Switch S_1 is switched 'on' and 'off' relative to the rotor position. When switch S_1 is closed the current builds up in the motor winding and the energy is taken from the d.c. supply. When S_1 is opened the current continues to flow in the winding, but now through the diode so that stored energy is either dissipated in the circuit or returned to the d.c. supply. The switch S_1 in practice can be a power transistor, thyristor, power MOSFET transistor or gate turn off thyristor depending on the power level, speed and applications. Brief discussions on these devices can be given as follows:[2.4,2.5,2.6]

The thyristor is suitable for high power levels because of its capability for handling high voltages and currents but the difficulty in turning it off when operating with 'd.c.' circuits makes it unattractive for low power level. The power transistor can generally switch faster than the thyristor, switching times of less than

1 to 2 μS being possible. The base drive requirements of the transistor are more onerous than those of gate requirements of the thyristor. The power and overload capabilities of the power transistor is less than that of large thyristors. The transistor by control of the base current is capable of turn-off while carrying load current, whereas in the thyristor the gate loses control after turn-on. The power MOSFET transistor is a new device that possesses many attractive characteristics. It can switch faster than the transistor, requires extremely low drive current and hence does not need the driver stages required for many power transistors, is capable of turn-off by the control of gate voltage in the same way as base current in the transistor. As it is a relatively new device the price is still high compared to the transistor. A significant disadvantage is that its 'on' resistance is higher than the transistor's (especially at voltage ratings more than 800 V), which results in higher losses and cooling problems. With the gate turn off thyristor, turn off is possible by reverse gate current. It can turn-off faster than the ordinary thyristor. Turn-on requirements are similar to those of the conventional thyristor, but present device cost, rating limitations and losses together with the need for added gate circuitry has so far slowed the introduction of the gate turn-off thyristor.

The power circuit for d.c. operation of a typical small SPSR motor operating from a 12 or 24 Volt d.c. supply is shown in Fig. 2.4.4. This circuit is

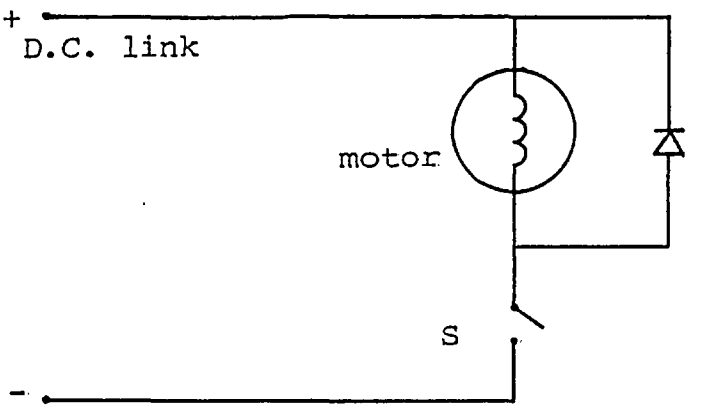

Fig. 2.4.3 Basic circuit for d.c. operation

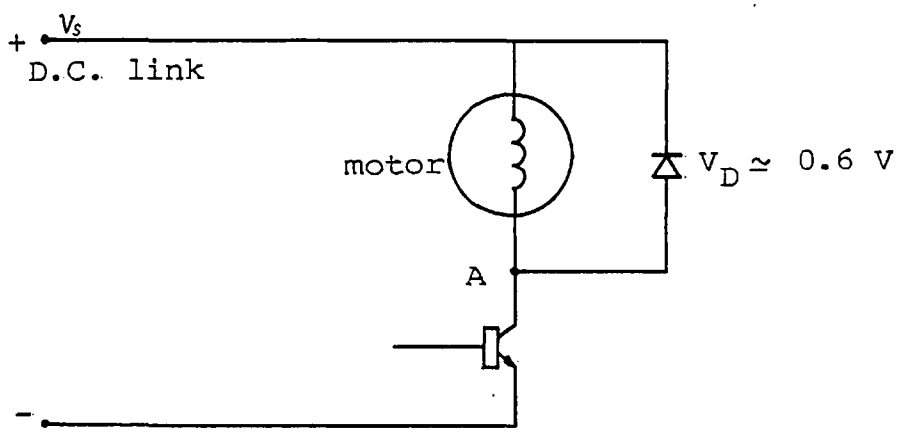

Fig. 2.4.4 Power circuit for low L/R motor

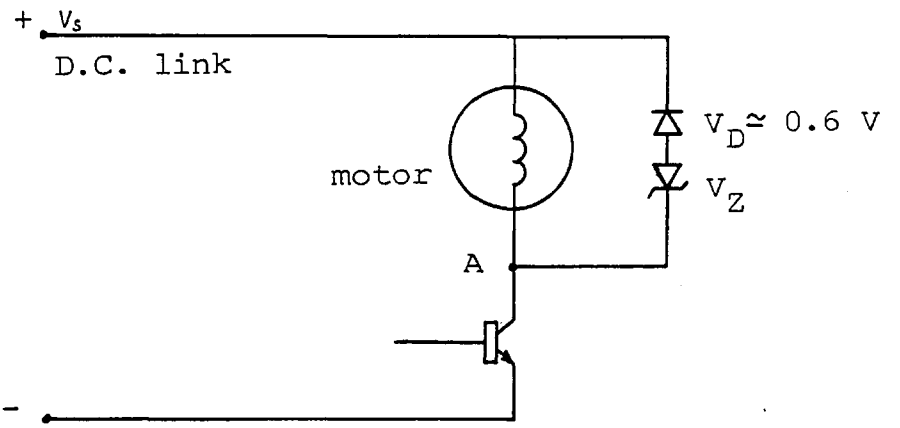

Fig. 2.4.5 Power circuit with zener diode to accelerate pull-down

recommended for relatively small motors because the low L/R ratio of small motor windings means that there is less need for a high voltage to pull the current down to zero. When the transistor in Fig. 2.4.4 is switched off, the voltage at point A rises to a value higher than V_s and the diode conducts. The voltage across the load will be clamped at about 0.6 V, and $V_A = V_s + 0.6$ V. The load current is clearly diverted from the transistor through the diode. The stored energy is returned to the d.c. supply or dissipated in the diode and circuit resistance. When the current falls to zero, V_A drops to V_s and the diode cuts off. The freewheeling action can be accelerated by increasing the reverse voltage across the load as shown in Fig. 2.4.5. In this circuit the freewheel path includes a zener diode connected back to back with the freewheel diode. With this arrangement, when the transistor is off the voltage at point A is clearly $V_s+V_z+0.6$ V. The dissipation in the diodes will be higher than in the previous circuit and the freewheel current is pulled down quicker.

For larger motors, the motor winding is more inductive (higher L/R ratio) and the stored magnetic energy will be higher. If the reverse voltage is low, the freewheel current can flow for a considerable time and can result in high negative torque pulses. Two circuits that can provide a pull-down reverse voltage equal to the d.c. rail voltage (V_s) are shown in Figs. 2.4.6 and 2.4.7.

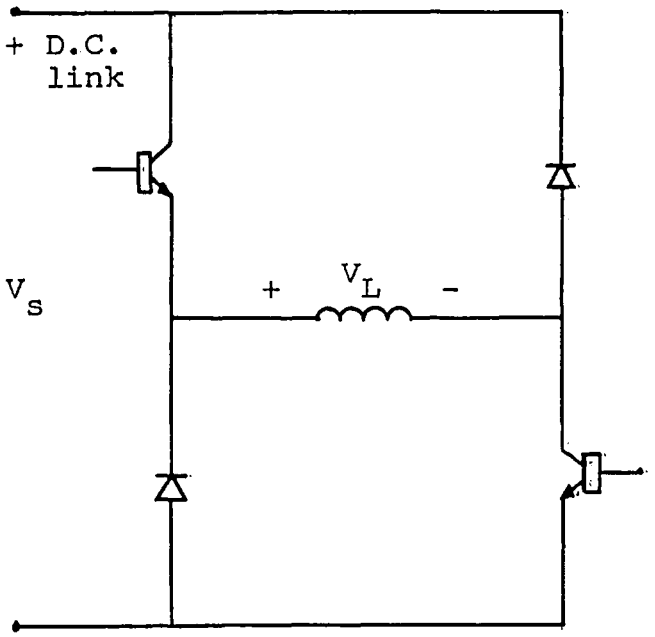

Fig. 2.4.6

The half bridge inverter circuit

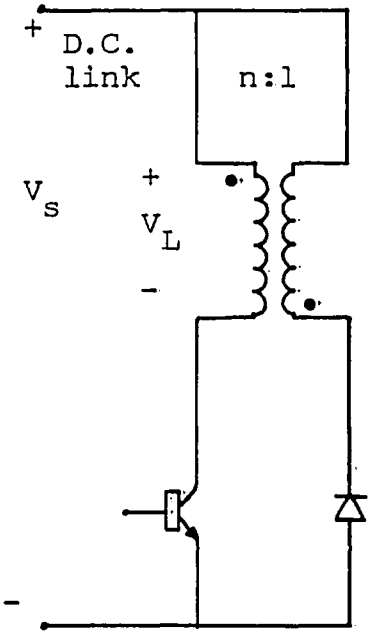

Fig. 2.4.7

The bifilar-wound pull-down circuit

Fig. 2.4.6 shows a half inverter bridge. The two transistors (one of which needs a floating base drive circuit) are switched on and off simultaneously and in synchronism with the rotor position. When the transistors are 'on' the current flows through the load via two transistors and the voltage across the load V_L is equal to V_s. When the transistors are 'off', the voltage V_L (in order to allow the current to flow in the same direction) reverses, the diodes conduct and clamp V_L to $-V_s$. Energy is returned to the power supply and the current is pulled down to zero.

In the circuit of Fig. 2.4.7 it is possible to halve the number of transistors and diodes and avoid

the need for a floating base drive to the top transistor by using a bifilar-wound pull-down winding on the stator (in effect a primary and secondary circuit wound together). In this citcuit when the transistor is 'off' the voltage V_L reverses, the diode conducts and the current in the primary transfers to the secondary flowing through the diode and again returning energy to the supply. The reverse voltage on the primary is also $-V_s$ if n = 1.

Comparing the two circuits, the bifilar-wound circuit[2.7] has the advantage of using only one transistor and diode. However:

a) an extra winding is needed. This increases the winding space requirement (only slightly since the wire can be thin) and/or slightly decreases the space available for the main coil, four rather than two leads are needed, and possibly extra slot insulation between the coils.

b) the voltage to be withstood by the transistor and diode is doubled w.r.t. to the single-coil circuit (assuming an equal number of turns on primary and secondary). This can clearly be a serious disadvantage for certain supply voltage and device combinations.

From the a.c. feed circuit options, the triac circuit (Fig. 2.4.2) was chosen for investigation with both an experimental six-saliency homopolar motor and a form 1 motor. Two options of d.c. feed circuit were examined: the single-coil transistor circuit and the bifilar-wound

pull-down transistor circuit. Tests were conducted with experimental form 1, form 2 and form 3 motors.

2.5 Position-sensor systems

As with 'brushless d.c.' motors, many types of position-sensing system are worth considering.[2.8] The possibilities include systems based on magnetic transducers of various types, electro-optical, inductive and capacitance sensors.

a) Magnetic transducer systems. Two common types of device used, capable (unlike the simple pick-up coil) of sensing 'd.c.' conditions (as at standstill) are, the Hall effect device which detects the magnitude and polarity of a magnetic field and the Magneto resistive device which gives a corresponding variation in resistance proportional to the flux density. Each system needs a separate magnet or other flux source and a rotor-mounted means for modulating the flux density such as a series of steel projections. If an a.c.-excited flux source is employed (unfortunately requiring its own supply), a pick-up coil-based system can also be considered (see later). Fringe flux phenomena tend to give rather rounded output waveforms when magnetic field sensors are used and Schmitt trigger or other thresholding circuits are often desirable.

b) Electro-optical systems. These comprise an

optical transmitter, sensor and some rotor-mounted means for modulating the light reaching the sensor. The transmitter can be an LED, filament bulb or infrared source and the sensor is normally a photodiode or phototransistor. The systems have the advantages of precise switching, low inertia and simplicity. Output waveforms are often quite sharp. For hostile environment, fibre optics allow the source and sensor to be kept away if necessary from heat, dust and vibration. Transmitter lifetimes have much improved and are now generally commensurate with typical motor lifetimes.

c) Capacitance sensors can be compact but require accurate parts-location and need to be custom-produced if costs are to be low. A high-frequency source (and leads) are required.

d) Inductive systems are based on inductive coupling between coils. A variety of inductive systems with varying degrees of sophistication are available. They range from simple co-axial stator mounted, bobbin coil pairs (used with steel projections on the rotor to modulate the coupling) to the pick-offs and resolvers used in high performance servo systems. Fig. 2.5.1 shows a typical arrangement of systems (a), (b) and (d).

After some preliminary work with a Hall-effect sensor prior to the present project, opto-electrical

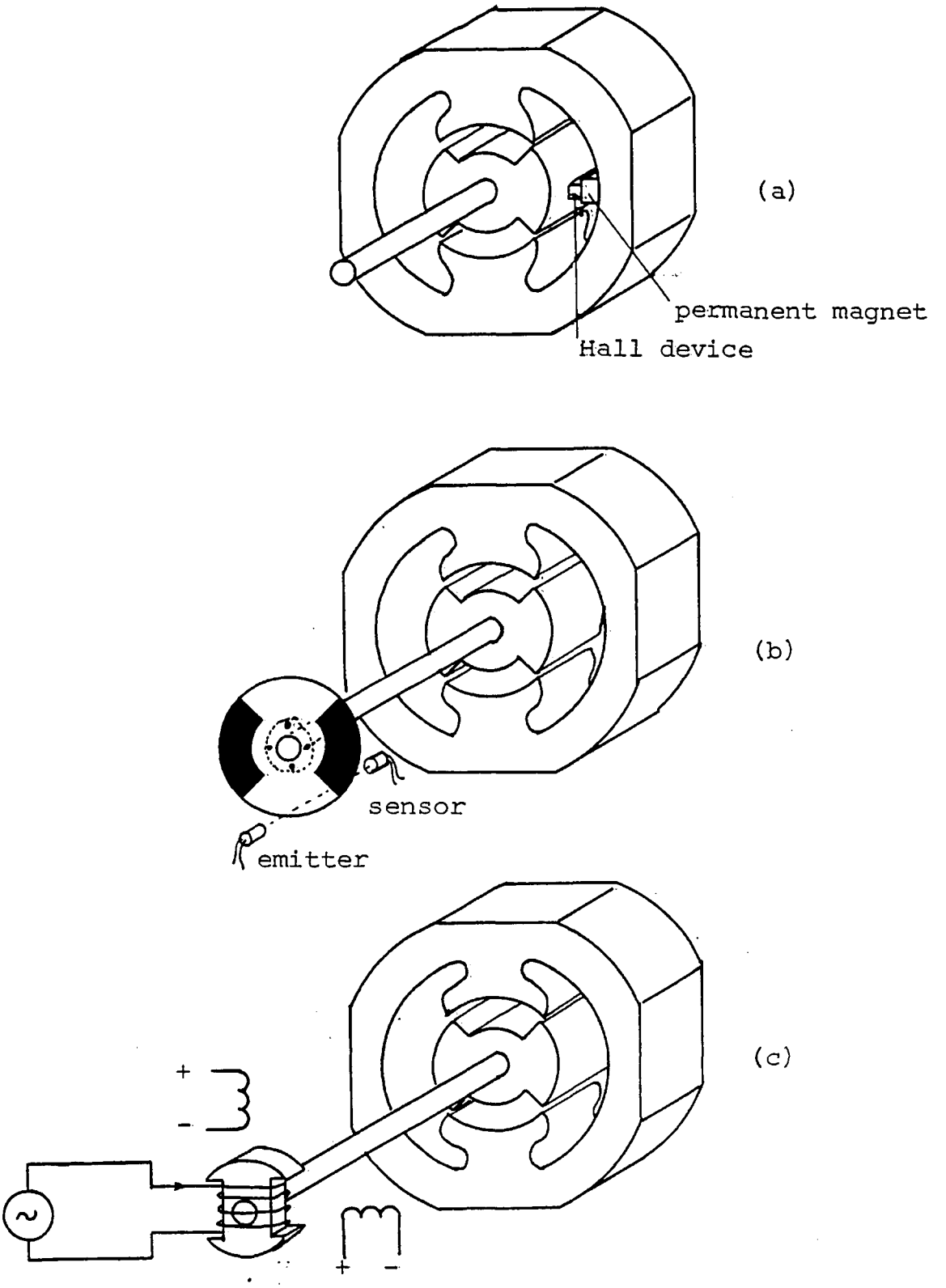

Fig. 2.5.1 Possible position-sensing systems
(a) Magnetic-transducer system
(b) Electro-optical system
(c) Inductive system

systems were adopted exclusively for the experimental program.

2.6 Speed-control methods

It is helpful in discussing the control of the SPSR motor by considering its natural characteristics. As shown in section 1.2.2 the constant voltage, constant switching-angle torque characteristic of the SPSR motor is similar to that of a d.c. series motor. The relation of torque τ and output power P vary with rotor speed for constant supply voltage and unsaturated conditions as:

$$\tau \propto \frac{1}{\omega^2} \quad \text{and} \quad P \propto \frac{1}{\omega^2}$$

and there is, of course, a family of series characteristics for varying supply voltages with an upper limit characteristic set by maximum rated voltage. The similarity between SRM and d.c. series motor characteristics immediately leads to the possibility of control through terminal voltage and current in the same way as with the d.c. series motor.

Open-loop control (of outer, speed loop) or closed-loop control can be implemented as desired. Open-loop control has no feedback path so no corrective action can be made against speed variations due to changes in load or supply disturbances. The open-loop control method would normally be used for the speed control of a low-cost

system where the absolute constant speed is not important and precise adjustment is not needed by the load, particularly when the load has a fixed, known torque versus speed characteristic (e.g. fan). Control of the SPSR motor can be implemented in both the power supply stage and power switching stage.

Voltage control possibilities include[2.9]

a) Rheostat control. This is perhaps the simplest method for controlling the input voltage of the motor. The variable resistor is inserted in series with the stator winding of the circuit to control the winding voltage. This method has the disadvantages of being relatively lossy and of giving poor load regulation.

b) Variable transformer control can be used to control the a.c. voltage supply to the motor with 'a.c.' feeds or to the rectifier with 'd.c.' feeds. Disadvantages here are the cost and bulkiness of the variable or tapped transformer.

c) Rectifier control. With 'd.c.' feeds, the d.c. link voltage can be varied compactly and efficiently by using thyristors in the rectifier. Cost is relatively low but the rate at which the link voltage can be reduced when the motor is on no or low load (given the presence of a link smoothing capacitor) might be slower than would be desirable in some cases.

d) Switching angle variation e.g. by mechanical 'cut-off' or 'advance and retard' adjustment of position sensor or by electronic means in the control circuit. Many possibilities here fall into the 'crude but effective' category. None have been investigated during the present project but it is considered that further work in this area would reap considerable dividends.

e) Sub-cycle switching modulation (PWM or PFM) of the winding supply voltage. This method, applicable to 'd.c.' feeds can most easily be implemented via the main power switches in the power switching unit using a PWM control chip or otherwise. The advantages of the method are that (1) no extra power components are needed, (2) closed loop control or manual control can be implemented if desired with little difficulty since the modulator can be controlled by means of a voltage signal. However transistor losses are somewhat increased and the control circuit cost is somewhat higher.

A relatively new technique, requiring a current sensor, is to operate the feed in the current source mode, the link current being controlled as desired by switching modulation of the main power switches or by phase control of the rectifier thyristors.

f) Phase control of triac or thyristor in 'a.c.' feed schemes. The thyristor or triac gate signal in 'a.c.' schemes is modulated primarily by the position

sensor. Average winding currents can clearly be controlled at minimal cost by the exercise of phase control on the same device in the usual way, but the detailed operation and analysis is complicated.

In the present project some open-loop measurements were made with scheme (f) on an 'a.c.' fed SPSR motor and scheme (e) (with PWM) on a 'd.c.' fed SPSR motor. Figs.2.6.1 and 2.6.2 show simplified diagrams of the two systems used. Circuit details will be described later and some remarks on'closed-loop' speed control are included in chapter 7.

2.7 Protection circuits[2.10,2.11]

2.7.1 Protection circuits for thyristor or triac

The principal measures necessary to ensure reliable operation in the context of the present project are:

a) Series HRC fuse. This can be used for protecting the device against large surge currents of relatively short duration.

b) Small saturable reactor or inductor. This, added in series with individual device, limits the rate of rise of current.

c) The peak voltage rating of a device used in particular operation must obviously be greater than the

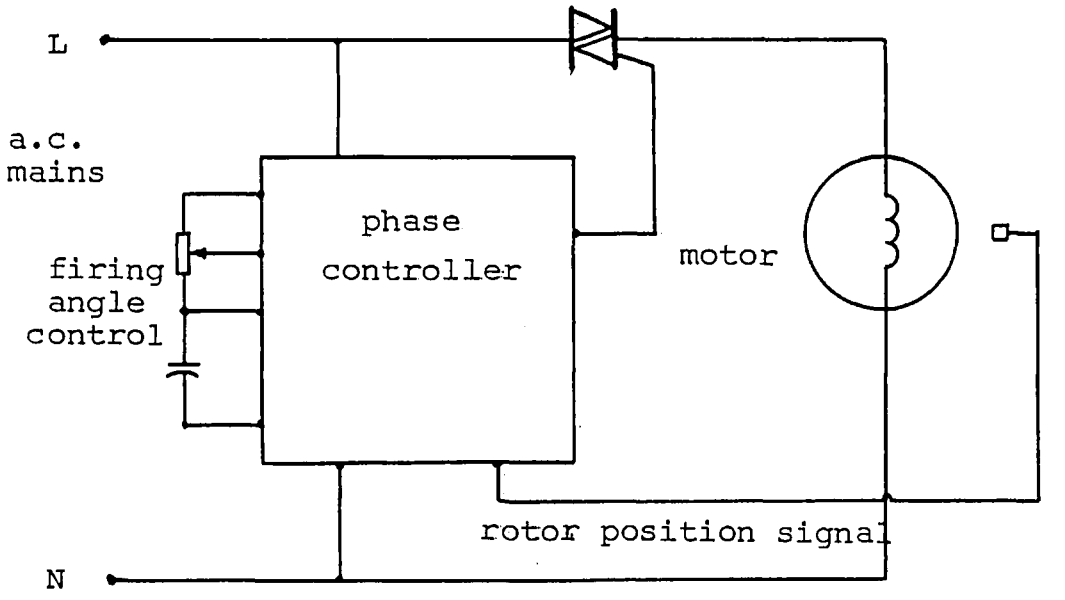

Fig. 2.6.1 Phase control of the 'a.c.' feed circuit

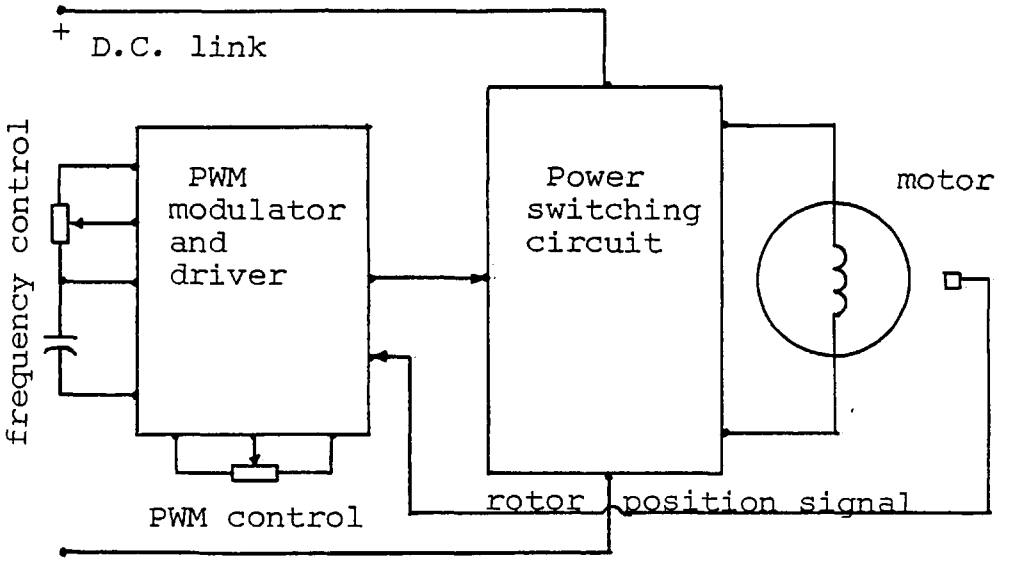

Fig. 2.6.2 PWM control of the 'd.c.' feed circuit

peak voltage it experiences during the course of the circuit operation. In practice, the safety factor is 1.5 or 2.0. Transients within the circuit may momentarily raise to several times the normal voltage, and it is these voltages which must be prevented from appearing across the off-state device.

A typical protection circuit is shown in Fig. 2.7.1. The capacitor C across the device ensures that any high dV/dt appearing at the thyristor terminals will set up an appropriate current in the capacitor. The inductance in the circuit will severely limit the magnitude of the current to the capacitor and hence limit dV/dt. When the thyristor is fired, any charge on the capacitor will be discharged into the thyristor, possibly giving an excessive high di/dt, but this can be suitably limited if needed by the inclusion of the resistor R. A diode D is included to by-pass R for improved dV/dt protection. The RC combination also serves to limit the induced voltage spike produced during the reverse recovery of the thyristor storage charge.

A nonlinear device such as a thyrector which has a reverse breakdown voltage similar to a zener diode can also be used for protection. If such a device is placed in parallel with a thyristor which has a higher peak reverse voltage value, then any transient voltage will be clipped at the safe level.

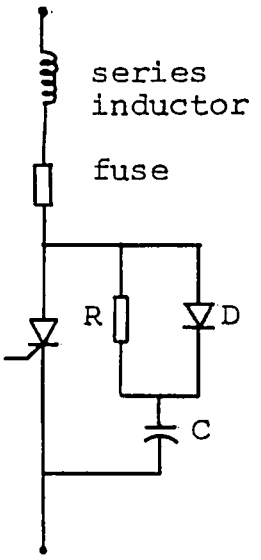

Fig. 2.7.1 Protection circuit for a single thyristor

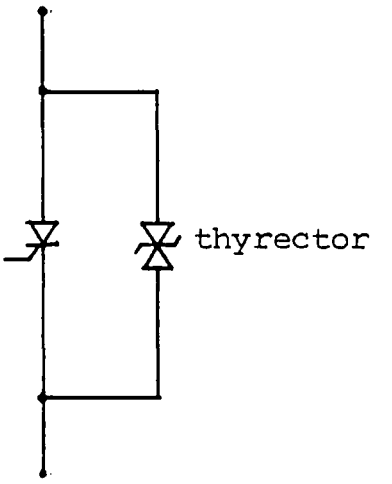

Fig. 2.7.2 Protection circuit using the thyrector diode

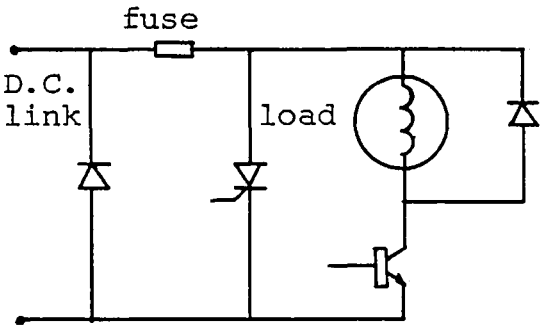

Fig. 2.7.3
Crow bar thyristor protection for power transistor

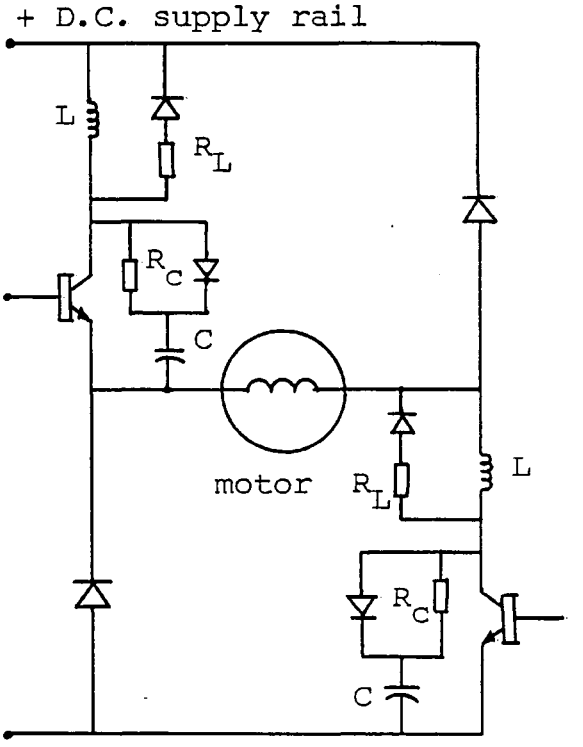

Fig. 2.7.4
Snubber ciruit for power transistor

2.7.2 Protection circuits for transistors

The overload capacity of the transistor is somewhat less than that of the thyristor so power transistor protection presents a more critical task. A rise in the collector current due to fault conditions may increase the collector-emitter voltage particularly if the base current is insufficient to match the increased collector current demand. As the transistor goes out of saturation, it is possible to have a high power loss within the transistor without there being sufficient current to cause the fuse to blow. It follows that a series fuse is insufficient for protection of the transistor. One well-known way of protection is by the use of a crowbar protection thyristor as shown in Fig. 2.7.3. Here fault conditions are sensed by a rise in the collector-emitter voltage, in conjunction with high collector current, which by suitable circuitry fires the crowbar thyristor, which in turn causes blowing of appropriate fuse link, hence rapidly relieving the transistors of the over-current.

Alternatively a current limiting circuit can be used to remove base drive as the collector current rises beyond a predetermined level, so permitting transistor turn-off.

Snubber circuits applied to the half bridge circuit used in the tests are shown in Fig. 2.7.4. The

snubber circuits greatly reduce the transistor's switching losses and provide some protection against voltage and current spikes emanating from the supply or motor winding. Switch-on losses are reduced because when the transistor switches on, the rate of rise of the collector current (di/dt) is limited by the series snubber inductor so that the transistor voltage drops before the peak current is reached. The switch-off losses are reduced because when the transistor switches off, the rate of rise of the transistor collector-emitter voltage (dV/dt) is limited by the parallel snubber capacitor so that the transistor collector current drops before the voltage reaches its peak value. The resistor R_L dissipates the energy stored in the inductor during 'off' period. The snubber resistor R_C limits the discharged current from the capacitor to the transistor during the 'on' period. To ensure successful operation of the snubber circuit, component values have to be calculated according to the transistor's parameters, load current and supply voltage. A design procedure for transistor snubber circuit compiled from Refs. 2.12 and 2.13 is shown in Appendix B1.

It should be emphasized that the reliable operation of power switching device also depends on the other factors such as temperature and interference. Sufficient cooling must be provided for the power switching devices (heat sink mounting) to allow the heat that results from forward voltage drop and switching losses to dissipate without excessive device temperature rise. The problems

of earthing, shielding particularly of the control circuit and mains filtering also need considering. Refs. 2.14 and 2.15 suggest some precautions and techniques for reducing harmonics, pick up and interference.

2.8 Merits of SPSRM drive system

The SPSRM drive system thus has a number of advantageous features, many of them possessed in common with polyphase SRM systems. Robustness, low cost, simplicity and ability to operate in adjustable speed applications are potential advantages in a general sense. In specific terms, one can cite a number of items:

(i) An absence of excitation or conductor-work of any kind on the rotor. This can allow the rotor to be easy to manufacture and to be cheap and robust. The motor can operate at relatively high speeds if required for enhanced power to weight applications such as high-speed hand tools, vacuum cleaners, some aerospace drives, etc. or for high-speed applications like centrifuges, gyro drives, etc.

(ii) There are no brushes or commutator. Hence, as with induction and brushless d.c. drives, the SPSRM has no problem with commutation, brush wear or electrical noise and can be used in hazardous areas.

(iii) The possession of a d.c.series motor type characteristic with fixed-voltage feeding makes the SPSRM potentially suitable for a wide range of applications such as fans, electrical drills, lawnmowers and washing machines. Like a.c. and d.c. commutator motors, the speed of a SPSRM can be controlled over a wide range by simple control of the voltage supply (e.g. by phase control or by pulse-width-modulation (PWM) control).

(iv) Unidirectional-current feed. In contrast with standard induction motors, synchronous motors and permanent-magnet brushless d.c. motor drives, the torques produced by SRMs are in most cases independent of the direction of winding currents. The unidirectional current permits the number of unidirectional solid-state switches such as thyristors or transistors to be reduced by half compared with the number required for an equivalent inverter. In the case of SPSR motor, it is possible to use only one switching element in the power circuit of the feed. This can reduce not only the cost of electronics but also the complexity of the control circuit. Higher reliability and easier maintenance are likely to result. Additionally this form of circuit where the switching devices are always connected in series with the motor winding avoids the possibility of short-circuit across the d.c.rails occurs in the bidirectional switching circuit for induction or synchronous motors when two devices connected in series between the d.c. rails become simultaneously conducting.

(v) The stator winding of the SPSRM can be of the concentrated-winding type, often the simplest and cheapest to form. With some SPSRM constructions, the winding can be wound on a former or bobbin prior to stator assembly thus avoiding the need for in-situ stator winding machines.

There are some drawbacks with SPSRM drives. The main ones are:

(i) Vibration. Fig. 2.8.1(c) shows a typical torque versus time waveform of a SPSRM for a particular operating voltage and particular switching angles. It can be seen that the instantaneous torque depends on both instantaneous current and rotor position, and that when the current is allowed to flow during negative dL/dt periods, negative torques are produced. Even when these are avoided, the pulsed nature of the torque can cause vibrations which might not be acceptable at high power or with particular loads. (In certain cases it would be possible to use suitable torsional compliances in the shaft or stator mounting to filter out the vibration if required over most of the speed range.) Torque pulsations occur with all SRM drives but the pulsation is bound to be high with SPSRM drives because it is impossible to avoid zero or even negative torques during some parts of the cycle.

(ii) Starting. Since positive torque can only developed for certain ranges of rotor position in a

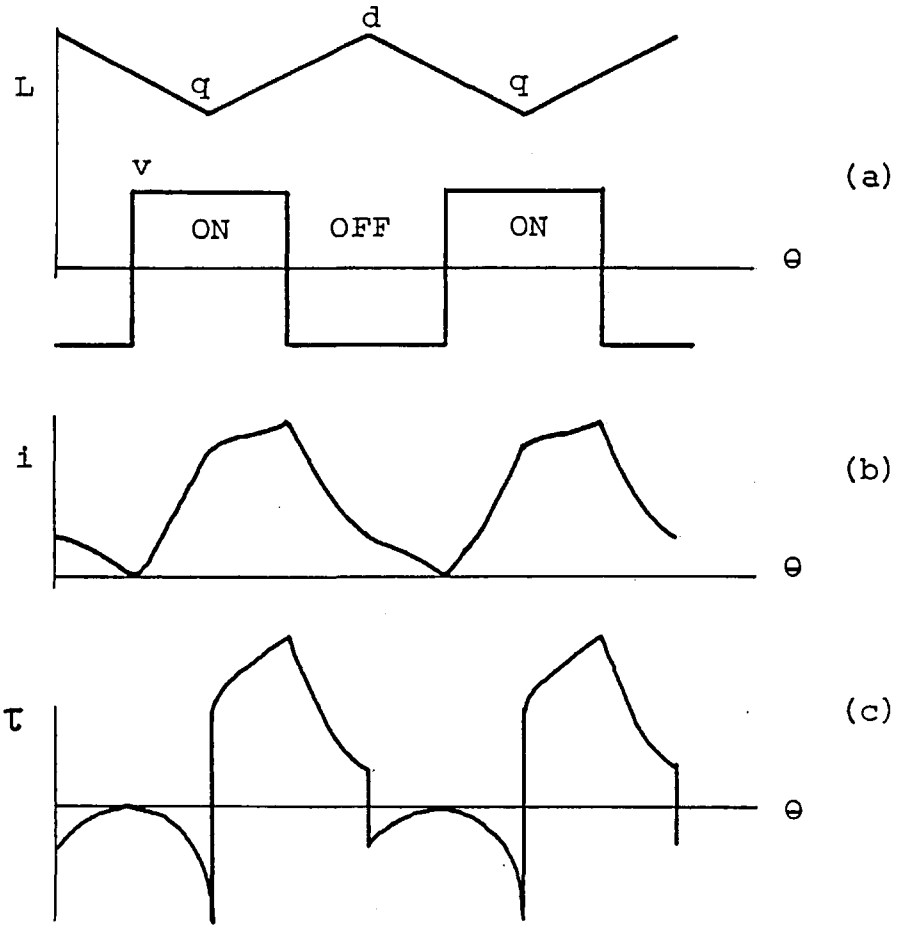

Fig. 2.8.1 Typical waveforms of current (b) and torque (c) pulses of the SPSR motor

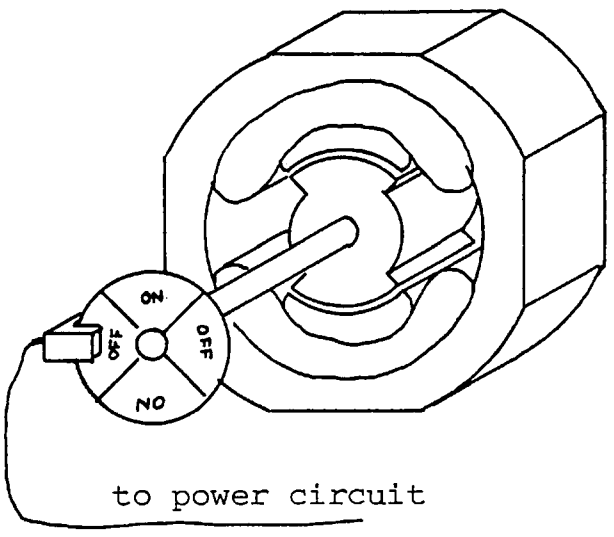

(a)

Off-position on the position sensor

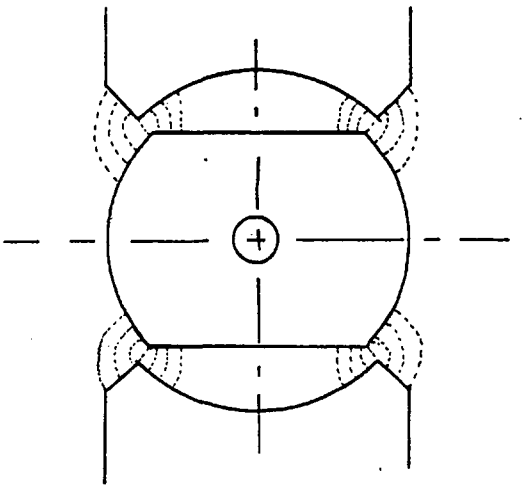

(b)

Unstable balanced position due to fringing flux

Fig. 2.8.2 Starting problems

SPSRM drive, the motor is able to start only when the rotor position falls within these ranges. Fig. 2.8.2 shows 2 rotor positions where starting is impossible. In the first case, the supply is normally 'off' since the torque developed would be negative. In the second case, the torque would be zero even with an energized coil since the $dL/d\theta$ is zero; the rotor is in q position and 'held' by the fringing flux in what would otherwise be an equilibrium position. At this position significance disturbance would cause the rotor to rotate in either directions. (It will eventually rotate in the direction set by the switching angles, perhaps after oscillations.)

A number of methods exist for starting. In one, a parking magnet is fixed onto the yoke or endplate of the motor facing the rotor as shown in Fig. 2.8.3. The rotor then comes to rest in a position favourable for the generation of positive torques at switch on. This method works well when the load and friction torques are low at low speed and standstill. When these conditions do not obtain, the starting magnet method can be used in conjunction with a viscous or compliant coupling element or a centrifugal or powder clutch in the shaft.

Another related idea is to employ another starting pole which would initiate rotor movement only if the rotor fails to start. This starting pole can be quite small, unlaminated and be wound with a few turns only. The starting pole would be excited only when a) the rotor

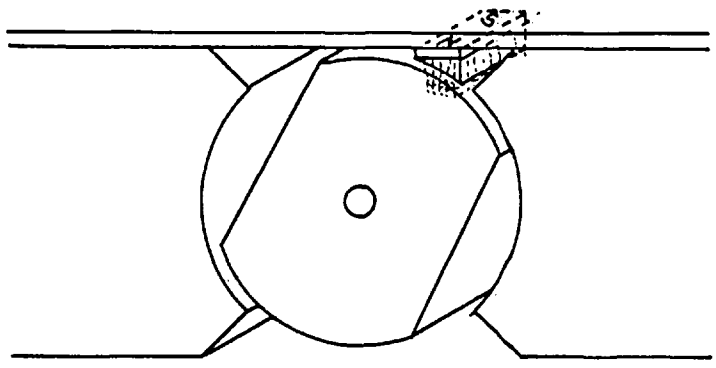

(a) Parking magnet on the motor housing

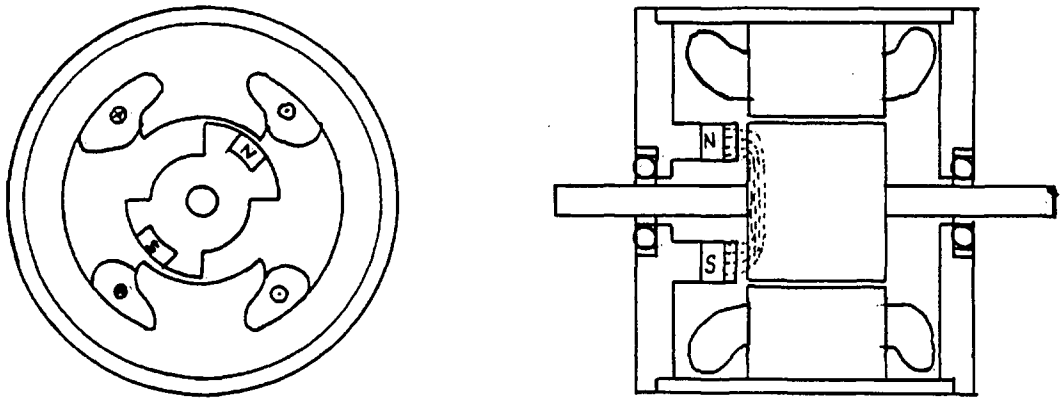

(b) Parking magnet at the end plate

Fig. 2.8.3 Arrangements of parking magnet on the stator for assisting starting. The starting pole location can be similar to that of the parking magnet.

is at rest and b) the rotor is in a non-start position. The starting pole idea compared with the parking magnet idea may seem inferior because it needs more components and is perhaps more difficult to implement. However, it does not interfere with the motor operation during running as does the parking magnet field (to a small extent) and there are no problems in procuring or fitting a suitable magnet.

The circuit and starting pole have been built and tested separately and the results are positive. However further modifications and tests are needed. Circuit details are shown in Appendix B2.

(iii) Power and size limits. The discontinuous nature of the torque and the use of a single-channel feed limit the maximum practicable size of SPSRM able to operate satisfactorily on two grounds:(a) noise and vibration: these tend to worsen as size increases,(b) power per channel: beyond a certain power rating, design trade-offs for obvious reasons would tend to favour multi-phase rather than single-phase operation. The topics of inherent power (size) limits for reluctance motors and of reluctance motor versus induction (and other) motor power to weight ratio are extremely controversial ones and outside the scope of this thesis. In some quarters it is held that, other things (including operating speed and frequency) being equal, the reluctance motor wins in power to weight terms

below a certain rated power threshold and the induction motor above. The matter is dealt with at some length in Ref. 2.16, from which Fig. 2.8.4 is taken. It is likely that in certain respects (e.g. core flux and maximum current loading per rated power) the single phase switched reluctance motor bears the same relationship to its multiphase counterpart as does the single phase induction motor to the multiphase equivalent.

(iv) Starting current. Fig. 2.8.5 shows a typical set of characteristic SPSRM curves for constant d.c. link voltage operation. At low speeds both mean torque and mean current rise to high values as in the case of d.c. and a.c. series motors. With d.c. link feeds, the starting current of a SPSRM will be only limited by winding resistance. Except with very small motors (where per unit winding resistance is relatively high), some form of current limiting circuit is needed to prevent the power circuit from overloading. If the supply is pulse-width-modulated for instance, the mark to space ratio can be set to be low at starting and gradually increased during the acceleration period. Alternatively (or additionally), the switching angles (on and off times) of the main supply pulse can be varied. Other techniques include the use of phase angle control on the d.c. link supply bridge rectifiers and the use of a starting impedance in the feed circuit.

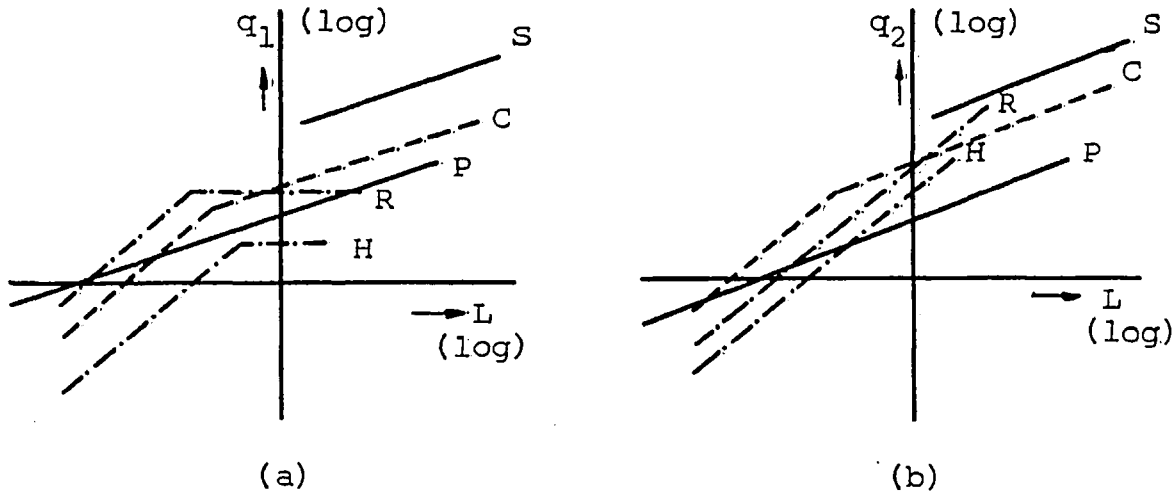

Fig. 2.8.4 Variation of figures of merit with linear dimension L. The discontinuity in some curves occurs at the critical dimension at which magnetic saturation starts.
(a) Power to weight ratio q_1
(b) The figure of merit q_2 which is $\frac{\eta}{1-\eta}$ where η is efficiency.
S = superconducting machines, C = conventional machines,
P = permanent magnet machines, R = reluctance machines,
H = hysteresis machines

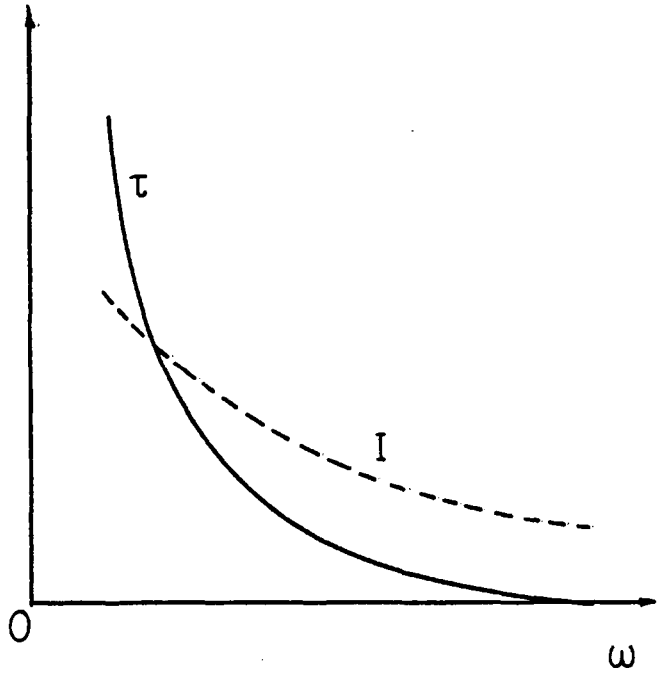

Fig. 2.8.5 Typical current and torque versus speed characteristics of the SPSR motor

Although the SPSRM has some disadvantages due primarily to the discontinuous nature of its torque, these do not always matter depending on the application, and partial solutions to some of the worse effects can be found without excessive costs. In some applications the advantages can outweigh disadvantages and the SPSRM system with its single-channel feed may be considered as a reasonably strong contender among other variable-speed brushless drive systems.

2.9 Concluding remarks

In this chapter the basic composition and merits of a SPSRM drive has been described and some of the options that exist for each part of a SPSRM system have been outlined. The large number of possible motor and feed circuit types has been indicated. It has shown that a number of low cost options exist though some of them introduce problems which may not always prove acceptable in a particular application.

CHAPTER 3

THEORY OF OPERATION OF THE SPSR MOTOR

3.1 Introduction

The analysis presented is based on a simplified equivalent circuit of the SPSR motor as shown in Fig. 3.1.1. The use of this circuit requires the following assumptions:

a) the effect of iron losses is negligible,

b) the magnetic circuit is linear.

These assumptions are perhaps to be expected in a first analysis. In hard driven SRMs, neither iron loss nor saturation effects would be at all negligible. However there are reasons to suppose that these assumptions are in fact unlikely to cause too much error, in respect of current and torque prediction for many practical SPSRM systems. The principal reasons are: (a) iron losses certainly affect input power levels significantly; currents and torques are less affected unless the iron losses are severe, (b) peak currents (on or off load) increase sharply with saturation. In order to maintain reasonable device utilisation in the power switching unit, it is often advisable (as it emerged during the experimental investigation) to operate the motor's magnetic circuit unsaturated throughout the cycle.

It may be noted that the fundamentals of reluctance device behaviour when significant amounts of saturation occur has been the subject of considerable attention in recent years and is well documented in the learned society literature and in many textbooks on machines fundamentals.[3.1, 3.2] In a more extended and/or narrow a study (typified for polyphase SRMs by that reported by Stephenson [3.3]) a developed version of the calculation method presented below could be evolved probably with little difficulty. Lengthiness would be inevitable in using such a method given the need for a two dimensional table of inductance values (versus current and rotor angle) for each motor investigated.

The winding resistance R (Fig. 3.1.1) can obviously be taken as fixed. The winding inductance $L(\theta)$ varies cyclically with the rotor position between maximum (L_d) and minimum (L_q) values. All the predictions made in the thesis assume a simple triangular variation of inductance with rotor position as shown in Fig. 3.1.2. This obviously simplifies the detailed algebra, computer program and input data needs, and was an assumption which was adhered to when early measurements on the experimental motors showed that inductance versus rotor angle curves were all in fact remarkably close to this ideal form. The 'secondary' assumptions corresponding to triangular variation of inductance with rotor angle are:

c) constant clearance (parallel airgap) between stator and rotor saliencies,

d) single concentrated excitation coil,

e) equal widths of stator and rotor saliencies,

f) equal numbers of stator and rotor saliencies,

g) negligible flux fringing.

Assumptions (c) to (f) were each substantially true for the experimental motors. It is very important to note that the state space analysis described below places no restrictions on the shape of the inductance versus rotor angle curve. Few changes would be required in the program listing to accommodate an arbitrary curve shape. The process of measuring or calculating and inputting a series of (rather than just two) inductance values would obviously be more lengthy.

From Fig. 3.1.1, the circuit equation is:

$$v = iR + \frac{d(Li)}{dt} \qquad (3.1.1)$$

which can be written in the form:

$$v = iR + L\frac{di}{dt} + i\frac{dL}{dt} \qquad (3.1.2)$$

It is interesting to note that for constant speed and a triangular variation of inductance with rotor angle, the dL/dt versus time relation is a square wave, dL/dt being positive during the increasing inductance period and negative during the decreasing inductance period. As Ref. 3.4 states:"At low speeds, dL/dt is small and the

motor behaves virtually as a simple R-L circuit. As the speed increases, dL/dt becomes significant, and then dominant alongside R and the circuit looks more resistive during the increasing inductance period and more subject to the negative resistance when L is decreasing. The back e.m.f. effects of a negative i(dL/dt) is unlike the one that occurs in a d.c. or synchronous machine because its existence depends on the flow of coil current i." The term L(di/dt) depends on the changes of coil current. The negative back e.m.f. L(di/dt) when the current is decreasing causes the current to flow through the freewheeling diode.

From eq.(3.1.2) the division of power can be obtained by multiplying by i on both sides:

$$vi = i^2R + \frac{d}{dt}(\tfrac{1}{2}Li^2) + \frac{1}{2}\, i^2\frac{dL}{dt} \qquad (3.1.3)$$

This equation shows that, when running as a motor, the input electrical power (vi) goes partly to increase the stored magnetic energy ($\frac{1}{2}Li^2$) and partly to provide mechanical output power ($\frac{1}{2}\, i^2\frac{dL}{dt}$). The remainder is dissipated in the winding resistance (i^2R). So the output power P_m is $\frac{1}{2}\, i^2\frac{dL}{dt}$ and at constant rotor speed (ω_r = constant) the equation for the instantaneous output torque is

$$\tau = \frac{1}{2}\frac{i^2}{\omega_r}\frac{dL}{dt} \qquad (3.1.4)$$

where ω_r is the angular rotor speed.

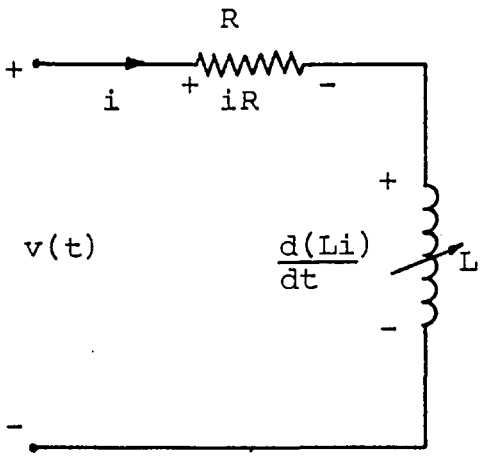

Fig. 3.1.1

Simplified equivalent circuit

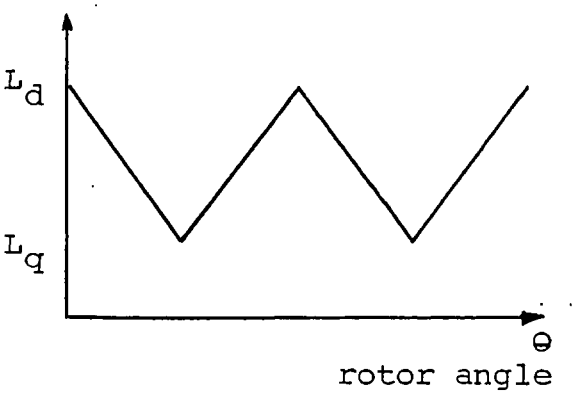

Fig. 3.1.2

Variation of inductance with rotor position

It can be seen clearly from equation (3.1.4) that the output torque of the unsaturated SPSR motor varies linearly with the square of the stator current and inversely with the rotor speed, a similar characteristic to that of the unsaturated d.c. series motor.

Before further attempts are made in finding the solutions for currents and torques, the significance of the switching angles should be briefly discussed. As mentioned in section 1.2, continuous rotation of the rotor is achieved by switching the supply voltage 'on' and 'off' in synchronism with the rotor position. Fig. 3.1.3(a) shows typical waveforms of voltage, current and torque

expected for an ideal (if 'naive') switching pattern where the excitation coil is switched 'on' just after the rotor reaches the q position and switched 'off' just after it reaches the d position. The equivalent circuit of the motor is assumed to be as shown in Fig. 3.1.1,a d.c. link type feed circuit is assumed with no pulse-width-modulation and the pull-down reverse voltage is equal the d.c. rail voltage. At constant speed the supply voltage is a square wave but the current pulse is far from a rectangular shape because of the circuit inductance. After the supply voltage has been switched on at the q position the stator current takes some time to build up. After the supply voltage has been switched off, the current continues to flow in the winding through freewheel diodes until pulled down to zero by the reverse applied voltage. The decreasing current that flows while the rotor is in what can be termed the 'negative inductance slope region' produces negative torque, and this can result in a low value of mean torque as shown.

The current waveform can clearly be improved by introducing an advance switching on angle (α) and an advance switching off angle (β) as shown in Fig. 3.1.3(b). In this case the supply voltage is switched on at α elec. deg. before the rotor reaches the q position and switched off at β elec. deg. before the rotor reaches the d position. After switch on, the current builds up rapidly due to low inductance and is maximum

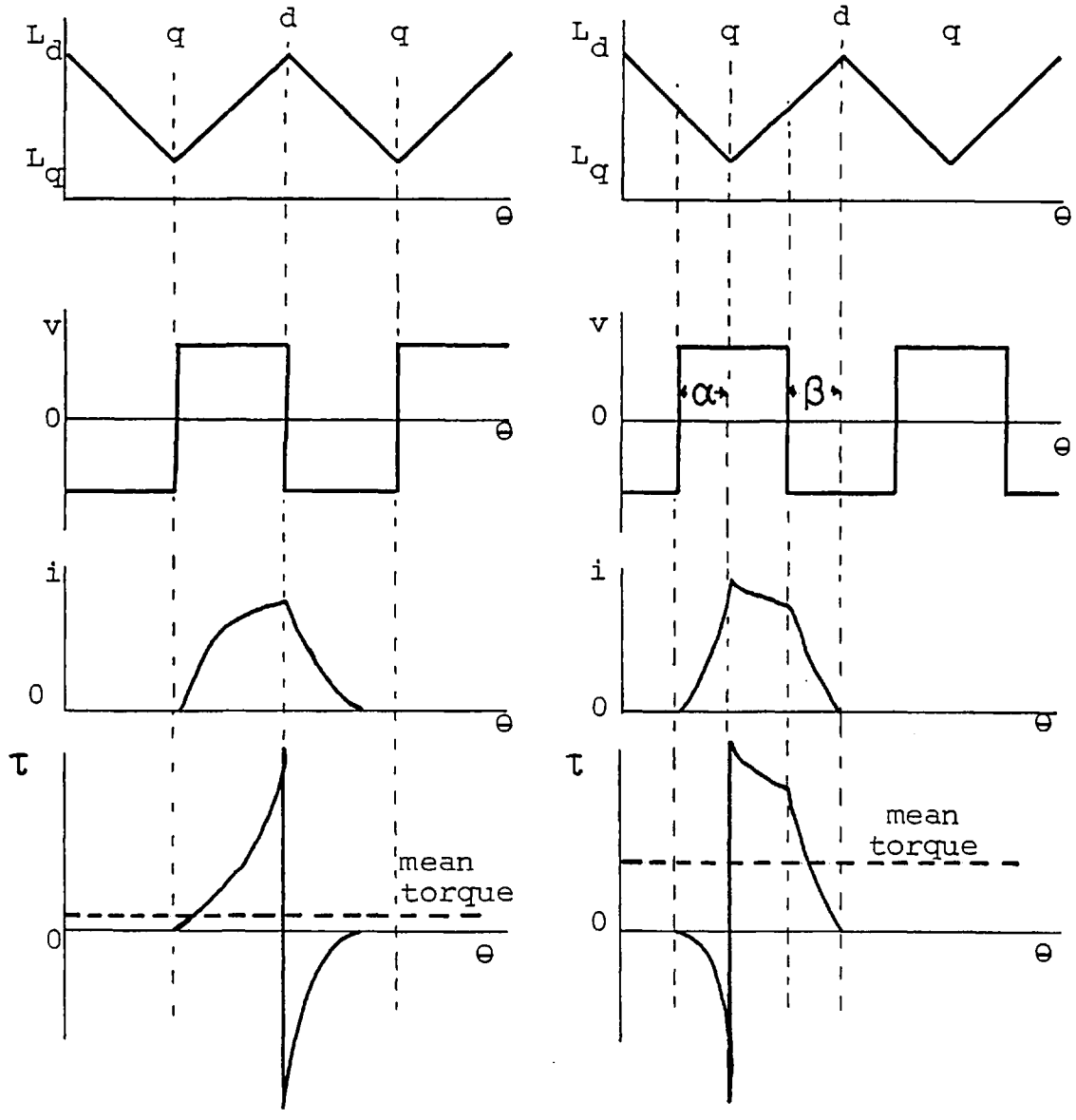

(a) ideal switching pattern (b) advance switching angle

Fig. 3.1.3 Comparisons of currents and output torques of the SPSR motor with different switching angles

Note The mean torque in case (b) (with advance switching angles) is higher than in case (a) (with zero advance switching angles)

when the rotor is at the q position. After the supply voltage is switched off the current still flowing in the coil is pulled down rapidly due to the combination of increasing inductance and reverse voltage. Although there is a negative torque produced at the start of the current pulse it is quite low because of the small instantaneous current. The current pulse is closer to a square wave in form and lies mainly in the positive inductance slope region which results in higher mean torque.

3.2 Steady-state analysis for 'd.c.' operation of the SPSR motor

For 'd.c.' operation where the power supply to the rotor is fed from a d.c. link, the voltage function v for equation (3.1.2) is the square wave as shown in Fig. 3.2.1. The analytic solutions of the simplified equations (3.1.2) and (3.1.4) for current and output torque become very lengthy and involve in solving differential equations with variable coefficients. Two alternative methods were then adopted in order to simplify the calculations: a) Simplified analytic method and b) Step by step method.

The simplified analytic method follows the method that has been described in Ref. 3.5, in which the resistance R of the winding is neglected. This assumption is reasonable as a first approximation for motors operating

with reasonably good efficiencies since if the motor efficiencies are to be acceptable the resistive voltage drop iR must be small compared with effective back e.m.f. $i(dL/dt)$ or compared with the reactive drop $L(di/dt)$. For low speeds the approximation is unlikely to be a good one since the current is high and the terms di/dt and dL/dt small. The approximation is also unfortunately unlikely to be a good one for the small motors with their relatively high R/L ratios investigated in the present project. However, the simplification enables the current waveform to be calculated analytically, either by hand or with a programmable calculator, together with the mean and r.m.s. current and mean torque. Rough trends can be examined with relatively little effort (valuable in choosing control strategies to suit particular drive systems) even if predictions of e.g. peak current levels are too approximate to be of much use.

The other method, based on a step by step approach takes into account the resistance of the winding. The usual (slight) approximations are made, viz: non derivative variables are replaced during each time step with their average values and time derivatives of variables with their differences divided by Δt, both average values and differences being taken over a small time interval Δt. A simple stepping computer program can then be written for point by point computation of the current and torque waveforms. The r.m.s. current and torque are calculated by standard means.

The step by step method is obviously more accurate than the simplified analytic method and can be applied to a motor with any R/L ratios, but involves more complicated calculations and longer computing times. As will be seen, current waveforms as well as trends are predicted to quite good levels of accuracy.

3.2.1 Simplified analytic method

This follows the general approach of Ref. 3.5 though differing in some important details at a number of stages (see end of this section). The simplified analytic solution of the voltage equation can be found for each regions A, B, C and D dictated by the inductance profile, and switching angles as shown in Fig. 3.2.1.

For generality the supply voltage is assumed to switch on to the stator winding when the rotor is at $\theta = \theta_o$, advanced by α elec deg from the q position and to switch off at $\theta = \theta_p$, advanced by β elec deg from the d position. So the applied voltage, dictated by the inverter under the control of the position sensor, has a rectangular waveform given by

$$v(\theta) = k_1 V_s \qquad (\theta_o < \theta < \theta_p) \quad (3.2.1)$$

$$v(\theta) = k_2 V_s \qquad (\theta_p < \theta < \theta_q) \quad (3.2.2)$$

where k_1, k_2 are the ratios of the voltage seen by the stator winding to the d.c. link voltage V_s. Normally

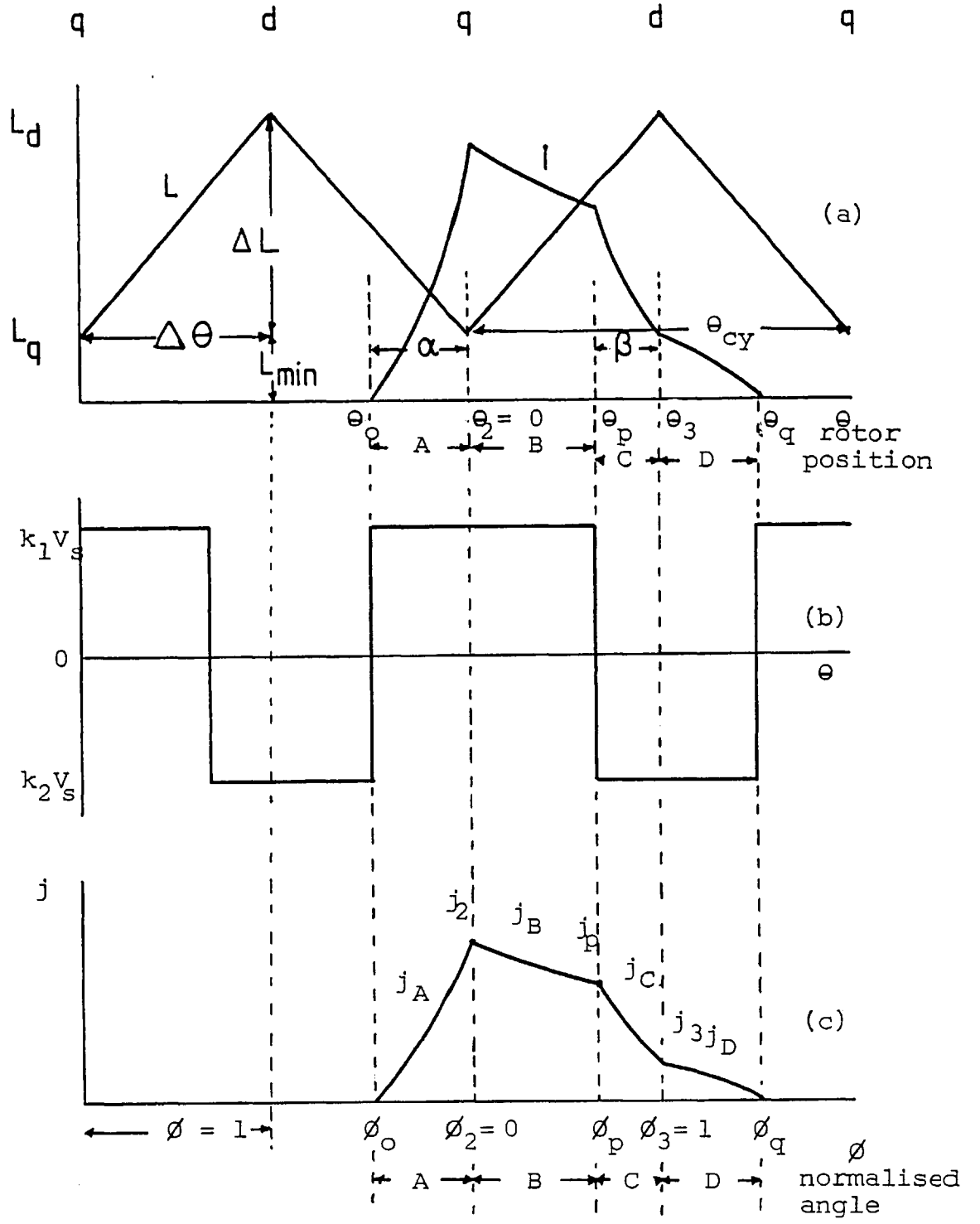

Fig. 3.2.1 (a) Inductance profile and current waveform

(b) Voltage waveform

(c) Normalised current

k_1 is equal to 1 and k_2 is -1 for a half bridge inverter or -n when the turns ratio of main coil to pull-down coil is 1:n (with bifilar-wound pull-down circuits)

θ_o and θ_p are the controlled switching angles and θ_q is the angle at which the current becomes zero.

As stated previously, the resistive drop iR is assumed negligible and it is now assumed in addition that:

a) The inductance variation follows a triangular waveshape with the equal and opposite slopes during the rising and falling inductance periods. The inductance is of course assumed to be independent of stator current.

b) The stator current transfers from the main transistors to the freewheel diodes over a negligible rotor angle, during which the stator current is constant.

c) In the case of a bifilar-wound pull-down circuit, the motor current is the sum of the main winding current and the pull-down current, leakage inductance effects being negligible.

The simplified equations for eqs(3.1.1) and (3.1.4) can then be rewritten as

$$v = \omega_r \frac{d}{d\theta}(iL) \qquad (3.2.3)$$

$$\tau = \frac{1}{2} i^2 \frac{dL}{d\theta} \qquad (3.2.4)$$

where $\omega_r = \frac{d\theta}{dt}$ is the rotor angular speed.

For the period of increasing inductance $\theta_2 < \theta < \theta_3$ during which positive torque is produced, the inductance function for $\theta_2 = 0$ (for convenience) is

$$L = \Delta L \left(b + \frac{\theta}{\Delta\theta} \right) \qquad (3.2.5)$$

and

$$\frac{dL}{d\theta} = \frac{\Delta L}{\Delta\theta} \qquad (3.2.6)$$

where ΔL is the change in inductance over the period $\Delta\theta$ of rising inductance as shown, and

$$b = \frac{L_{min}}{\Delta L} \qquad (3.2.7)$$

a) Current waveform derivation

The calculation of the current waveforms can be simplified still further by the introduction of a normalised current j and a normalised angle ϕ which is independent of speed. In this way, a set of normalised waveforms may be computed which are applicable at any speeds with appropriate scaling.

The unit angle is defined as $\Delta\theta$ such that the normalised angle ϕ is equal to $\frac{\theta}{\Delta\theta}$. The increasing inductance region $\theta_2 < \theta < \theta_3$ can then be defined to be the region $0 < \phi < 1$. The inductance function for this region with respect to normalised angle is then,

$$L = \Delta L \left(b + \phi \right) \qquad (3.2.8)$$

and the voltage and torque equations are

$$v = \omega_r \frac{\Delta L}{\Delta\theta} \frac{d}{d\phi} \left(i \left(b + \phi \right) \right)$$

and $$\tau = \frac{1}{2} i^2 \frac{\Delta L}{\Delta \theta}$$

The normalised current can be defined as $j = \frac{i}{I}$ where I is the unit current and defined as:

$$I = \frac{V_s \Delta \theta}{\omega_r \Delta L} \qquad (3.2.9)$$

and the normalised equations for current and output torque become

$$\frac{v}{V_s} = \frac{d}{d\phi}(j (b + \phi)) \qquad (3.2.10)$$

and $$\tau = \frac{1}{2} \frac{V_s I j^2}{\omega_r} \qquad (3.2.11)$$

for $0 < \phi < 1$

In the decreasing inductance region ($\phi < 0$ and $\phi > 1$) the inductance function is

$$L = \Delta L (b - \phi)$$

and the voltage equation for this region becomes

$$\frac{v}{V_s} = \frac{d}{d\phi}(j (b - \phi)) \qquad (3.2.12)$$

for $\phi < 0$ or $\phi > 1$

The current equations can then be derived by applying suitable voltage function for each regions as follows :

Region A ($\phi_o < \phi < 0$)

The voltage function (from Fig. 3.2.1) is

$$v = k_1 V_s$$

substituting into equation (3.2.12) the normalised equation becomes,

$$k_1 = \frac{d}{d\phi}(j(b-\phi)) \qquad (3.2.13)$$

and the solution for region A is

$$j_A = k_1 \frac{(\phi-\phi_o)}{(b-\phi)} \qquad (3.2.14)$$

where j_A is the current in region A which is zero at $\phi = \phi_o$ and the current at boundary j_2 where $\phi = \phi_2 = 0$ can be calculated by substituting $\phi = 0$ in j_A, which yields

$$j_2 = - \frac{k_1 \phi_o}{b} \qquad (3.2.15)$$

Region B ($0 < \phi < \phi_p$)

The voltage function is the same as in region A but the inductance function changes from negative slope to positive slope so the voltage equation is

$$k_1 = \frac{d}{d\phi}(j(b+\phi)) \qquad (3.2.16)$$

and the current equation for region B is

$$j_B = \frac{k_1\phi + bj_2}{b + \phi} \qquad (3.2.17)$$

and the current at boundary j_p where $\phi = \phi_p$ is

$$j_p = \frac{k_1\phi_p + bj_2}{b + \phi_p} \qquad (3.2.18)$$

Region C ($\phi_p < \phi < 1$)

Since ϕ_p is the switching off angle, the voltage function for this region is

$$v = k_2 V_s$$

and the voltage equation becomes

$$k_2 = \frac{d}{d\phi}(j(b+\phi)) \qquad (3.2.19)$$

and the current equation for region C is

$$j_C = \frac{k_2(\phi-\phi_p)+(b+\phi_p)j_p}{b+\phi} \qquad (3.2.20)$$

and j_3 can be found for $\phi = 1$ as

$$j_3 = \frac{k_2(1-\phi_p)+(b+\phi_p)j_p}{b+1} \qquad (3.2.21)$$

Region D ($1 < \phi < \phi_q$)

The voltage function is still $v = k_2 V_s$ but the region lies in the negative inductance slope and the inductance function in terms of rotor position is

$$L = L_{max} - \frac{\Delta L}{\Delta \theta}(\theta - \theta_3) \qquad (\theta > \theta_3)$$

and with normalised angle, the inductance function is

$$L = \Delta L\ ((b+1)-(\phi-1)) \qquad (\phi_3=1)$$

so the voltage equation becomes

$$k_2 = \frac{d}{d\phi} j((b+1)-(\phi-1)) \qquad (3.2.22)$$

and the current equation for region D is

$$j_D = \frac{(\phi-1)k_2+(1+b)j_3}{(1+b)-(\phi-1)} \qquad (3.2.23)$$

The angle ϕ_q where the current falls to zero can then be calculated from eq. (3.2.23) by equating j_D to zero, hence

$$\phi_q = 1 - \frac{(1+b)}{k_2} j_3 \qquad (3.2.24)$$

It should be noted that the normalised current waveform depends only on the switching angles ϕ_o and ϕ_p. And with the half bridge inverter circuit or bifilar-wound pull-down circuit with equals turns ratio where $k_1=1$ and $k_2= -1$, the transistor conduction angle $\phi_p-\phi_o$ is equal to the diode conduction angle $\phi_q- \phi_p$. From equation (3.2.3) the increase in flux up to ϕ_p caused by the supply voltage V_s must equal the flux decrease after ϕ_p due to $-V_s$.

b) Derivation of torque and power

The last section shows that once the switching angles ϕ_o and ϕ_p are defined the normalised current

waveform is defined irrespective of speed. Since the instantaneous torque τ at a given speed is proportional to j^2 (eq. 3.2.11), the mean torque τ_{mean} and developed power P are given by

$$\tau_{mean} = \frac{1}{2} \frac{V_s I}{\omega_r} j^2_{\tau rms} \qquad (3.2.25)$$

$$P = \frac{1}{2} V_s I j^2_{\tau rms} \qquad (3.2.26)$$

where $$j_{\tau rms} = \left[\frac{1}{\emptyset_{cy}} \int_{\emptyset_o}^{\emptyset_q} j^2 \, d\emptyset \right]^{\frac{1}{2}}$$

and $$\emptyset_{cy} = \frac{\theta_{cy}}{\Delta\theta} = 2$$

i.e. the mean torque and power are proportional to the normalised r.m.s. value of the torque producing current over a complete angular cycle $\emptyset_{cy}$ of the rotor geometry. It should be made clear at this point that the $j_{\tau rms}$ is not the same as the r.m.s. value of the current because $j_{\tau rms}$ takes into account the effect of negative torque production in the negative inductance slope regions.

Using the symbols $SS = \int j^2 d\emptyset$ and $S = \int j d\emptyset$ over four regions A, B, C and D, the expressions for torque producing r.m.s. current and mean currents can be written as follows:

i) Torque producing r.m.s. current

$$j_{\tau rms} = \left[\frac{1}{\emptyset_{cy}} \left(-SS_A + SS_B + SS_C - SS_D \right) \right]^{\frac{1}{2}} \qquad (3.2.27)$$

ii) Transistor and diode r.m.s. and mean currents:

$$
\begin{aligned}
j_{Trms} &= \left[\frac{1}{\phi_{cy}}\left(SS_A+SS_B\right)\right]^{\frac{1}{2}} \\
j_{Tmean} &= \frac{1}{\phi_{cy}}\left(S_A+S_B\right) \\
j_{Drms} &= \left[\frac{1}{\phi_{cy}}\left(SS_C+SS_D\right)\right]^{\frac{1}{2}} \\
j_{Dmean} &= \frac{1}{\phi_{cy}}\left(S_C+S_D\right)
\end{aligned}
\qquad (3.2.28)
$$

iii) Interrelationship between $j_{\tau rms}$, j_{Tmean} and j_{Dmean}:

The mean power P previously defined by eq. (3.2.26) is also given by

$$P = V_s I \left(j_{Tmean} - j_{Dmean}\right)$$

Hence

$$j^2_{\tau rms} = 2\left(j_{Tmean} - j_{Dmean}\right) \qquad (3.2.29)$$

iv) Expressions for current integrals for each regions:

$$
\begin{aligned}
S_A &= k_1 b\left[\frac{\phi_o}{b} + \left(1-\frac{\phi_o}{b}\right)\ln\left(1-\frac{\phi_o}{b}\right)\right] \\
S_B &= k_1 b\left[\frac{\phi_p}{b} - \left(1+\frac{\phi_o}{b}\right)\ln\left(1+\frac{\phi_p}{b}\right)\right] \\
S_C &= k_2(1-\phi_p) + \left[(k_1-k_2)\phi_p - k_1\phi_o - k_2 b\right]\ln\frac{(b+1)}{(b+\phi_p)} \\
S_D &= -k_2(\phi_q-1) - \left[(k_1-k_2)\phi_p - k_1\phi_o + k_2(b+2)\right]\ln\frac{(b+2-\phi_q)}{(b+1)}
\end{aligned}
\qquad (3.2.30)
$$

$$SS_A = k_1^2 b \left[M_1^2 - 1 - 2M_1 \ln M_1\right]$$

$$\text{where} \quad M_1 = 1 - \frac{\phi_o}{b}$$

$$SS_B = k_1^2 b \left[M_2 - 1 + \frac{J_2^2(M_2-1)}{M_2} - 2J_2 \ln M_2\right]$$

$$\text{where} \quad M_2 = 1 + \frac{\phi_p}{b}$$

$$J_2 = 1 - \frac{j_2}{k_1}$$

$$SS_C = k_2^2(b+\phi_p) \left[M_3 - 1 + \frac{J_p^2(M_3-1)}{M_3} - 2J_p \ln M_3\right]$$

$$\text{where} \quad M_3 = \frac{(b+1)}{(b+\phi_p)}$$

$$J_p = 1 - \frac{j_p}{k_2}$$

$$SS_D = -k_2^2(1+b) \left[M_4 - 1 + \frac{J_3^2(M_4-1)}{M_4} - 2J_3 \ln M_4\right]$$

$$\text{where} \quad M_4 = 1 - \frac{(\phi_q - 1)}{(1+b)}$$

$$J_3 = 1 + \frac{j_3}{k_2}$$

(3.2.31)

As previously stated, the foregoing analysis method follows the general approach given in Ref. 3.5 except that, in the author's opinion:

The current pulse is defined in section 10.2 of the paper by i_p and θ_p from which θ_o and θ_q are obtained. Equation(10) for the current in the rising inductance region in the paper is

$$i = \frac{k(\theta - \theta_p) + i_p(b + \theta_p)}{(b + \theta)}$$

$\theta = \theta_o$, $i = 0$ and $k = 1$ are then set to give

$$\theta_o = \theta_p - i_p(b + \theta_p)$$

and $\theta = \theta_q$, $i = 0$ and $k = -n$ set to give

$$\theta_q = \theta_p + \frac{i_p}{n}(b + \theta_p)$$

If the current is switched on before the instant at which the inductance starts to rise (as is usually the case at speed), the above relations for θ_o and θ_q seem not to be valid, since θ_o, the switch-on angle is inevitably set by the θ_o relation within the rising inductance region. Similarly the θ_q relation implies that the current extinguishes before the inductance has attained its maximum value. This is often not so.

The current at the boundaries in the paper are also derived from the i_p, θ_p parameters and the equations for current and current integrals are then defined once i_p, θ_p, θ_o and θ_q are defined. However i_p emerges only from a complete solution and is therefore very difficult (except by working backwards) to fix at this stage as a parameter. A 'missing link' between these parameters is suspected.

In the author's analysis only θ_o and θ_p

are used as parameters and i_p and θ_q are solved for, together with other quantities. Finally, a different inductance waveform is used (pure triangular). All these matters result in appreciable differences between the equation for current and current integrals in the paper and in this thesis.

3.2.2 Step by step method[3.6]

The step by step method is based on the simplified equations for current (3.1.2) and instantaneous output torque (3.1.4), the resistance of the winding being taken into account. Those equations are

$$v = iR + L\frac{di}{dt} + i\frac{dL}{dt} \qquad (3.2.32)$$

and

$$\tau = \frac{1}{2}\frac{i^2}{\omega_r}\frac{dL}{dt} \qquad (3.2.33)$$

As stated previously, the other main assumptions are the same as in the previous method. For a small time interval Δt, (between the time t_1 and t_2), the approximation is made, as indicated in Fig. 3.2.2 that the variables' derivatives can be expressed as:

$$\frac{di}{dt} = \frac{\Delta i}{\Delta t} = \frac{i_2 - i_1}{\Delta t}$$
$$\frac{dL}{dt} = \frac{\Delta L}{\Delta t} = \frac{L_2 - L_1}{\Delta t} \qquad (3.2.34)$$

and nonderivative variables as:

$$v = \frac{v_1 + v_2}{2} \quad , \quad L = \frac{L_1 + L_2}{2}$$

$$i = \frac{i_1 + i_2}{2} \quad , \quad \tau = \frac{\tau_1 + \tau_2}{2} = \tau_{ave} \qquad (3.2.35)$$

where subscript 1 denotes the value of the quantities at the beginning of Δt, t_1; and
subscript 2 denotes the value of the quantities at the end of Δt, t_2.

For a square wave supply V_s, $v_1 = v_2 = V_s$.

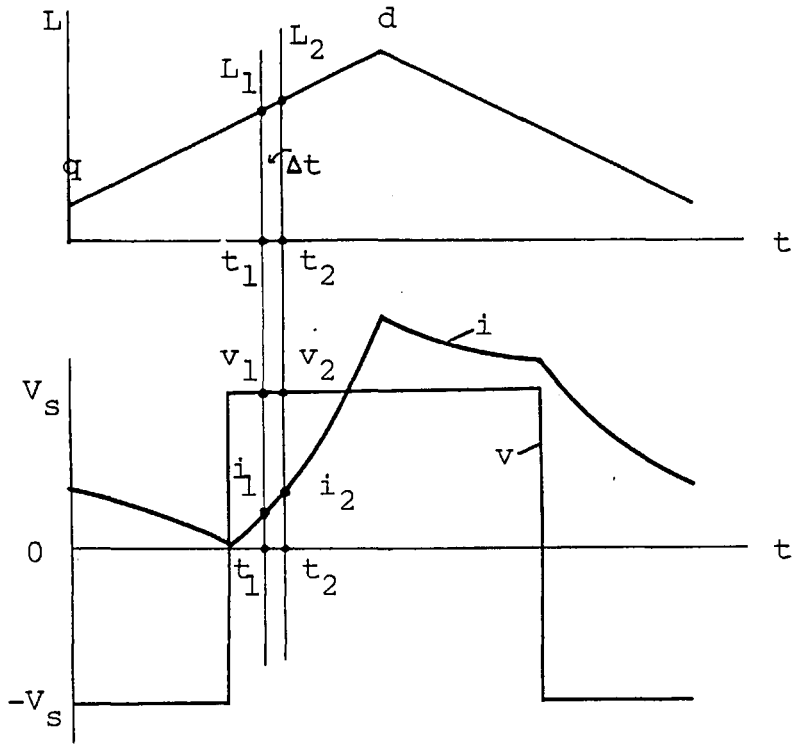

Fig. 3.2.2 Time step approximation for inductance, voltage and current over a small time interval Δt between t_1 and t_2

Substituting equations (3.2.34) and (3.2.35) into equations (3.2.32) and (3.2.33), yields

$$V_s = \frac{(i_1+i_2)}{2} R + \frac{(L_1+L_2)}{2} \frac{(i_2-i_1)}{\Delta t} + \frac{(i_1+i_2)}{2} \frac{(L_2-L_1)}{\Delta t}$$

Expanding and rearranging gives the current i_2 at the end of Δt as:

$$i_2 = \left(2V_s-(R- \frac{2L_1}{\Delta t})i_1 \right)/\left(R+ \frac{2L_2}{\Delta t} \right) \qquad (3.2.36)$$

and from equation (3.2.33), the instantaneous torque is

$$\tau_{ave} = 0.125 \frac{(i_1+i_2)^2}{\omega_r} \frac{(L_2-L_1)}{\Delta t} \qquad (3.2.37)$$

The flow chart of the main program used to perform the calculations is shown in Fig. (3.2.3). The number of time steps used for one cycle of inductance is 100 and proved to be sufficient to give accurate average results. It may be noted that the CPU time for calculating the whole performance curves for a set of parameters is 0.58 CPU seconds (typical).

Although the flow chart shows the program for the half bridge inverter circuit where the positive supply voltage is equal to negative pull-down voltage, it needs only slight modification in order for predictions to be made for the single transistor circuit or the bifilar-wound pull-down circuit (in which the pull-down reverse voltage is generally not equal to the supply voltage). In the case of the bifilar wound circuit, the bifilar

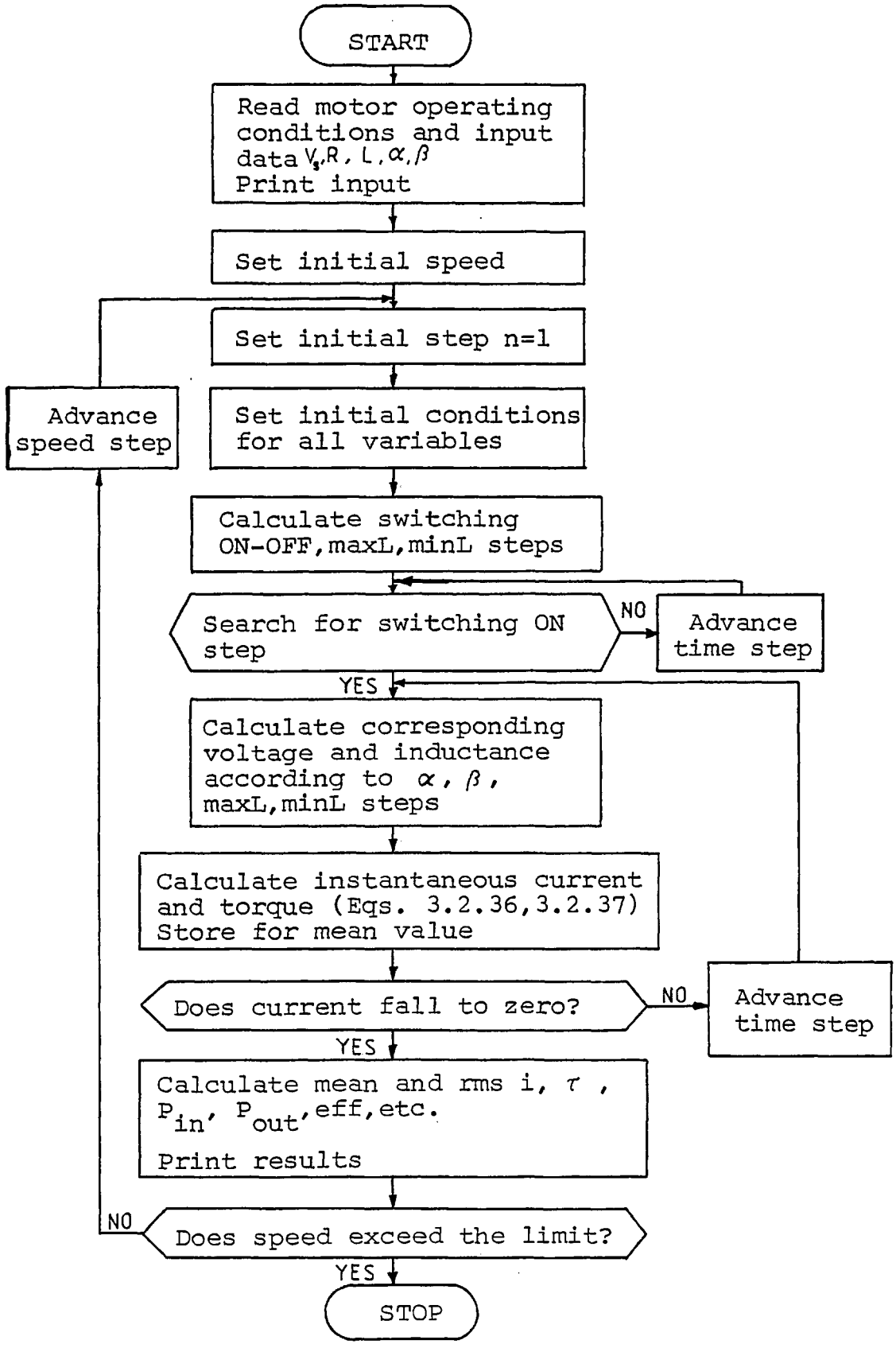

Fig. 3.2.3 Flow chart of the computer program for d.c. operation of SPSR motor

coil can usually be wound with thinner wire to save winding space and because the pull-down r.m.s. current is normally considerably less than main r.m.s. current. The resistance of the bifilar coil is then higher than the main coil and this results in the freewheel current being pulled down somewhat quicker. The effect can easily be taken into account by the program with appropriate resistance values used for switch on and switch off periods.

An important advantage of the step by step method over the simplified analytic method is relevant when the current waveform does not reduce to zero even at the end of the cycle. This continuous current mode of operation (which is not always completely undesirable) can occur if the switch-on period is relatively long or the reverse pull-down voltage is too low. The current waveform can take many cycles to settle to a repetitive pattern and Fig.3.2.4 shows a typical case with a two-pole SPSR motor. The peak current increases from 0.2 A in the first cycle to 1 A in the 19th. cycle and to 1.2 A in the 61st. cycle. For such a case it is possible, when steady state information is required, to allow the computation to proceed until the difference between two consecutive cycles is negligibly small. (e.g. Here, the difference between the currents at the beginning of 61st. and 62nd. cycle is 0.00025 A)

Other quantities calculated for performance predictions were:

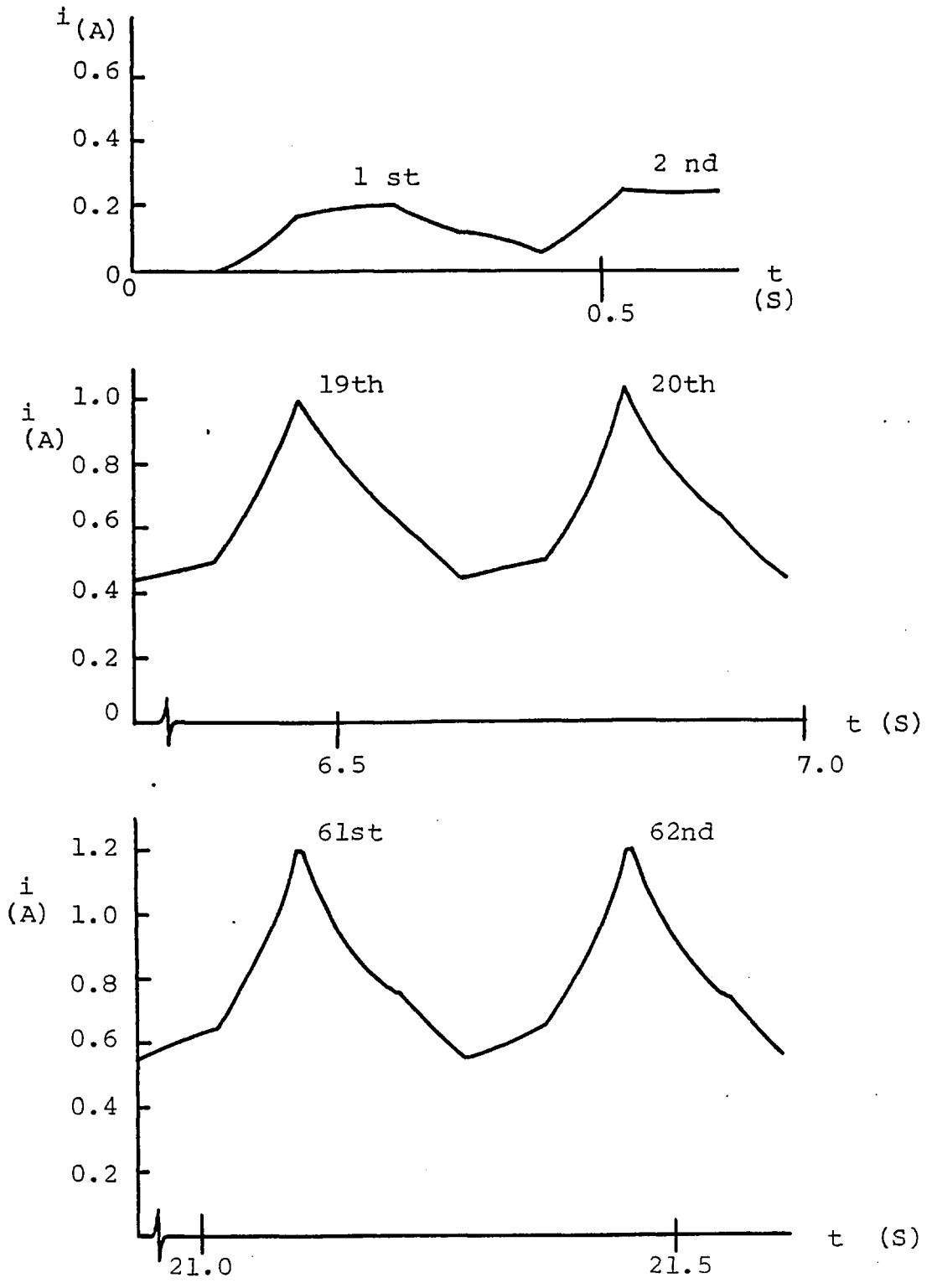

Fig. 3.2.4 Continuous current waveform of a typical 2 pole SPSR motor (at 8600 rev/min $\alpha = 90^{\circ}$ $\beta = 60^{\circ}$) at 1st, 2nd, 19th, 20th, 61st and 62nd cycle respectively

Power input = Average of $(v_n i_n)$ for two cycles

Power output = Average torque(N-m)xSpeed(rad/sec)

I^2R loss = Average of $(i^2)R$

Power loss = Power input - Power output

Efficiency = $\frac{\text{Power output}}{\text{Power input}}$ x 100 %

The computer listing of the program is given in Appendix B3.

Fig. 3.2.5 compares the current waveform obtained from the simplified analytic method and the step by step method for a typical two pole SPSR motor. The machine data used in the calculations is: R= 34.2 Ω, L_{max} = 1.98 H, L_{min} = o.84 H, α,β = 90°elec. The supply voltage is 165 V and the feed circuit is the single coil half bridge inverter type. The rotor speed is set at 2500 rev/min. The current waveforms are not continuous and the peak current obtained from simplified analytic method is higher than obtained from step by step method due to the absence of the winding resistance. Comparisons between the numerical values of calculated mean torques and mean and r.m.s. currents also show higher values from the simplified analytic method, the percentage differences based on the step by step method being 21.3% for mean torque, 15.8% for mean current and 10.9% for r.m.s. current. The calculated value of $j^2_{\tau rms}$ was compared with $2(j_{Tmean}-j_{Dmean})$ and found to be equal (both values are 0.177) to the third decimal point as proved in eq.(3.2.29).

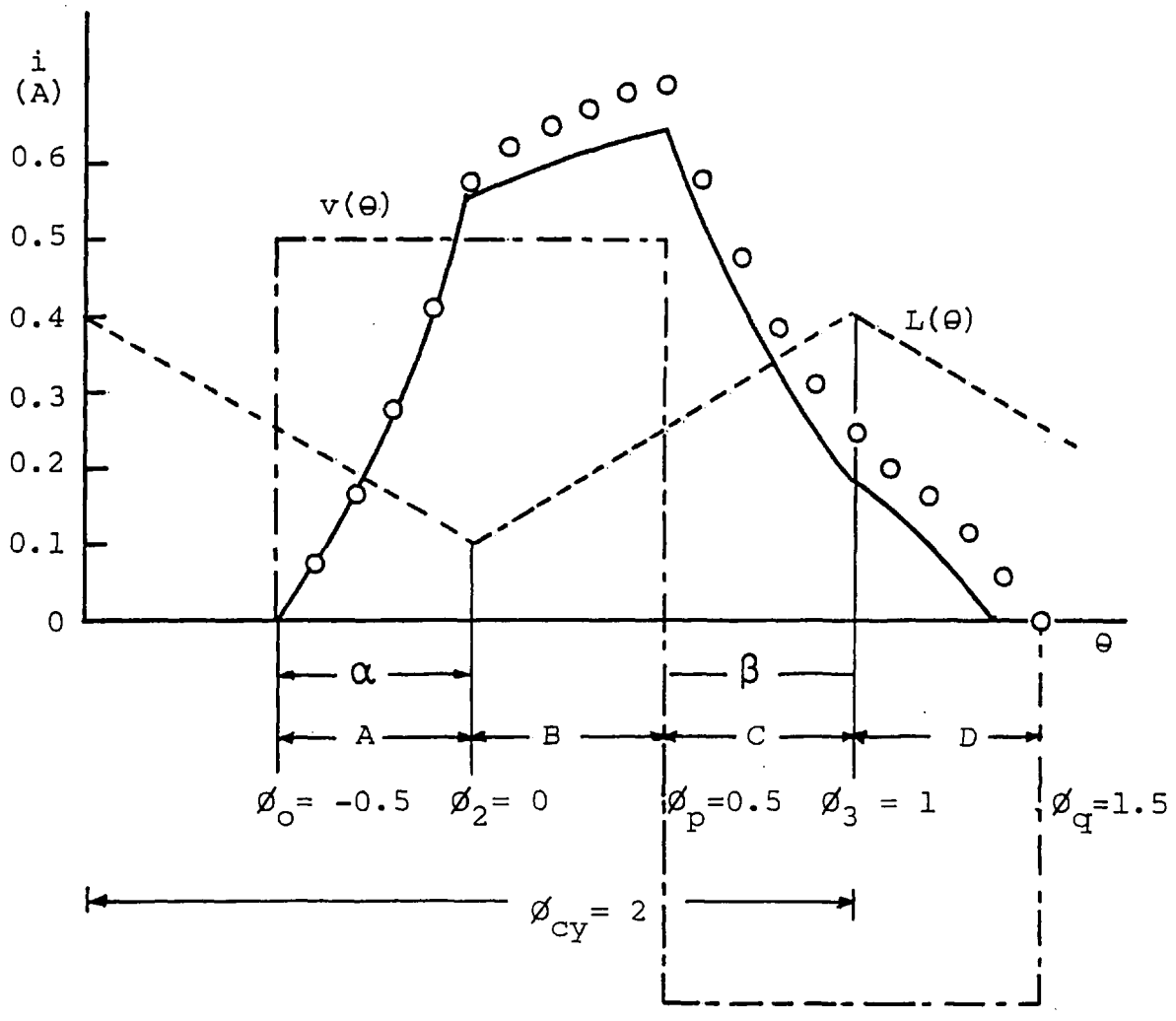

Results	τ_{mean} N-m	i_{mean} A	i_{rms} A	i_{rms}/i_{mean}
Step by step	0.0399	0.322	0.393	1.22
Analytic	0.0484	0.373	0.436	1.17
Error %	21.3	15.8	10.9	4.1

Analytic method $j^2_{\tau rms} = 0.177$

$2(j_{Tmean} - j_{Dmean}) = 0.177$

Fig. 3.2.5 Comparison of the current waveforms obtained Step by step method (———) and from Simplified analytic method (o)

Input data are: V = 165 V, R_a = 34.2 Ω, L_d = 1.98 H, L_q = 0.84 H, α = 90°, β = 90°, speed 2500 rev/min

This confirms the derivation of the current integral expressions in equations (3.2.30)and (3.2.31).

3.3 Steady-state analysis for 'a.c.' operation of the SPSR motor

Consideration of the analysis for steady-state, 'a.c.' operation of the SPSR motor will be limited to operation with the triac feed circuit (Fig. 3.3.1). This circuit option is seen as the best within the 'a.c.' feed category as discussed in section 2.4.1. The equivalent circuit of the motor is the same as before, the effects of iron losses and saturation again being neglected. Only the step by step method is used because of the difficulty in representing the voltage supply function and delay phase angle within the simplified analytic method.

The current i_2 at the end of a short time step Δt can be defined as before (eq. 3.2.36) as

$$i_2 = (2v-(R-2L_1/\Delta t)i_1)/(R+2L_2/\Delta t) \qquad (3.3.1)$$

where v is now the supply voltage function and the average torque during a step is

$$\tau_{ave} = 0.125(i_1+i_2)^2(L_2-L_1)/\ \omega_r \Delta t \qquad (3.3.2)$$

which is the same as in eq(3.2.37). Other variables and subscripts are the same as described in section 3.2.2.

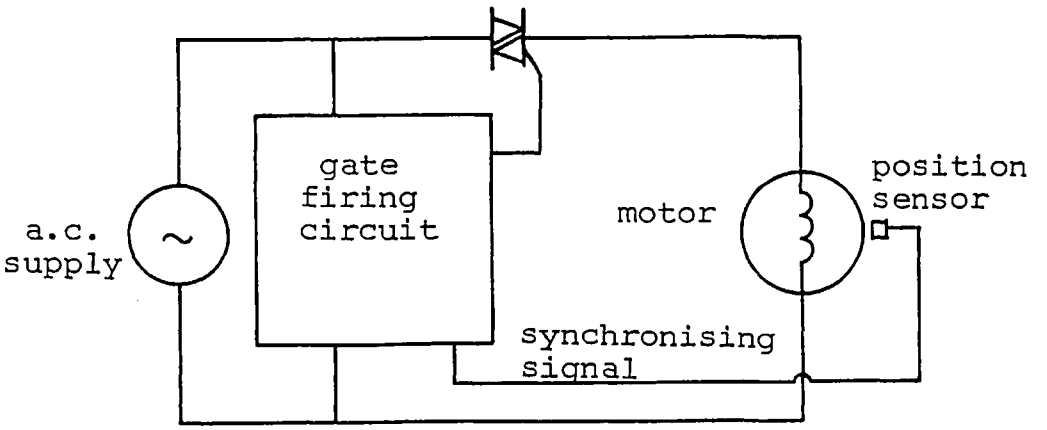

Fig. 3.3.1 Simplified a.c. triac-fed circuit

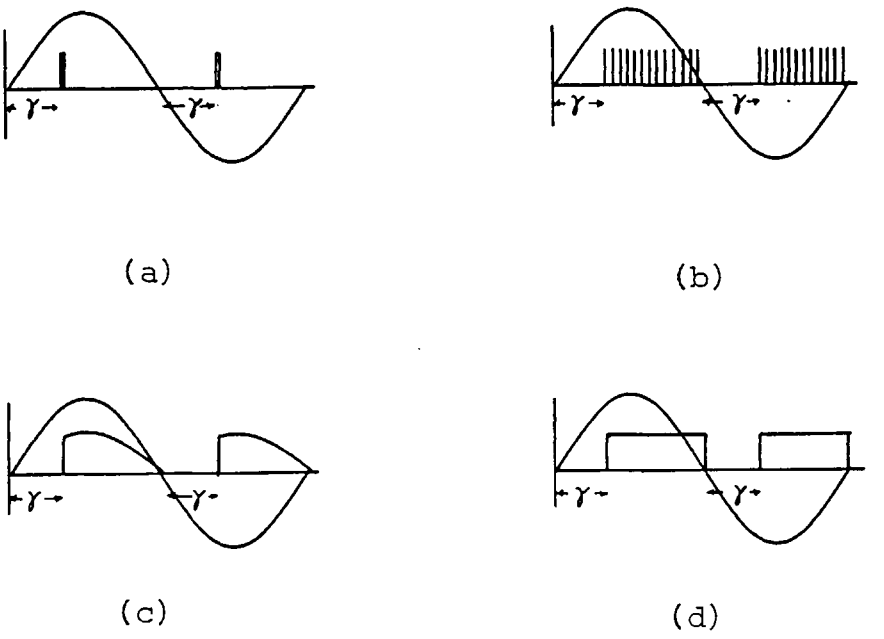

Fig. 3.3.2 The firing signal of a triac can be (a) a short pulse or (b) a train of short pulses. A part of sinusoidal pulse (c) is better and a half-cycle square pulse (d) is better still.

As shown in Fig. 3.3.1, the current and torque with the 'a.c.' triac-fed circuit are controlled by the combination of two signals: the synchronising signal from the position sensor and the gate firing signal from the gate triggering circuit. The exact form of the gate firing signal can influence the motor's operation and this thus therefore be considered. The gate firing signal normally takes one of the forms shown in Fig. 3.3.2 in which the delay angle γ can be varied for power control.[3.7] The simplest firing signal (3.3.2(a)) provides two pulses per cycle of the supply. The pulse must have a dura-tion longer than the switch on time of the triac. This type of circuit functions satisfactorily on controlled d.c. or a.c. resistive loads, but difficulties can arise with inductive loads and loads containing back e.m.f.s such as batteries, capacitors or motors. A train of pulses (control being exercised by phase variation of the leading edge of the pulse train as shown in Fig. 3.3.2(b)) is sometimes used to improve switching operation but if the inductance of the circuit is high it can prevent the triac from reaching the holding current within the first (or first few) pulses and a false trigger can occur. To overcome these difficulties half sine-wave (3.3.2(c)) or half-cycle cycle square-wave (3.3.2(d)) gate signals with variable-phase leading edges are used. The square-wave signal is prefer-able, since if the sine wave is to give sufficient gate firing current at near maximum or minimum firing angles, excessive gate power dissipation can occur.

In this analysis a gate signal of the single pulse per half cycle type is used (Fig. 3.3.2(a))to simplify the simulation of the switching action but modification in the simulation program will be indicated to cater for a d.c. gate signal of Fig. 3.3.2(d) type.

Modulated gate signals of both the single pulse and the d.c. types are shown in Fig. 3.3.3. The firing signal is essentially derived from the supply voltage waveform, the phase-delay angle being related to the zero crossing point of the supply voltage. The signal is then modulated by the synchronising signal from the position sensor; only the mains-derived firing signals falling within the 'on' periods of the synchronising signal appear at the gate and fire the triac. (Fig. 3.3.4 corresponds to a motor speed which is relatively high, 180° (elec) of rotor rotation occurring every $1\frac{1}{4}$ mains cycles)

According to the system shown in Fig. 3.3.1, the sinusoidal voltage supply can be expressed as

$$v = V_s \sin(\omega t+\theta) \qquad (3.3.3)$$

where V_s is the peak value of the voltage supply ($\sqrt{2}$ of Vr.m.s.) and

$\omega = 2\pi f$ where f is the supply frequency (Hz).

Designation of phase relationships is a critical matter. The $t = 0$ instant is set to coincide with the d position of the rotor. The electrical angles α and β are

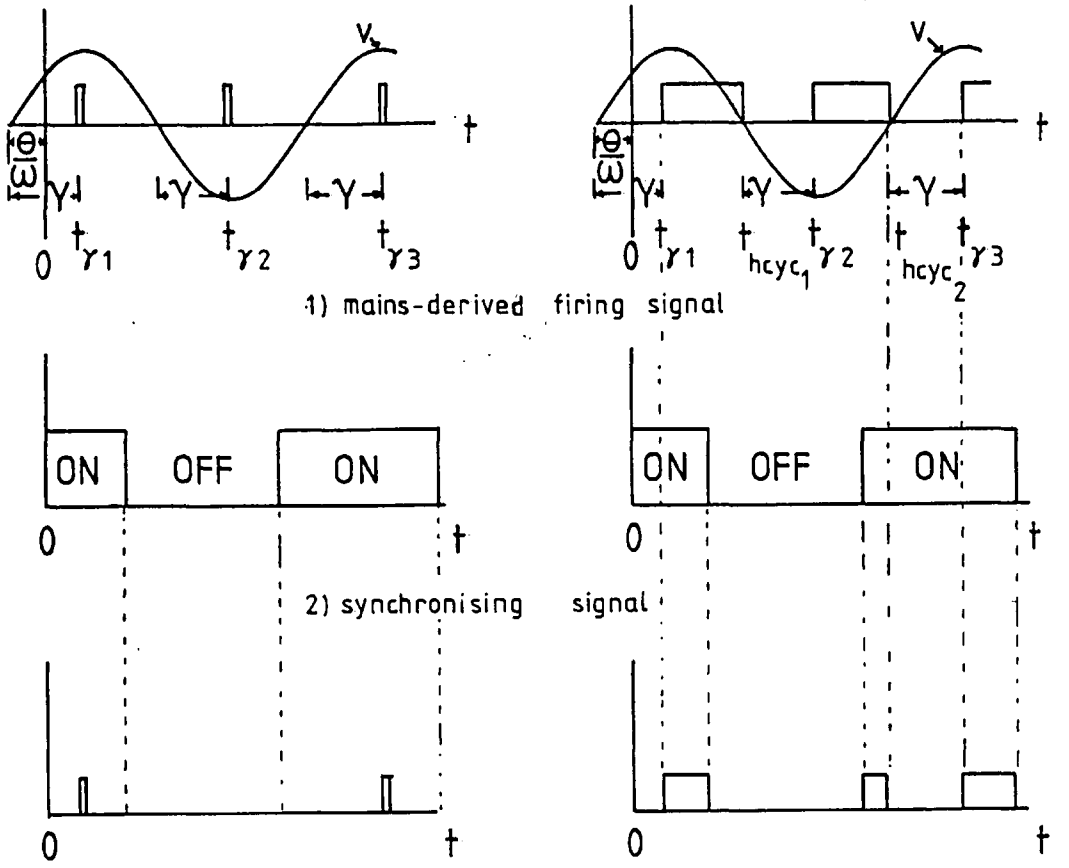

(a) single-pulse signal

(b) d.c. triggering signal

Fig. 3.3.3 Modulation of firing signal and synchronising signal in the a.c. triac-fed circuit

related to the d and the q rotor positions respectively (e.g. α is rotor advance angle with respect to the q position at which the supply is switched on). θ is the angle between the $t = 0$ instant and the instant at which the supply voltage positive-going zero crossing occurs. The zero crossing instant can then be related to α and β as required. The relations between the inductance profile, the voltage supply function and switching angles are shown in Fig. 3.3.4.

In order to simulate the modulation of the phase delay signal by the synchronising signal the following steps have to be defined:

a) Phase-delay signal. In the case of the single-pulse gate signal (Fig. 3.3.3(a)) the time t_γ for the phase-delay signal (which is related to the zero crossing point of the voltage supply) is expressed in terms of the delay angle γ and the voltage phase angle θ as follows

i) for $\gamma < \theta$ and $\theta < \pi$

$$t_{\gamma_1} = \frac{\pi - \theta + \gamma}{\omega}$$

ii) for $\gamma > \theta$ and $\theta < \pi$

$$t_{\gamma_1} = \frac{\gamma - \theta}{\omega}$$

where γ is the delay angle referred to the positive going zero crossing point of the voltage supply in radians and ω is the angular frequency in rad/sec ($\omega = 100\pi$ for 50Hz)

For both cases (i) and ii)) , the times for the subsequent phase delay signals are

$$t_{\gamma_n} = t_{\gamma(n-1)} + \frac{\pi}{\omega} \qquad n=2,3,..m.$$

For the d.c. triggering signal the phase delay signal is defined by the times for the leading and trailing edges. The time for the leading edge can be calculated in the same way as for single pulse triggering. The time for the trailing edge, as shown in Fig. 3.3.3(b), is the end of each half cycle (which is related to θ). The time for the first half cycle $t_{hcyc}(1)$ is then:

$$t_{hcyc}(1) = \frac{\pi - \theta}{\omega}$$

and the subsequent half cycle times are

$$t_{hcyc}(n) = t_{hcyc}(n-1) + \frac{\pi}{\omega} \qquad n=2,3,..m$$

b) Synchronising signal. The advance switching 'on' time t_{α}' and advance switching 'off' time t_{β}' are related to the advance angles α and β respectively as shown in Fig. 3.3.4. If the d position is taken as reference the first switch on time t_{α_1} and switching off time t_{β_1} can be defined as

$$t_{\alpha_1} = \frac{t_p}{2}\left(1 - \frac{\alpha}{\theta_p/2}\right)$$

and

$$t_{\beta_1} = \frac{t_p}{2}\left(2 - \frac{\beta}{\theta_p/2}\right)$$

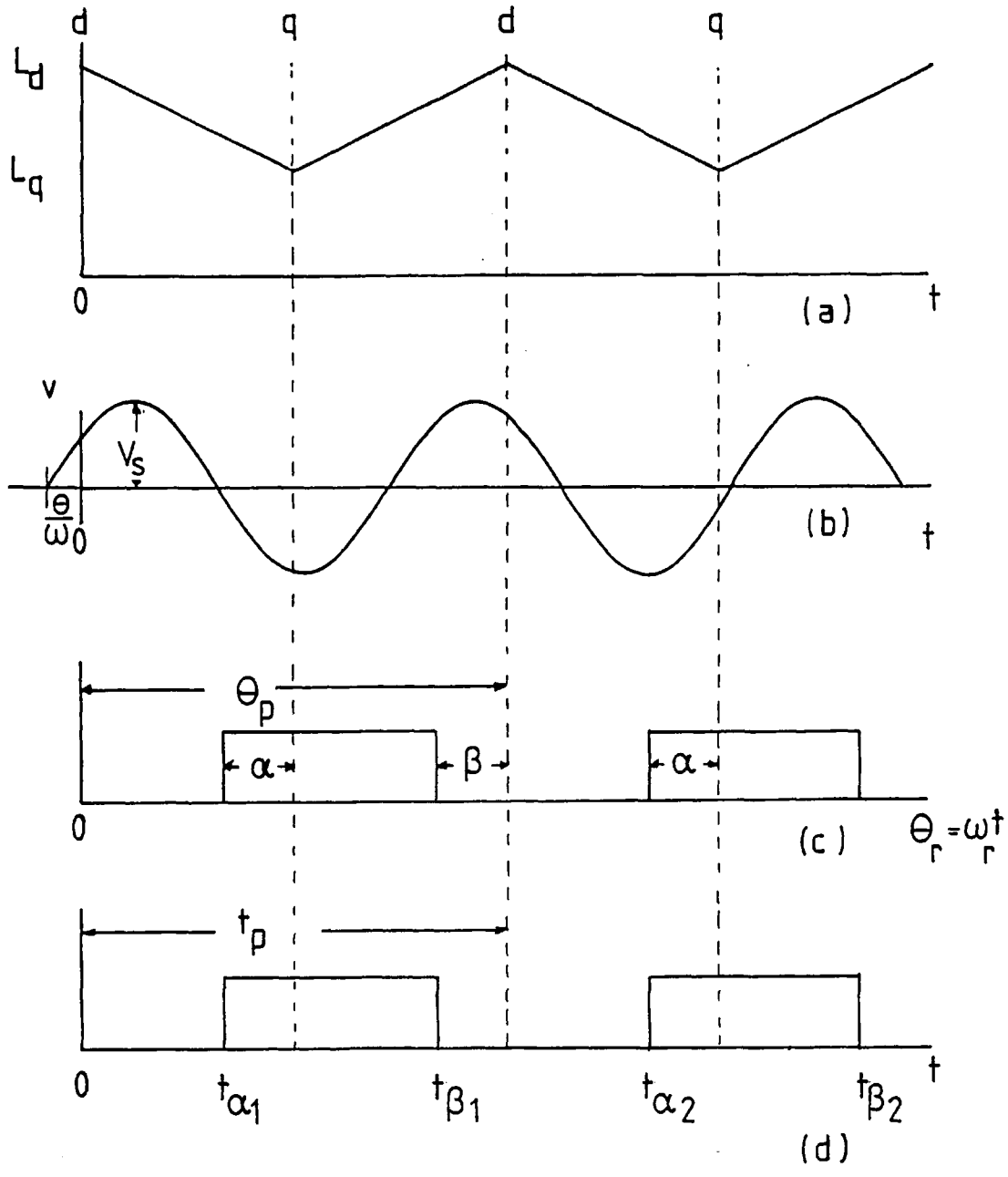

Fig. 3.3.4 Relations between rotor position, inductance variation, supply voltage and switching angles
(a) Variation of inductance with time
(b) Supply voltage
(c) Synchronising signal (space)
(d) Synchronising signal (time)

where t_p is the time required for the rotor to move move from one maximum alignment position to the next maximum alignment position.

θ_p is the angle between two maximum alignment positions.

α , β and θ_p are all in electrical degrees.

The subsequent 'on' and 'off' times are:

$$t_{\alpha n} = t_{\alpha(n-1)} + t_p \qquad n=2,3,..m$$

$$t_{\beta n} = t_{\beta(n-1)} + t_p$$

A computed current and torque waveforms for the a.c. triac-fed operation of a SPSR motor with single pulse triggering signal is shown in Fig. 3.3.5 for a set of typical operating condition and machine parameters. The bidirectional nature of the triac allows both positive and negative current pulses to flow depending on the mains polarity at turn-on, only a single half cycle of current per current-pulse occurs, the reverse mains polarity pulling down the current to zero during the following mains voltage half cycle. The magnitude of torque pulses is proportional to the square of the magnitude of the corresponding current pulses and the polarity depends only on the polarity of the slope of the inductance. The series of torque and current pulses can be seen to repeat over an interval of time depending on the supply frequency and the synchronising signal frequency (which is of course

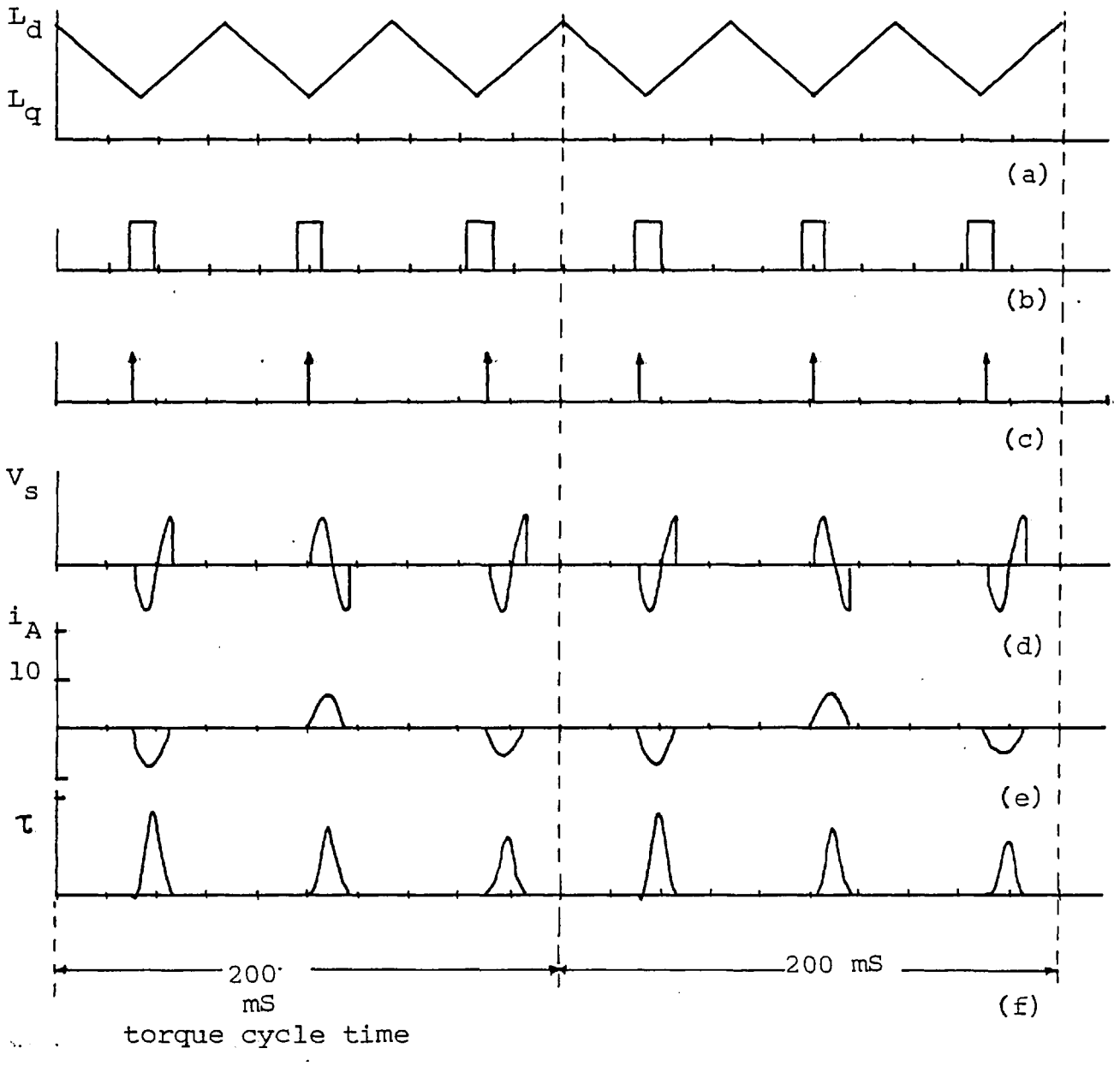

Fig. 3.3.5 Calculated waveform for a.c. operation of the SPSR motor with single-pulse firing circuit (6-saliency motor, 240 V a.c., R = 5.18 Ω L_d = 450 mH, L_q = 177 mH, α = 24°, β = 150° 150 rev/min)

(a) Inductance
(b) Synchronising signal
(c) Triggering signal
(d) Voltage supply
(e) Current
(f) Torque

related to the rotor speed). The periodic time of this repeating sequence of torque bursts will be called the 'torque cycle time' T_t and can be calculated from

$$T_t = \text{LCM} (T_e, T_m) \quad \text{mS}$$

i.e. the period of T_t is the lowest common multiple of the periods T_e and T_m where:

T_e is the period of the supply frequency equal to $\frac{1000}{f}$ in mS (f is the supply frequency in Hz);

T_m is the numerator of the smallest ratio of $\frac{60000}{p \cdot rpm}$ in mS , where p is the number of rotor saliencies (the higher of the two saliency numbers for stator and rotor if unequal on the two parts of the motor) and rpm is the rotor speed in rev/min.

(Note that only k:1 or 1:k (k is an integral number) rotor to stator saliency ratios are normally practicable with single phase SRMs. Vernier type k:m ratios require multiphase excitation)

For example, Fig. 3.3.5 corresponds to a six saliency motor operating with 50 Hz a.c. mains supply, with a rotor speed of 150 rev/min.

$$T_e = \frac{1000}{f} = \frac{1000}{50} = 20 \text{ mS}$$

The smallest ratio of $\frac{60000}{p.rpm} = \frac{60000}{6x150} = \frac{200}{3}$

Hence T_m which is the numerator of the smallest ratio of $\frac{60000}{p.rpm}$ = is 200 mS, and

$$T_t = \text{LCM}\ (\ 20\ ,\ 200\ ) = 200\ \text{mS}$$

i.e. the series of torque and current pulses repeat in every 200 mS as shown.

The flow chart of the computer program is summarised in the Fig. 3.3.6. The triac conduction characteristic is simulating by setting the instantaneous supply voltage v equal to $V_s \sin(\omega t+\theta)$ after the triac is fired until such time as i falls or is reduced to zero. The current i is then set equal to zero until the next firing instant. A time step of 1 mS was found to give sufficient accuracy and to be reasonably economic in computing time. Other quantities such as mean power input, efficiency and mean torque are calculated by standard means. It may be noted that a typical CPU time depends on the length of the torque cycle time, for example 0.675 S and 1.37 S are typical CPU times for the calculation at two speeds which the torque cycle time are 100 mS and 400 mS, respectively.

The mean torque and mean current of the SPSR motor at a given speed when operated with an a.c. triac-fed circuit are found to be not only the switching angles and phase delay angle but also dependent on the voltage

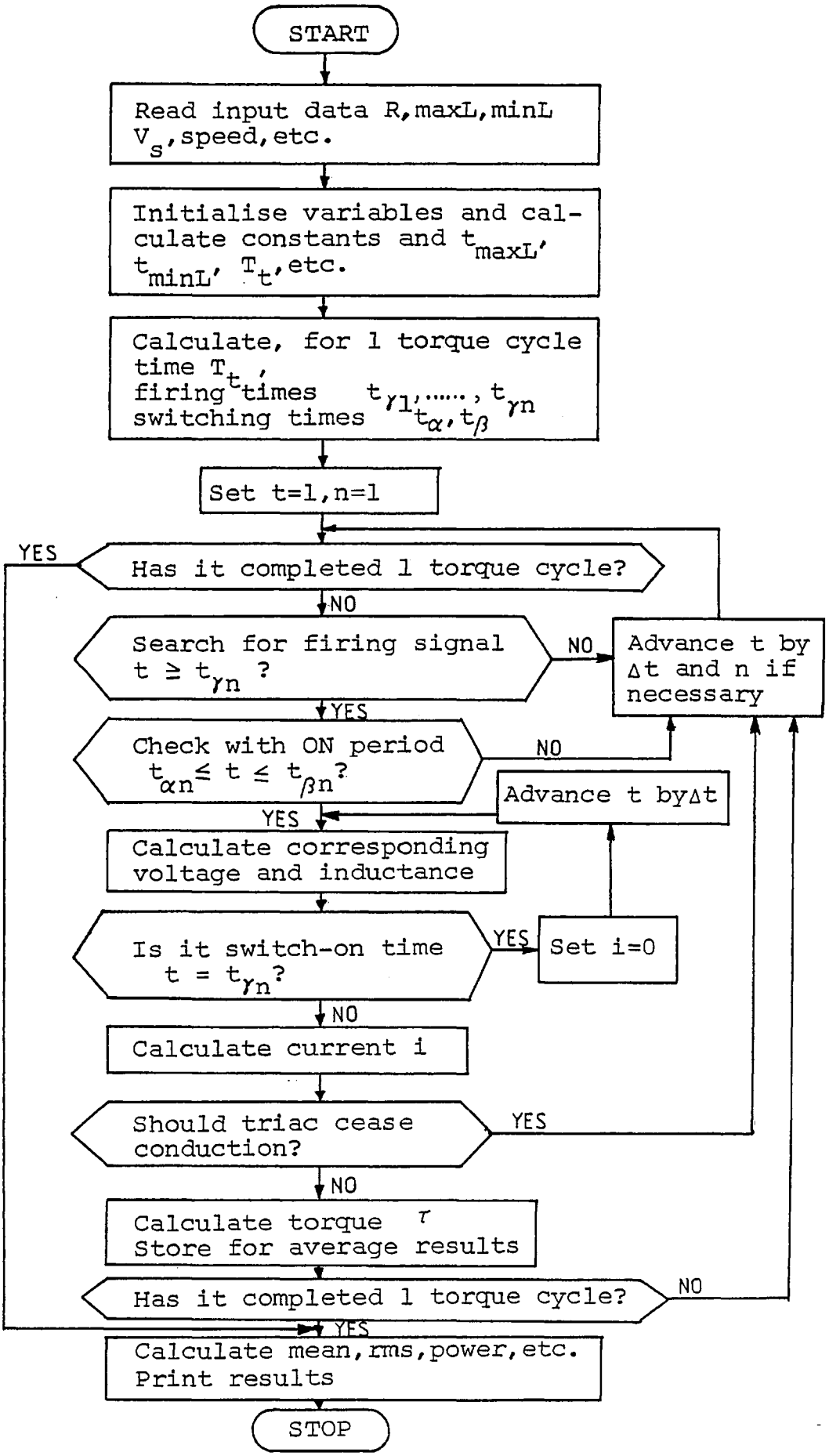

Fig. 3.3.6 Flow chart of the program for a.c. triac operation

phase angle 'θ' at the original switch on time. Fig. 3.3.7 shows the waveforms of current and torque pulses computed from identical operating conditions for two values of 'θ'. It can be seen that for this case where the torque cycle time is short (20 mS) and the current pulses are repeated in every mains cycle, the mean torque for $\theta = 36^{o}$ elec is more than three times bigger than the mean torque for $\theta = 0^{o}$ elec. For speeds where the torque cycle time is long and the current and torque pulses take many mains cycles to repeat, the effect of 'θ' changes on mean values tends to cancel out and changes in mean current and mean torque are virtually absent.

In summary, the beating effects that occur between the mains and the switching frequency produce a repeating sequence of torque and current pulses. If the sequence repetition time is short, the values of mean torque and current vary considerably according to the exact phase relationship between the first switching instant and the mains supply zero crossing. If the sequence repetition time is long, the effects tend to cancel out. The beating effects also give rise to current and torque sub-harmonics in addition to current ('super') harmonics that occur with any mains-fed, triac or thyristor-controlled load.

The a.c.triac operation program listing is given in Appendix B4.

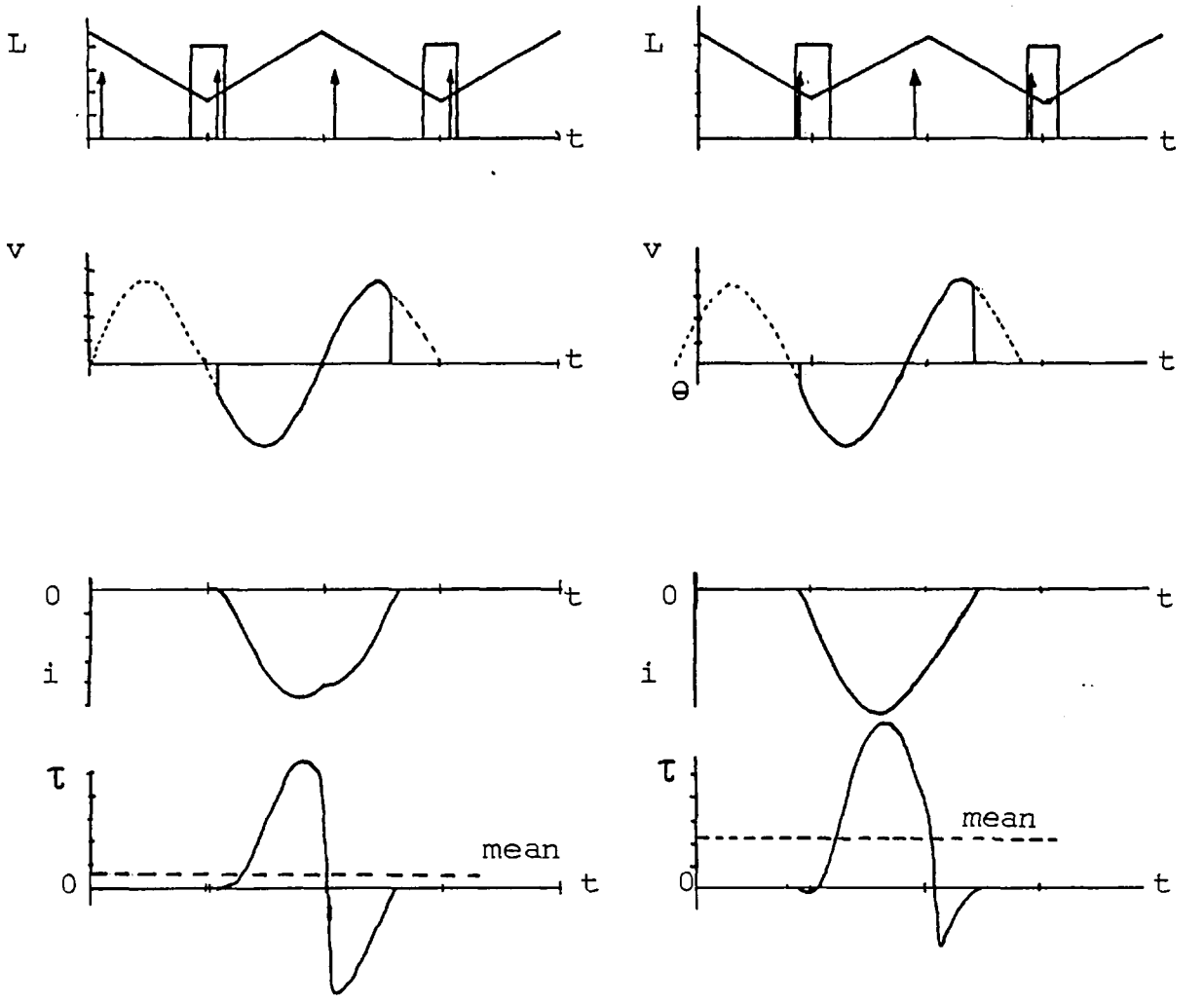

(a) $\theta = 0^{o}$
mean torque 0.62 N-m

(b) $\theta = 36^{o}$
mean torque 2.114 N-m

Fig. 3.3.7 Comparisons of the current and torque waveforms of a particular SPSR motor at the same speed, supply volts, phase-delay angle, switching angles but with different voltage phase angle 'θ'

3.4 Discussion of phenomena adversely affecting the accuracy of the analysis and predictions

The most important phenomena can be listed as follows:

1) Fringing flux: This will cause the variation of inductance to deviate from the triangular waveshape assumed to one having more rounded changes at the d and q positions. The slopes near to the d and q positions will hence be somewhat less than the one assumed. The inductance characteristic may even possess a flat top and bottom. These deviations can lead to errors in the waveform prediction of current and torque though for given L_d and L_q, mean torque may not be too much affected.

2) A comprehensive discussion about the effects of saturation on motor performance is beyond the scope of this thesis, though the matter has been dealt with briefly in chapters 1 and 2. Saturation obviously decreases the available airgap flux particularly when the rotor is at or near the d position and the maximum inductance at the d position is correspondingly reduced. Heavy local saturation can occur at the pole tips when the rotor and stator poles are partially overlapped and can result in local hot spots. How this affects the torque is strongly dependent on the location of the saturated material and

how the location and degree of saturation change with rotor position.

Perhaps the key factor to consider is the effect on the feed circuit. A lower maximum inductance due to saturation lowers the impedance seen by the voltage source and this can lead to an unexpectedly high peak current. This peak current normally occurs just at the instance of switching off where the rotor is close to the d position. Damage of switching devices can occur unless generously rated devices are used. As stated previously this may be uneconomic.

The effects of fringing flux and saturation can be taken into account in the same way as in the stepping motor as summarised in Ref. 3.8 and Ref. 3.3 contains a method for calculating the torque and current of a variable-reluctance stepping motor from measured or computed nonlinear magnetisation data.

3) Small errors in current and torque predictions may arise from changes in winding resistance during operation due to temperature changes and skin effect. The former effect can be of first order significance (40% change with 100°C rise) particularly when comprehensive monitoring of temperature changes during tests (not always easy) is not done. Significant skin effect phenomena may occur when the motor is operating at high speeds and the

winding wire diameter is appreciate (as might be the case for instance when a low voltage supply is used). Fundamental frequencies as high as 700 Hz were used during tests and maximum rates of change of current, given the non-sinusoidal nature of the winding current, would hence have corresponded to frequencies several times this. Calculation of skin depth and increase in resistance are shown in Ref. 3.9, but skin depth effects were neglected in the predictions made in the present work since wire sizes on the experimental motors were small.

4) The series R-L equivalent circuit used in the analysis means that only copper loss is considered in determining the calculated efficiencies. In practice there are other major losses, viz: friction & windage losses and iron losses.

The friction and windage losses can be said to include all those factors which produce a mechanical drag on the machine, such as bearing friction and air resistance. The combined effects can be experimentally determined for a particular machine from the Retardation or Running-down test.[3.10] Prediction of friction and windage losses is difficult, especially when wide speed range is involved.

Iron losses are normally regarded as comprising hysteresis loss due to the cycling of the material through

its hysteresis loop, and eddy current loss resulting from the induced currents circulating within the material. Standard semi-empirical formulae can be found in most a.c. machines textbooks and iron data sheets, but the relationships apply only when excitation conditions are sinusoidal. This is far from being the case in SRMs. However two brief attempts were made in the present project to estimate iron losses.

In the first, flux density waveforms are predicted from the predicted current waveform, inductance variation, leakage factors and cross-sectional areas of the various parts of the magnetic circuit. The iron losses in each part of the magnetic circuit at each frequency is then found using the standard semi-empirical formulae, and the total iron loss for a particular operating condition found by summation. The process is repeated for other operating conditions as required.

The second proposed method was partly inspired by the approach outlined in Ref. 3.11 which develops the idea of a modified equivalent circuit for d.c. machines and partly by the method of including iron losses in the standard equivalent circuit of 3 phase induction motors. The modified equivalent circuit of a SPSRM will be of the form shown in Fig. 3.4.1, where R represents the winding resistance, L the total winding inductance and R_c a shunting resistor in which the iron loss is thought of as taking place. This concept can perhaps be adopted for the SRM (as it is for induction motors) with the iron loss resistor

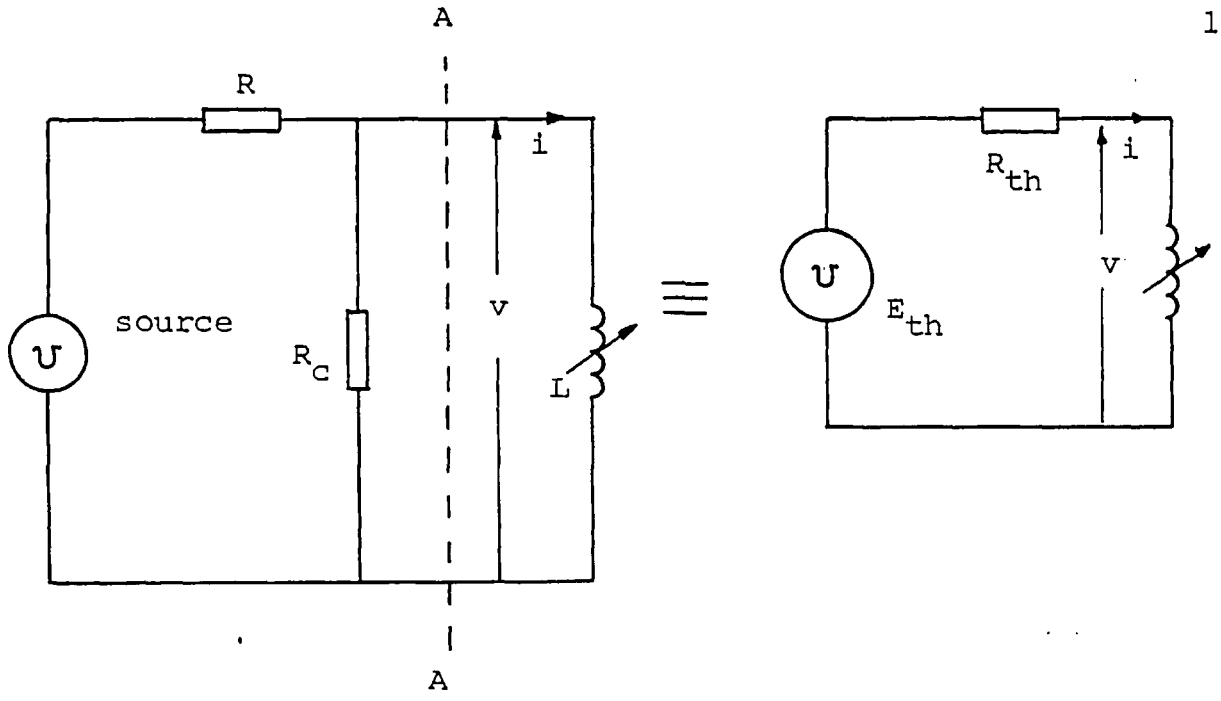

Fig. 4.3.1 Proposed equivalent circuit taking into account the iron losses

being placed across the motor's total inductance L. Some justification can be made as follows:

The voltage across R_c is

$$v = \frac{d}{dt}(Li)$$

so the power loss in R_c (P_{Rc}) can be written as

$$P_{Rc} = \frac{v^2}{R_c} = \frac{1}{R_c}\left(\frac{d}{dt}(Li)\right)^2 \qquad (3.4.1)$$

but the total flux 'ϕ_t' is

$$\phi_t = \frac{Li}{N}$$

where N is the number of turns of the winding, and hence $\frac{d(\phi_t)}{dt}$ is

$$\frac{d(\phi_t)}{dt} = \frac{1}{N}\frac{d(Li)}{dt}$$

and

$$\left(\frac{d(\phi_t)}{dt}\right)^2 = \frac{1}{N^2}\left(\frac{d(Li)}{dt}\right)^2 \quad (3.4.2)$$

Now the iron loss P_i to a first approximation varies as $\left(\frac{d(\phi_t)}{dt}\right)^2$. Hence from equations (3.4.1) and (3.4.2)

$$P_{Rc} \propto P_i$$

Although the equivalent circuit of this form results in somewhat more complexity (Thevenin source approach to the circuit on the left of A-A of Fig. 3.4.1, or simultaneous first order differential equations) the time stepping method can still be used.

Unfortunately lack of time and the need to investigate other, perhaps more important aspects of SPSRM behaviour, did not permit the validity of either method to be investigated. It did not seem sensible to include the calculation procedure of the first method or the more complex equivalent circuit of the second in the main prediction method, prior to validation, and no predictions of iron losses were therefore made.

3.5 Concluding remarks

Methods of predicting the current and torque waveforms for both 'd.c.' operation and 'a.c.' triac operation of the SPSR motor have been developed.

The simplified equivalent circuit based on a linear model of the SPSR motor was used throughout. For 'd.c.' operation, the simplified analytic method provides a short and easy way of predicting approximate current and output torque waveforms. These are useful in determining design trends for both motor and supply unit. The step by step method requires a computer but yields more accurate solutions especially for small machines with their relatively high R/L values. For 'a.c.' triac operation, the repetition pattern of current and torque pulses and mean current and torque levels were found to be dependent on the exact phase relationship between a reference switching instant and the nearest mains supply positive-going zero crossing. Calculations often need to be made over a number of mains cycles in view of the relatively large torque cycle times that can occur.

The effects of nonlinearity have been discussed and possible improvements to the analysis method have been suggested. The predicted results are compared with test results in the chapters 4 and 5.

CHAPTER 4

PERFORMANCE OF A LOW-SPEED, 6-SALIENCY MOTOR

4.1 Introduction

In the early stages of the project, work was done on a SPSRM that had been the subject of a previous industrially-sponsored feasibility study[4.1]. The principal objective of the study was to investigate the prospects for an improved drive system for ceiling fan units. The traditional type of drive consists of a 'capacitor-run' 'single-phase' induction motor. The motor uses an external rotor configuration, has a high diameter to length ratio and has a fairly high pole-number. A tapped-autotransformer or phase-controlled triac is used for speed control. Efficiency is fairly low and winding cost, due to the rather large number of stator coils, relatively high.

Previous work in 1974-5 in the laboratory on a specially designed and built reluctance rotary actuator for an industrial application possessing a solid iron, axial/radial magnetic circuit and a single circumferential coil excitation system led to the idea that perhaps this type of structure could find application, suitably excited, as a low speed switched reluctance motor. The absence of laminations, squirrel cage and multi-coil winding, would give very low costs, and iron losses would perhaps not be

too high given a reasonably low switching frequency and a reasonably low choice of design peak flux density. The original specified speed :150 rev/min. was low enough to make the risk, as regards iron losses, worth taking, and a motor and feed was 'designed' to meet the outline torque and speed requirements.

Many features of the motor and feed were chosen to bring costs (target total factory price £8) to an absolute minimum : use of a solid iron magnetic circuit (as stated above), use of a configuration that enabled a single, easy to wind, circular coil suffice for excitation, use of a simple, mains-fed triac or thyristor feed circuit, etc. The external rotor layout employed is convenient for ceiling fan drives and follows previous practice. The experimental motor was constructed from a number of machined steel and dural pieces though it was envisaged that, in production, the stator and rotor would each be made from a steel casting with a minimum number of machining (turning) operation being necessary to true up the airgap and bearing surfaces.

Although the motor design and construction had been completed before the start of the present project, together with a certain amount of preliminary testing, work remained to be done under a number of headings and it is with the further progress made that this chapter is concerned. The principal headings are:

a) design, construction and testing of a d.c. link feed system, as an alternative to the previously-investigated mains-fed triac system;

b) investigation of system operation with d.c. link feed and of effect of switching angle variation;

c) further measurements of system operation with triac feed;

d) evolution of prediction methods and correlation of measured and predicted results;

e) assessment, with triac feed, harmonic current levels in the mains.

The details of the motor are shown in Fig. 4.1.1, and the principal dimensions are:

overall diameter	279.4	mm.
overall height	71.5	mm.
airgap length	0.7	mm.
shaft diameter	12.7	mm.
rotor active length	19.05	mm.
pole arc/pole pitch ratio	0.42	
stator saliency width/rotor saliency width	1.13	

The rotor segments were made of 6 mild steel pieces cut from a preformed loop of 127 mm. internal radius and machined down to the size shown in Fig. 4.1.2. The rotor segments were fixed between a dural star wheel and a dural ring. The stator pole pieces were also made of mild steel with the slot of 19mm. wide for accommodating

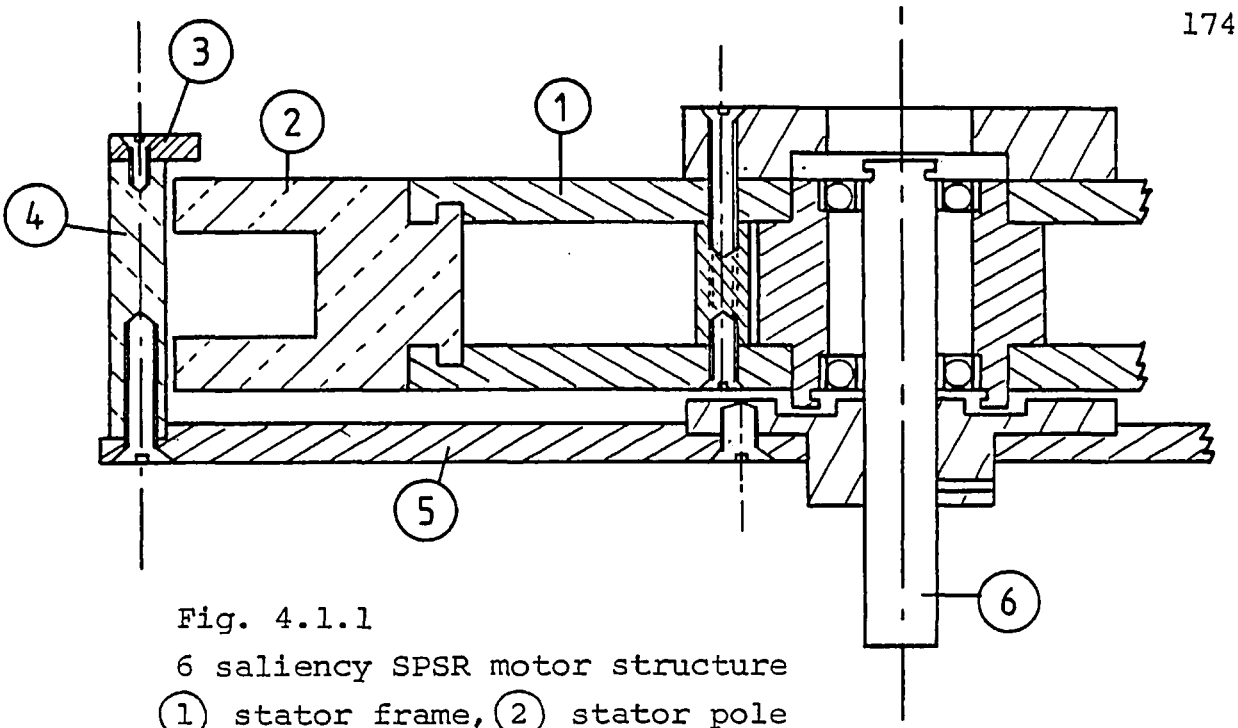

Fig. 4.1.1
6 saliency SPSR motor structure
(1) stator frame, (2) stator pole piece, (3) rotor holding ring, (4) rotor pole piece, (5) rotor star wheel and (6) shaft

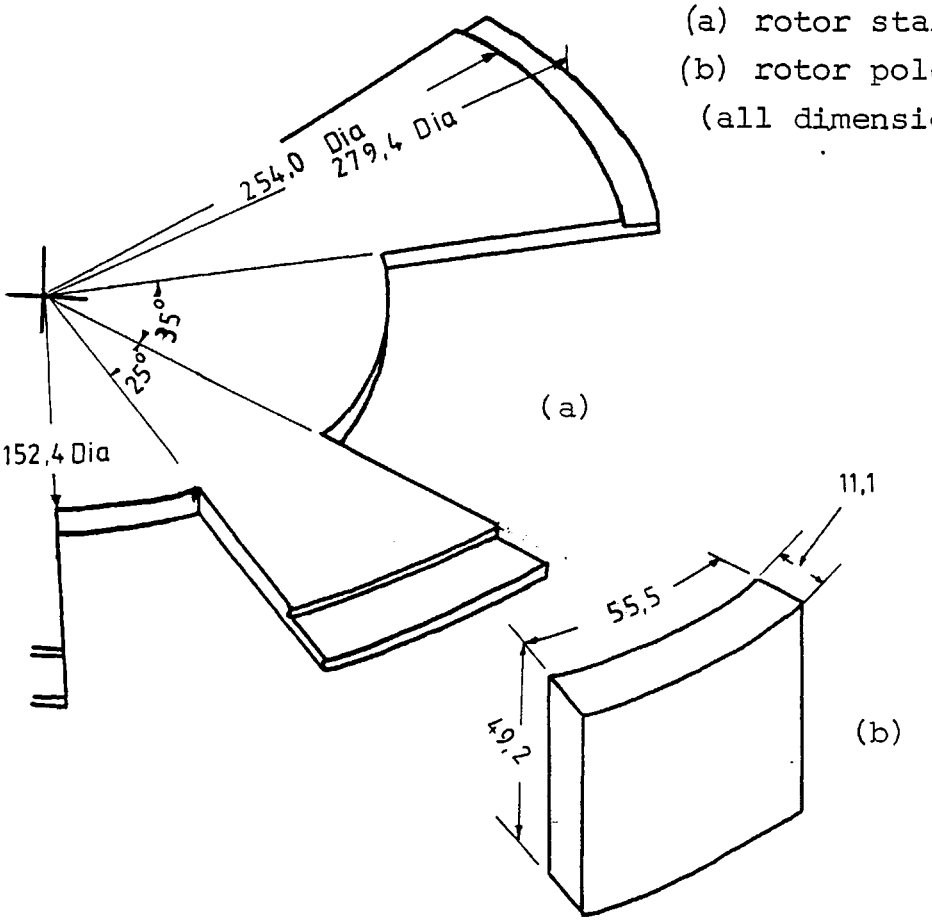

Fig. 4.1.2
(a) rotor star wheel
(b) rotor pole piece
(all dimensions are in mm.)

the excitation coil as shown in Fig. 4.1.3. The stator pole pieces were slitted to reduce eddy current losses.

A 1:1 ratio of stator to rotor saliency number was chosen to minimise switching frequency (discontinuous torque not mattering in this application) and the saliency number of six was a compromise between the need for low switching frequency and for high torque.

The excitation coil comprises 2 similar, co-axial coils. Each had 170 turns of grade M of 0.71 mm. diameter enamelled copper wire with 2 strands in parallel. The two coils were connected in series to give a total of 340 turns. The total coil weight of the prototype is 1.52 kg.

Fig. 4.1.4 shows the test rig. The motor was mounted on the support beam, a pulley was fixed on to the shaft and two spring balances and a cord were wrapped round the pulley for torque measurements.

Two methods of mounting the position sensor are shown in Fig 4.1.5 (a) and (b) . Fig 4.1.5 (a) shows the hall-effect device used for position sensing. The ferrite-magnet, steel pole piece and hall crystal are bonded and fixed on the motor support beam. The rotor position is sensed by means of small, steel projections on the rotor ring. These modulate the device's output

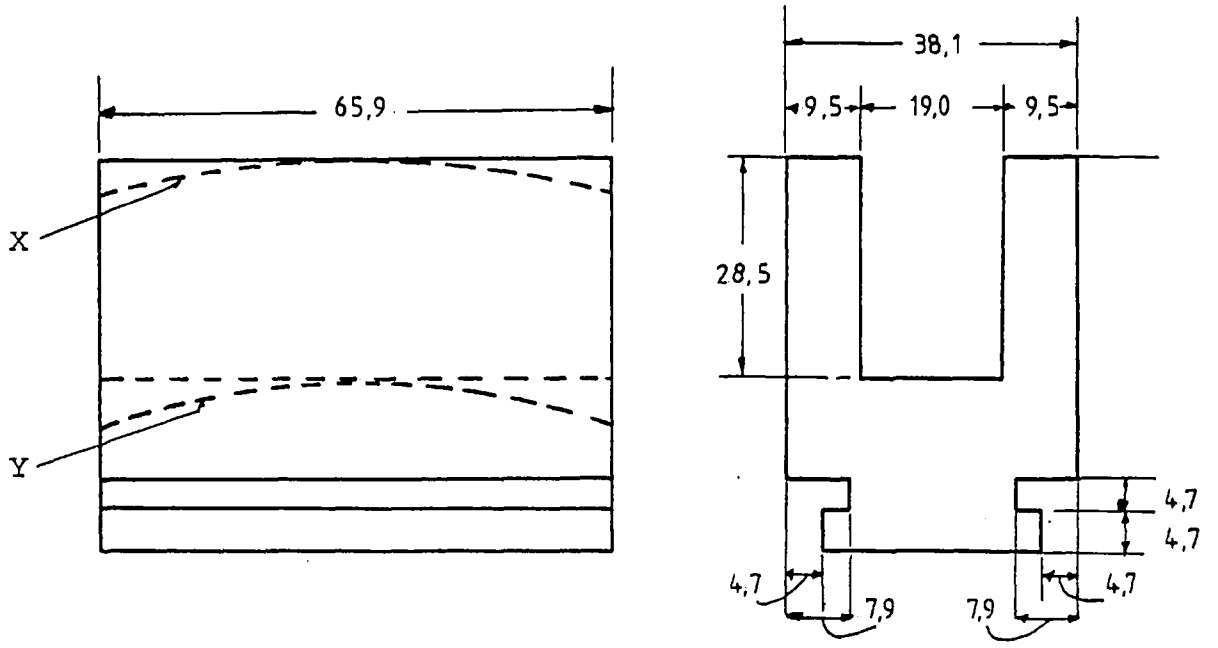

Fig. 4.1.3 Stator pole piece (before milling)
(X finally turned down to 127 mm radius,
Y finally turned down to 98.4 mm radius,
all dimensions are in millimetres)

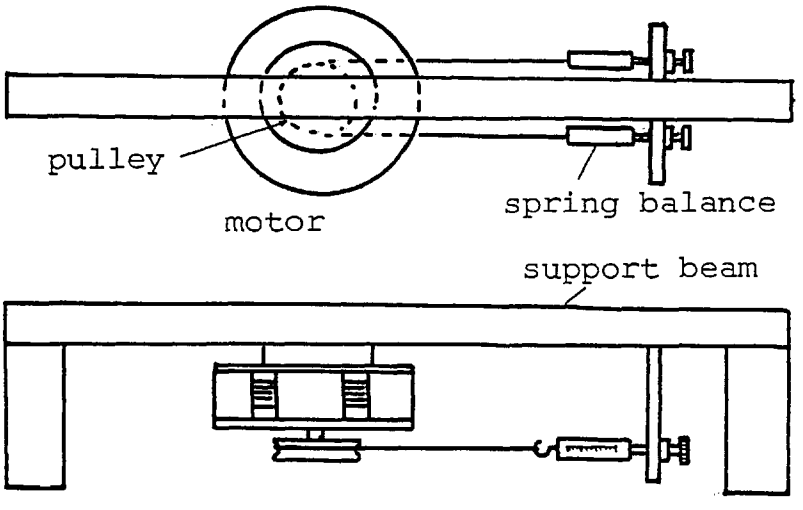

Fig. 4.1.4 Test rig for low-speed, 6-saliency motor

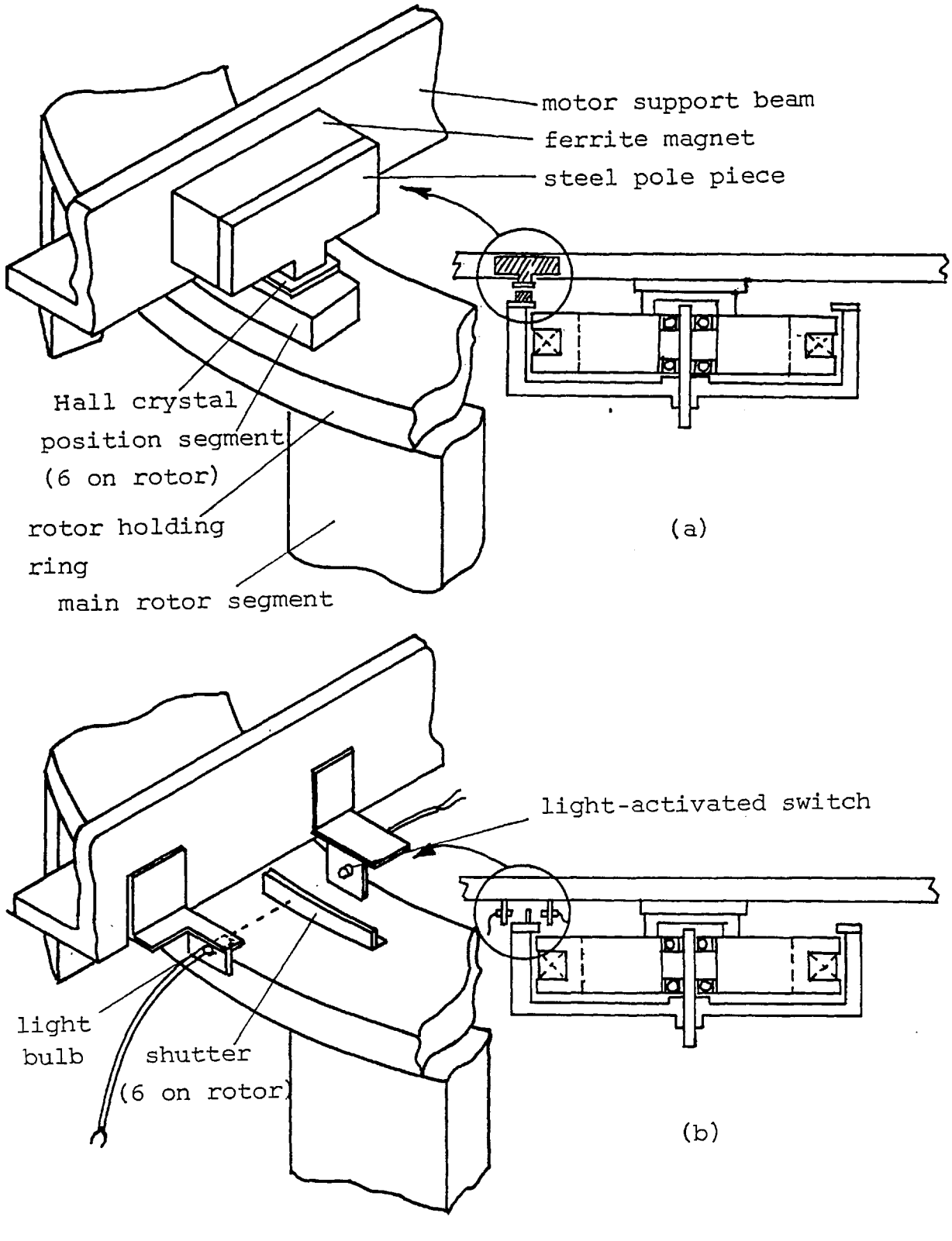

Fig. 4.1.5 Position sensor location on experimental motor
(a) Hall-effect device
(b) Light-activated switch

in the required fashion. Fig. 4.1.5 (b) shows the alternative arrangement incorporating an opto-electrical system. The transmitter (light bulb) and the receiver (light activated switch with associated circuit) are fixed on the support beam, and small plastic shutter are provided on the rotor ring to mark the rotor position. Switching angles on both systems are fixed by the circumferential lengths of the projections.

The principal tests carried out on this experimental motor were:

a) Measurement of equivalent circuit parameter,
b) Load test with d.c. link PWM transistor-fed circuit,
c) Load test with a.c. triac-fed circuit.

4.2 Measurement of equivalent circuit parameters

The solid-iron nature of the magnetic circuit causes great difficulties in using equivalent circuit that are at all exact and it was decided to make the fairly drastic assumption that a simple R-L circuit with fixed parameters would suffice for first order predictions. There is perhaps more excuse than with fixed frequency and/or sine-wave fed machines for making this assumption since the derivation of a realistic equivalent circuit

able to model accurately the phenomena over the tremendous ranges of flux and frequency (fundamental and harmonics) occurring in the actual motor was reckoned to be beyond the scope of a project in which other SPSRM types and many feed circuit aspects were being tackled.

The d.c. resistance of the stator coil was measured with 'Kelvin Bridge' and was found to be 5.18 Ω. With the assumption that the equivalent circuit of the motor comprises only a variable inductor connected in series with a resistor, the circuit for measuring the motor inductance was set up as shown in Fig. 4.2.1 (a). With a 50 Hz a.c. supply applied to the circuit, the stator power losses, coil currents and coil voltages were read for a number of rotor positions (24 electrical degree intervals) for a complete cycle of inductance waveform.

The apparent inductance for each position of the rotor was then calculated according to the phasor diagram of Fig. 4.2.1 (b) as follows:

The impedance of the coil is

$$Z = \frac{V_1}{I} \qquad (4.2.1)$$

where V_1 is the coil voltage and I is the coil current.

The apparent resistance of the coil

$$r = \frac{P}{I^2} \qquad (4.2.2)$$

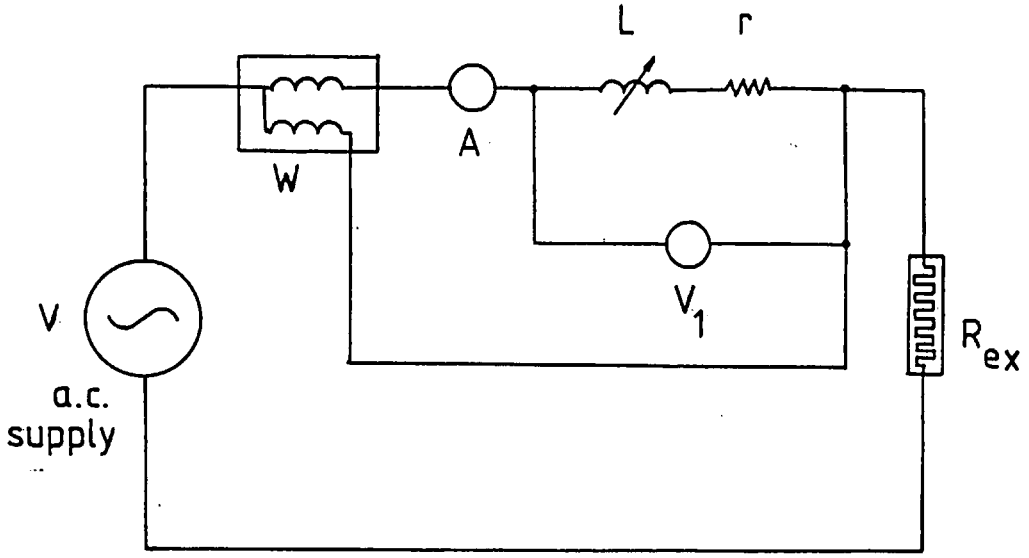

(a)

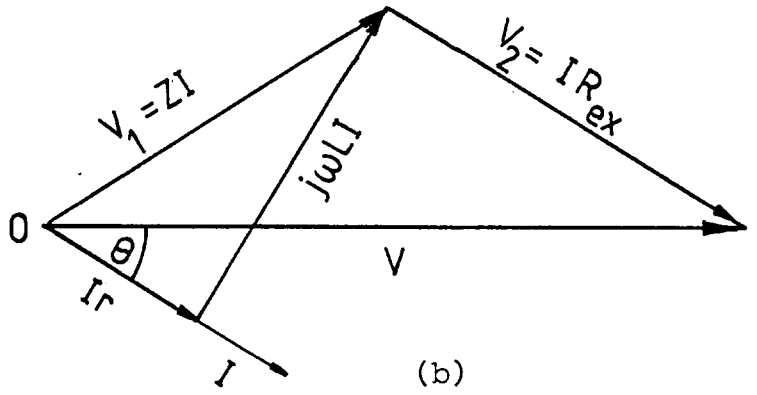

(b)

Fig. 4.2.1 (a) Inductance measuring circuit
(b) Corresponding phasor diagram

where P is the coil power losses.

Coil apparent inductive reactance

$$X_L = \sqrt{Z^2 - r^2} \qquad (4.2.3)$$

The inductance L is then equal to

$$L = \frac{X_L}{2\pi f} \qquad (4.2.4)$$

where f is the supply frequency.

The same procedure was carried out to other lower frequencies of 28.57 Hz and 11.11 Hz, power being supplied from a variable frequency generator. Reduced voltages were used to avoid saturation.

The variation of apparent inductance with rotor position for different supply frequencies is shown in Fig. 4.2.2 (a). Extrapolation of inductance versus frequency in Fig. 4.2.2 (b) gave the value of maximum and minimum inductance at zero frequency corresponding to zero iron losses assumed in the analytic model.

The maximum and minimum inductances at d and q positions respectively are

$$L_{max} = 450 \text{ mH} \quad , \quad L_{min} = 177.5 \text{ mH}$$

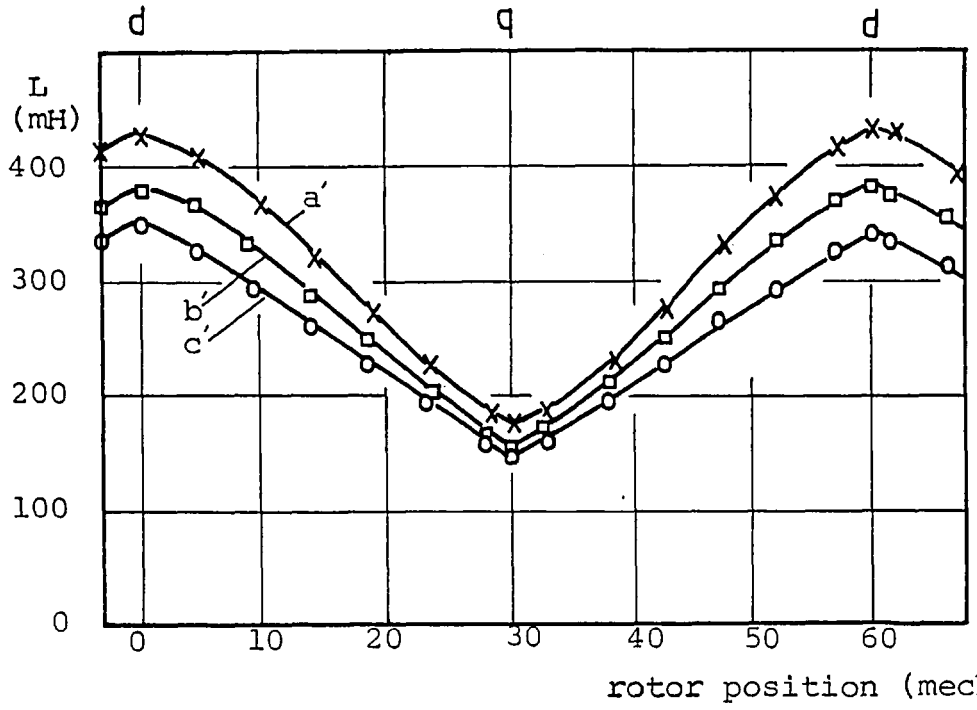

a') measuring frequency of 11.1 Hz
b') measuring frequency of 28.57 Hz
c') measuring frequency of 50.0 Hz

(a)

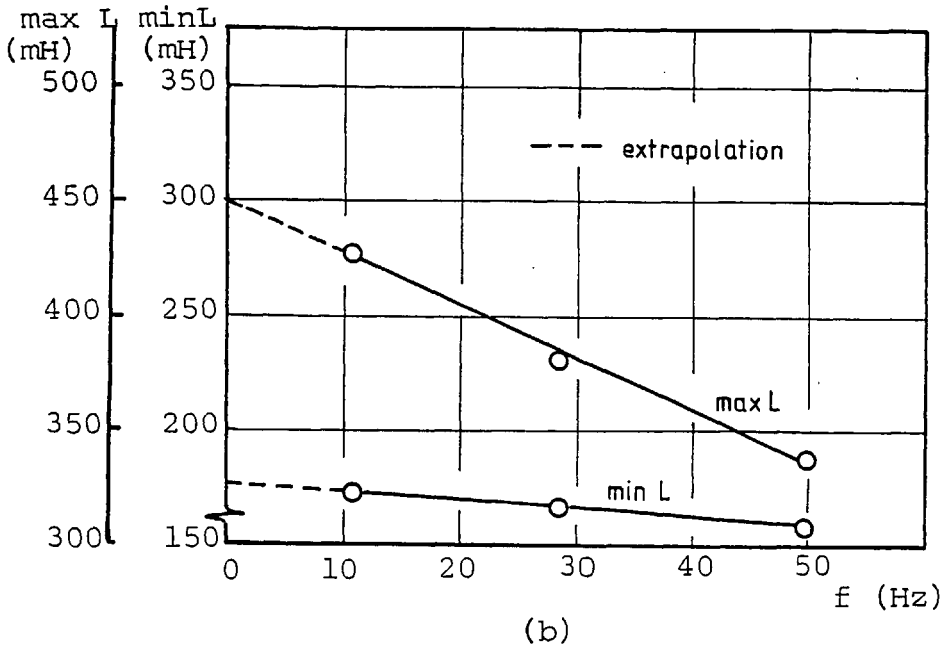

(b)

Fig. 4.2.2 (a) Variation of inductance with rotor position
(b) Variation of maximum and minimum inductances with frequency

Calculation of the total inductance at the maximum alignment position from the basic lumped circuit theory on the assumptions that the permeability of iron is infinity and the fringing flux is zero can be made as follows:

The inductance per segment of rotor and stator can be considered to result from the main airgap flux and the slot leakage flux. As shown in Fig. 4.2.3, the airgap inductance for one segment of the stator with the rotor in the d position ,

$$L_g = N^2 \mu_o \frac{wL_1}{2g} \quad H \quad (4.2.5)$$

where
- N is the number of turns of the winding,
- μ_o is the permeability of air,
- g is the airgap length,
- L_1 is the length of the rotor piece,
- w is the width of the active volume.

With $N = 340$ turns, $\mu_o = 4 \times 10^{-7}$, $g = 0.7 \times 10^{-3}$ m, $w = 9 \times 10^{-3}$ m and $L_1 = 60 \times 10^{-3}$ m; the airgap inductance per segment is

$$L_g = 56.03 \quad mH$$

The slot leakage inductance per segment of stator can be calculated from the standard formula for the leakage inductance of an open rectangular slot[4.2] (Fig 4.2.3), the expression for the slot leakage inductance is

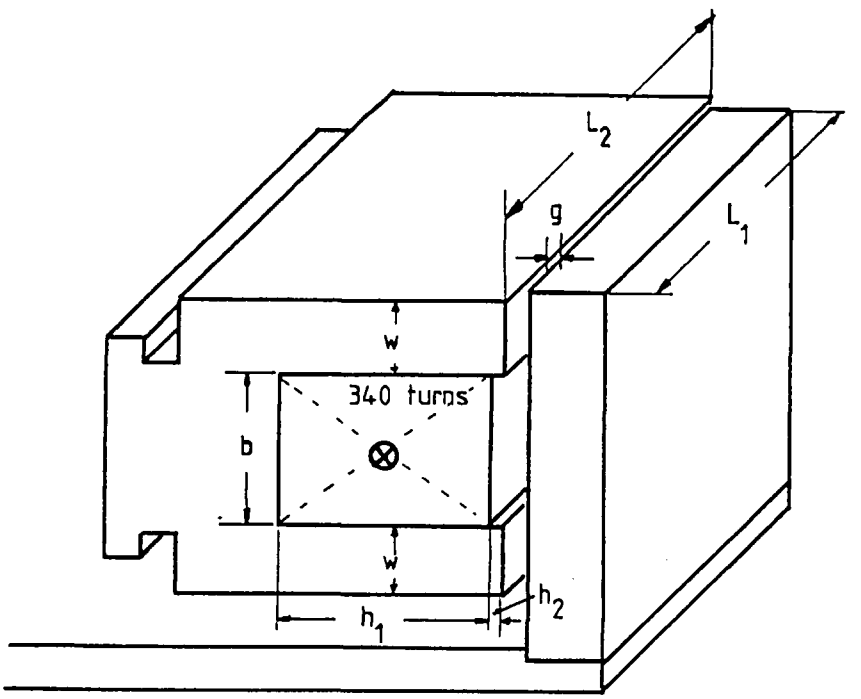

Fig. 4.2.3 Model for calculating maximum inductance, the fringing flux and overhang flux are neglected and $\mu_{r\ iron} = \infty$ is assumed

$$L_s = N^2 \mu_o \left(\frac{h_1}{3b} + \frac{h_2}{b} \right) L_2 \quad H \quad (4.2.6)$$

for stator pole piece $h_1 = 29 \times 10^{-3}$ m, $b = 19 \times 10^{-3}$ m, $h_2 = 1 \times 10^{-3}$ m, $L_2 = 68 \times 10^{-3}$ m ; the slot leakage inductance per segment is

$$L_s = 5.54 \quad mH$$

Hence total inductance per segment = 56.03+5.54 mH

= 61.57 mH

The experimental motor has 6 saliencies and this gives the total inductance of 6x61.57 = 369.4 mH.

The calculated inductance is 18 % less than the extrapolated value obtained from the set of measurements. The difference is probably due to the neglected

fringing and overhang fluxes. The neglect of airgap curvature and of the slight non-rectangularity of the stator slots are also likely to contribute errors in the calculated value.

4.3 Motor performance with d.c. link PWM transistor-fed circuit

4.3.1 The d.c. link PWM transistor-fed system

Fig. 4.3.1 shows a simplified diagram of the d.c. link PWM transistor-fed system used in the experiments. The system can be roughly divided into : (i) rectifier, filter and smoothing circuit; (ii) power switching circuit and (iii) sensor and control circuit. The control circuit was isolated from the power circuit by means of opto-isolators on the signal side and isolation transformers on the supply side.

For the tests, the rectifier was supplied from a single-phase variac transformer to allow d.c. link voltage to be adjusted (see Fig. 4.3.2). The power switching circuit's components were chosen for experimental purposes only and it is realised that the circuits can be greatly improved, particularly when the load and performance are specified. The rectifier and smoothing circuit consists of a bridge rectifier with an electrolytic capacitor as a smoothing component. The power switching

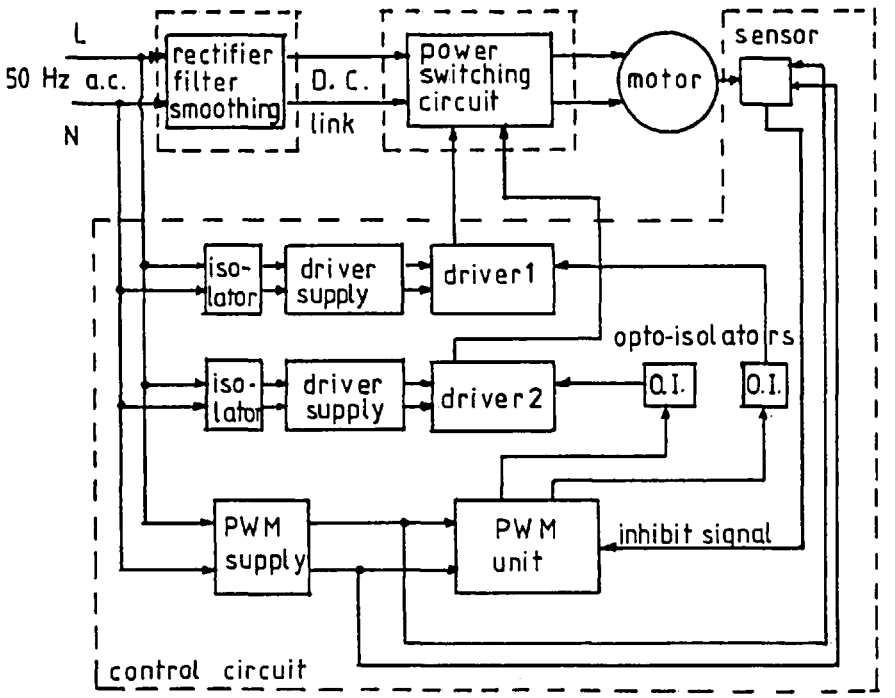

Fig. 4.3.1 Schematic diagram of the PWM transistor-fed system

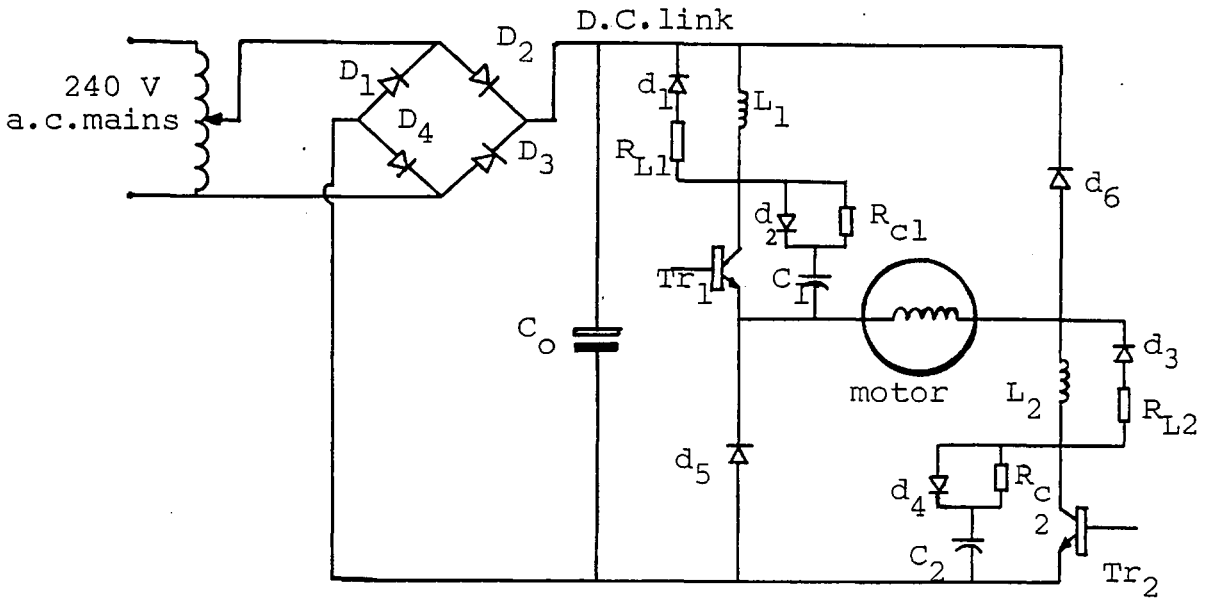

Fig. 4.3.2 The rectifier and power switching citcuit D_1-D_4 600 V 6 A; C_o 1160μF; d_1-d_6 BYX 71-600; L_1,L_2 50 μH; C_1,C_2 0.022 μF; R_{L1},R_{L2} 30 Ω 27 W; R_{c1}, R_{c2} 120 Ω 46 W

circuit is a half bridge inverter type with power darlington SVT 6002 Series TRW transistors used as switching elements. These have a high gain and a fast switching time. Fast-recovery silicon diodes BYX 71-600 were used in the main freewheel path.

The outline characteristics of the transistor and diode are :

SVT 6002 Series TRW transistor

$I_{c\ cont}$	=	15	A
V_{ceo}	=	500	V
$V_{ce}sat$	=	1.5	V
t_r	=	0.4	μS
t_f	=	1	μS
I_s	=	3	A
I_{ceo}	=	1	mA
V_s	=	450	V
V_{sn}	=	$V_{ceo}-V_s$ = 50	V
T_j	=	150	^oC
T_{amb}	=	30	^oC
$\theta_{j\ amb}$	=	2.4	$^oC/W$

BYX 71-600

Encapsulation SOD-38

$I_{F(av)max}$	=	7	A
$V_{rrm\ max}$	=	600	V
$I_{FSM\ max}$	=	60	A
$t_{rr\ max}$	=	450	nS
$V_{F\ max}$ at I_F	=	1.25	V
at 5 A			

Suitable snubber circuits were provided to protect the transistors. Fast-recovery diodes were used in both freewheel circuits and snubber circuits. Polypropylene capacitors were used in the snubbers because of their good high frequency performance, ability to withstand high voltage, fast rise-time pulses and their low loss.

Rotor-position sensing was achieved by the light-activated switch and the associated circuit shown in Fig. 4.3.3 (a). The signal is fed to the inhibit terminal of the PWM chip as shown in Fig. 4.3.3 (b), the PWM chip is the switching regulator control and drive unit ZN 1066 by Ferranti. The full descriptions of the circuit and performance of the chip are shown in ref. 4.3 and only brief explanations will be given here.

As the data sheet states : " The ZN 1066 is a 24 lead D.I.L package, designed to satisfy the requirement for a general purpose control and drive unit in switching power supplies, transformer coupled DC/DC converters, motor speed control and other power control applications. The circuit includes a voltage reference, current control amplifier, voltage control amplifier, oscillator, pulse width modulator, pulse steering flip-flop, dual alternating outputs, cross coupled output inhibits and a synchronising and shut down facility. The output frequency is adjustable up to 500 KHz with 0-100 % duty cycle control."

As shown in Fig. 4.3.3 (b), the pulse width of the output signal is controlled by the difference of the voltage inputs of amplifier 2 . The soft-start circuit is provided to prevent output voltage overshoots. This feature forces the duty cycle of the switching transistors to increase gradually from zero to their normal

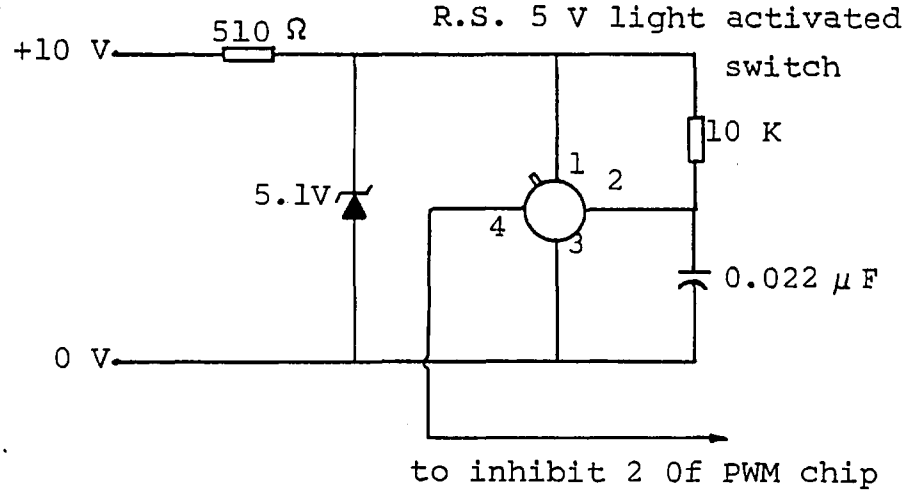

(a)

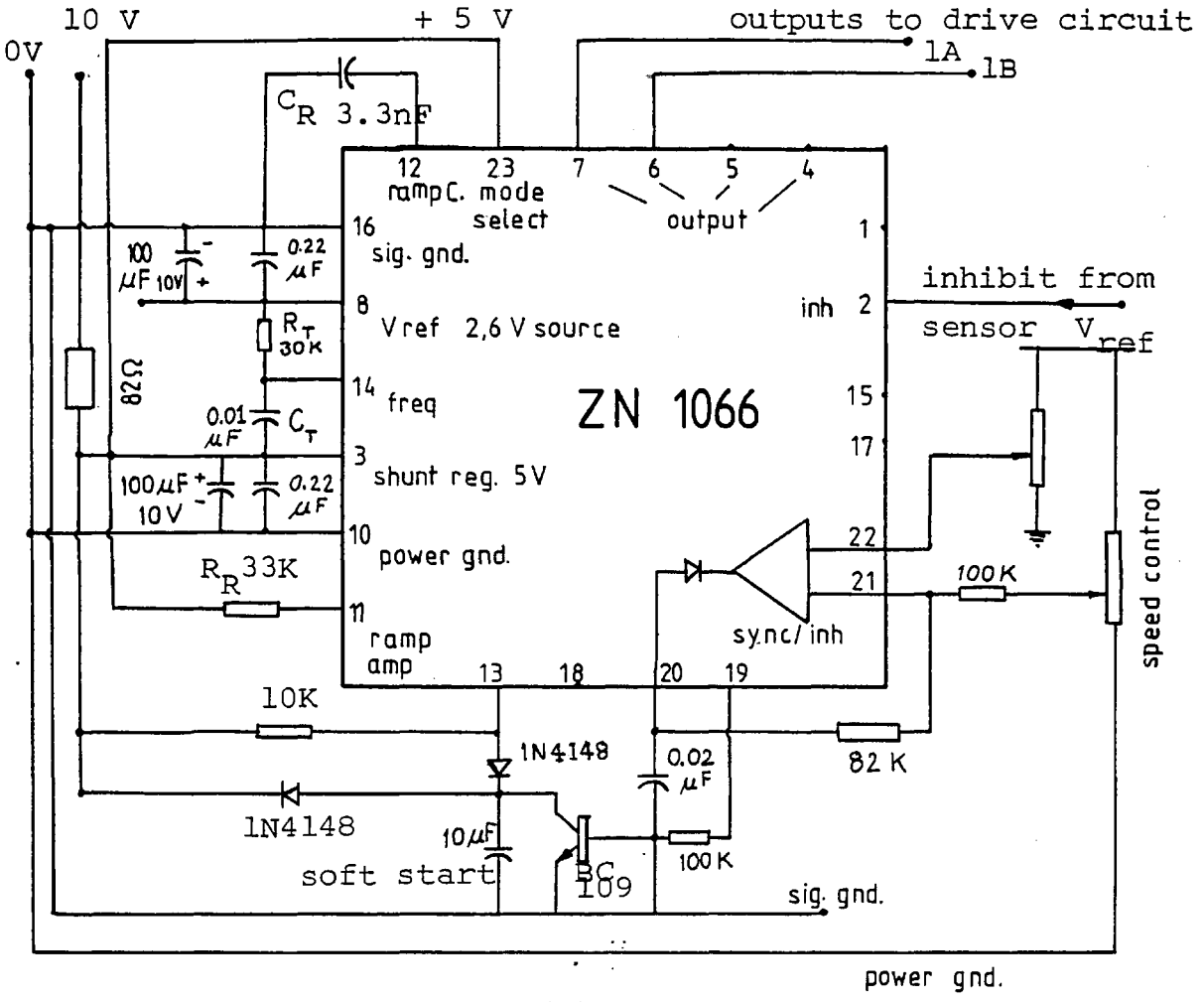

(b)

Fig. 4.3.3 (a) Position-sensor circuit
(b) PWM circuit

condition
operating during system power up or after an inhibit.

The oscillator frequency can be programmed by means of an external timing resistor R_T and capacitor C_T to define any time period in the range 2 seconds to 2 microseconds (0.5 Hz to 500 KHz). The oscillator period is approximately

$$T_{osc} = 0.33\ C_T R_T \qquad (4.3.1)$$

where T_{osc} is in microseconds,

R_T is in ohms and C_T is in microfarads,

with the limits $3K \leq R_T \leq 100K$ and $C_T \geq 1500$ pF.

The output-pulse width is infinitely variable from 0 to 50 % when mode control (pin 23) is at 0 V, or 0 to 100 % when mode control is at 5 V. If mode control is at 0 V , the output waveform frequency is approximately equal to

$$f_o = 1.5/C_T R_T \qquad (4.3.2)$$

Note that f_o refers to the frequency of the outputs 1A, 1B (pins6 and 7) or outputs 2A, 2B (pins 4 and 5). The frequency of the oscillator and ramp generator waveforms is twice f_o .

If the mode control is at 5 V the output waveform pulse width is variable from 0-100% and the output waveform frequency

$$f_o = \frac{1}{0.33\ C_T R_T} \quad \text{KHz} \qquad (4.3.3)$$

With mode control at 5 V and C_T = 0.01 μF and R_T = 30 K, the output frequency was set at 10 KHz.

In general, 0-50% duty cycle control is sufficiency for PWM controlled load as 0 % duty cycle is equivalent to full voltage applied to the load and 50% duty cycle is equivalent to zero mean voltage applied to the load.

As the 120 mA output from the PWM chip was considered to be insufficient to drive the power darlington transistor, the driver circuits and opto-isolators of Fig. 4.3.4 were used. A totem pole output configuration was adopted to speed up the switch-off time of the transistor. The isolation transformer was used in the power supply circuit of the driver to prevent short-circuits.

4.3.2 Load tests of low-speed, 6-saliency motor with different switching angles

The test circuit used in the experiments is shown in Fig 4.3.5. Wattmeter W, voltmeter V_1 and ammeter A_1 were used for measuring the corresponding a.c. quantities of the system. Voltmeter V_2 and ammeter A_2 were used for measuring d.c. rail voltage and average

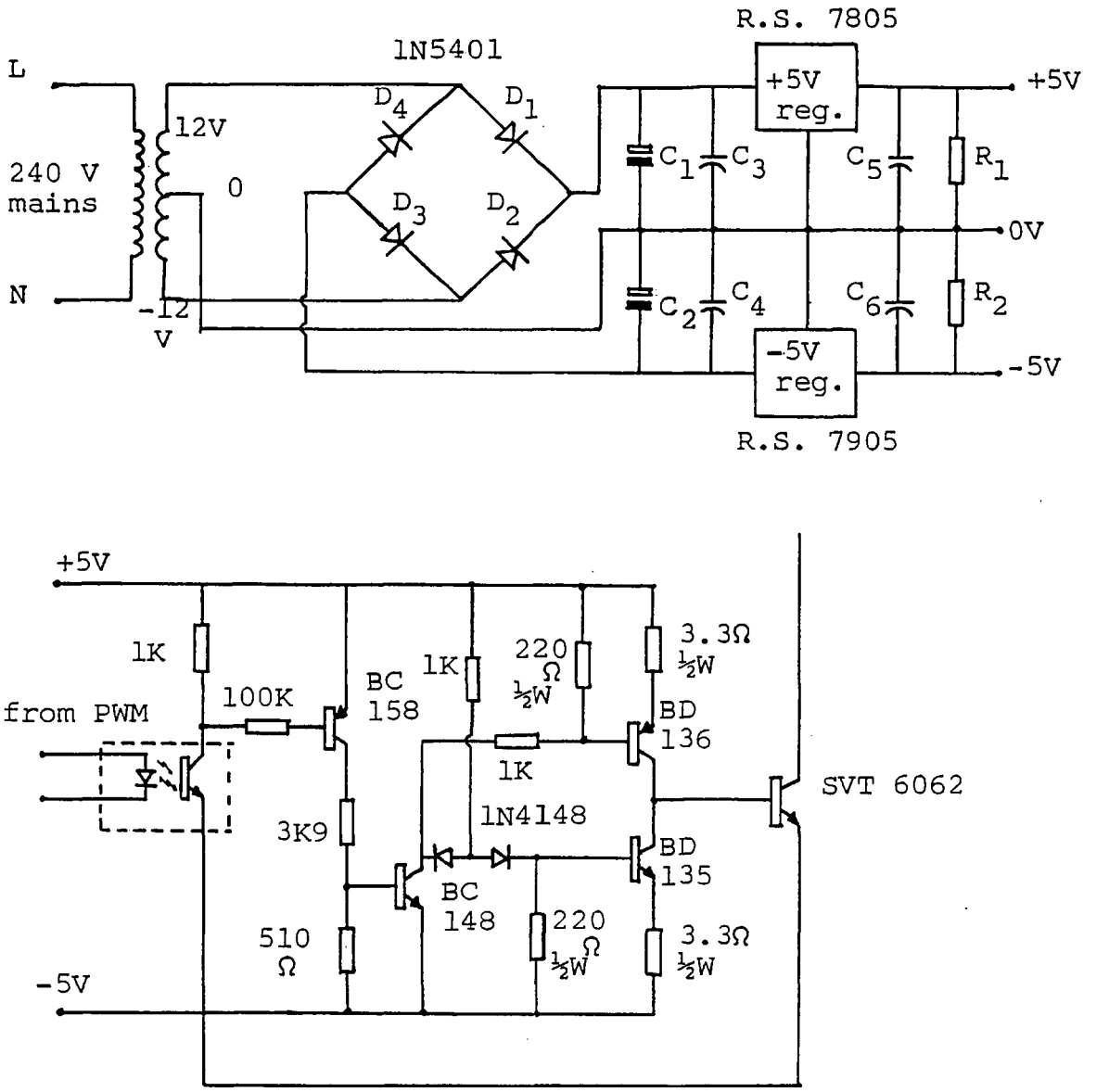

Fig. 4.3.4 Driver circuit

C_1,C_2 2200 μF 16V; C_3,C_4 0.22 μF;
C_5,C_6 0.47 μF; R_1,R_2 4K7

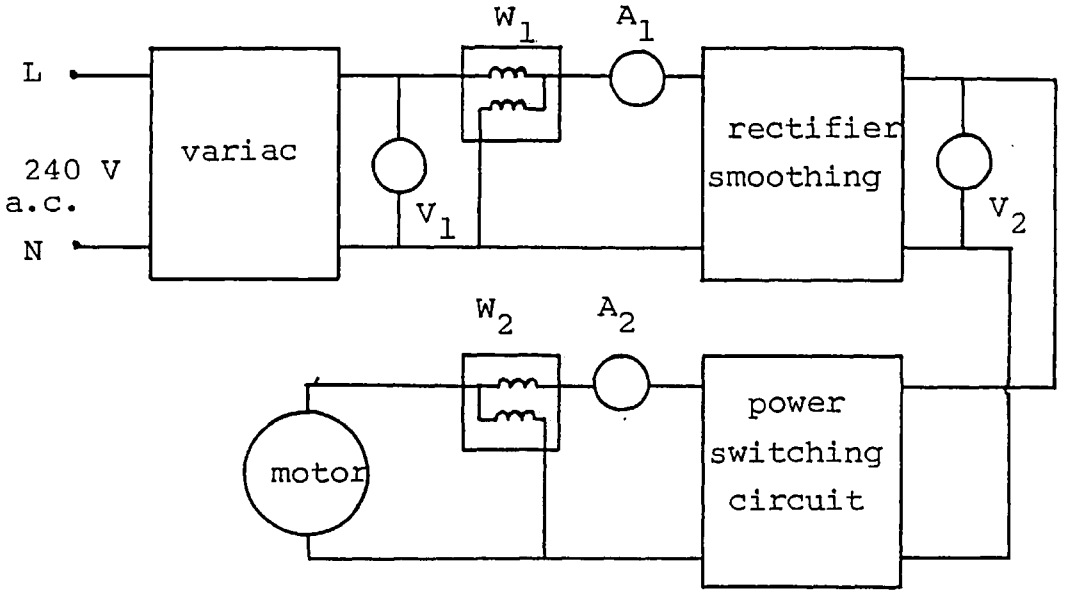

V_1, A_1 moving-iron type
V_2, A_2 moving-coil type

Fig. 4.3.5 Test circuit

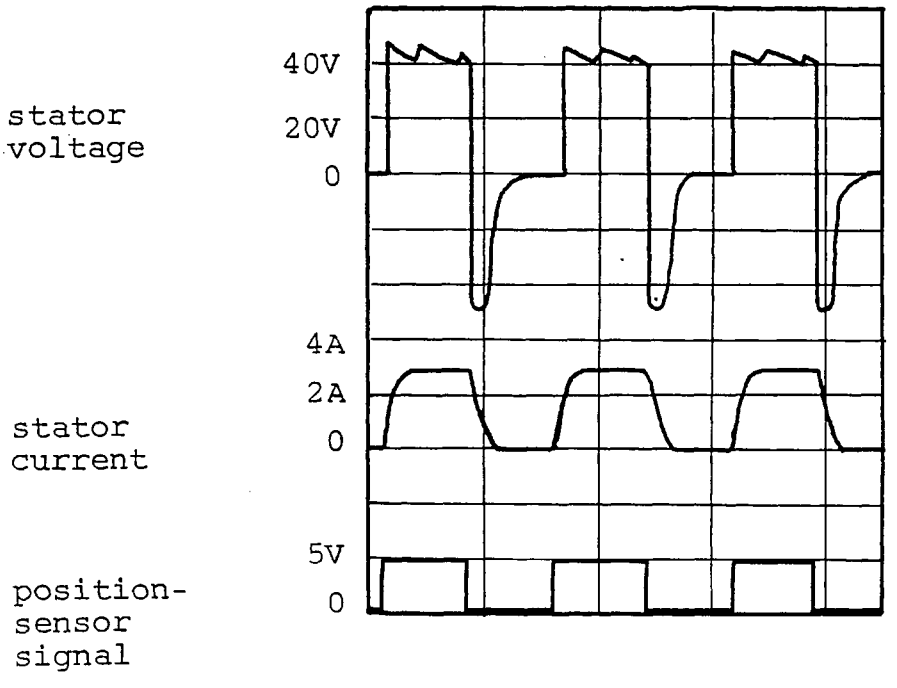

Fig. 4.3.6 Stator voltage, stator current and position-sensor signal waveforms
($\alpha = 24^{\circ}$, $\beta = 24^{\circ}$, 150 rev/min)

coil current respectively. The rotor speed was calculated from the frequency of the signal of the position sensor circuit (speed in rev/min is equal to $10xf_{LAS}$, where f_{LAS} is the frequency of the signal in Hz). Two spring balances and a cord around the pulley on the motor shaft were used as a brake for torque measurement.

Tests were then carried out for two settings of PWM mark/space ratio :

a) full mark/space ratio

b) 87.3% mark/space ratio

In each case the d.c. rail voltage was set at 50 V. with $\alpha = 24^{o}$elec and $\beta = 24^{o}$elec. Powers, voltages, currents and speeds were then recorded for each load setting. The tests were repeated for two different values of β (48 ^{o}elec and 72 ^{o}elec) with the same α .

Fig. 4.3.6. shows the waveforms of the stator voltage and current for $\alpha = 24^{o}$ and $\beta = 24^{o}$ at 150 rev/min. The voltage waveform shows fairly sharp rising and falling edges corresponding to the 'on' and 'off' signals from the position sensor. The ripple at the top of positive half cycle results from the rectification ripple in the d.c. rail, and the percentage of ripple increases with load current. When the sensor switches 'off' the coil voltage is suddenly pulled down to $-V_s$ due to the action of the freewheel diodes. The coil current then drops

exponentially (due to coil inductance) to zero. When the stator current equals zero, the freewheel diodes stop conducting and because the transistors are still 'off', the stator coil is now effectively disconnected from the circuit so the stator coil voltage is zero. The whole cycle repeats for the next 'on' signal from the sensor.

4.3.3 Results and discussion

a) Full mark/space ratio

The results of the tests with full mark to space ratio PWM are shown in Fig. 4.3.7 for three values of β . The no-load speeds are about the same (550 rev/min) and the motor torque-speed curves are similar in form to those of a series d.c. motor. For the same value of β the motor mean torque varies linearly with the square of the stator current and roughly inversely with rotor speed. Increasing β from 24 ^{o}elec to 48 ^{o}elec (i.e. decreasing the 'on' period) can reduce the current considerably without significant reduction in torque and can also improve efficiency.

Further increase in β (from 48 ^{o} to 72 ^{o}) reduces the mean torque appreciably especially at low speeds. This suggests that the optimum 'advance off-angle' for the best operation of $\alpha = 24^{o}$ is $\beta = 48^{o}$.

The numerical values of mean torque, mean current

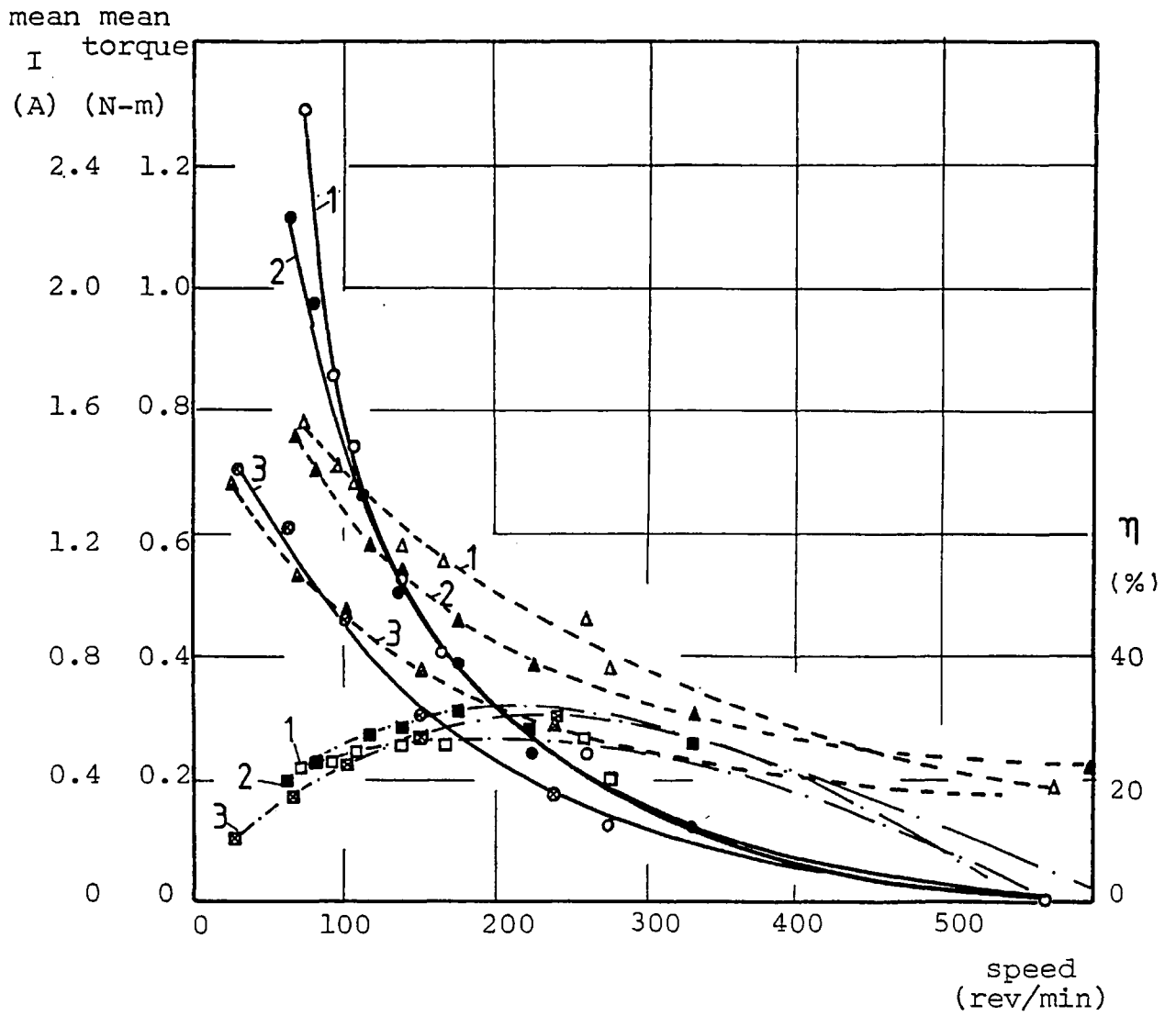

Fig. 4.3.7 Performance curves at 50 V d.c. rail

α = 24°, full m/s ratio

1. β =24°, 2. β =48°, 3. β =72°

——— mean torque

– – – – – mean current

—·—·— efficiency

and efficiency are given for low speed (150 rev/min) and for the speed which gives maximum efficiency (250 rev/min) in Table 4.1. The maximum output torque at 150 rev/min is 0.48 Nm for α = 24° and β = 24°. This is rather low for this motor because the operating voltage (50 V) used in the tests was rather low. The output torque can certainly be increased by increasing the supply voltage since the mean current is only 1.2 A compared with the 3.7 A rating of the winding (assume J = 3000 A/in^2). The efficiencies are undoubtedly low because of the solid structure of rotor and stator, the maximum efficiency with a 50 V feed being approximately 31% at 250 rev/min with α = 24° and β = 48°.

The power distribution curves are shown in Fig. 4.3.8. It can be seen that, generally the power inputs are proportional to the length of switch 'on' period set by the switching angles but not the power outputs. This is because of the negative torque produced by the 'carry-over' current in the negative inductance slope region as explained before. If the advance-off angle 'β' is too small, the negative torque may cause reduction in mean torque and also output power. The overall (motor +drive) efficiencies are around 20-23% for most loads.

b) 87.3% mark/space ratio

The same test circuit together with the same test procedure except that a PWM mark to space ratio

Table 4.1 Performance data with PWM transistor-fed circuit

speed rev/min	150			250		
α / β deg.	24/24	24/48	24/72	24/24	24/48	24/72
mean torque N-m	0.48	0.46	0.29	0.25	0.22	0.16
mean current A	1.20	1.00	0.74	0.92	0.74	0.56
efficiency %	25.0	29.0	26.7	27.3	31.0	30.0

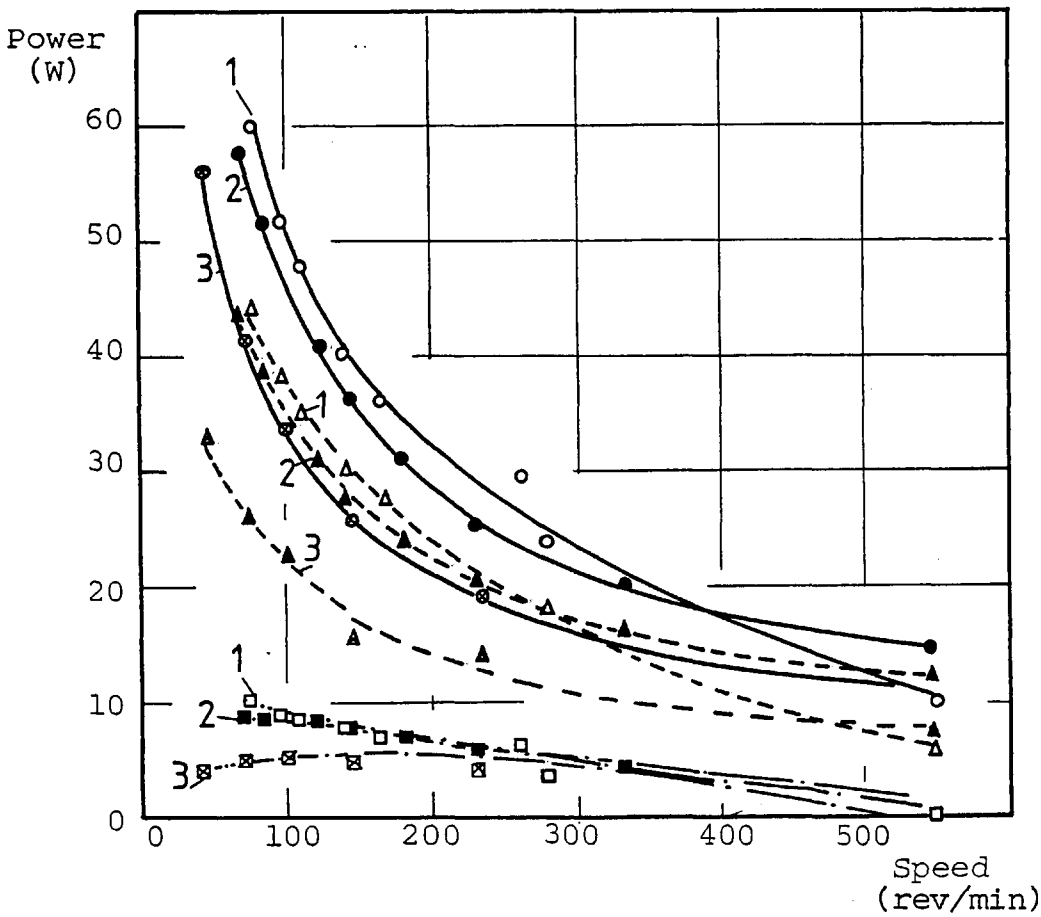

Fig. 4.3.8 Power versus speed curves at 50 V d.c. rail, α = 24° full m/s ratio
1. β = 24°, 2. β = 48°, 3. β =72°

——— power input to the system
- - - - - - - power input to the motor
—·—·— power output

set at 87.3% was used in this test. The results are shown in Fig. 4.3.9 and 4.3.10 for α = 24° and β = 24° and 48° . At β = 72°, the output torque was too small to be measured with the brake. The output torque-speed curves are similar to those of full mark/space. The speed can be controlled smoothly (at 0.4 Nm the speed dropped about 80 rev/min from full mark/space case). As expected, the mean power input reduces with decreasing mark/space ratio. The motor efficiencies are comparable with those for full mark/space operation.

The computer prediction based on the method described in section 3.2.2 was made with the machine parameters obtained in section 4.2 (R=5.18 Ω , L_{max} = 450 mH, L_{min} = 177 mH). The predicted results are compared with the measured results for the case of α =24° and β = 24° with full mark/space ratio in Fig. 4.3.11. The predicted torque and current characteristics although higher than the measured values possess the same shape for the whole range of speeds. The higher predicted currents are perhaps due to the use of the d.c. resistance value in the predictions. Variation of coil temperature and skin effect would increase the resistance of the coil in the tests . Because the motor torque varies roughly with the square of the current, calculated torques are also higher than the measured values. Neglected iron losses will also have contributed to the errors between the predicted and measured torques. Since the iron losses

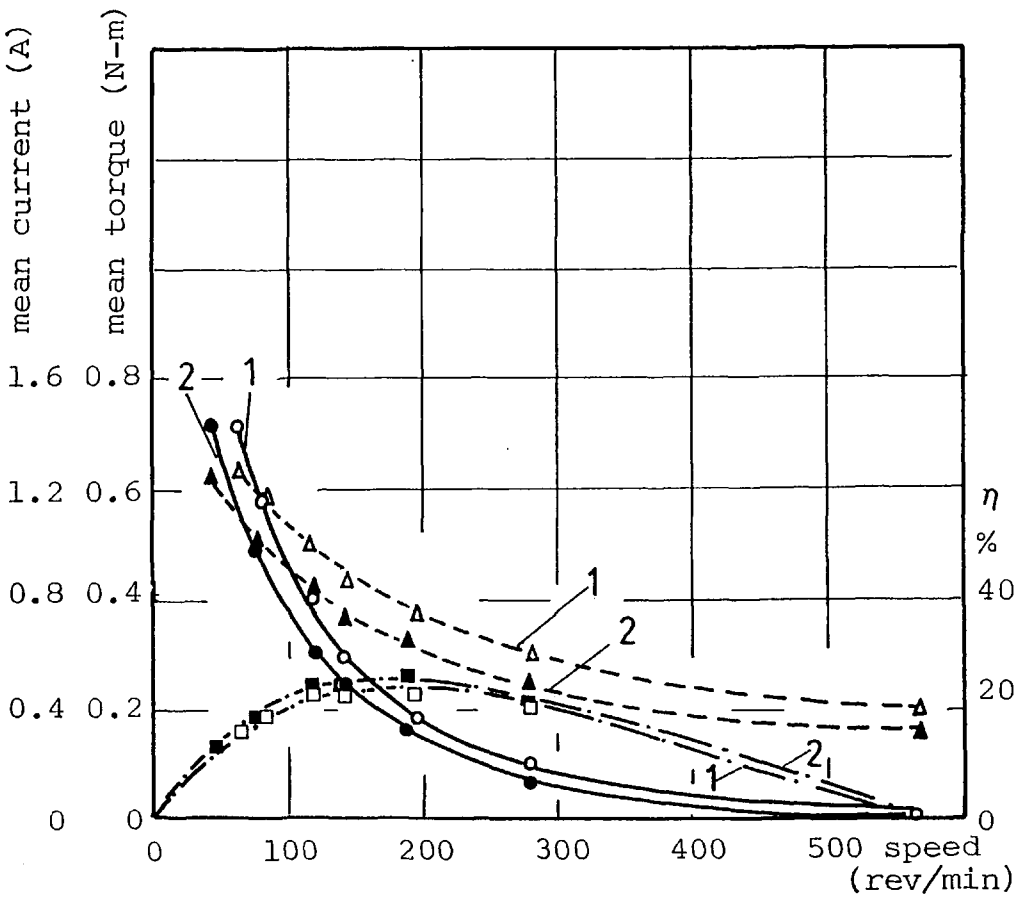

Fig. 4.3.9 Performance curves at 50 V d.c. rail α = 24°, 87.3% m/s ratio
1. β = 24°, 2. β = 48°
——— mean torque
– – – – mean current
—·— efficiency

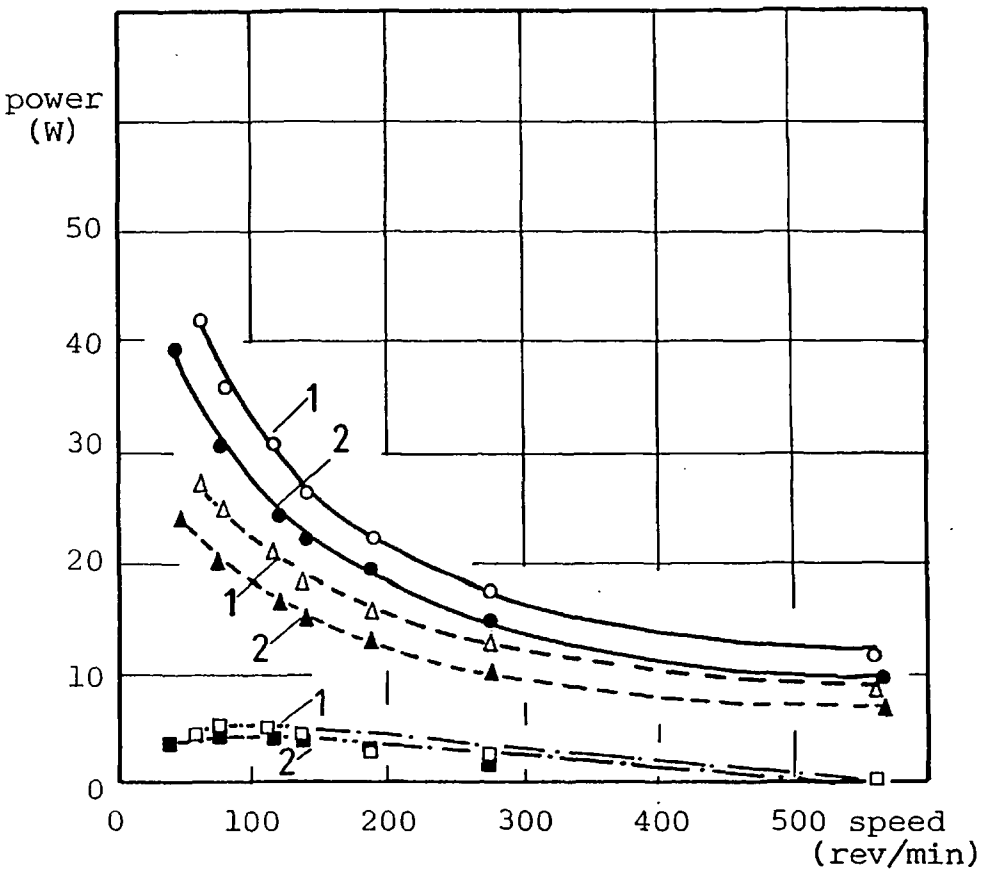

Fig. 4.3.10 Power versus speed curves at 50 V d.c. rail, 87.3% m/s ratio
α = 24°
1. β = 24°, 2. β = 48°
——— power input to the system
– – – power input to the motor
—·— power output

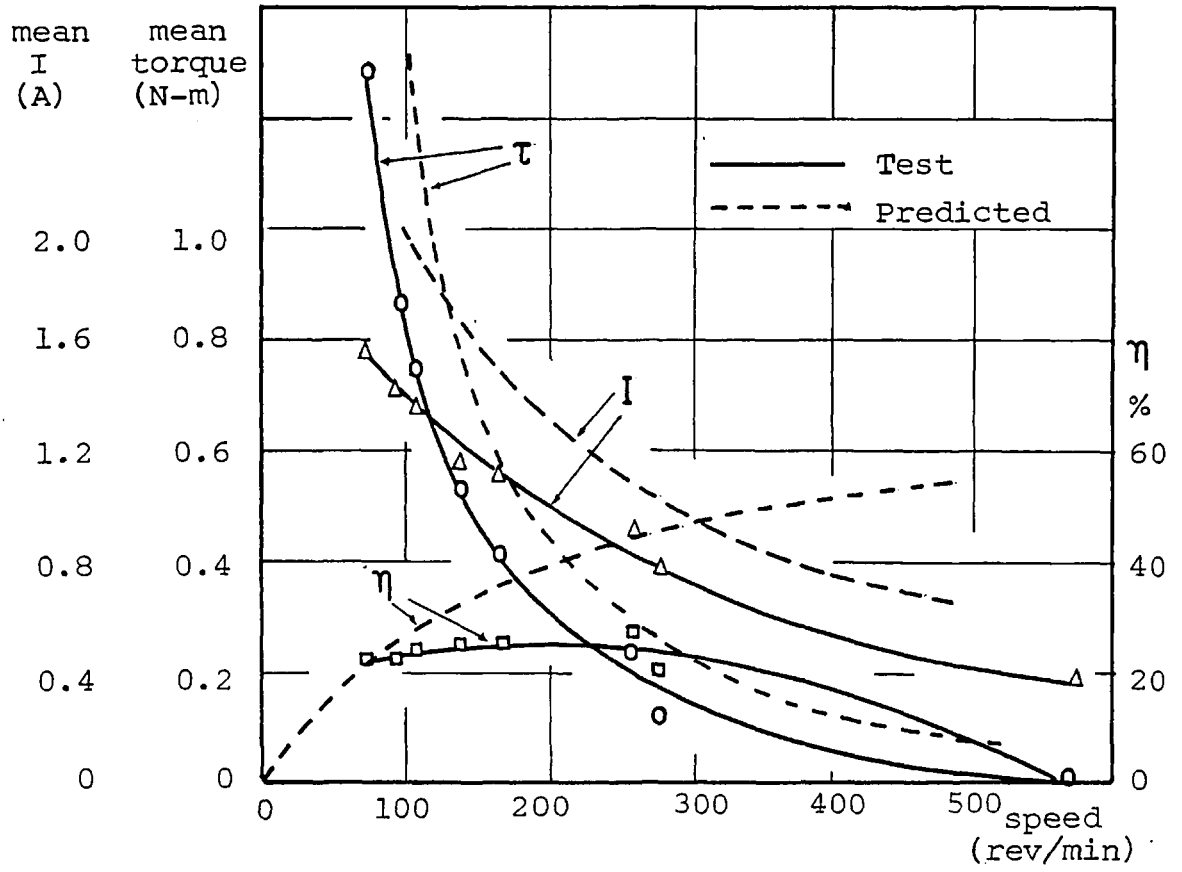

Fig. 4.3.11 Performance curves at 50 V d.c. rail full m/s ratio, $\alpha = 24^{\circ}$, $\beta = 24^{\circ}$

together with the friction and windage losses are neglected, it is obvious that the calculated efficiency is inevitably considerably higher than the measured value.

Predicted performance for full mark/space operation of the same operating condition (i.e. the same average motor supply voltage) are shown in Fig. 4.3.12 and 4.3.13 . The effect of changes in current and torque with increasing β from 24° to 48° and 72° can be seen to be similar to the measured results i.e. increasing β from 24° to 48° helps to reduce stator current without appreciable effect on output torque.

The exact prediction for the case of PWM supply voltage would be lengthy, even with a neglect of the iron losses. The L/R time constant of the winding is in any case so large compared to the PWM cycle time that little would be gained by so doing.

The effect on performance of supply voltage variation ($T \propto V^2$, $I \propto V$), of decrease in airgap length (both affecting flux levels, the latter affecting R/L ratios) and of adjustment to the switch on and switch off times relative to the instant at which rotor passes through the q and d positions are shown in Fig. 4.3.14 and 4.3.15 for another set of machine parameters.[4.4] As reference 4.4 states :"There is some advantage in decreasing the airgap length but this is limited by mechanical considerations. Varying the switch on and off times(α and β)

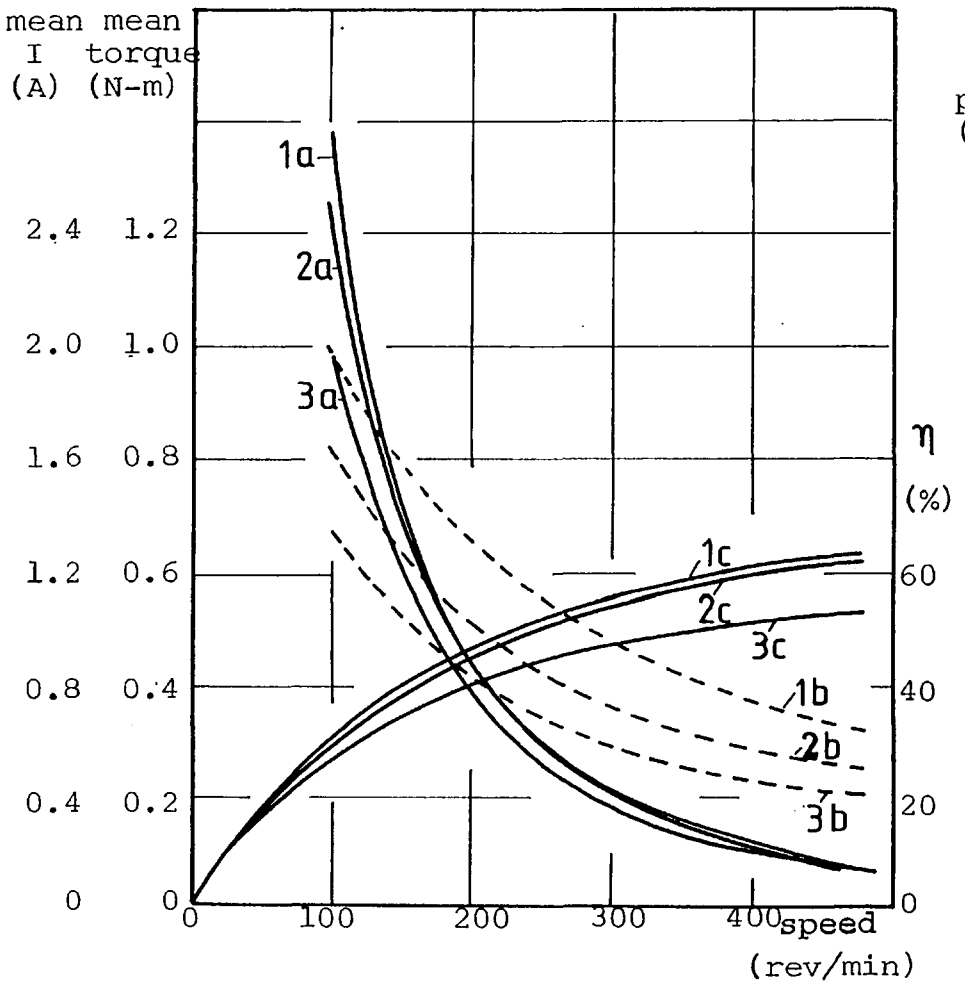

Fig. 4.3.12 Predicted performance curves at 50 V d.c. rail, full m/s
1. $\beta = 24^{o}$, 2. $\beta = 48^{o}$, 3. $\beta = 72^{o}$
a. mean torque, b. mean current
c. efficiency

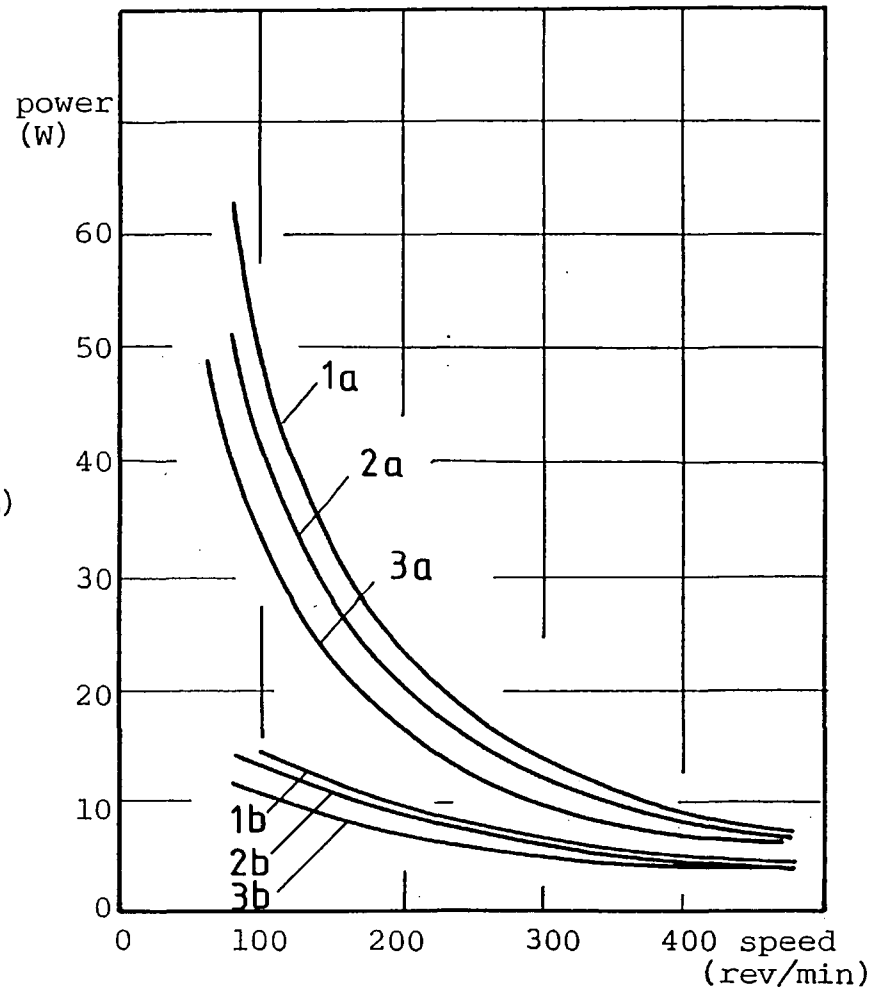

Fig. 4.3.13 Predicted power versus speed curves at 50 V d.c.rail, $\alpha = 24^{o}$ full m/s
1. $\beta = 24^{o}$, 2. $\beta = 48^{o}$, 3. $\beta = 72^{o}$
a. power input to the motor
b. power output

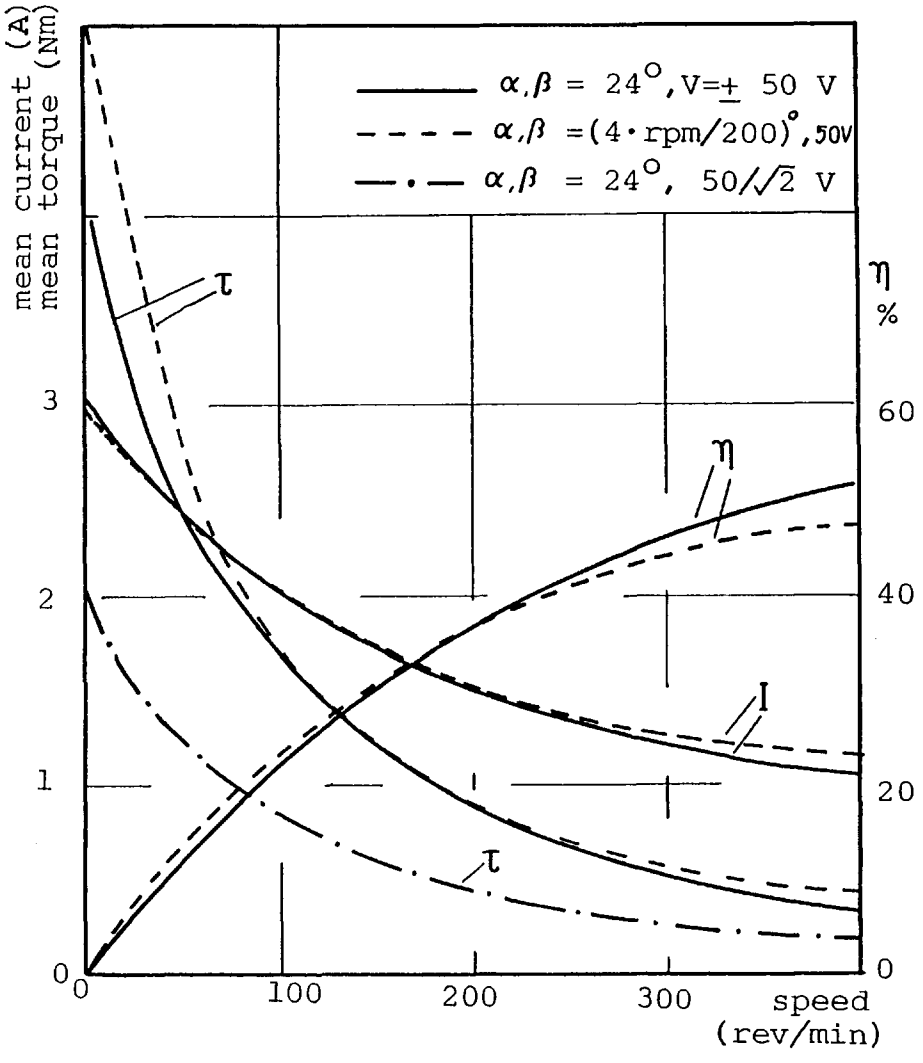

Fig. 4.3.14 Effect of supply voltage and switching angle variation on motor performance

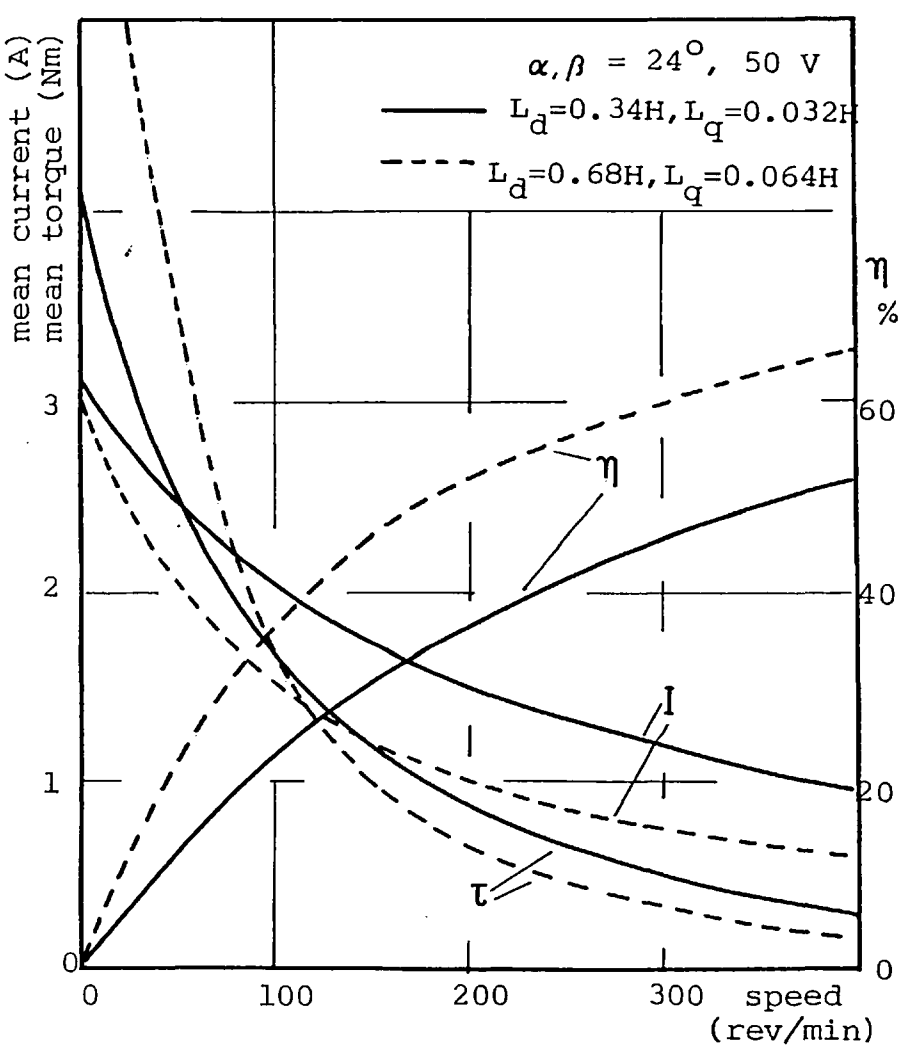

Fig. 4.3.15 Effect of decrease in airgap length

according to speed can improve the motor speed characteristic over the whole speed range as shown for a typical case. With large motors, it is almost essential to decrease supply volts in some way at low speeds. However in small motors, including the one used for these predictions, per unit coil resistance tends to be relatively high and this holds down mean currents and torque levels with fixed voltage d.c. rail and simple switching feed systems to somewhat lower value."

4.4 Motor performance with a.c. triac-fed circuit

4.4.1 The a.c. triac-fed system

In the a.c. feed system the excitation coil is supplied directly from the a.c. 50 Hz mains with a triac connected in series acting as a switching element. The triac firing signals are controlled both by the phase-delay angle (relative to the zero crossing point of the voltage supply), and by the sensor's switch on and off angles (relative to q and d position of the rotor).

Fig. 4.4.1 (a) shows the complete control circuit for the full-wave, single-pulse triggerring scheme used in the experiments.[4.5] This circuit was designed to meet the objectives of simple configuration and low cost. It was realised that these advantages would be to some extent offset by reduced motor performance.

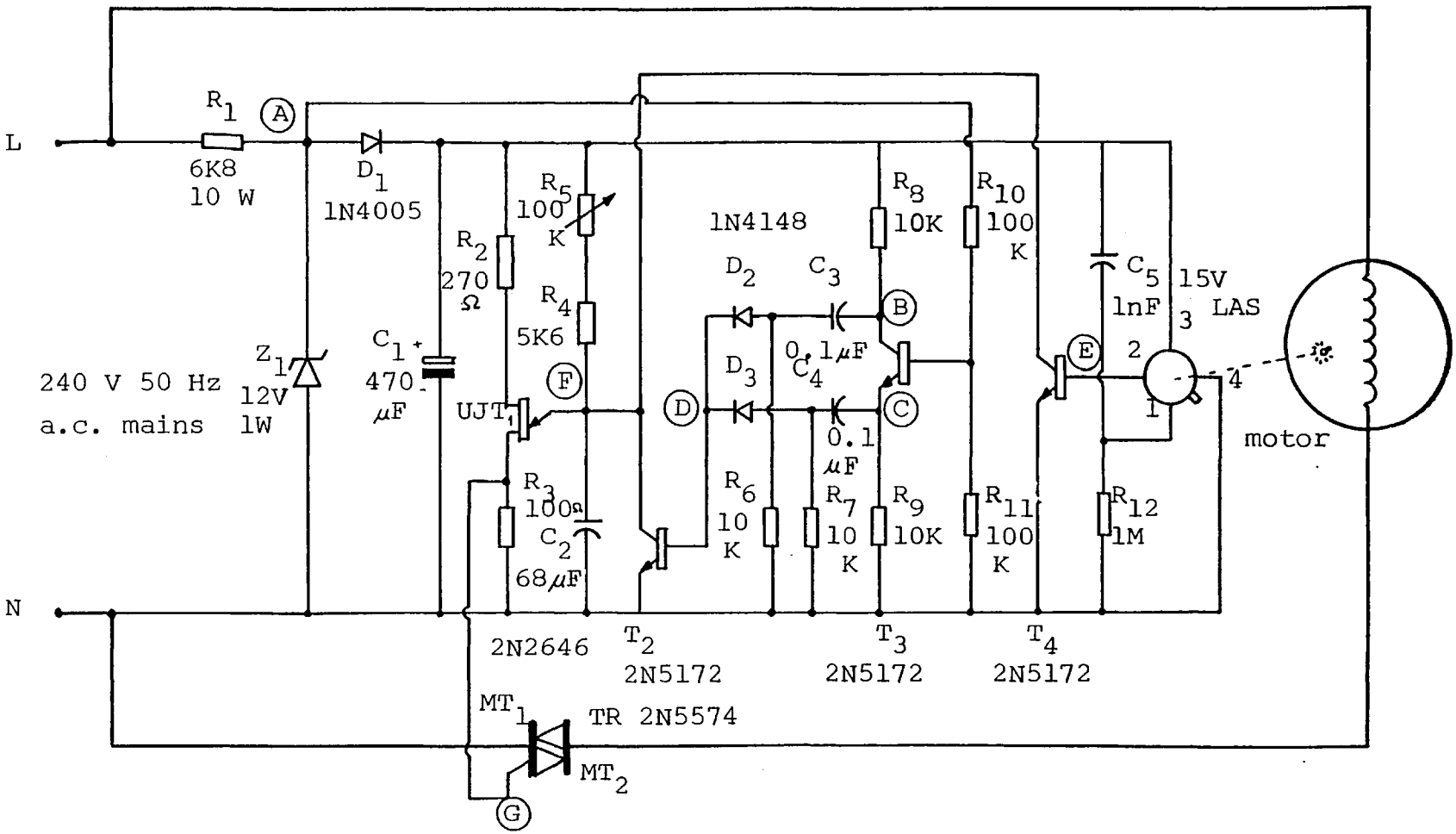

Fig. 4.4.1(a) Control circuit of a.c. triac-fed system

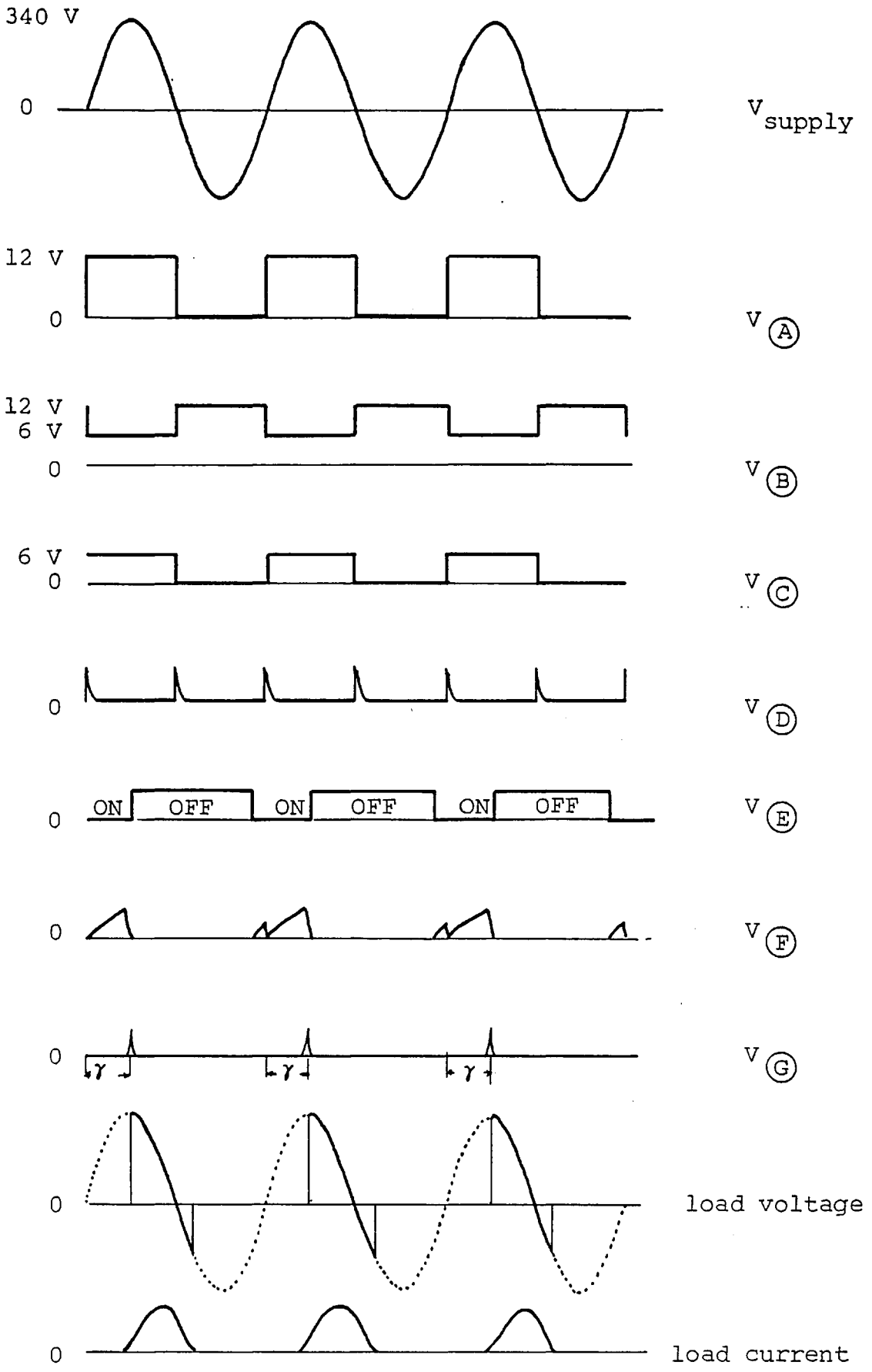

Fig. 4.4.1(b) Waveforms in the control circuit of a.c.triac-fed system

The main circuit consists of a single triac (2N5574) connected in series with the excitation coil. The triac rating chosen for the experimental purposes only is 15 A , 400 V. The triac was connected such that terminal MT_1 is at neutral to avoid high voltages in the non-isolated gate firing circuit. R_1 and zener Z_1 form a potential divider which transforms 240 V mains to 12 V. positive pulses. The voltage across the zener Z_1 is then fed through D_1 to the smoothing capacitor C_1 to provide the d.c. supply to the rest of the circuit. The 50 Hz, 12 V positive going square wave across the zener Z_1 serves as a reference signal for the phase delayed action. This signal is fed to the high gain amplifier with dual differentiator (T_3, C_3, C_4 and D_2, D_3) which produces pulses at both the rising edge and the falling edge of the square wave. The rising edge and the falling edge of the square wave clearly coincide with the zero crossing point of the a.c. mains voltage. R_4, R_5, C_2 and UJT_1 form a relaxation oscillator[4.6] with the period of 380 μS to 7 mS ($T = RC \ln \left(\frac{1}{1 - \eta} \right)$ and $\eta \simeq 0.63$ for UJT 2N2646).

The beginning of the period is controlled by the pulses from the differentiators via T_2 and the period is controlled by R_5. Hence, the firing signal is modulated with the synchronising signal from the position sensor at the base of UJT_1 which will short-circuit C_2 during the off periods and stop oscillation. The waveforms are shown in Fig. 4.4.1 (b).

It should be noted that although the circuit was called the single-pulse firing circuit, in fact the number of pulses produced in one half cycle varies according to the period set by R_4, R_5 and C_2. Fig. 4.4.2 (a) shows the ideal firing signal for the single-pulse circuit where only one pulse occurs in each half cycle regardless of the phase-delay angle. But in practice if the period of the relaxation oscilltor is at its minimum (380 μs which corresponds to 7 ^{o}elec delay angle) a train of 25 pulses appears at the gate (Fig. 4.4.2 (b)). On the other hand if the period of oscillation is set at maximum (7 mS, which corresponds to 126 ^{o}elec delay angle) only one pulse will appear in each half cycle (Fig.4.4.2 (c)). For phase-delay angles between these two extremes the number of pulses varies from 25 to 1. Variation in the number of pulses normally has no effect on the operation of the triac with ordinary a.c. power control because once the triac is fired the pulses that follow the first one will have no effect on the operation of the triac. But in switched reluctance motor operation, in which the firing signal is modulated with the synchronising signal, the train of pulses will increase the chances of burst firing in the 'on' periods. Its effect will be discussed later when the test results are compared with the predicted results.

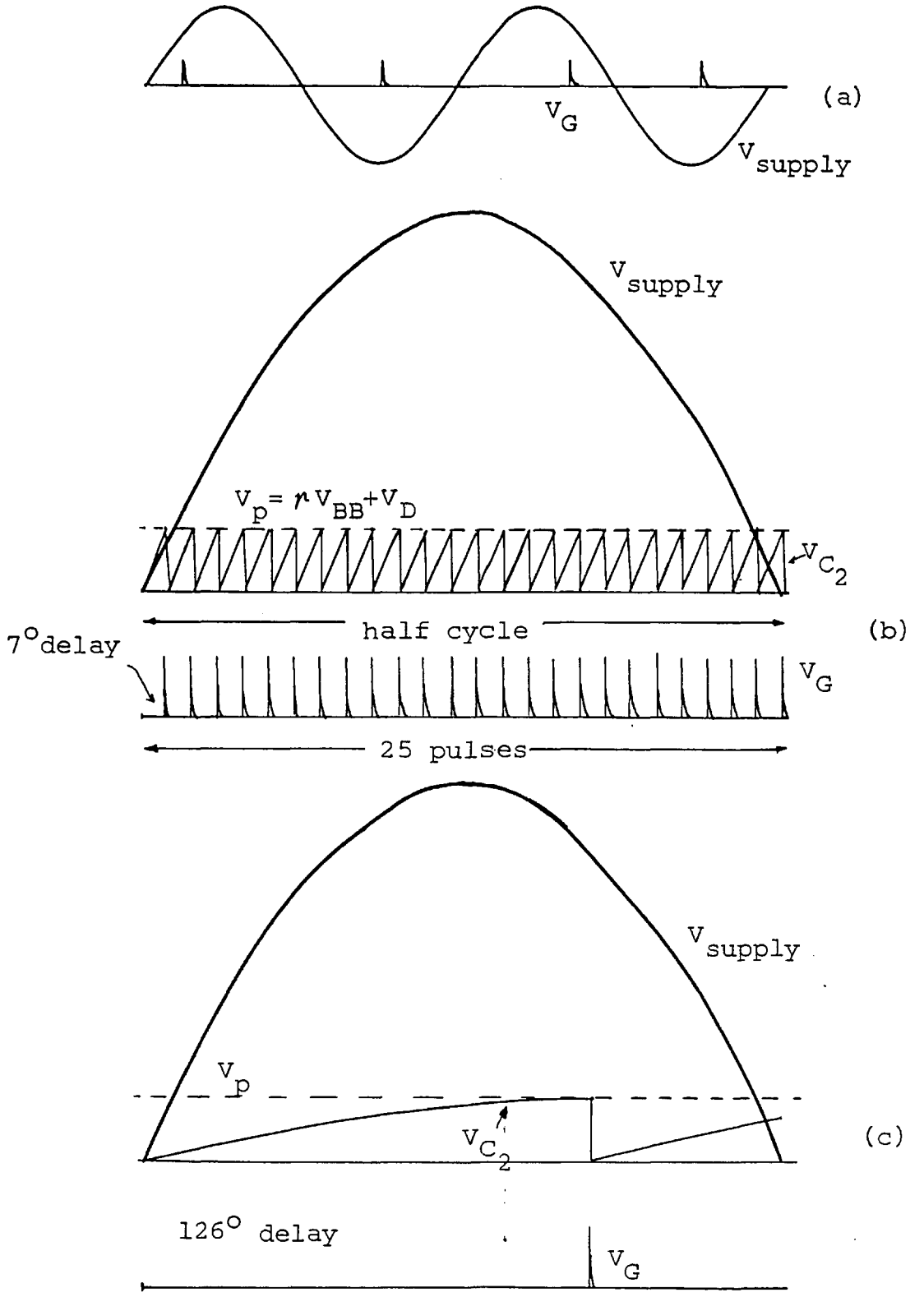

Fig. 4.4.2 (a) Ideal single-pulse firing signal
(b) Firing signal at minimum oscillating period
(c) Firing signal at maximum oscillating period

4.4.2 Load tests of low-speed 6-saliency motor with triac feed - effect of firing angle and switching angle variation

The same test rig was used in the experiments with two spring balances for measuring torque. The test circuit is shown in Fig. 4.4.3. In this case, the currents and power measured are the total currents and powers to the system (motor+drive).

Tests were carried out with two settings of switching angle, each with two different firing angles as follows:

1) $\alpha = 24^{\circ}$ and $\beta = 150^{\circ}$ with
   a) $\gamma = 18^{\circ}$
   b) $\gamma = 45^{\circ}$
2) $\alpha = 24^{\circ}$ and $\beta = 105^{\circ}$
   c) $\gamma = 36^{\circ}$
   d) $\gamma = 72^{\circ}$

For all cases, the voltage supply was set at 240 Volts.

Test results show that the triac-fed circuit with open-loop-phase-angle-control method would give stable operating points for most types of load, including the 'square law' fan load of the original specification. The coil voltage and the coil current waveforms are shown in Fig. 4.4.4, for $\alpha = 24^{\circ}$ and $\beta = 150^{\circ}$ with $\gamma = 0^{\circ}$.

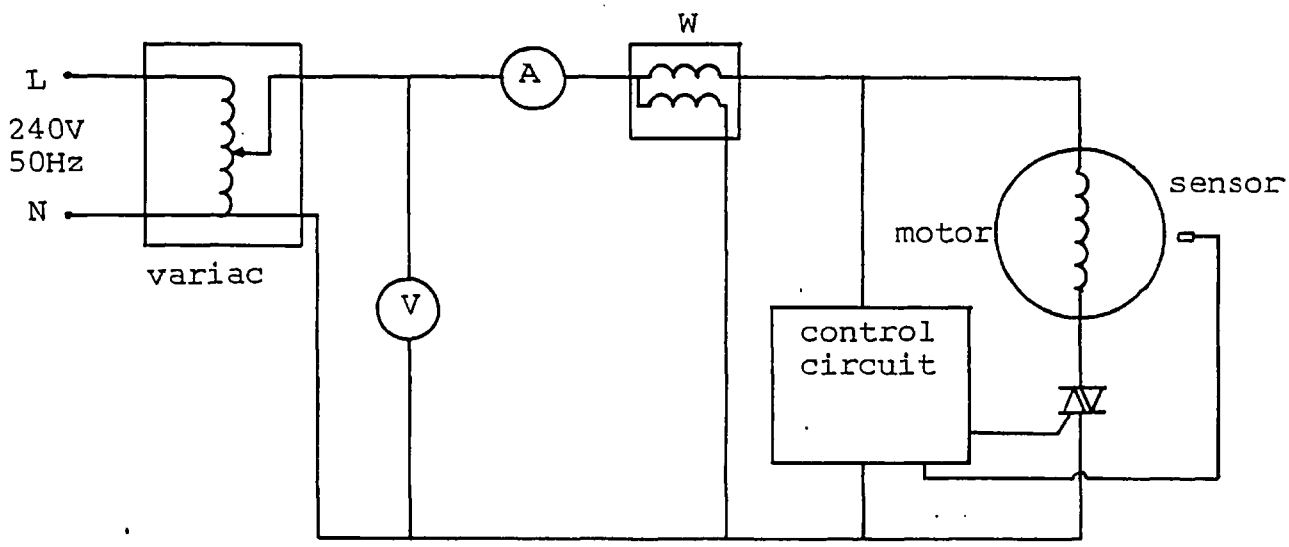

Fig. 4.4.3 Test circuit

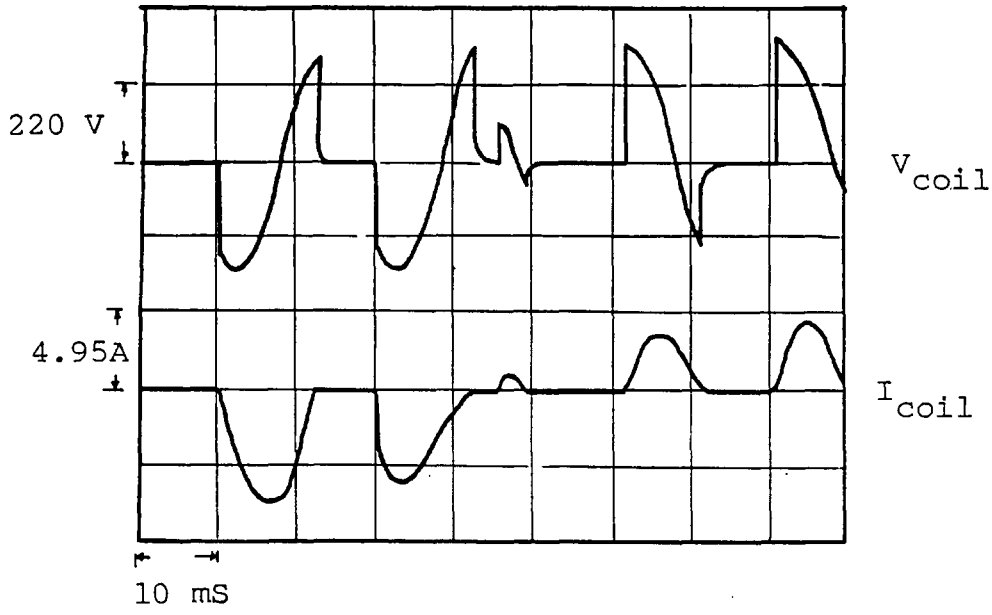

Fig. 4.4.4 The coil voltage waveform and the coil current waveform of the low-speed, 6-saliency SPSR motor at no-load with 240 V a.c.mains supply, the no-load speed was 580 rev/min

The switch-off angle β was deliberately set to a bigger value than in the d.c. link operation to compensate for the uncontrolled switch-off characteristic of the triac and to minimise the carry-over current. At this no-load speed (580 rev/min), the current waveform comprises both positive and negative pulses and is non-repetitive. It thus contains harmonics of a large range of orders. The sharp rising edges of the voltage waveform correspond to the commencement of the conduction state of the triac. At i=0 the voltage does not drop simultaneously to zero perhaps because of the effect of the stray capacitance of the winding.

4.4.3 Results and discussion

The mean torque, mean current, power output and efficiency characteristics of the 6 saliency motor for the tests at 240 V are shown at Fig. 4.4.5 and 4.4.6 for 1) $\alpha = 24^{\circ}$, $\beta = 150^{\circ}$ with $\gamma = 18^{\circ}$ (1a), $\gamma = 45^{\circ}$ (1b), and 2) $\alpha = 24^{\circ}$, $\beta = 105^{\circ}$ with $\gamma = 36^{\circ}$ (2c), $\gamma = 72^{\circ}$ (2d). Although the torque-speed curves are dissimilar from the d.c. series motor shape obtained with the d.c. link feed system, it can be seen that stable operation can be obtained for most load with fairly good variable speed characteristics. The maximum no-load speed is 560 rev/min. The operating condition of case 2c gives the highest output torques and the specified load of 1.1 N-m is obtained at 310 rev/min. The beating effect

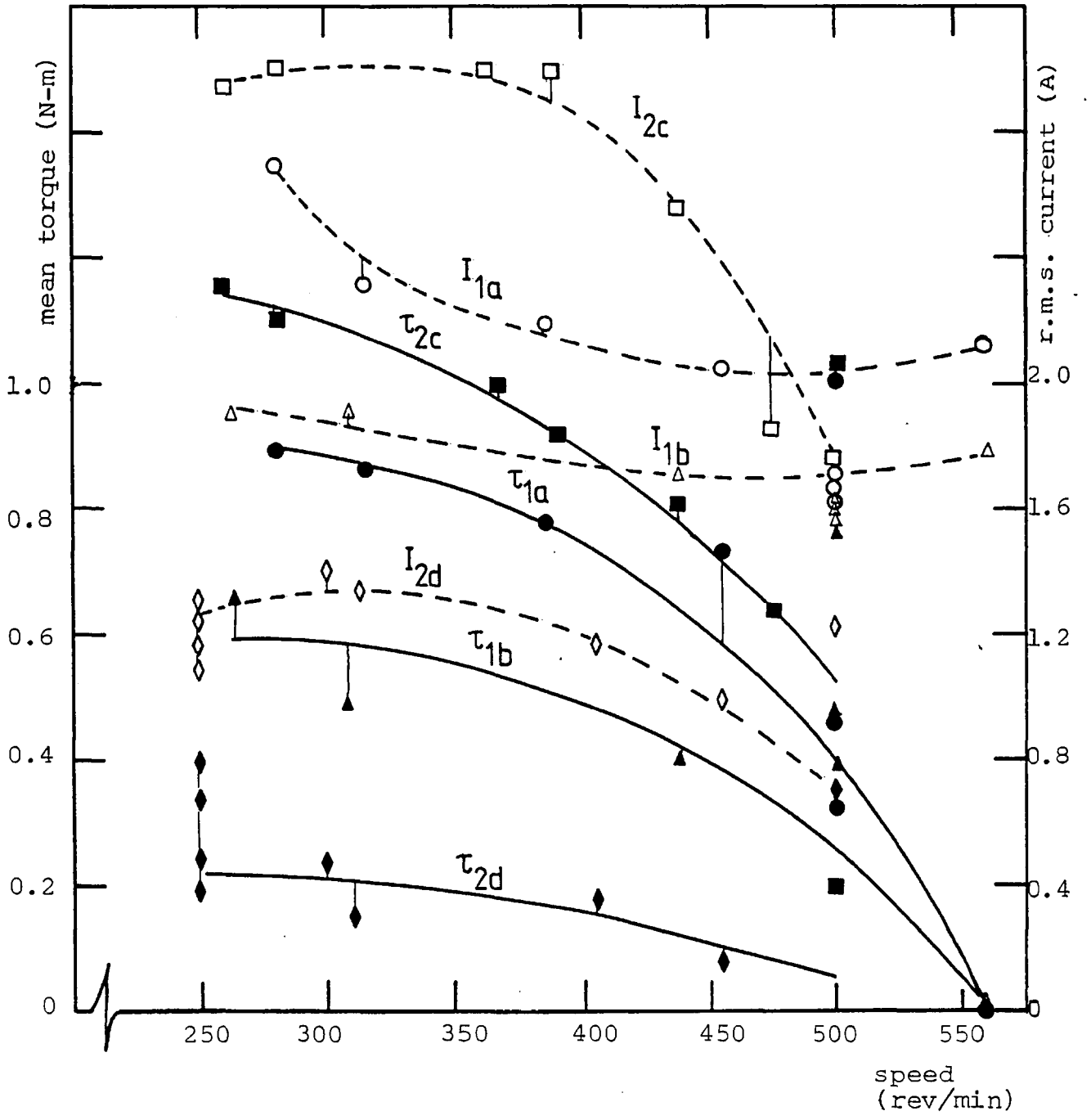

Fig. 4.4.5 Performance curves of 6-saliency motor with a.c. triac-fed circuit at 240 V mains
1. $\alpha = 24^{\circ}$, $\beta = 150^{\circ}$; 2. $\alpha = 24^{\circ}$, $\beta = 105^{\circ}$
a. $\gamma = 18^{\circ}$, b. $\gamma = 45^{\circ}$, c. $\gamma = 36^{\circ}$, d. $\gamma = 72^{\circ}$
——— torque - - - - - - current

(mentioned in chapter 3) occurs between the supply frequency and the switching frequency and 'quasisynchronous' speeds occur at 250 rev/min and 500 rev/min where the torque pulse repetitions are short (40 msec and 20 msec respectively). The wide range of average torques available these quasisynchronous speeds (0.3-1.0 N-m in case 1a at 500 rev/min) could be used with certain loads and/or mechanical transmissions to make a synchronous type drive system. The mean torques at other speeds vary with each setting of α , β and γ . For this set of tests, α $=24^{o}$, β $= 150^{o}$ seems to give too short an on-period and hence too low an output torque level, but it should be reminded that a large ' α ' produces higher negative torque pulses at low speeds while a small ' β ' will adversely affect the high-speed torque characteristic because of the carry-over currents.

The current levels do not change much over the test speed range for each case except at the quasi-synchronous speeds where the currents tend to vary linearly with load torques. The maximum output powers (Fig. 4.4.6) occur at about the same speed : 435 rev/min, and are 40, 35,18 and 7 watts for cases 2c,1a,1b and 2d respectively.

The overall efficiencies (motor+drive) are rather low (15-17%) because of the higher than normal level of iron loss. This in turn can be ascribed to the solid iron magnetic circuit and the high harmonic content in the coil current.

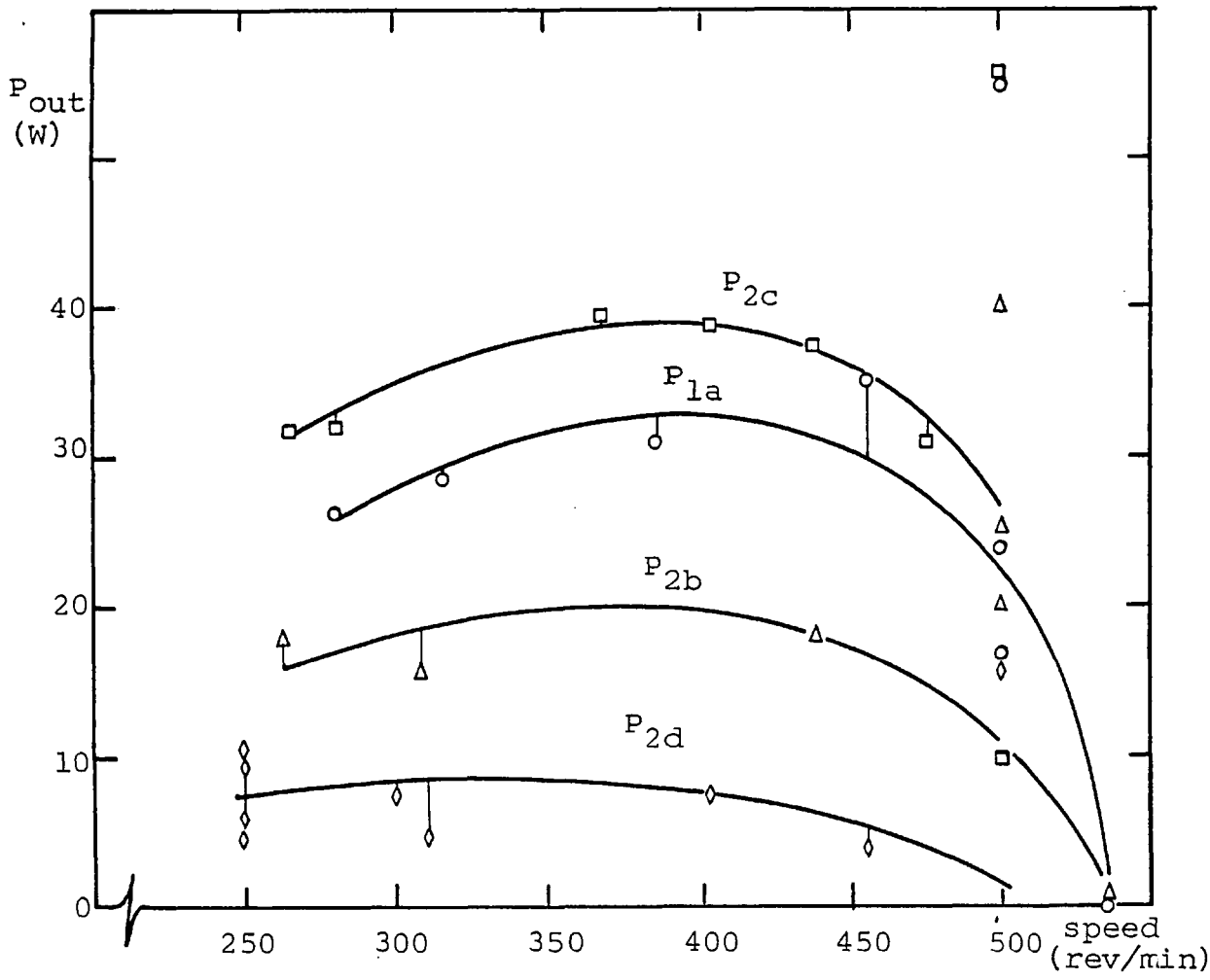

(a)

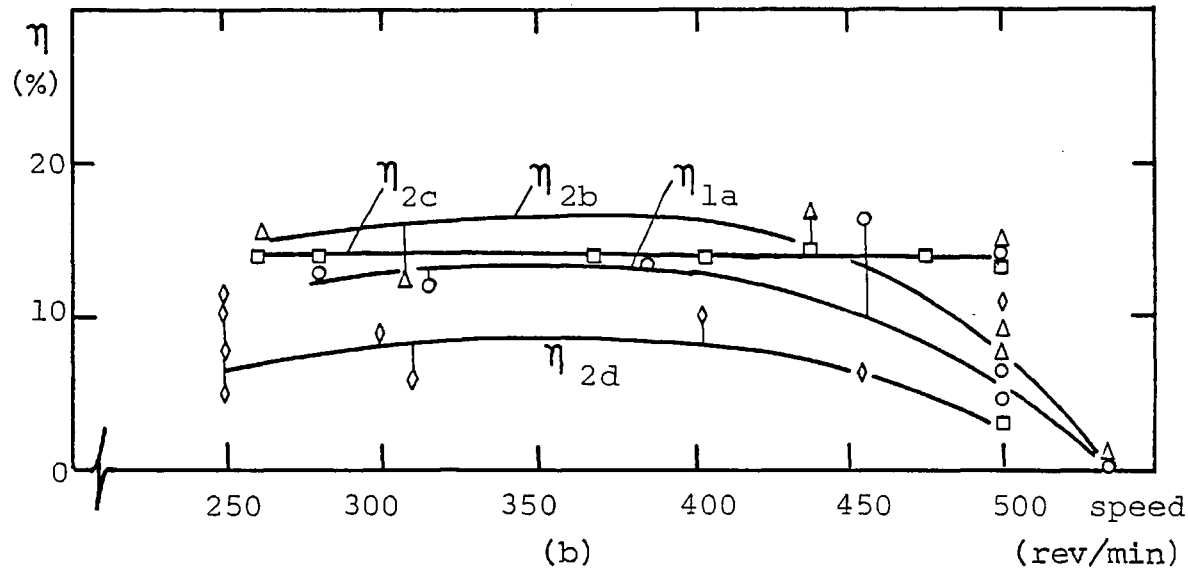

(b)

Fig. 4.4.6 (a) Power output speed characteristics
(b) Efficiency speed characteristic of 6-saliency SPSR motor with a.c. triac-fed circuit at 240 V (for subscripts see Fig. 4.4.5)

Predictions have been made using the method explained in section 3.3, with the machine parameters obtained in section4.2. In the computation an ideal, single-pulse firing signal was assumed for convenience. The torque-speed curve shown in Fig. 4.4.7 is the average of the results obtained from predictions with two values of voltage phase angle 'θ' ($\theta = 0^{o}$ and $\theta = 36^{o}$). The α , β and γ values used were the same as in case 1a whose measured results are shown in comparison. Since the prediction method neglects iron losses, friction and windage losses, the prediction mean torques would again be expected to be considerably higher than the measured values. However, the prediction assumes that only a single pulse rather than a pulse train is produced by the firing circuit and the number of predicted torque bursts are hence sometimes lower than the actual number of torque bursts particularly when 'γ' is small (as explained earlier). This produces a somewhat lower predicted mean torque for test speed region than would otherwise be the case.

Quasisynchronous phenomena are found at 500, 400, 300, 250, and 200 rev/min where the repetition period of the torque cycle is less than or equal to 5 cycles of the mains supply. The occurrence of a wide range of average torques at each quasisynchronous speed is similar to the behaviour of a synchronous motor and the effect of 'θ' on the mean output torque of the switched reluctance motor torque is comparable to the effect of torque

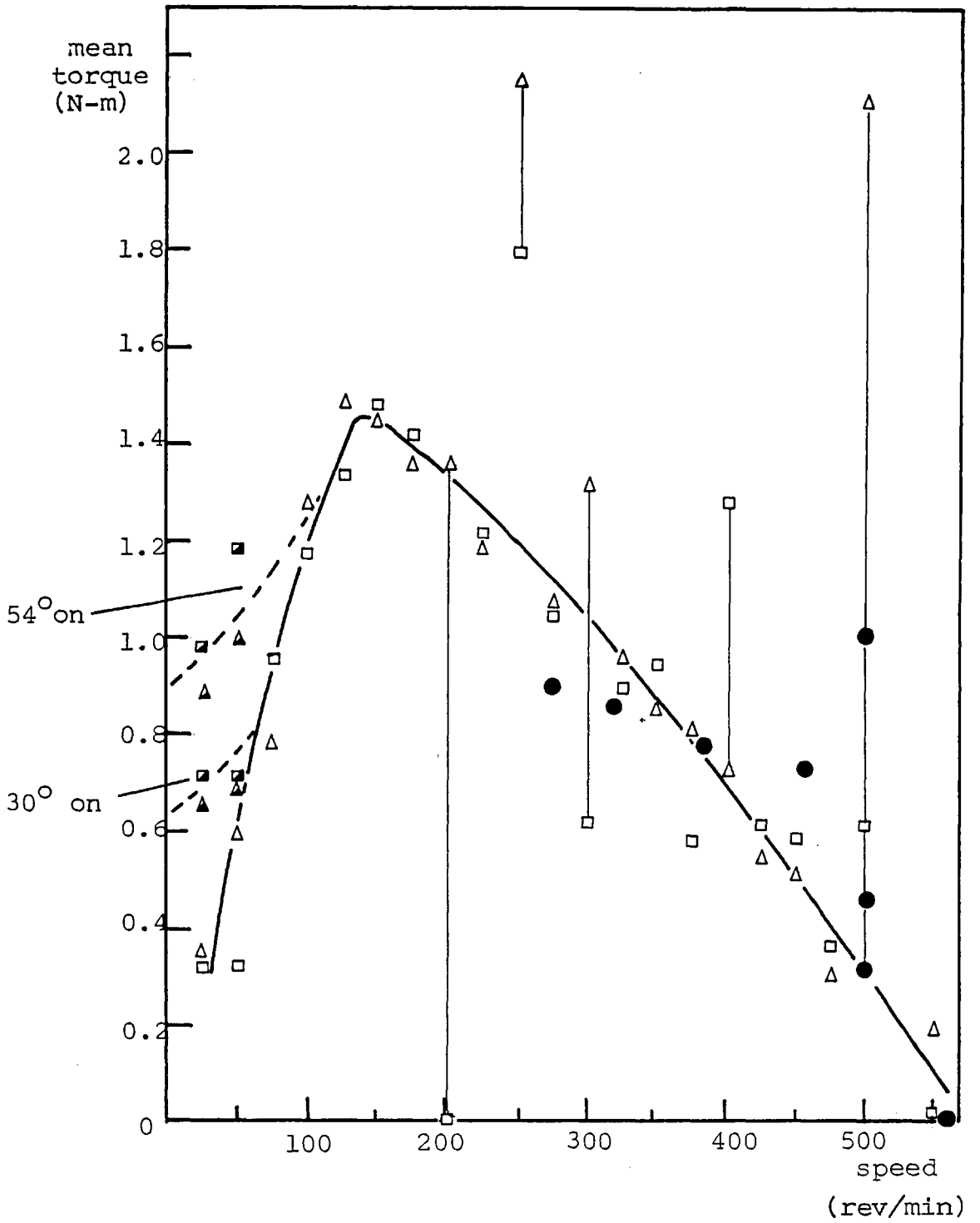

Fig. 4.4.7 Predicted torque-speed characteristic of the SPSR motor with a.c. triac-fed single-pulse trigger signal at 240 V, $\alpha = 24^{\circ}$, $\beta = 150^{\circ}$, $\gamma = 18^{\circ}$, □, $\theta = 0^{\circ}$, Δ, $\theta = 36^{\circ}$; ● measured results

------ improved performance at low speeds

54° on = $\alpha = 0^{\circ}$, $\beta = 126^{\circ}$

30° on = $\alpha = 0^{\circ}$, $\beta = 150^{\circ}$

angle in a synchronous motor. At other speeds where the period of torque cycles are more than 5 cycles of mains supply the effects tend to cancel out. Fig. 4.4.8 shows the variation of mean torque with 'θ' for quasi and non-quasisynchronous speeds. For non-quasisynchronous speeds, the maximum torque of 1.45 N-m occurs at 150 rev/min. At speeds lower than 150 rev/min, the average of the mean torques, surprisingly, drops sharply with decreasing speed. Investigation of the current and torque waveforms shows that this is because of the way that the switching angles have been set.

As explained previously, the switch-on angle 'α' was set to allow a high current build up in the positive torque region, while the switch-off angle 'β' was deliberately set to avoid 'carry-over' currents. This works well at relatively high speeds where the mechanical period is very much longer than the period of the supply frequency. At low speeds, however, the mechanical period is very much longer than the period of the supply frequency and with $\alpha = 24^{o}$ and $\beta = 150^{o}$ the on period is only 15% of the period of a mechanical cycle. Nearly 45% of this on period lies in the negative torque region (α). For example, at 50 rev/min both the mechanical period and the torque cycle are equal to 200 mS, and with $\alpha = 24^{o}$ and $\beta = 150^{o}$, the on period is only 30 mS and about 13.5 mS of this falls in the negative torque region. Hence there would be only one or two (at the

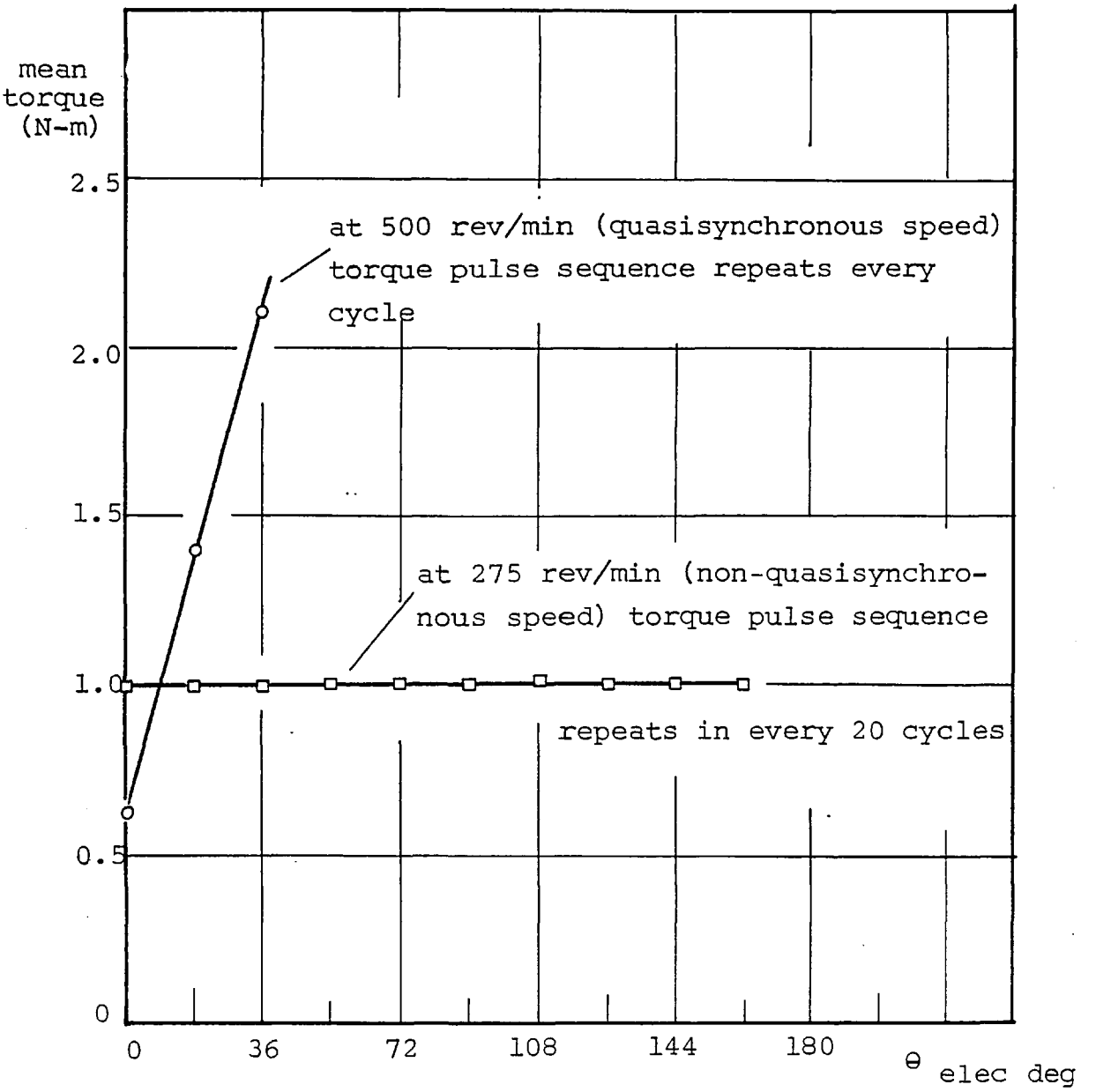

Fig. 4.4.8 Variation of computed mean torques at quasi- and non-quasi-synchronous speeds

maximum) pulses per pole or only 5 to 10 pulses per sec compared to about 50 pulses per sec at 500 rev/min (see Fig. 4.4.9). Furthermore about 45% of torque pulses produced are negative.

An improved low speed torque characteristic was found to be possible by setting $\alpha = 0^{o}$ and increasing β as speed decreased. Two low-speed torque curves with $\alpha = 0^{o}$ and $\beta = 30^{o}$ and 45° are shown in Fig. 4.4.7. At 25 rev/min, for example the average of the mean predicted torques were found to be increased from the original 0.32 N-m to 0.7 N-m and 0.95 N-m for $\beta = 30^{o}$ and 45° respectively.

Although it seems that the average mean torques are very low at low speed, in practice with inertia-only loading, the motor was found to be able to accelerate from standstill to maximum no-load speed without difficulty. The ability of motor to be able to accelerate well while outputting only a relatively low mean torque may be related to the fact that although the mean torques are low they consist of very large pulses of positive and negative torque and the rotor gains sufficient additional speed during a positive torque pulse to attain a speed where the mean torque is higher and hence able to maintain continuous operation.

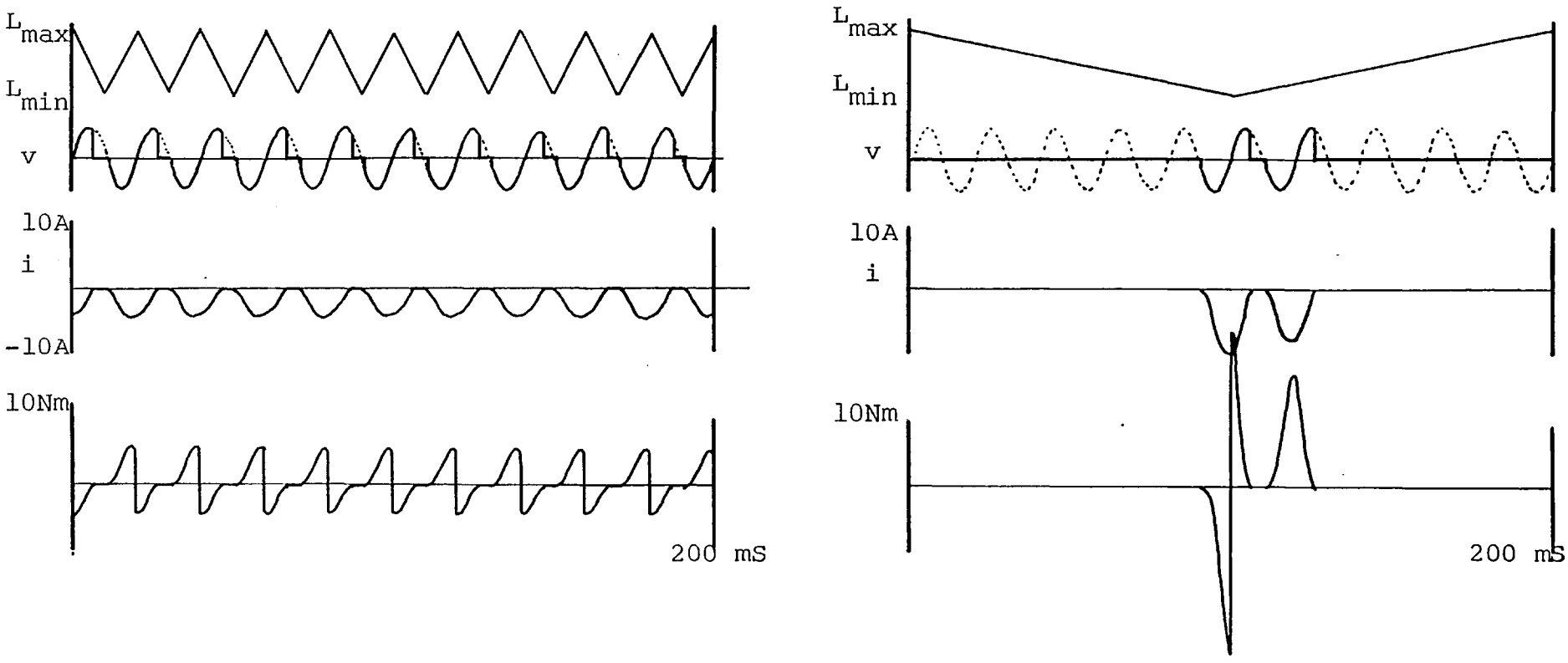

(a) at 500 rev/min (50 torque pulses/S)

(b) at 25 rev/min (10 torque pulses/S)

Fig. 4.4.9 Comparison between the number of torque pulses/second at high speed (a) and low speed (b) for single-pulse trigger a.c. triac operation at 240 V (predicted)

The predicted current and power output characteristics for the same operating condition are shown in Fig. 4.4.10 and 4.4.11. The average predicted mean coil current levels (shown in solid line) are lower than the measured values (shown in dots) for the same reason as explained in the torque-speed characteristics. The average predicted currents are also relatively constant over the whole speed range. With the decrease in average output torques at low speeds, the output powers also drop to very low values at speeds below 100 rev/min, the maximum predicted average power output (at non-quasisynchronous speed) is 37 W at 300 rev/min.

4.4.4 Theoretical investigation of the motor performance with 'd.c.' trigger firing circuit

As stated previously in section 3.3, the use of a 'd.c.' trigger firing signal (where each firing pulse consists of a single square-wave pulse lasting to the end of the mains half cycle) can give the best operation of a triac-controlled circuit, particularly when the load is significantly inductive and particularly in this drive system where an opto 'enable' signal of uncertain duration also plays a part in the control circuit. The previous theory assumed 'single-pulse' firing signal and it has been explained and demonstrated how this leads to generally pessimistic torque predictions of operation with the usual

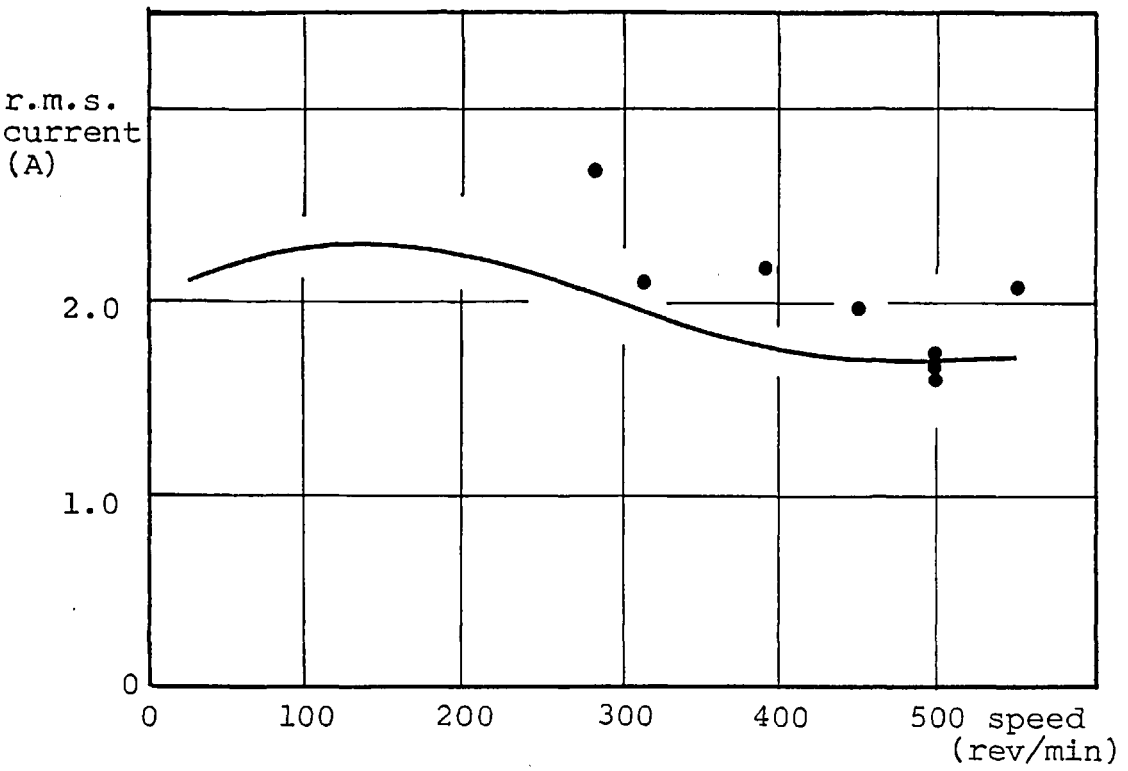

Fig. 4.4.10 Predicted current-speed characteristic for the same operating condition as in Fig. 4.4.7, • measured results

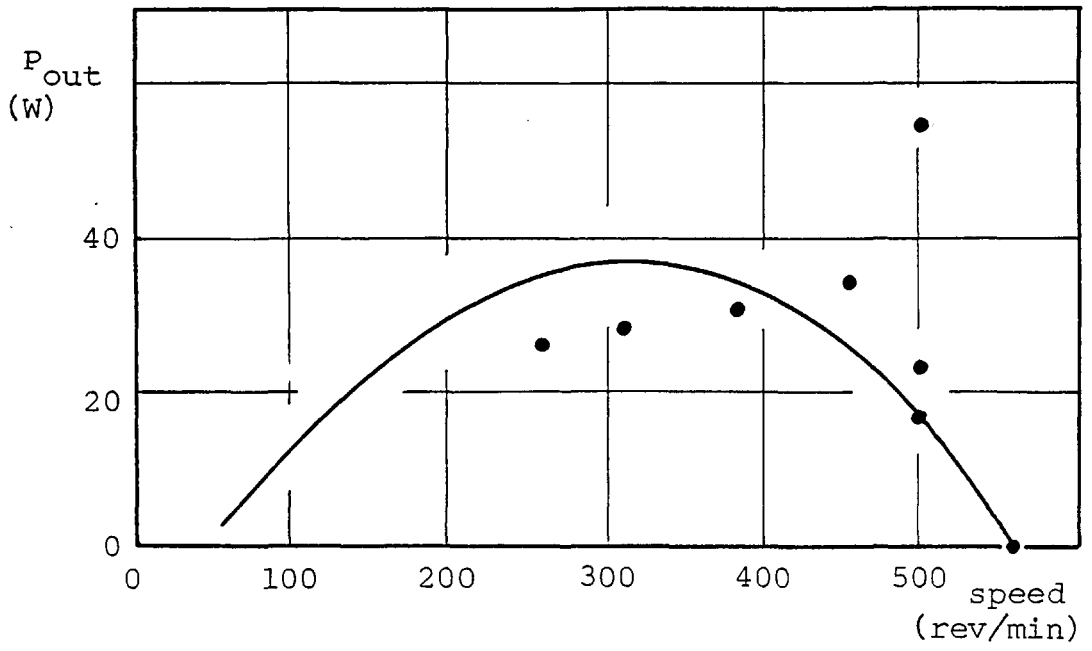

Fig. 4.4.11 Predicted power output-speed characteristic for the same operating condition as in Fig. 4.4.7, • measured results

'pulse-train' firing signals. Since the experimental feed circuit did in fact incorporate a 'pulse-train' firing circuit, rather than a single-pulse circuit, it was obviously desirable to make new predictions based on a different firing basis. Rather than attempting to simulate the exact operation of the pulse-train generator, predictions were made assuming that the trigger signals were of the 'd.c.' type. The only error caused here is likely to be due to the fact that the commencement of triac conduction in the real case can occasionally be slightly delayed when the synchronising signal (opto-sensor) switches to the enable state just after the end of one of the pulses in the train. The pulse-train frequency was approximately 2.5 KHz (see Fig. 4.4.2(b)) so the maximum delay (assuming negligible pulse-width) would be only 0.4 mS or 7° on the 50 Hz waveform. This was not considered to be likely to cause significant prediction error.

Fig. 4.4.12 shows the predicted torque-speed characteristic (the average of the mean torque with two different voltage phase angles 'θ') of d.c. trigger operation in comparison with single-phase operation, for the same operating voltage. Improved output torque levels can be seen clearly at high speeds (approximately 0.4 N-m gain in output torques in the speed range between 300 rev/min and 500 rev/min) resulting from the higher number of torque bursts with the d.c. trigger triac scheme.

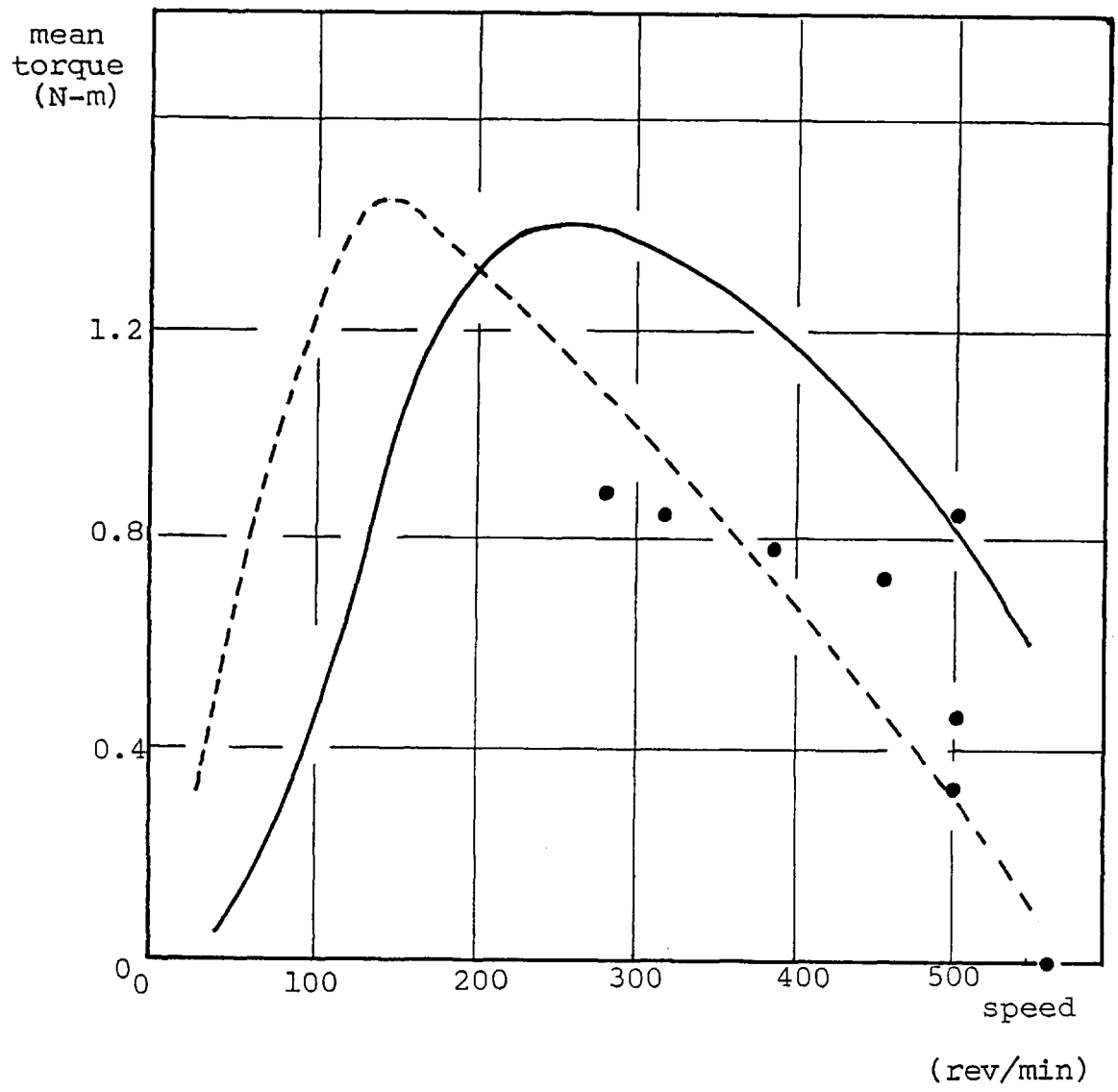

Fig. 4.4.12 Comparison between the average of the mean predicted torque versus speed of the motor with d.c. trigger firing signal and single-pulse firing signal at 240 V for the same switching angles and firing angle ($\alpha = 24^{\circ}$, $\beta = 150^{\circ}$, $\gamma = 18^{\circ}$)

———— d.c. trigger

- - - - - - single-pulse trigger

● measured results with pulse-train trigger

The maximum output torque of 1.4 N-m occurs at 250 rev/min and is comparable with the maximum torque with the single pulse scheme. At low speeds, torque levels are lower for d.c. trigger scheme. Although this is partly due to the rather large ' α ' and ' β ' settings as explained in the previous section, the main factor is likely to be that the d.c. trigger scheme creates more negative torque bursts at low speed. The predictions with d.c. trigger scheme can be seen to agree with the measured results better than the 'single pulse' scheme as expected. Higher predicted values are obviously due to the neglect of iron losses, friction and windage losses in the computation.

The comparisons are also made between r.m.s. currents and efficiencies in Fig. 4.4.13 and 4.4.14. The predicted motor efficiencies do not improve much with the d.c. trigger scheme. The predicted motor maximum efficiencies (iron, friction & windage losses neglected) for non-quasisynchronous speeds occur at 375 rev/min and are approximately 42% for both cases. Higher efficiencies can be expected at quasisynchronous speeds.

4.4.5 Mains Harmonics with triac-fed circuit

Another important factor apart from the general performance (power, circuit, efficiency etc.) concerning the use of the switched reluctance motor with an 'a.c.' triac-fed circuit is the harmonic contents of the current

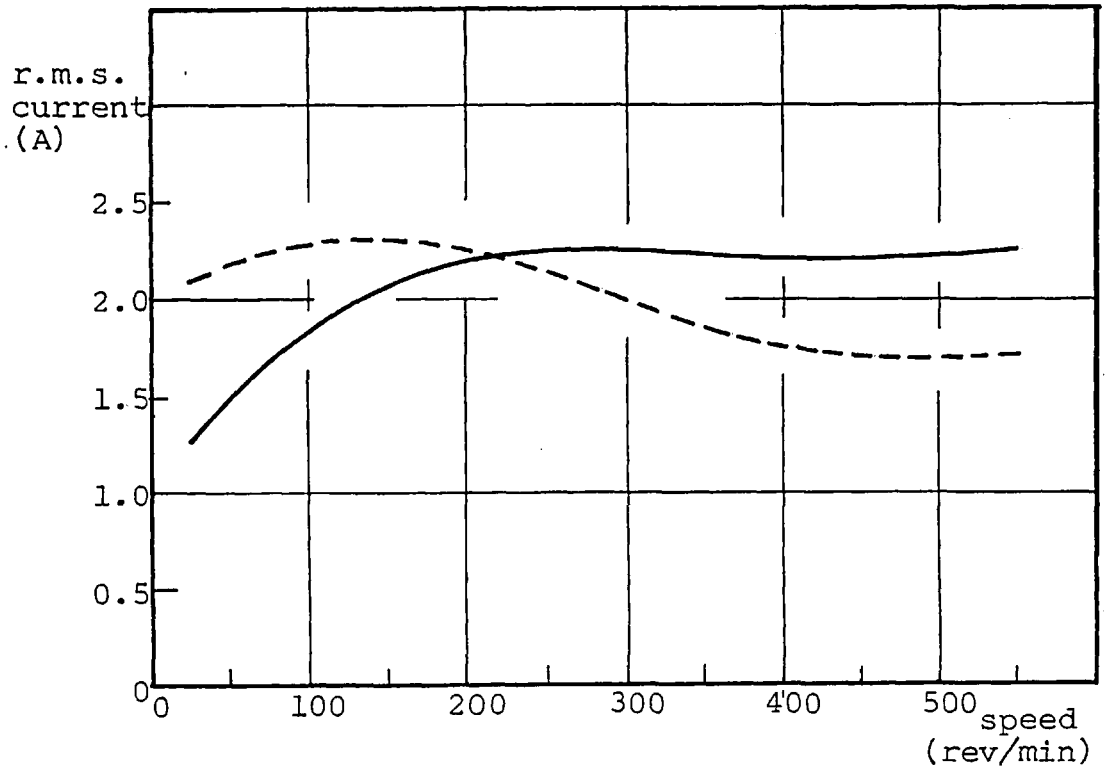

Fig. 4.4.13 Predicted average r.m.s. current curves

——— d.c. trigger

- - - - - - single-pulse trigger

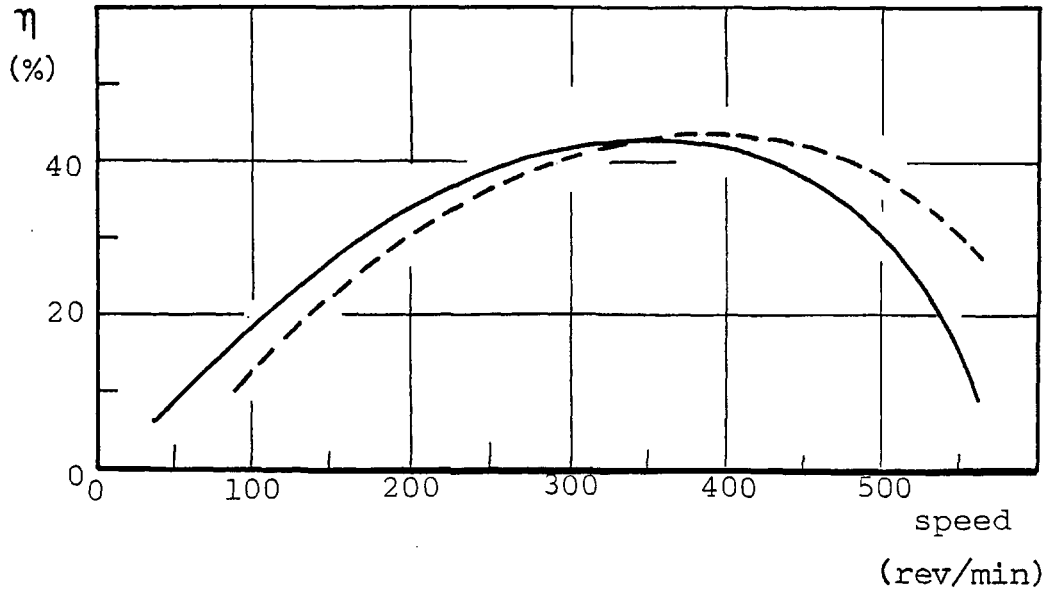

Fig. 4.4.14 Predicted average motor efficiency curves

——— d.c. trigger

- - - - - - single-pulse trigger

waveform supplied to the motor. The regulations and recommendations covering the allowable magnitudes of harmonic currents supplied to thyristorised and other nonlinear equipment connected to the mains are given in references 4.7-4.10.

As stated in reference 4.11: "In the case of a single-phase switched reluctance motor supplied from the mains with a.c. triac control, the current contains harmonics of a large range of orders from d.c. upwards and although it is similar to the current drawn by half-wave, full-wave and phase angle controlled rectifiers, burst-fired and phase-controlled a.c. regulators and arc-furnace loads often of substantial powers ratings, the fact that it is a single phase load and the relatively large harmonic amplitudes means that harmonic effects must be considered at an early stage."

In assessing whether the harmonics amplitudes fall below the recommended limiting values, the whole range of operation has to be tested for both current harmonics of frequencies greater than 50 Hz and those on 'voltage fluctuations' for the subharmonic currents. Difficulties arise because of the very wide variety of current waveforms occuring as speed, switching angles, firing angles and also voltage phase angle 'θ' vary. A full investigation would hence be very difficult and time-consuming. This section deals with some preliminary work

that has been done in assessing harmonics levels for some typical speeds and operating conditions. The regulations laid down in B.S. 5406 were consulted as a guideline for assessment procedures and limitations. The assessment here is made on predicted rather than measured current waveforms partly because of the difficulty in obtaining suitable measuring and recording equipment complying with the recommended specification.

Fig. 4.4.15 shows the predicted current waveform of the motor with 240 V mains supply, α =24°, β =150°, γ =18° and θ =0° at a speed of 550 rev/min and delivering 26 W power output. This is typical of those for operation at non-quasisynchronous speeds and reasonably high switching frequencies. (Section 5.4.3.7 confirms that predicted/measured waveform correlation is generally quite good.)

Fourier analysis of the waveform can be made by a standard package.[4.12,4.13] The result obtained from the most basic analysis method[4.14] is shown in Fig. 4.4.16. The harmonics amplitudes are shown as percentages of the fundamental (5 Hz). For this particular operating condition the harmonics range from d.c. upwards. The maximum amplitude occurs at 5 Hz, this being the beat frequency between the supply and the switching frequencies (and the frequency of torque cycle). The next dominant frequency is that of the supply : 50 Hz. The higher order

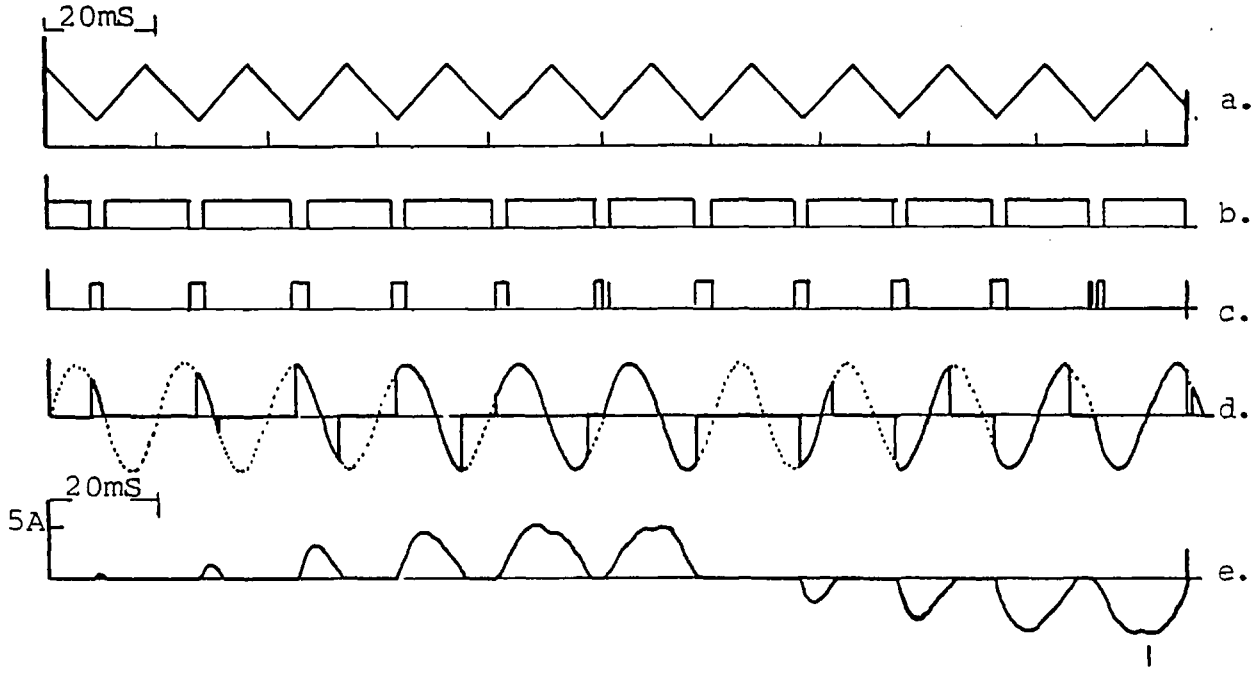

a. inductance, b. switching signal, c. gate signal,
d. load voltage and e. load current

Fig. 4.4.15 Computed load voltage and load current of the motor with a.c. triac d.c. trigger feed circuit at 240 V, 550 rev/min, 26 W

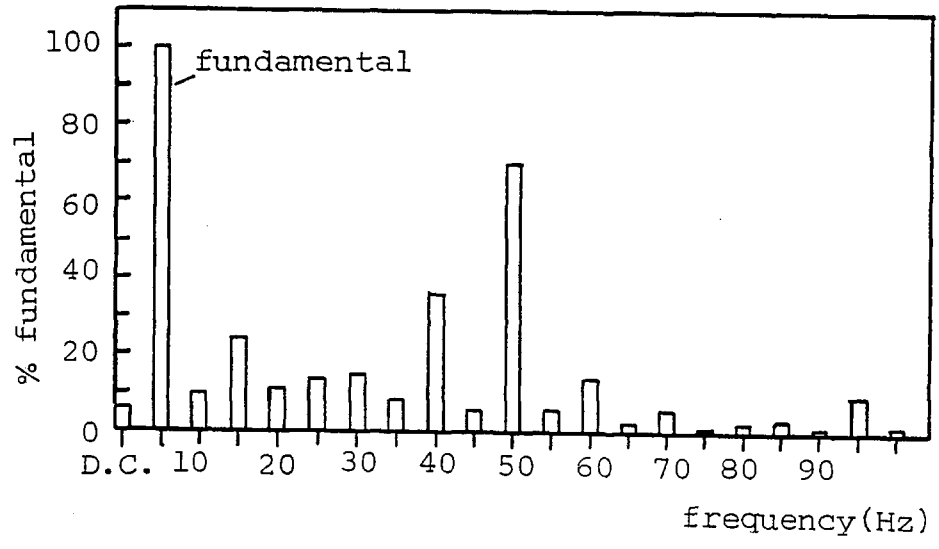

Fig. 4.4.16 Harmonic amplitudes of the above motor current

harmonics are relatively small in amplitude.

In accessing the acceptability of these harmonic amplitudes, reference is made to B.S. 5406. This makes a number of relevant statements as follows:

" a) General considerations:

The use of phase control system is prohibited for control of the power of heating elements in thermal appliances. However, this prohibition does not apply to : a) appliances having a rated power not exceeding 200 W and b) motor controls, but they must comply with the limits in harmonics and voltage fluctation.

b) Harmonics of the current

The harmonics of the current input to the appliance shall be such that if the appliance were to be connected to the artificial network as shown in Fig. 4.4.17 and supplied at nominal voltage, the resulting harmonic content of the phase-to-neutral voltage of the artificial network would be equal or less than the values shown in Table 4.2.

The voltage harmonic content of order n, H_n, resulting from an appliance is calculated as indicated by the following formula:

For single phase appliance 220 V (240 V) rated voltage

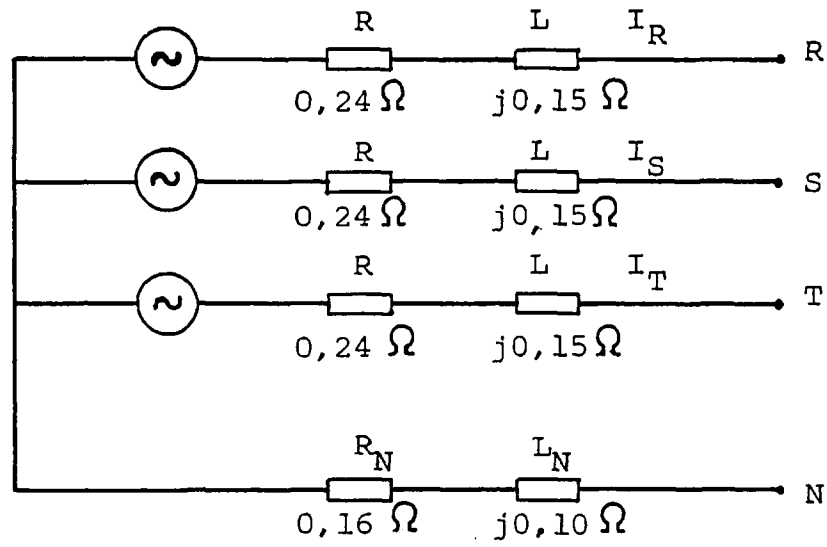

The impedance of the phase-neutral loop is:

$Z_1 = (0,40 + j0,25)\ \Omega$ at 50 Hz

Fig. 4.4.17 Artificial network

Table 4.2

	Harmonic Order (n)	Maximum harmonic content (%)
odd harmonics	3	0,85
	5	0,65
	7	0,60
	9	0,40
	11	0,40
	13	0,30
	15	0,25
	"	"
	"	"
	39	0,25
even harmonics	2	0,30
asymmetrical control	4	0,20
	"	"
	"	"
	40	0,20

$$H_n = \frac{100 \sqrt{(0,40)^2 + n^2.(0.25)^2}}{U} I_n \quad \%$$

where n is the order of the harmonic concerned;

H_n is the voltage harmonic content of order n resulting from the appliance, existing between phase and neutral of artificial network, in %;

I_n is the r.m.s. value of the harmonic component of order n of the line current supplied to the appliance, in amperes;

U is the r.m.s. value of the voltage applied between phase and neutral in volts, corresponding to the nominal voltage of the appliance considered."

Table 4.3 compares the harmonic contents 'H_n' calculated for three motor operating points (with 240 V supply and $\alpha = 24^\circ$, $\beta = 150^\circ$, $\gamma = 18^\circ$ and $\theta = 0^\circ$) with the recommended limits. For these three cases (high speed, speed for maximum output power, low speed) all harmonics content shown fall below the recommended limits. Higher order harmonic currents are very small and can be negligible.

c) Voltage fluctuation

The voltage fluctuation is assumed to be caused by the (subharmonic) pulses of current and is of the type 'a' (as defined in B.S. 5406) in which the intervals between

Table 4.3 Harmonics contents of higher order

speed rev/min	harmonic order(n)	I_n rms (A)	H_n calculated (%)	H_n limit (%)
100	2	0.0493	0.013	0.30
	3	0.0436	0.015	0.85
	4	0.0395	0.017	0.20
	5	0.0063	0.003	0.65
250	2	0.1193	0.032	0.30
	3	0.0657	0.023	0.85
	4	0.0172	0.007	0.20
	5	0.0241	0.013	0.65
	6	0.0379	0.024	0.20
550	2	0.0095	0.002	0.30
	3	0.0395	0.012	0.85
	4	0.0148	0.006	0.20

resultant voltage changes are regular and the magnitude is nominally constant. The voltage changes caused by the appliance can be calculated from the following formula where:"

-underlined quantities denote vector quantities (e.g. $\underline{U}$ is a voltage vector). Quantities between bars are resultant vector lengths (e.g.: $|\underline{U}_2|$).

-suffix 1 refers to the condition when current is not flowing.

-suffix 2 refers to the condition when current is flowing.

For a single-phase appliance of 220 V (240 V) nominal voltage (see Fig. 4.4.18)

$$\frac{\Delta U}{\underline{U}_1} = \frac{100\ |(0,4+j0,25)\underline{I} + \underline{U}_2| - |\underline{U}_2|}{|(0,4+j0,25)\underline{I} + \underline{U}_2|} \quad \%$$

where:

$\frac{\Delta U}{\underline{U}_1}$ is the relative resultant voltage change in % of the no load voltage $\underline{U}_1$;

$\underline{U}_2$ is the voltage at the terminals of the appliance when current is flowing;

$\underline{I}$ is the current supplied to the appliance.

It is suggested that normally the magnitude and the phase angle of the current input is obtained from the nominal rating and the power factor of the apparatus,

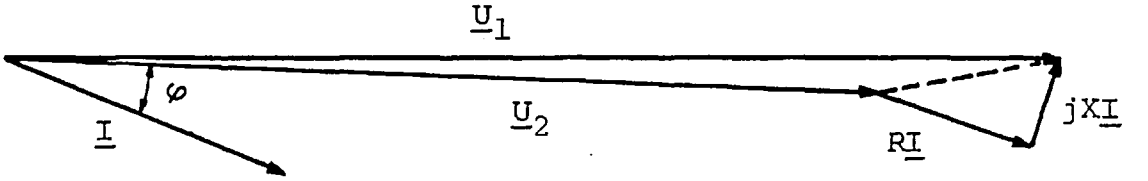

$$R + jX = (0,4 + j0,25)\ \Omega$$

Fig. 4.4.18 Phasor diagram for voltage changes calculation for single-phase appliance of rated voltage 220 V (240 V)

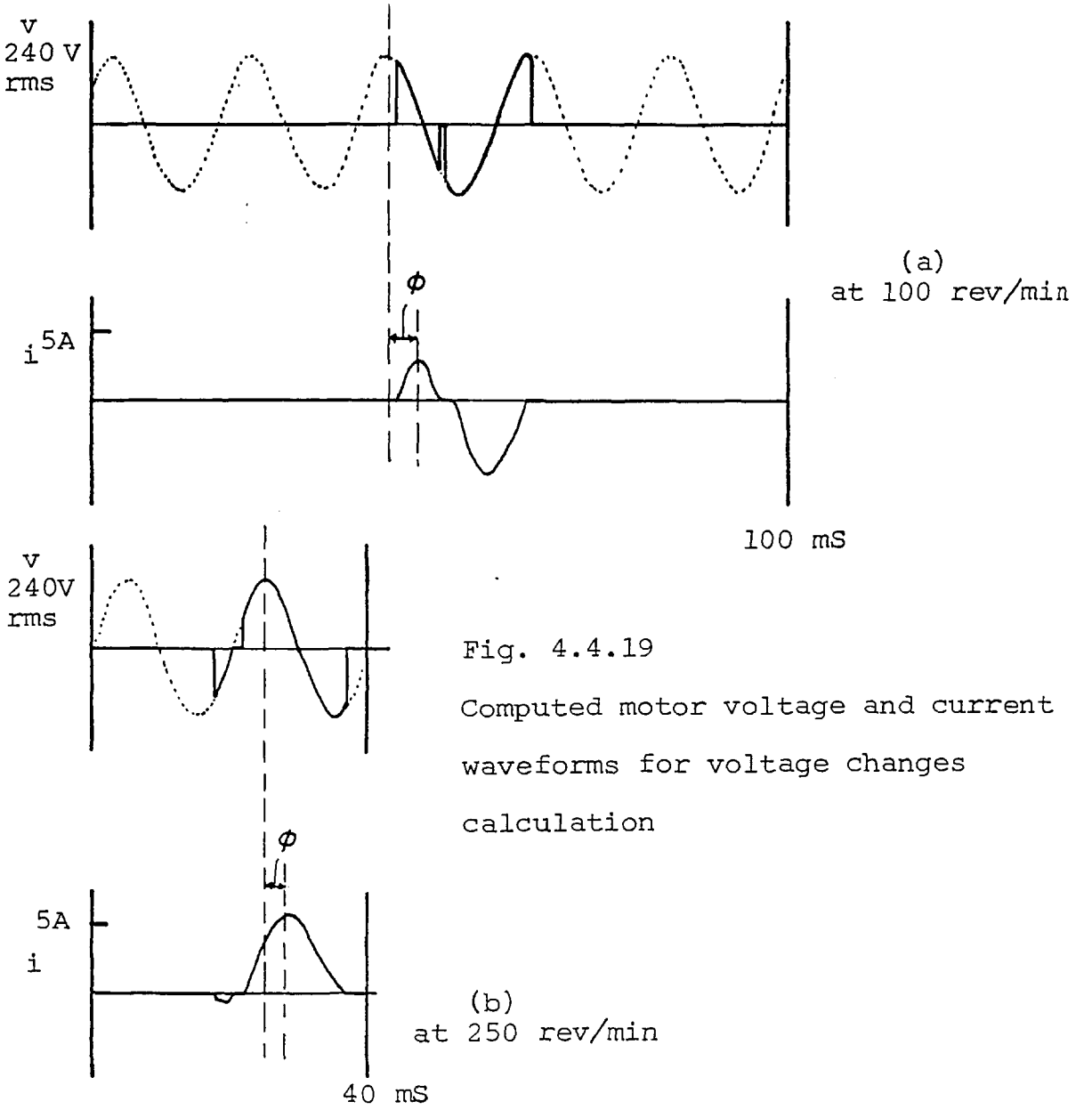

Fig. 4.4.19
Computed motor voltage and current waveforms for voltage changes calculation

and the value of $\underline{U}_2$ is set at 240 V . However, because of the unusual current pattern that occurs in the SPSR motor (Fig. 4.4.19) the following assumptions will be used to simplify the calculation:

1) The magnitude of the current is calculated from the actual root mean square of the current pulse.
2) The phase angle is the relative angle of the current pulse with respect to the corresponding voltage pulse.
3) The number of voltage changes per minute is equal to the number of current pulses per minute.

On the above assumptions, the magnitude and phase angle of the input currents and the number of voltage changes per minute for the two speeds of 100 rev/min and 250 rev/min are:

speed rev/min	I A	ϕ deg (lag)	γ changes/ min
100	2.84	72	600
250	3.24	54	1500

For operation at the designated high speed (550 rev/min) the current waveform in Fig. 4.4.15 shows that the period of time between two successive changes is less than 40 mS and the two changes are considered as one.

Comparisons between the calculated resultant

voltage change in % and the maximum permissible magnitude of relative voltage changes at the particular fluctuation frequencies are shown in Table 4.4.

Table 4.4

speed	calculated value	maximum permissible value
rev/min	%	%
100	0.419	0.43
250	0.579	0.45

For this particular case, the voltage fluctuation at 100 rev/min is less than the maximum permissible value but at 250 rev/min is greater by about 28%. It should be noted that the number of changes that occurs in the case of 250 rev/min is corresponding to the maximum number of changes examined in the B.S. 5406 (see Fig. 4.4.20).

d) d.c. components

B.S. do not give limits for the d.c. component of input currents, so no assessment has been made here. However B.S. state that such limits are under consideration so d.c. current levels may need examining at some stage in the future.

Overall it would seem therefore that for the specific drive system and operating conditions considered, the higher order harmonic currents are within maximum

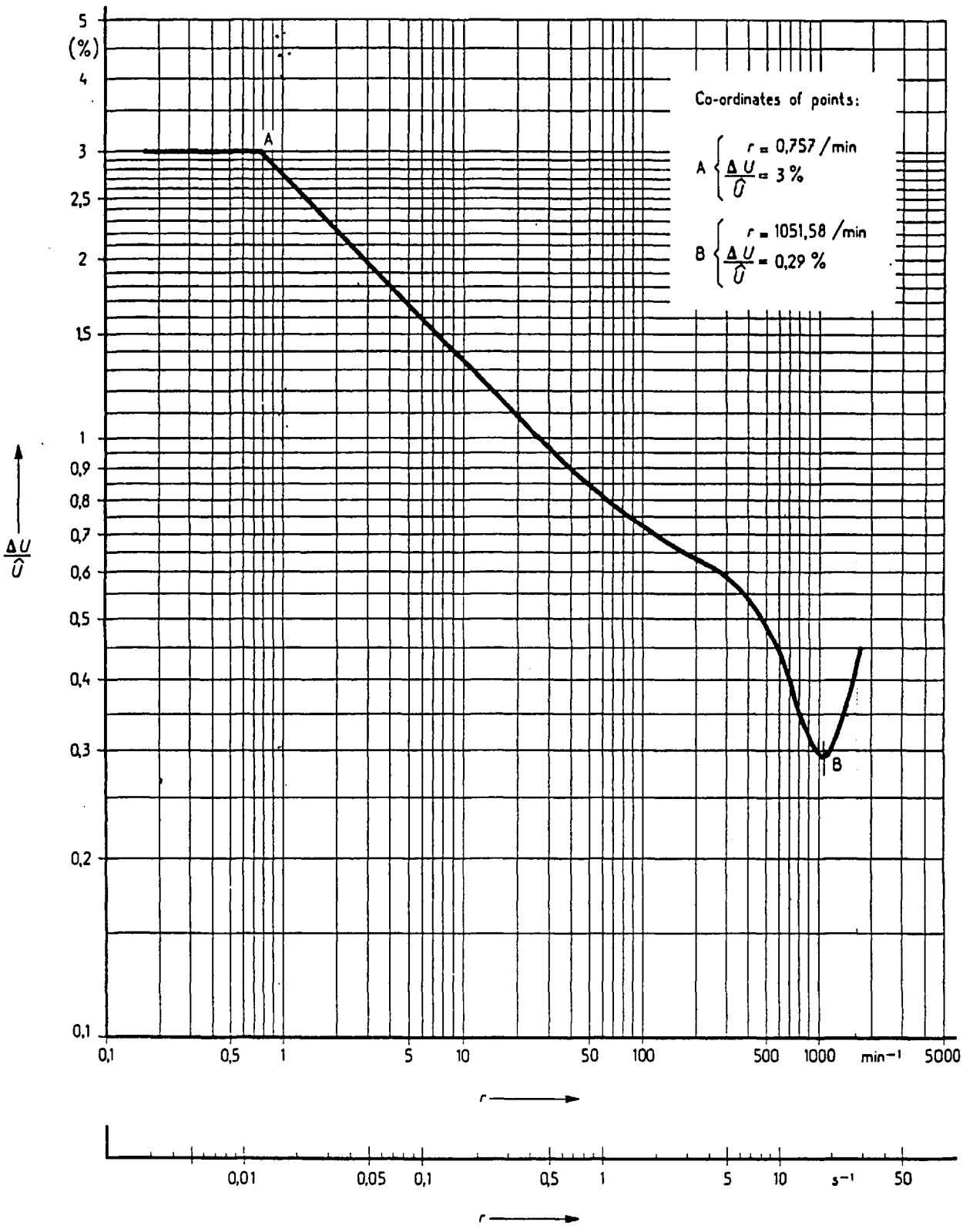

Fig. 4.4.20 Magnitude of maximum relative voltage changes with respect to number of voltage changes per minute or per second (reproduced from B.S.)

permissible limits. The voltage fluctuation effects might exceed the maximum permissible values for certain parts of the operating speed and load range. This suggests that maximum output ratings of the motor with this type of operation would be somewhat limited or that some harmonic reduction method, perhaps similar to the triac control of a single phase fan motor[4.15], might be needed to improve the current waveform.

Measurements of actual harmonic currents and voltage fluctuations over the entire operating range are of course desirable to confirm the calculated results before any firm conclusions can be made concerning the effects of harmonics on the supply and it was unfortunate that time did not permit this to be done within the present project.

4.5 Conclusions

1. A variable-speed, brushless drive system for low-power, low-speed application has been described. Although motor output levels were sufficient to meet the specific application requirements for which the motor was originally designed, and temperature-rise levels within acceptable limits, the effect of high iron losses on overall efficiency was somewhat too significant for commercial viability. In fact the gamble taken in using a solid steel magnetic circuit would probably have paid off

if the motor had only been required for a speed range up to 150 rev/min (as originally specified). Even at 250 rev/min the efficiency is a little worse than that of the existing capacitor-run, high pole number, high diameter to length, external-rotor, single-phase induction, direct-drive motors generally used at present for ceiling fans. However, an improved performance is clearly required of a replacement product where possible.

2. A laminated magnetic circuit could certainly be used, but the options are narrow unless the radial/axial flux, single-coil configuration is abandoned. The use of U'strip cores' was considered, but was thought to be too costly at this torque (hence size) level. As can be seen in chapter 5, this idea was persued (form 3 motor) in connection with low torque high speed motor where the magnetic circuit volume per output is smaller and the relative cost penalty correspondingly less.

3. Similar remarks also apply to the adoption of permanent magnets in the rotor, though it was decided for reasons of time not to persue this idea in the project.

4. In comparing the direct mains-fed, triac-controlled feed system with the d.c. link system, the most important factor is the usual cost versus performance trade-off. It is important to add that certain operating features of the triac scheme would completely rule it out

of consideration for the majority of applications. However for a few application where the torque, operating speed range, load inertia, starting condition and power level were appropriate (the power level for instance would have to lie below certain figure for the mains harmonic currents to be acceptable), the cheap and robust triac scheme should not be forgotten. In certain application, advantage could perhaps be taken of the quasisynchronous phenomena.

CHAPTER 5

PERFORMANCE OF THE HIGH-SPEED TWO-POLE MOTORS

5.1 Introduction

This chapter presents the results of investigations into three experimental SPSRM. Operation both with 'a.c.' and 'd.c.' feed circuits was examined and many of the experimental results are correlated with predictions using the procedures described in chapter 3.

As indicated in chapter 1, following the work on the rather special low-speed motor with its solid iron magnetic circuit, high diameter to length ratio and relatively large size to output ratio, it was decided to orientate the investigation towards smaller motors of more conventional layout and towards the possibilities of effective operation over a speed range extending to 10,000 or 20,000 rev/min. Funds were limited and the experimental motors were all of small physical size. Two of the three motors were workshop-modified single-phase shaded-pole inductance motors, only the third being constructed from scratch.

5.1.1 Experimental motors

A different configuration is used in each (designated form 1, form 2 and form 3) and this enables

comparisons to be made on matter such as production cost, magnetic and electric loadings, leakage levels and performance.

a) Form 1 motor

The form 1 motor has a similar layout to that of a well-known type of single-phase shaded-pole induction motor as used for driving, e.g., pumps in washing machines, fans in overhead projectors and fan-heaters. The experimental motor as purchased is shown in Fig. 5.1.1 and contains a closed magnetic circuit with a detachable top portion, two shaded rings on each pole, a squirrel cage rotor and a bobbin-wound excitation coil. During manufacture the bobbin coil is wound on the detachable portion and this is then slid into position as a unit between the two side-arm portions of the pre-assembled core. Both stator and rotor are laminated.

The principal dimensions of the motor are:

stator core dimensions	=	63.5 x 63.5 x 37.5	mm^3
shaft size	=	6.35	mm
airgap length	=	0.4	mm
stator bore diameter	=	31.8	mm
rotor diameter	=	31.0	mm
rotor active length	=	37.5	mm

Modifications were made in the workshop on the as-purchased unit to change its construction from a single-

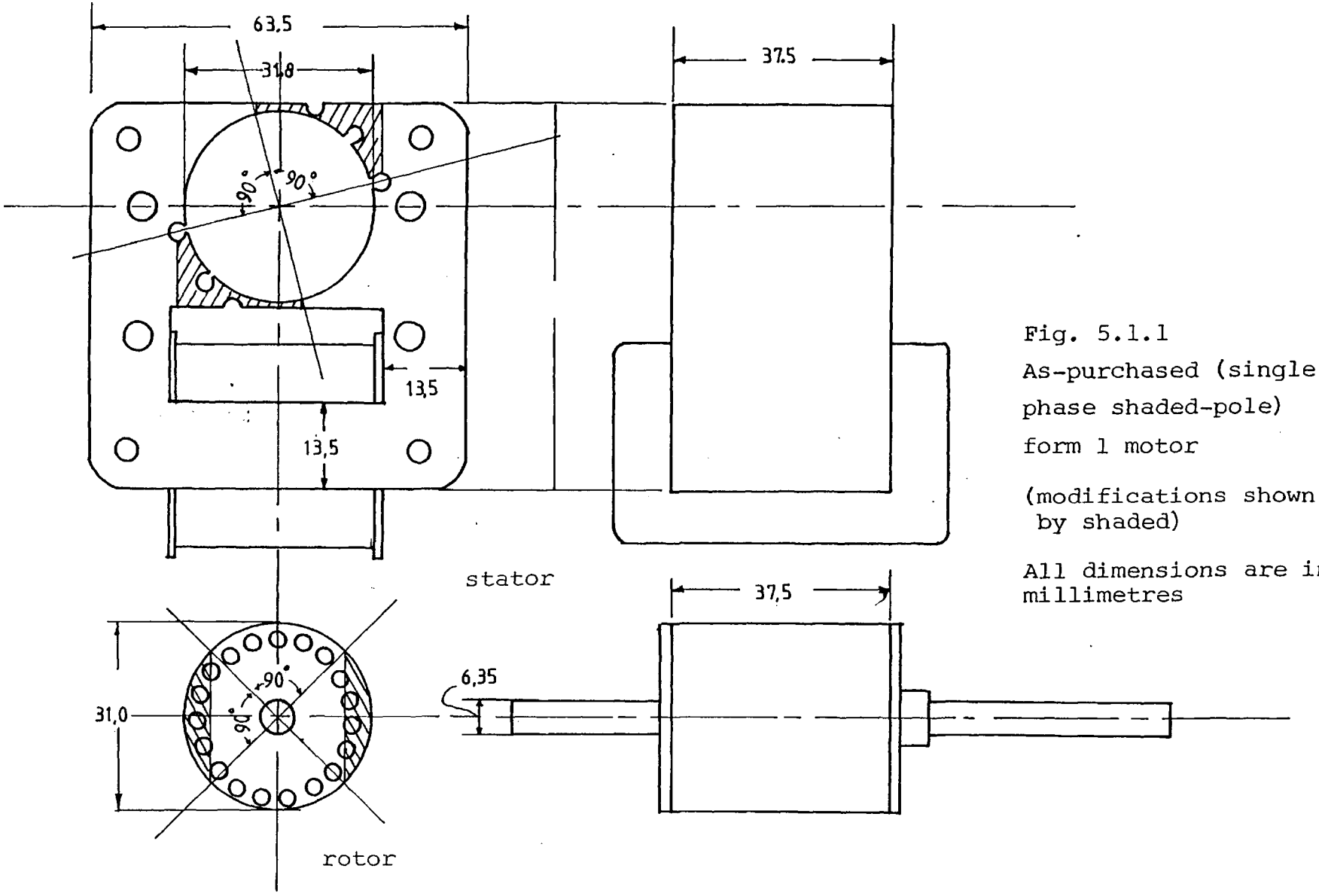

Fig. 5.1.1
As-purchased (single-phase shaded-pole) form 1 motor

(modifications shown by shaded)

All dimensions are in millimetres

phase shaded-pole induction motor to a single-phase switched reluctance motor. The main operations were:

1) The shading rings on the stator were removed and the bridge section on the stator core cut-away to reduce leakage flux particularly when the rotor lies in the q position and hence to improve the L_d to L_q ratio of the motor. The cut-away sections are shown shaded. The pole arcs remaining have smooth surfaces, uninterrupted by shading-ring slots. The ratio of pole arc to pole pitch is 0.5.

2) The end-rings on the rotor were removed and the rotor flats milled to produce a two-pole salient rotor. The rotor bars were left intact to help hold the lamination stack together, but play a negligible role electrically.

b) Form 2 motor

The form 2 layout is also similar to that of a well-known type of single-phase shaded-pole induction motor, often used as an extractor-fan drive. The experimental unit shown in its as-purchased form in Fig. 5.1.2 has a conventional two-pole laminated stator with one shading ring on each pole arc. The rotor is standard. The principal dimensions of the motor are:

diameter of the stator bore	=	28.1	mm
rotor diameter	=	27.1	mm
rotor active length	=	25.4	mm

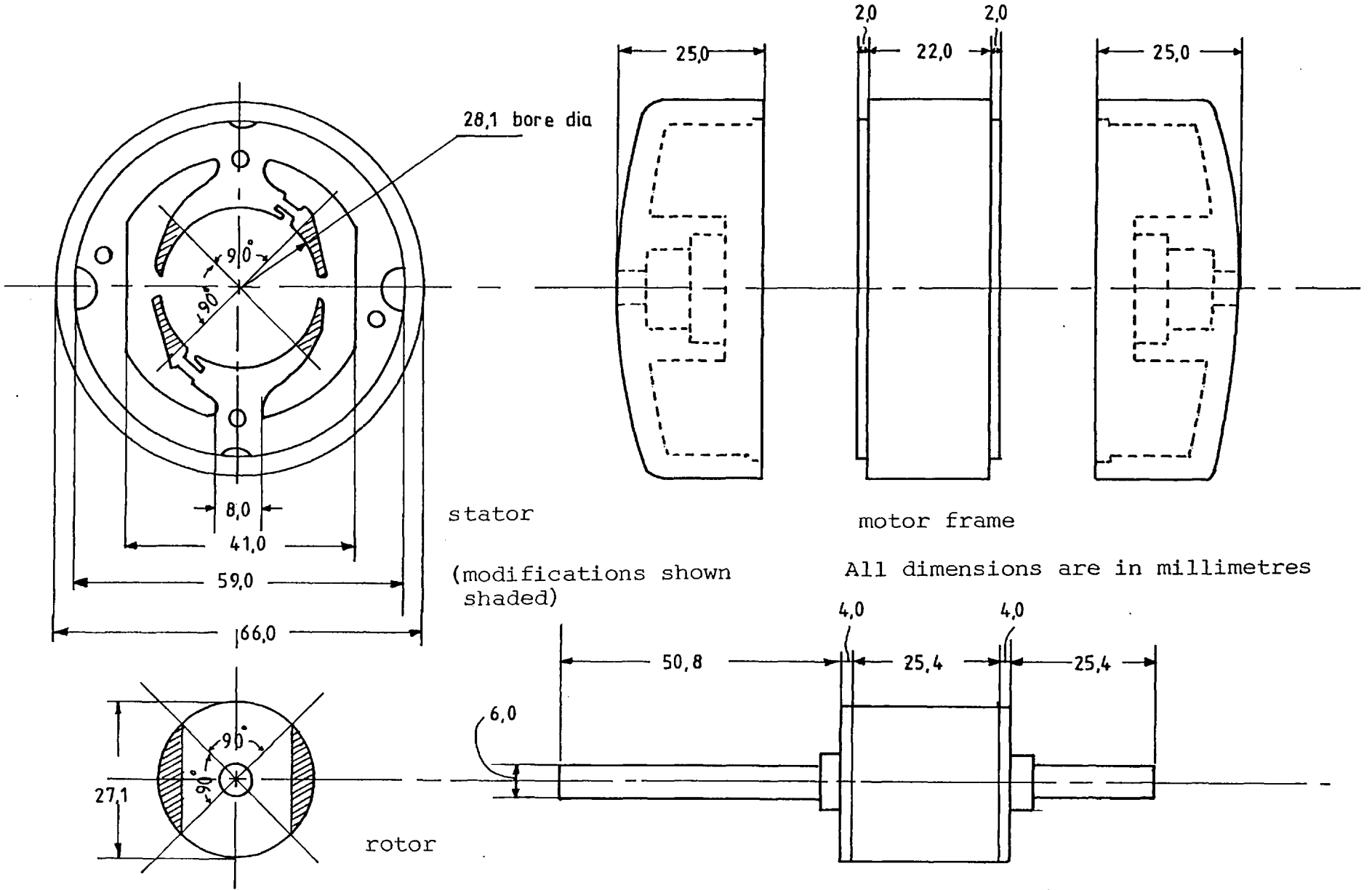

Fig. 5.1.2 As-purchased (single-phase shaded-pole) form 2 motor

airgap length	=	0.5	mm
stator stack length	=	26.0	mm
shaft diameter	=	6.0	mm

Modifications were made in the same way as the form 1 motor, the shading rings being removed and the stator pole arcs cut down. The final pole arc to pole pitch ratio was 0.5. Two new rotors were made for this form 2 motor with laminations stacked in a direction parallel to the shaft and in the conventional direction respectively. It was expected that the former stacking arrangement would result in a higher L_d to L_q ratio, but the problem of holding the lamination stack together against centrifugal forces is introduced. Burrs occurred during the machining process and caused short-circuited paths on the surface of the lamination pack. After a number of tests, heat from the resulting eddy current loss burnt the bonding epoxy resin and the lamination pack split. Hence formal experiments were conducted on the conventionally stacked rotor only. A new rotor was made to the same overall dimensions as the old one with the same ratio of pole arc to pole pitch as the stator, the saliencies being created by milling flat the shaded areas as shown in Fig. 5.1.2.

c) Form 3 motor

The form 3 motor is the result of an attempt to develop a novel motor that is effective but is simple,

cheap and easy to manufacture. A radial/axial flux path is used as in the low-speed, six-saliency motor described in chapter 4. This enables the excitation winding to be of the same form, i.e. a very simple single, concentrated, circular coil or quasi-circular coil which can be wound on a simple former in the pre-assembled stage. The single-concentrated coil is not only easy to manufacture but may often possess somewhat better heat dissipation properties than standard types of windings and hence be able to carry higher current densities for the same temperature limit.

Radial/axial flux paths can lead to lamination problems and it was realised that one way of avoiding these was to use strip wound C cores to form the stator magnetic circuit. In the experimental motor, TELMAG C core HWR 30/16 (Q6.3 in BS 5347) normally used as a small transformer core was employed. The lamination thickness is 0.1 mm. The dimensions of the core before and after machining are shown in Fig. 5.1.3. The rotor was made of a pack of laminations stacked parallel to the axis of the shaft. Epoxy resin was used to bond the laminations and 4 transverse bolts incorporated to increase the strength. The rotor block was treated with acid to partly remove the burrs caused by machining. It was realised that this type of rotor construction would perhaps always be more expensive and less strong than the standard rotor construction, even in production, but better performance levels were envisaged as being quite possible. (Chapter 2 gives details of an interesting alternative construction)

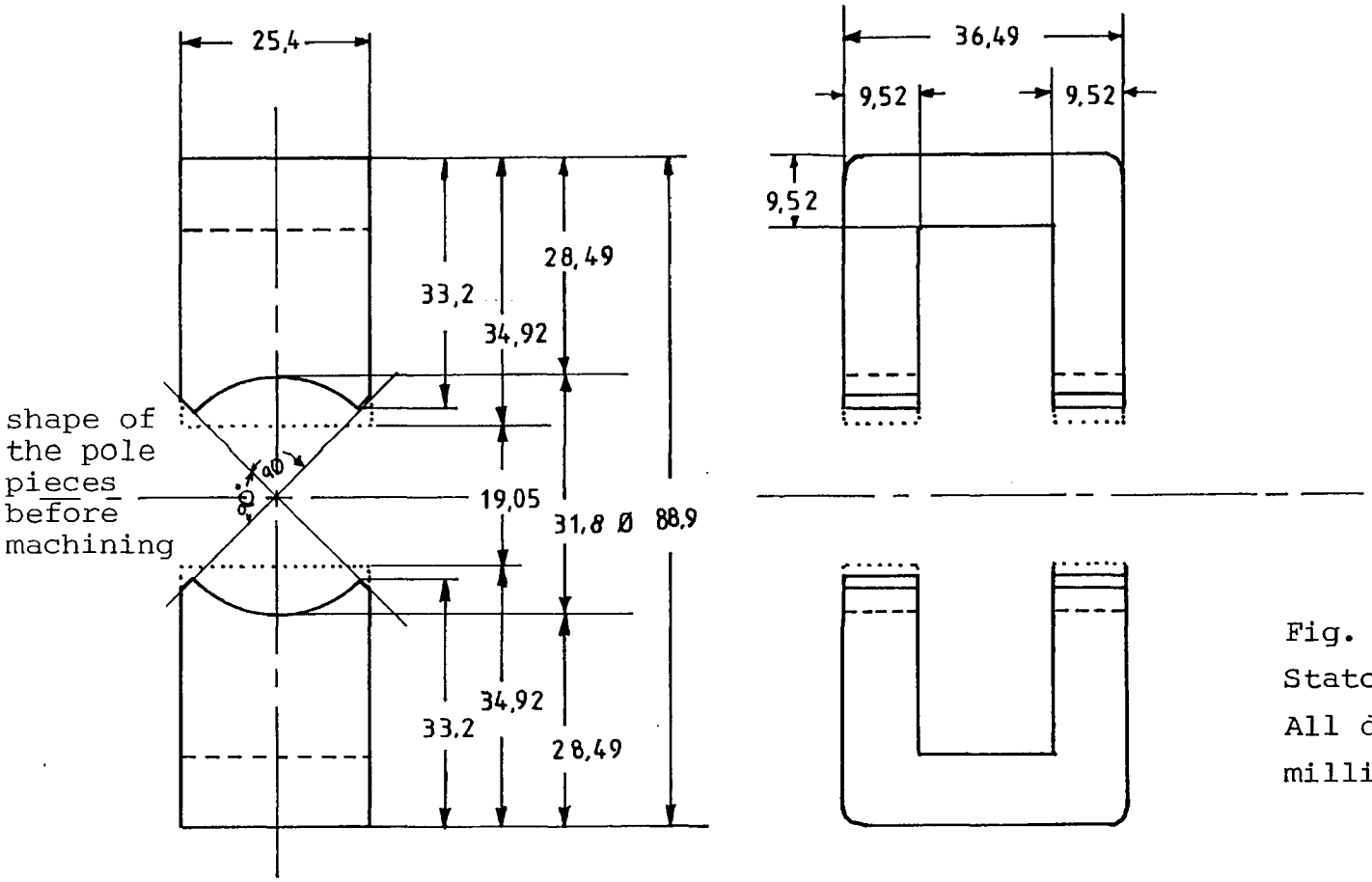

Fig. 5.1.3
Stator pole pieces
All dimensions are in millimetres

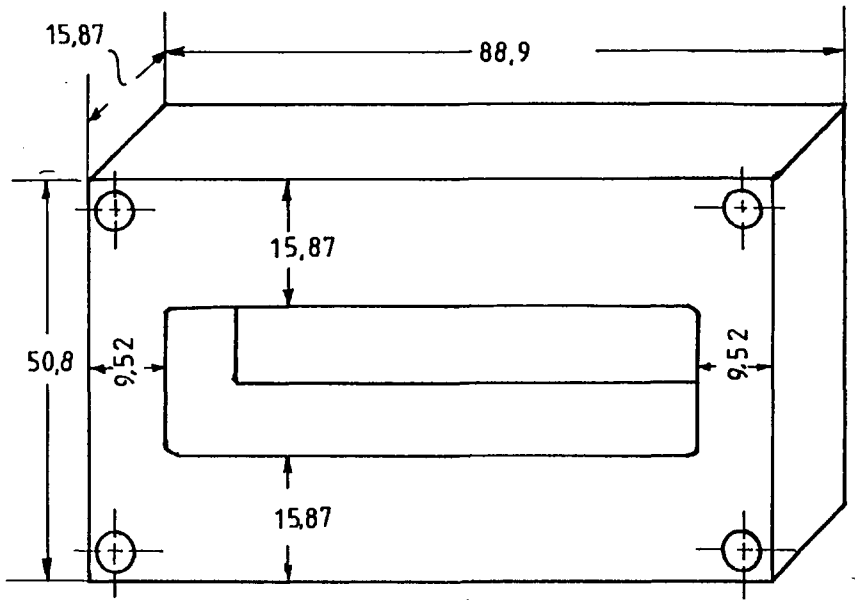

(a) Clamping piece (Dural)

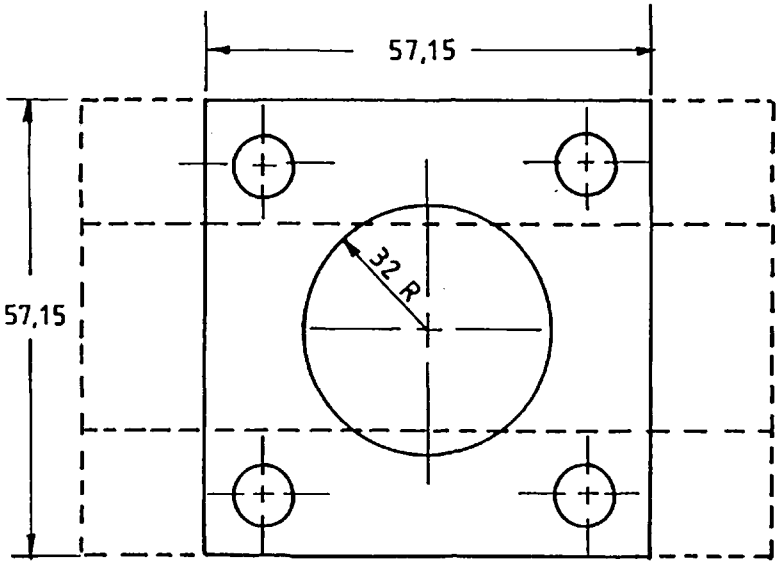

(b) Bridge piece (Dural)

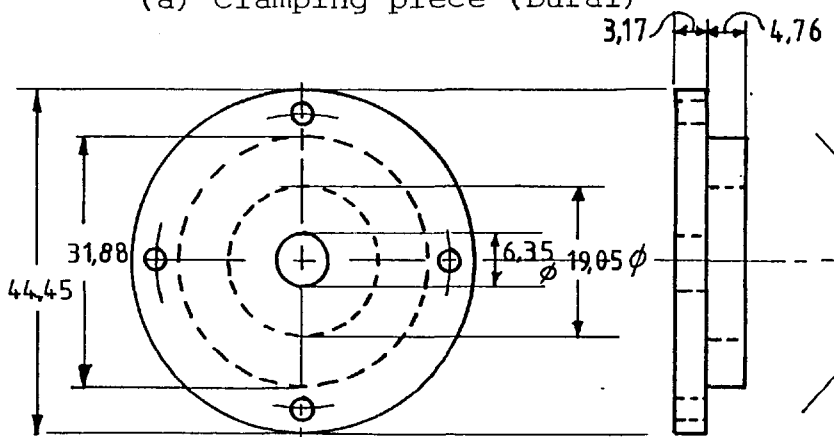

(c) Bearing housing (Dural)

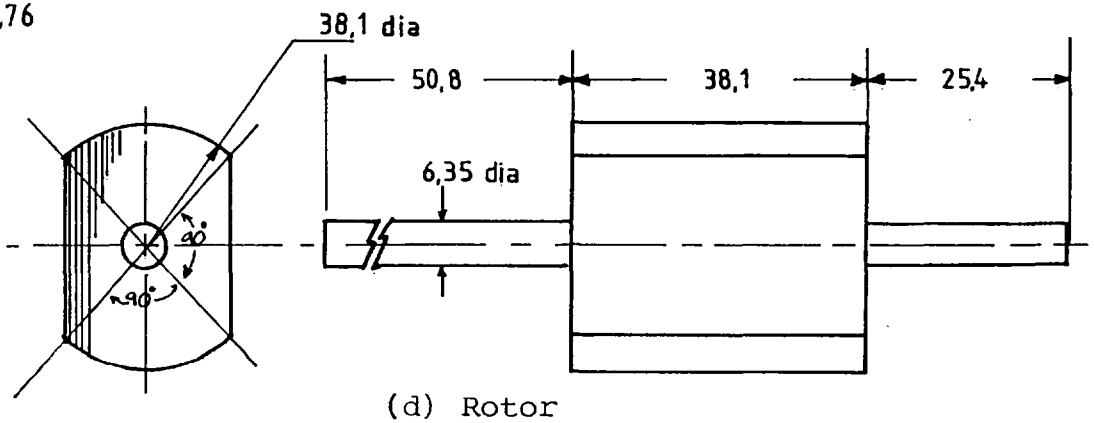

(d) Rotor

Fig. 5.1.4 Form 3 motor components

All dimensions are in millimetres

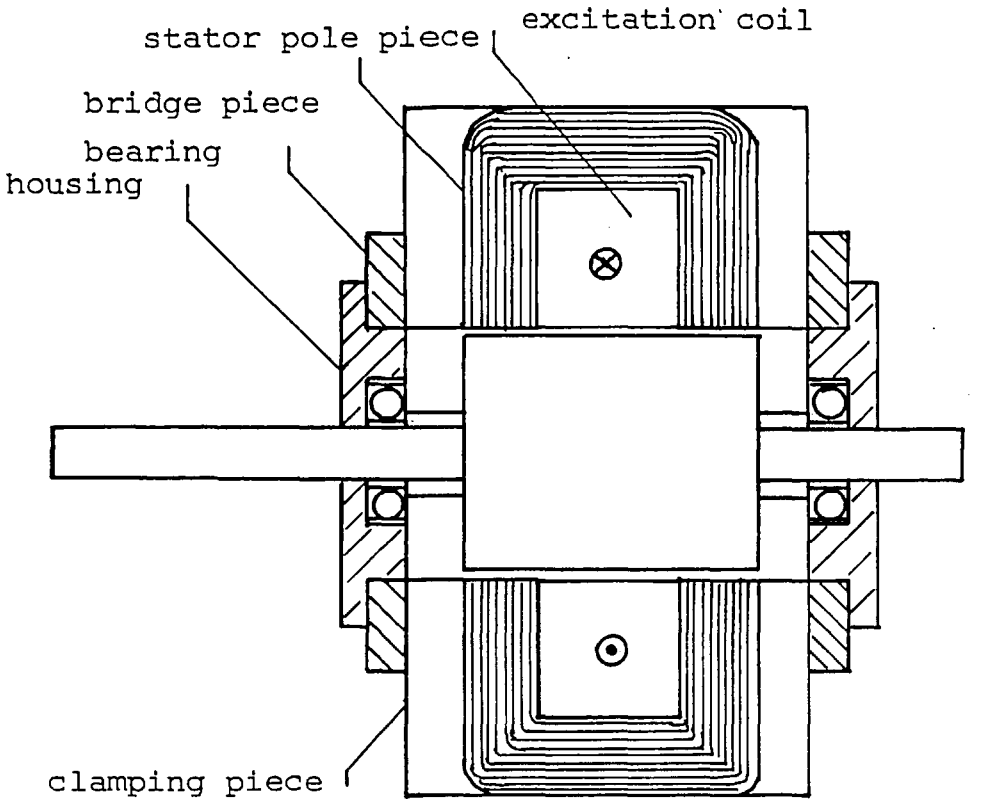

Fig. 5.1.5 Cut-away view of the form 3 motor

Two clamping pieces were used to hold the stator pole pieces in place. The window in each clamping piece allows the excitation coil to be inserted after assembly.

In the construction, the clamping pieces and pole pieces were assembled first with two bridge pieces on the top and bottom. The whole unit was then lined up on a lathe and the bridge pieces drilled through to make the stator bore, pole arcs and location surfaces for the bearing housings. In this way, eccentricity was kept to minimum. The two bearing housings were then fitted to the bridge pieces. Fig. 5.1.4 shows the components of the

form 3 motor and Fig. 5.1.5 shows a cut-away view of the complete unit.

The principal dimensions of the experimental unit are:

overall dimensions (excluding clamping pieces)	= 88.9x36.5x69.8	mm^3
stator bore diameter	= 31.8	mm
rotor diameter	= 31.0	mm
airgap length	= 0.4	mm
rotor active length	= 19.0	mm
shaft size	= 6.35	mm

Fig. 5.1.6 shows the form 1 and form 2 motors after modification together with the form 3 motor.

5.1.2 Test on the original form 1 motor

A load test was carried out on the original form 1 motor (in its single-phase shaded-pole induction motor form) with the purpose of using the results obtained as a reference for subsequent comparisons. A standard test circuit and a spring balance brake system was used which was carried out at the mains supply voltage of 232 V and a winding temperature of 60°C. The performance curves obtained are shown in Fig. 5.1.7. Characteristics typical of those of small induction motors are shown. The no-load speed of 2950 rev/min corresponds to a slip of 0.016. The pull-out is 60 mN-m at 2375 rev/min. At this speed the corresponding power output is 15 W with 25 % efficiency,

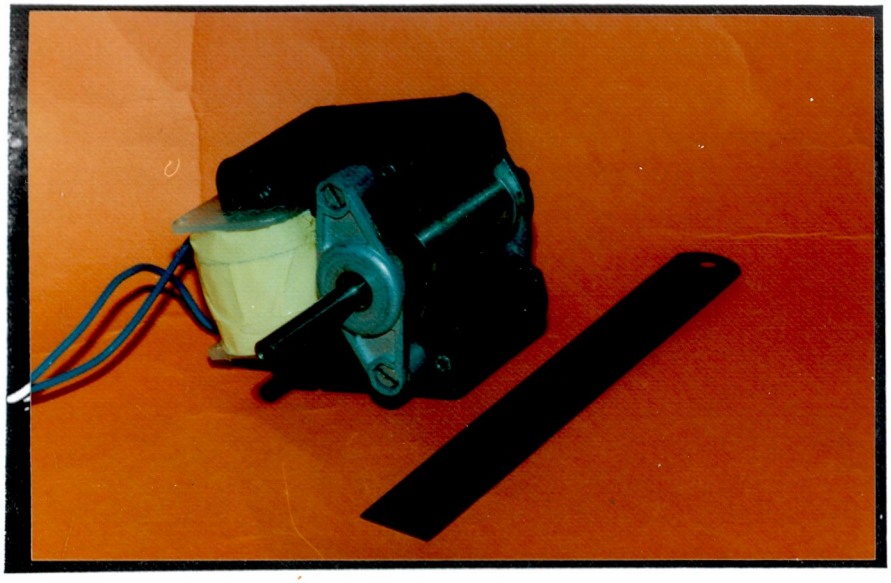

(a)
Form 1 motor

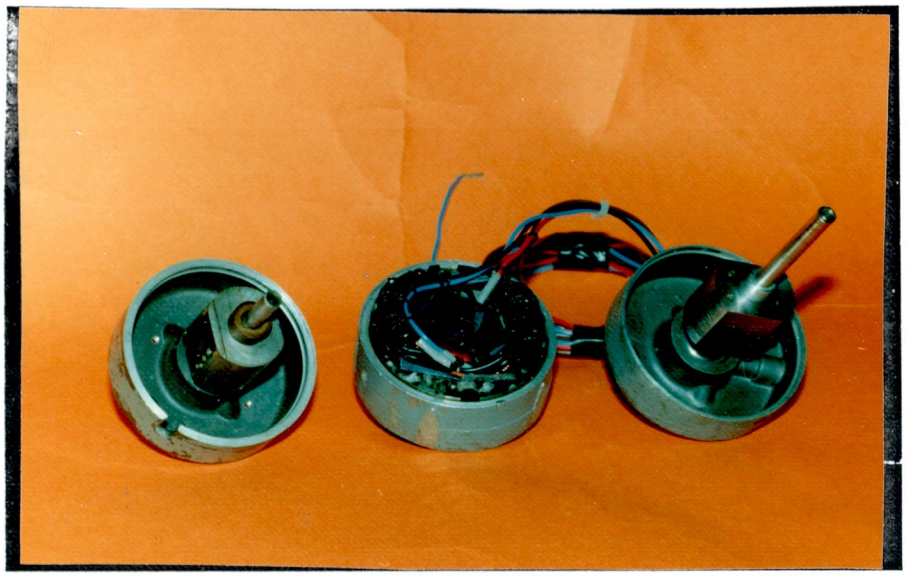

(b)
Form 2 motor

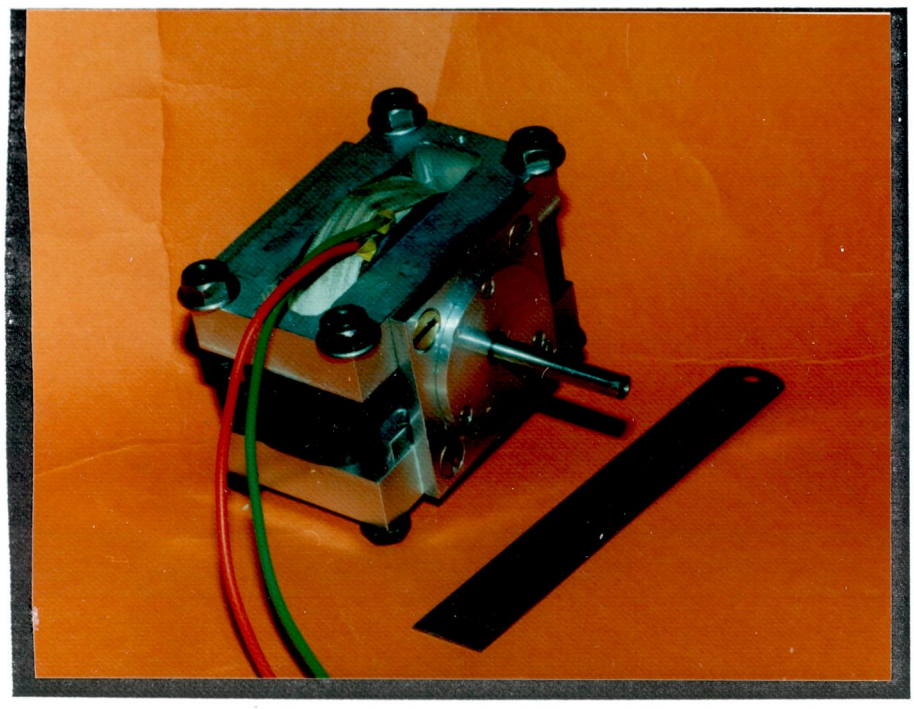

(c)
Form 3 motor

Fig. 5.1.6 Experimental motors

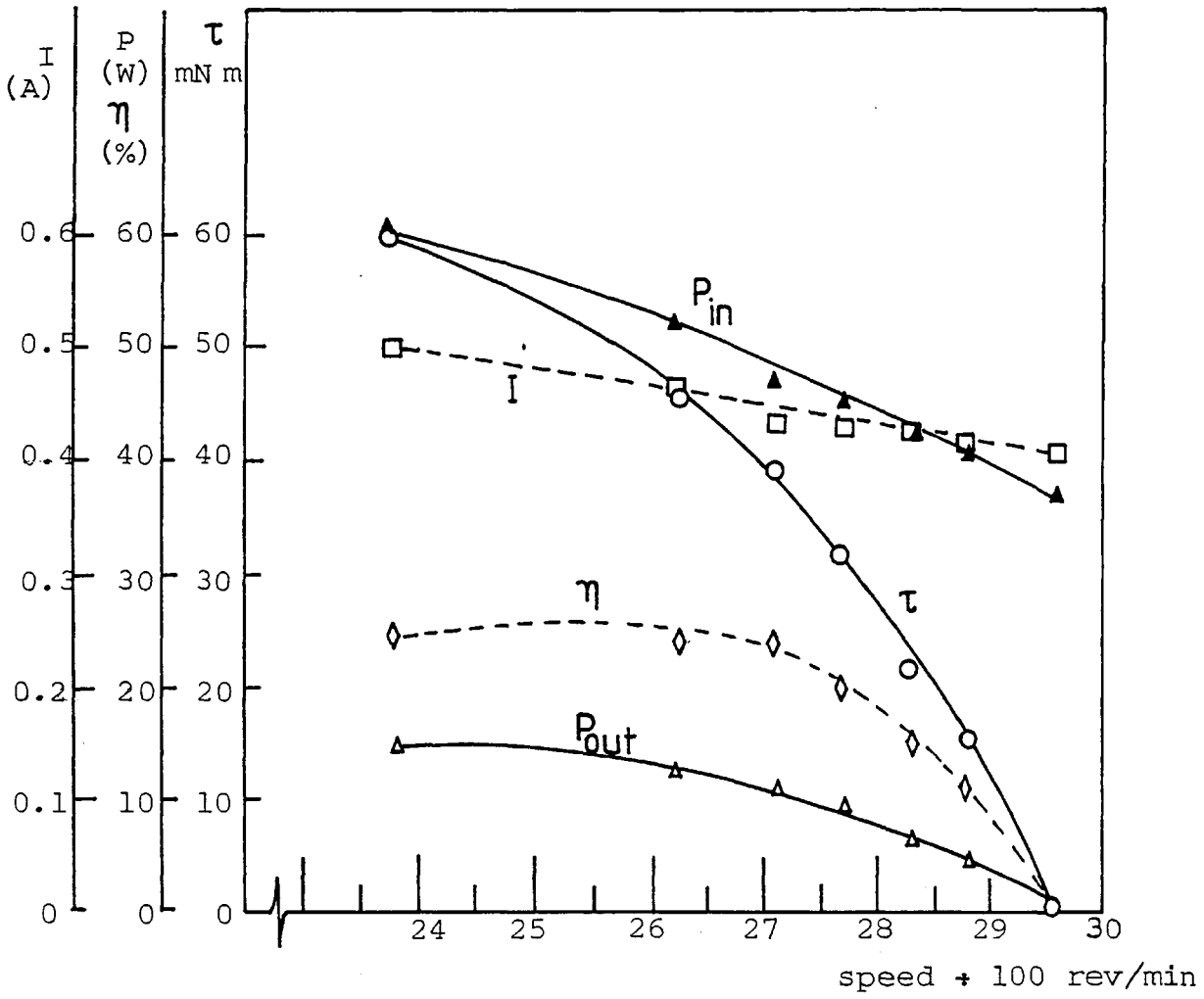

Fig. 5.1.7 Preformance curves of the as-purchased single-phase shaded-pole induction form 1 motor on 232 V a.c. mains, 60° absolute temperature

a figure which is common for a machine of this size. The power factor ranges from 0.4 at no-load to 0.52 at pull-out. The input current increases from 0.4 A at no-load to about 0.5 A at pull-out. The steady state winding temperature was approximately 60°C (40°C rise).

5.1.3 Introduction to the experimental work on the small SPSRMs

Work commenced with a preliminary investigation into the performance of the form 1 motor with its as-purchased winding fed from a feed circuit of the d.c. link type. As a result of this work, and of some predictions, modifications were made to the motor to improve its performance and further tests conducted.

The extremely low cost and simplicity of the a.c. triac-fed circuit previously investigated with the low speed motor, encouraged the study of its operation with the two pole form 1 motor. It was realised that the system's limited speed range (to 3000 rev/min at best) and propensity for drawing supply currents containing sub-harmonics would probably continue to prove unavoidable disadvantages, but the possibility of specific applications being found where the disadvantages would matter little could not be ruled out. (for instance, sub-harmonic currents are not envisaged as causing problems for say sub-200 W drives)

Subsequent the work on the 'a.c.'-fed form 1 motor system, investigations were conducted into the operation of the form 2 and form 3 motors with two types of 'd.c.' feed. Heat runs were carried out in all cases.

In order to achieve continuity in presentation, the performance of the form 1 motor with 'a.c.' triac-fed circuit will be described first in section 5.2. In section 5.3 the performance of the form 1 motor, the form 2 motor and the form 3 motor with 'd.c.' transistor-fed circuit will be presented. Finally in section 5.4 the performance at the class E temperature limit of all the motors with 'd.c.' transistor-fed circuits will be compared in terms of rated power, efficiency, and other performance factors.

5.2 Performance of the form 1 motor with 'a.c.' triac-fed circuit

5.2.1 'A.C.' triac-fed circuit with d.c. trigger

Section 4.4.4 showed how the use of a d.c. trigger tended to give more bursts of torque pulses than when the single pulse firing circuit was used. This is considered to be beneficial, especially at high speeds where the 'on' period is generally kept short to avoid carry-over currents and negative torque pulses, and the chance of the firing signal being completely missing when the single pulse trigger circuit is used is high.

The d.c. trigger circuit for a.c. triac control used in the experiments is shown in Fig. 5.2.1. The control circuit is supplied by a dual voltage +12, 0, -12 V external d.c. supply. The input signal (1) is fed from the mains supply voltage via the voltage divider R_1 and R_2. The first stage of the circuit which is formed by R_1, R_2, R_x, R_3, R_4 and Tr_1, Tr_2, Tr_3 gives positive pulses at point (3) which occur at the zero crossing points of the input supply voltage. With the resistor values used, the rising and falling edges of each pulse occur at 100 μS before and 100 μS after the zero crossing point of the input signal. The action at this stage of the circuit can be briefly explained as follows. At the start of the positive half cycle of the input voltage V(1) is equal to zero and Tr_1 is off. The voltage at the base of Tr_3 is then approximately 6 V due to R_3 and (R_2+R_x), hence Tr_3 is on and C_1 is short-circuited. After a short time ($\simeq$ 100 μS), input voltage V(1) increases to a value which is high enough to turn Tr_1 on. This will turn off Tr_3 and C_1 is charged up via R_4 . C_1 continues charging until the input voltage V(1) drops below the value that is sufficient to supply base current to keep Tr_1 on ($\simeq$ 100 μS before V(1) = 0). So Tr_1 is off, Tr_3 is on and C_1 is then short-circuited to ground.

Operation for the negative half cycle is similar to that in the positive half cycle with Tr_2 operating in the same way as Tr_1. The voltage across C_1 is hence a 100 Hz ramp waveform of approximately 4.5 V peak.

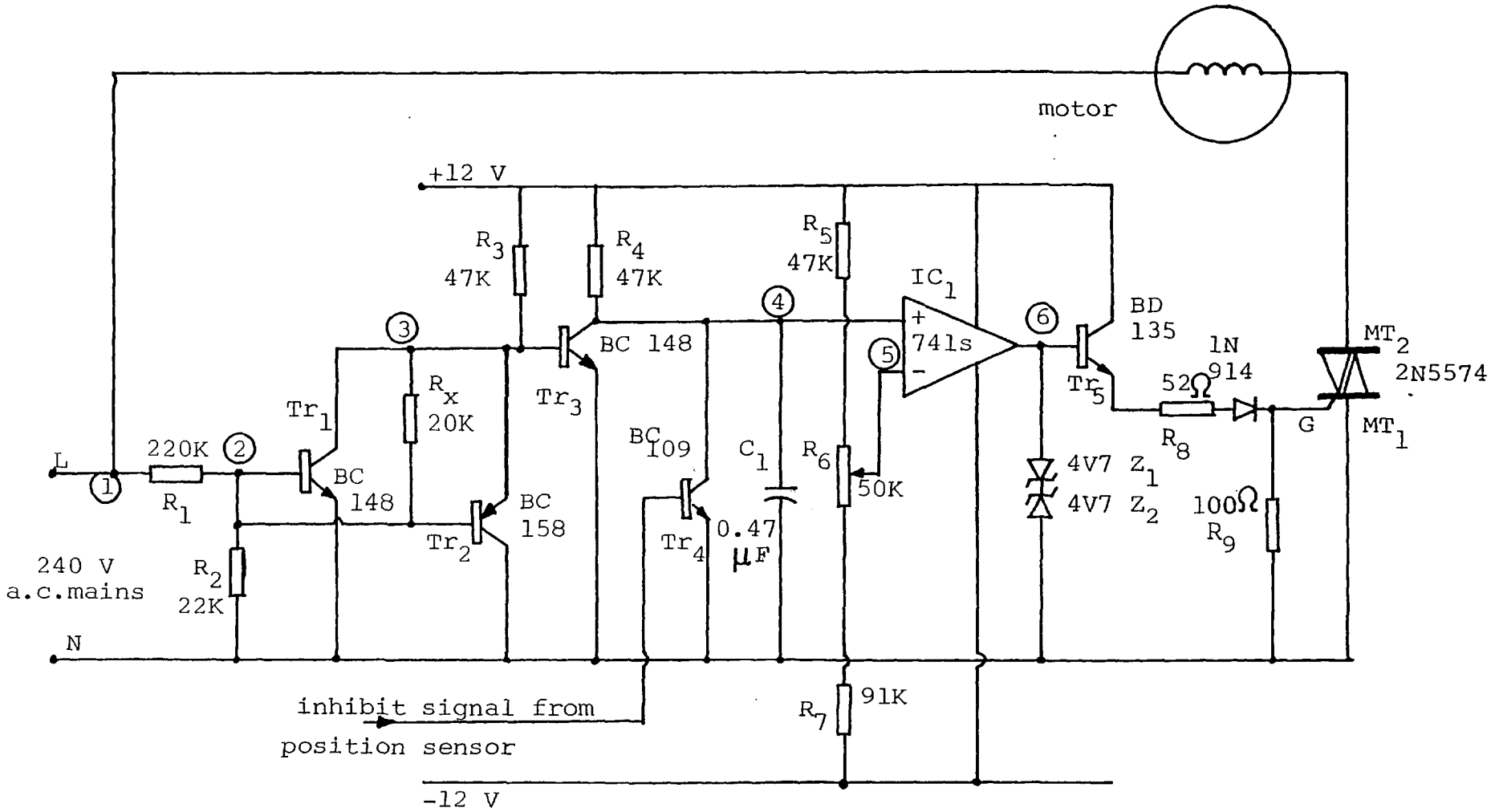

Use 2 % component for R_1 to R_4

Fig. 5.2.1 The 'a.c.' triac-fed circuit with d.c. trigger firing control

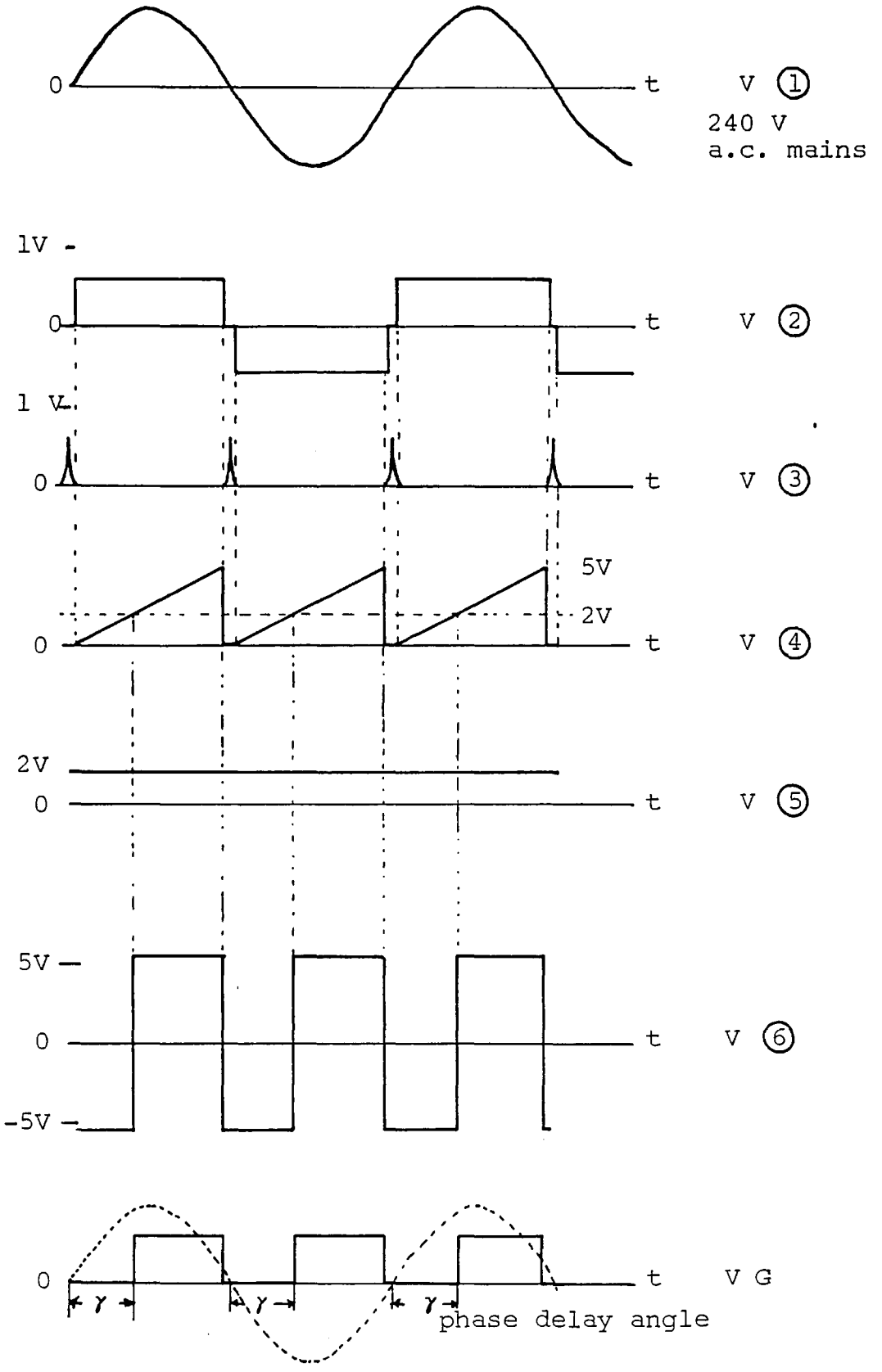

Fig. 2.5.2 Waveforms at the points indicated in the a.c. triac control circuit (without synchronising action)

The ramp signal is then compared with the reference voltage from the phase-delay control potentiometer and the output at point (6) will be a square wave of $\pm$ 5.3 V. The positive half cycle of the square wave will turn Tr_5 on and a corresponding positive pulse appears at the gate of the triac.

The gate signal is hence a positive pulse whose rising edge can be adjusted relative to the zero crossing point and whose duration extends to the end of the half cycle. At maximum width, the gap between each consecutive pulse is approximately 200 μS. Tr_5 is added to provide enough gate drive for the triac with R_8 as a current limiter. R_9 is provided to prevent the gate from floating. The synchronising signal is fed to the base of Tr_4 which serves to short-circuit the capacitor C_1 during the off periods.

Waveforms at each point described in the circuit are shown in Fig. 5.2.2.

5.2.2 Experimental system

Investigation of the theoretical torque speed characteristics of the a.c.-fed 6-saliency motor in Fig. 4.4.10 (in section 4.4) shows that the average of the mean output torque for fixed switching angle operation increases from zero at no-load to a maximum value at about half no-load speed and then drops to a very low value at low speeds.

Since output torque measurements within the positive slope region of the torque-speed characteristic are very difficult to obtain using the pulley and spring balance system used in the previous experiments, a dynamometer system based on closed-loop speed control of a permanent magnet d.c. motor was developed and built.

A block diagram of the closed loop speed controller is shown in Fig. 5.2.3. The details are as follows:

a) Dynamometer. A 24 V, ferrite-field d.c. permanent magnet motor (commercial vehicle windscreen wiper motor) was chosen for the dynamometer because of its size and speed range. The variation of no-load speed against input voltage of the motor is shown in Fig. 5.2.4. Its linear characteristic makes it suitable for armature voltage speed control. Because the shaft of the dynamometer is small (6 mm), the conventional method of supporting the motor with a bearing on each end of the shaft could not be followed. Instead, four trunions were used, bearing on the smooth cylindrical frame of the motor. The torque arm, of 3 mm duraluminium sheet was attached to the front end of the motor frame. A flexible aliminium coupling was used to couple the dynamometer to the test motor and a spring balance used to measure the torque. The test rig is shown in Fig. 5.2.5.

b) Summing amplifier. In practice the summing point shown in the diagram forms part of the summing

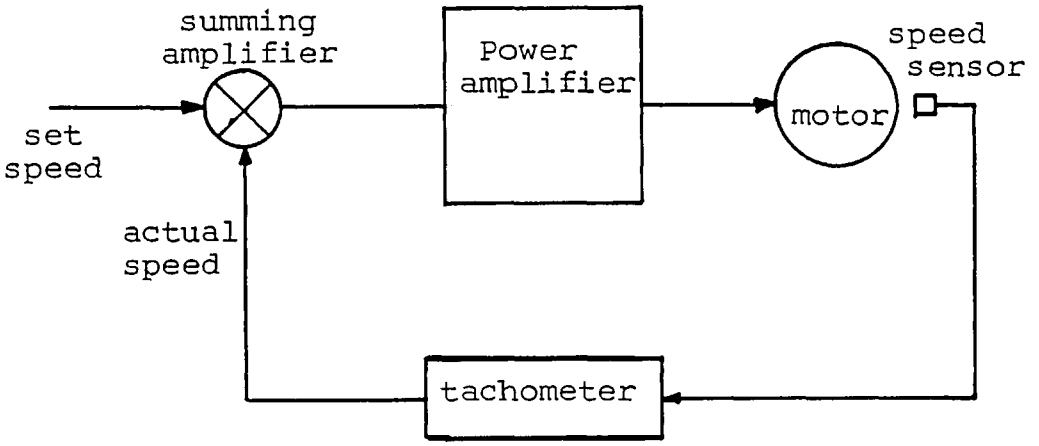

Fig. 5.2.3 Block diagram of the speed control system of a d.c. motor

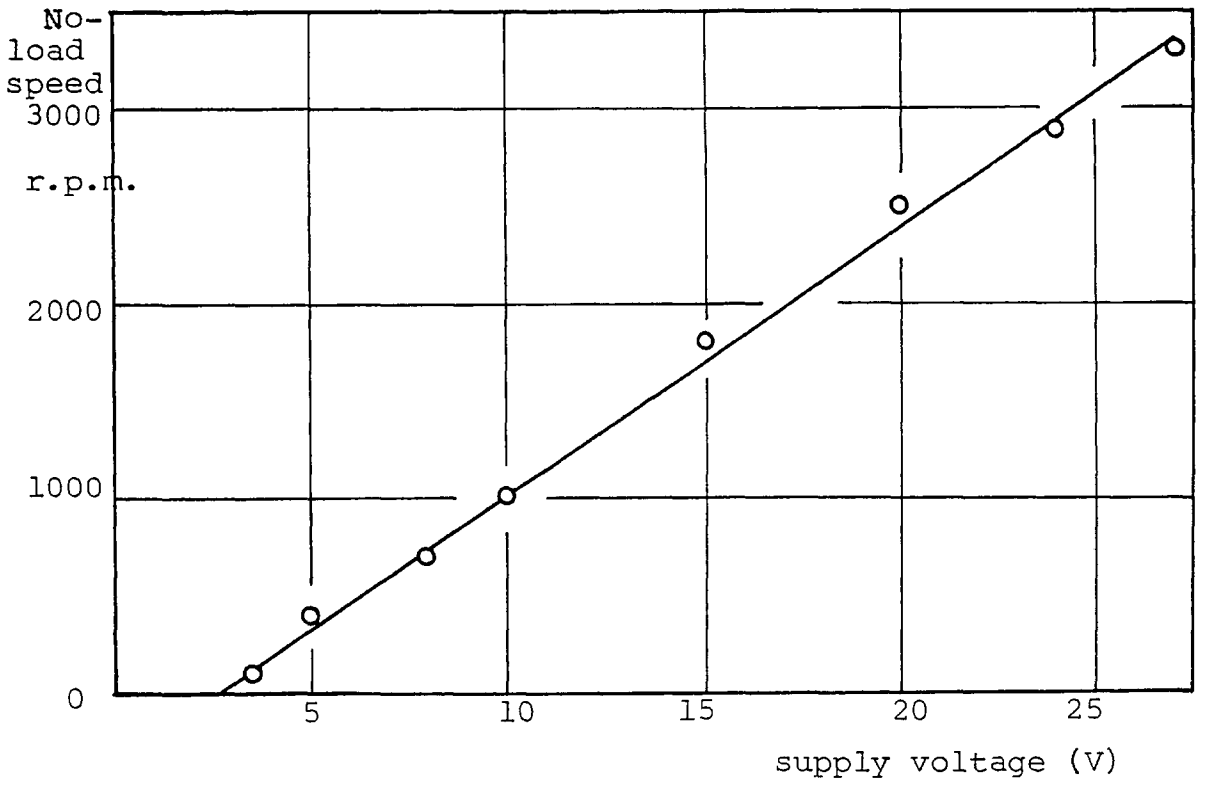

Fig. 5.2.4 Variation of no-load speed against supply voltage of the dynamometer

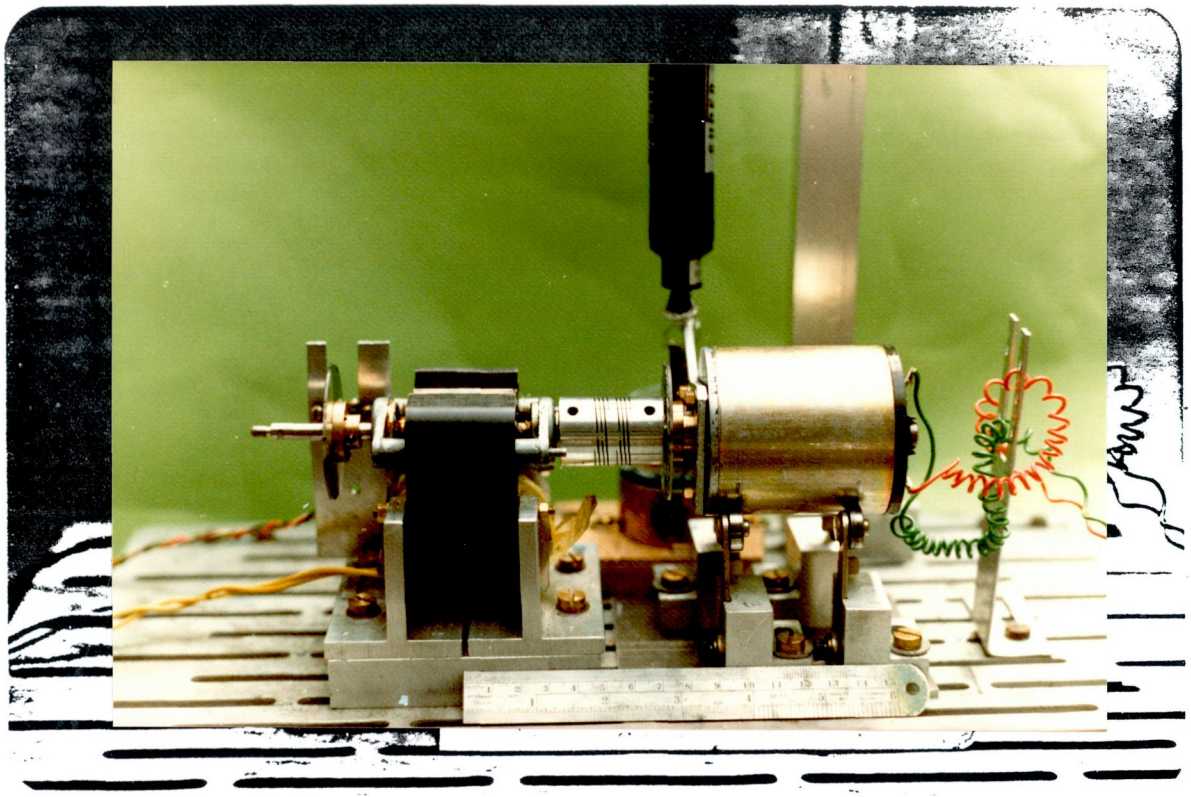

Fig. 5.2.5 Test rig

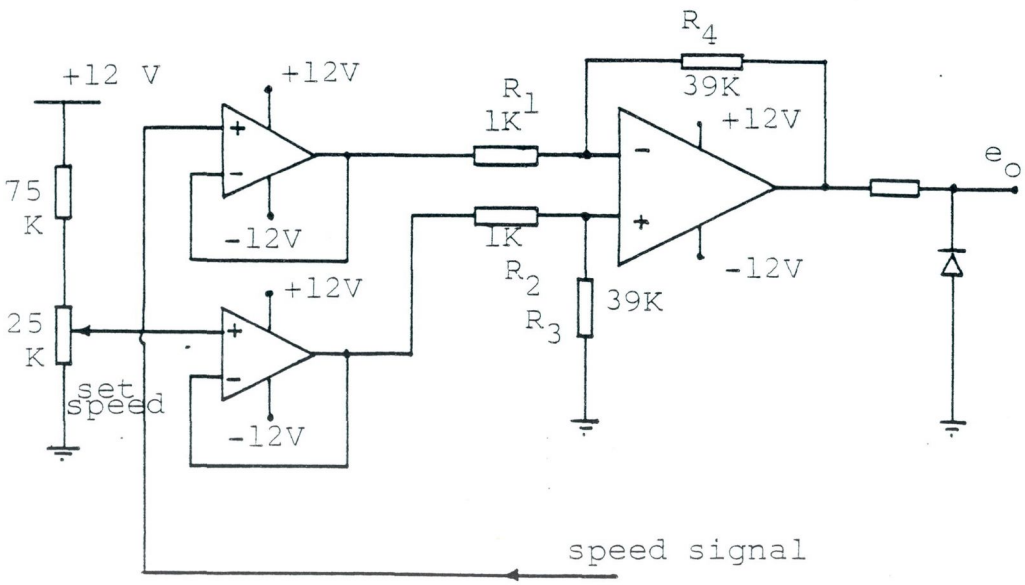

Fig. 5.2.6 Summing amplifier

amplifier. The power amplifier has a very low voltage gain ($K \simeq 1$-5) and the greater part of the gain required for good speed accuracy is provided by the summing amplifier. (Note that the overall gain was not made so large that the system became unstable due to noise or ripple. An overall gain of 100 to 200 was found suitable.) The summing amplifier which has been arranged as a high input impedance differential amplifier[5.1] is shown in Fig. 5.2.6. Two unity gain followers on the input from very high input impedance buffers. With $R_4/R_1 = R_3/R_2$ and $R_1 = R_2$, the output voltage

$$e_o = \frac{R_4 \, (e_1 - e_2)}{R_1} \qquad (5.2.1)$$

The gain of the summing amplifier is hence 39.

The diode at the output stage will prevent negative output voltages being fed to the power amplifier. This prevents the motor from rotating in the opposite direction.

c) Power amplifier. A standard laboratory power amplifier with DC-20,000 Hz bandwidth and variable gain (AMCRON DC 300 A) was used.

d) Speed sensor and electronic tachometer. An optical speed sensor with F/V converter was preferred to an electromechanical tachometer to avoid loading problems. A perspex disc with a black and white pattern as shown in Fig. 5.2.8 was fixed on to the shaft of the motor

and an R.S. slotted optical source and sensor fixed to the rig.

In order to convert the output signal of the slotted opto switch to a voltage proportional to speed an R.S. voltage to frequency converter 307-070 was used in its F/V mode. The F/V converter (Ref. 5.2) with its associated circuit is shown in Fig. 5.2.7. The input signal of the F/V converter must cross zero in order to trip the comparator. Because the output signal of the slotted opto switch (Fig. 5.2.8(b)) is only unipolar (positive going pulses), a differentiator circuit (R_1 and C_1) is provided at the input terminal of the F/V circuit. In order to overcome hysteresis the amplitude of the input signal must be greater than $\pm$ 200 mV. If the input voltage exceeds -2.5 V then the op-amp output will go to its maximum voltage for the duration of this over-voltage. To overcome this a pair of back to back diodes and series resistor is incorporated to limit the voltage to $\pm$0.7 V.

The number of strips on the perspex disc and the value of C_{ref} and R_{int} in the converter circuit can be calculated from the ranges of motor speed and required output voltage as follows.

The operating speed range is approximately from 100 to 3600 rev/min. The output voltage of the F/V converter is fixed by the rail supply and the range is from 0 to 4 V. The operating frequency is from 10 Hz to

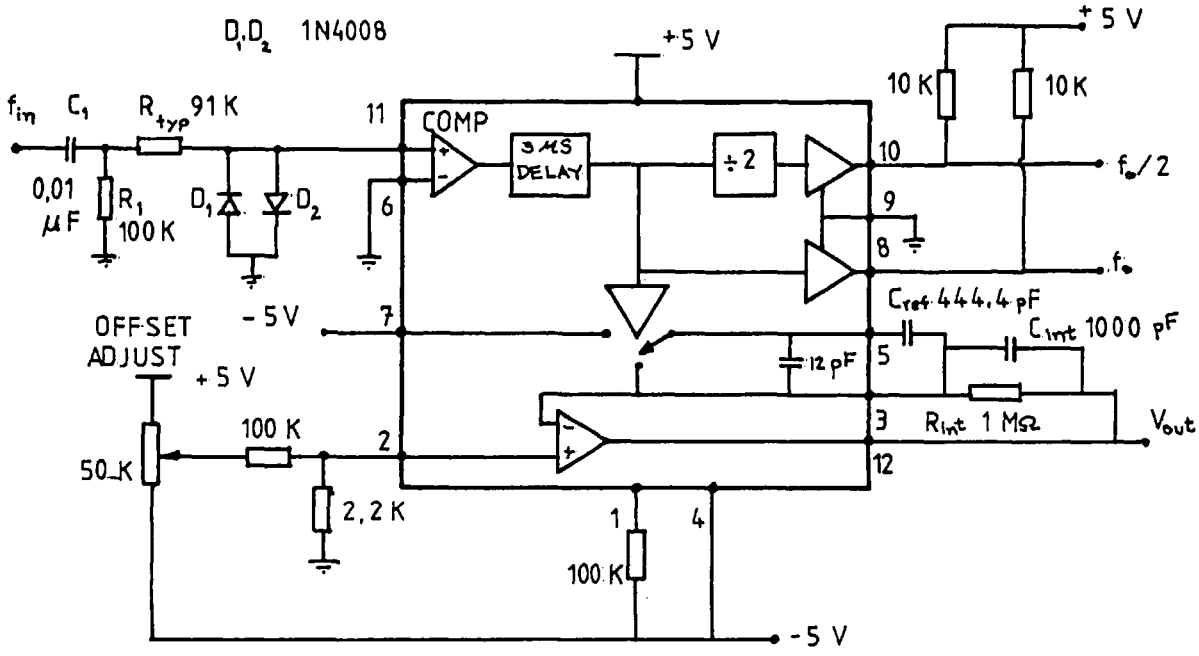

Fig. 5.2.7 F/V converter circuit

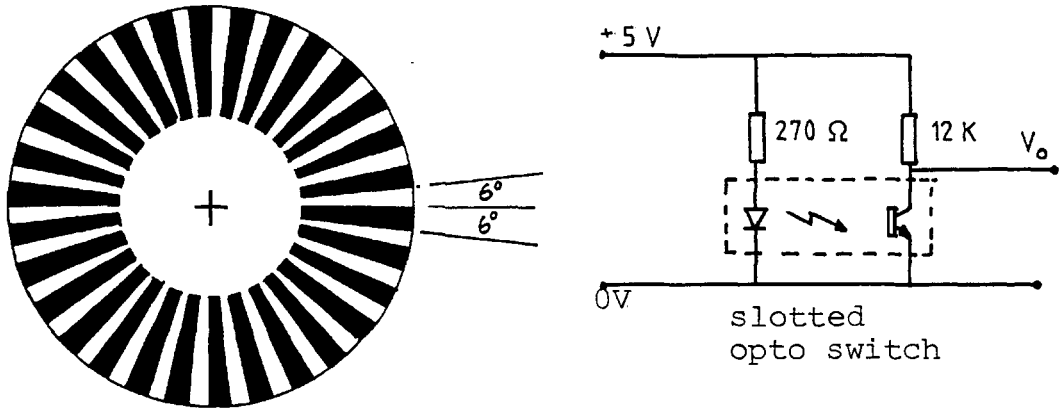

(a) (b)

Fig. 5.2.8 (a) Speed-sensor disc (perspex)

(b) Slotted-opto switch with its associated circuit

10 KHz or 100 KHz. The chosen number of strips on the disc should be high for the ripple in the output at low speed (e.g. 100 rev/min) to be easily smoothed. However since the size of the perspex disc is only 50 mm in diameter, the maximum number of strips is limited due to the appreciable active width of the opto sensor. 30 strips corresponding to a strip width and spacing width of 6° each (Fig. 5.2.8(a)) was the number chosen, giving a range of output frequency from 50 Hz to 1.8 KHz over a speed range of 100 rev/min to 3600 rev/min.

A value of C_{ref} was chosen from the output voltage equation for the F/V converter:

$$V_{out} = f_{in}(V_{ref}C_{ref}R_{int}) \quad (5.2.2)$$

and V_{ref}= 5 V, R_{int}= 1 MΩ to give V_{out} equal to 4 V at a f_{in} of 1.8 KHz.

Hence $C_{ref} = 444.4$ pF

and the conversion factor V/Hz is 2.22 mV.

The tachometer circuit was tested both with a signal from the signal generator as input and a signal from the slotted opto switch, in the latter case the speed of the motor being checked by a handheld tachometer. The characteristic obtained is shown in Fig. 5.2.9. The measured relation between the output voltage and the input frequency or the motor speed is 2.4 mV/Hz or 1.2 mV/(rev/min).

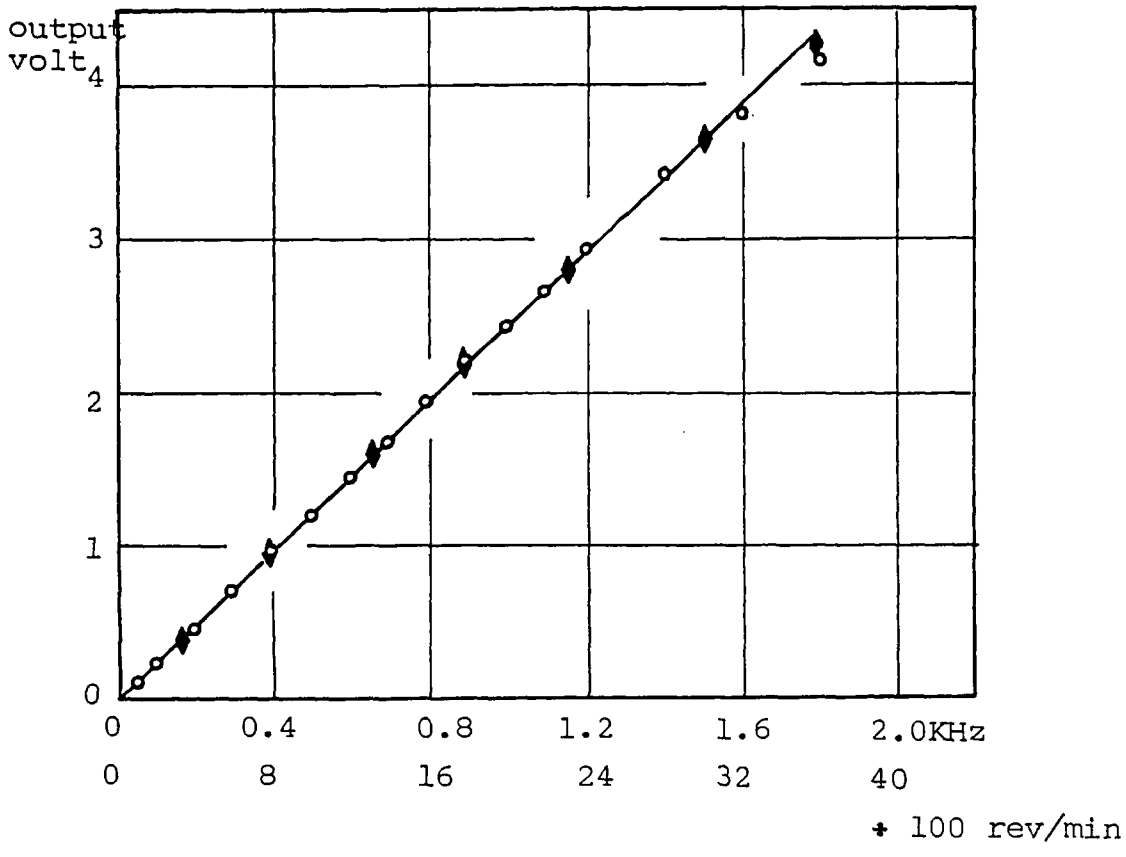

Fig. 5.2.9 Electronic tachometer characteristics

○ F/V characteristic calibrated with the signal generator

♦ F/V characteristic calibrated with the motor

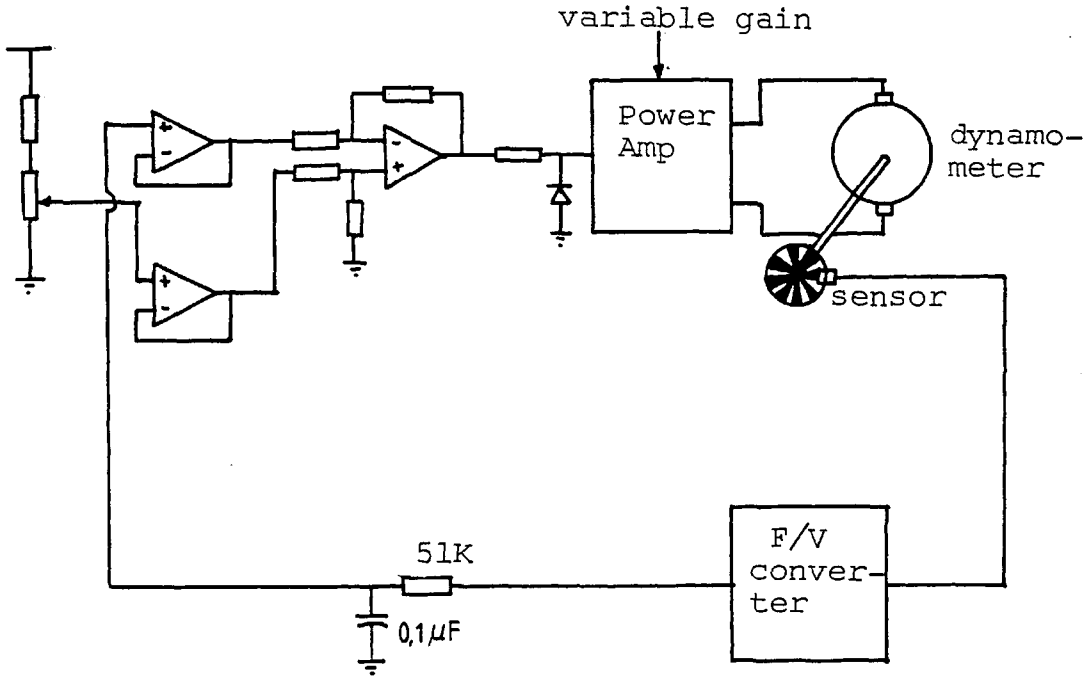

Fig. 5.2.10 Dynamometer system with closed-loop speed control

Although the average value of the F/V converter output voltage is proportional to the frequency of the input signal, the actual voltage waveform contains ripple of the same frequency as the input signal whose magnitude is frequency dependent. The ripple voltage is undesirable for the summing amplifier, so the output signal is fed to a low-pass filter. The time constant of the filter is approximately 5 mS (R = 51 KΩ C = 0.1 μF).

The complete control system is shown in Fig. 5.2.10.

5.2.3 Load test with 'a.c.' triac-fed circuit

The operation of the form 1 motor with 'a.c.' triac circuit was tested both with the single pulse firing circuit (as used with the low-speed, 6 saliency motor) and the 'd.c.' trigger firing circuit described in section 5.2.1. During these tests the motor was wound with a reduced number of turns (130 of 1.12 mm diameter enamelled copper wire) in order to match better the current and voltage ratings of the 'd.c.' feed circuit used later to those of the motor winding.

The test circuit is shown in Fig. 5.2.11. The motor was supplied from 240 V a.c. 50 Hz mains through a variac. The variac output supply was adjusted to 25 V because of the low impedance of the motor circuit. The

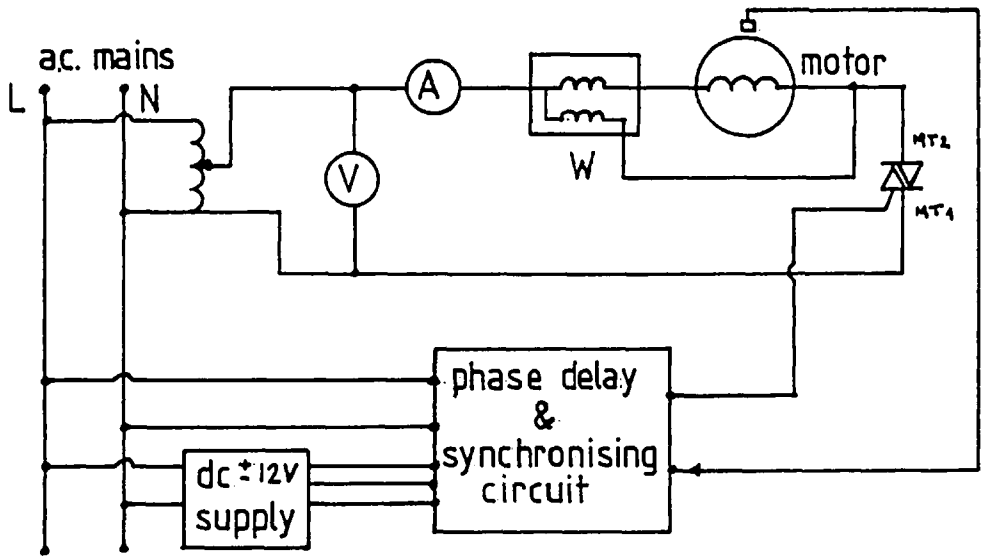

Fig. 5.2.11 Test circuit

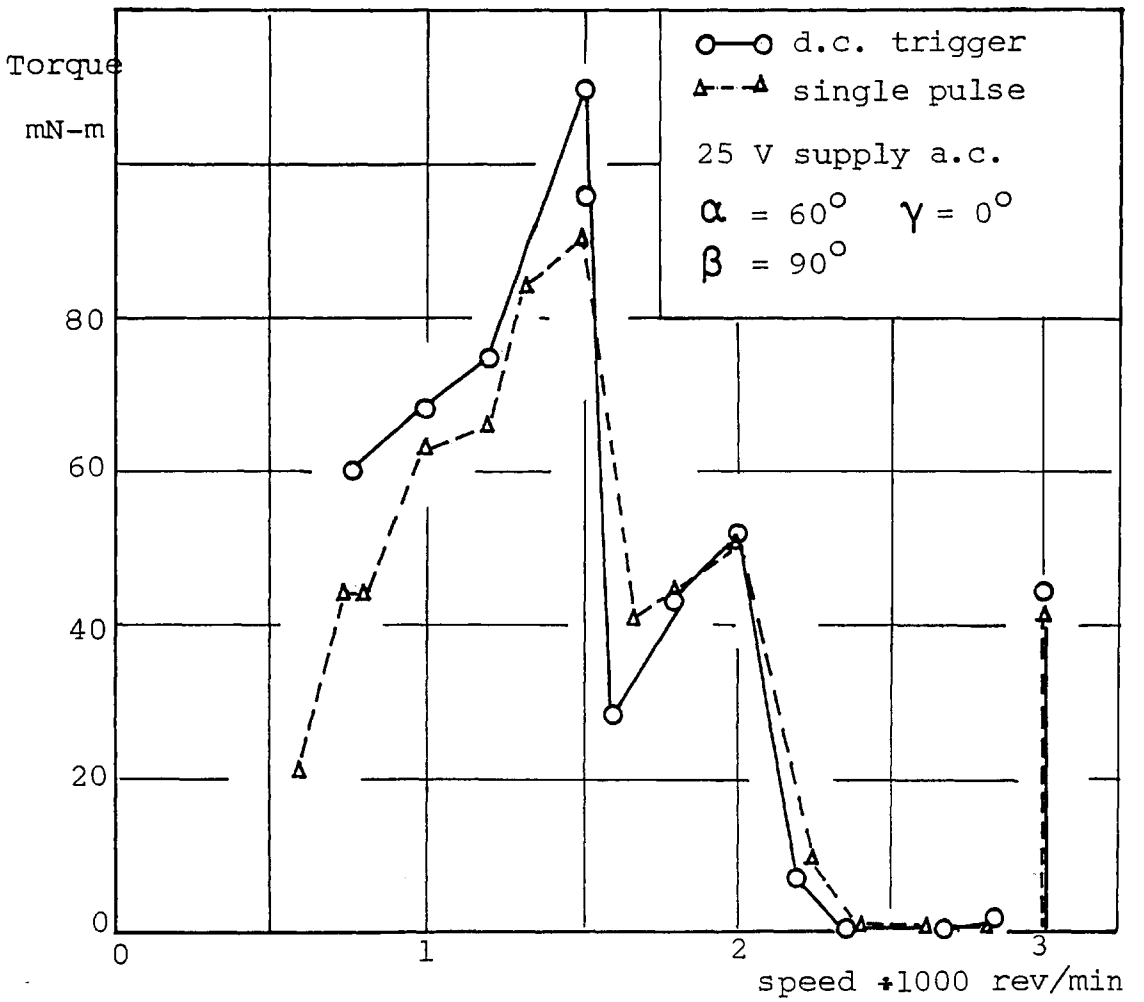

Fig. 5.2.12 Torque versus speed characteristic of the form 1 motor with a.c. triac-fed circuit

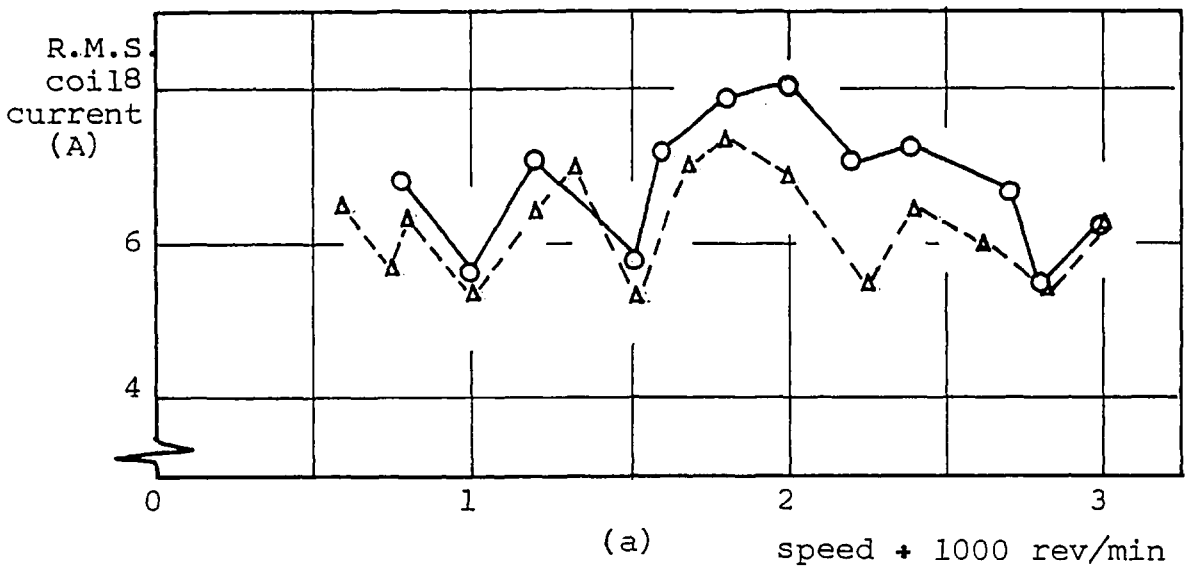

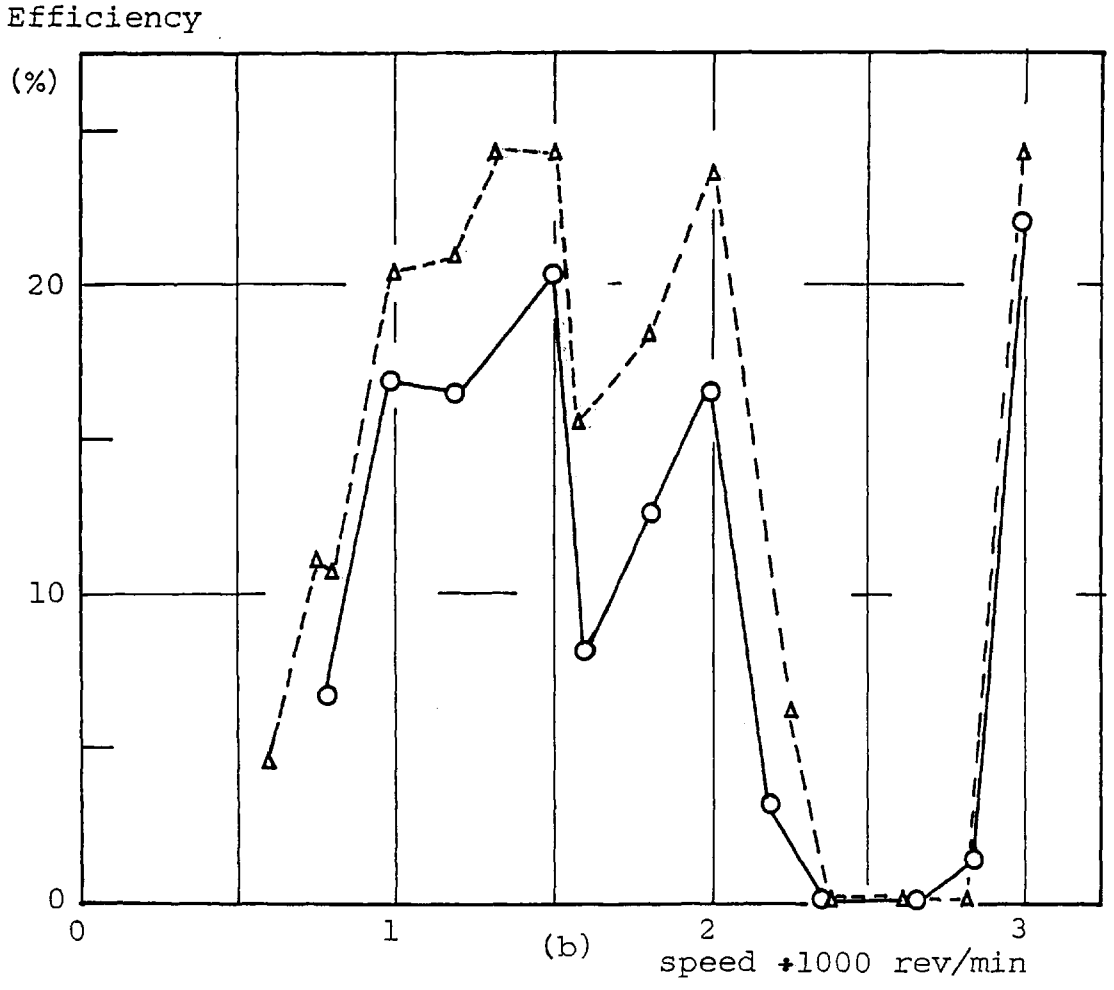

Fig. 5.2.13 (a) Motor r.m.s. current (b) motor efficiency characteristics of the form 1 motor (25 V, α = 60°, β = 90°, γ = 0°)

o——o d.c. trigger
Δ- - - -Δ single pulse

phase-delay and synchronising circuit was seperately supplied from 240 V a.c. mains. A dual rail $\pm$ 12 V d.c. supply was provided for the d.c. trigger firing circuit.

The motor was first tested with the d.c. trigger firing circuit and switching angles of $\alpha = 60^{o}$elec, $\beta = 90^{o}$elec, and zero phase-delay angle. It was found that the maximum operating speed of the motor was 3000 rev/min. Between 3000 and 2300 rev/min, the output torque oscillated, with an average value around zero. The output torque became positive again between 2000 and 1500 rev/min with smaller oscillations and the highest putput torque occurred at 1500 rev/min. Quasisynchronous phenomena were observed at 3000 and 1500 rev/min. For speeds lower than 1500 rev/min, the oscillations were high and no measurements could be made. The amplitudes of the oscillations at these low speeds increased with decreasing speed but the oscillating frequencies generally decreased.

Appreciable speed hunting occurred, this effect clearly being the result of both the nature of beating torque and the overall system response to it. Speed hunting and the beating effects were particularly noticeable at low speeds (due partly to the high percentage changes in speed inevitable at low speeds) and at speeds near to quasisynchronous ones (where beat frequencies are low). The tachometer smoothing circuit, by introducing a phase lag in the feedback loop, was also thought to be contributing to speed hunting and the time constant of the low-pass

filter was later reduced to 4 mS.

To reduce oscillations, a dash pot (with water as damping fluid) was built and fitted at the end of the torque arm. With the damper, further tests were carried out with each firing circuits. The oscillations were reduced and measurements were made from 3000 rev/min down to 800 rev/min. The results are as shown in Fig. 5.2.12 and Fig. 5.2.13.

In order to reduce speed hunting and to enable the torques to be more accurately measured, an inertia in the form of a steel disc of 4 " diameter and ½ " thickness was fitted on to the motor shaft. The flywheel and the damper reduced speed hunting and oscillations and further tests conducted. With the single-pulse firing circuit tests were done with $\alpha = 90^{\circ}$, $\beta = 90^{\circ}$ and zero phase-delay angle γ. With the d.c. trigger firing circuit tests were done with four sets of α and β with zero phase-delay angle. The results are shown in Figs. 5.2.14 and 5.2.15.

5.2.4 Results and discussion

5.2.4.1 Test results

The results of load tests on the form 1 motor with a 25 V a.c. supply and $\alpha = 60^{\circ}$, $\beta = 90^{\circ}$ and $\gamma = 0^{\circ}$ with both d.c. trigger firing circuit and single-pulse

firing circuit are shown in Figs 5.2.12 and 5.2.13. Comparison of the torque-speed characteristics in Fig 5.2.12 shows that output torque is little affected at least at zero phase-delay angle by the choice of firing circuit, and no advantage is gained by using a d.c. trigger circuit at zero phase-delay angle. The similarity between the actions of the single-pulse circuit and the d.c. trigger circuit at zero phase-delay angle has already been discussed in Section 4.4.1 (see Fig. 4.4.2). It can be seen that although the maximum operating speed is 3000 rev/min, there is a narrow band of zero average torque between 2400 and 3000 rev/min. It is obvious that the motor can not be used to drive a load within this band.

Quasisynchronous phenomena occur at 3000, 2000, 1500 and 1000 rev/min and at these speeds relatively high output torques are available with an absence of low frequency beating phenomena. The maximum output torque occurs at 1500 rev/min and is 110 mN-m with the d.c. firing circuit. The average r.m.s.currents lie between 6 and 8 A over almost the entire measured speed range but lower currents occur at quasisynchronous speeds (Fig. 5.2.13(a)). Fig. 5.2.13(b) shows that motor efficiencies are rather low in absolute terms and only 25 % maximum efficiency was achieved at quasisynchronous speeds. (Note though that the efficiency levels are comparable with those measured with the motor in its original induction form) Fig 5.2.14 shows the corresponding torque-speed characteristics (again with V = 25 V, $\alpha = 90^{\circ}$, $\beta = 90^{\circ}$, $\gamma = 0^{\circ}$) obtained with

the single-pulse firing circuit with two loads of differing inertia. With higher inertia, the oscillations and hunting are reduced and a band of zero torques now shows clearly in the speed range between 2400 and 3000 rev/min. The inertia level seems to affect the measured mean torque value particularly at speeds near 1600 rev/min. This is presumably due to changes in the amplitude of the speed limit cycle and the effect this has on the torque pulse sequence. With the lower inertia it was found that whereas at speeds just above the quasisynchronous speed of 1500 rev/min (1500 to 1600 rev/min) the output torque decreases to a low value, at speeds beyond this (e.g. 1666.67 rev/min at which the torque cycle time is only 180 mS and 2000 rev/min at which the torque cycle time is only 60 mS) the output torque increases sharply. A substantial higher measured torque was also recorded with the higher inertia at 750 rev/min.

Fig. 5.2.15 shows comparisons of the torque-speed characteristics for four different α and β settings, of the form 1 motor with higher inertia load operating with the d.c. trigger firing circuit. Besides the general characteristics mentioned ealier the effects of α and β on high-speed and low-speed performances can be clearly seen. It can also be seen that with large α (a and b), high negative torque pulses causing low output mean torques occur at low speeds, whereas large β (a and c) gives better performance at high speeds. If switching angles must be left fixed a reasonable compromise in overall performance

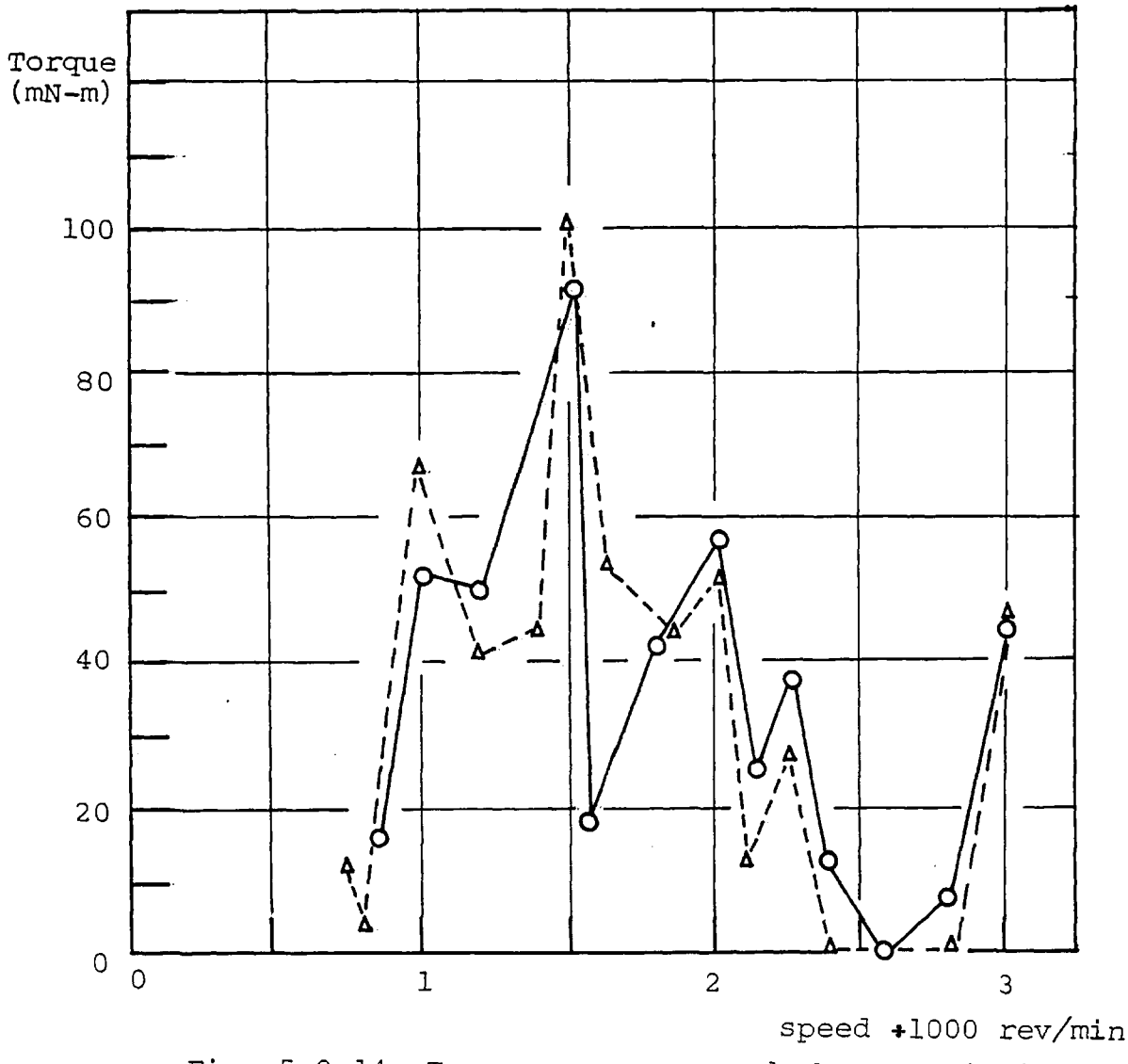

Fig. 5.2.14 Torque versus speed characteristics obtained with single-pulse firing circuit (25 V, $\alpha = 90^{\circ}$, $\beta = 90^{\circ}$ $\gamma = 0^{\circ}$) but with two loads with differing inertia

o——o damper only

Δ----Δ flywheel and damper

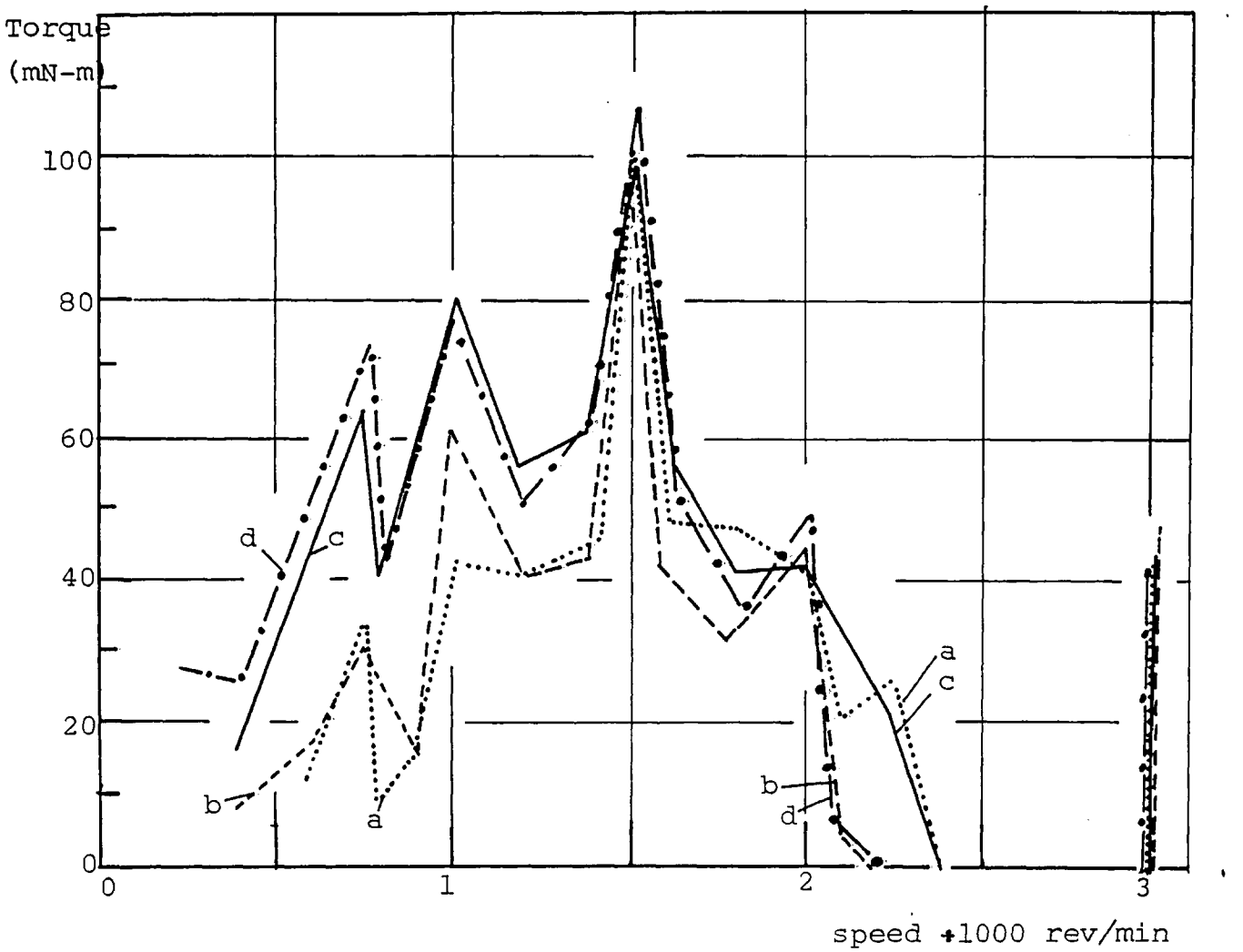

Fig. 5.2.15 Variation of torque versus speed characteristics with different switching angles

		α°	β°
a	.....	90	90
b	- - - - - -	90	60
c	———	60	90
d	—·—·—	60	60

(25 V, $\gamma = 0^\circ$ with damper and flywheel)

can be obtained (for this set of switching angles) with the case c values (α = 60°elec and β = 90°elec).

Fig. 5.2.16 shows the performance curves for case c where α = 60° and β = 90°elec. The maximum power output obtained at 1500 rev/min is 16 W with a maximum efficiency of 30 %. The efficiencies are higher at quasisynchronous speeds because at these speeds the input currents are less than at the non-quasisynchronous speeds (5.0 A at 1500 rev/min compared to 7.0 A at 1800 rev/min). The r.m.s. current can again be said to be approximately constant (at 6 A) virtually throughout the whole operating speed range.

A test was carried out to investigate the effects of the zero average torque bands (at very low speed and at speeds near 3000 rev/min) on the acceleration of the motor. In this test the motor shaft was disconnected from the dynamometer and a pure inertial load put on the shaft. Test conditions were: 25 V supply, α = 90°, β = 90° and γ = 0°. The motor was the same form 1 motor but with a new winding having 8.6 % fewer turns than before (115 turns of 1.12 mm diameter copper wire). Different inertial loads were examined and the motor switched on at standstill and allowed to run up to maximum speed in each case. It was found that despite the zero average zero torque bands the motor was able to accelerate from standstill to synchronous speed (3000 rev/min) with added inertial loads of up to 160×10^{-7} kg-m^2 (about 88 % of the

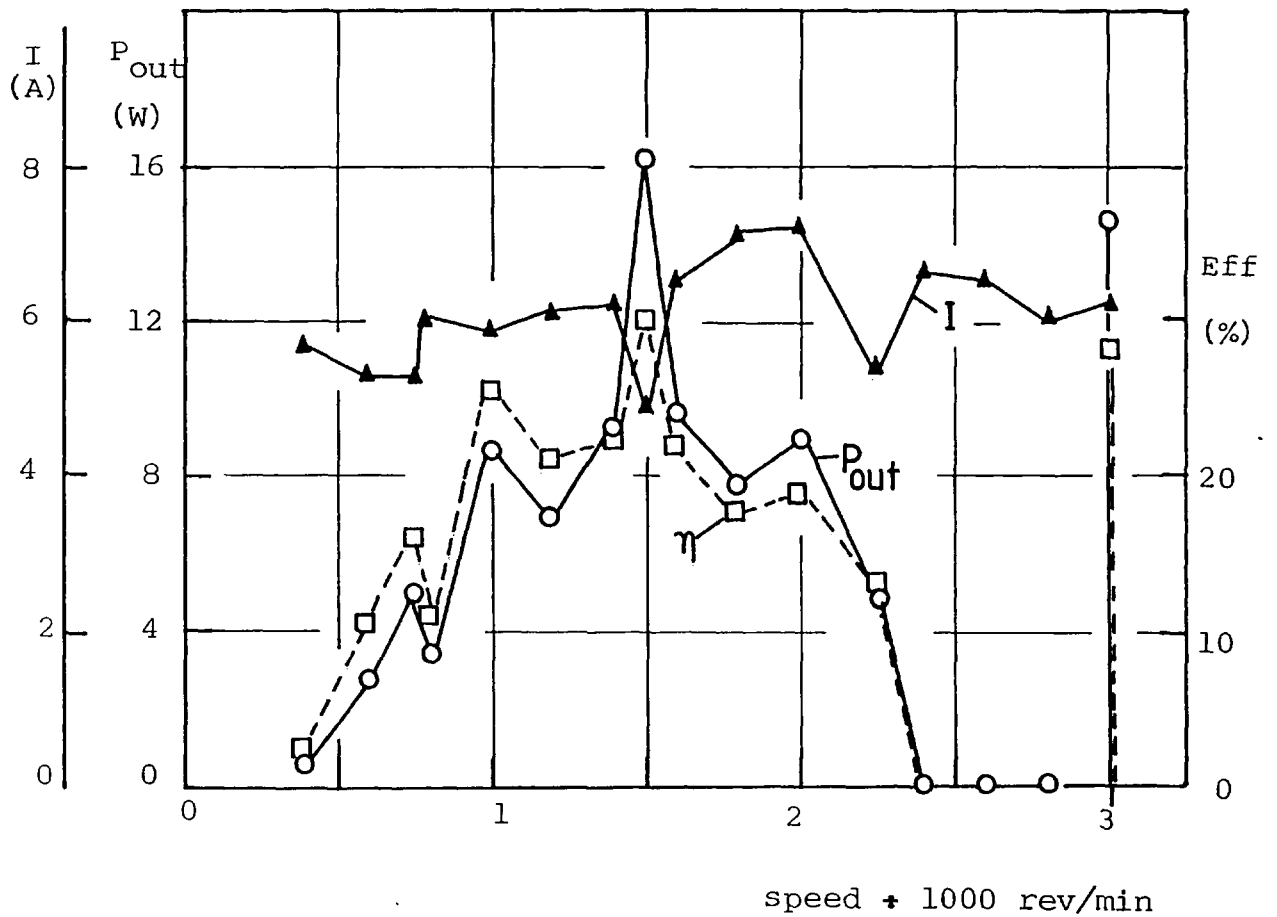

Fig. 5.2.16 Performance curves for case c ($\alpha = 60^{o}$, $\beta = 90^{o}$)

inertia of the rotor : rotor inertia being estimated as 180×10^{-7} kg-m^2).

Fig. 5.2.17 shows the coil voltage and coil current waveforms of the motor operating (with the single pulse firing circuit) with $\alpha = 90^{\circ}$ and $\beta = 90^{\circ}$ elec and zero phase-delay angle. All traces correspond to quasi-synchronous speeds because of the difficulties in dealing with non-repetitive waveforms on an ordinary oscilloscope. At quasisynchronous speeds the current pulses are of course repetitive though some pulses may have negative polarity as in case d and f. At 3000 rev/min with zero phase-delay angle, the winding sees full mains voltage and the motor behaves in the same way as a reluctance motor with fixed frequency supply. In case b , the corresponding switching signal waveform is shown and the carry-over current into the 'off' periods can be clearly seen. The current waveforms were monitiored from a 0.15 Ω current shunt connected in series with the motor coil.

5.2.4.2 Predictions

Theoretical investigations were carried out using the step by step approach explained in section 3.3 on the steady state operation of the form 1 motor with d.c. trigger firing circuit. It is important to note that the equivalent circuit parameters used in the predictions obtained from measurements (Clearly the use of calculated

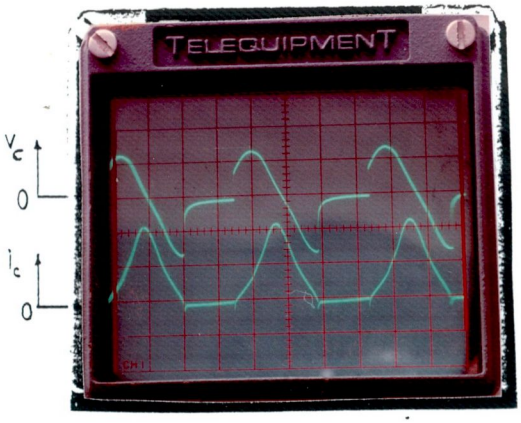

(a) 1500 rev/min (no load)

I_{rms} = 4.3 A

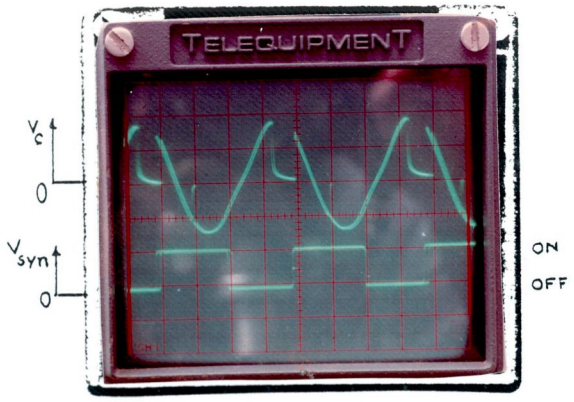

(b) 1500 rev/min

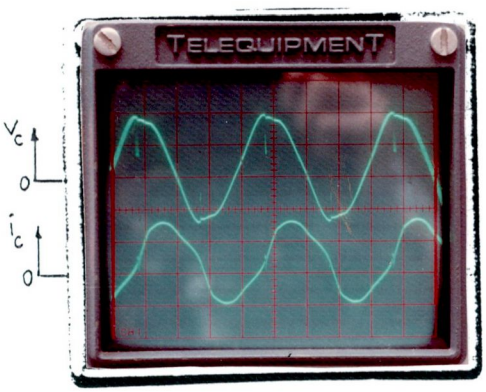

(c) 3000 rev/min (no load)

I_{rms} = 5.7 A

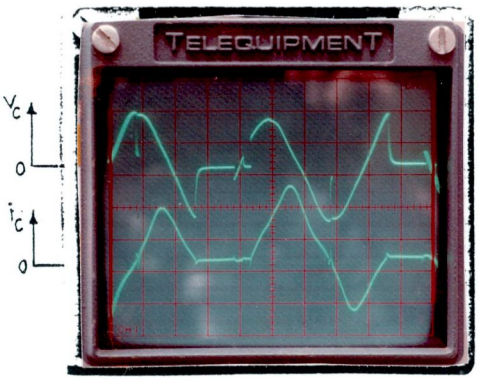

(d) 2000 rev/min

I_{rms} = 6.7 A

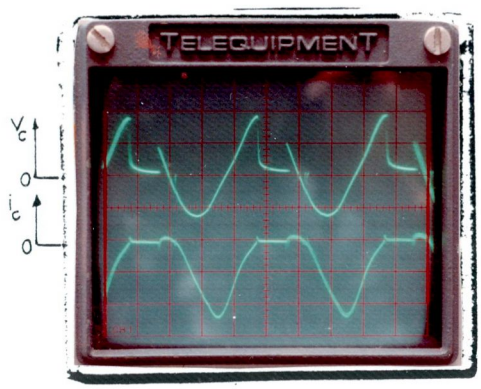

(e) 1500 rev/min (on load)

I_{rms} = 4.7 A

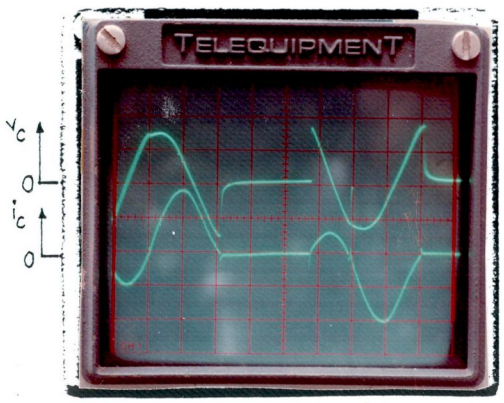

(f) 1000 rev/min (on load)

I_{rms} = 5.2 A

Fig. 5.2.17 Waveforms of coil voltage, coil current and switching signal (b)
Scale: v 20 V/div, switching signal 5 V/div,
i 6.66 A/div, t 5 mS/div

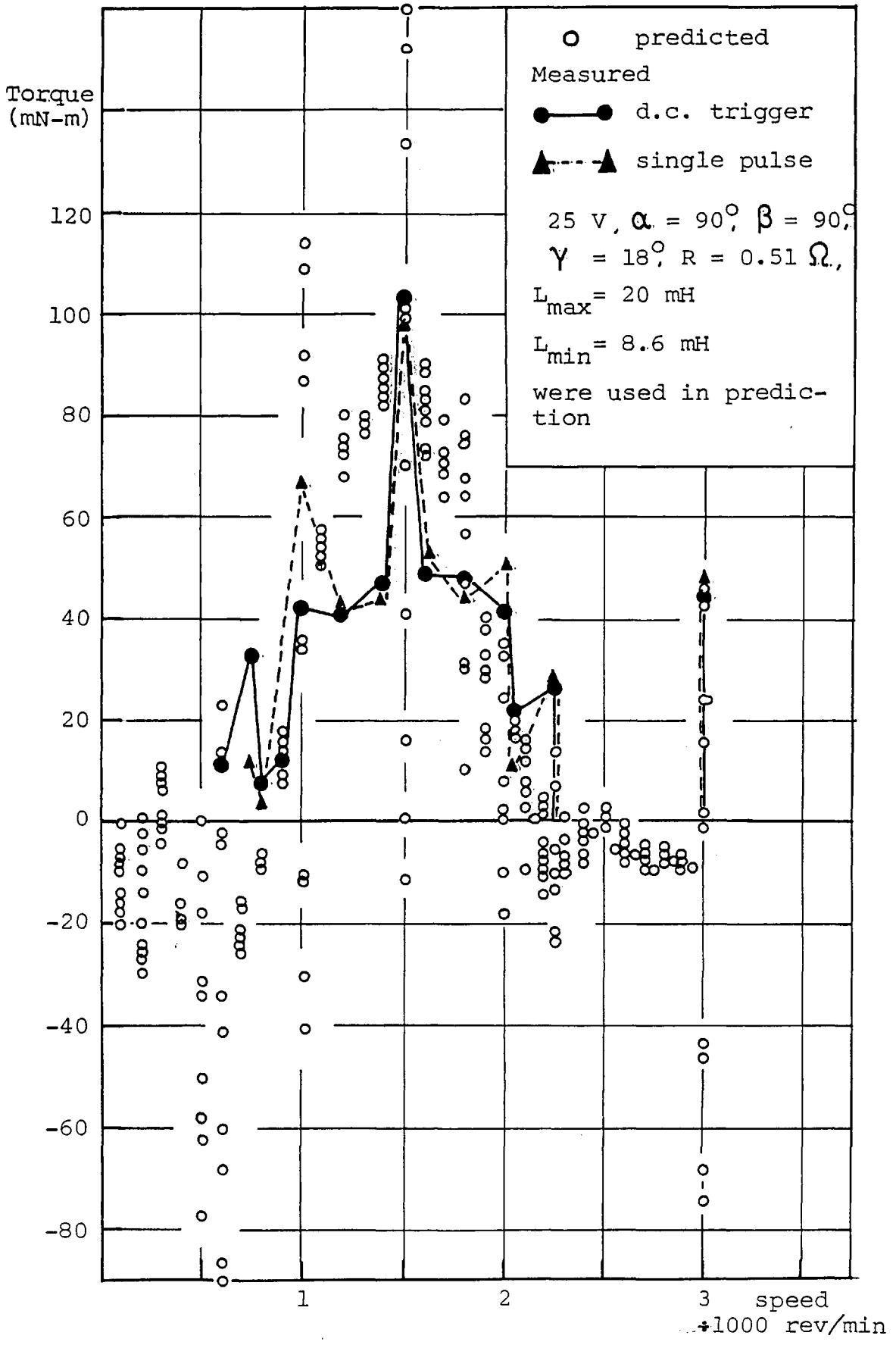

Fig. 5.2.18 Comparisons between the predicted characteristics and the test results with both firing circuits

parameters would have been preferrable, but the primary objective was to check the validity of the performance prediction method, and to exclude consideration of correlation errors due to inaccuracies in parameter prediction methods. The measured parameters are $R = 0.51\ \Omega$, $L_{max} = 20$ mH and $L_{min} = 8.6$ mH). Although the quite long time step of 1 mS was used in the computations as a compromise between accuracy and computing time, the calculation was lengthy especially for the non-quasisynchronous speeds. The program also had to calculate a number of operating points (corresponding to the whole range of possible voltage phase angles 'θ') at each speed in order to find the possible range of developed torques. A range of 'θ' from 0° to 180° with 18° interval was used in the calculations.

Comparisons between the predicted characteristics and the test results with both firing circuits are shown in Figs. 5.2.18 and 5.2.19. In each case results were obtained for $\alpha = 90^{\circ}$, $\beta = 90^{\circ}$ with minimum phase-delay angle. According to the firing circuit configuration previously explained, the minimum phase-delay angle for the d.c. firing circuit was approximately 4° and for the single pulse firing circuit was 7°. The predictions were hence made with 18° phase-delay angle, this being the minimum phase-delay angle that can be set in the program due to the 1 mS time step used. There is a clear evidence of zero and/or even negative torques bands at low speeds and at speeds near synchronous speed (3000 rev/min).

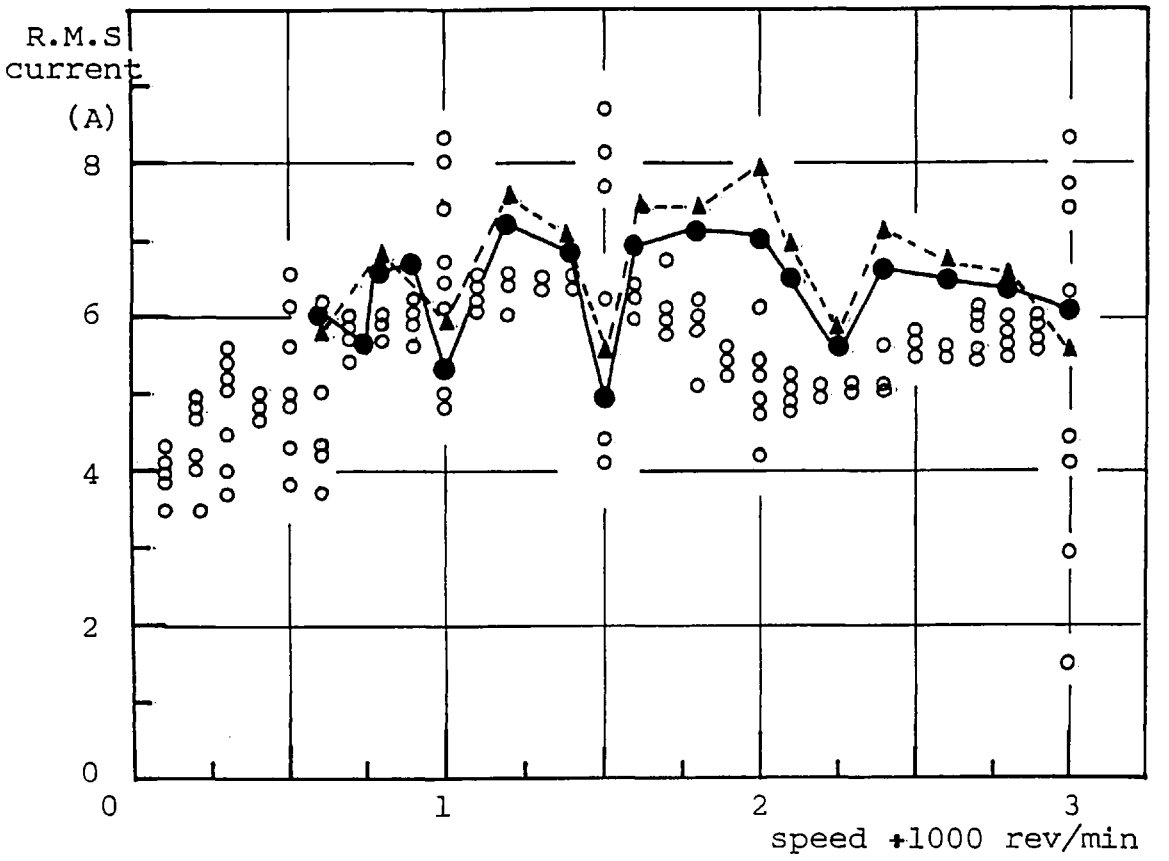

Fig. 5.2.19 Comparisons between predicted characteristics and test results with both firing circuits

o predicted, measured ●——● d.c. trigger
▲- - -▲ single-pulse

Examinations were made of predicted instantaneous torque waveforms and two typical cases (2700 rev/min and 400 rev/min each in zero average torque bands) are shown in Fig. 5.2.20. The following additional data applies:

$I_{rotor} = 181.6 \times 10^{-7}$ kg-m^2 (friction neglected)

Case		(a)	(b)
speed	rev/min	2700	400
average torque	mN-m	+5.9	-8.8
biggest forward torque pulse ($\int T\,dt$ N-m-S)		1440×10^{-6}	2560×10^{-6}
$\Delta\omega = \frac{\int T\,dt}{I_{rotor}}$	rev/min	757	1340

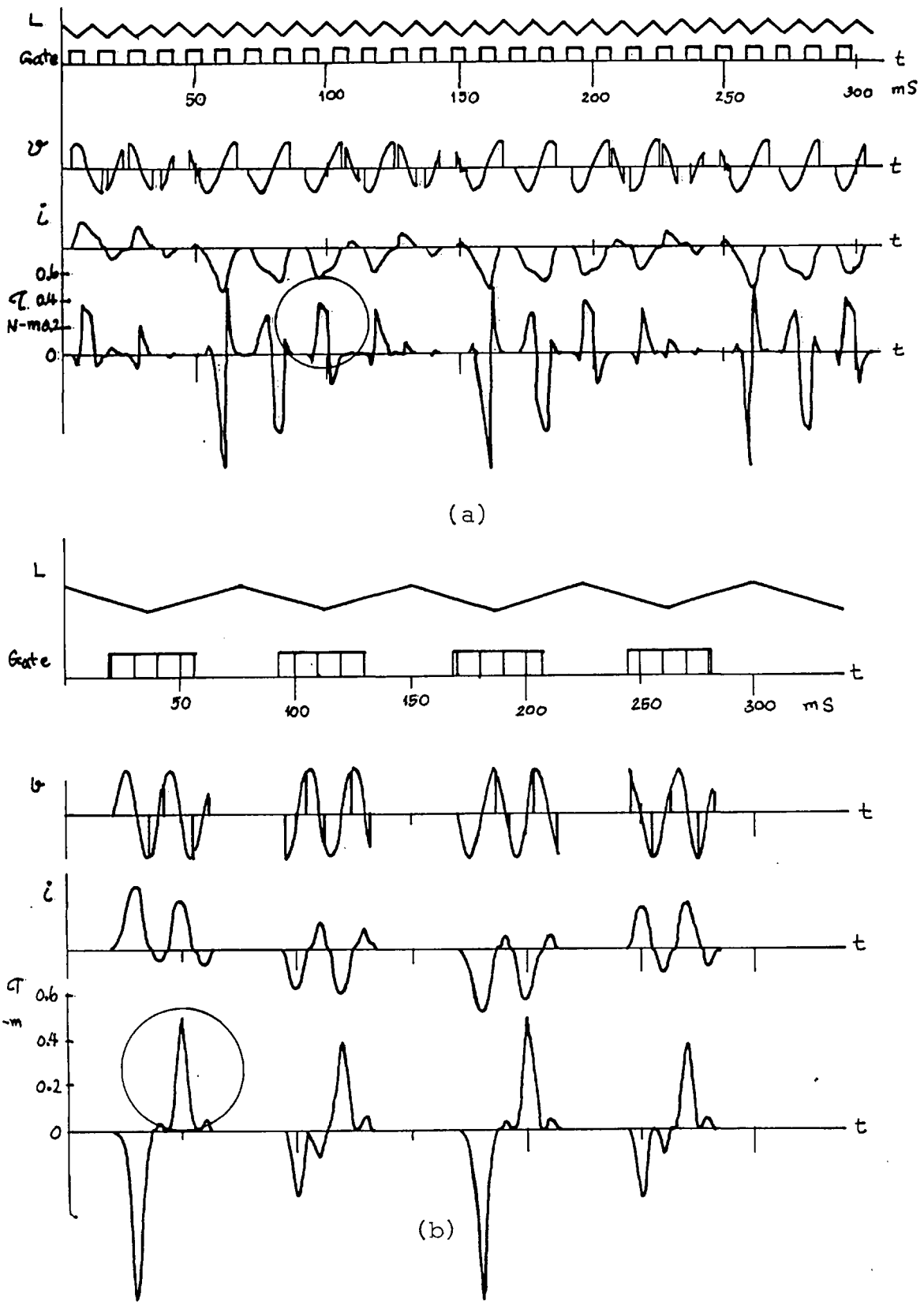

Fig. 5.2.20 Predicted current and torque waveforms
(a) at 2700 rev/min
(b) at 400 rev/min

Hence, although the average torques for these two speeds are low or negative, the biggest forward torque pulses are able to accelerate the rotor to higher speeds before the next negative torque pulses occurs. From this investigation, which is supported by the fact that in the test the motor was able to accelerate quite significant inertial loads to synchronism, it would seem that this ability is closely related to synchronising ability of synchronous and reluctance motors on fixed frequency supplies whereby the rotor gains sufficient speed during a positive torque pulse to attend a speed where the mean torque is positive and sufficiently large to maintain continued operation.

It should be noted that although an absolutely constant speed is assumed during the prediction process, in practice the motor speed and torque will follow limit cycles whose magnitudes will partly depend on the nature of load. This is because of the presence of both positive and negative torque pulses in the instantaneous torque. The analysis of the nature of the variation in speeds is reckoned to be possible with the time stepping approach developed, simply by adding another equation relating torque, inertia and acceleration. Unfortunately, further investigations on this topic have not been made due to the lack of time.

A final comment should be made about current levels particularly since this affects harmonic amplitudes

in the mains. Current levels in the investigation described above are quite high (6 - 7 A) for the voltage level used (25 V) because of the low number of winding turns (130). However, it is of course possible to operate the motor, rewound, at a higher voltage and lower current.

If for instance the number of turns is increased by a factor k, the impedance of the winding Z will increase by k^2 and hence if the motor is run on a supply voltage of k times the original, coil current will be only 1/k times the original. The power output $P \propto VI$, flux density (V/k) and the current density remain constant.

Hence, if the voltage supply is increased by a factor of 9.6 from 25 V to 240 V and the number of turns from 130 turns to 9.6x130 = 1248, the current will be approximately (6/9.6) = 0.62 A with the same power output.

It is interesting to note from this that the motor would now be comparable with the as-purchased shaded-pole motor operating from the mains (1300 turns of winding and operating current of 0.5 A). Some comparisons between the as-purchased shaded-pole motor and the form 1, triac-fed motor rewound for 240 V operation are shown in Table 5.1.

Table 5.1

Motor		as-purchased shaded-pole	form 1 triac-fed rewound
mode of operation (speed)		fixed	variable
operating current	(A)	0.5	0.62
operating voltage	(V)	232	240
max speed	(rev/min)	3000	3000
max power output	(W)	15	16
max efficiency	(%)	25	30
power factor*	(p.u.)	0.5	0.36

* as calculated from (watt-meter reading)/ $V_{rms}I_{rms}$

5.3 Performance of the two-pole motors with 'd.c.' link transistor-fed circuit

5.3.1 Introduction

Investigations started with the form 1 motor, the early stages involving modifications to its structure (stator, rotor, winding) to improve its performance as a SPSRM. The following changes were made to the original structure of the motor shown in Fig. 5.3.1:

Step 1. The shading rings were removed and the rotor was milled flat on both sides to form two salient poles each 90° mech arc. The permanent magnetic bridges

on the stator and the end rings were still left intact. The permanent magnetic bridges are said to improve the performance of the motor in its shaded-pole form[5.3] due perhaps to the resulting smoothness in the airgap flux distribution. The closed stator structure also has the advantage of being stronger and the laminations are easier to punch. Because of these advantages the bridges were at first left on the stator. The minimum width of the bridge section is only 2 mm compared with the 35 mm of the entire pole, so in normal operation the bridge sections should be well-saturated and the leakage flux limited to a low value. The rotor bars and rings remaining after milling were also not removed in order to preserve the rotor's strength and because it was hoped that the effect of the cage in interfering with the motor's operation would be small. Preliminary tests carried out with the simple circuit of Fig. 5.3.2 at 30 V with $\alpha = 30^{\circ}$ and $\beta = 60^{\circ}$ disproved this, the motor failing to start or run even with an initial spin applied to the shaft.

Step 2 . A gap of 5 mm width was cut at the middle of the top bridge of the stator to reduce the leakage flux. The motor still failed to operate.

Step 3. Another gap of the same width (5 mm) was cut at the middle of the lower bridge of the stator. At this stage, the two stator poles were completely separate with 5 mm gaps. The motor then ran slowly with the same test circuit. The maximum speed was approximately

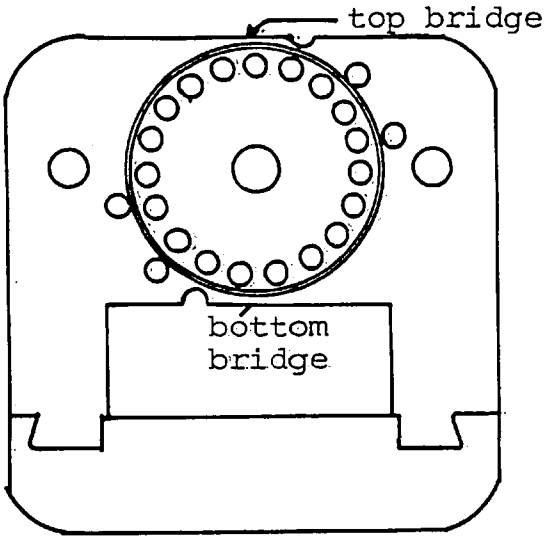

Fig. 5.3.1 The form 1 motor stator

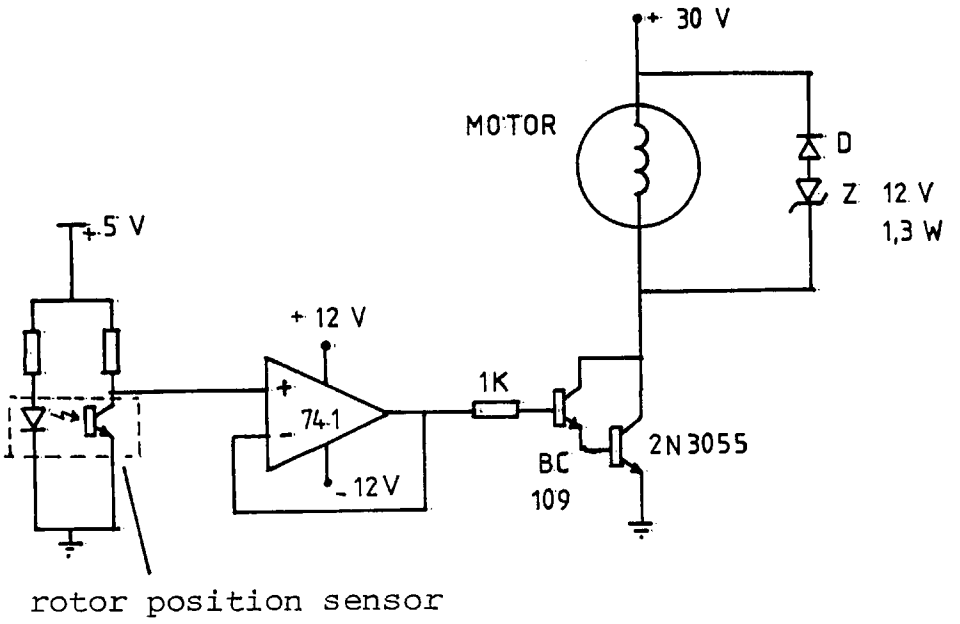

Fig. 5.3.2 Low voltage d.c.fed circuit

300 rev/min with a very small torque.

Step 4. It was concluded that the stator pole gap of 5 mm was not wide enough. The leakage flux was still high because even with the rotor in the q position the leakage flux could travel from one stator pole to other via the rotor without difficulty due to the appreciable overlap between the stator and rotor poles. The stator poles were hence cut to the same width as the rotor pole arc (90°mech). When tested with the same circuit, the motor started and ran up to a no-load speed of 470 rev/min with a coil current of 100 mA on 30 V supply. The motor was also tested at other voltage levels from 10 to 60 V and it was found that the motor operated at voltages between 10 and 30 V but failed to operate at the voltages between 35 and 60 V. The rotor cage was suspected to be the cause of trouble at the higher voltages, high braking torque presumably being produced. It was hence decided that in order to get better performance out of the motor: 1) the rotor end rings should be removed to open circuit the cage and 2) a better coil-current pull-down method and 3) a higher supply voltage level circuit were needed.

Inductance measurements were made at each stage using the P, I, V method at 50 Hz (as used with 6 saliency motor) and are shown in Table 5.2. An increase in L_d to L_q ratio can be seen for each stage of the development and the final ratio was 2.35.

Table 5.2

The winding resistance measured with 'Kelvin bridge' is 34.2 Ω .

Step		Test voltage (V)	L_d (H)	L_q (H)	L_d/L_q ratio
1	 complete stator rotor with end rings	235	1.67	1.30	1.28
2	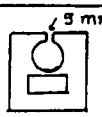 rotor same as in 1	240	1.52	1.18	1.28
3	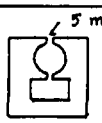 rotor same as in 1	234	1.32	1.10	1.20
4	 rotor's end rings removed	150	1.98	0.84	2.35

Note In step 4 the test voltage was reduced from 240 V to 150 V to avoid excessive currents in the q position.

L_d increased at step 4 perhaps because of the increase in airgap flux due to the absence of the cage.

5.3.2 The PWM circuit and driver circuit for the two-pole motors

During the development a new PWM and driver circuit with cheaper PWM and driver chips were designed and constructed. The main components of the circuit are the regulating pulse width modulator chip SG 3524 and the dual high current output driver chip SG 3627. The control circuit was designed to drive power darlington transistors in the half bridge inverter configuration. An isolated driver circuit is still required for the top transistor connected between positive rail and load so only half of the dual driver chip can be used to drive the bottom transistor.

Full details of both PWM and driver chips are given in Refs. 5.4 and 5.5 but extracts from these are included for reference purposes.

" a) The regulating pulse width modulator SG 3524 contains all the control circuitry needed for a regulating power inverter or switching regulator. Fig. 5.3.4 shows the block diagram of the circuit in the package which includes voltage reference, error-amplifier, oscillator, pulse width modulator, pulse steering flip-flop, dual alternating output switches and current limiting and shutdown circuitry.

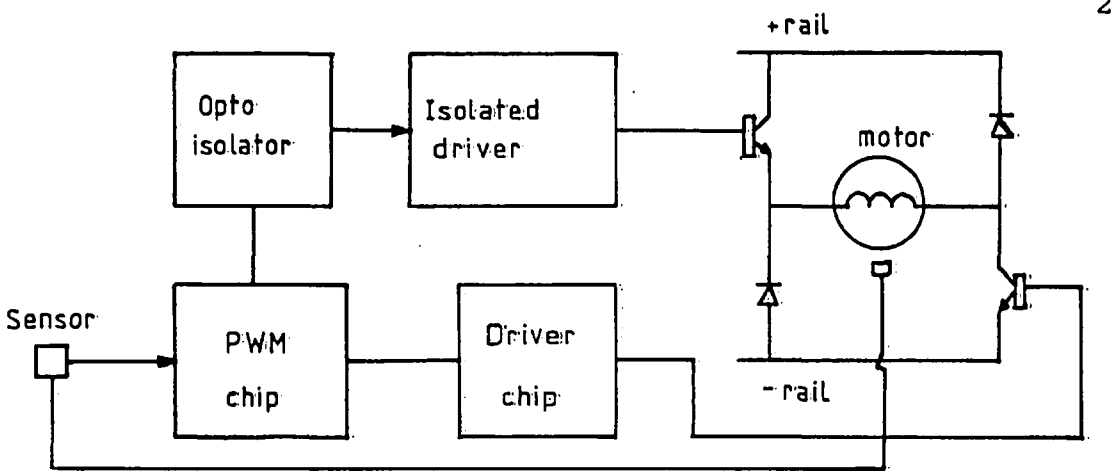

Fig. 5.3.3 Schematic diagram of the PWM transistor-fed circuit

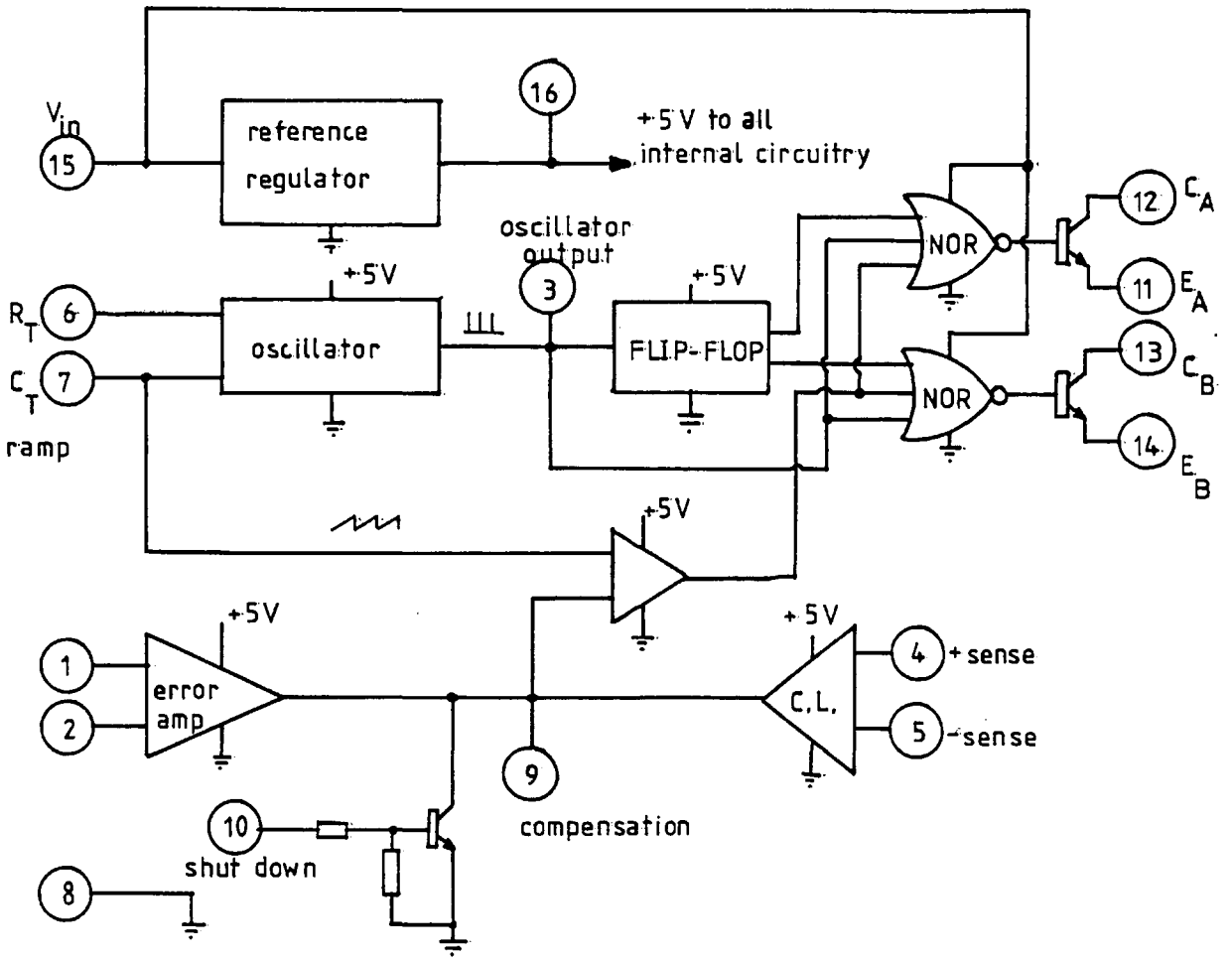

Fig. 5.3.4 Block diagram of the internal circuit of the PWM chip SG 3524

approximately 30 μA to 2 mA, i.e. 1.8 k $\lesssim R_T \lesssim$ 100 k. The range of values for C_T also has limits as the discharge time of C_T determines the pulse width of the oscillator output pulse. The pulse is used (among other things) as a blanking pulse to both outputs to insure that there is no possibility of having both outputs on simultaneously during transitions. Practical values of C_T fall between 0.001 and 0.1 μF. The oscillator period is approximately $t = R_T C_T$ where t is in microseconds when R_T = ohms and C_T = microfarads." With 0.1 microfarads and 10 k used in the circuit, the oscillator frequency was set to 1 KHz. The two outputs were connected in parallel for an effective 0-90 % duty cycle and the frequency of output was equal to the frequency of the oscillator.

" The mark to space ratio of the output signal is controlled by means of the voltage at pin 2 which is then compared with the ramp voltage across C_T and the output signal from the comparator is used to control two NOR gates at the output stage. Synchronisation with the switching signal is possible via pin 10 which will shut down the input signal if sufficient current is supplied to it (in this circuit +5 V switching signal is fed through a 2.2 K resistor).

The current limiting circuitry is provided through pin 4 and pin 5 with pin 4 at positive potential and pin 5 at negative potential and the threshold voltage is approximately 200 mV. Although the circuit provides

a relatively small threshold with a negligible temperature coefficient, there are some limitations to its use, the most important of which is ± 1 volt common mode range which requires sensing in the ground line."

The output signal from the collector of the output transistor of the PWM chip was coupled to the inverting input of the driver chip through a small diode. The output stage of the driver was arranged as a totem pole switching circuit with -5.3 V negative pull down.

The driver circuit for top transistor is shown in Fig. 5.3.7 with its isolated power supply. The opto isolator provides isolation between the PWM chip and the driver stage. A totem-pole switching circuit was also used at the output stage.

5.3.3 Performance of the form 1 motor (with original winding)

5.3.3.1 Load tests

The tests which were carried out with the form 1 motor can be divided into two stages. In the first stage, the motor was tested at a fixed voltage level but with different switching angles in order to find the optimum angle for high speed performance. In the second stage further tests were done at the optimum angles.

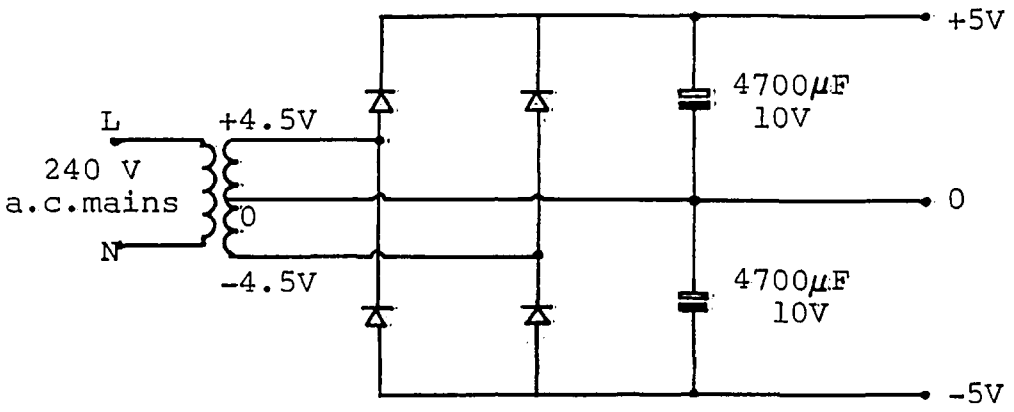

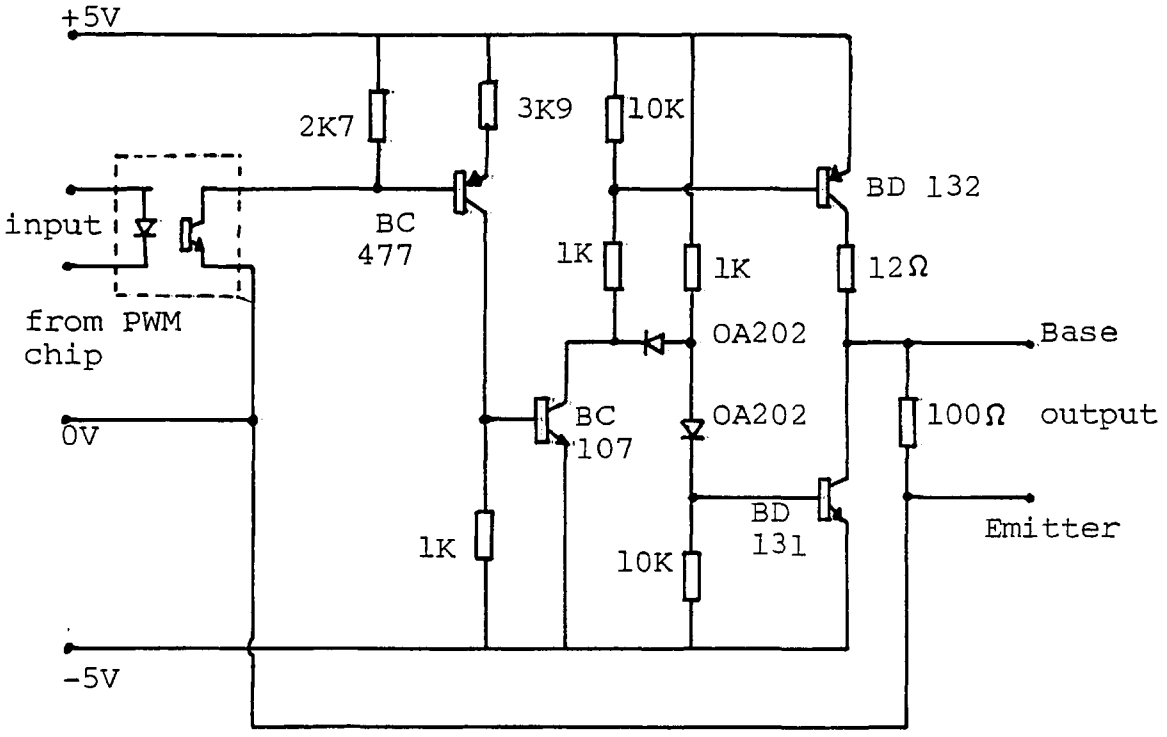

Fig. 5.3.7 Isolated driver circuit

Fig. 5.3.8 shows the arrangement of the test circuit in which the mains supply was stepped down, rectified and fed to the d.c. rail of the inverter bridge. The d.c. voltmeter, moving coil ammeter and wattmeter were used to measure d.c. rail voltage, input current and input power to the motor respectively. The motor output torque was measured by pulley and spring balances as shown in Fig. 5.3.9 (a) and the motor speed by an electronic stroboscope calibrated using the switching signal. The rotor position was sensed by means of an optical switch and a rotor-mounted disc made of perspex. The switching angles were adjusted by varying the position and length of the black tape on the disc. Fig. 5.3.9 (b) shows the actual size of the rotor position disc. The black patches correspond to 'off' periods. The PWM and driver unit and the isolated driver circuit were housed in cast aluminium boxes to protect the circuits from interference caused by the switching action of the main transistors and electromagnetic interference from the motor itself. The main transistors were protected against high rates of rise of current and voltage by snubber circuits (not shown in the diagram).

5.3.3.2 Results and discussions

The measured torque-speed characteristics of the form 1 motor with its original (1300 turns) winding with different switching angles and a 165 V rail are shown in Fig. 5.3.10. The d.c. rail voltage of 165 V gave

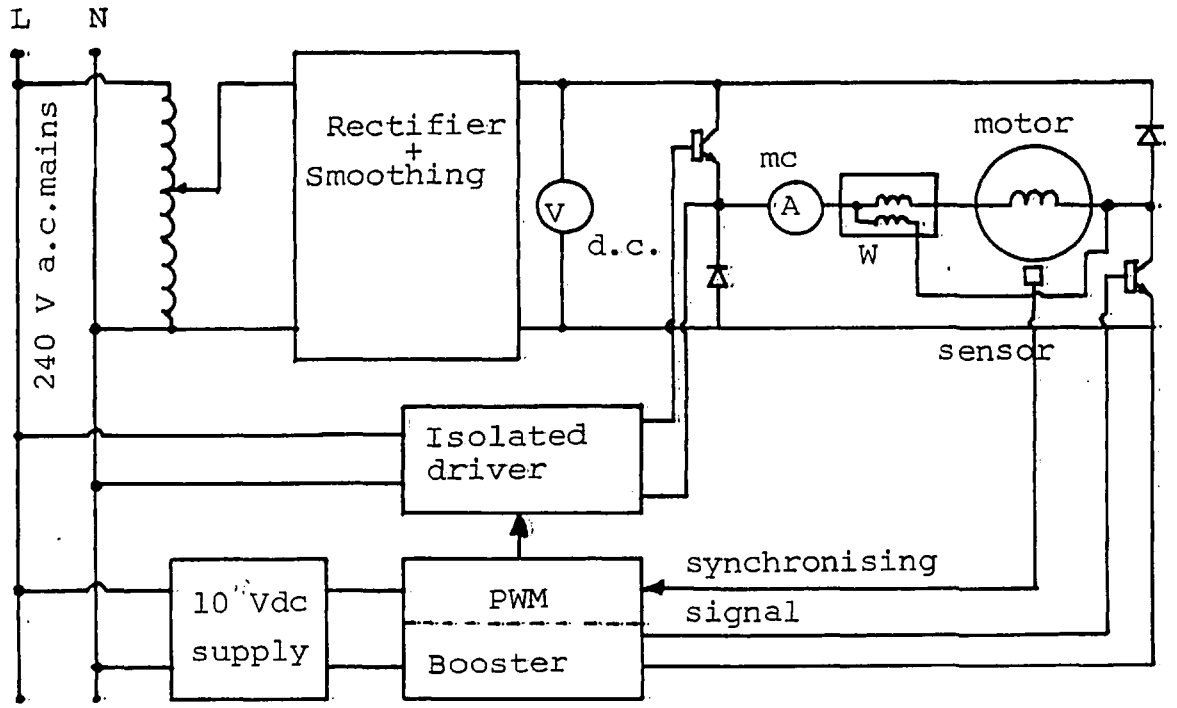

Fig. 5.3.8 Test circuit

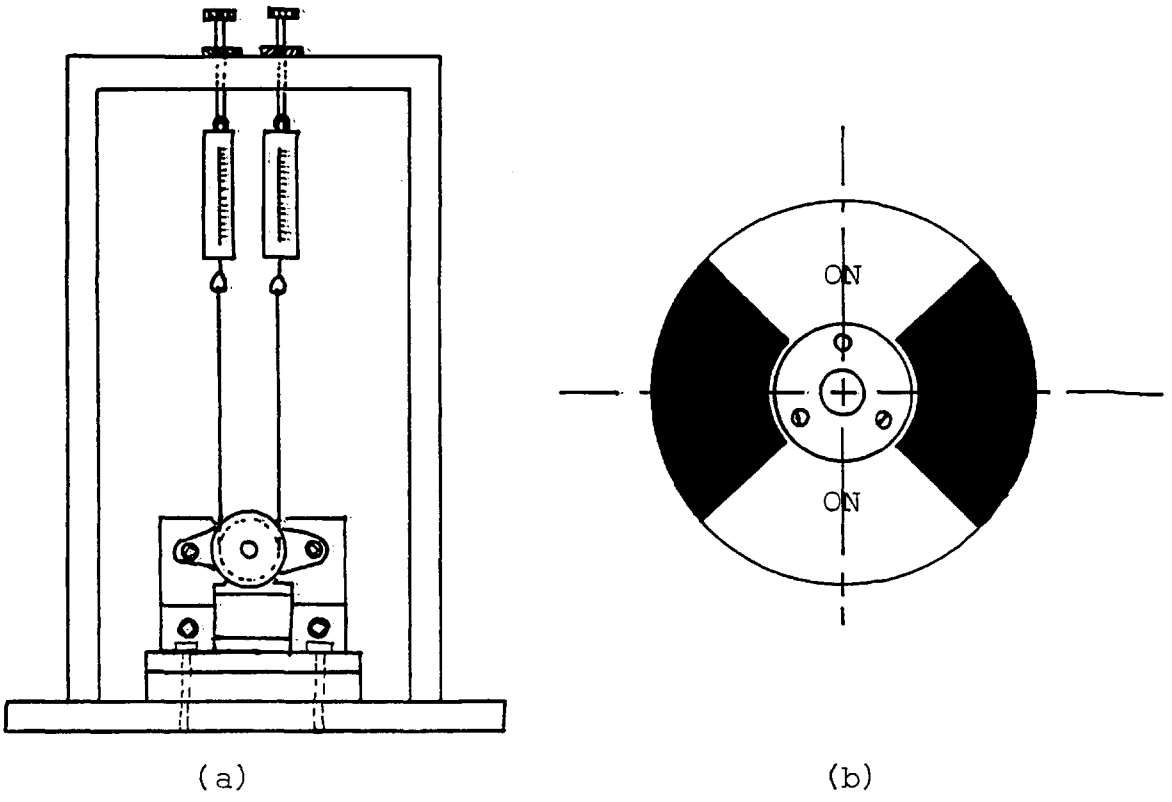

(a) (b)

Fig. 5.3.9 (a) Test rig with spring balance system (pulley diameter = 25.4 mm)
(b) Rotor position disc (perspex)

sufficient current at high speeds. Overheating of the motor coil at low speeds was prevented by the 0.5 A current limit. Curves 1,2 and 3 show the improvement in output torques with increasing advance switching angles for the same 'on' period. The no-load speeds can be seen to increase from 2100 rev/min for $\alpha = 0^{\circ}$ and $\beta = 0^{\circ}$ to 5700 rev/min for $\alpha = 60^{\circ}$ and $\beta = 60^{\circ}$. Curves 4,5,6 and 7 show the effects of advance 'on' angles α for a fixed advance 'off' angle β of 85°. With fixed β, increasing α will increase the length of 'on' period and hence more power is fed to the coil. Although the use of an advance 'on' angle means that the current is switched on in the negative torque region, the overall effect can be positive due to the increase brought about in the current during the positive torque region. It can be seen that the no-load speed has increased from 6400 rev/min for $\alpha = 35^{\circ}$ to 8400 rev/min for $\alpha = 95^{\circ}$. Further increase in α to 115° gives still higher torque and power but the no-load speed drops to 8100 rev/min. Comparisons between two characteristic curves 8 and 9 in which the 'on' periods ($\alpha + 180 - \beta = 210^{\circ}$) are equal show that more torque is available with curve 9 where α and β are each 20° less than the values used for curve 8.

Fig. 5.3.11 shows the corresponding mean currents and efficiencies. Curves 1,2, and 3 in (a) show that the advance switching strategy not only improves output power but also improves the motor efficiency. For a fixed β

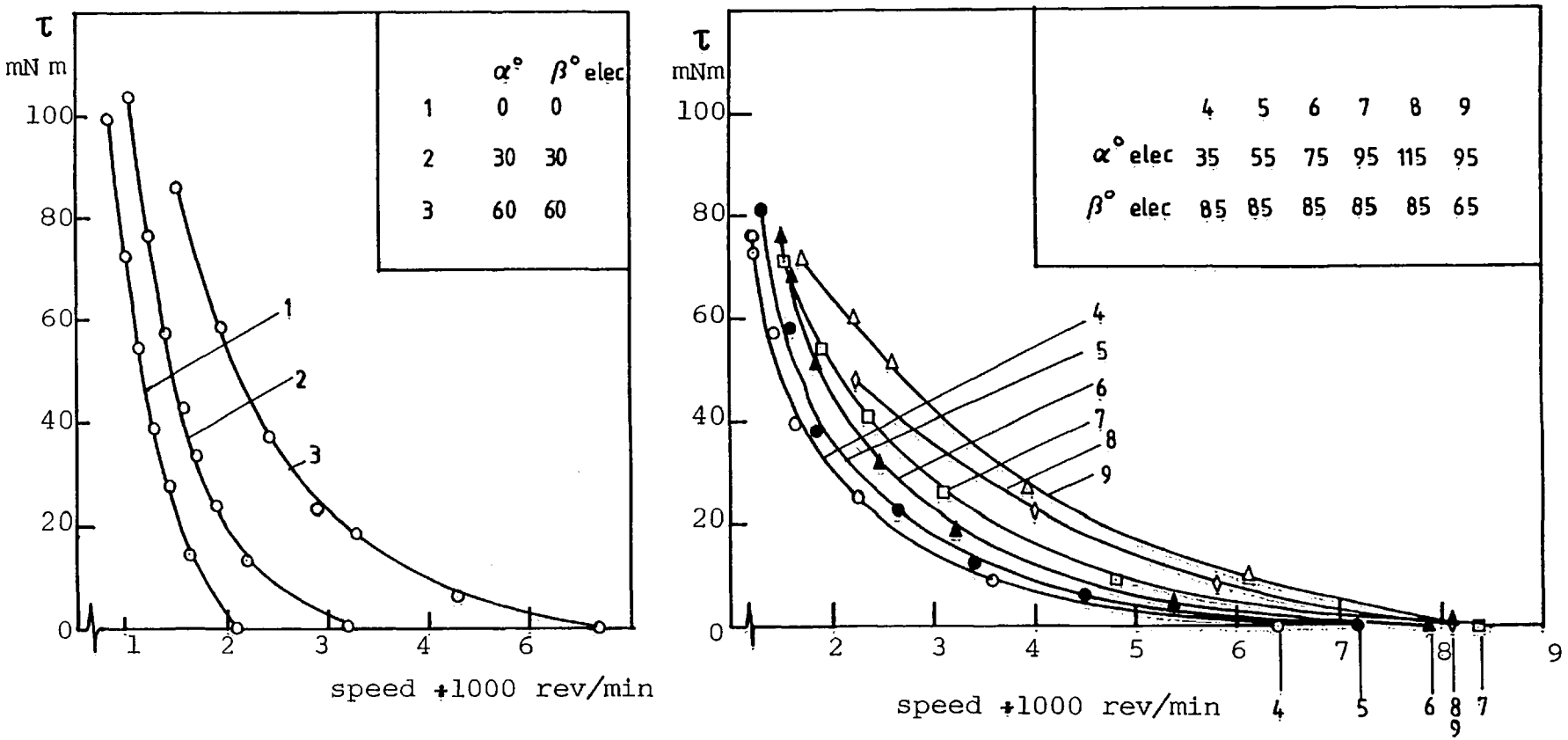

Fig. 5.3.10 Measured torque versus speed characteristics of the form 1 motor with its original winding and with different switching angles (165 V d.c. rail)

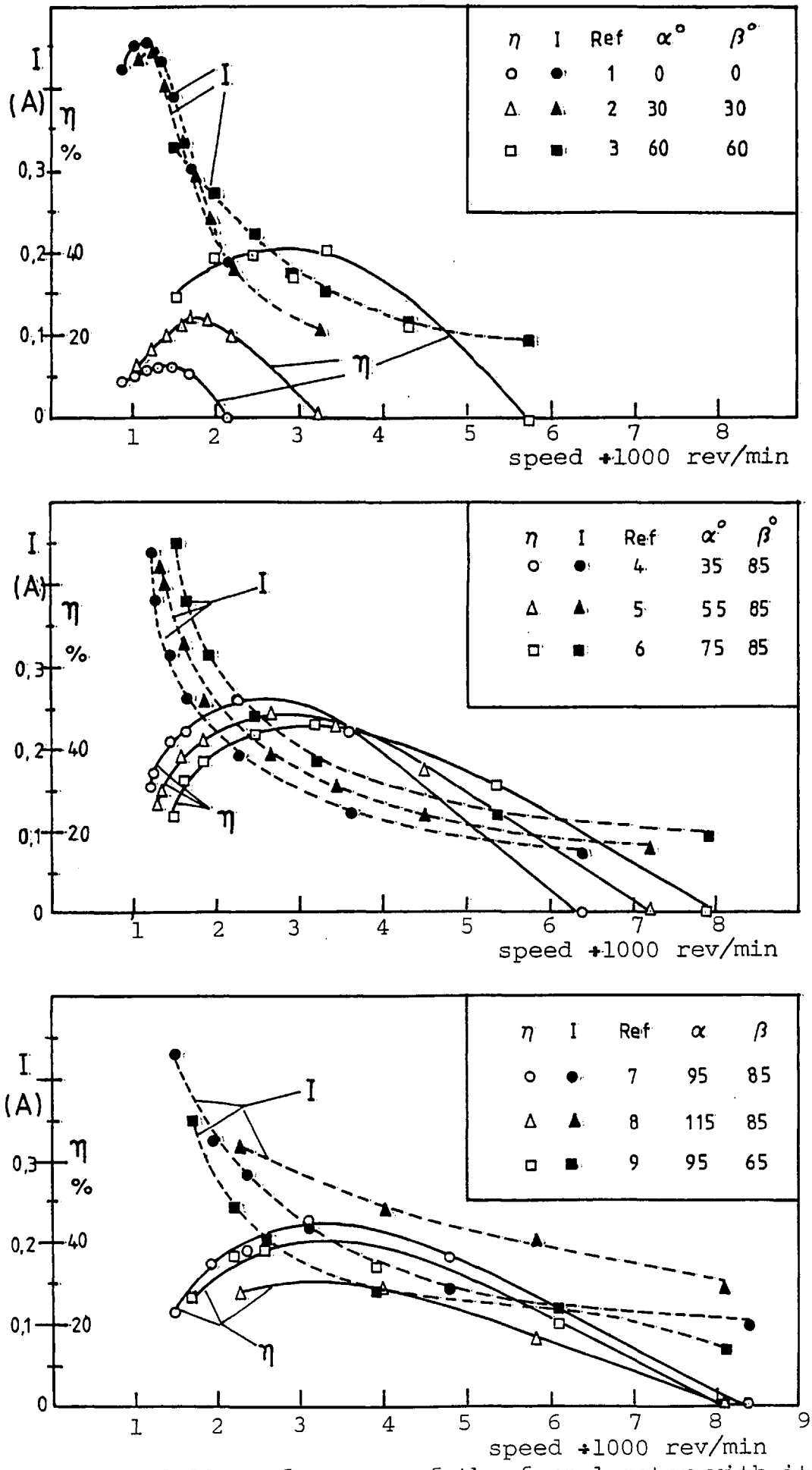

Fig. 5.3.11 Performance of the form 1 motor with its original winding and with different switching angles (165 V d.c.rail)

of 85° the mean currents increase with increasing 'on' periods and although the motor efficiencies are improved at high speeds, they are worse at low speeds. The limiting value of α can be seen to be around $\alpha = 95°$. Further increases (e.g. to 115°) result in lower efficiencies for the whole speed range. An improvement in efficiency can be seen with curve 9 for which α and β were reduced by 20°.

The tests were then repeated for 1) $\alpha = 90°$ and $\beta = 90°$ and 2) $\alpha = 90°$ and $\beta = 60°$. The first set of switching angles is close to those for curve 7 which gave the maximum no-load speed and best overall efficiencies, and the second is close to those for curve 9 where maximum output torques are obtained. The results of the tests at 170 V d.c. rail are shown in Fig. 5.3.12. With a small advance 'off' angle β, higher output torques are seen to occur together with a higher no-load speed (9400 rev/min as opposed to 8100 rev/min with $\beta = 90°$) but this is done at the expense of higher losses and hence lower efficiencies. The maximum efficiencies of the motor which in either case occurs at around 3500 rev/min are 55 % for $\beta = 90°$ and 33 % for $\beta = 60°$. The motor mean current with $\beta = 60°$ is approximately constant at 0.7 A except at very low speeds whereas with $\beta = 90°$ the mean current increases with load. This is because for $\beta = 60°$ the 'off' period is shorter (off period = $180 - \alpha + \beta$) and for this particular case is not long enough to allow the current to drop to zero

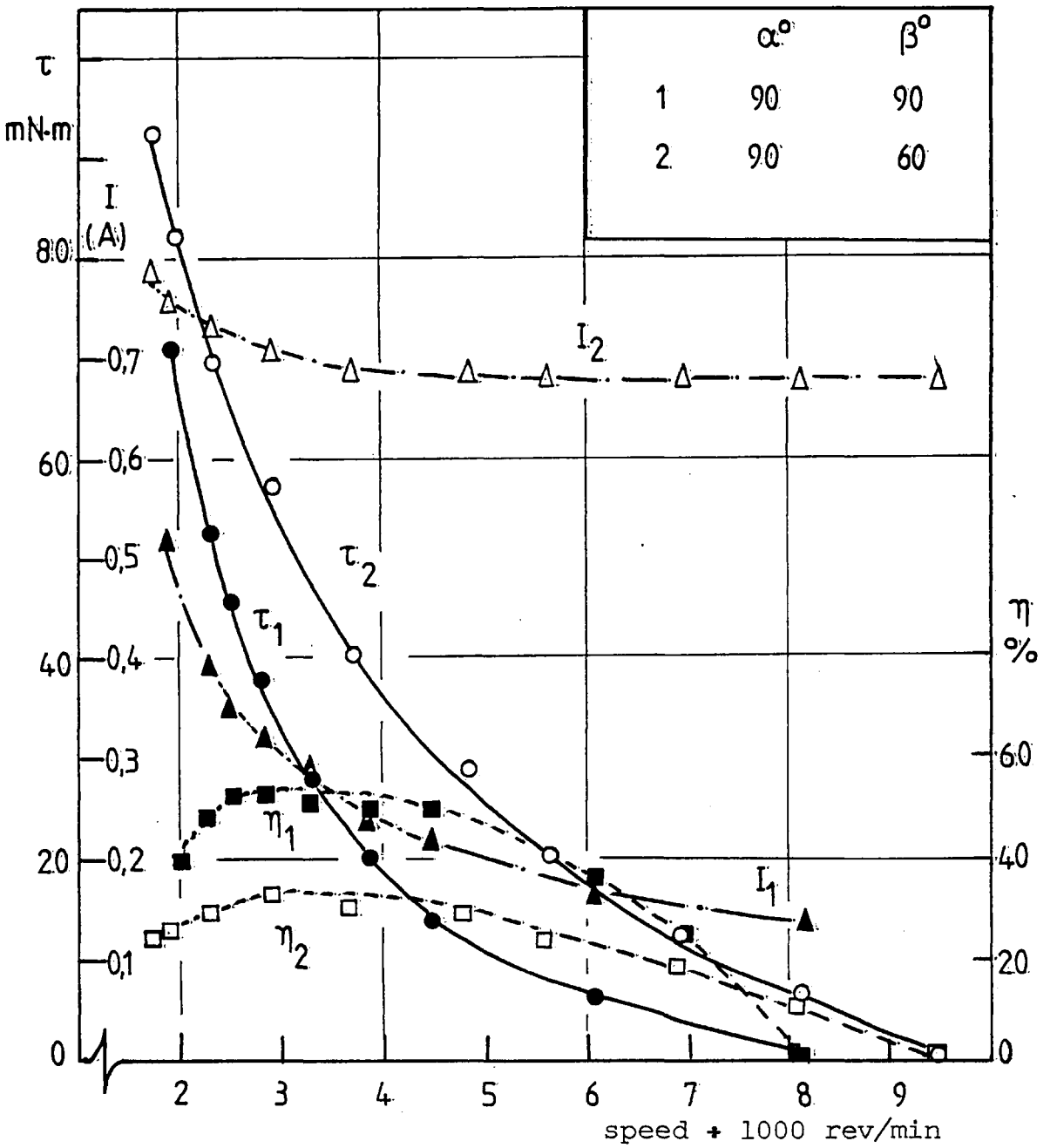

Fig. 5.3.12 Performance curves of the form 1 motor with different switching angles (170 V d.c.rail)



(a) α = 90°, β = 90°, speed 7800 rev/min



(b) α = 90°, β = 60°, speed 4200 rev/min

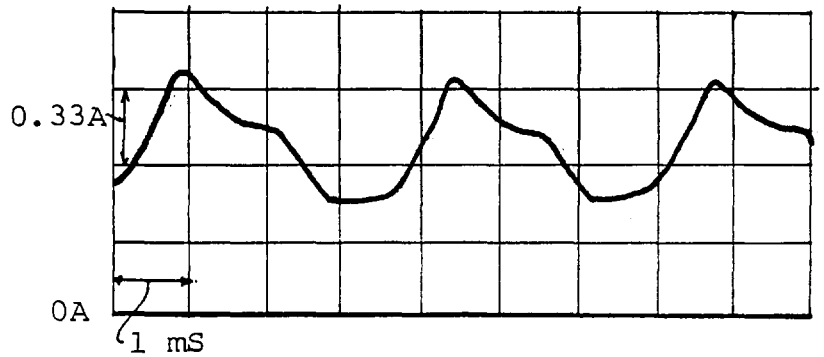

(c) α = 90°, β = 60°, speed 8600 rev/min

Fig. 5.3.13 Measured waveforms of the coil current of the form 1 motor (170 V d.c.rail)

before the start of the next 'on' period. The current waveform instead of consisting of a train of seperate positive pulses is hence continuous (Fig. 5.3.13(b) and(c)). The effect of the d.c. current component as such on the mean torque is zero (saturation neglected), but the higher than normal peak currents might be expected to result in higher output torques and higher copper losses (each related to the square of the current).

Fig 5.3.14 shows the total power losses for $\beta = 60^{\circ}$ to be approximately 4 times higher than for $\beta = 90^{\circ}$. The power losses of course tend to limit the rated output power of the motor (usually defined as the maximum output where the winding temperature rise on continuius operation reaches the maximum allowable figure). Hence, a comparison between two sets of operation is best made on the basis of the same temperature rise. With the assumption that the temperature rise is proportional to the total power loss comparisons can be made as follows:

1) The total power losses at 3500 rev/min (maximum efficiencies for both cases) which is taken as a reference speed are 34 W and 8.5 W for $\beta = 60^{\circ}$ and $\beta = 90^{\circ}$ respectively.

2) Assume again that the efficiency of the motor does not change with the voltage level and that the output torque, the power losses, the power output and the

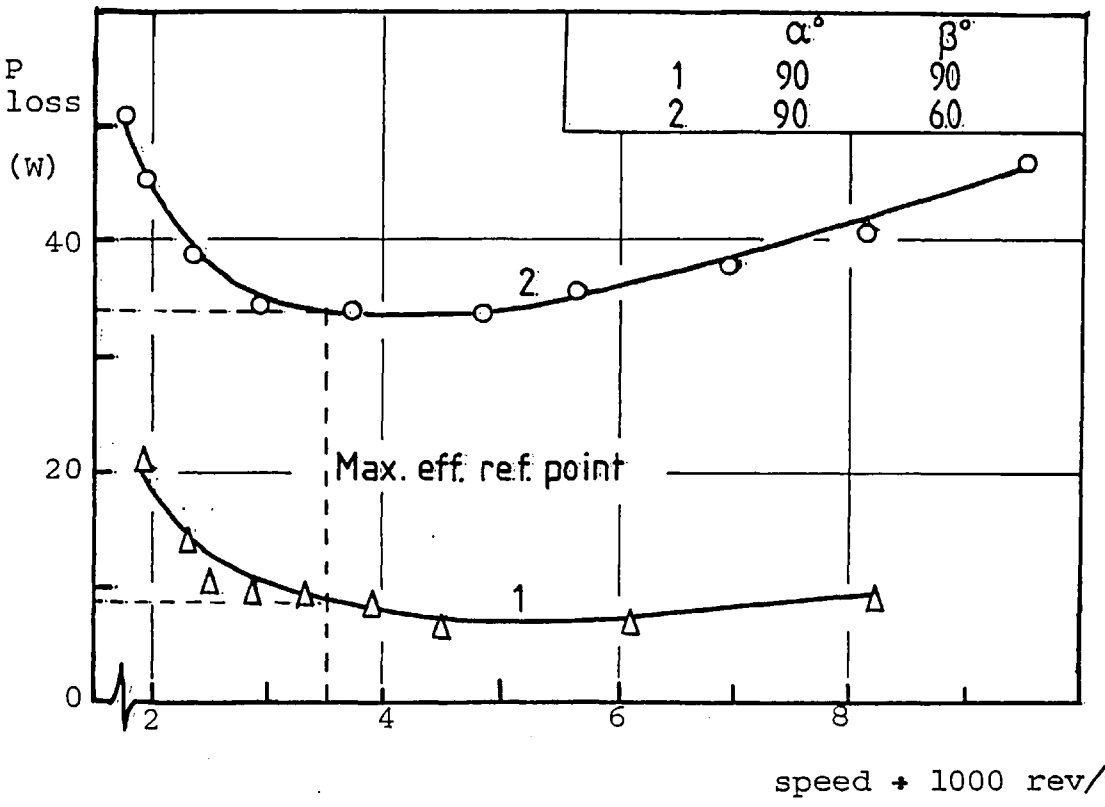

Fig. 5.3.14 Total power losses-speed curves (170 V d.c.rail)

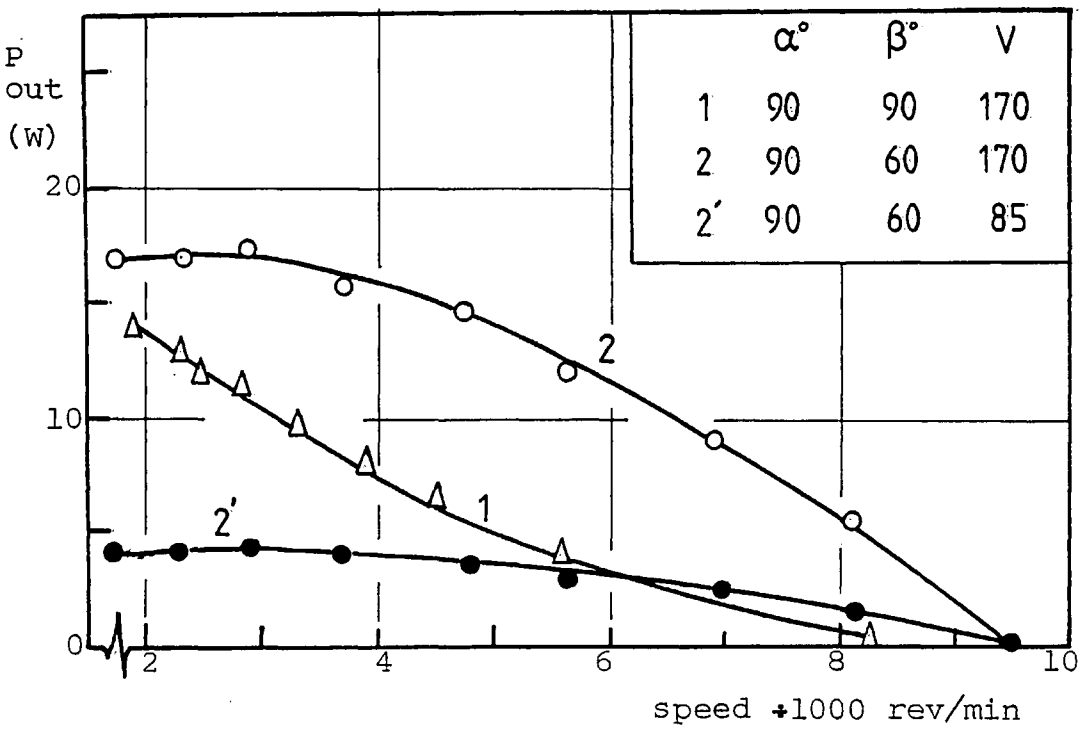

Fig. 5.3.15 Power output characteristics of the form 1 motor at the same supply voltage (1 and 2) and for the same power losses (1 and 2')

power input are all proportional to V^2.

i.e. $$P_{loss} \propto V^2 \qquad (5.3.1)$$

and $$P_{loss} = kV^2 \qquad (5.3.2)$$

3) For the motor to operate at the same power loss (same temperature rise) of 8.5 W, a lower voltage must be used when $\beta = 60^\circ$ which can be calculated from

$$V_{new} = V_{old}\sqrt{\frac{P_{lnew}}{P_{lold}}} \qquad (5.3.3)$$

where V_{old} = 170 V
P_{lnew} = total power losses at lower voltage
= 8.5 W
P_{lold} = total power losses at 170 V
= 34 W

Hence, $$V_{new} = 85 \quad V$$

4) With the assumption that $P_{out} \propto V^2$, the new output power for $\beta = 60^\circ$ for the same losses with $\beta = 90^\circ$ can be calculated from

$$P_{onew} = P_{oold}\left[\frac{V_{new}}{V_{old}}\right]^2 \qquad (5.3.4)$$

The power outputs are compared in Fig. 5.3.15 for a) the same voltage of 170 V (1 and 2) and b) for the same total power losses at 3500 rev/min (1 and 2'). It can be seen that for the same temperature limit the scheme with $\beta = 90^\circ$ gives a higher output power at low speeds

(up to approximately 6000 rev/min) but at higher speeds (up to 9400 rev/min) power output is higher with $\beta = 60^{\circ}$.

Overall, the results lead to the conclusion that for good high speed performance, at least with the motor tested, the current should certainly be switched on before the rotor reaches the q position ($\alpha > 0^{\circ}$) and that α can in fact be set as large as 90° elec (halfway between the d and the q position). Further increases in α seem to be unprofitable. With an appreciable switching angle α it is necessary to switch the current off before the rotor reaches the d position to allow the current to drop to zero before the beginning of the following 'on' period. If β is too small or smaller than α , the current pulses will not fall to zero and a d.c. component in the coil current (continuous current) results. The d.c. component causes excessive losses and lowers the rated power of the motor. However higher torques are available and there can be an advantage in allowing a d.c. component to occur at high speeds.

5.3.3.3 Predictions

Predictions using the step by step method explained in Chapter 3 were made. Again the machine parameter values used were obtained from measurements (for the same reason as explained in Section 5.2.4.2). The values were: a) winding resistance measured by 'Kelvin bridge'

at ambient temperature: 34.2 Ω and b) winding inductance at the d and q positions measured by P, I , V method at 50 Hz: L_d = 1.98 H and L_q = 0.84 H.

Apart from the assumption made about the trigular waveform of inductance with rotor position explained in Chapter 3, the following assumptions were also made in the calculations:

a) In the case of $\alpha = 90^\circ$ and $\beta = 90^\circ$:

1) The resistance used in the calculation was 34.2 Ω as measured. This was because in this test the current level was rather low and temperature rise was so small that the effect of increase in resistance could be neglected.

2) The increase in L_d at low frequency was assumed to be 20 % with L_q constant as measured.

3) Saturation was neglected.

b) For the case of $\alpha = 90^\circ$ and $\beta = 60^\circ$:

1) The resistance of the current shunt for monitoring the current waveform (in this test only) of 1.7 Ω was added to the measured winding resistance.

2) An increase in resistance of the coil of 10 % was assumed corresponding to temperature rise observed during the tests.

3) Because the test currents were generally high, 10 % reduction in L_d was assumed in an attempt to

allow for saturation. L_q was not modified.

For both cases, the following assumptions were made on the matter of losses:

1) Constant iron losses of 5 W were added to the power inputs at all speeds.

2) A constant friction and windage loss torque of 2.98 mN-m was assumed for the whole speed range. This was deducted form the calculated developed torque to give output torque and output power.

Comparisons between the predicted and measured performance are shown in Fig. 5.3.16 - 5.3.19. It can be seen that although the assumptions are rather crude, in the case of $\alpha = 90^\circ$ and $\beta = 90^\circ$ where the coil currents are rather low and saturation effects are small or negligible, the predictions agree well with the measured results. In the case of $\alpha = 90^\circ$ and $\beta = 60^\circ$ the effects of saturation and iron losses at the higher current levels (and perhaps the presence of d.c. (continuous) current component) causes higher discrepancies which can be seen clearly in input powers and output torques at high speeds. Another cause of error is perhaps related to the mechanism of calculation which starts from a zero current initial condition. With $\alpha = 90^\circ$ and $\beta = 60^\circ$, the current does not fall to zero at the end of the cycle and the calculation has to be repeated until the current waveform is repetitive and the d.c. level stable. This may take as long as 60 cycles and

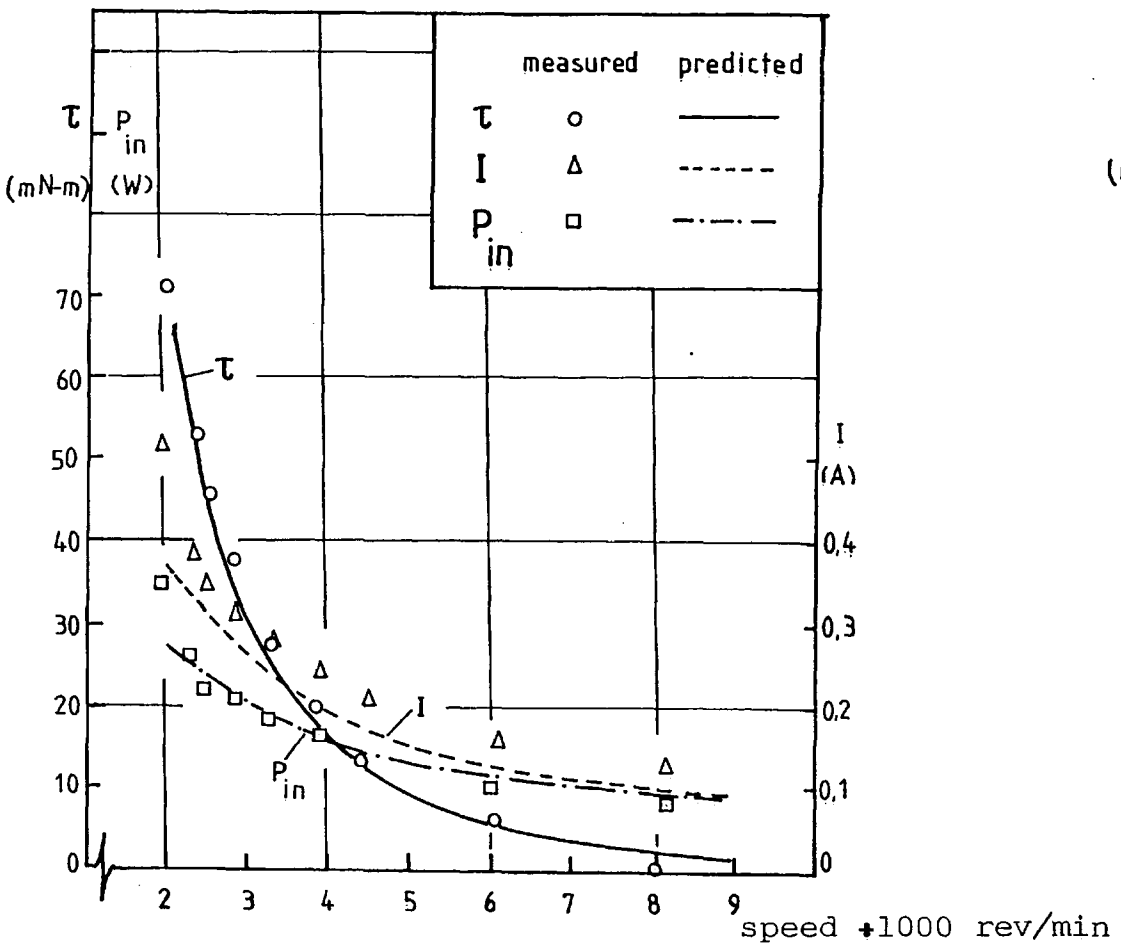

Fig. 5.3.16 Comparisons between predicted and measured performances of the form 1 motor (α = 90°, β = 90°, 170 V)

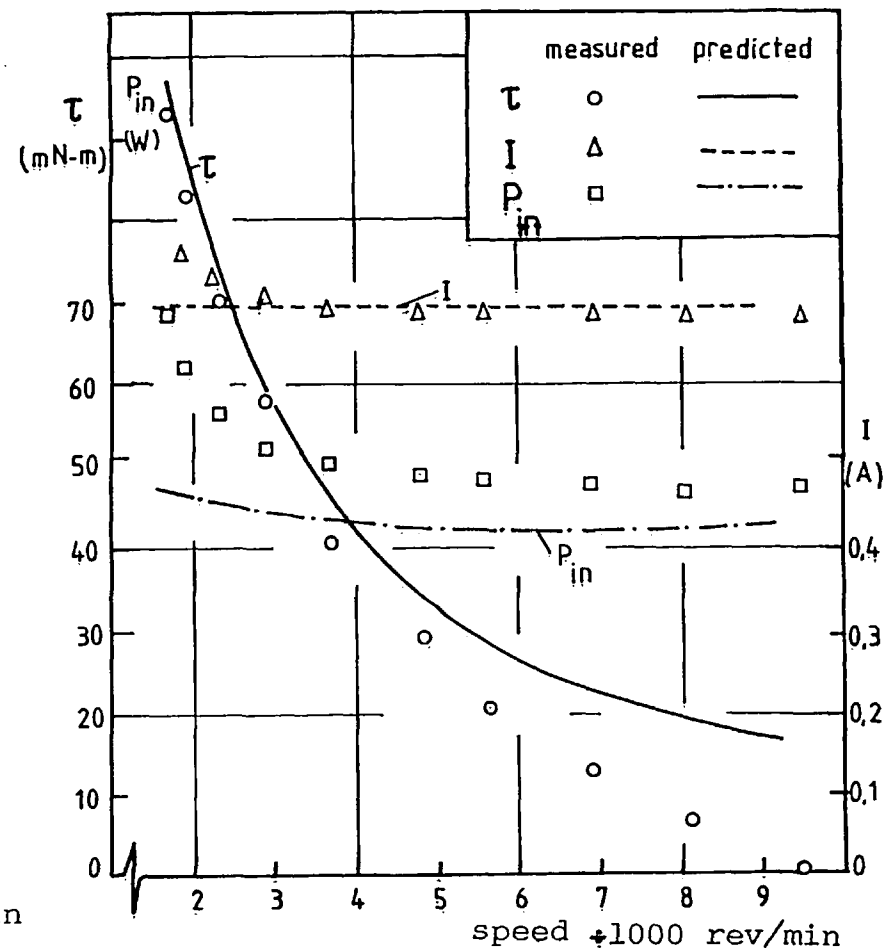

Fig. 5.3.17 Comparisons between predicted and measured performances of the form 1 motor (α = 90°, β = 60°, 170 V)

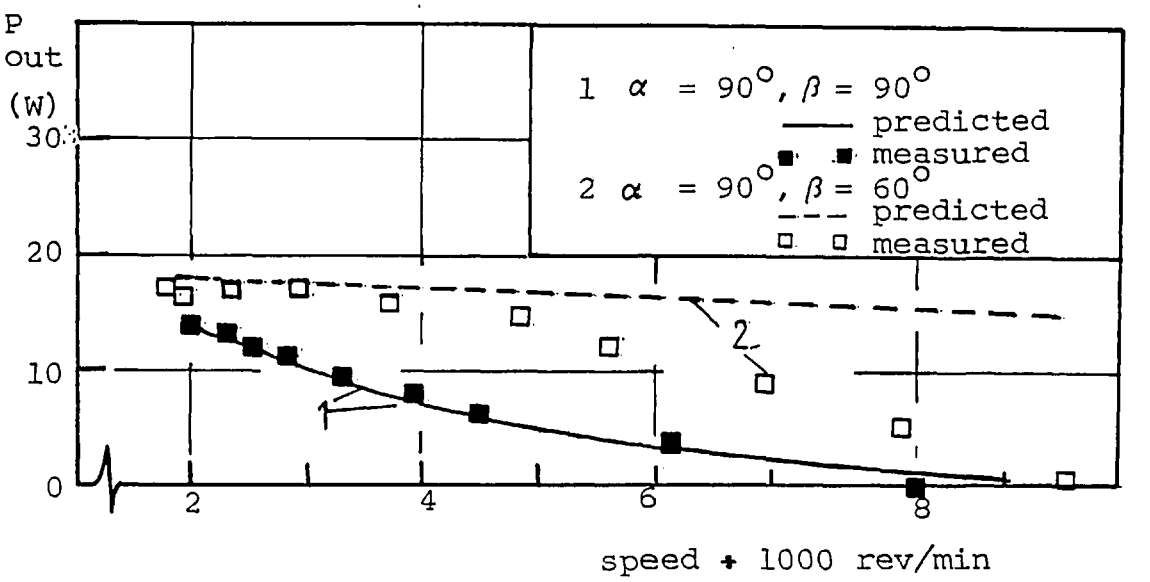

Fig. 5.3.18 Comparisons between predicted and measured output power characteristics of the form 1 motor at 170 V

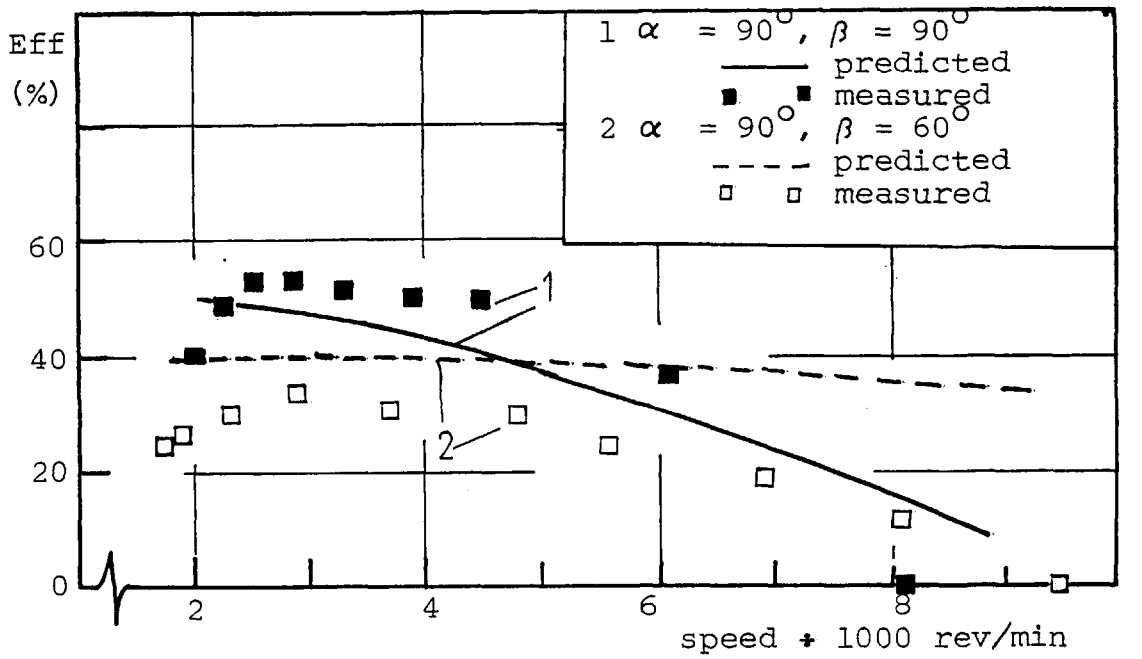

Fig. 5.3.19 Comparisons between predicted and measured motor efficiencies (form 1 motor, 170 V)



(a) α = 90°, β = 90°, 7800 rev/min



(b) α = 90°, β = 60°, 4200 rev/min

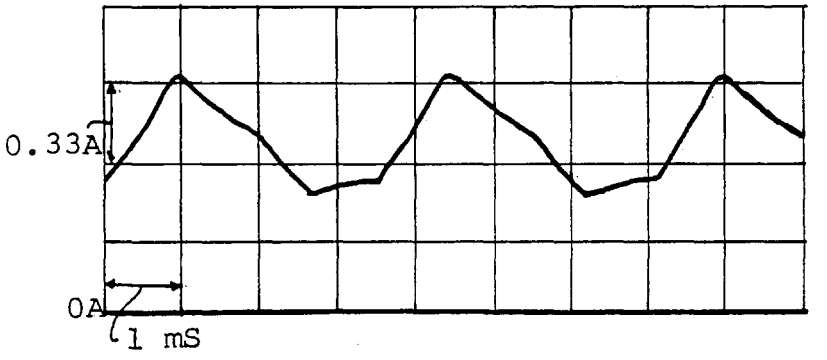

(c) α = 90°, β = 60°, 8600 rev/min

Fig. 5.3.20 Predicted current waveforms with the step by step method (form 1 motor, 170V)

The chance of cumulative errors cannot be ruled out. The predicted current waveforms for both operating conditions are shown in Fig. 5.3.20 and the d.c. component can be seen in (b) and (c) for $\alpha = 90^{\circ}$ and $\beta = 60^{\circ}$.

5.3.4 Performance of the form 1, form 2 and form 3 motors

5.3.4.1 Introduction

The work outlined in the previous section led to a drive system which developed a maximum power output of 17 W at 3000 rev/min and a no-load speed of 9400 rev/min. The next stage involved the determination of the rated output and the maximum no-load speed of the motor. The rating of a machine partly depends upon the amount of heat due to losses it can dissipate without the winding mean temperature exceeding the nominal limiting value for the particular class of insulation involved, and beyond which an unacceptable rate of insulation deterioration occurs. Maximum permissible temperatures for different classes of insulation are[5.6]

Insulation class	Y	A	E	B	F	H	C
Maximum temp $^{\circ}C$	90	105	120	130	155	180	180

For small motors the most usual insulations used for the winding are class E synthetic-resin enamels

and the maximum permissible temperature is 120°C abs. In its as-purchased state the motor full load current and absolute temperature values were 0.5 A and 60°C respectively. This temperature is way below the 120°C permissible and it is hence almost certainly possible to get more output power from the motor than that achieved as a SPSRM in the previous section where the current was little larger at 0.7 A. Rather than do this by raising the voltage level of the d.c. rail, (considered to be undesirable since the inverter then has to withstand higher voltage) the alternative method of reducing the coil turns was adopted. The relations between the output power, current, etc. and turns (N) for a given motor are as follows:

The impedance $$Z \propto N^2 \qquad (5.3.5)$$

, coil current $$I \propto \frac{V}{N^2} \qquad (5.3.6)$$

and the output power P which is proportional to VI is

$$P \propto V . \frac{V}{N^2}$$

$$P \propto \frac{V^2}{N^2} \qquad (5.3.7)$$

The current density δ given by

$$\delta = \frac{I}{a}$$

can be expressed in term of total winding area A_c as

$$\delta = \frac{I}{A_c/N} = \frac{I\,N}{A_c}$$

Hence $$\delta \propto \frac{V}{N^2} \cdot \frac{N}{A_c}$$

and for the same winding area A_c

$$\delta \propto \frac{V}{N} \qquad (5.3.8)$$

The magnetic flux density B which is the total flux ϕ per cross-sectional area of the magnetic circuit A_i is

$$B = \frac{\phi}{A_i}$$

and can be expressed in term of volt/turn $(\frac{V}{N})$ as

$$B \propto \frac{V}{N A_i}$$

and hence for a given motor

$$B \propto \frac{V}{N} \qquad (5.3.9)$$

a) Hence if V is kept constant and the number of turns (N) is reduced by a factor of k (assuming taht the magnetic circuit is not saturated)

Z decreases by a factor of k^2
I increases by a factor of k^2
P increases by a factor of k^2
δ increases by a factor of k
B increases by a factor of k

b) If the voltage per turn is kept constant i.e. the voltage is changed in the same sense and same proportion as the changes in number of turns (as explained in Section 5.2.4.2) the following relations hold:

Z	changes by a factor of k^2
I	changes by a factor of $1/k$
P	is constant
δ	is constant
B	is constant

The winding turns were hence reduced to a value low enough for the existing feed circuit to supply the motor when operating at its temperature limit at the designated operating speed/s. (This summarised quite a complex sequence of adjustment, calculation and test.) Measurements of voltage and current at this 'rated' operating point are then usable if required to further adjust turns (on a constant volts per turn basis) to enable the motor to develop the same power (at the same temperature rise etc.) with a supply of any desired voltage.

5.3.4.2 Preliminary test with the form 1 motor with reduced turns

The motor was accordingly rewound with a new excitation coil of 130 turns of 1.12 mm diameter enamelled copper wire, (reduced by a factor of 10:1 from the original 1300 turns) and a convenient, reference, initial operating voltage chosen (50 V). Switching angles $\alpha = 90^{\circ}$ and $\beta = 90^{\circ}$ which previously produced a discontinuous current waveform were chosen.

With the number of turns reduced by a factor

of 10 and the voltage level reduced from the previous value by a factor of 3.4, a reduction of 100:1 in impedance (R & L) was expected together with an increase in coil current of 29 times and an increase in power output of 8.6 times, all with reference to the values obtained in the previous experiment with $\alpha = 90^{o}$ and $\beta = 90^{o}$. (In practice the increase in power output will of course be less if saturation occurs.)

The measured resistance and inductances of the motor at the test frequency of 50 Hz for the new winding were $R_{amb} = 0.396\ \Omega$, $L_d = 20.3$ mH and $L_q = 8.6$ mH. When compared with $R_{amb} = 34.2\ \Omega$, $L_d = 1.98$ H and $L_q = 0.84$ H measured with the old winding at the same frequency, the relation between impedance and turns can be seen to predict values well.

Minor changes were made to the feed circuit. Because of the higher current level expected (up to 10 A) the rectifier diodes were replaced with a new set having a higher rating of 13 A average. The snubber diodes BYX 71-600 (t_{rr} of 450 nS) were replaced with the faster EF 150 n6 (t_{rr} of 40 nS) to protect the main transistors from the high voltage spikes at switch-off. The snubber components were replaced with ones calculated for the new operating current and voltage.

The performance of the form 1 motor measured

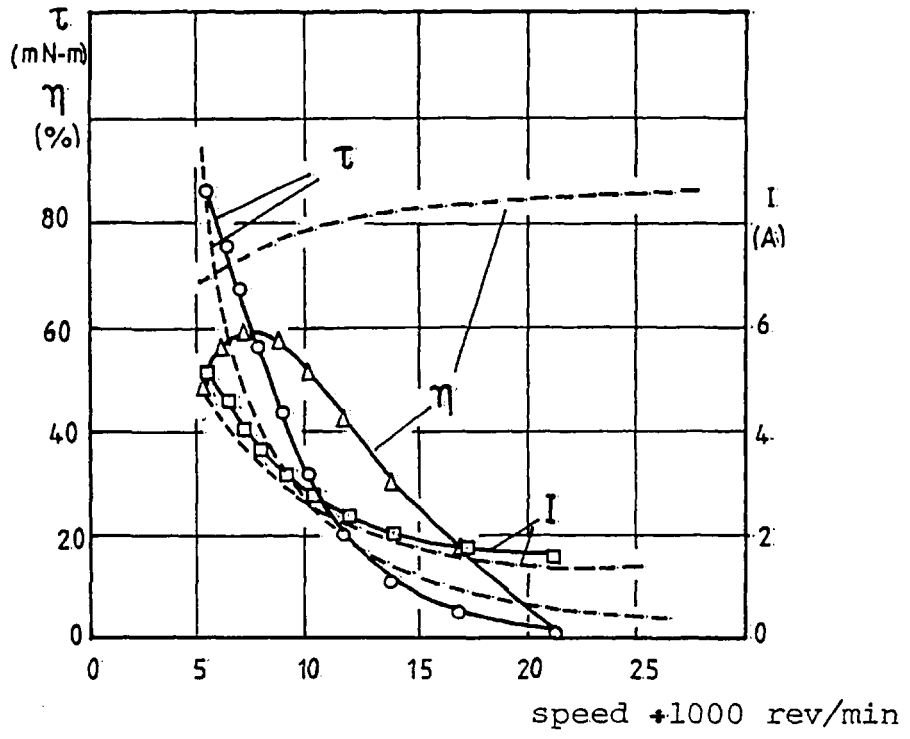

Fig. 5.3.21 Performance curves of the form 1 motor (reduced turns) with the d.c. transistor-fed circuit ($\alpha = 90^{\circ}$, $\beta = 90^{\circ}$, 50 V)

——— test
------- predicted

with the same test rig and test circuit as in Section 5.3.3 in shown in Fig. 5.3.21 in comparison with the predicted results. The extremely high speed of 21000 rev/min at no-load was demonstrated. The original bearings were not replaced and hence friction losses, vibrations and noise were significant. The lack of special laminations led to high iron losses especially at speeds above 10000 rev/min. The maximum power output at 6500 rev/min was 50 W. Maximum motor efficiency of 58 % and overall efficiency (motor +drive) of 44 % occurred at 7500 rev/min.

In the predictions the hot resistance of 0.51 Ω was used instead of the ambient temperature figure of 0.396 Ω. The inductances were taken from the 50 Hz measurement: L_d = 20.3 mH and L_q = 8.6 mH. Measurements of inductance at different frequencies with the same V/f ratio unfortunately showed a wide range of variation in L_d and L_q perhaps due to the eddy current losses caused by the presence of the rotor conductor left in the rotor. The values at 50 Hz were chosen because this frequency lay well within the operating frequency range and because of the good quality of the tie up with the previous tests. The exclusion of iron, friction and windage losses from the predictions inevitably led to poor correlation between predicted and measured efficiencies especially at higher speeds.

5.3.4.3 Preliminary measurements of all test motors

Following the results achieved in developing the form 1 motor as a high speed drive system, the investigation was extended to include the other experimental motors and the use of a bifilar-wound pull-down coil. The motors tested in this extended program were:

1) Form 1 motor with a bifilar coil of 115 turns (No. 1)
2) Form 1 motor with single coil of 160 turns (No. 2)

3) Form 2 motor with a bifilar coil of 200 turns

4) Form 3 motor with single coil of 160 turns

Before the tests were carried out, preliminary measurements were made to determine the equivalent circuit parameters and the saturation level of each motor.

a) The test circuit for the inductance measurements is shown in Fig. 5.3.22(a). I, E_2 and the phase angles between $-E_1$ and E_2 (α') were recorded for each rotor position and the inductance and each position of rotor calculated from the phasor diagram (b) using:

$$L = \frac{E_2 \sin (180-\alpha')}{\omega I}$$

therefore,

$$L = \frac{E_2 \sin \alpha'}{\omega I} \qquad (5.3.10)$$

where L is the inductance of the motor winding
E_2 is the voltage across the motor winding
ω is equal to $2\pi f$ and $f = 50$ Hz
I is the current in the winding
α' is the phase angle at which $-E_1$ leads E_2 (positive).

The measurements were made at 50 Hz and in the linear region of the magnetisation characteristic as in the previous predictions. The variation of inductance with rotor position is shown in Fig. 5.3.23 in comparison with the triangular waveform approximation. The values of d.c. resistances, and maximum and minimum inductances are shown in Table 5.3.

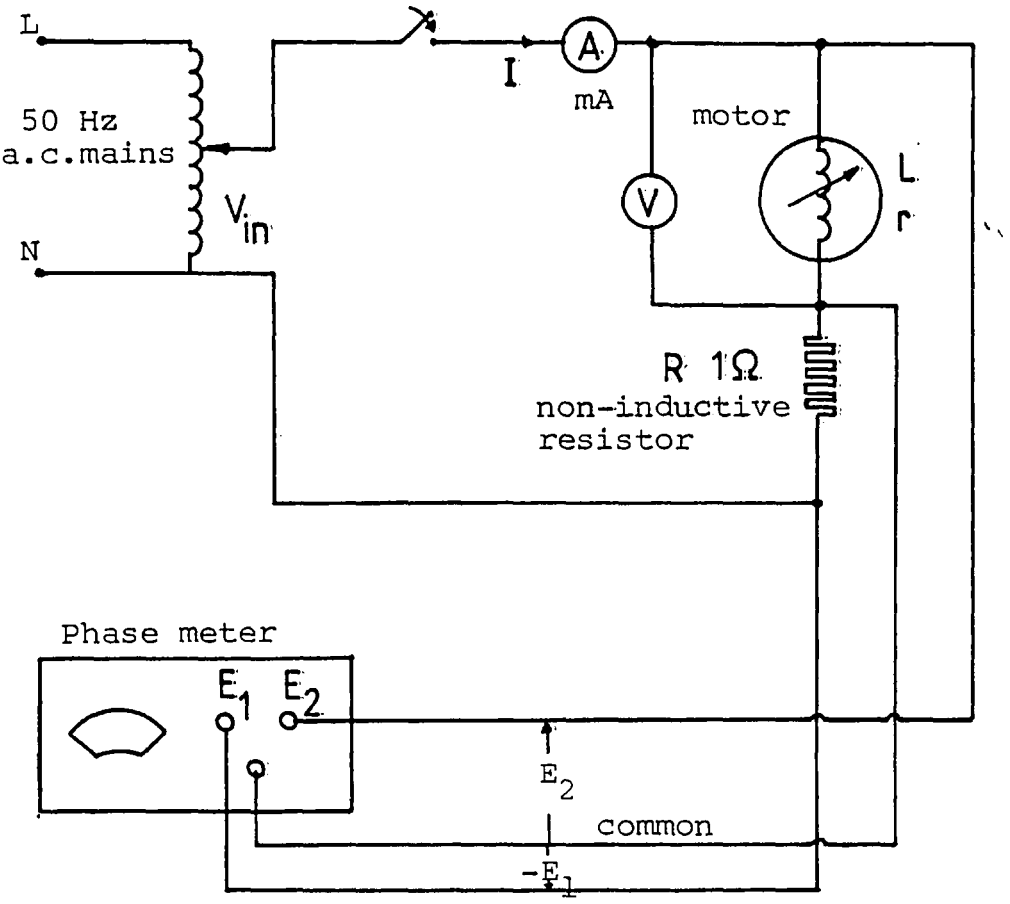

(a)

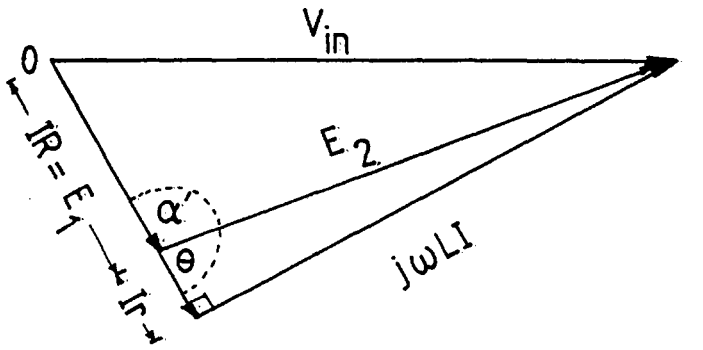

(b)

Fig. 5.3.22 (a) Circuit for inductance measurement

(b) Corresponding phasor diagram

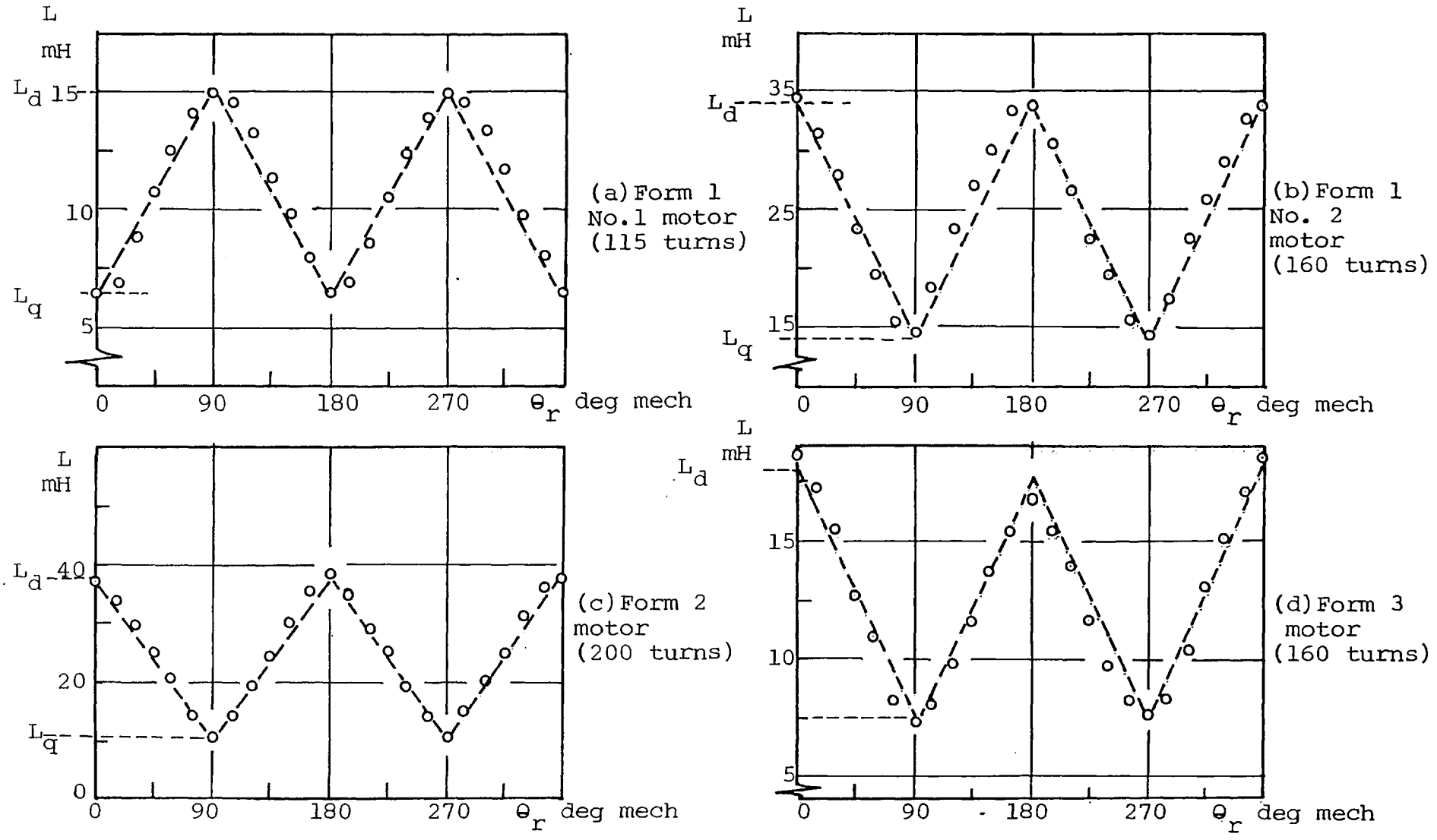

Fig. 5.3.23 Variation of inductances with rotor positions (no saturation)
o measured points ------ approximation

Table 5.3

Motor	wire dia. (mm)	no.of turns	R_{amb} (Ω)	L_d (mH)	L_q (mH)	L_d/L_q
Form 1 No.1 (bifilar)	1.12	115	0.344	15.0	6.5	2.31
	0.56	115	1.276			
Form 1 No.2	1.12	160	0.500	34.0	14.0	2.43
Form 2 (bifilar)	0.376	200	4.54	37.5	10.8	3.47
	0.345	200	5.35			
Form 3	1.12	160	0.498	18.0	7.5	2.40

An attempt was made to use a longitudinal laminated stack rotor with the form 1 No.2 and form 2 motor but was later abandoned due to the problem related with the strength of the rotor lamination. It is however interesting to note that the longitudinal stack rotor did not improve the L_d/L_q ratio as expected. The L_d to L_q ratios of the form 1 No.2 and form 2 measured with longitudinal stack rotor were only 2.41 and 2.06 compared to 2.43 and 3.47 achieved with the conventional rotor, respectively.

The winding resistances and inductances of the motors can be calculated to a first degree of approximation from the windings and physical dimensions of the motor; using the following standard relations:

$$R = \frac{\rho N L_t}{a_w} \qquad (5.3.11)$$

where the symbols take their normal meanings, and ρ for copper is 1.7×10^{-8} Ω-m at 20°C.

$$L = \frac{\lambda}{i} = \frac{N\phi}{i} = \frac{N^2\phi}{Ni} = \frac{N^2}{\mathcal{R}} \quad H \qquad (5.3.12)$$

where λ is the total flux linkage
i is the current in one conductor
$\mathcal{R}$ is the total reluctance of the magnetic circuit.

The reluctance of a parallel airgap with the length g_a and cross-section A_a is

$$\mathcal{R} = \frac{1}{\mu_o} \frac{g_a}{A_a} \quad \frac{A\text{-}T}{Wb} \qquad (5.3.13)$$

Fig 5.3.24 shows the assumptions made in calculating the mean length/turn (L_t) of the winding and the d axis reluctance. (Magnetic flux concentrated in the airgap volume defined by the overlapped area and the active core length l_a only; fringing and leakage fluxes and iron reluctance neglected.) Table 5.4 gives the details of winding and airgap dimensions of each motor and also the comparisons between the calculated values and measured values of the d.c. resistance and the d axis inductance.

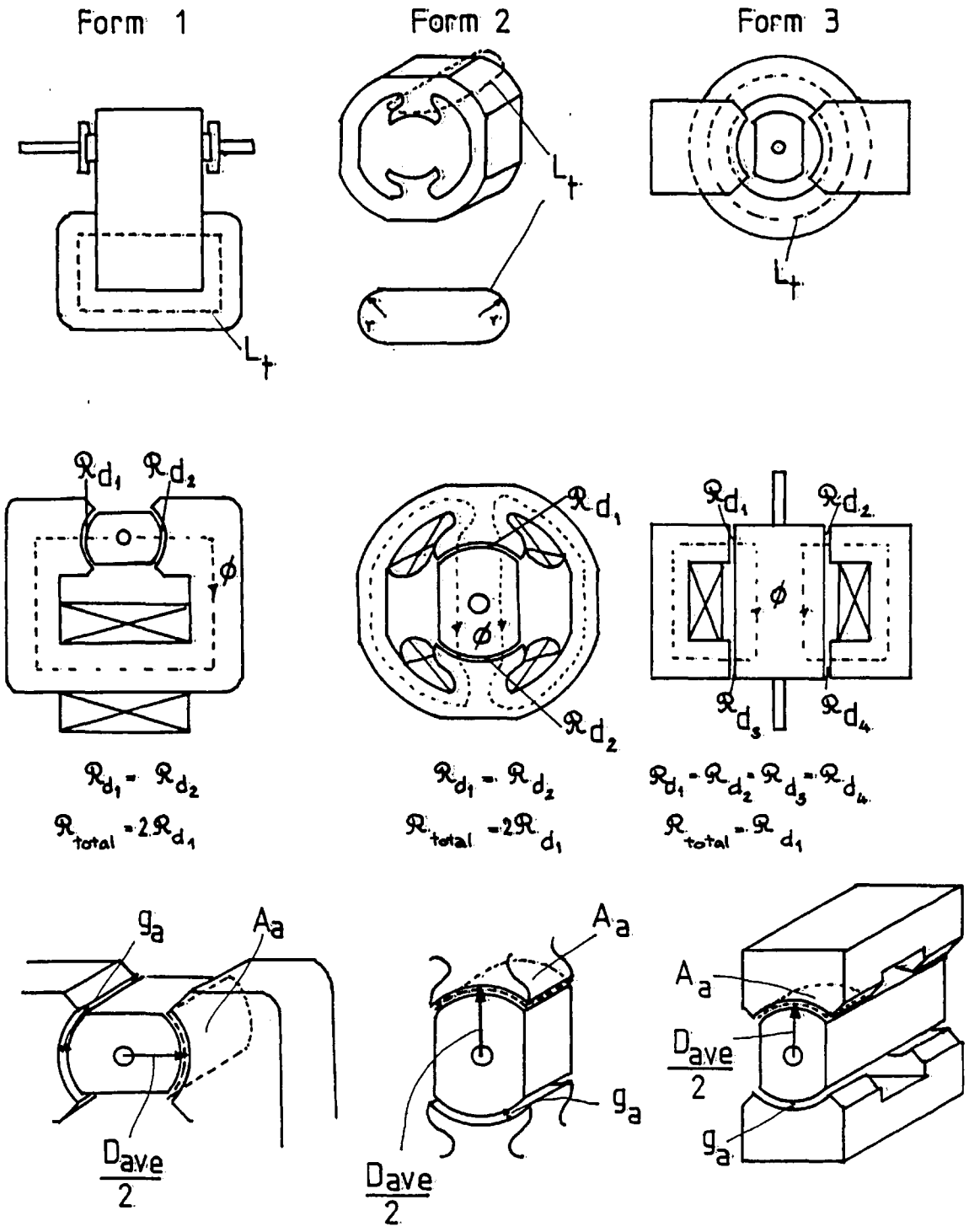

Fig. 5.3.24 Approximations made in the calculation of winding resistances and airgap inductances of the motors

Table 5.4

Quantity	Form 1 No.1	Form 1 No.2	Form 2	Form 3
N (turns)	115	160	200	160
L_t (m)	14.65×10^{-2}	14.65×10^{-2}	12.42×10^{-2}	16.45×10^{-2}
a_w (m^2)	9.85×10^{-7} / 2.46×10^{-7}	9.85×10^{-7}	1.11×10^{-7} / 0.93×10^{-7}	9.85×10^{-7}
g_a/gap (m)	0.43×10^{-3}	0.43×10^{-3}	0.52×10^{-3}	0.43×10^{-3}
A_a (m^2)	9.24×10^{-4}	9.24×10^{-4}	5.63×10^{-4}	2.35×10^{-4}
$\mathcal{R}_{total}$ (AT/Wb)	7.41×10^{5}	7.41×10^{5}	14.68×10^{5}	14.56×10^{5}
$R_{d.c.}$ (Ω) calc.	0.289 / 1.159	0.403	3.80 / 4.52	0.454
$R_{d.c.}$ (Ω) meas.	0.344 / 1.276	0.500	4.54 / 5.35	0.498
L_d (mH) calc.	17.85	34.56	27.24	17.58
L_d (mH) meas.	15.0	34.0	37.5	18.0

Leakage flux, fringing flux, saturation and inaccuracy in measuring the small gap length are probably the chief factors in the discrepancies between measured and calculated inductance values. Improvements here and a prediction method for the calculation of the q axis inductance perhaps by using Roter's approach[5.7] or by analytic or numerical solution of the field distributions[5.8] would be desirable but were not persued due to lack of time.

b) The magnetisation characteristics of the motors were measured using the d.c.method as shown in Fig. 5.3.25. The average flux density 'B_{av}' was calculated by dividing the measured flux by the smallest cross-section area of the magnetic circuit. Measurements were made with the rotor in both d and q axis positions. The results are shown in Fig. 5.3.26 in terms of average flux density 'B_{av}' against magnetomotive force 'F'.

The slope of the airgap line is

$$\frac{B_{av}}{F} = \frac{\phi_{av}}{A_{siron}\,F} \quad .$$

The ratio $\frac{\phi_{av}}{F}$ can be assumed to be equal to the permeance of the airgap (leakage, fringing flux and iron reluctance neglected) which in terms of the dimensions of the airgap is $\mu_o A_a / g_a$.

The slope of the airgap line is thus $\frac{\mu_o A_a}{A_{siron} g_a}$

(5.3.14)

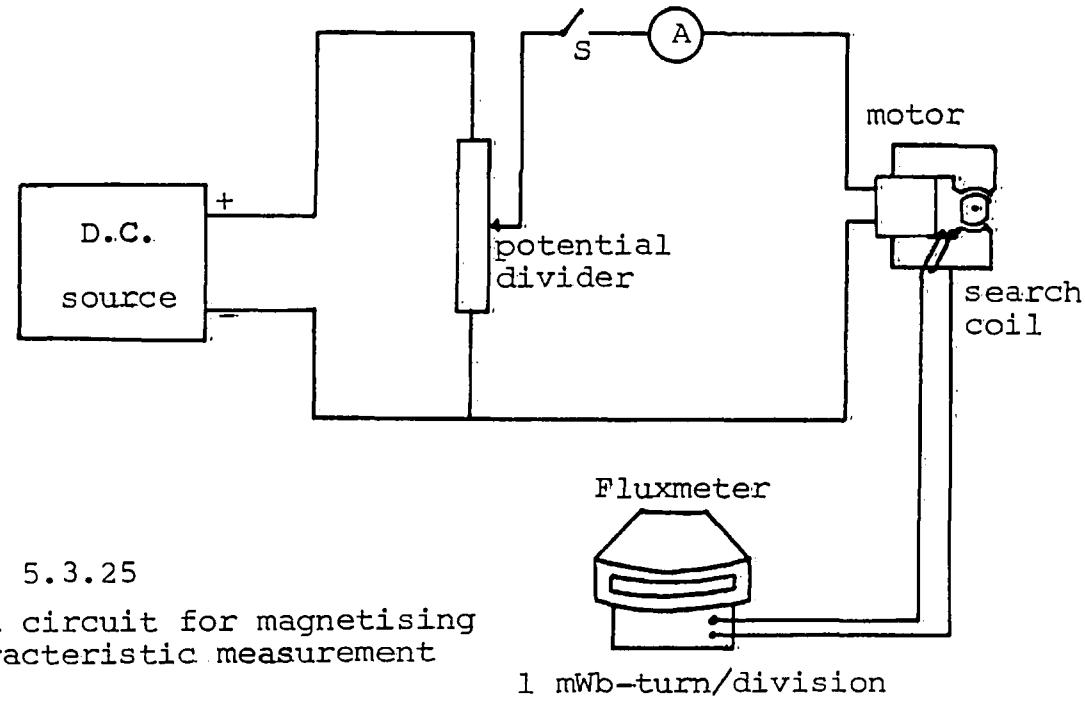

Fig. 5.3.25
Test circuit for magnetising characteristic measurement

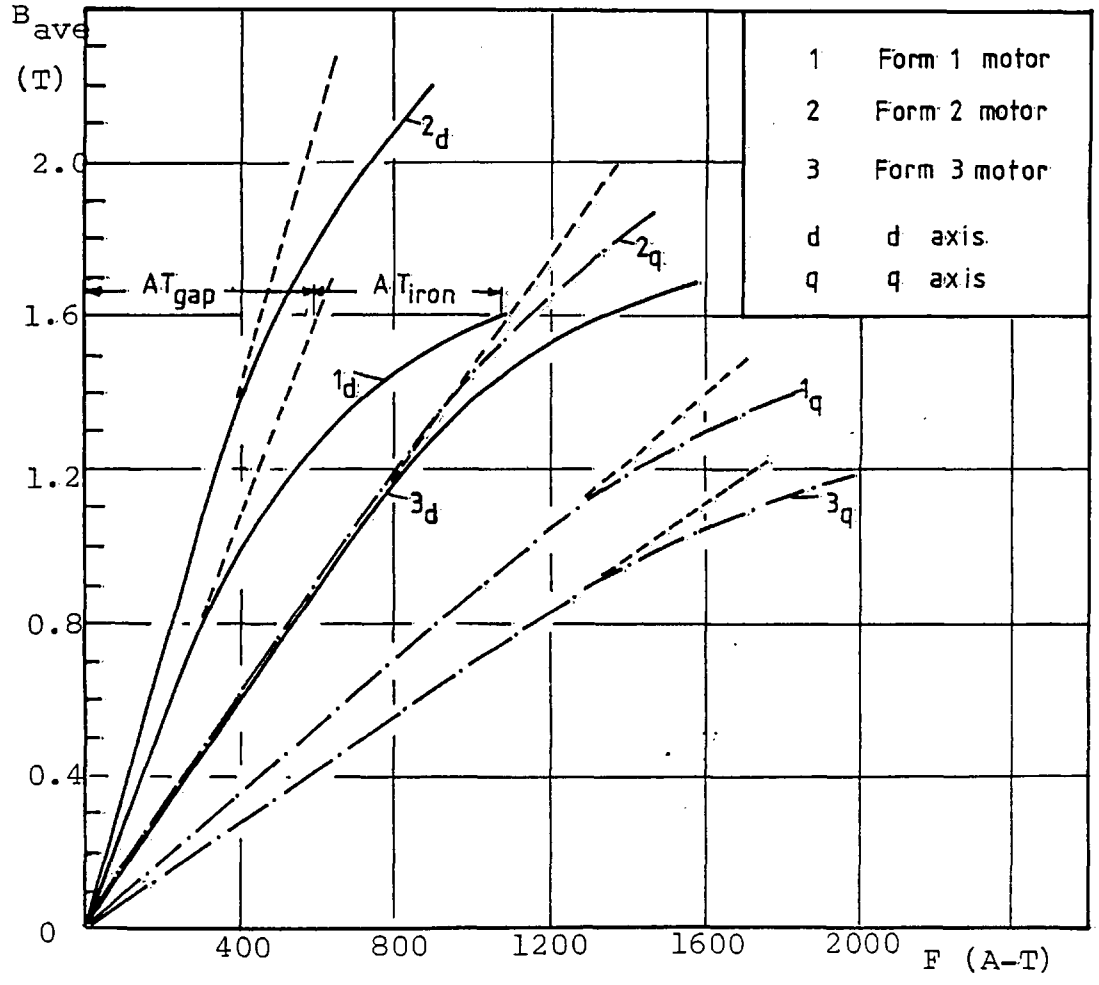

Fig. 5.3.26 Magnetising characteriatics of the form 1, form 2 and form 3 motors at the d and q positions

Comparisons between the actual slope of the d axis airgap lines and the values calculated from eq. (5.3.14) are shown in Table 5.5. It is likely that the low prediction for the form 2 motor is due to 'low' measurement of the gap.

Table 5.5 Magnetising characteristics

Quantity	form 1	form 2	form 3
g_a total m	0.86×10^{-3}	1.04×10^{-3}	0.86×10^{-3}
A_a m^2	9.24×10^{-4}	5.63×10^{-4}	2.35×10^{-4}
A_{siron} m^2	5.06×10^{-4}	2.08×10^{-4}	2.42×10^{-4}
$\frac{\mu_o A_a}{A_{siron} g_a}$	2.66×10^{-3}	3.27×10^{-3}	1.42×10^{-3}
actual slope	2.66×10^{-3}	3.55×10^{-3}	1.48×10^{-3}

The relative significance of saturation can be defined as

$$\text{Relative significance of saturation at particular operating point} = \frac{AT_{iron} \times 100}{AT_{iron} + AT_{gap}} \quad \% \qquad (5.3.15)$$

where AT_{iron} is the m.m.f. drop in the iron
AT_{gap} is the m.m.f. drop in the airgap

$AT_{iron} + AT_{gap}$ is the total m.m.f. needed to drive the magnetic circuit to that operating flux density.

From the curves, the relative significance of saturation in each motor when 1.6 Tesla is present in the smallest area portion of the magnetic circuit is:

Table 5.6

	form 1	form 2	form 3
	43.3 %	10.0 %	15.6 %
at total	1060 A-T	500 A-T	1280 A-T

Hence at this operating flux density (1.6 T), The form 1 motor can be said to be the most heavily saturated. Although the power output of similar-sized motors is not accurately proportional to the A-T needed to fully flux the motor, one nevertheless might expect from the A-T figures that the form 3 motor would be able to develop the highest output power followed by the form 1 and form 2 motors in descending order.

c) In order to be able to compare the relative merits of the two motors of conventional structure (form 1 and form 2) measurements were carried out to determine the percentages of leakage flux. The test circuit is shown in Fig. 5.3.27(a). The stator of the motor was supplied

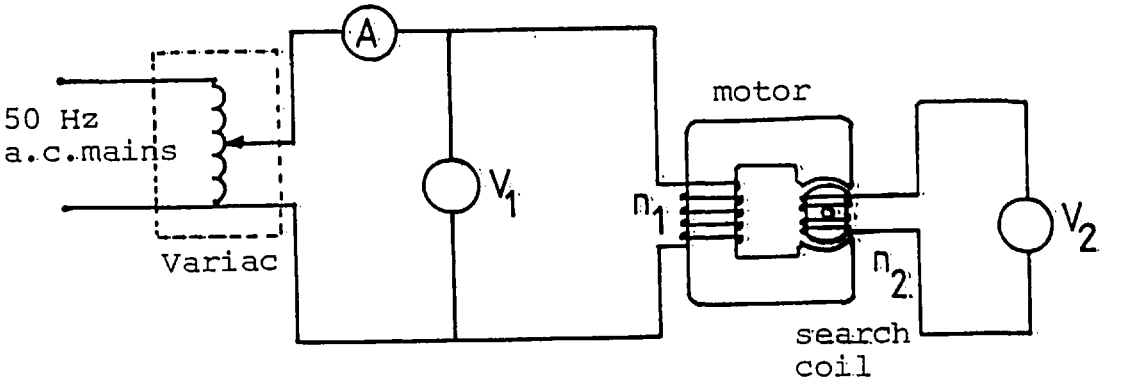

(a)

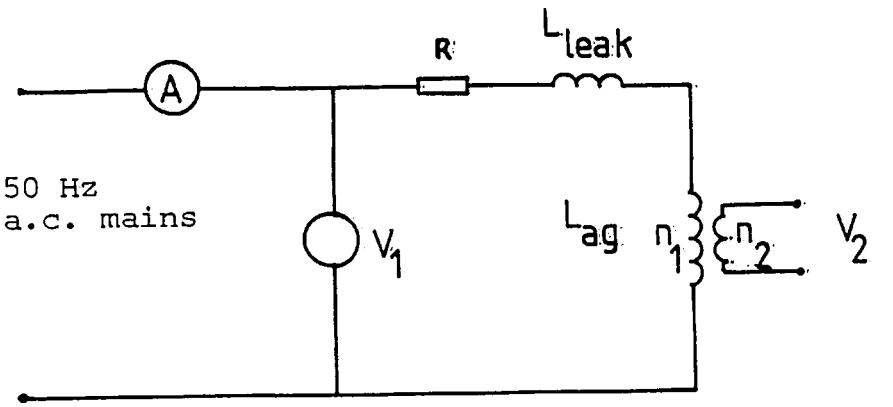

(b)

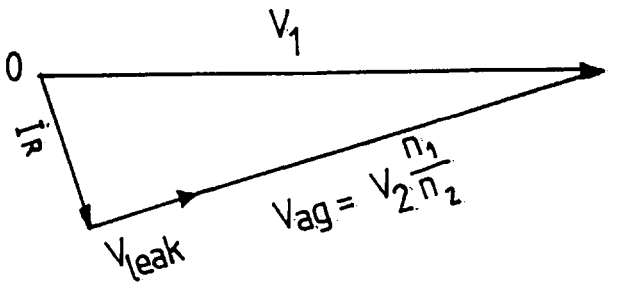

(c)

Fig. 5.3.27 (a) Test circuit
(b) Equivalent circuit
(c) Phasor diagram

from 50 Hz a.c. mains via a variac and a search coil of 10 turns was wound on the rotor at right angles to the flux path. On the assumption that the equivalent circuit of the motor is as shown in Fig. 5.3.27(b), the ratio of the airgap flux to total flux can be calculated in terms of the induced voltages as shown in the phasor diagram (c) as

$$\frac{\text{airgap flux}}{\text{total flux}} = \frac{(n_1/n_2)\ V_2}{\sqrt{V_1^2 - (I_1 R)^2}} \qquad (5.3.16)$$

where n_1 is the number of turns of the excitation coil
n_2 is the number of turns of the search coil
V_2 is the voltage induced in the search coil
V_1 is the supply voltage
I_1 is the supply current
R is the resistance of the winding,

and the percentage of the leakage flux σ can be defined as

$$\sigma = \left(1 - \frac{\text{airgap flux}}{\text{total flux}}\right) \times 100\ \% \qquad (5.3.17)$$

The average of σ values taken from measurements at three different excitation currents (I_1) with the rotor in the d position are

	form 1	form 2
% leakage σ	20.4 %	26.6 %

From the results shown above, the form 1 motor which is a lot cheaper to manufacture than the form 2 motor, does not at first sight seem to be leakier even though the excitation coil's location is quite remote from the airgap. The comparison is however somewhat misleading because the airgap permeance of the two experimental motors are rather different, the form 2 motor permeance being only half that of the form 1 motor (Table 5.4) and one per unit leakage permeance is thus twice as significant. With equal airgap permeances, the form 2 motor can still be considered as a better configuration as far as the leakage flux is concerned.

5.3.4.4 Modification to drive circuit and test rig

Following previous load tests with the form 1 motor, modifications were made to both the drive circuit and the test rig to enable it satisfactorily to feed the motor at higher speeds and power levels. The modifications made included a higher power driver circuit, a single-output-transistor switching circuit for the bifilar wound motor, a tachometer for high speed measurement and an eddy-current brake dynamometer.

a) The driver circuit

During load tests on the form 1 motor with reduced turns, it was found that the main transistor which

was driven from the driver chip failed several times. On each occasion the driver chip was also burnt out and examinations of the load current, voltage across the main transistor and base drive signal waveforms showed that trouble was being caused by a) unexpectedly high peak load currents as high as three times the average current, b) insufficient base drive and c) insufficient pull-down voltage at the base of the transistor at switch-off. The insufficient base drive of course caused the transistor to come out of saturation and the driver chip was hence replaced by a driver circuit of the Fig. 5.3.7 configuration, the new driver circuit being supplied from a separate d.c. regulated power supply unit of 1 A rating. The d.c. supply was considered to be important for the driver circuits which were modified to be able to source or sink load currents of 500 mA. The output transistors (BD 131 and BD 132) were fitted with small heatsinks to assist heat dissipation. The driver circuits were isolated and protected by high speed fuses at both output and supply rails. The new circuit is shown in Fig. 5.3.28.

b) Single-output-transistor switching circuit for bifilar-wound motors

This was built to operate from a d.c. rail voltage of 100 V to supply a load current of approximately 10 A. The circuit, with snubbers, is shown in Fig. 5.3.29. Component details are as follows:

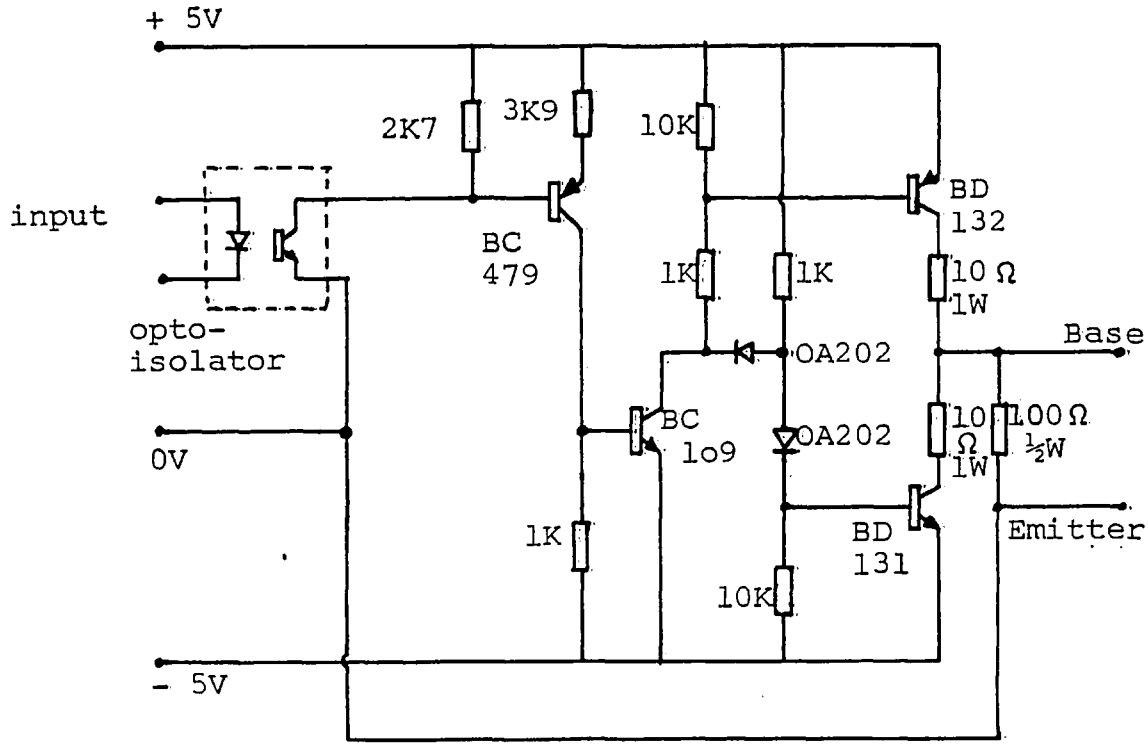

Fig. 5.3.28 Driver circuit

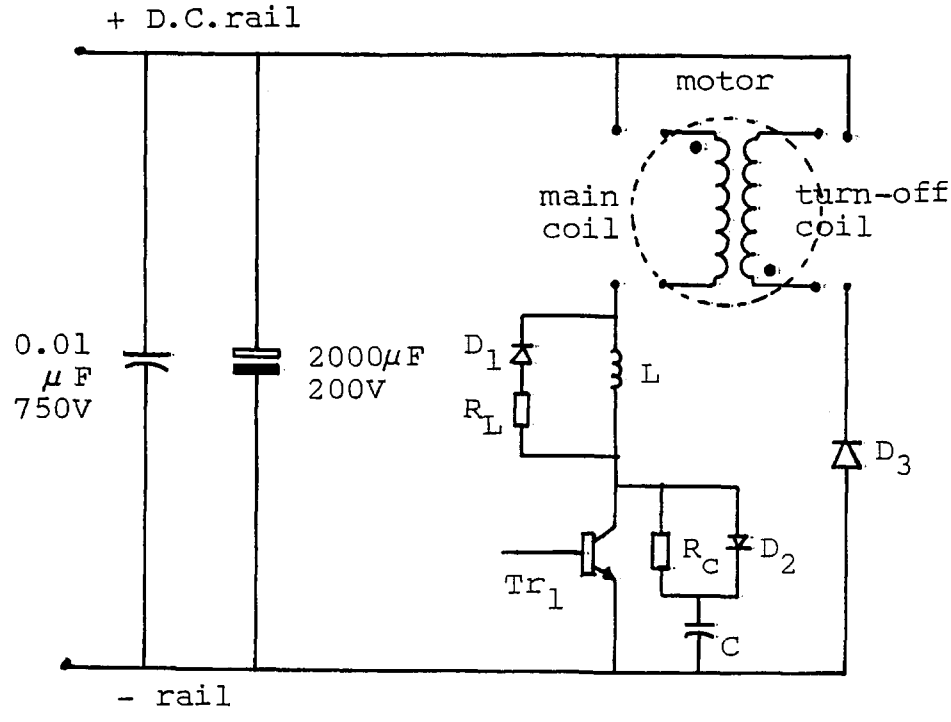

Fig. 5.3.29 Switching circuit for the bifilar-wound motor (with snubber)

Main transistor	: IR 6062, 400 V, 20 A
All diodes	: BYX 50-300, 300 V, t_{rr}= 100 nS
Snubber L	: 20 μH, 7 A
Snubber C	: 0.047 μF 630 V (polypropylene)
R_C	: 28 Ω 2 W
R_L	: 1.95 Ω 2 W

The layout of the experimental circuit is shown in comparison with the circuit for single-coil motors in Fig. 5.3.30. In order to reduce the voltage spikes that might damage the main transistor: a) the snubber capacitors were placed as near as possible to the main transistors, b) all wiring was kept short and c) the rail smoothing and rail decoupling capacitors were placed near the inverter.

c) Tachometer

The high top speed and small size of the motor makes speed measurements using stroboscope or normal mechanical tachometer particularly inconvenient and the previously built optical tacho used for the speed-control system of the d.c. machine dynamometer (Fig. 5.2.8) was modified. An 8-tooth aluminium disc was fitted on to the shaft and the timing RC of the F/V converter circuit selected to give a ratio of output voltage to input frequency of 1 mV/Hz. The output of the tachometer was hence 7500 rev/min/V and the speed range for linear output extended from 75 rev/min to 26000 rev/min.

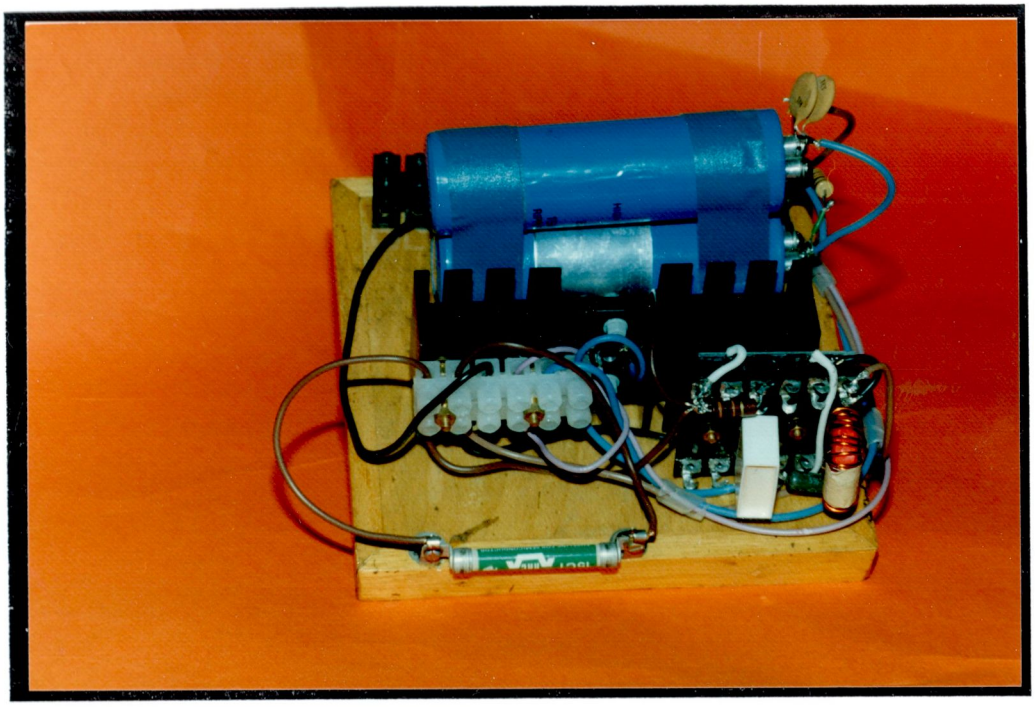

(a)

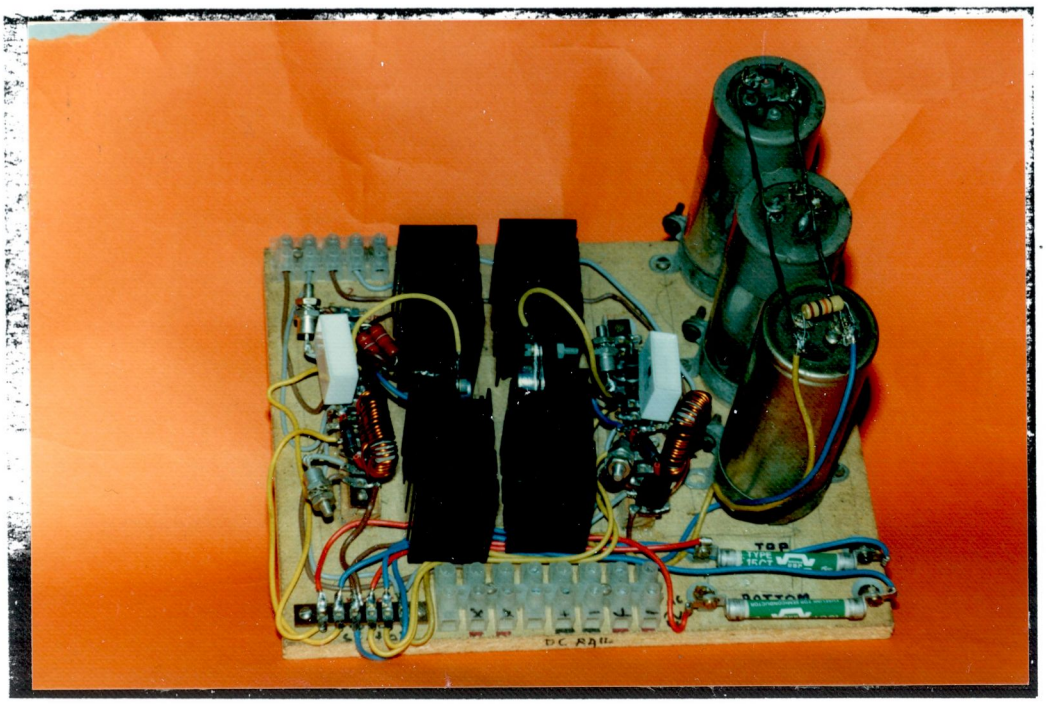

(b)

Fig. 5.3.30 Layout of the components in the switching circuits
(a) Single-transistor switching circuit
(b) Two-transistor switching circuit

d) Eddy-current brake dynamometer

To overcome the problems of stray friction and load-to-motor couplings-matters which can become extremely significant with small motors at high speeds, an eddy-current brake dynamometer was developed. A diagram of the experimental unit shown in Fig. 5.3.31 is based on a stator of 4 strip wound C cores, and a circular disc rotor. The excitation coil on each C core was wound with 110 turns of 1.12 mm diameter copper wire and mild steel pole pieces were added. The rotor disc was made of non-magnetic material to avoid unbalanced-magnetic pull. For the form 1 and form 3 motor tests, a 3.1 mm copper disc was used but for the form 2 motor tests a 1.6 mm disc was used to keep the cantilever weight and friction loss low. The diameter of both discs was 101 mm. The excitation coils were connected in series and supplied from a d.c. source. The reaction torque on the dynamometer was measured by a 200 gm spring balance with a torque arm of 96 mm. The dynamometer unit is shown with the motor in Fig. 5.3.32. In setting up the dynamometer, the disc was located on the motor shaft as near to the bearing as possible and no coupling was used in order to reduce vibration. The disc was secured firmly and checked for truth. A damper was fitted as before to the torque arm to damp down vibration transmitted from the motor through the bedplate to the dynamometer unit.

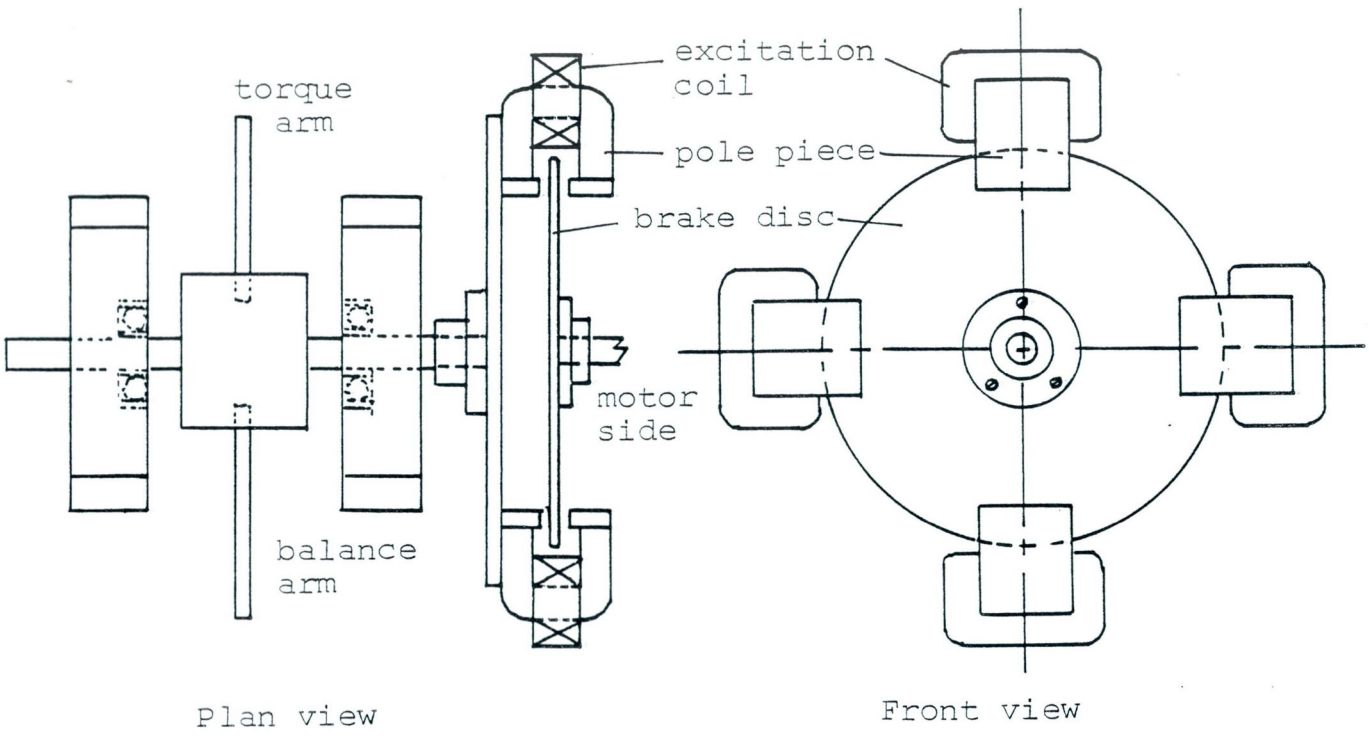

Fig. 5.3.31 The eddy-current brake dynamometer

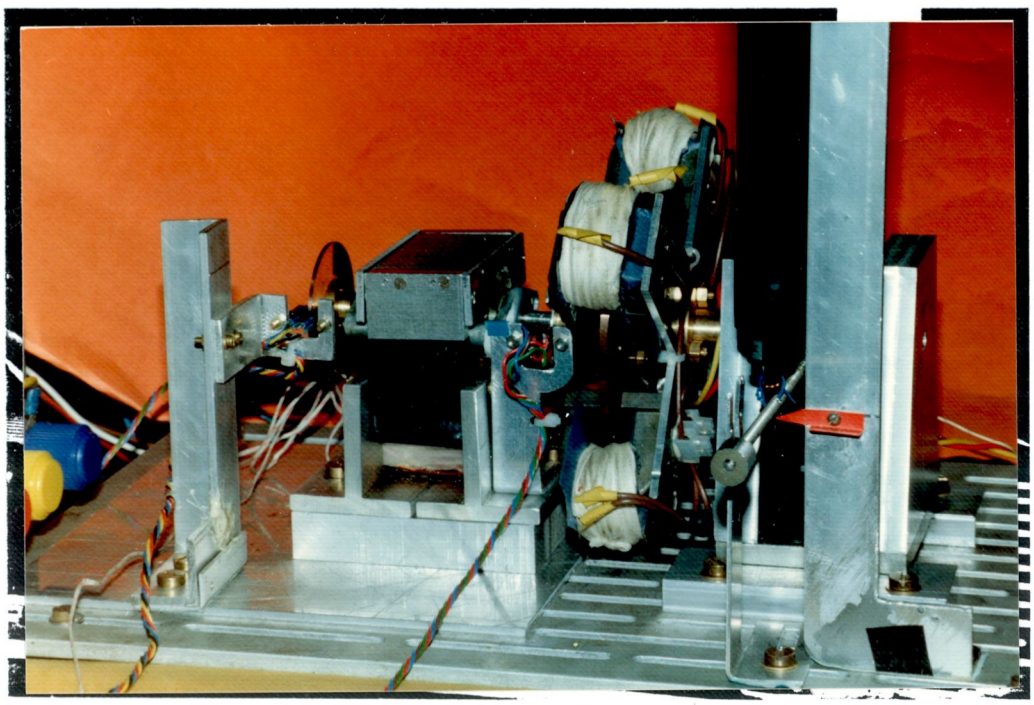

Fig. 5.3.32 Test rig with the form 1 motor

5.3.4.5 Retardation tests

The objective of the retardation test is to estimate the friction and windage losses in the system. For normal operation of small motors at low speeds (up to 3000 rev/min) with proper bearings, the friction and windage loss is normally small and can often be neglected. But for the SPSR motors tested, the lack of high speed bearings, the presence of the eddy-current brake disc of appreciable diameter (and windage) and the high speeds of the motor increase the friction and windage losses considerably and it was important to determine this loss if the motor's gross output power to be found.

The motor with all the discs (i.e. speed-sensor, position-sensor and dynamometer disc) was run up to the maximum no-load speed, and the power supply then switched off. (Note in order to eliminate the possibility of damage to the main transistors due to the voltage spikes that might occur when the mains is interrupted, the motor was switched off by removing the synchronising signal to the switching unit.) The motor speed was recorded by means of the speed sensor and F/V tachometer and plotted against time using an X-Y plotter. The deceleration curve of the form 1 motor is shown in Fig. 5.3.33(a). From the deceleration curve the friction and windage torque can be calculated from

$$J\dot{\omega} - T_f = 0 \qquad (5.3.18)$$

where J is the total moment of inertia of the system
ω is the angular speed of the motor
$\dot{\omega}$ is the angular acceleration or deceleration
T_f is the friction and windage torque.

For a small Δt eq(5.3.18) can be written as

$$T_f = J \frac{\Delta \omega}{\Delta t}$$

and hence $$T_f = J.\Delta\omega\left(\frac{1}{\Delta t}\right) \qquad (5.3.19)$$

Hence if the ω axis of the X-Y plot is divided into equal steps of $\Delta\omega$, the corresponding Δt can be found for each step. Values of $1/\Delta t_n$ are then plotted against ω_o (the average of ω_1 and ω_2 for each step) as shown in Fig 5.3.33(b) for the form 1 motor. From the smoothed deceleration characteristic, the friction & windage torque 'T_f' can be calculated by multiplying $J\Delta\omega$ and the ordinates of the deceleration curves (b). The T_f versus ω characteristic is then obtained as shown in Fig. 5.3.33(c). A typical moment of inertia calculation for the rotor is shown in Appendix B5. Fig. 5.3.34 (a), (b) and (c) shows the friction and windage loss characteristics for the form 1 No.2, form 2 and form 3 motors respectively. The friction and windage power losses are also given.

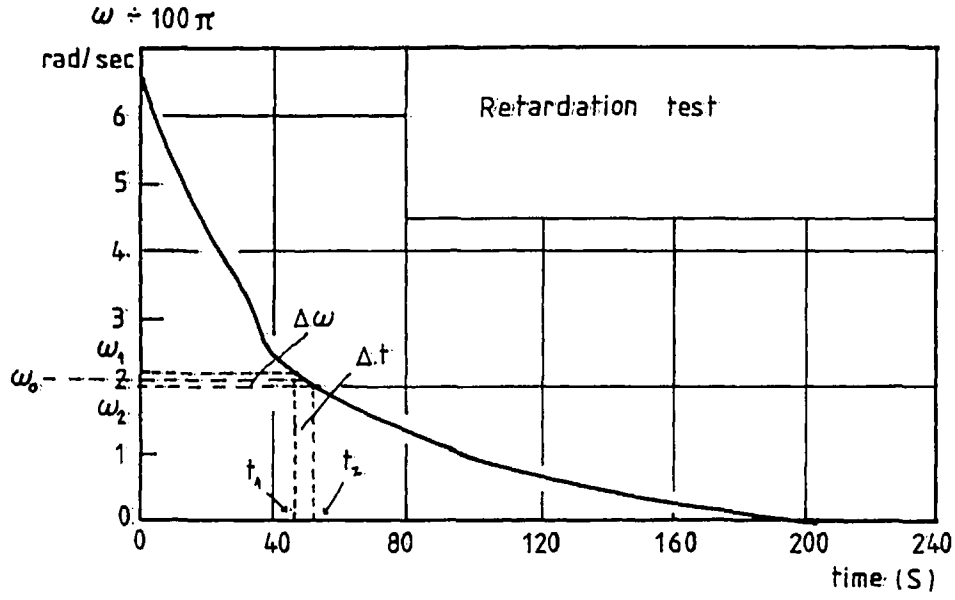

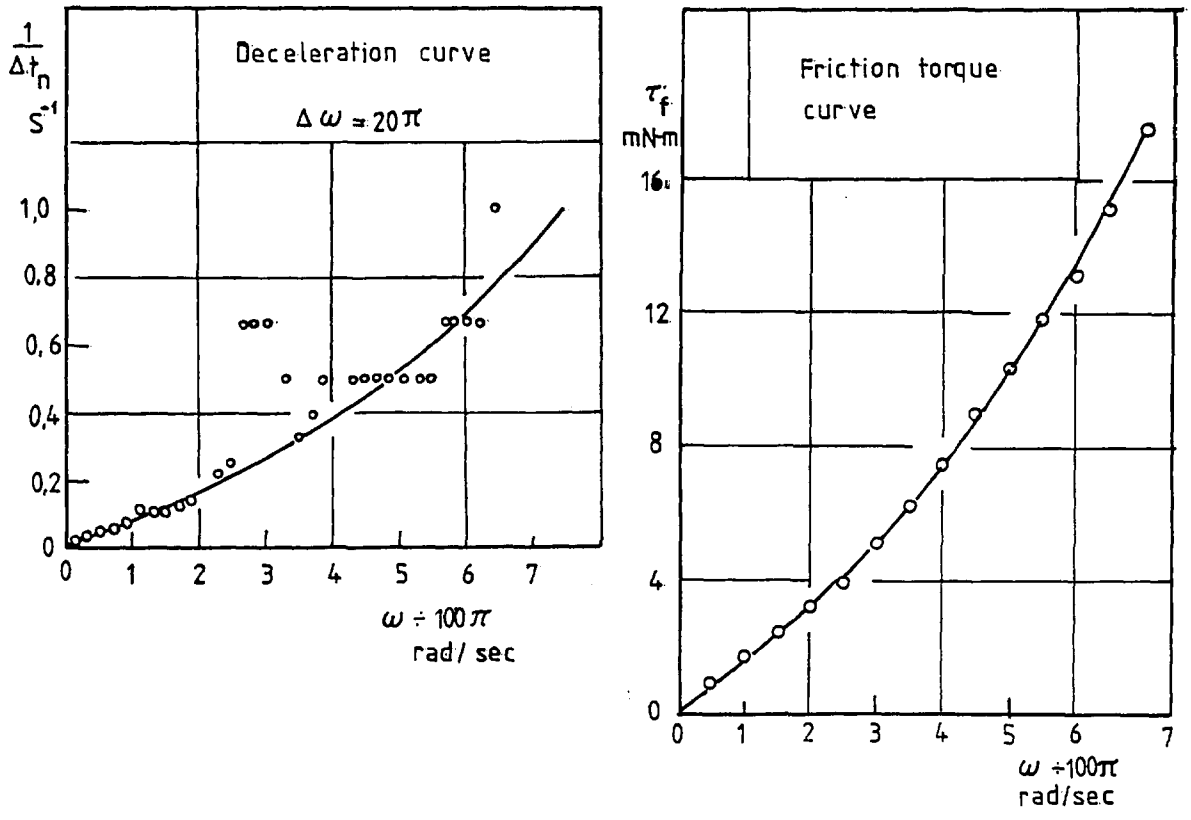

Fig. 5.3.33 Results from the Retardation test on the form 1 No. 1 motor

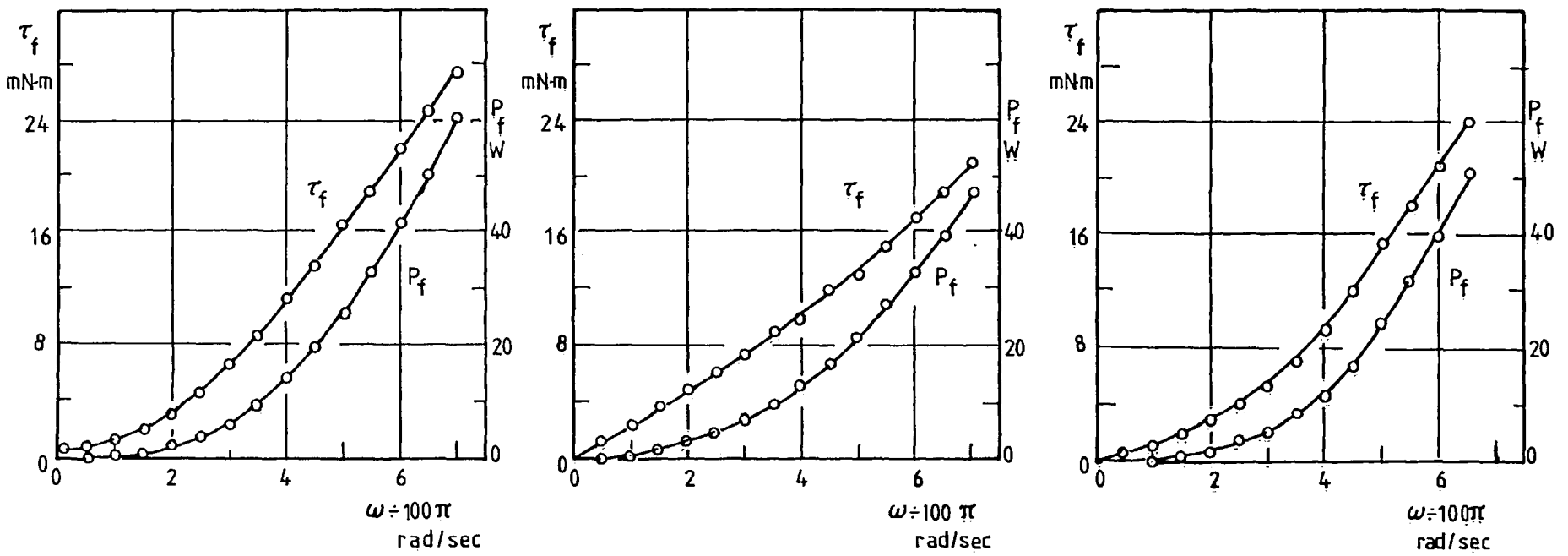

(a) Form 1 No.2 motor (b) Form 2 motor (c) Form 3 motor

Fig. 5.3.34 Friction torque and power loss curves obtained from the retardation tests

5.3.4.6 Load tests of the two-pole high speed motors with d.c. feed circuit

The principal tests carried out were:

a) Form 1 No.1 motor on 40 V d.c. rail

b) Form 1 No.2 motor on 80 V d.c. rail

c) Form 2 motor on 70 V d.c. rail

d) Form 3 motor on 80 V d.c. rail

All tests were made with $\alpha = 90^{\circ}$ and $\beta = 90^{\circ}$, and full m/s ratio.

The switching angles were chosen according to preliminary test to give maximum no-load speed (Section 5.3.4.2) without continuous coil-current operation. The voltage level was chosen in each test to avoid excessive currents at low speeds. The voltage and current waveforms are shown in Fig 5.3.35 to 5.3.38. In Fig. 5.3.35, the transistor current (main-coil current) is shown in (a) and the diode current (pull-down current) in (b). With a rail voltage of 40 V the peak voltage across the main transistor can be seen to be approximately 80 V. This is twice the rail voltage and results from the transformer action and 1:1 ratio of the pull-down coil. The drop in V_{CE} at the trailing edge corresponds to the instant at which the diode current drops to zero and the transformer action ceases. The change in current waveform from a flat top shape at 16000 rev/min no-load in (a) and (b) to a peaky waveform in (c) at 12000 rev/min due to magnetic saturation can be

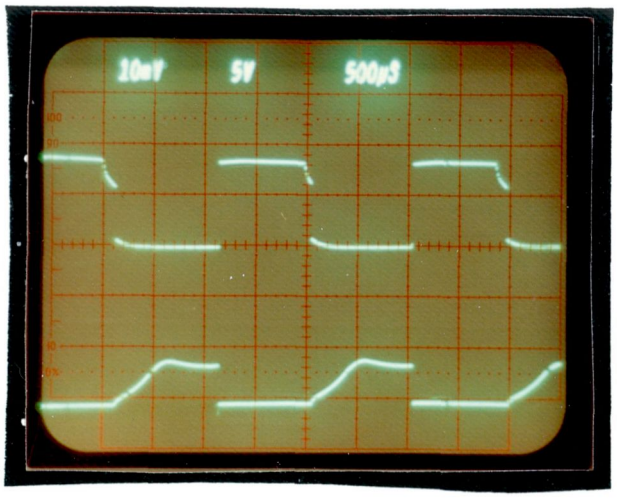

(a)

v_{CE} 50V/div

i_T 5A/div

t 0.5mS/div

Voltage across main transistor and main-coil current (40 V d.c.rail, 16000 rpm., P_{out} 21 W, I_{coil} mean 1.97 A)

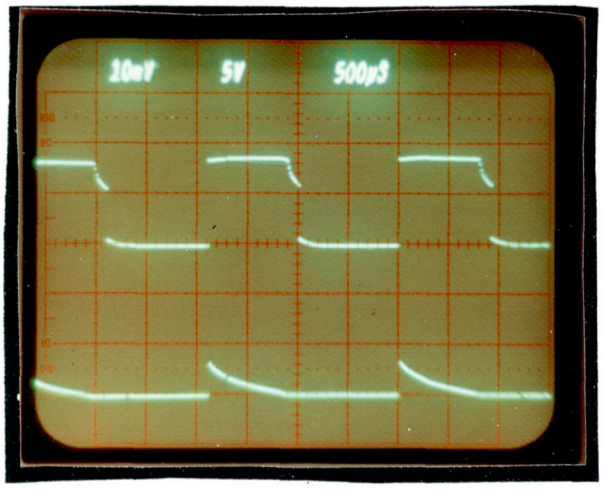

(b)

v_{CE}

i_D

Voltage across main transistor and turn-off-coil current (same condition and same scale as in (a))

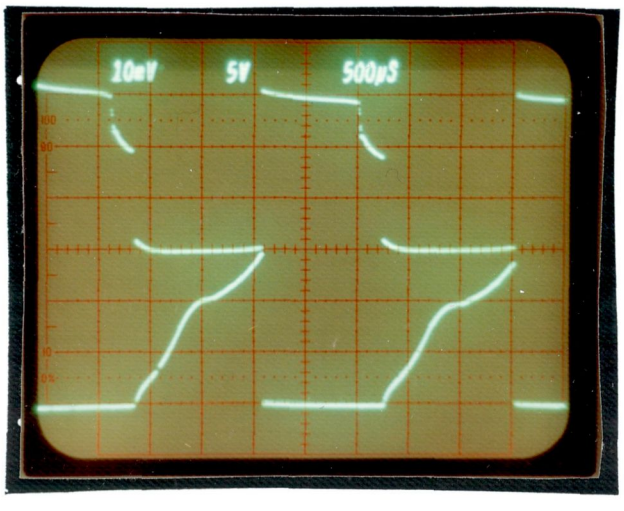

(c)

v_{CE}

i_T

Voltage across main transistor and main coil-current (70 V d.c.rail, 12000 rpm, P_{out} 75.8 W, mean current 4.3 A)

:same scales as in (a)

Fig. 5.3.35 Voltage and current waveforms of the form 1 No.1 motor (bifilar winding)

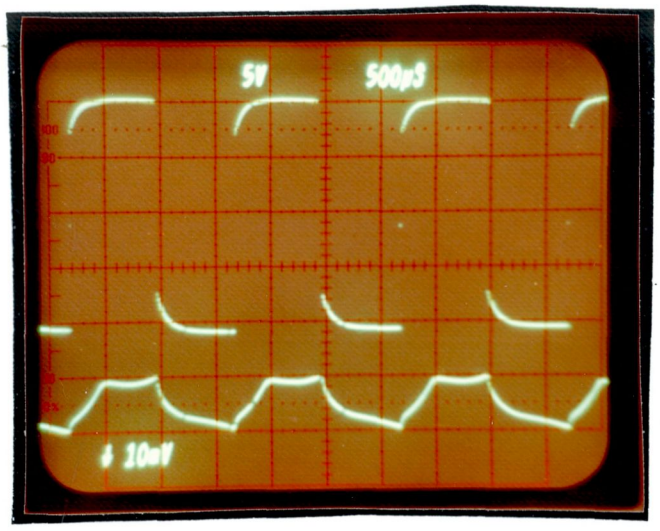

(a)

v_{coil} Coil voltage and coil current (100 V d.c. rail, 20400 rpm., no load, mean I 2.72A)
Scale: v 50V/div
i 5A/div
t 0.5mS/div

i_{coil}

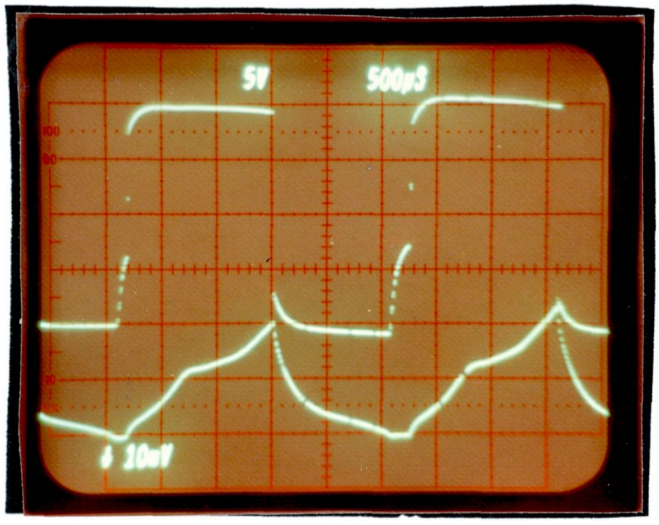

(b)

v_{coil} Coil voltage and coil current (100 V d.c. rail, 12000 rpm., P_{out} 72 W, mean I 4 A) same scales as in (a)

i_{coil}

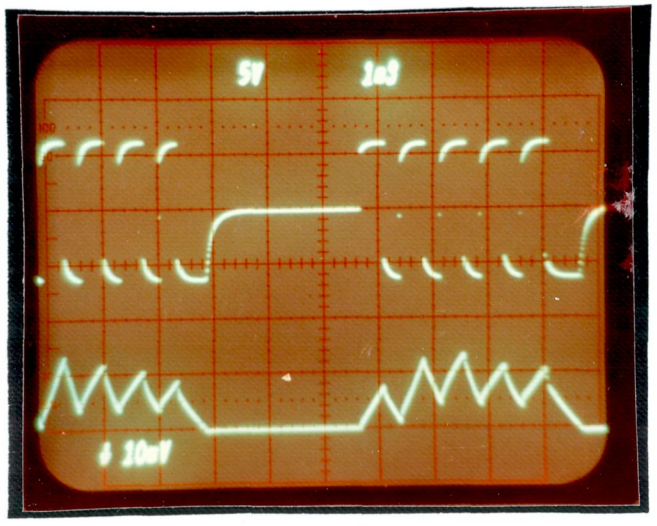

(c)

v_{coil} PWM action on coil voltage and coil current (60 V d.c. rail, 4500 rpm., mean I 0.7 A)
Scale: v 50V/div
i 2A/div
t 1mS/div

i_{coil}

Fig. 5.3.36 Voltage and current waveforms of the form 1 No.2 motor (single coil)

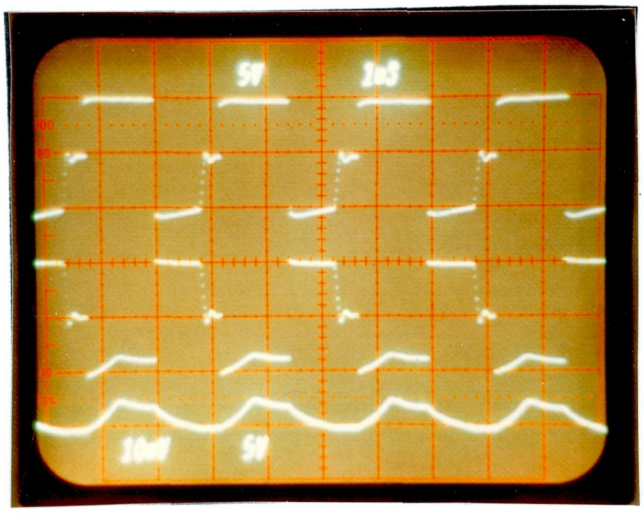

v main-coil

v pull-down coil

$i_T + i_D$

(a) Main-coil and pull-down coil voltage and transistor and diode current waveforms (50 V d.c.rail, 14000 rpm., no load):Scale v 50 V/div, i 5 A/div, t 1mS/div

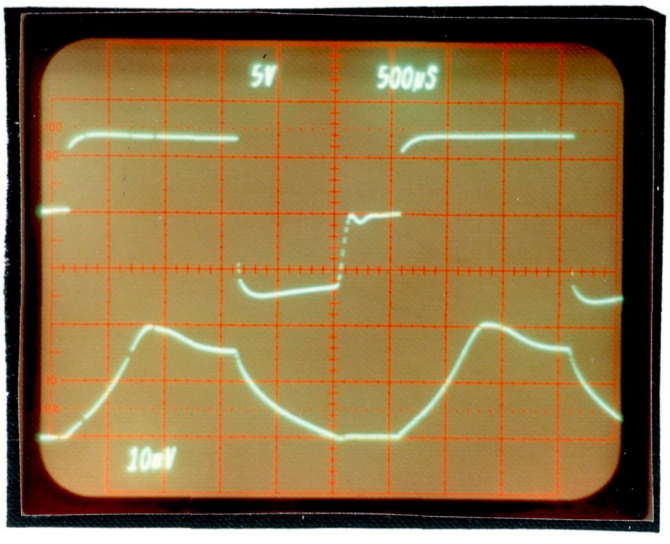

v main-coil

$i_T + i_D$

(b) Main-coil voltage and transistos and diode currents (67 V d.c.rail, 10800 r m., P_{out} 26.7 W):Scale v 50 V/div, i 2 A/div, t 0.5 mS/div

Fig. 5.3.37 Voltage and current waveforms of the form 2 motor (bifilar winding)

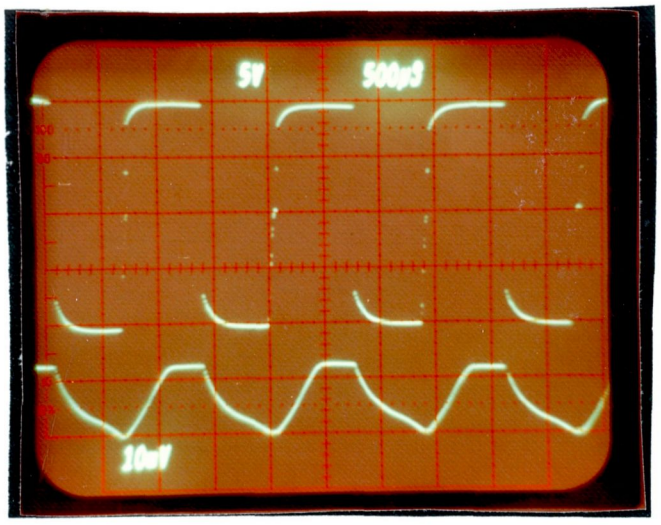

v coil

i coil

(a) Coil voltage and coil current (100 V d.c.rail, 22000 rpm., no load, maen I 3.2 A):Scale v 50 V/div, i 5 A/div, t 0.5 mS/div

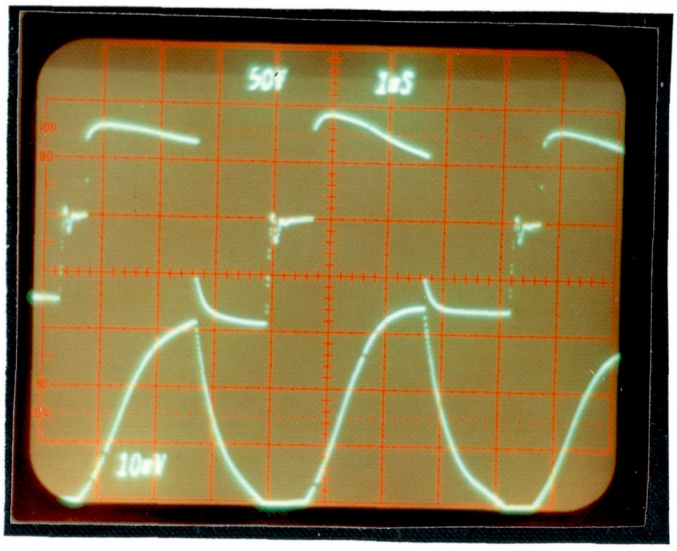

v coil

i coil

(b) Coil voltage and coil current (80 V d.c.rail, 7500 rpm., P_{out} 95 W, mean I 7.0 A):Scale v 50 V/div, i 5 A/div, t 1 mS/div

Fig. 5.3.38 Voltage and current waveforms of the form 3 motor (single coil)

seen clearly, the peak value being 15 A compared with a mean current of 4.3 A. The magnetisation characteristic has been discussed in Section 5.3.4.3(c).

The same characteristic of peaky current waveforms developing as the motor is slowed up by the load and draws larger currents is also shown in Fig. 5.3.36(a) and (b) for the form 1 No.2 motor. The voltage across the coil of the motor can be seen to be twice the rail voltage but with two transistors connected in series with the load (one to the top rail and another to the bottom rail), each device now has to withstand a voltage only equal to rail voltage. Fig. 5.3.36(c) shows the chopping action when operated in the PWM mode. Fig. 5.3.37(a) shows the voltage waveform of the main coil and pull-down coil of the bifilar wound form 2 motor and the current waveform shown is the combined current flow in the main coil and pull-down coil. Even at 10800 rev/min with a peak current of 4 A no saturation is shown in the current waveform in (b). For the single coil form 3 motor the waveforms are shown in Fig. 5.3.38. A slightly peaky waveform can be seen in (b) in comparison with the flat top currnt waveform in (a) but the peak to mean current ratio was not as high as in the form 1 motor although the A-T was higher. The relative significance of saturation shown in the current waveforms for the form 1, form 2 and form 3 motors agrees with the trends indicated in Table 5.6. The test rigs of the form 2 and form 3 motors are shown in Figs 5.3.39 and 5.3.40 respectively.

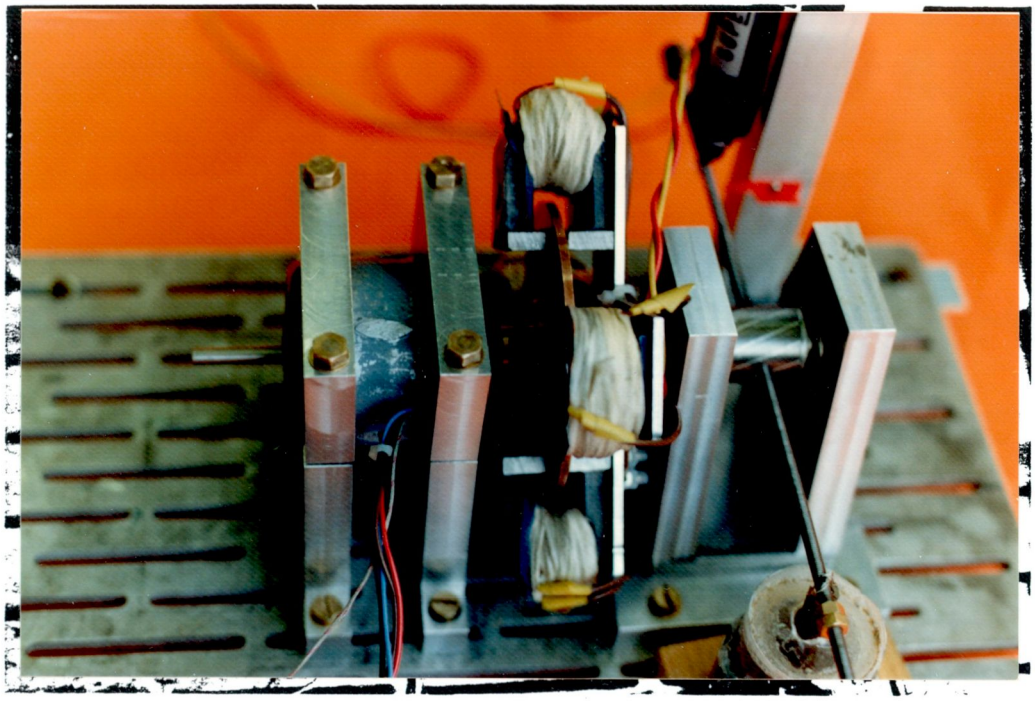

Fig. 5.3.39 Test rig with the form 2 motor (position and speed discs are not shown)

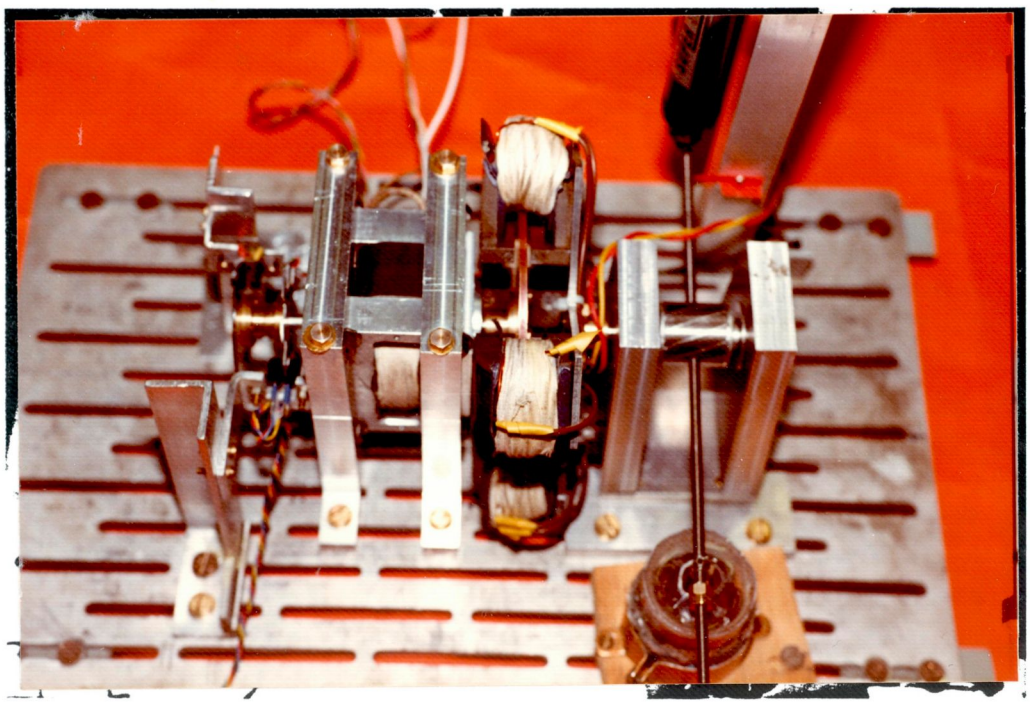

Fig. 5.3.40 Test rig with the form 3 motor

The performance curves of each motor are shown in Figs. 5.3.41 to 5.3.44. Curves of gross torque (output torque+friction+windage torque), gross power (output power + firction + windage losses), d.c. rail current and motor efficiency against speed are shown (Note however that in Fig. 5.3.41 the overall (motor + drive) efficiency is plotted). The mean d.c. rail current can be seen to be lower than the mean coil current because the former is the average of difference between the positive current supplied to the coil and the negative current from the coil fed back to the rail. The form 3 motor had the best efficiency (approximately 55 %). The power distribution curves are shown for the form 2 and form 3 motors in Fig. 5.3.45 (a) and (b) respectively. Unfortunately, inadequate metering in the tests with the form 1 No.1 and form 1No.2 made it impossible to present their power distribution characteristics. The curves presented show both measured characteristics and calculated characteristics with some approximations. The measured quantities were a) power input from the d.c. rail (motor + inverter), b) power input to the motor (by electronic wattmeter) and c) the output power of the motor (from torque). The differences between a) and b) were taken as the power losses in the inverter and the differences between b) and c) were taken as the total power losses in the motor which were treated as the summation of copper losses, iron losses and friction & windage losses. The friction and windage losses were obtained from the retardation tests, the copper losses

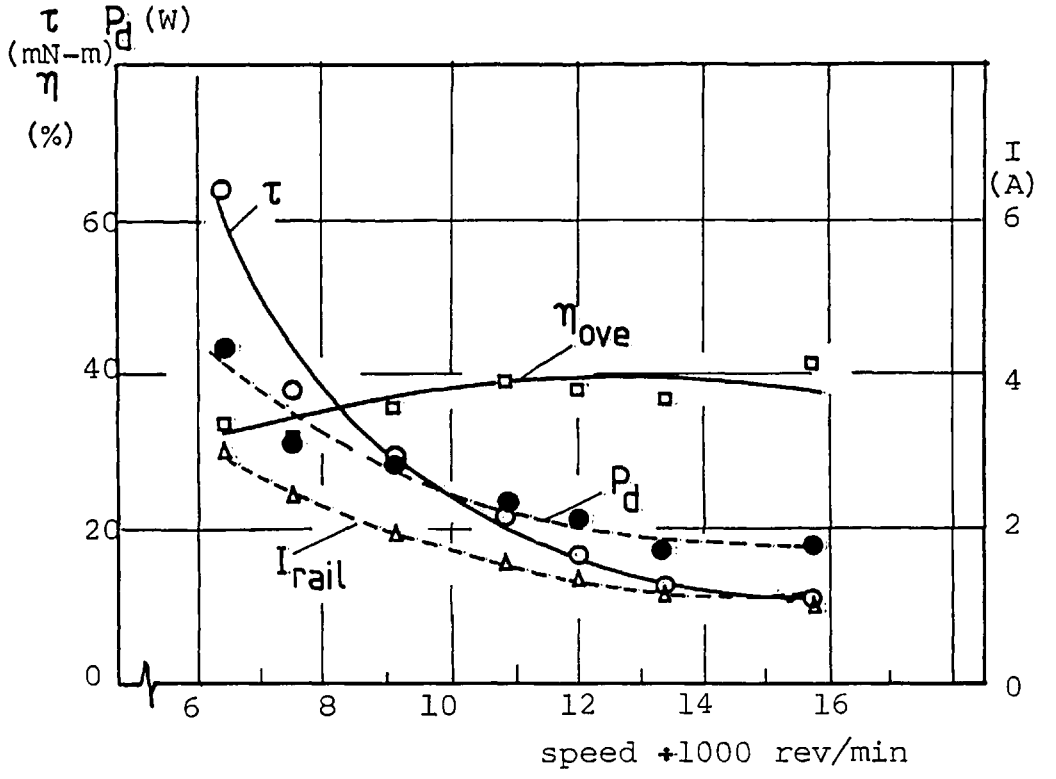

Fig. 5.3.41 Performance curves of the form 1 No.1 motor (40 V)

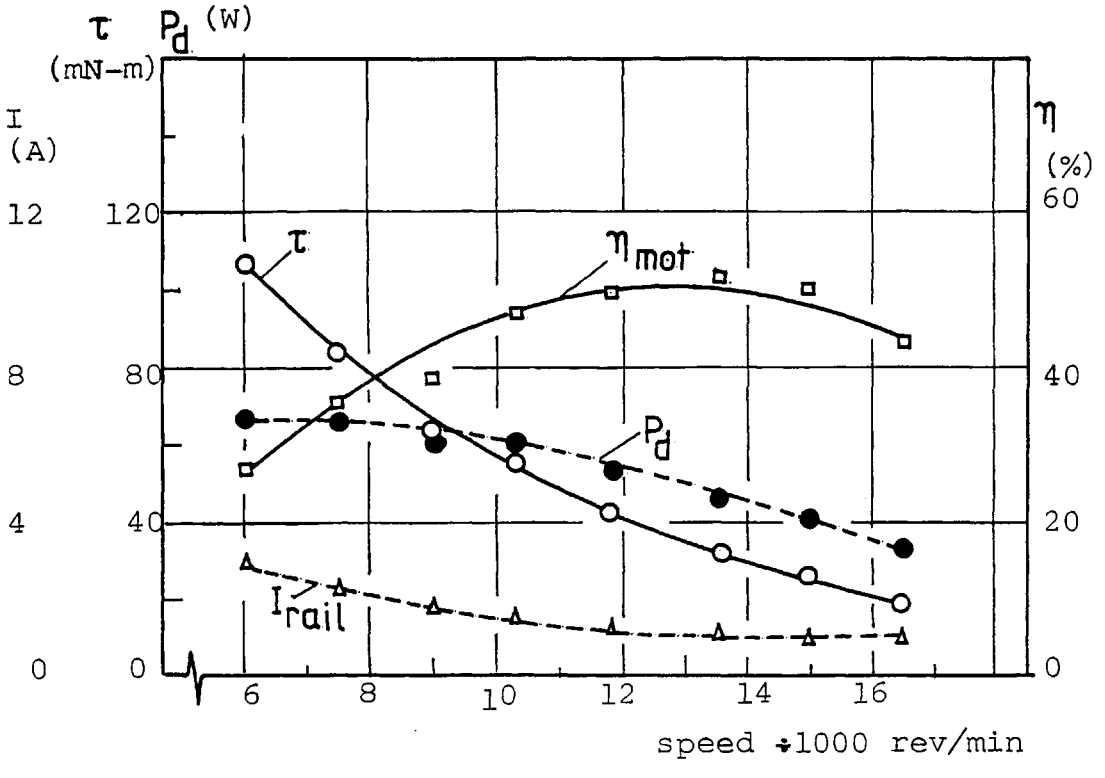

Fig. 5.3.42 Performance curves of the form 1 No.2 motor (80 V)

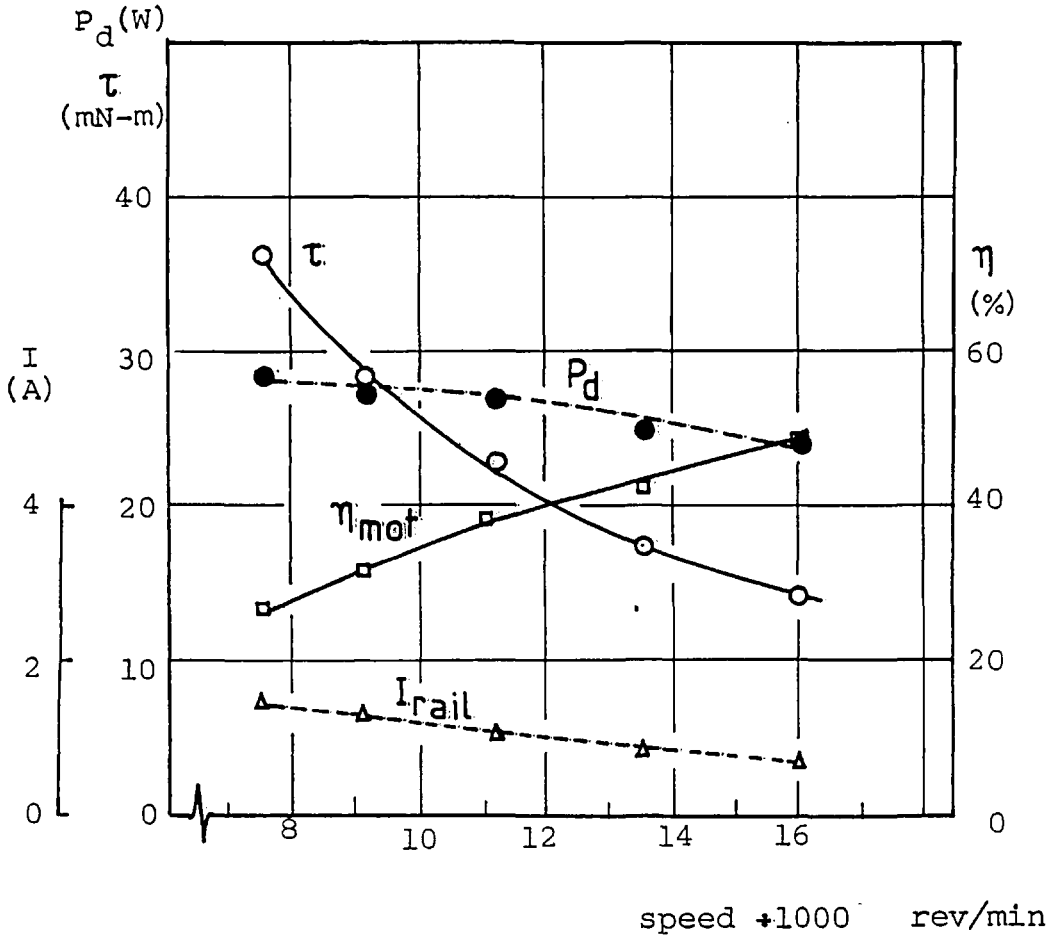

Fig. 5.3.43 Performance curves of the form 2 motor (70 V)

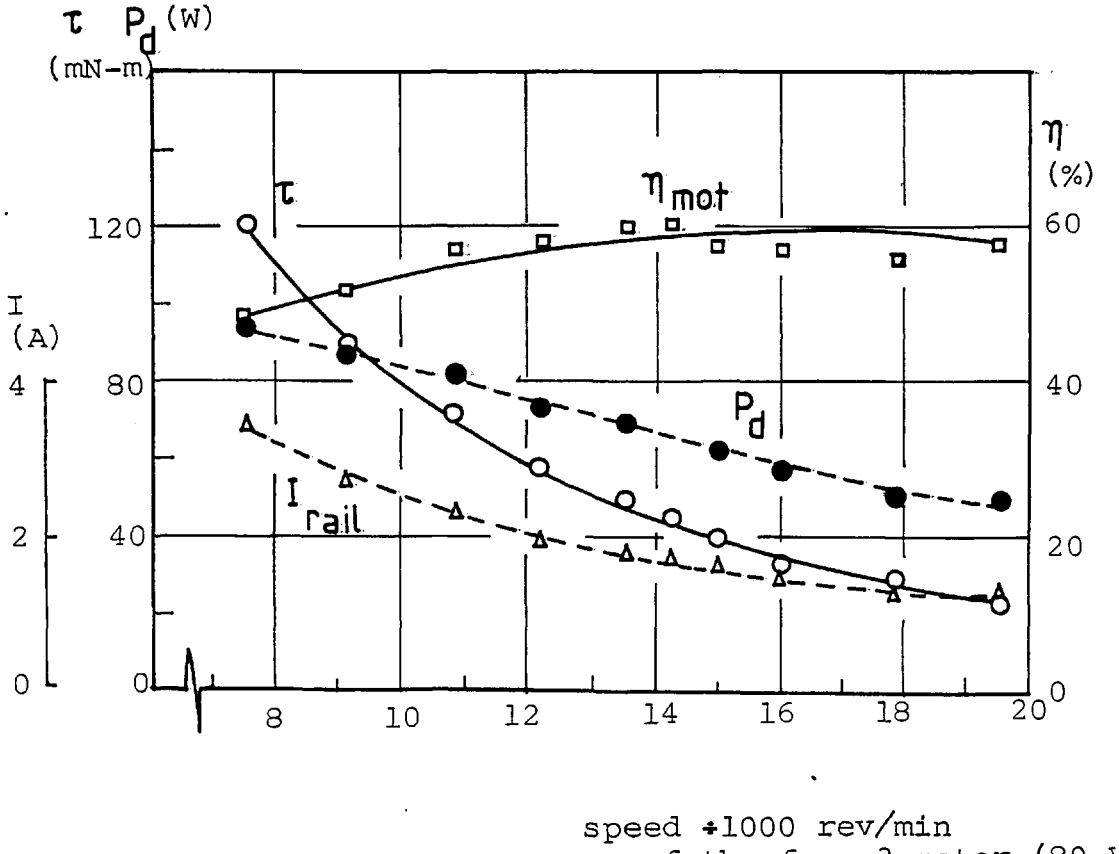

Fig. 5.3.44 Performance curves of the form 3 motor (80 V)

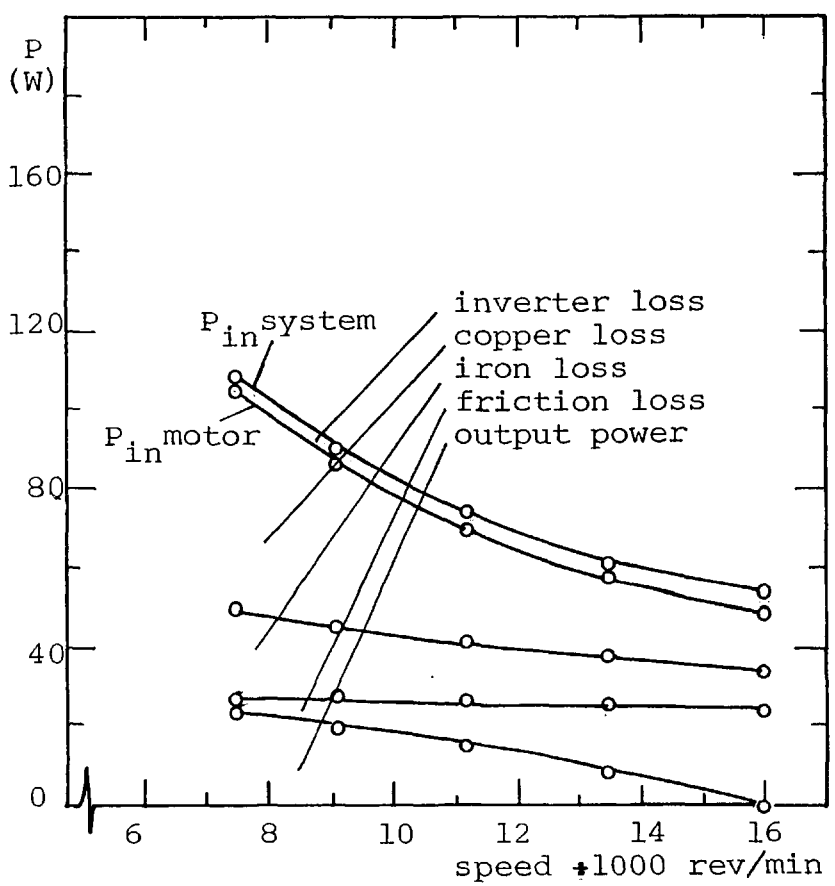

(a) Form 2 motor (70 V)

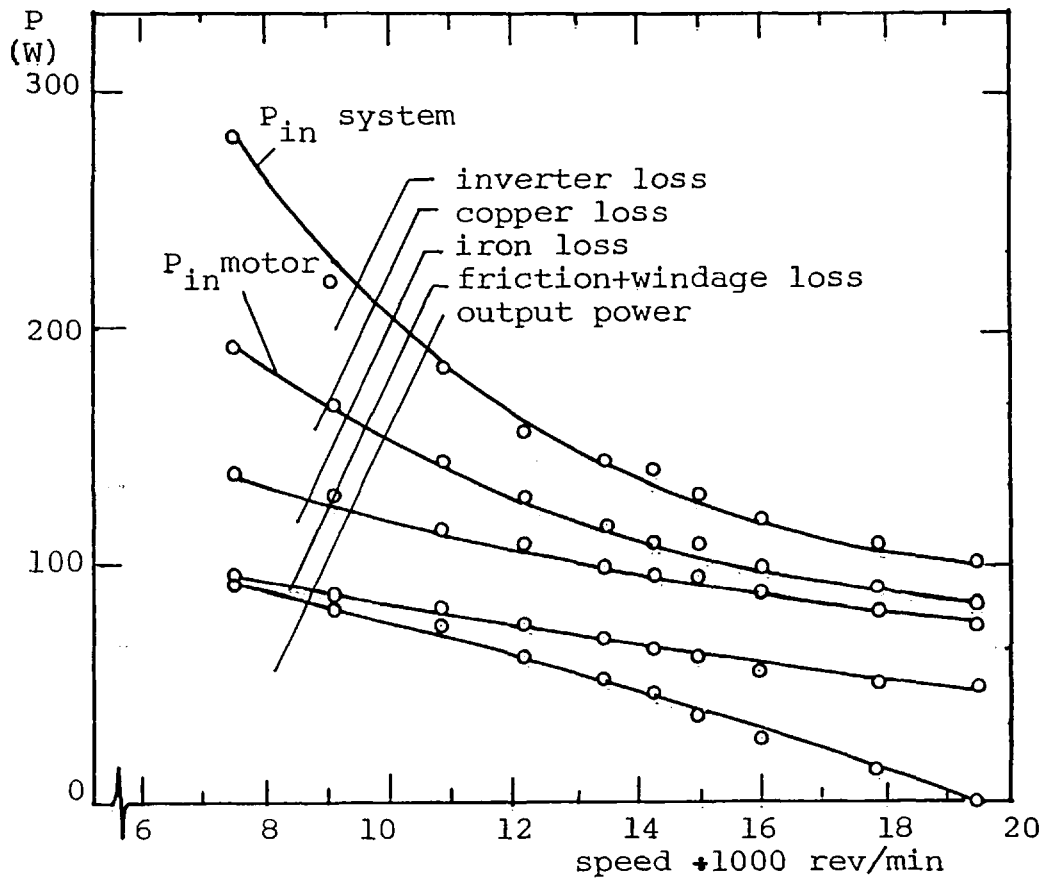

(b) Form 3 motor (80 V)

Fig. 5.3.45 Power distribution curves

were calculated from the measured r.m.s. coil currents (in the form 2 motor the r.m.s. currents were measured separately for each coil) and the d.c. resistance of the coil with an assumed 60°C temperature rise. The iron losses were calculated by substracting the copper losses and friction & windage losses from the total power losses in the motor. The inverter losses in the form 2 motor (a) can be seen to be small in comparison with the power losses in the form 3 motor (b) due to the very low inverter current. However because of a very high resistance of the winding, the motor copper loss turned out as the biggest single loss, and this suggests a maximum efficiency operating point in the range 15000 rev/min to 16000 rev/min. At speeds higher than this the friction and windage losses inevitably lead to efficiency reductions. For the form 3 motor, the iron losses can be seen to be fairly constant with speed, perhaps due to a balance between the increase in losses with higher frequencies and the decrease in losses with lower flux densities as the current falls. The operating point at which iron losses and copper losses were approximately equal was at a lower speed than with the form 2 motor, maximum efficiency occurring around 13000 rev/min.

5.3.4.7 Predictions

Performance predictions of the two-pole high-speed motors were made with both the simplified analytic

method (neglected resistance) and the step by step approach explained in Sections 3.2.1 and 3.2.2. Apart from the previously mentioned assumptions, viz: negligible iron losses and a triangular inductance waveform, the following further assumptions were made:

a) For the form 1 No.1, form 1 No.2 and form 3 motors where the coil currents were high, the effect of the return currents to the rail caused the voltage supply to the coil at the instant of switch on to be slightly higher due to the rail's impedance than the d.c. rail voltage set in the experiments. An increase of + 5 V in the rail voltage was hence assumed in the calculations for these cases.

b) Winding resistance values were assumed to be equal to the d.c. values measured at ambient temperature. This was assumed because each point of measurement was made separately, quickly and with the winding virtually at ambient temperature in order to prevent changes in output torques due to increase in resistance. This was a particular hazard at low speeds. This assumption is of course only necessary with the step by step approach since resistance is neglected in the simplified analytic method.

c) A 10 % decrease in L_d was assumed to 'account' for d axis saturation. L_q was left unmodified.

Comparisons between predicted and measured coil current waveforms are shown in Figs. 5.3.46 to 5.3.48 for the form 1 No.1, form 1 No.2, form 2 and form 3 motors respectively. In general the peak values of the measured current were higher than predicted perhaps due to the neglect of iron losses and saturation in the predictions. When peak currents are relatively low and saturation is absent the entire predicted waveform correlates well. However for the case with the form 2 and form 3 motors where saturation is not marked, good agreement can be seen even at low speeds. However Fig. 5.3.47(b) for the form 1 No.1 motor at 12000 rev/min shows a 50 % underestimate of peak current.

The limitations of the simplified analytic method can be seen in the case of the form 2 motor (the smallest of the motors with a high winding resistance) where the observed period of zero current is predicted by the step by step method but not by the simplified analytic method. The latter method also tends to overestimate somewhat the peak current (Fig. 5.3.48(a)). When the effect of saturation on the predictions of mean current are considered, it would seem that although saturation results in a faster rise and fall in the leading and trailing edges of the current pulses and higher peak currents (than in predictions), mean current levels are predicted fairly well (Fig. 5.3.48 (b)).

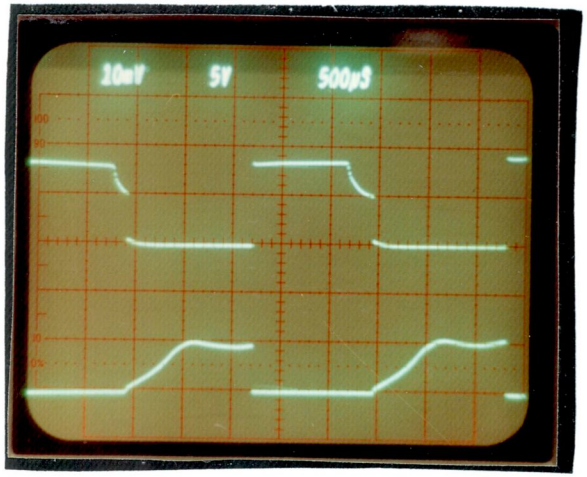

v_{CE}
50V/div

i_T
5A/div

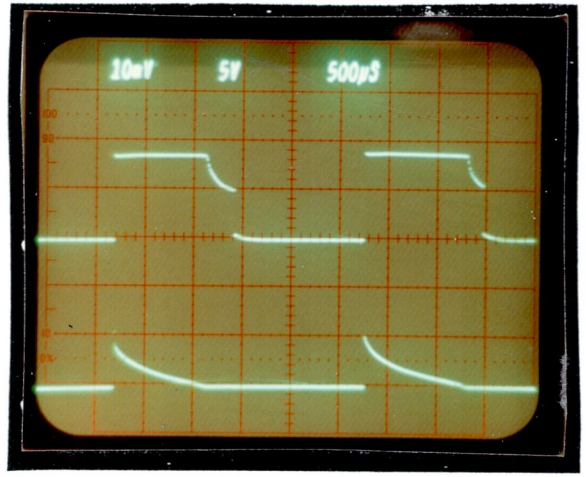

v_{CE}
50V/div

i_D
5A/div

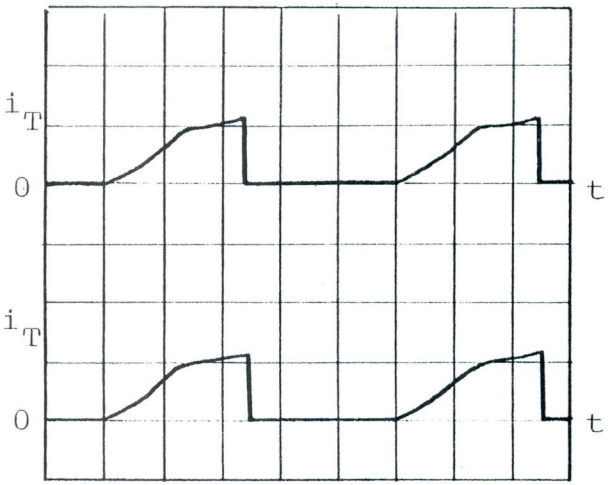

(a) Transistor current

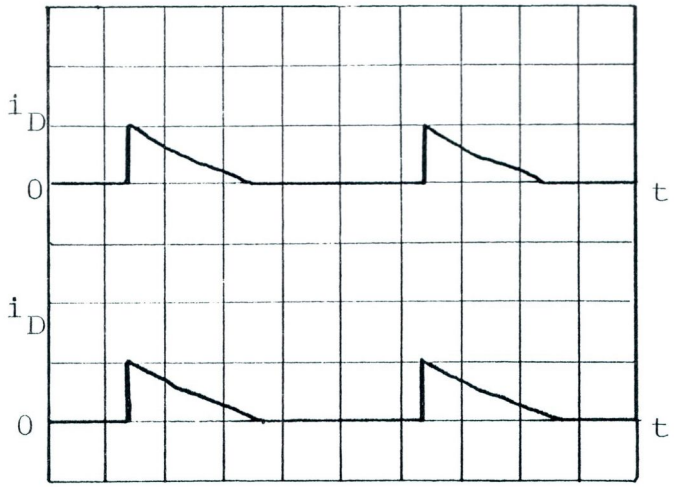

(b) Diode current

Step by step prediction

Analytic prediction

i 5 A/div
t 0.5mS/div

Fig. 5.3.46 Comparisons between predicted and measured current waveforms of the form 1 No.1 motor (40 V, 12000 rev/min)

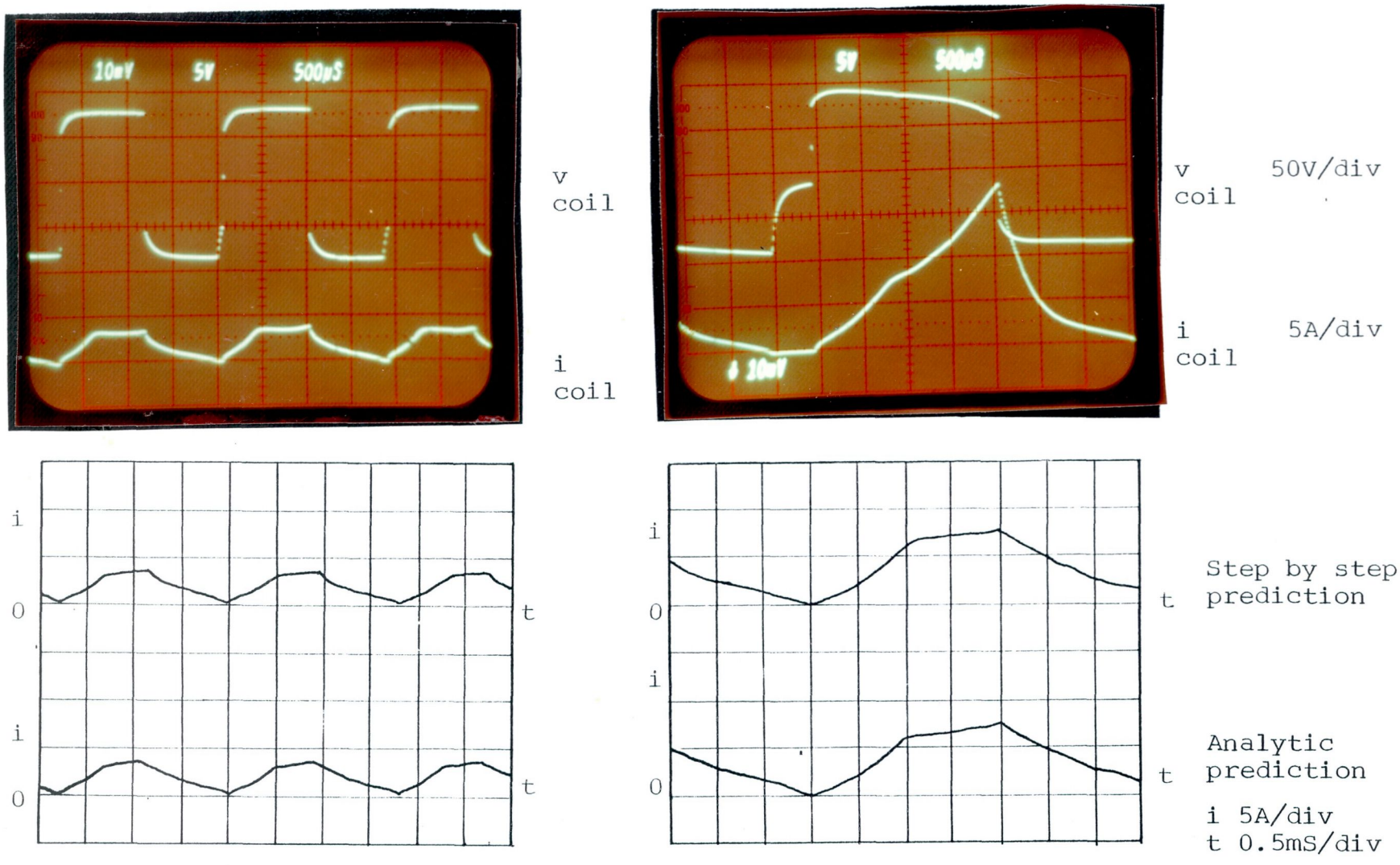

(a) 17000 rev/min (b) 7500 rev/min

Fig. 5.3.47 Comparisons between predicted and measured current waveforms of the form 1 No.2 motor (80 V)

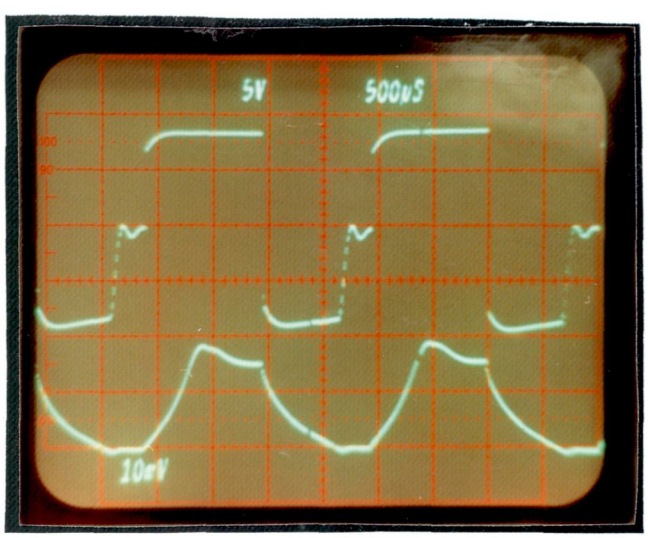

v main
coil
50V/div

i_T+i_D
2A/div

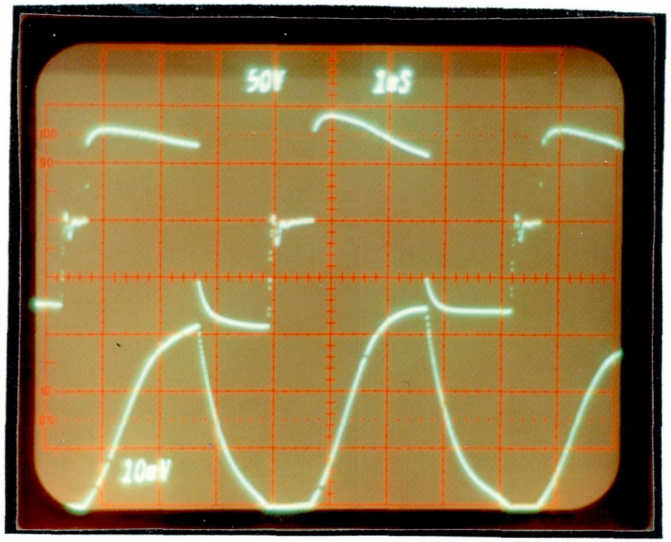

v
coil
50V/div

i
coil
5A/div

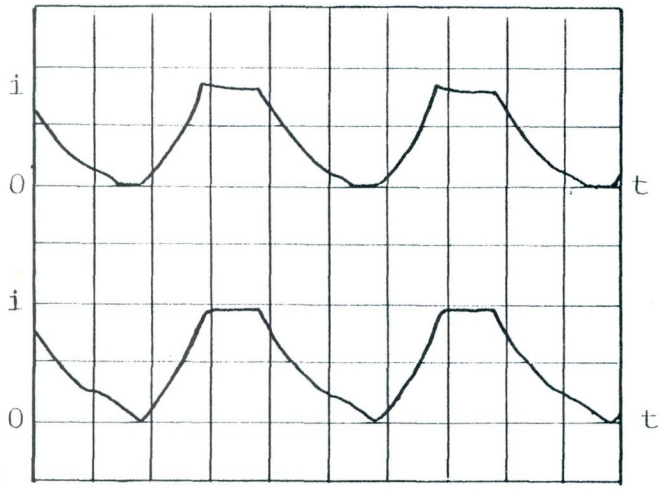

i
2A/div
t
0.5mS/
div

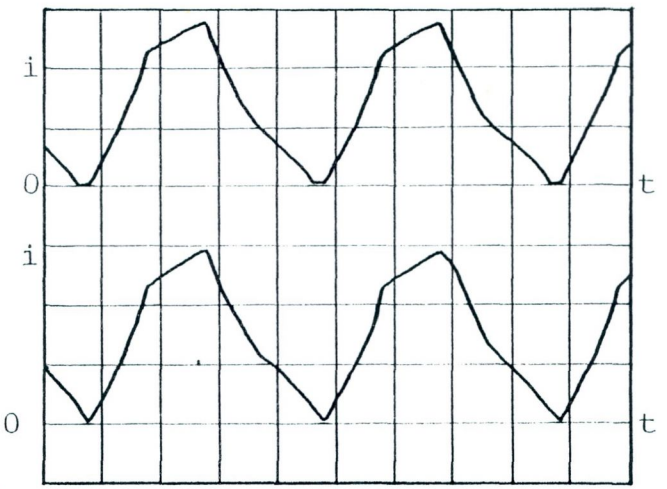

Step by step
prediction

Analytic
prediction

i 5A/div
t 1mS/div

(a) Form 2 motor (83 V,15000 rev/min) (b) Form 3 motor (80 V, 7500rev/min)

Fig. 5.3.48 Comparisons between predicted and masured current waveforms

The predicted gross torque versus speed curves are compared with the measured results (output torque + friction & windage loss torque) in Fig. 5.3.49. For the form 1 No.1 motor at 40 V (a) and the form 3 motor at 80 V (d), the predicted curves and measured points tie up well and perhaps demonstrate the validity of the L_d, L_q and supply voltage assumptions. In (b) the measured points at high speed can be seen to be higher than predicted and this perhaps suggests that although saturation reduces the gap flux density per amp and a reduced winding inductance, the resulting increase in peak current leads to a net torque gain. However when the saturation level is severe as at low speeds, the effect of the decreases in flux is dominant and results in a net drop in output torque. However, the torque gains at lower saturation levels may rarely be worth aiming for in practice in view of the higher copper losses and the need for switching devices of larger current rating. The predicted and measured characteristics shown in (c) for the form 2 motor where saturation is probably absent tie up well. In general it would seem that the simplified analytic method normally gives higher predicted torques than the step by step method due to the neglect of resistance. The difference is small for a low resistance motor but for a small, high resistance such as the form 2 motor, the errors can be significant (here up to 25 %). It should be mentioned that the friction and windage torques, which were added to the measured output torques to give the gross measured torque points in the comparisons,

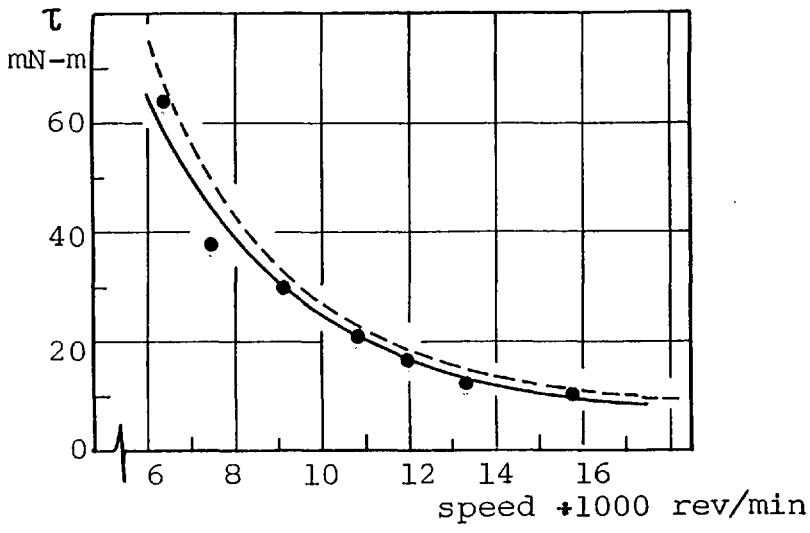

(a) Form 1 No.1 motor (40 V)

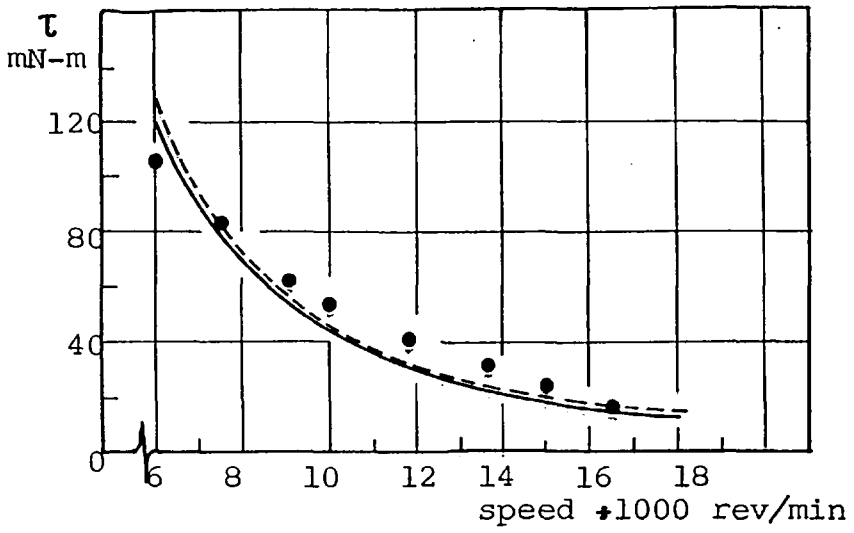

(b) Form 1 No.2 motor (80 V)

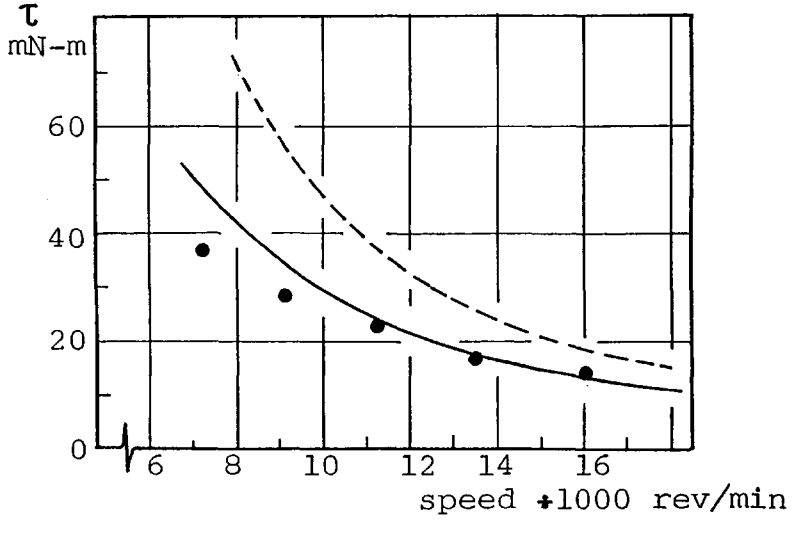

(c) Form 2 motor (70 V)

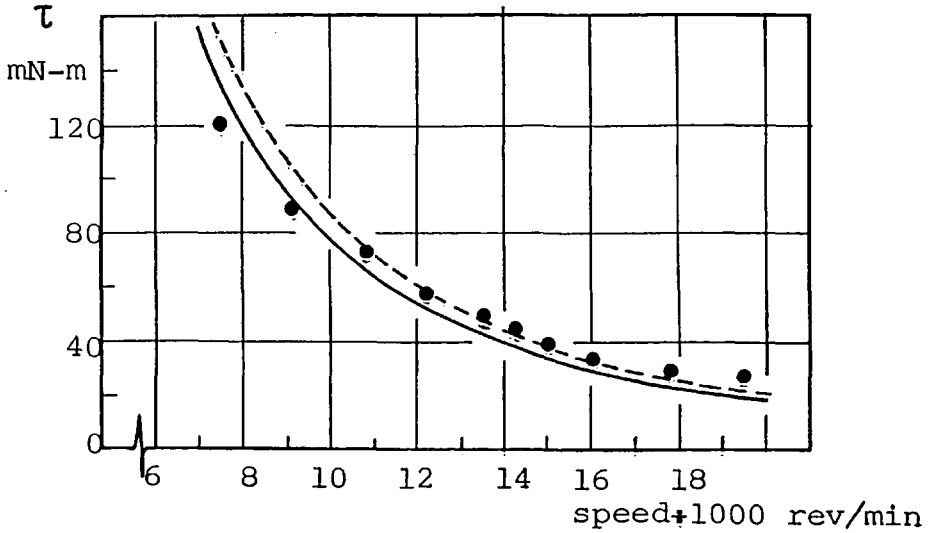

(d) Form 3 motor (80 V)

Fig. 5.3.49 Comparisons between the predicted and measured gross torque characteristics
● measured point ——— step by step prediction ------analytic prediction

were obtained from the smoothed curves through the retardation test results and from the calculated moments of inertia of the systems. Error might be introduced here and could account for the gross torque point at high speeds being a little too high.

The increase in mean coil currents at low speeds due to the effect of saturation can again be seen clearly in Fig. 5.3.50 (a) for the form 1 No.2 motor. As before, mean current levels correlated well for the form 3 motor in spite of differences between the waveshapes. Fig. 5.3.51 shows the comparisons between the copper losses calculated from a) measured r.m.s. currents (shown by the points), b) r.m.s. current predicted by the step by step approach (solid line), and c) r.m.s. current predicted by the simplified analytic method (broken line) for the form 3 motor. The same assumed value of the coil resistance was used in each case and the predicted and measured coil r.m.s. currents and the losses can be seen to be in good agreement. R.m.s. current comparisons are not included for the bifilar wound motors due to insufficient test data.

Since iron losses were neglected in the predictions, overall efficiency predictions are not made.

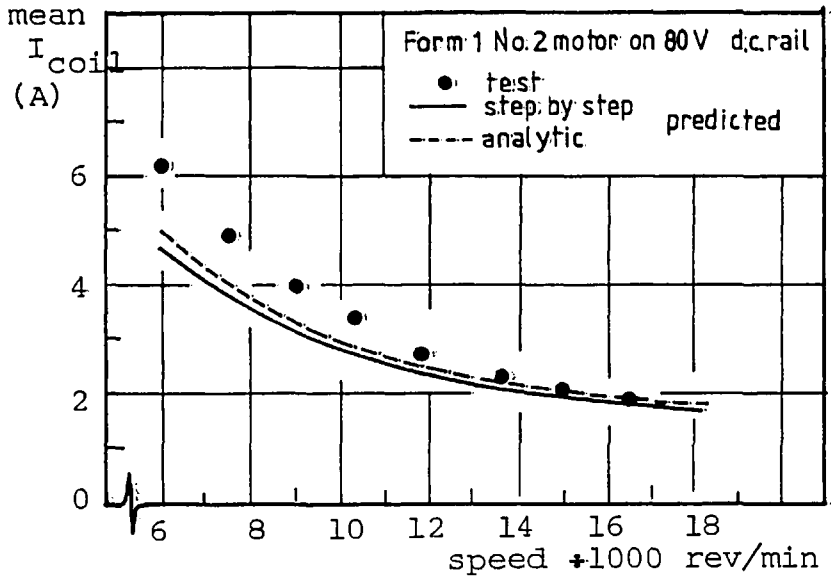

(a)

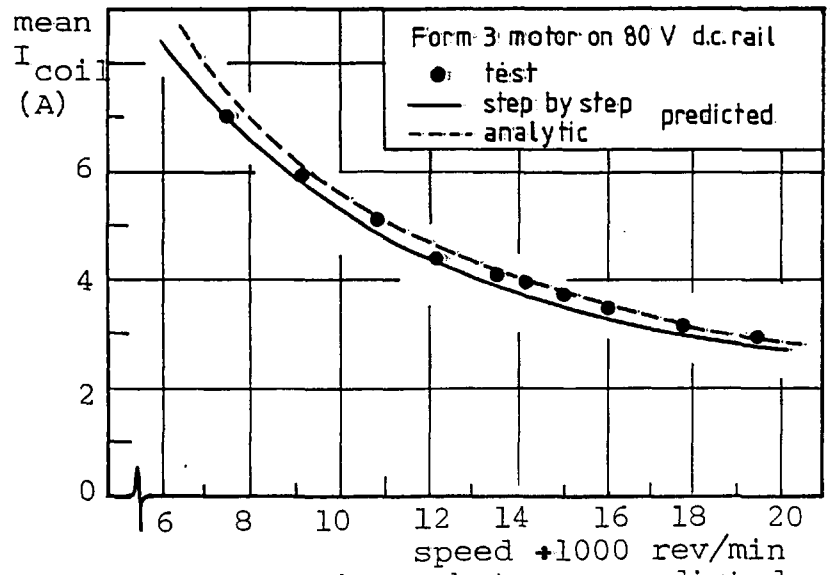

(b)

Fig. 5.3.50 Comparisons between predicted and measured mean coil current characteristics

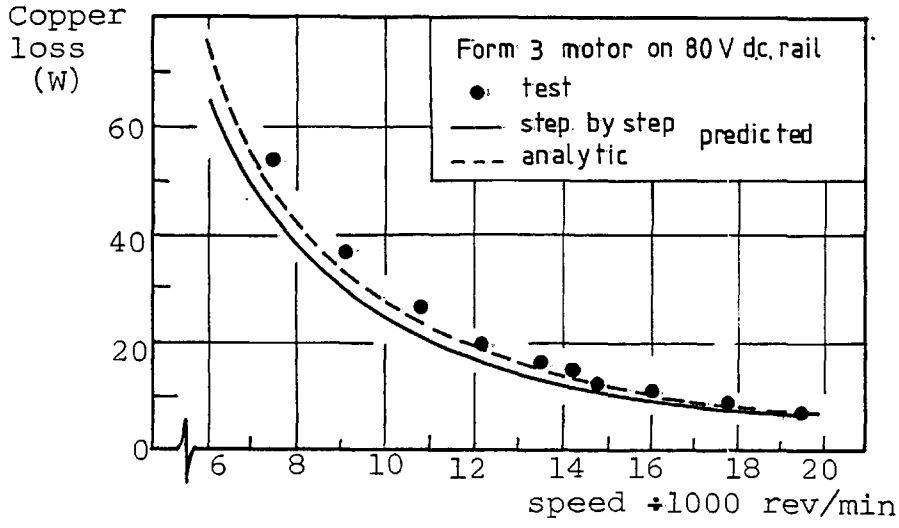

Fig. 5.3.51 Comparisons between predicted and measured copper loss of the form 3 motor

5.4 Performance of two-pole motors with d.c. feed at temperature limit

5.4.1 Test results

The objective of this part of study is to determine the rated output power of each motor by operating it at the class E insulation temperature limit (120°C absolute or 95°C rise with 25°C ambient).

From the results of the previous test the following nominal speeds were chosen, somewhat arbitrarily: 12000 rev/min for the form 1 No.1, 12000 rev/min for the form 1 No.2, 15000 rev/min for the form 2 and 12000 rev/min for the form 3 motors. These are typical speeds for commutator motors and for the form 1 and form 3 motors 12000 rev/min is near to the speed where the motors operate at maximum efficiency. For the form 2 motor, because of high copper loss, the maximum efficiency occurred at higher speed and the speed of 15000 rev/min was chosen as lying between the speeds for maximum output power and efficiency.

The procedure for determining rated output power at maximum permissible temperature rise is as follows:

a) A thermocouple temperature monitor was inserted into the winding and fixed with araldite.

b) The motor was run up to its operating speed and put under increasing loads (supply volts being raised to maintain constant speed) until the temperature of the coil monitored by the thermocouple wire was constant and approximately equal to the temperature limit. The motor was kept running for a while to ensure temperature stability and the operating conditions and other quantities then recorded.

c) The motor was next switched off and the winding resistance quickly measured by means of a change over switch and a measuring circuit (DC V,I method).

d) The mean temperature rise Δt rise was then calculated from the value of the hot resistance R_2 and the resistance at ambient temperature R_1 from:

$$\Delta t \text{ rise} = \frac{1}{\alpha} \left(\frac{R_2}{R_1} - 1 \right) \qquad (5.4.1)$$

where α is the temperature coefficient (0.00393 $/^{\circ}C$ for copper). (It is well known that the mean temperature rise calculated from the winding gives no information about hot spots, but the mean temperature rise is the figure universally regarded (in small and integral KW motor work) as limiting power ratings.)

A sequence of load adjustments and winding resistance measurements should then have been made on each motor until stable operation at $95^{\circ}C$ rise (by resistance) was achieved. Unfortunately this was not done, partly

due to lack of time and the thermocouple (spot) temperature was used as the basis for fixing the load. However only in the case of the form 1 motor did this lead to appreciable error, the temperature rises by resistance being 110, 100, 89 and 94°C for the form 1 No.1, form 1 No.2, form 2 and form 3 motors respectively.

The performances at the temperature limit of the four motors are shown in Table 5.7 and 5.8. Column 5 refers to the mean coil current in the main winding only. Unfortunately the power input to the form 1 No.1 motor (power input to the main coil minus the power returned from the pull-down coil) was not recorded in the test and hence the efficiency of the motor (in Table 5.8 column 17) was not calculable. In Table 5.8 the friction and windage power losses were calculated from the results of the retardation test in Section 5.3.4.5 and the copper losses were calculated from the measured r.m.s. currents and the hot resistance of the windings. The friction and windage power losses were added to the measured output powers to give the gross power and the efficiencies of the motors. The overall efficiencies were based on the gross output power figures. A power loss separation was not possible for the form 1 No.1 and form 1 No.2 motors due to an insufficient number of measurements and the total power losses are hence given as shown. The maximum gross power can be seen to be 137 W at a motor efficiency of 57 % for the form 3 motor. These are considered to be good figures given the motor's size

Table 5.7 Test results

	1	2	3	4	5	6	7	8	9
Motor	T_{rise}	speed	Vd.c. rail	I d.c. rail	I coil mean	P d.c. rail	P in motor	T out	T f+w
	^{o}C	rev/min	V	A	A	W	W	mN-m	mN-m
Form 1 No.1 (bifilar)	110	12000	70.0	3.10	4.45 ①	224	N.R. ②	52.7	7.6
Form 1 No.2 (single coil)	100	12000	118.0	2.25	5.00	268	228	62.15	11.6
Form 2 (single coil)	89	15000	83.0	1.0	1.27 ①	78	75	9.41	13.6
Form 3 (single coil)	94	12000	105.0	2.85	6.30	300	240	99.8	9.24

Note ① Main coil only ② No record

Table 5.8 Test results

	10	11	12	13	14	15	16	17	18
Motor	speed	P_{out}	P_{f+W}	P_d	P_{cu}	P_{iron}	P_{inv}	Eff motor	Eff overall
	rev/min	W	W	W	W	W	W	%	%
Form 1 No.1 (bifilar)	12000	66.22	9.55	75.77	148.23 ③			④ N.A.	33.8
Form 1 No.2 (single coil)	12000	78.09	14.57	92.67	135.33 ⑤		40.0	40.64	34.57
Form 2 (bifilar)	15000	14.78	21.36	36.14	27.19	11.66	3.0	48.18	46.33
Form 3 (single coil)	12000	125.4	11.6	137.0	45.53	57.45	60.0	57.08	45.60

Note ③ $P_{cu} + P_{iron} + P_{inv}$ ④ Not applicable ⑤ $P_{cu} + P_{iron}$

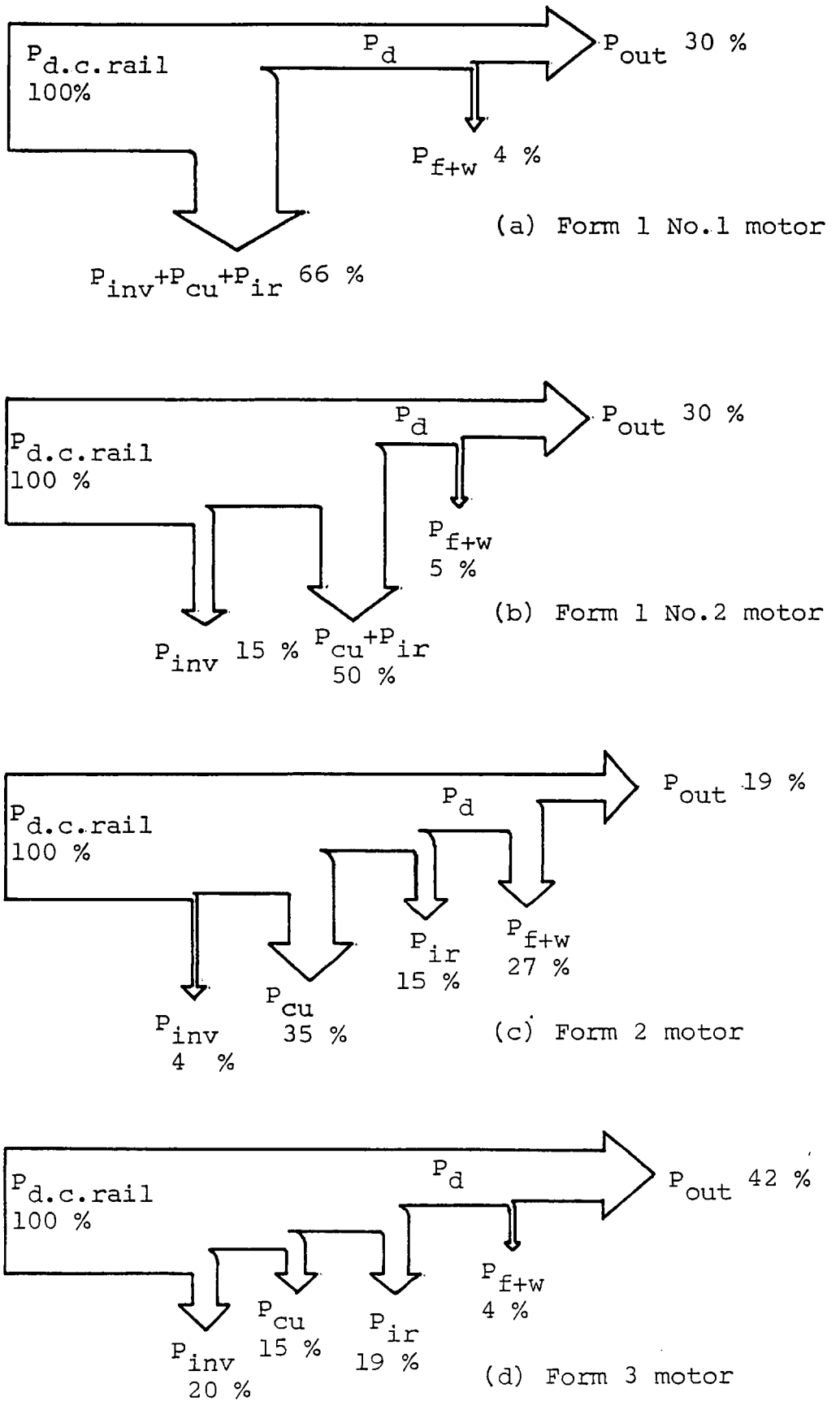

Fig. 5.4.1 Power distribution diagrams at temperature limit

and the fact that it was the first experimental unit of an unusual configuration to be constructed.

The power distribution diagram for each motor is shown in Fig. 5.4.1 in percentage of d.c. rail power input. The inverter power losses plus the motor's copper and iron losses can be seen to be roughly the same for all motors at approximately 55 % to 66 % of input power. The friction and windage loss in the form 2 motor was high because of its small size relative to the dynamometer disc used in the torque measurements. For other motors it was approximately 5 %. Copper losses can be seen to be the biggest component in the form 2 motor even at 15000 rev/min due to the high number of turns of fine wires used in the winding and it would hence be beneficial to operate the form 2 motor at higher speeds. The power losses in the inverter can be seen to be proportional to the coil current over the ranges examined, but a faster rate of increase would have occured had peaky current waveforms been present.

5.4.2 Discussion

Assessments can now be made about the relative merits of the drive systems investigated in terms of a number of performance criteria. It should be emphasised that authoritative judgements are not really possible without specific applications in mind and certainly not when the evidence is based on test results from non-

optimal-designed motors of differing size. However some general discussion is possible and is felt to be worthwhile.

Table 5.9 gives details of the physical structures of the motors. Some comments are necessary about the data:

a) The dimensions given in column 1 refer to the active parts of the motor and exclude the end plates and bearing housings (see note (1)). The overall volumes are given in column 2. Column 3 presents normalised volumes with respect to the form 1 No.1 motor. The significantly smaller overall volume of the form 2 motor can be observed.

b) The 'active rotor volumes' were calculated using $\frac{\pi}{4} D^2L$. The 'salient rotor volume' is the actual volume of metal in the salient rotor. (column 6 and 7)

c) The 'active rotor ratios' are based on the form 1 No.1 rotor and for the form 2 and form 3 rotors it can be seen that the active rotor volume is only half of the form 1.

d) The rotor inertias were calculated from the geometry of the rotor and an assumed density figure.

e) Column 11 gives only weight of the active portion of the motors.

The performance of the motors at the temperature limit are given in Table 5.10. The main conclusions

Table 5.9 Physical structure

Motor	1 ① dimensions active	2 overall vol. axbxc	3 ② overall vol. ratio	4 airgap length	5 active rotor length	6 active rotor $\frac{\pi}{4}D^2L$	7 ④ active rotor salient	8 ⑤ active rotor ratio	9 ⑥ act.rot ove.vol	10 ⑦ rotor inertia	11 ⑧ total weight
	mm^3	cm^3	p.u.	mm	mm	cm^3	cm^3	p.u.	p.u.	10^{-7} kg-m^2	kg
Form 1 No.1 bifilar	63.5 x 63.5 x 60.0	241.9	1	0.43	38.1	28.3	23.16	1	0.117	181.6	1.20
Form 1 No.2 single coil	63.5 x 63.5 x 60.0	241.9	1	0.43	38.1	28.3	23.16	1	0.117	181.6	1.20
Form 2 bifilar	59.0 x 59.0 x 46.0	160.1	0.66	0.52	25.4	14.65	11.98	0.51	0.091	70.2	0.53
Form 3 single coil	88.9 x 69.8 x 36.5	226.8	0.94	0.43	19.0 ③	14.34	11.73	0.50	0.063	181.6	0.79

Note ①

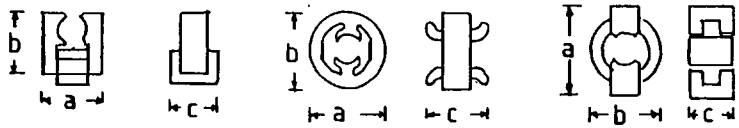

② base on form 1 ③ 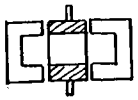 active rotor ④ 

⑤ base on form 1 ⑥ $\frac{\text{column 6}}{\text{column 2}}$ ⑦ calculated ⑧ stator+rotor+coil only

Table 5.10 Performance near temperature limit

	1	2	3	4	5 ②	6	7	8	9
Motor	gross power P_d	Eff motor	Eff overall	peak VA	energy density	P_d/ weight	P_d/ overall volume	$P_d/\hat{\psi}\hat{i}$ ③	P_d/ peak VA
	W	%	%	KVA	KJ/m^3	W/kg	MW/m^3	W/Wb-t-A	%
Form 1 No.1 bifilar	75.77	N.A. ①	33.80	1.05	1.64	63.14	0.31	56.64	7.21
Form 1 No.2 single coil	92.67	40.64	34.57	1.77	2.01	77.22	0.38	46.80	5.23
Form 2 bifilar	36.14	48.18	46.33	0.29	1.23	67.55	0.23	168.09	12.09
Form 3 single coil	137.0	57.08	45.60	1.57	5.97	173.4	0.60	137.20	8.69

Note ① Not applicable ② See text ③ See Table 5.11

can be outlined as follows:

a) Power output.

The bifilar-wound pull-down winding used in the form 1 No.1 and form 2 motors enables only one main transistor to be used in the drive circuit but some disadvantages occur as far as the motor is concerned. Winding space for the main coil will be reduced so the motor rating is adversely affected. The low output power of the form 2 motor is also due to its small size in comparison with the others.

b) Efficiency.

For the form 2 and form 3 motors where saturation levels were low and hence where the ratios of peak/mean coil current were correspondingly low, high efficiencies were achieved both for motor and system.

c) Energy density.

Some comparison between motors of different sizes and speeds can be made by considering a parameter which is largely independent of the size and speed. One such parameter can be termed the "energy density" C which can be defined as

$$C = \frac{\text{Power output}}{D^2L \times \text{operating speed}} \qquad (5.4.2)$$

where D^2L is the rotor active volume. This is closely related to the 'output coefficient'. The term energy density is somewhat more explanatory and is justified by the units of C which are N-m per m^3 or Joules per m^3.

C can be defined in terms of the specific mean magnetic and electric loadings B and J since

$$\tau = F \frac{D}{2}$$

$$\tau = BJ(\pi DL)\frac{D}{2}$$

Hence
$$P_{out} = BJ(\pi DL)(\frac{D}{2})\omega \qquad (5.4.3)$$

$$= (\frac{\pi}{2} BJ)(D^2L\omega)$$

where ω is the operating speed in rad/sec

Hence
$$C = \frac{P_{out}}{D^2L\omega} = \frac{\pi}{2} BJ \qquad (5.4.4)$$

Hence for conventional motors, C, in effect will indicate the electrical and magnetic loadings in the machines.

For a doubly-salient switched reluctance motor, the relation between the gross output power and the machine parameters is somewhat less direct than in the conventional motor due to its goemetry and the process of torque production. However, a simplified relation can be derived in general form similar to the one associated with conventional motors as follows:

Fig. 5.4.3 shows the basic doubly-salient

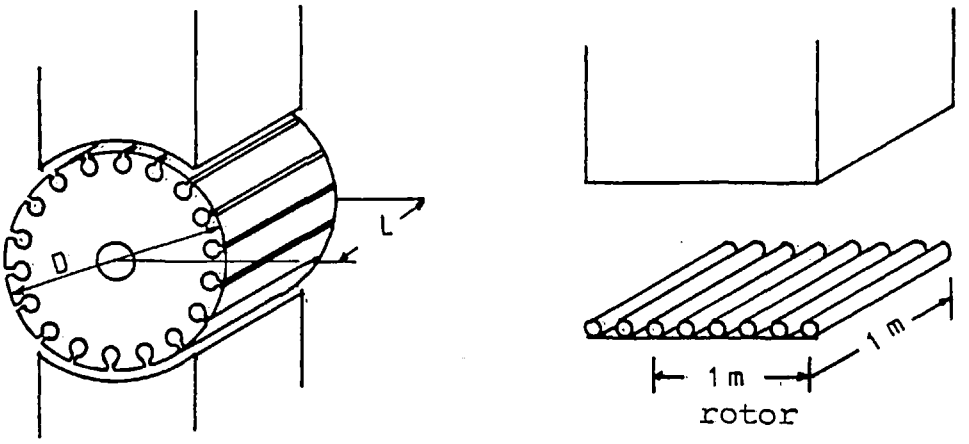

(a) Simplified diagram of a conventional machine

(b) Developed view

Fig. 5.4.2 The output power of a conventional machine can be calculated from the interaction between the current in the rotor and the flux set up by the stator

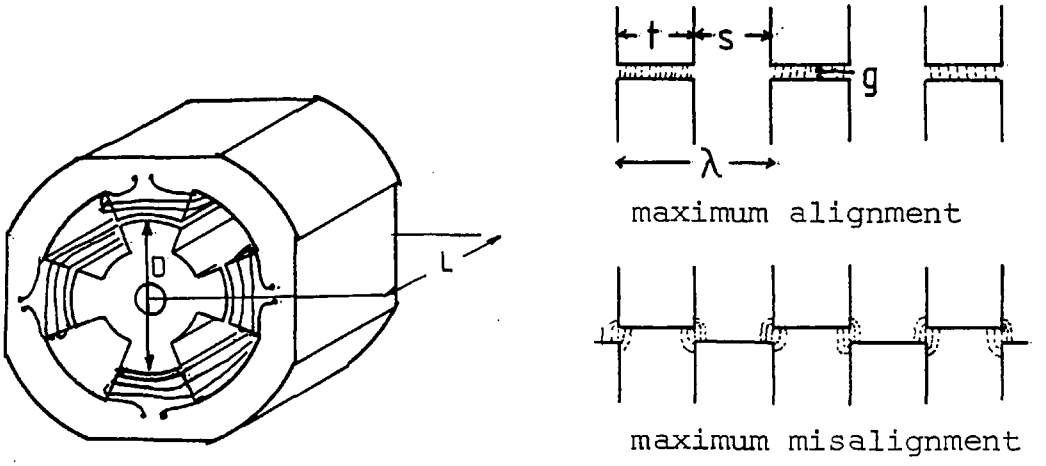

(a) Basic SR motor

(b) Developed view

Fig. 5.4.3 The SR motor has no conductor work on the rotor and the power output is proportional to the changes in the energy stored in the airgap

switched reluctance motor and a developed view. The machine diameter at the extremity of the teeth is 'D', the core length is 'L' and the airgap length is 'g'. The machine is assumed to have identical rotor and stator saliencies with a tooth width 't' to tooth pitch 'λ' ratio equal to 'γ' and number of saliencies equal to 'p'. The m.m.f. 'F' per gap is exerted across each set of rotor and stator teeth. P_1 is the permeance per gap at the maximum alignment position (assumed no fringing) and P_2 is the permeance per gap at misalignment position.

If it is assumed that the iron does not saturate, the power developed 'P_d' can be written in terms of the change in stored energy between the maximum misalignment and maximum alignment positions '$E_c.p$' and the switching frequency 'f', as

$$P_d = E_c.p.f \qquad (5.4.5)$$

where E_c is the change in stored magnetic energy/gap/switching cycle
p is the number of saliencies (gap)
f is the switching frequency in Hz

If E_1 is the energy stored per gap at maximum alignment and E_2 is the energy stored per gap at maximum misalignment then E_c can be written as

$$E_c = E_1 - E_2 \qquad (5.4.6)$$

Hence

$$E_c = \frac{1}{2} F^2 P_1 \left(1 - \frac{P_2}{P_1} \right) \qquad (5.4.7)$$

If a uniform flux density at the maximum alignment position 'B_1' is assumed in each airgap cross-section 'A_1' (i.e. B_1 is the flux density/gap), then

$$B_1 = \frac{FP_1}{A_1}$$

and so

$$F = \frac{B_1 A_1}{P_1} \qquad (5.4.8)$$

substituting eq(5.4.8) into (5.4.7) yields

$$E_c = \frac{1}{2} \frac{B_1^2 A_1^2}{P_1} \left(1 - \frac{P_2}{P_1} \right) \qquad (5.4.9)$$

With the assumption of negligible fringing flux, P_1 can be expressed in terms of gap geometry as

$$P_1 = \frac{\mu_o A_1}{g} \qquad (5.4.10)$$

Substituting (5.4.10) into (5.4.9), yields

$$E_c = \frac{1}{2\mu_o} B_1^2 A_1 g \left(1 - \frac{P_2}{P_1} \right) \qquad (5.4.11)$$

The switching frequency f is related to the rotor speed ω_r in rad/sec as

$$f = p \frac{\omega_r}{2\pi} \qquad (5.4.12)$$

So the developed power P_d in(5.4.5) becomes

$$P_d = \frac{1}{4\pi} \frac{B_1^2}{\mu_o} A_1 g \left(1 - \frac{P_2}{P_1} \right) p.p \omega_r \qquad (5.4.13)$$

The factor $(A_1 g\ p)$ which is the total airgap volume can be expressed in terms of the ratio of tooth width/ tooth pitch γ and the approximated rotor peripheral annular volume πDLg as

$$A_1 g\ p = \gamma \pi DLg \qquad (5.4.14)$$

Substituting into (5.4.13) yields

$$P_d = \frac{1}{4} \frac{B_1^2}{\mu_o} \gamma g\ D\ L\left(1 - \frac{P_2}{P_1}\right) p\ \omega_r \qquad (5.4.15)$$

The flux density per gap B_1 can also be expressed as

$$B_1 = \mu_o \frac{F}{g}$$

or

$$B_1 = \mu_o \frac{NI}{pg} \qquad (5.4.16)$$

where NI is the total m.m.f. , and if J is defined as the mean surface current density in A-T/m at the airgap diameter then

$$J = \frac{NI}{\pi D} \qquad (5.4.17)$$

and the flux density B_1 can be expressed in terms of J as

$$B_1 = \mu_o \frac{J \pi D}{pg} \qquad (5.4.18)$$

Hence P_d in eq(5.4.15) becomes

$$P_d = \frac{\pi}{4} (B_1 J)(D^2 L)\ \gamma \left(1 - \frac{P_2}{P_1}\right) \omega_r \qquad (5.4.19)$$

For a homopolar switched reluctance motor where the homopolar m.m.f. acts across all the gaps at the same time as shown in Fig. 5.1.5, the expression for the output power can be written (subject to the assumption of the previously stated) as

$$P_d = \frac{\pi}{4}(JB_d)(D^2L)\,\gamma\,\left(1 - \frac{P_2}{P_1}\right)(p\,\omega_r) \qquad (5.4.20)$$

with all parameters as previously defined except that in this case

$$B_d = \frac{\text{total airgap flux}}{\text{total airgap cross section}}$$

The expressions for C show that whether the motor is homopolar or heteropolar, geometrically similar motors having equal magnetic and electrical loadings and gap flux densities at aligned and misaligned positions, will be proportional to operating speed and the motor's D^2L or rotor volume.

The energy density as defined by gross output/ $D^2L\omega_r$ for each motor is shown in column 5 of the Table 5.10 in KJ/m^3. The form 3 motor which developed the highest output power for quite a small active rotor volume (comparable to that of the form 2 motor and only half that of the form 1 motor) gives the highest energy density: 5.97 KJ/m^3.

d) Power/size

The energy density normally gives a strong indication of the power/overall size of the motor because for conventional motors the total volume of the motor is proportional to the volume enclosed by the airgap surface. However for the unconventional configurations of the form 1 and form 3 motors, the relation is not quite straightforward and another parameter of power/overall volume for each motor is given in column 7. Although the differences between the overall volume levels of the form 3 motor and the other motors are less than the differences between their energy density ratios, the best power/overall size is still shown for the form 3 motor ($6MW/m^3$).

e) Power/weight

The best power/weight (which was considered as the ratio of the gross power to the weight of the motor's active parts) was also achieved by the form 3 motor, perhaps due to the very economical utilization of the iron in the magnetic circuit. However special arrangements for clamping the pole pieces and the excitation coil have to be made in the form 3 motor and these take up extra space and reduce the motor's power/weight advantage over the inherently strong, straightforward, simple but rather bulky form 1 motor. The form 2 motor's relatively low power/weight is probably due to its small size and the totally enclosed nature of its construction. (As its windings are totally enclosed in the motor frame, their

ability to dissipate heat is not as good as with the rather exposed windings of the form 1 and form 3 motors.)

f) Gross power/(peak flux.peak current) ratio.

As shown in chapter 1, the mean torque developed by a SPSR motor operating under cyclic conditions is proportional to the area enclosed by the ψ, i trajectory between the magnetisation characteristics (ψ-i) of the d and q axes. The shape and size of the trajectory depends on the voltage and current waveforms (i.e. voltage fed or current fed), the magnetisation characteristics and the speed.

By comparing the values of the parameter:
mean gross torque/(peak flux $\hat{\psi}$ x peak current $\hat{i}$)
for different motors, an idea of how much the area enclosed by the ψ , i magnetisation curves is enclosed or swept by the trajectory can be formed. For operation at a given speed comparisons of the parameter (gross power / $\hat{\psi}$ $\hat{i}$) are just as revealing and these values are given in column 8.

The products of peak linkage flux ($\hat{\psi}$) and peak current ($\hat{i}$) were derived from the measured magnetisation characteristics at the d and q positions of each motor in Fig. 5.3.26. The assumed magnetisation characteristics at peak currents shown in Fig. 5.4.4 were derived from the characteristics in Fig. 5.3.26 with the following

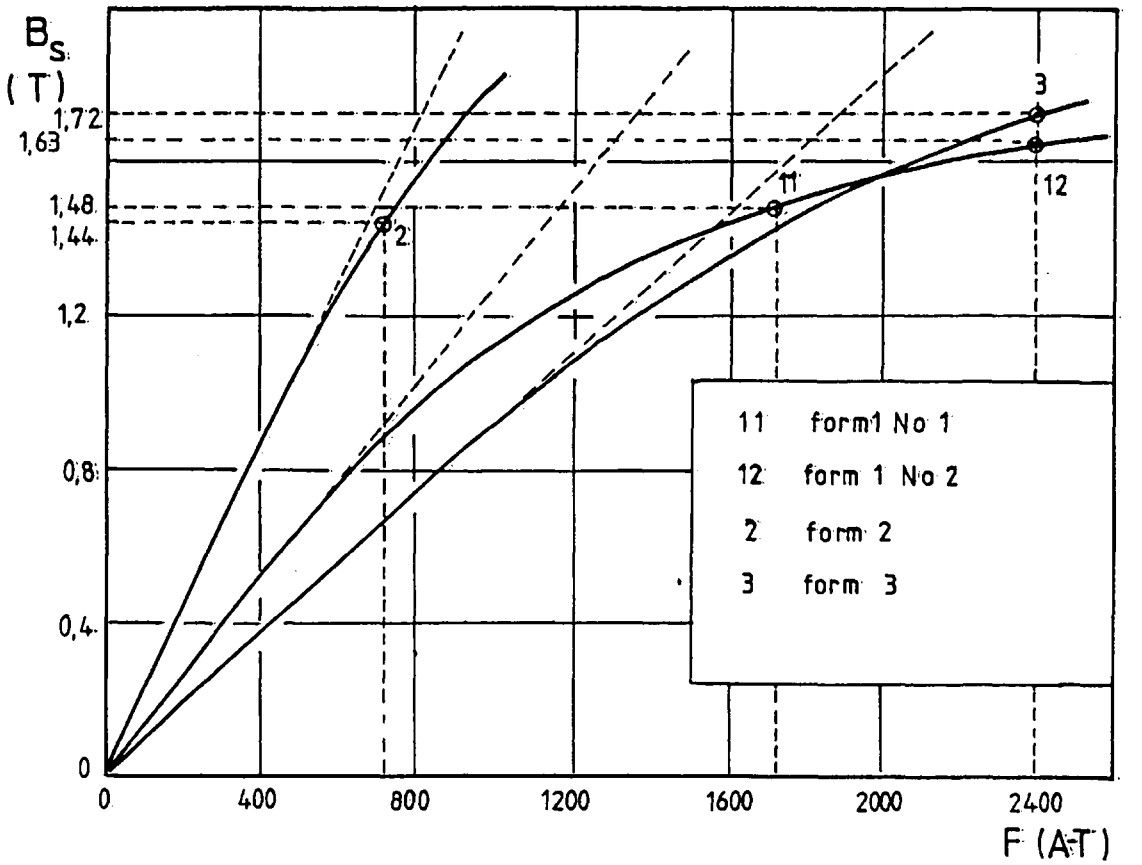

Fig. 5.4.4 Derived magnetising characteristics of the form 1, 2 and 3 motors at peak currents

Table 5.11 Calculation of P_d/peak ψ .peak i

Parameters	Form 1 No.1	Form 1 No.2	Form 2	Form 3
peak i (A)	15.0	15.0	3.6	15.0
N (turns)	115	160	200	160
peak A-T	1725	2400	720	2400
peak B_s (T)	1.48	1.63	1.44	1.72
A_{siron} (m^2)	5.06×10^{-4}	5.06×10^{-4}	2.08×10^{-4}	2.42×10^{-4}
peak ψ (Wb-t) ($\hat{B}_s A_{siron} N$)	0.0861	0.132	0.0598	0.0665
$\hat{\psi}\ \hat{i}$ (Wb-t-A)	1.292	1.98	0.215	0.998
P_d (W)	75.77	92.67	36.14	137.0
$P_d/\hat{\psi}\ \hat{i}$ (W/Wb-t-A)	56.64	46.80	168.09	137.2

assumptions: a) the peak current occurred when the rotor was halfway between the d and q positions (this is true for the form 1 and form 3 motors as shown in Fig. 5.3.35 and 5.3.38) since peak current occurs just before the switching off instant for $\beta = 90^{o}$elec, b) the airgap line slope varies linearly with rotor angle between the d and q positions and c) the saturation factor at peak current is the same as that with the rotor in the d position (Table 5.6). From the assumptions above, the airgap line at peak current was obtained by linear interpolation of the airgap lines at the d and q positions, and the saturation factor (Table 5.6) was calculated at 1.6 T to determine the saturation curve for each motor.

Table 5.11 shows the steps in calculating the peak $\hat{\psi}$ and peak $\hat{i}$ in which:

1) the peak A-T was calculated from the peak current,

2) the peak flux density $\hat{B}_s$ (in the smallest iron section) was then obtained from the saturation curve,

3) and by multiplying $\hat{B}_s$ with the smallest cross-section of the magnetic circuit (A_{siron}) and N (turns) the peak flux linkage $\hat{\psi}$ was obtained.

For this case, it can be seen that the highest value of $P_d/\hat{\psi}\,\hat{i}$ was achieved by the form 2 motor. This developed the smallest output but because it operated at the lowest flux density and also with little saturation,

gave the highest ratio of $P_d / \hat{\psi}\hat{i}$. The ratios are rather low for the form 1 motors and because of saturation and its effect on $\hat{i}$, very little is gained from pushing the A-T up as shown for the form 1 No.1 and form 1 No.2 cases.

g) Power/peak VA

The cost of the switching unit depends greatly on the peak voltage and peak current that the output devices must be able to withstand, and it is hence interesting to see how good the SR motor system is in comparison with other drive schemes involving a variable frequency solid state supply. The ratio of P_d/peak VA for each tested SPSR motor is given in column 9 . The form 2 motor which operates with the lowest saturation factor gave the best ratio of P_d/peak VA (12 %). The figures for the other motors were 8 % with the form 3 and 7 % and 5 % for thr form 1 No.1 and No.2 motors respectively. The P_d/peak VA figure seems to be adversely affected by saturation (as with the form 1 motor).

A P_d/ peak VA figure was derived for a standard inverter supplied 1 phase induction motor as follows:

Fig. 5.4.5 shows a standard inverter drive induction motor scheme. For 1 phase operation, the motor voltage waveform and the voltage across a transistor are as shown in (c). If the induction motor is assumed to operate at a power factor of 0.8 and an efficiency of

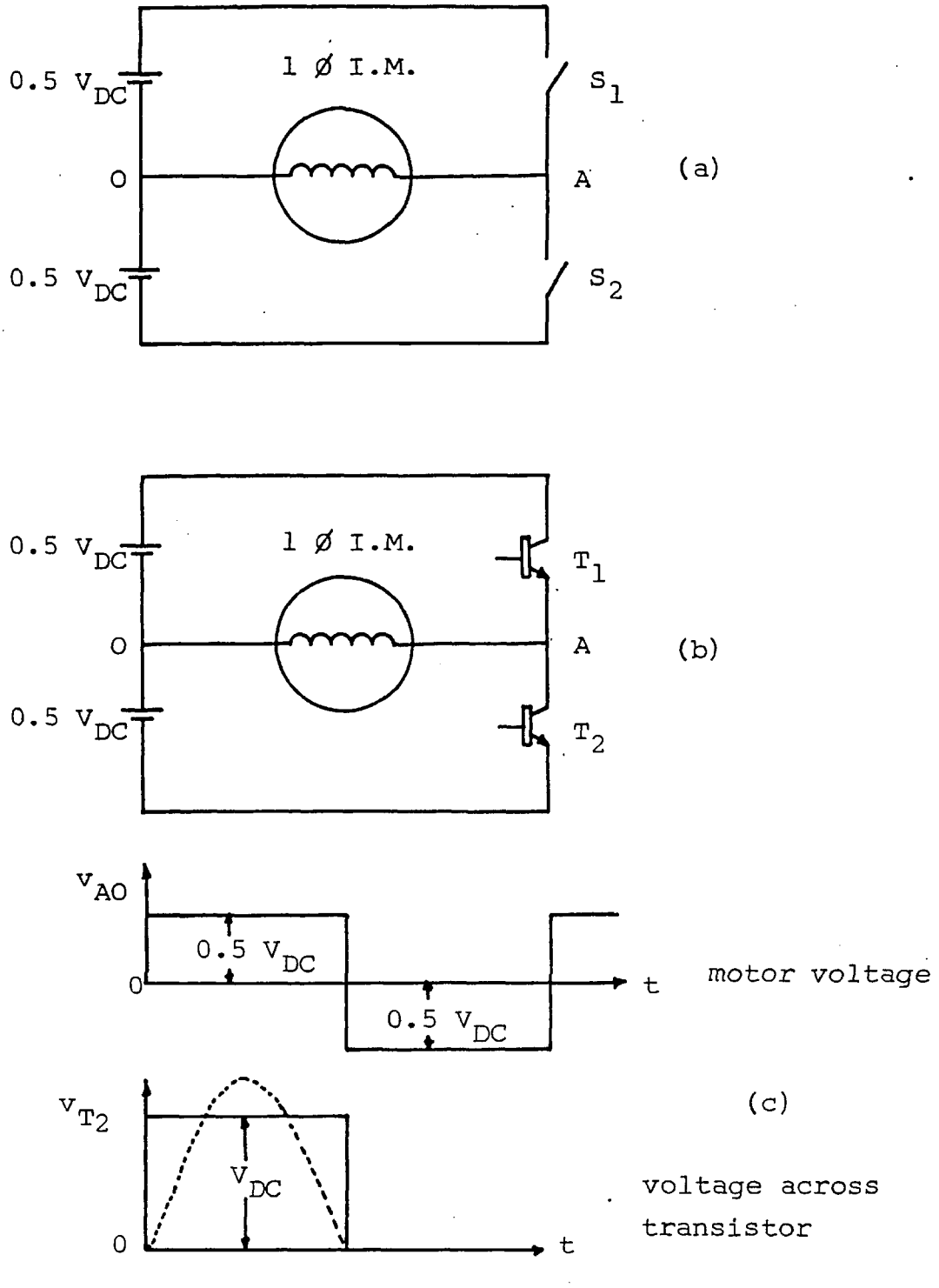

Fig. 5.4.5 A standard inverter supplied single-phase induction motor system
(a) Simplified diagram
(b) Circuit configuration
(c) Ideal voltage waveforms

60 % (typical values for small motors), the power input of the motor is

$$P_{in} = V_{ph} I_{ph} \cos \phi \qquad (5.4.21)$$

Hence $$P_{out} = 0.48 V_{ph} I_{ph} \qquad (5.4.22)$$

The peak voltage that the transistor has to withstand is shown in Fig. 5.4.5(c), hence the peak transistor voltage

$$\hat{V}_T = V_{DC} \qquad (5.4.23)$$

where $\hat{V}_T$ = peak transistor voltage
and the peak transistor current is

$$\hat{I}_T = I_{DC} \qquad (5.4.24)$$

(assuming square wave current).

To simplify the derivation, the sine form factor is assumed and the ratio of peak to r.m.s. value of the voltage and current is taken as $\sqrt{2}$, which gives

$$\begin{aligned} V_{ph} &= \frac{V_{DC}}{2} \frac{4}{\pi} \frac{1}{\sqrt{2}} \\ I_{ph} &= I_{DC} \frac{4}{\pi} \frac{1}{\sqrt{2}} \end{aligned} \qquad (5.4.25)$$

Substituting eq.(5.4.25) into eqs. (5.4.23) and (5.4.24) gives

$$\begin{aligned} \hat{V}_T &= 2\sqrt{2} \frac{\pi}{4} V_{ph} \\ \hat{I}_T &= \sqrt{2} \frac{\pi}{4} I_{ph} \end{aligned} \qquad (5.4.26)$$

So the ratio of $P_{out} / \hat{V}_T \hat{I}_T$ or $P_d /$ peak VA is

$$\frac{P_{out}}{\hat{V}_T \hat{I}_T} = \frac{0.48\ V_{ph} I_{ph}}{2\sqrt{2}.\sqrt{2}\ V_{ph} I_{ph} (\frac{\pi}{4})^2} \times 100\ \%$$

$$= 19.45\ \%$$

It can be seen that, the 12 % achieved by the form 2 SPSR motor scheme is not too bad compared with the inverter driven induction motor scheme of similar power and size.

For all round performance, the form 3 motor came out as the best in terms of efficiency, energy density, power/weight and power per volume. Although it came second best in the last two categories of $P_d/\hat{\psi}\hat{i}$ and P_d/peak VA, it was not very far behind the form 2 motor and when its other merits are considered this would be acceptable. Some comparisons between the specific outputs of the experimental SPSR motors and some conventional, commercially available motors are given in Table 5.12 for interest.

5.5 Conclusions

The performance of two-pole motors with an a.c. triac-fed circuit and with d.c. link transistor-fed circuits have been presented. For medium speeds (3000 rev/min), the simple low-cost a.c. triac-fed can be used as a fixed-or variable-speed drive for certain type of loads. Efficiency is comparable with or better than a

Table 5.12 Comparison of the specific output values of the experimental SPSR motors with the commercially available conventional motors

	1	2	3	4	5	6 ①	
Motor type and make	output KW	speed rev/min	output W/kg	output W/litre	output T/wt Nm/kg	output T/vol. $Nm/_{m^3}$	Remarks
3 Ø squirrel cage 50Hz ind. mot. NECO TEFC RB frame (5.9)	3.73	1425	74	208	0.5	6440	Standard, commercially available machine. Data relates to continuous rating. Examples chosen are all 'small', somewhat larger specific values would be obtained for larger sizes or higher temperature insulated.
D.C. motor drip proof comp. field NECO 78 frame (5.9)	1.5	1400	30	89	0.204	3010	
Universal(a.c./d.c.) motor drip proof NECO frame 5 (5.9)	0.75	8000	40	122	0.048	714	
Exp. SPSR motor Form 1 No.1 bifilar	0.075	12000	63	310	0.050	2100	Specific vaues near temperature limit class E insulation. Note ① output torque/ active rotor volume
Exp. SPSR motor Form 1 No.2 single coil	0.092	12000	77	380	0.061	2600	
Exp. SPSR motor Form 2 bifilar	0.036	15000	67	230	0.043	1570	
Exp. SPSR motor Form 3 single coil	0.137	12000	173	600	0.138	7600	

single phase shaped pole motor of similar size. Supply current harmonics may cause problems, though at this power level this is unlikely (cf. colour T.V. receiver set and light dimmer unit). With the d.c. link feed circuits, extremely high speeds can be achieved with fewer and smaller harmonics. Although the cost of drive circuit is higher its characteristics made it suitable for a wide range of applications. Of the three forms of motor tested the radial/axial flux form 3 motor showed good performance, although, in view of its unusual construction, special consideration would have to be given to assembly and production factors. Full-load efficiencies (hot) up to 57 % were achieved. These are considered to be quite good considering the small size and low cost of the motor.

As far as predictions are concerned, the step by step approach has been proved to be quite accurate in predicting both current waveforms and general characteristics of both the a.c. fed and d.c. link fed schemes in spite of the rather crude assumptions made during the calculating process. The work is considered to form a good base for investigations into more comprehensive prediction methods, factors of particular concern being machine parameter prediction and measurement, and the simulation and prediction of friction, windage and iron losses and of saturation. The simplified analytic method has been proved to be useful for hand calculated estimation of general characteristics in some cases.

CHAPTER 6

SOME DESIGN ASPECTS OF SPSRM DRIVE SYSTEMS

6.1 Introduction

A comprehensive design study is beyond the scope of this thesis but some discussions of the principle design options is possible, partly based on the experience gained and results obtained during the experimental investigations.

In selecting the design of s SPSRM drive system, the followings are the principle choices to be made:

i) magnetic-circuit configuration
   e.g. axial/radial flux path, radial/circumferential flux path and axial/circumferential flux path;
ii) excitation-winding configuration
   e.g. conventional one coil/pole, concentrated ring coil;
iii) rotor configuration
   e.g. conventional disc lamination, axial lamination, flux barrier, etc.;
iv) stator and rotor pole number;
v) number of teeth per pole (castellation);
vi) rotor geometry

e.g. pole arc/pole pitch, airgap width, slot depth slot shape, etc.;

vii) number of winding turns;

viii) feed configuration

e.g. 'a.c.' feed, d.c. link feed, half bridge switching unit, quarter bridge switching unit, etc.;

ix) type of switching devices;

x) choice of control method

e.g. (i) link voltage or current control by mains transformer, SCR phase-angle-controller or chopper

(ii) switching unit control by switching modulation within each on-period or by switching angle control via electronic, mechanical or electromechanical means.

The fixing of the design of a complete system is complicated by the usual factors encountered by system designers, viz: (a) the frequent lack of a clear choice and (b) the frequent tendency of one design decision to affect others. Some of the trends, trade-off and 'pros and cons' under each heading are discussed below and some topics are considered in combination.

6.2 Magnetic-circuit, excitation-winding and rotor configuration

Fig. 6.2.1 shows simplified diagrams of the three basic magnetic-circuit configurations for SPSR motor i.e.: axial/radial flux path (a), conventional radial/circumferential flux path (b1), 'U' core radial/circumferential flux path (b2) and possible axial/circumferential flux path (c), together with the possible configurations of the rotor based on the use of conventional, straight-edge laminations (d), conventional slotted-disc laminations (e), axially stacked laminations (f), flux barrier laminations (g) and 'strip cores' (h) and (i).

According to present manufacturing techniques, the 'U' core radial/circumferential stator (b2) is the cheapest configuration to manufacture, is strong and allows bobbin-coil excitation windings to be used. However, the motor is rather bulky and inductance leakage levels can be high. Hence this configuration might not be suitable for motors of larger power. Although, the test results on this type of motor were marred by high iron losses, it is believed that if somewhat thinner and higher-grade laminations are used, performance can be improved. Motors having more than 2 poles are difficult to make with this form of stator.

For the conventional radial/circumferential

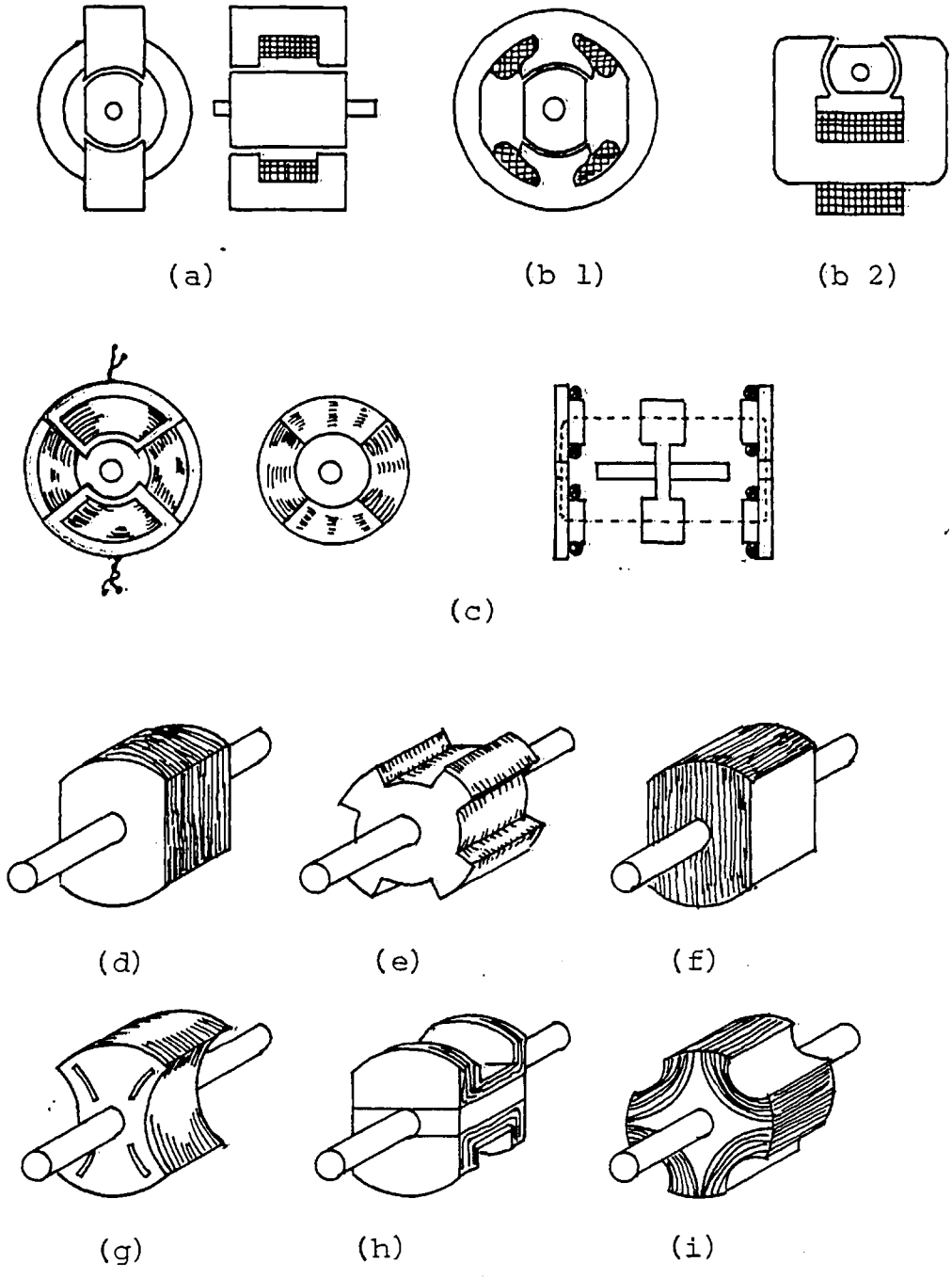

Fig. 6.2.1 Three basic magnetic-circuit configurations for SPSR motor (a, b1&b2, c) and possible configurations for rotor (d, e, f, g, h and i)

stator (b1), the lamination can be manufactured cheaply (stamping) but winding assembly is more difficult and its heat dissipation properties are unlikely to be as good as with options (b2) or (a) with their exposed windings. Leakage inductance levels can be expected to be lower, particularly for larger power motors. There is no restriction on pole number and the configuration may therefore be more suitable for larger power motors.

Both radial/circumferential configurations (b1 and b2) allow conventional disc laminations (d), (e) and (g) to be used on the rotor. The rotor is hence inherently cheap and strong, and this is considered to be a distinct advantage of this configuration.

The stator and rotor of the radial/axial flux configuration (a) are rather more difficult to manufacture. The use of strip cores can help here though means of holding these can add to costs. The possibilities for productionising this form of stator still need to be thought about and assessed. A strip core (h and i) or axially laminated (f) type of rotor must be used with this configuration. With the axially laminated rotor, there are problems in holding the laminations together and the inevitable rotor turning operation causes surface short-circuits which increase iron losses. However the radial/axial configuration enables the single concentrated ring coil type of excitation system to be used with its advantages of low winding

cost and also good heat dissipation. Experimental results from the prototype of the form 3 motor suggests that the configuration can give a motor that is relatively light and one which possesses relatively (and surprisingly) low levels of leakage. These advantages are believed to hold up to moderate sizes, but strip core costs might be a problem particularly in larger sized-motor.

The author has no experience with the axial/circumferential configuration (c) but it is believed that some of manufacturing techniques used for the disc pump[6.1] are applicable and could make it possible to build this type of motor at moderate cost.

Rotor configuration, choice is of course heavily constrained by the stator type adopted. A number of points are worth putting on record:

1) of the rotor using disc laminations, the slotted rotor is better in terms of minimising q axis zig-zag leakage with its adverse effect on L_q;

2) for radial/axial flux path, the axially laminated rotor can in practice only be made with 2 saliencies (f). If more than a 2 pole rotor is needed, a wound strip core has to be used;

3) the flux barrier type of rotor(g) is worthy of further exploration for SPSRMs since L_d/L_q ratio and output torque levels are likely to be improved.

Solid iron magnetic circuits are only worth considering for applications involving low switching frequencies (low speed and low number of poles). The choice between internal rotor or external rotor configuration depends primarily on application factors. The external rotor configuration may be a convenient one mechanically for some applications (e.g. ceiling fan, axial flow ducted fan) and inherently high rotor inertia might be desirable in others (e.g. gyro and gramophone turntable drives). The winding on the internal stator can be easier to wind but winding area might be less and heat dissipation poorer.

It should be noted that the build up of unbalanced magnetic pull (UMP) with rotor eccentricity is likely to be larger in radial/axial motors (pole fluxes in parallel) than in radial/circumferential motors (poles magnetically in series) where UMP is essentially caused by leakage flux only.

6.3 Stator number of poles and castellation

Equations (5.4.19) and (5.4.20) for output power are:

for the heteropolar SPSRM:

$$P_d = \frac{\pi}{4} (B_1 J)(D^2 L) \gamma \left(1 - \frac{P_2}{P_1} \right) \omega_r \qquad (6.3.1)$$

for the homopolar SPSRM:

$$P_d = \frac{\pi}{4} (B_d J)(D^2 L) \gamma \left(1 - \frac{P_2}{P_1} \right) p \omega_r \qquad (6.3.2)$$

Hence for the heteropolar motor, and given the assumptions implicit in equation (5.4.19). there is no power gain to be had by increasing the number of poles 'p! If the number of poles 'p' is increased, either the A-T/pole ($\frac{J\pi D}{p}$) has to be increased or the gap length 'g' decreased to keep the flux per pole (B_1) fixed. However no power is gained from doing so and the operating frequency 'f' has to be increased with the number of poles to keep the speed constant. This leads to higher iron and switching losses. An overiding consideration with large motors (perhaps not relevant with SRMs of the SP type) is that saturation is difficult to avoid with the large A-T per pole inevitable with the large pole pitches that occur with small pole numbers and the choice of a high pole number may be desirable particularly if the operating speed is not necessary high.

Output power increases can be gained by castellation of the poles in homopolar and heteropolar motors as indicated by eq.(6.3.2) (where p = teeth per pole) but this is done at the cost of an increased operating frequency and for many variable speed drives where no particular angular resolution needs occur, the arguments for and against castellation may be finally balanced. Heavy castellation leads to fringing and leakage effects becoming dominant and to levels of P_1/P_2 ratio and output torque seriously lower than predicted using simple methods. As is the case with high speed, multi-phase stepper motor

operation, high speed running of castellated SPSRMs, would tend to require the use of special drive circuit techniques if current waveforms and torques are not to suffer unduly.

6.4 Ratio of stator pole number to rotor pole number

In the case of SPSR motor (both heteropolar and homopolar motors) where all the coils are excited simultaneously, maximum torque occurs when all the alignment forces in the gaps are in the same direction. In general, the use of unequal stator and rotor pole numbers (e.g. $N_s/N_r = \frac{2}{3}, \frac{4}{6}, \frac{3}{4}$ etc.), is not reckoned to be viable due to the large backward torques or torque 'gaps' that will occur (depending on the excitation arrangement tried). Although this remark does not apply to the special case of 2n:1 and 1:2n ratios of stator and rotor pole numbers, torque per size and speed are reduced and output power doubly affected. For polyphase SRMs, this topic is discussed in Ref. 6.2.

6.5 Ratio of stator pole width to rotor pole width

A diagrammatic description of possible values for stator and rotor pole arcs (reproduced from Ref. 6.2) is shown in Fig. 6.5.1 where θ_s is the stator pole arc and θ_r is the rotor pole arc. θ_{smax} is equal to stator pole pitch. As far as the variation of inductance with rotor position is concerned, there will be a point in the lower

triangle XWZ which gives the same inductance profile as given by a point in the upper half triangle XYW. But values of θ_s and θ_r in the lower half triangle ZWX are preferred since the stator has to carry the excitation winding and it is hence more practical to have a smaller pole arc on the stator. Fig. 6.5.2 shows the inductance profiles corresponding to points X, Z and W in (a), (b) and (c) respectively. Point X where θ_r and θ_s are minimum, and rotor low inertia is low, is not perhaps to be considered as a practical design point since the positive torque production region is short. At point Z where θ_r is maximum and θ_s is minimum, the zero torque production region is long and occurs at the point where the current is high (assuming a square wave voltage to be switched on in the positive torque region or earlier) and this is hence another poor design point. At point W where $\theta_s = \theta_r$ there is no zero torque production region and in order to get a high output torque, the square wave voltage should be switched on at a certain angle prior to q position ('α') and switched off before the rotor reaches d position ('β'). However, negative torques still occur at the rising and falling edges of the current waveform. The ideal inductance profile seems to be of the form of Fig. 6.5.3 where there are small zero torque production zones at minimum and maximum inductance positions (AB and CD). For this case, if the square wave voltage is switched 'on' at A, the current can be built up without negative torque; and if the voltage is switched 'off' at C, the current can reduce to a low value

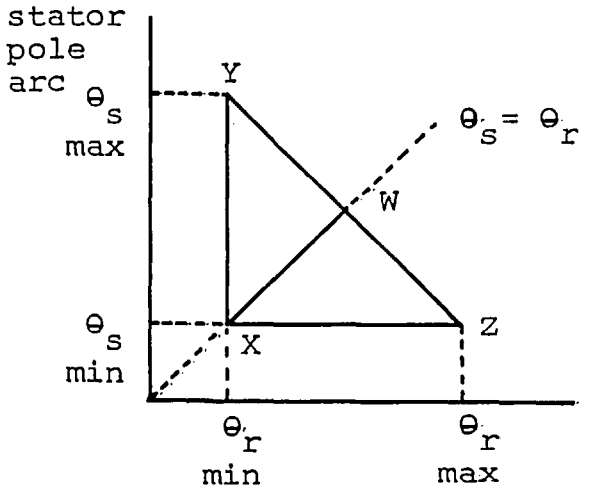

Fig. 6.5.1

Diagramatic description of possible values for stator and rotor pole arcs

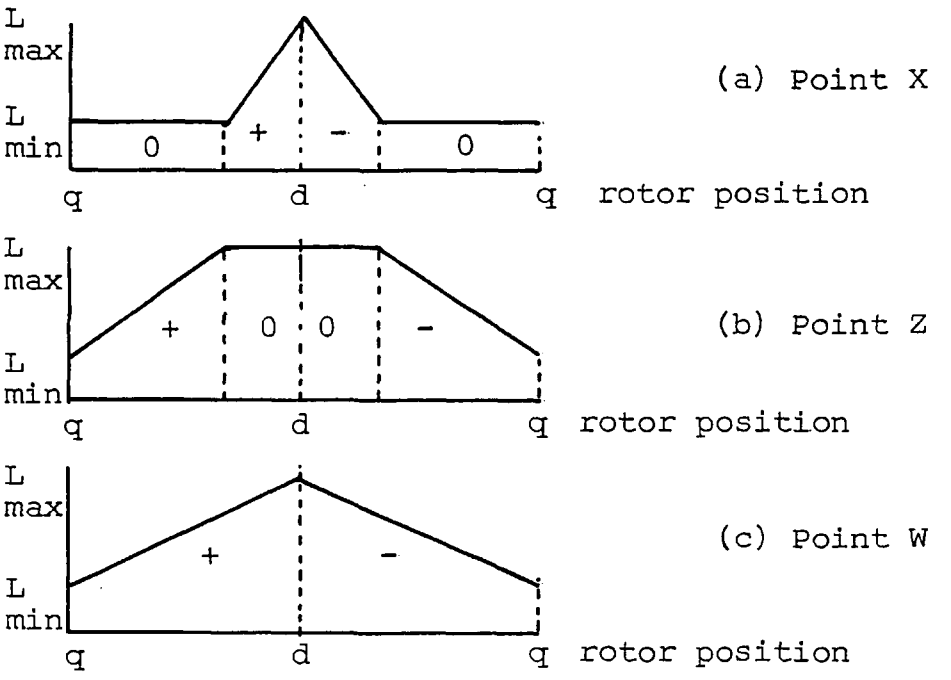

Fig. 6.5.2 Inductance profiles corresponding to the points in the Fig. 6.5.1 diagram: + positive torque production zone, - negative torque production zone and 0 zero torque zone

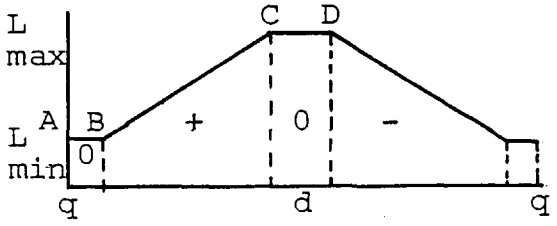

Fig. 6.5.3 Ideal inductance profile for square wave voltage supply ($\theta_s < \theta_r$, pole arc:pole pitch < 0.5)

by D and hence negative torque caused by the 'carry-over' current in the negative torque production region is kept low. This implies $\theta_s < \theta_r$ and the ratio of pole arc to pole pitch is less than 0.5.

6.6 Airgap length, slot, gap geometry

The effect of gap geometry on the static output torques of doubly salient reluctance machines has been widely investigated in connection with the stepper motors. [6.3,6.4,6.5] Ref. 6.5 in particular shows the variation of the permeance for aligned teeth 'P_1' and for symmetrically misaligned teeth 'P_2' with slot geometry ratios $\frac{t}{\lambda}$ and $\frac{\lambda}{g}$, where λ = tooth pitch, t = tooth width and g = airgap length. As shown in eqs. (6.3.1) and (6.3.2), the output torque of the SPSRM is proportional to $\gamma\left(1 - \frac{P_2}{P_1}\right)$ where $\gamma = \frac{t}{\lambda}$ and the variation of $\frac{t}{\lambda}\left(1 - \frac{P_2}{P_1}\right)$ (which has been derived from the data given in Ref. 6.5) with slot geometry can be shown in Fig. 6.6.1. It can be seen that due to the effect of fringing and leakage the function $\frac{t}{\lambda}\left(1 - P_2/P_1\right)$ does not vary too much with t/λ (rather flat variation). The values of t/λ for maximum $(t/\lambda)(1 - P_2/P_1)$ varies with λ/g ratio (t/λ = 0.45 for λ/g = 20, t/λ = 0.50 for λ/g = 200) and the smaller the gap the higher the numerical value of the function $(t/\lambda)(1 - P_2/P_1)$. It is assumed throughout that saturation is absent. The optimum t/λ for saturated working of doubly-salient machines is given in Ref. 6.4. It can be concluded that, if the machine is not working

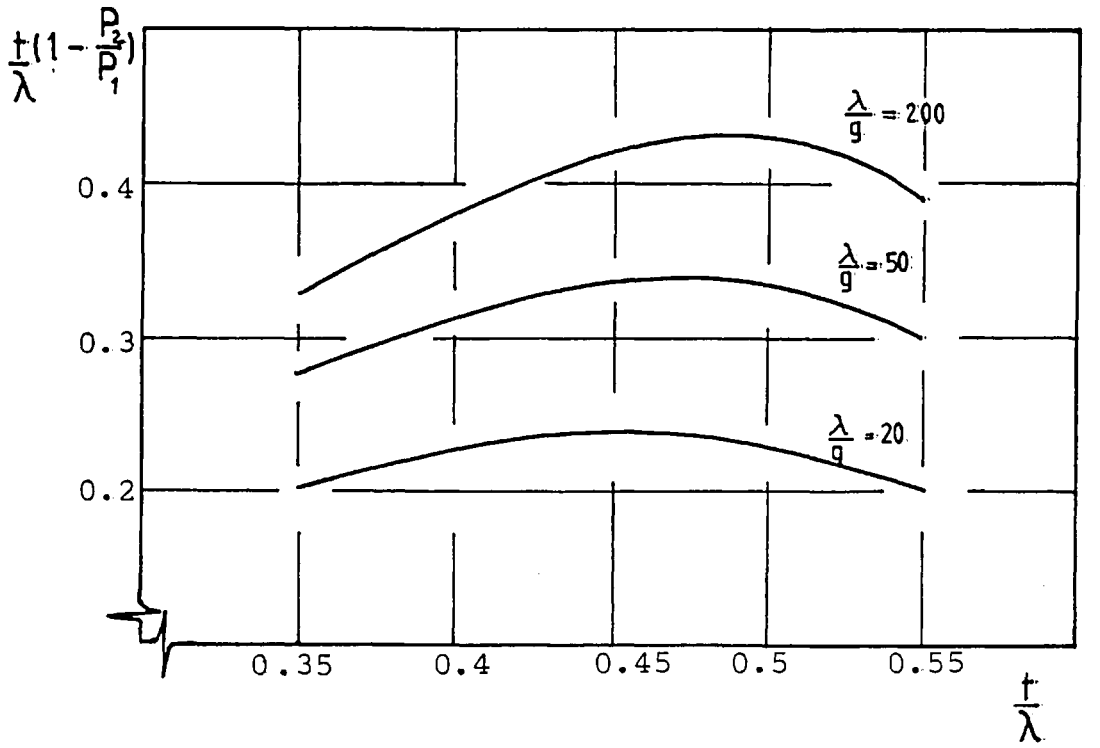

Fig. 6.6.1 Variation of $(t/\lambda)(1 - P_2/P_1)$ with slot geometry (non-saturated case)

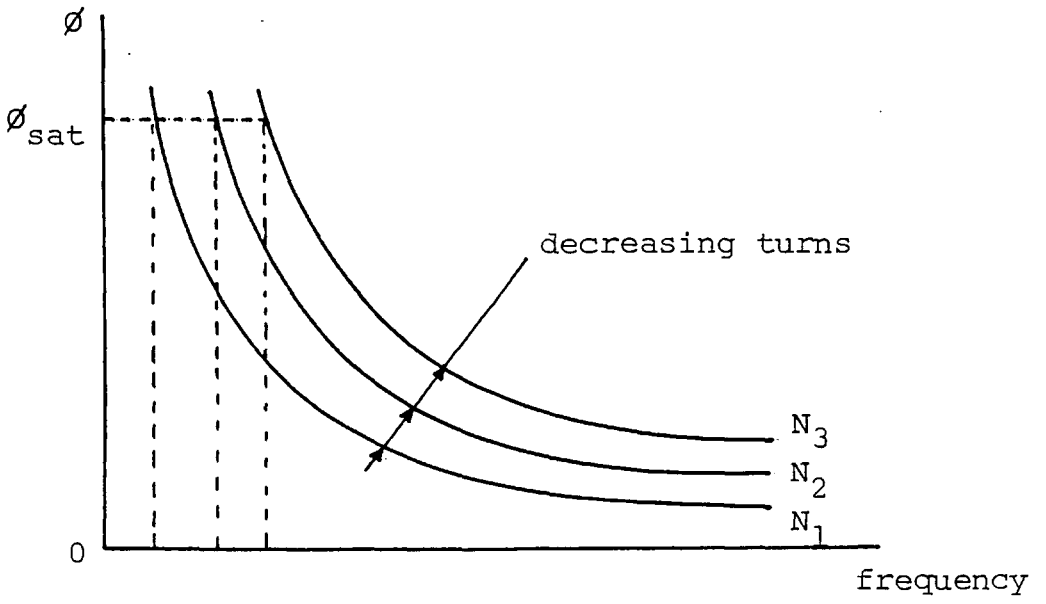

Fig. 6.8.1 Theoretical variation of flux level with frequency for different values of N (turns) (assume fixed E_{av}) :Reduction in E_{av} at low speed can keep the flux to be not higher than $Ø_{sat}$ for low number of turns

at a high saturation level, choice of t/λ in the range of 0.4 to 0.5 is acceptable and the smaller the gap the higher the output torque. In practice the smallness of the airgap length will be limited by mechanical considerations such as the cost of high precision machining, special bearings, etc. and a range of 0.2 - 0.4 mm is suggested for small, non-precision motors.

6.7 Choice of lamination and wire

Excessive iron losses are a particular hazard in high speed SPSRMs and the use of thin and/or low-loss laminations (0.3 mm or less) may often be worth considering.

The usual factors are considered when selecting the winding wire and its insulation grade.

6.8 Number of turns of the excitation coil

If, for simplicity ϕ_{min} is assumed as negligible, the average back e.m.f.

$$E_{av} \simeq N \phi_{max} 2f \qquad (6.8.1)$$

Hence the number of turns can be approximated to be equal to

$$N \simeq \frac{E_{av}}{2\phi_{max} f} \qquad (6.8.2)$$

Relation (6.8.2), then enables the number of turns to be estimated from the supply voltage level ($V_s \simeq E_{av}$ with neglected resistance) and the design (or saturating) flux level at the operating frequency for full volts operation. Fig. 6.8.1 shows the corresponding variation of flux level with frequency for different number of turns and fixed E_{av}.

The choice of coil turns is hence bounded by the need to maintain torque at the desired top speed and to avoid too much saturation (and current peakiness) at some desired low speed (or at standstill). The choice is hence affected by whether supply volts or other regulation methods are intended.

6.9 Choice of feed circuits, pull-down circuits, sensors and switching devices

a) 'a.c.' or 'd.c.' feed

The advantages and disadvantages of these two broad categories of feed have been fully discussed in Chapters 4 and 5 , so only a summary of 'pros' and 'cons' is given (see Table 6.1)

b) pull-down method

Factors affecting the choice between bifilar pull-down circuit and single coil half bridge circuit with d.c. link feeds are summarised in Table 6.2.

Table 6.1

Feed circuit	'pros'	'cons'
a.c. triac-fed	-cheap -straightforward	-can only be used to drive certain loads -limited max speed -high ripple torque -beating effect -high mains harmonics -limited max power
d.c.link transistor-fed	-wide speed range -high speeds possible -low harmonic currents -fine control possible	-more expensive and complex circuit

Table 6.2

pull-down circuit	'pros'	'cons'
bifilar quarter bridge	-only one device needed -reduces cost in driver or commutating circuit and snubber circuit	-high voltage device needed(expensive) -problem with spikes is more serious -winding required more space and more expensive
single-coil half bridge	-cheaper winding -better use of winding area -lower voltage rating device -less serious spike problem	- 2 devices needed -higher cost for driver or commutating and snubber circuits

c) choice of sensors and switching devices

Feasible sensors include opto-electrical devices, Hall-effect devices, inductive and capacitive effect devices. Feasible switching devices include thyristor, triac, bipolar transistor, power MOSFET transistor and gate turn-off device. Brief descriptions of these components and of their usage in SPSRM drives have been given in Chapter 2, and because the numerous factors that affect the choice of these devices (e.g. new devices, new circuits, improved devices) have been widely investigated and reported, Refs. 6.6 and 6.7 are suggested for consultation.

6.10 Choice of control methods

The principal possibilities are tabulated in Table 6.3. A full investigation of control methods must await another project but a few comments can be made at this stage:

With switching unit control, the choice between PWM and switching angle variation finely balanced. With the latter current waveform form factors are worse; with PWM on the other hand switching losses are higher and higher speed devices are needed.

Some interesting possibilities for non-electronic switching angle control exist, such as:

Table 6.3

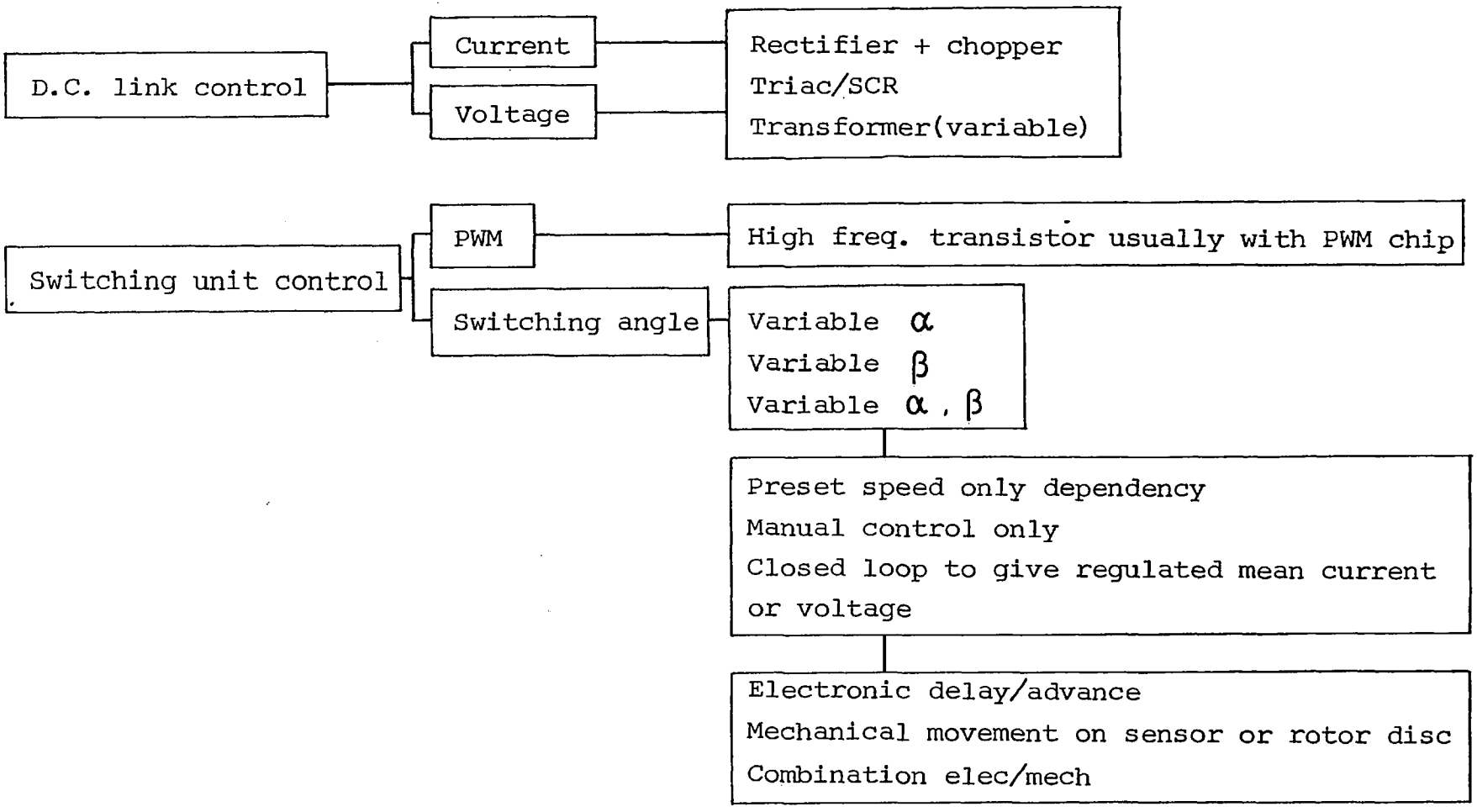
D.C. link control
Current
Voltage
Rectifier + chopper
Triac/SCR
Transformer(variable)
Switching unit control
PWM
High freq. transistor usually with PWM chip
Switching angle
Variable α
Variable β
Variable α , β
Preset speed only dependency
Manual control only
Closed loop to give regulated mean current or voltage
Electronic delay/advance
Mechanical movement on sensor or rotor disc
Combination elec/mech

i) position sensor moveable radially plus multi-track (or spiral-track) disc

ii) centrifugally-operated, circumferentially-moveable disc, car (similar to ignition back-plate) C.B. or twin disc arrangement (one fixed to rotor, the other moveable on the rotor) giving a net pattern whose mark to space varies with speed.

iii) multi-track, multi-sensor system with electronic signal selection.

6.11 Conclusions

A short-list of factors affecting the design of a SPSRM drive has been discussed. The major effort of the present project has been devoted to the construction and testing of a number of motors and drive circuits, together with the derivation and extensive varification of a steady-state analysis and it has hence not proved possible to devote much time to wider aspects, one of the most important of which is the evolution of design procedures. This would not be an easy task, given the variety of feasible feed circuits, control circuits, motor configurations and modes of operation. However, with appropriate development resources, this same variety undoubtedly offers extensive opportunities for developing well-integrated and well-tuned SPSRM motor/drive/control solutions to specific application needs.

CHAPTER 7

CONCLUSIONS AND SUGGESTIONS FOR FURTHER WORK

7.1 Conclusions

Part B of this thesis has reported an investigation relating to a class of SPSRM drive systems. Four experimental motors of differing configurations have been built and tested. Operation both with a triac-fed circuit connected directly to the 50 Hz mains and with a d.c. link, variable frequency switching circuit has been investigated. For each scheme tested, predictions of steady-state operation using two methods, based respectively on a simplified analytic approach and a step by step approach, have been made and correlations with test results have been presented. The quality of many of the correlations has generally been good and has indicated that each prediction method is valuable, though it is clear that further work into iron loss and saturation effects is needed if a fully comprehensive method, valid for all operating conditions is to be developed.

Assessments have been made of the experimental motors' power ratings by means of load tests near the temperature limit, the ratings have been presented alongside other performance-indicating figures such as power/volume, power/weight, energy density, etc. A number of motor,

drive circuit and control-unit configurations have been explored and the factors affecting the design of a SPSRM drive system briefly examined and summarised.

SPSRM devices certainly possess one or two undesirable features which in some circumstances can totally negate their advantages. Specifically, one can state that the penalty paid for the low cost and simplicity of the single phase feed circuit and single phase motor is the discontinuous nature of output torques and the absence of starting torque that results for some rotor positions. Vibration, noise and high torque ripple were not serious factors, at speed, in the motors tested but could be so in larger motors.

However the performance levels obtained from the experimental SPSRM drives have generally been encouraging and suggest that SPSRM drives are likely to prove viable in a number of application areas. Whether SPSRM drives can compete successfully in the domestic drives market presently served by a.c. commutator motors and thyristor-regulated d.c. motors remains to be seen. Much depends on how far the cheaper SPSR motor (no rotor windings, no commutator, no commutator connections, no brushes, no rotor slot insulation, no rotor flash test or heat run required during manufacture) can compensate for the more expensive feed circuit (typically d.c. link system versus thyristor phase angle regulator), on what level of

'premium price' people are prepared to pay for a high quality, quiet drive, and on the attitudes of manufacturers many of whom have substantial investments in commutator motor production plant.

The estimated costs for simple d.c. link feed circuits in Ref. 7.1 shows that these can be remarkably low but commutator motor drives for domestic equipment are also very cheap (developed and improved over many years; very large production volumes per annum) and the task of a 'newcomer' in establishing a significant position may hence be difficult.

In certain non-domestic application areas, the cost constraints are much less onerous and easier progress may occur. (The project reported in section 7.2 involves a typical such application area.)

Whatever the application area, the rate of progress is likely to be significantly affected by improvements in SPSRM system costs and performance. The continuing developments in power switching technology and the fact that the systems tested so far were based on non-optimised, first-version experimental units make it very likely that such improvements will occur and the results of future projects are eagerly awaited.

7.2 An example of industrial application of SPSRM drive system

During the course of the project, a miniature SPSR motor system for an inertia-load drive application was developed in collaboration with an industrial concern in the aerospace sector. One of the principal performance targets involved the acceleration of a 24 gm-cm^2 inertia-load up to 12000 rev/min within 5 seconds. The available power supply consisted of a 12 V d.c. rail with a nominal maximum capacity of 300 mA. A two pole SPSR motor and feed circuit featuring a simple closed speed loop and a single output switching device in the form of a power MOSFET transistor was designed, built and tested. The system performed satisfactorily and extracts from the test results are shown in Table 7.1. The motor and test rig are shown in Fig. 7.2.1. The development of an improved version of the motor and feed system is in progress.

Table 7.1 Performance of the miniature motor

operating speed (rev/min)	total current (mA)	run up time (S)	speed drift %		
			at operating speed	through 90° rot/ sec	20 mins running
12000	61	7	0.024	0.072	0.048
18000	134	14	0.031	0.32	0.062

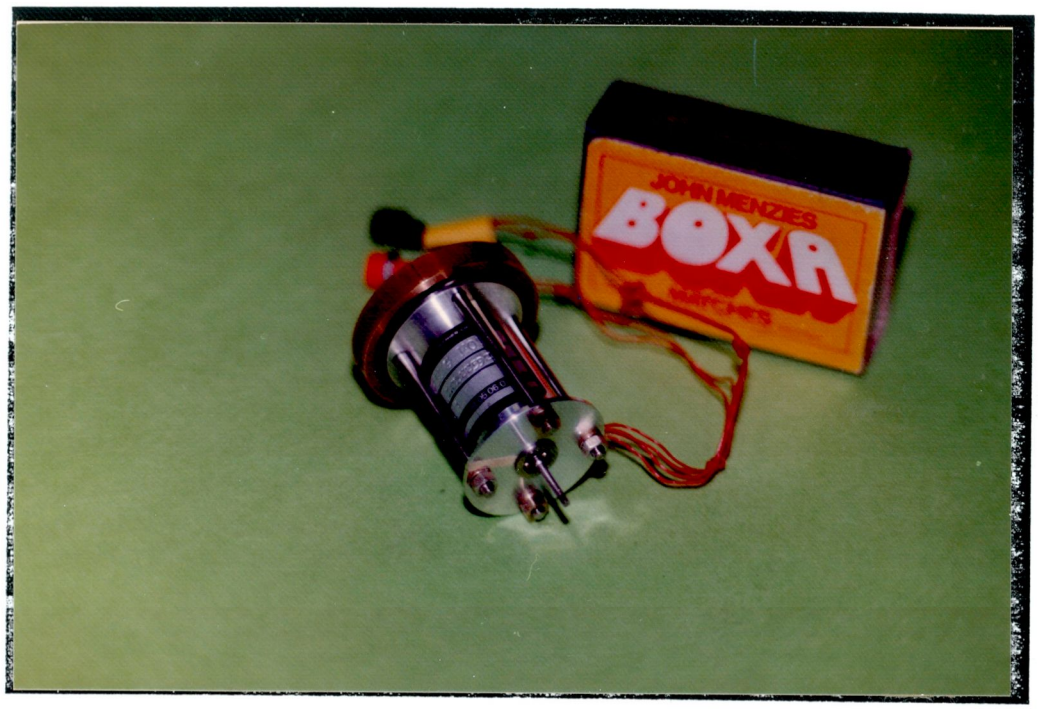

(a)

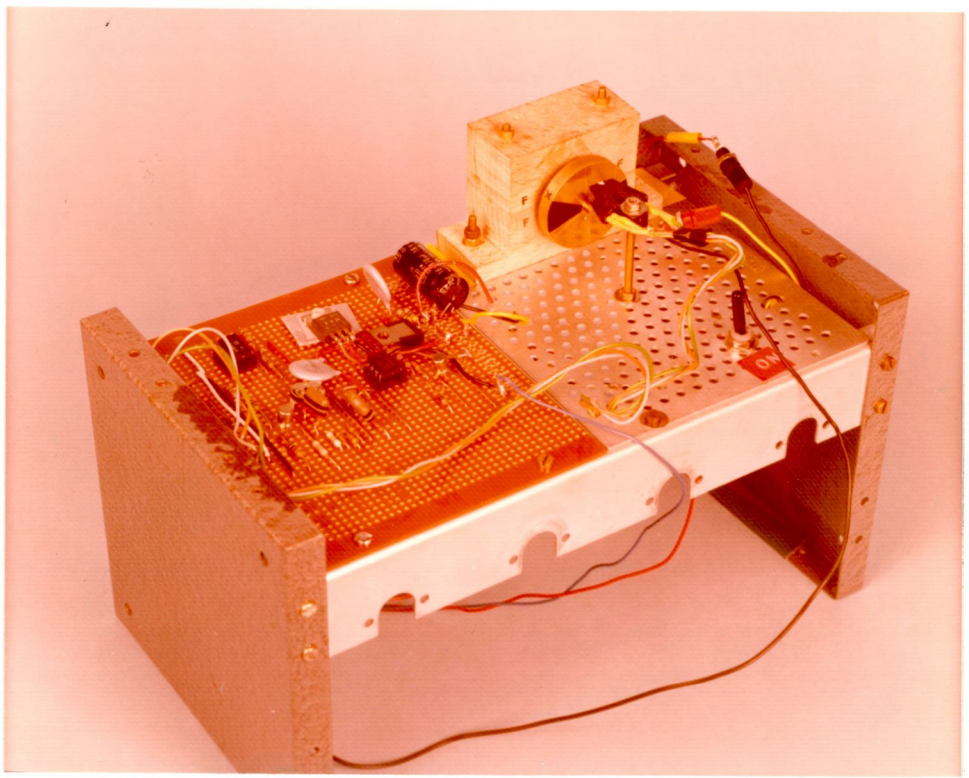

(b)

Fig. 7.2.1 (a) Miniature SPSR motor
(b) Control circuit and test rig

7.3 Suggestions for further work

The main priorities would seem to occur in six areas:

a) Improvement of motor analysis.

Relations for the calculation of iron losses, quadrature axis inductance and leakage inductance for each type of motor configuration are required. Beyond this, the development of techniques for the calculation of sets of ψ versus i and rotor angle curves to allow the prediction of motor performance under saturated conditions would be desirable, even though saturated operation would normally be avoided in practice to reduce peak current levels.

b) Investigation of lower-cost, d.c. link feed circuits.

These are considered to be a number of avenues for reducing feed circuit costs. Systems in which link voltage or current is controlled by means of thyristors in the rectifier are worthy of investigation as a possibly cheaper alternative to the use of PWM techniques in the switching unit. The development of cheap switching-angle control method is desirable. The economies obtainable by the use of the more recently-available switching devices could be examined.

c) Development and testing of motor starter techniques.

Further work could be conducted into the development of cheap, reliable starting methods which involve minimum disturbance to the motor's 'run' operation.

d) Investigation of the effects of scale on SPSRM system viability, and the behaviour of systems of larger power rating than the ones tested.

Investigations in the ½ KW to 1 KW power range probably represent a sensible next step, and would enable comparisons between traditional and SPSRM drives to be made for applications that absorb a significant proportion of the motors currently manufactured for high speed (10000 to 20000 rev/min) and controlled speed drives.

e) Assessments of the viability of variants on the basic SPSRM scheme.

An interesting suggestion here involves the use of a tandem motor arrangement fed from a single-channel feed. Regenerated energy from one motor at turn off is fed to the other at turn on.[7.2]

f) Design optimisation and general comparisons between cost effectiveness of different motor and drive circuit configurations.

Preliminary work in these areas has been reported

in the thesis but the scope for further work is very great and could perhaps proceed in parallel with investigation under some of the headings (b) to (e), subject to a satisfactory outcome of work under (a).

APPENDIX A1

RANGE OF SLIPS OVER WHICH GENERATION TAKES PLACE

Range of slip over which generation takes place for single-phase operation of a three-phase induction generator (Fig. A1) can be derived from the equivalent circuit of Fig. A2 as follows:

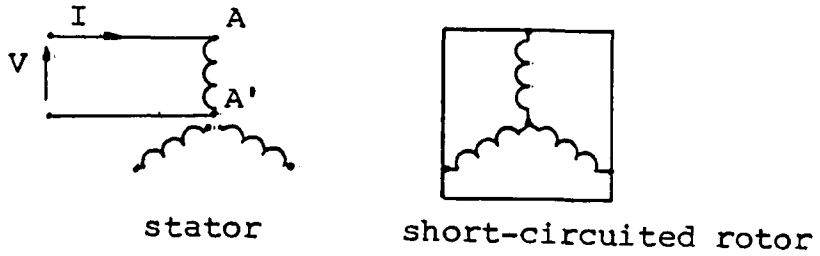

Fig. A1 Connection diagram

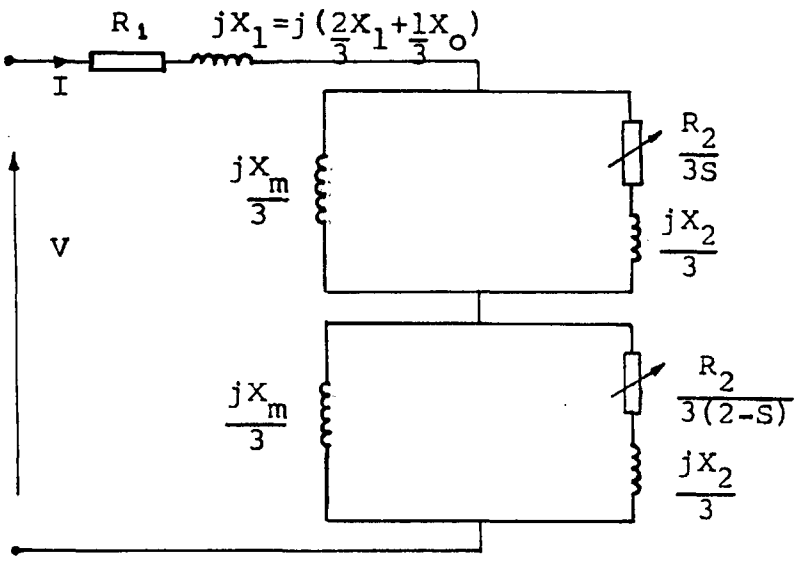

Fig. A2 Corresponding equivalent circuit

From the equivalent circuit, the electrical power P_e is equal to the real part of (VI^*). the operating generating slip range can then be found from the characteristic equation

$$\mathrm{Re}\ (VI^*) = 0 \tag{1}$$

to simplify the derivation, let

$$Z_1 = R_1 + jX_1$$

$$Z_f = \frac{jX_m}{3} \,//\, \frac{R_2}{3S} + \frac{jX_2}{3} \tag{2}$$

$$Z_b = \frac{jX_m}{3} \,//\, \frac{R_2}{3(2-S)} + \frac{jX_2}{3}$$

in which Z_f and Z_b may be written as

$$Z_f = \frac{jX_m}{3} \frac{(R_2 + jSX_2)}{(R_2 + jS(X_2+X_m))}$$

$$Z_b = \frac{jX_m}{3} \frac{(R_2 + j(2-S)X_2)}{(R_2 + j(2-S)(X_2+X_m)} \tag{3}$$

These can be further simplify by assigning the following variables :

$$X_2 + X_m = X_{2m}$$

$$SX_2 = a \qquad SX_{2m} = c$$

$$(2-S)X_2 = b \qquad (2-S)X_{2m} = d \tag{4}$$

Hence Z_f and Z_b are reduced to

$$Z_f = \frac{jX_m}{3} \frac{(R_2+ja)}{(R_2+jc)}$$

$$Z_b = \frac{jX_m}{3} \frac{(R_2+jb)}{(R_2+jd)} \qquad (5)$$

If the voltage phasor V is taken as a reference ($V \angle 0^\circ$) the current I in the equivalent circuit is

$$I = \frac{V}{Z_1+Z_f+Z_b} \qquad (6)$$

substituting the expressions for Z_1, Z_f, Z_b ; (6) becomes

$$I = \frac{3V}{3(R_1+jX_1)+jX_m\left[\frac{(R_2+ja)(R_2+jd)+(R_2+jb)(R_2+jd)}{(R_2+jc)(R_2+jd)}\right]}$$

Factorising the terms in the square bracket, we obtain:

$$I = \frac{3V}{3(R_1+jX_1)+jX_m\left[\frac{(2R_2^2-ad-bc)+jR_2(a+b+c+d)}{(R_2^2-cd)+jR_2(c+d)}\right]} \qquad (7)$$

which can be shortened by assigning

$$2R_2^2-ad-bc = X \quad ; \quad R_2^2-cd = P$$

$$R_2(a+b+c+d) = Y \quad ; \quad R(c+d) = Q \qquad (8)$$

substituting (8) into (7) the expression for current I is

$$I = \frac{3V}{3R_1+j3X_1+jX_m\frac{(X+jY)}{(P+jQ)}}$$

which may be rewritten as

$$I = \frac{3V(P+jQ)}{(3R_1P-3X_1Q-X_mY)+j(3X_1P+3R_1Q+X_mX)} \tag{9}$$

Assigning R and T for the denominator of (9) as:

$$\begin{aligned} R &= 3R_1P-3X_1Q-X_mY \\ T &= 3X_1P+3R_1Q+X_mX \end{aligned} \tag{10}$$

then (9) becomes

$$I = \frac{3V(P+jQ)}{R+jT} \tag{11}$$

Multiplying (11), both numerator and denominator, by R-jT which is the conjugate of R+jT, we obtain :

$$I = \frac{3V((PR+QT)+j(QR-PT))}{R^2+T^2}$$

and the conjugate of I (I^*) is

$$I^* = \frac{3V((PR+QT)-j(QR-PT))}{R^2+T^2}$$

substituting into (1) , the electrical power is

$$P_e = Re\ (VI^*)$$

$$= \frac{3V^2(PR+QT)}{R^2+T^2}$$

For the conditions $P_e = 0$ and $V \neq 0$, the characteristic equation is

$$PR+QT = 0 \qquad (12)$$

Substituting the expressions for R and T , and cancelling like terms , (12) becomes on factorisation:

$$3R_1(P^2+Q^2)+X_m(XQ-YP) = 0 \qquad (13)$$

Note that X_1 has been eliminated from the equation, hence X_1 has no effect on the slip range.

From the expressions of P and Q in eq. (8)

$$P^2+Q^2 = R_2^4+c^2d^2+R_2^2(c^2+d^2) \qquad (14)$$

and from the expressions for c and d in (4) ; (14) may be written as

$$P^2+Q^2 = R_2^4+S^2(2-S)^2X_{2m}^4+(S^2-(2-S)^2)X_{2m}^2 \qquad (15)$$

simslarly, the term (XQ-YP) can be expanded according to the expressions given in (8) as

$$XY-PQ = R_2\left[R_2^2\left[(c+d)-(a+b)\right]+c^2(d-b)+d^2(c-a)\right]$$

and with the expressions given in (4)

$$XY-PQ = 2R_2^3X_m+2R_2S(2-S)X_mX_{2m}^2 \qquad (16)$$

Substituting both (15) and (16) into (13), the characteristic equation may then be written as

$$3R_1R_2^4+3R_1S^2(2-S)^2X_{2m}^4+3R_1X_{2m}^2(S^2-(2-S)^2)$$

$$+2R_2^3X_{2m}^2 + 2R_2S(2-S)X_m^2X_{2m}^2 \qquad = \ 0 \qquad (17)$$

Dividing both sides of (17) by $X_{2m}^4 \neq 0$, we obtain:

$$3R_1\left(\frac{R_2}{X_{2m}}\right)^4 + 3R_1S^2(2-S)^2$$

$$+ \frac{3R_1}{X_{2m}^2}(S^2-(2-S)^2)$$

$$+ 2R_2^3\frac{X_m^2}{X_{2m}^4} + 2R_2S(2-S)\frac{X_m^2}{X_{2m}^2} \qquad = \ 0 \qquad (18)$$

With the assumptions that

$$R_2 \ll X_{2m} \quad ; \quad X_m \simeq X_{2m}$$

the following terms are negligible :

$$\left(\frac{R_2}{X_{2m}}\right)^4 \longrightarrow 0 \quad , \quad \frac{R_1}{X_{2m}^2} \longrightarrow 0,$$

$$\left(\frac{R_2^3 X_m^2}{X_{2m}^4}\right) \longrightarrow 0$$

and (18) is reduced to

$$3R_1(S^2(2-S)^2)+2R_2S(2-S)\left(\frac{X_m}{X_{2m}}\right)^2 = 0$$

which gives

$$S(2-S)\left[\, 3R_1S(2-S)+2R_2\left(\frac{X_m}{X_{2m}}\right)^2 \right] = 0$$

Hence the first and second roots are

$$S_o = 0 \quad \text{and} \quad S_o = 2 \qquad (19)$$

For slips other than 0 and 2 , roots can be found from the equation;

$$3R_1S(2-S)+2R_2\left(\frac{X_m}{X_{2m}}\right)^2 = 0$$

or after rearranging,

$$S^2-2S-\frac{2}{3}\frac{R_2}{R_1}\left(\frac{X_m}{X_{2m}}\right)^2 = 0$$

or $$S^2 - 2S - K = 0$$

where $$K = \frac{2}{3}\frac{R_2}{R_1}\left(\frac{X_m}{X_{2m}}\right)^2$$

$$= \frac{2}{3}\frac{R_2}{R_1}\left(\frac{X_m}{X_2+X_m}\right)^2$$

Hence the other roots are

$$S_o = 1 \pm \sqrt{1 + K} \qquad (20)$$

From (19) and (20), the slips where the electrical power is equal to zero are

$$S_o = 0, \quad 2, \quad 1 \pm \sqrt{1 + K}$$

and $$K = \frac{2}{3}\frac{R_2}{R_1}\left(\frac{X_m}{X_2+X_m}\right)^2$$

APPENDIX A2

MAXIMUM AIRGAP POWER CONDITION

The maximum airgap power condition for single-phase operation of a three-phase induction motor in Fig. A 2.1 can be derived from the equivalent circuit of Fig. A 2.2 as follows :

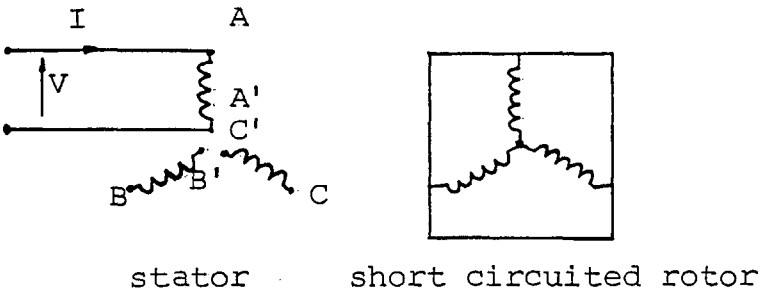

Fig. A2.1 Connection diagram

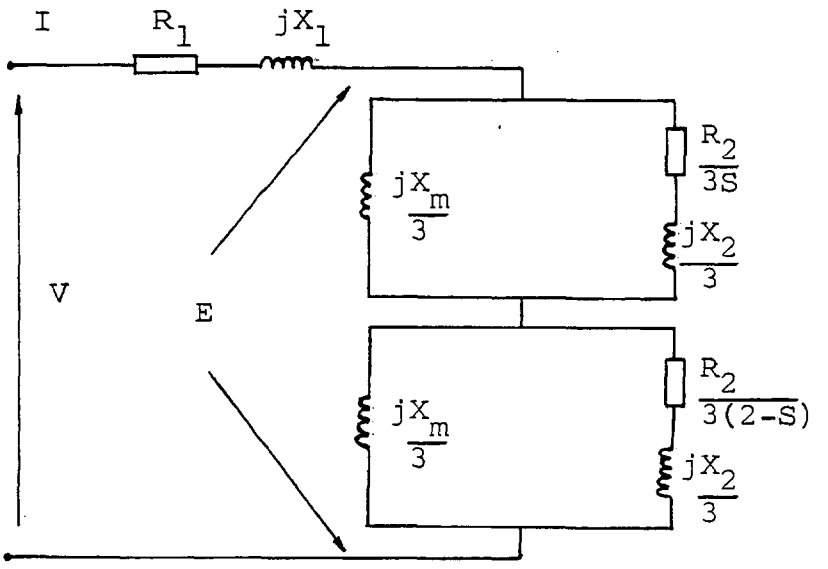

Fig. A2.2 Equivalent circuit

The airgap power can be defined as

$$P_{airgap} = Re\ (\ E\ I^{*}) \qquad (1)$$

where E is the voltage drop across Z_f and Z_b, if E is taken as a reference ($E \angle 0^{\circ}$) the expression for current I related to E is

$$I = \frac{E}{Z_f + Z_b} \qquad (2)$$

where

$$Z_f = \frac{jX_m}{3} \frac{(\ R_2+jSX_2\ )}{(\ R_2+jS(X_2+X_m)\ )}$$

$$Z_b = \frac{jX_m}{3} \frac{(\ R_2+j(2-S)X_2\ )}{(\ R_2+j(2-S)(X_2+X_m)\ )}$$

The following variables are assigned to simplify the equations in the same way as in Appendix A1 , i.e.

$$\begin{aligned} X_{2m} &= X_2+X_m \\ SX_2 &= a \\ (2-S)X_2 &= b \\ SX_{2m} &= c \\ (2-S)X_{2m} &= d \end{aligned} \qquad (3)$$

and

$$\begin{aligned} 2R_2^2 - ad - cb &= X \\ R_2(a+b+c+d) &= Y \\ R_2^2 - cd &= P \\ R_2(c+d) &= Q \end{aligned} \qquad (4)$$

Substituting Z_f and Z_b into (2) and with the assigned variables in (3) and (4) , the equation for current I becomes

$$I = \frac{3E}{X_m(X^2+Y^2)} ((QX-PY)-j(PX+QY)) \qquad (5)$$

which gives the conjugate of I as

$$I^* = \frac{3E}{X_m(X^2+Y^2)}((QX-PY)+j(PX+QY)) \qquad (6)$$

Substituting into (1) , the expression for airgap power becomes

$$P_{airgap} = \frac{3E^2(QX-PY)}{X_m(X^2+Y^2)}$$

or

$$P_{airgap} = -\frac{3E^2(PY-QX)}{X_m(X^2+Y^2)} \qquad (7)$$

The condition for maximum or minimum airgap power is

$$\frac{d}{dS}(P_{airgap}) = 0 \qquad (8)$$

which may be written as

$$-\frac{3E^2}{X_m}\frac{d}{dS}\frac{(PY-QX)}{(X^2+Y^2)} = 0 \qquad (9)$$

Because $-\frac{3E^2}{X_m} \neq 0$, hence

$$\frac{d}{dS}\frac{(PY-QX)}{(X^2+Y^2)} = 0 \qquad (10)$$

which may be expanded to

$$(X^2+Y^2)\left(P\frac{dY}{dS} + Y\frac{dP}{dS} - Q\frac{dX}{dS} - X\frac{dQ}{dS}\right)$$

$$-(PY-QX)\left(2X\frac{dX}{dS} + 2Y\frac{dY}{dS}\right) = 0 \qquad (11)$$

The expressions for derivative terms can be derived from (3) and (4), which give

$$\frac{dP}{dS} = -2(1-S)X_{2m}^2$$

$$\frac{dQ}{dS} = 0 \qquad (12)$$

$$\frac{dX}{dS} = -4(1-S)X_2X_{2m}$$

and

$$\frac{dY}{dS} = 0$$

substituting expressions given in (12) into (11), we obtain :

$$(X^2+Y^2)\left(Y \frac{dP}{dS} - Q \frac{dX}{dS} \right) - (PY-QX)\left(2X \frac{dX}{dS} \right) = 0 \qquad (13)$$

Each term in the bracket may then be derived as follows:

$$X^2+Y^2 = 4\left[(R_2^2-S(2-S)X_2X_{2m})^2+R_2^2X_{3m}^2 \right] \qquad (14)$$

where $X_{3m}=X_2+X_{2m}$;

$$Y \frac{dP}{dS} - Q \frac{dX}{dS} = -4(1-S)R_2X_mX_{2m}^2 \qquad (15)$$

$$PY - QX = -2R_2X_m(R_2^2+S(2-S)X_{2m}^2) \qquad (16)$$

and $$2X \frac{dX}{dS} = -16(R_2^2-S(2-S)X_2X_{2m})(1-S)X_2X_{2m} \qquad (17)$$

Substituting (14) → (17) into (13) and factorising, we obtain :

$$\left[-16(1-S)R_2X_{2m}X_m \right] \left[X_{2m}(R_2^2-S(2-S)X_2X_{2m})^2 + R_2^2X_{3m}^2 + 2X_2(R_2^2+S(2-S)X_{2m}^2)(R_2^2-S(2-S)X_2X_{2m}) \right] = 0 \qquad (18)$$

Hence the first root is

$$S = 1$$

For other roots , the characteristic equation is

$$X_{2m}(R_2^2-S(2-S)X_2X_{2m})^2+ R_2^2X_{3m}^2$$

$$+ 2X_2(R_2^2+S(2-S)X_{2m}^2)(R_2^2-S(2-S)X_2X_{2m}) = 0 \qquad (19)$$

Let $A = S(2-S)$ and substitue A in (19) , the characteristic equation may be written as

$$- A^2X_2^2X_{2m}^3- 2AR_2^2X_{2m}X_2^2$$

$$+(R_2^4X_{2m}+2X_2R_2^4+R_2^2X_{3m}^2X_{2m}) = 0 \qquad (20)$$

Dividing both sides of (20) by $-X_2^2X_{2m}^3 \neq 0$, we obtain,

$$A^2 + 2A\frac{R_2^2}{X_{2m}^2} -\left(\frac{R_2^4}{X_2^2X_{2m}^2} + \frac{2R_2^4}{X_2X_{2m}^3} + \frac{R_2^2X_{3m}^2}{X_2^2X_{3m}^2} \right) = 0 \qquad (21)$$

with the assumption that $R_2 \ll X_{2m}$, these terms are negligible:

$$\frac{R_2^2}{X_{2m}^2} \quad , \quad \frac{R_2^4}{X_2^2X_{2m}^2} \quad , \quad \frac{2R_2^4}{X_2X_{2m}^3} \longrightarrow 0$$

and (21) reduces to

$$A^2 - \frac{R_2^2 X_{3m}^2}{X_2^2 X_{2m}^2} = 0 \qquad (22)$$

or $$A^2 - K^2 = 0 \qquad (23)$$

where $$K = \frac{R_2 X_{3m}}{X_2 X_{2m}}$$

$$= \frac{R_2(2X_2+X_m)}{X_2(X_2+X_m)}$$

Four more roots can then be found from (23) as

$$S = 1 \pm \sqrt{1+K}$$

$$S = 1 \pm \sqrt{1-K}$$

But the slip where maximum airgap occurs in the generating region is given only by

$$S_{max} = 1 - \sqrt{1+K} \qquad (24)$$

where $$K = \frac{R_2(2X_2+X_m)}{X_2(X_2+X_m)}$$

The expression for maximum generating airgap power can now be derived by substituting the expression for S_{max}

into the expression for airgap power given in (7).

Hence, from

$$P_{airgap} = \frac{-3E^2 (PY-QX)}{X_m (X^2+Y^2)} \tag{25}$$

for maximum P_{airgap}, S is equal to $1 - \sqrt{1+K}$.

Substituting the expression for S_{max} in (3) and (4) yields

$$\begin{aligned} P &= R_2 (R_2 + \frac{X_{2m}X_{3m}}{X_2}) \\ Q &= 2R_2X_{2m} \\ X &= 2R_2(R_2+X_{3m}) \\ Y &= 2R_2X_{3m} \end{aligned} \tag{26}$$

and $$PY - QX = 2R_2^2X_m (\frac{X_{3m}X_{2m}}{X_2} - R_2)$$

$$X^2 + Y^2 = 4R_2^2 (R_2^2+2R_2X_{3m}+2X_{3m}^2)$$

and (25) becomes

$$P_{max} = \frac{-3E^2}{2} \frac{(\frac{X_{3m}X_{2m}}{X_2} - R_2)}{(R_2^2+2R_2X_{3m}+2X_{3m}^2)} \tag{27}$$

With the assumption that $R_2 \ll X_{2m}$,

R_2 can be neglected when compared to $\frac{X_{3m}X_{2m}}{X_2}$

and R_2^2 can be neglected when compared to $2X_{3m}^2$,

and (27) reduces to

$$P_{max} = \frac{-3E^2}{2}\left(\frac{X_{3m}X_{2m}}{X_2}\right)\left(\frac{1}{2R_2X_{3m}+2X_{3m}^2}\right) \qquad (28)$$

which gives the approximate airgap power

$$P_{max} = \frac{-3E^2}{4}\frac{X_{2m}}{X_2X_{3m}}$$

or

$$P_{max} = \frac{-3E^2}{4}\frac{(X_2+X_m)}{X_2(2X_2+X_m)} \qquad (29)$$

APPENDIX B1

TRANSISTOR SNUBBER CIRCUIT[2.12,2.13]

It is generally necessary to connect an RC snubber across a power transistor to absorb the energy associated with the recovery current of the device, to limit the resulting voltage spike and delay the voltage rise. In conjunction with the RC snubber, an RL snubber is used to delay the rise of current di/dt during the turn-on period.

a) dV/dt limiting snubber

Consider the circuit in Fig. B1.1. It is assumed that during the turn-off period the load current remains constant and that it transfers to the capacitor immediately the switching off procedure is initiated. The 'worst case' capacitor is chosen so that capacitor voltage does not rise above the allowable collector-emitter voltage when maximum load current I_L is flowing, i.e.

$$C = \frac{I_L}{dV/dt} \qquad \text{(B1.1)}$$

or approximately

$$C = \frac{I_L \Delta t}{\Delta V} \qquad \text{(B1.2)}$$

where I_L is the maximum load current,

ΔV is the maximum acceptable V_{CE} at the end of turn-off. D.C. rail to rail voltage (V_{cc}) can be used for convenience.

t is turn-off time of the transistor or t_f (fall time) given in the transistor data sheet.

So eq.(B1.2) can be written as

$$C = \frac{I_L \, t_f}{V_{cc}} \qquad \text{(B1.3)}$$

R_c is chosen to limit the peak discharge current through the transistor to a safe value when the transistor is turned on again, i.e.

$$R_c \geq \frac{V_{cc}}{I_p} \qquad \text{(B1.4)}$$

where V_{cc} is initial capacitor voltage (d.c. rail voltage)
I_p is transistor peak current (I_L can be used)

so

$$R_c \geq \frac{V_{cc}}{I_L} \qquad \text{(B1.5)}$$

It should be noted that the time constant should be small enough for C to discharge completely during the turn-on time of the transistor. In case of PWM mode of operation $t_{on}(min)$ is chosen to be 10 % of the operating frequency, i.e.

$$5 \, R_c \, C \leq t_{on}(min)$$

or

$$R_c \leq \frac{t_{on}(min)}{5 \, C} \qquad \text{(B1.6)}$$

From eqs. (B1.5)and(B1.6), the condition for R_c is

$$\frac{V_{cc}}{I_L} \leq R_c \leq \frac{t_{on}(min)}{5 \, C} \qquad \text{(B1.7)}$$

The power rating of the resistor can be calculated from the total energy stored in the capacitor which has to be dissipated through it, i.e.

$$P_{RC} = \tfrac{1}{2} C V_{cc}^2 f \qquad \text{(B1.8)}$$

where f is the operating frequency.

b) di/dt limiting snubber

During the turn-on period of the transistor, diode D_1 starts to turn-off but takes a finite time (the reverse recovery time t_{rr}) to do so due to stored charge. Thus D_1 appears as short-circuit as far as the transistor is concerned. A large current spike will flow and a series inductor must be connected in series with the transistor to limit this spike amplitude. The 'worst case' inductor is chosen so that the currnt that builds up from zero is limited to the maximum allowable current spike (I_s) in time t_{rr}. Using

$$L = \frac{V}{di/dt}$$

or approximately $$L = \frac{V_{cc}\,\Delta t}{\Delta I} \qquad \text{(B1.9)}$$

where V_{cc} is rail to rail voltage,
Δt is t_{rr} of the freewheel diode,
ΔI is the maximum allowable current spike(I_s).

Eq.(B1.9) can be rewrittened as

$$L = \frac{V_{cc} t_{rr}}{I_s} \qquad \text{(B1.10)}$$

R_L is chosen so that the time constant of the LR_L circuit is shorter than the minimum off time of the transistor. When operating in PWM mode t_{off}(min) is chosen to be 10 % of the period of the operating frequency, i.e.

$$\frac{5L}{R_L} \leq t_{off}(min) \qquad \text{(B1.11)}$$

or

$$R_L \geq \frac{5L}{t_{off}(min)} \qquad \text{(B1.12)}$$

The voltage drop across R_L caused by freewheeling current from L through the resistor when the transistor is switched off must not be higher than a certain value. If V_{SN} is the allowable superimposed voltage spike, then

$$R_L \leq \frac{V_{SN}}{I_L} \qquad \text{(B1.13)}$$

From eqs. (B1.12) and (B1.13) the condition for R_L is

$$\frac{5L}{t_{off}(min)} \leq R_L \leq \frac{V_{SN}}{I_L} \qquad \text{(B1.14)}$$

and the power dissipation in R_L can be calculated in the same way as in R_c , i.e.

$$P_{RL} = \tfrac{1}{2} L I_L^2 f \qquad \text{(B1.15)}$$

It may be noted that in the other (non-bridge) feed circuits, power diode recovery currents are absent and the need for the snubber L etc. greatly reduced.

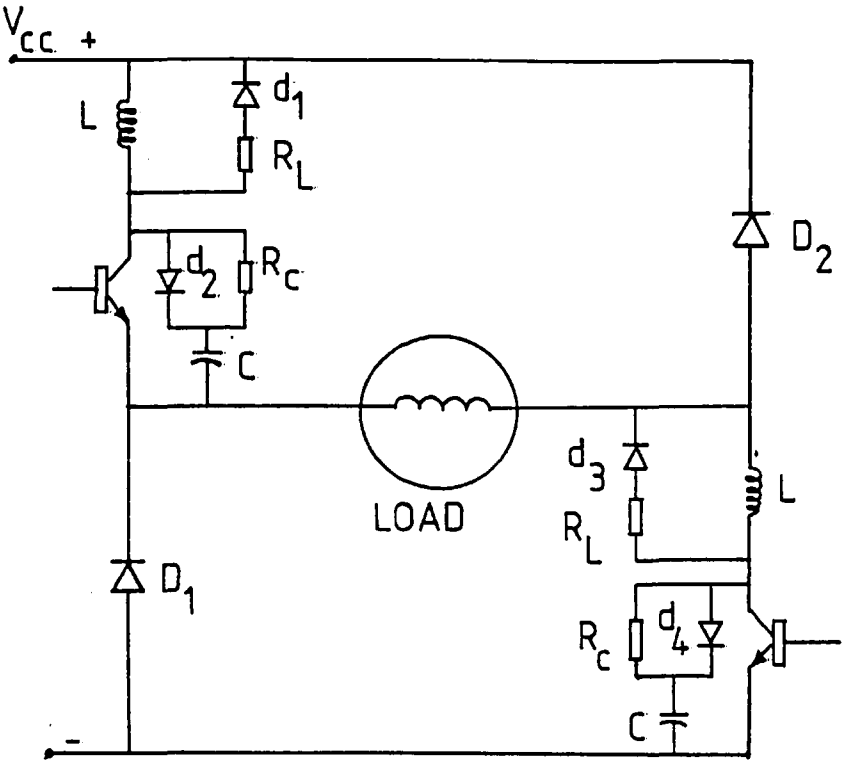

Fig. B1.1 Transistor snubber circuit

APPENDIX B2

CONTROL CIRCUIT FOR STARTING POLE

The control circuit for the starting pole has to distinguish between three conditions:

a) the rotor position enables the motor to start on the main winding alone;

b) the rotor position is such that it would be unable to start on the main winding (torque would be zero or negative);

c) the motor is rotating.

It is only in case (b) that the starting circuit must operate and switch on the supply to the starting pole so as to pull the rotor into a position in which positive torque is generated when the main winding is excited. For case (a) and (c) the control circuit must switch off the supply to the starting pole to prevent it from interfering with the motor operation.

In order to perform these functions a circuit of Fig. B2.1 is used. This circuit consists of 2 D type FLIP-FLOPs and 4 two-input NAND Schmitt triggers (1 DUAL D type CMOS FLIP-FLOP 4013 B and 1 QUAD 2 input NAND Schmitt trigger CMOS 4093 B). The input terminal of the circuit receives the signal from the rotor position sensor and the output terminal is connected to the power supply of the starting pole.

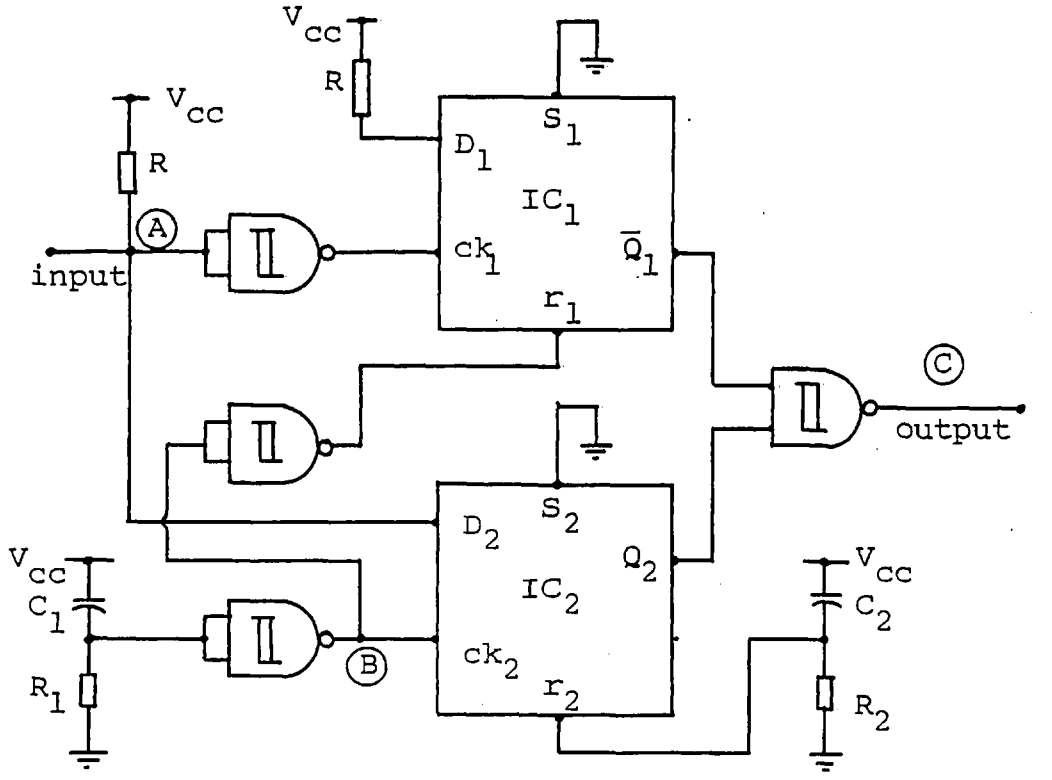

Fig. B2.1 Control circuit for starting pole

Table B2.1 Table of operation of the control circuit

time mS	case	Ⓐ	Ⓑ	D_2	r_2	ck_2	Q_2	r_1	ck_1	D_1	$\bar{Q}_1$	Ⓒ
$0 \prec t \prec 1$		Rdm	0	Rdm	1	0	0	1	Rdm	1	1	1
$1 \prec t \prec 10$		Rdm	0	Rdm	0	0	0	1	Rdm	1	1	1
$t \succ 10$	a	0	1	0	0	1	0	0	1	1	0	1
		1	Un	1	0	Un	0	0	0	1	0	1
$t \succ 10$	b	1	1	1	0	1	1	0	0	1	1	0
		0	Un	0	0	Un	1	0	1	1	0	1
		1	Un	0	0	Un	1	0	0	1	0	1

The conditions of the input signal are:

signal 0 (low) for condition (a), and

signal 1 (high) for condition (b).

The output conditions are:

signal 1 (high) for starting pole off, and

signal 0 (low) for starting pole on.

Two timing circuits are used to prevent a random output state. These have time constants $T_1 = \frac{1}{R_1 C_1}$ = 10 mS and $T_2 = \frac{1}{R_2 C_2}$ = 1 mS.

The operation of the circuit can be described with the aid of Table B2.1 where the logic '0' represents 'low' state and the logic '1' represents 'high' state, Rdm represents random state and Un means unchanged.

For the period of time between switch on and 1 mS later, the state of Ⓐ, ck_2 and ck_1 are random. Both r_1 and r_2 are at 1 which results in $\bar{Q}_1 = 1$ and $Q_2 = 0$. So the output is at 1 and the starting pole is shut-off.

For the period between $1 < t < 10$ mS, r_1 is still at 1 but r_2 changes to 0. Because no clock pulse appears at ck_2 and s_2 is inactive, the state of Q_2 is unchanged. Both $\bar{Q}_1$ and Q_2 are hence at the same state as before together with the output and the starting pole hence stays off.

The starting pole is hence inactive for 10 mS no matter what happens to the input signal or motor. This arrangement is necessary to prevent false activation due to the random state of IC_1 and IC_2.

After 10 mS the circuit will operate according to the input condition whidh can be divided into two cases as follows:

Case (a): the motor is able to start on main winding

For this case Ⓐ is 0 and ck_1 equals to 1. With r_1 changing from 1 to 0, IC_1 is able to clock D_1 to $\overline{Q}_1$ and results in $\overline{Q}_1$ equal to 0.

IC_2 will also get the clock pulse because Ⓑ changes from 0 to 1. So IC_2 clocks D_2 which is 0 to Q_2 and results in Q_2 equal to 0.

With $\overline{Q}_1$ equal to 0 and Q_2 equal to 0 the output stays at 1 and the starting pole stays off.

So for this case the starting pole is inactive and the main winding will get the motor started on it own.

After the first pulse point Ⓑ is unchanged so Q_2 stays at 0 no matter what happen to $\overline{Q}_1$, so the output is always off.

Case (b): the motor can not start on the main winding

For case(b), point Ⓐ is at 1 and after 10 mS from switch on Ⓑ changes from 0 to 1. With Ⓑ changing

to 1, r_1 changes to 0 but ck_1 is at 0 so IC_1 is unable to clock and stays at the previous state ($1 < t < 10$ mS) which is 1. Change in Ⓑ from 0 to 1 enables IC_2 to clock D_2 which is 1 to Q_2. With both $\overline{Q}_1$ and Q_2 at 1, the output is 0 and the starting pole is activated.

This in effect will tend to pull the rotor round towards the starting pole and out of the 'non start' region. This motor is then be able to start on the main winding.

At this time the input signal changes from 1 to 0, so IC_1 clocks D_1 to $\overline{Q}_1$ and changes $\overline{Q}_1$ to 0. The output Q_2 will stay the same at 1 because no change occurs in Ⓑ . The output then changes to 1 and shuts off the starting pole.

After this the state of $\overline{Q}_1$ will be at 0 because everytime IC_1 clocks, it will clock D_1 to make $\overline{Q}_1$ at 0. Q_2 is also at 1 because no clock signal appears after 10 mS. So the output will stay at 1 after the first pulse and the starting pole stays off.

From the explanation above it can be seen clearly that the starting pole will assist starting only when the rotor is in the off period and will not interfere with the main operation after the rotor rotates. Fig. B2.2 shows a possible arrangement of the starting pole with the form 1 motor and Fig. B2.3 a possible output circuit operating from mains with a triac as the controlled switch.

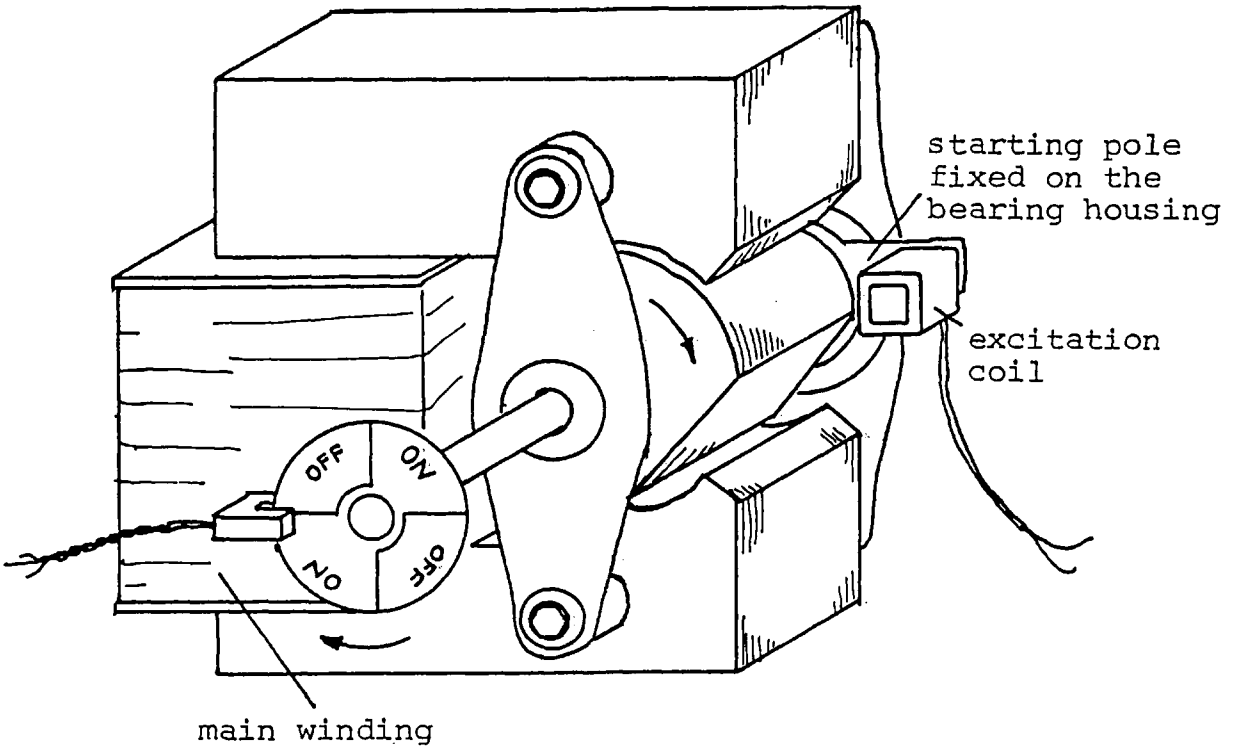

Fig. B2.2 Possible starting pole arrangement

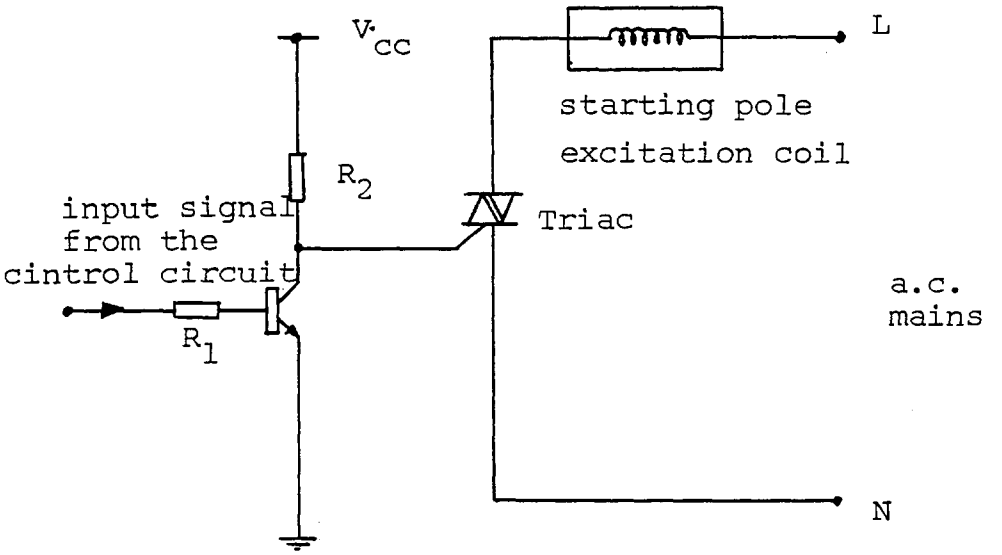

Fig. B2.3 Possible output stage

APPENDIX B3

```
MNF 5
C***** MINIATURE MOTOR *****
C***** TORQUE PREDICTIONS *****
C*****  OF THE 2 POLES SINGLE PHASE
C*****  SWITCH RELUCTANCE MOTOR
C*****  USING STEP BY STEP METHOD
C
C
      DIMENSION TM(500),V(500),XL(500),C(500),T(500),
     1RPM(100),ALPHA(20)
      DATA VSP,VSN/11.6,0.6/
      DATA R,XLMAX,XLMIN/1.22,0.013,0.0865/
      DATA BETA/60.0/
      DATA  NI/100/
      WRITE(6,200) VSP,VSN
      WRITE(6,210) R,XLMAX,XLMIN
      WRITE(6,220) BETA
      NJ=1
      ALPHA(1)=15.0
      N=1
      RPM(1)=1000.0
      WRITE(6,280)  ALPHA(1),RPM(1)
      GO TO 490
  480 RPM(N)=1000*N
C*****  INITIAL CURRENT AND TORQUE AT FIRST CYCLE *******
  490 NR=1
      C(1)=0.0


      T(1)=0.0
      GO TO 580
C*****  INITIAL CURRENT AND TORQUE AT THE FOLLOWING CYCLE
  500 C(1)=C(201)
      T(1)=T(201)
C*****  OTHER INITIAL CONDITIONS *******
  580 XL(1)=XLMAX
      TM(1)=0.0
      SP=6.0*RPM(N)
      P=180.0/SP
      ANI=NI
      DT=P/ANI
      DL=(XLMAX-XLMIN)/(ANI/2.0)
      V(1)=-VSN
      Q=0.0
      CMAX=0.0
      PI=3.1415926
      TMAX=0.0
      SUMC=0.0
      SUMT=0.0
      FC=0.0
      PIN=0.0
      ATC=0.0
      AVC=0.0
      AVT=0.0
      CMS=0.0
      E=0.0
      OUTP=0.0
      RLOSS=0.0
      W=0.0
      Z=0.0
C*****  ADVANCED ON AND OFF STEPS
      N1=(ANI/2.0)-((ALPHA(NJ)*ANI)/180.0)+1.0
      N2=ANI-((BETA*ANI)/180.0)+1.0
      N3=N1+NI
      N4=N2+NI
C*****  STEPS FOR MAX AND MIN  INDUCTANCE *******
      NI1=(NI/2)+1
      NI2=NI+1
      NI3=(3*NI)/2+1
      NI4=2*NI+1
C******* STARTING ITERATIONS
      K=2
  600 TM(K)=TM(K-1)+DT
      IF(K-N1)  660,660,610
  610 IF(K-N2) 670,670,620
  620 IF(K-N3) 660,660,630
  630 IF(K-N4) 670,670,660
  660 V(K)=-VSN
      GO TO 700
  670 V(K)=VSP
  700 IF(K-NI1)  750,750,710
  710 IF(K-NI2)  770,770,720
  720 IF(K-NI3) 750,750,730
  730 IF(K-NI4) 770,770,750
  750 XL(K)=XL(K-1)-DL
      GO TO 780
  770 XL(K)=XL(K-1)+DL
C*****  CURRENT **********************/
  780 ANUME=2.0*V(K)
      BNUME=C(K-1)*(R-2.0*XL(K-1)/DT)
      DENI=R+2.0*XL(K)/DT
      C(K)=(ANUME-BNUME)/DENI
      IF(C(K).GT.CMAX) CMAX=C(K)
      IF(C(K).LT.0.0) C(K)=0.0
C*****  TORQUE **********************
      CNUME=0.125*(C(K)+C(K-1))**2
      DNUME=XL(K)-XL(K-1)
      DENII=DT*SP*(PI/180.0)
      T(K)=(CNUME*DNUME)/DENII
      IF(T(K).GT.TMAX)  TMAX=T(K)
      IF(K.LT.NI1) GO TO 790
      IF(K.GT.N3) GO TO 790
      SUMC=SUMC+C(K)
      SUMT=SUMT+T(K)
      PIN=PIN+V(K)*C(K)
C*****  SUM OF SQUARE OF THE CURRENT
      FC=FC+C(K)**2
      Q=Q+1.0
  790 K=K+1
      IF(K.LE.NI4) GO TO 600
C*****  SQUARE OF THE RMS MOTOR CURRENT


      CMS=FC/Q
      AVC=SUMC/Q
      AVT=SUMT/Q
      PW=PIN/Q
C*****  NO LOSSES ****
      PWL=PW
      AVTT=AVT
C*****  CALCULATE OUTPUT ****
      OUTP=AVTT*SP*(PI/180.0)
      W=PWL-OUTP
      RLOSS=R*CMS
      Z=OUTP/PWL
      E=100.0*Z
      ATC=AVTT/AVC
```

```
C***** CHECK FOR REPETITION OF CURRENT *****
      CDIFF=ABS(C(N1)-C(N3))
      NCYC=2*NR-1
      IF(CDIFF.LT.0.0001) GO TO 795
      IF(NR.GT.30) GO TO 795
      NR=NR+1
      GO TO 500
  795 WRITE(6,300) CDIFF,NCYC
      WRITE(6,240)
      WRITE(6,250) AVTT,AVC,TMAX,CMAX,RPM(N),
     1PWL,OUTP,W,RLOSS,E,ATC,N1
C*****  PRINT FORMAT
  200 FORMAT(10X,"SUPPLY VOLTAGE =",F10.2,"V.",5X,
     1"PULL-DOWN VOLTAGE =",F10.2,"V.")
  210 FORMAT(10X,"R=",F10.4,"OHMS",3X,
     1"MAXL=",F10.4,"H",3X,"MINL=",F10.4,"H")
  220 FORMAT(10X,"BETA=",F10.4,"DEG")
  240 FORMAT(//,2X,"AVG-T-NM  AVG-AMPS  MAX-T-NM",
     12X,"MAX-AMPS    SPEEDS",12X,"INPUT POWER OUTPOWER",
     21X,"POWERLOSS  RES-LOSS  PER-EFFY T/C")
  250 FORMAT(1X,4F10.5,F10.2,12X,5F10.2,F6.3,1X,I2)
  280 FORMAT(//,1X,"ALPHA",F10.2,"SPEED",F10.2)
  300 FORMAT(/,10X,"CURRENT DIFFERENCE=",F10.8,"AMPS",
     110X,"AT",2X,I4,2X,"CYCLES")
C***** REPEAT FOR OTHER SPEEDS ***
      IF(N.GT.19) GO TO 900
      N=N+1
      GO TO 480
  900 STOP
      END
```

APPENDIX B4

```
MNF 5
C***** S. CHAIRATANA, **********
C***** SOLUTION OF TORQUE AND CURRENT EQUATIONS *****
C***** TRIAC POWER CIRCUIT
C***** SINGLE PHASE SWITCHED RELUCTANCE MOTOR
C***** O.C. TRIGGER SCHEME ****
C*****
      DIMENSION TGAM(200),TALP(200),TBET(200)
      DIMENSION TMAXL(300),TMINL(300)
      DIMENSION THCYC(300)
C*****
      DATA VS,F /25.0,50.0/
      DATA R,XLMAX,XLMIN/0.51,0.0200,0.0086/
C***** CETA AND GAMMA MUST BE THE MULTIPLE OF 18 DEGS
      GAMMA=0.0
      WRITE(6,800) VS
      WRITE(6,801)R,XLMAX,XLMIN
      WRITE(6,804) GAMMA
      CETA=0.0
   60 IF(CETA.GT.108.0) GO TO 990
C*****
      WRITE(6,803) CETA
      WRITE(6,850)
C***** SET ROTOR SPEED
      RPM=3000.0
   70 CONTINUE
      ALPHA=45.0
      BETA=45.0
C***** INITIAL CONDITIONS *****
  110 COLD=0.0000
      TORQ=0.0
      PI=3.1415926
      CMAX = 0.0
      TMAX=0.0
      SUMC=0.0
      SUMT=0.0
      CSQ=0.0
      TM=0.0
      PIN=0.0
      AVC=0.0
      AVT=0.0
      AVCSQ=0.0
      TOSTP=0.0
      RMSC=0.0
      OUTP=0.0
      RLOSS=0.0
      AMVS=0.0
      ANUME=0.0
      BNUME=0.0
      CETR=0.0
      CNEW=0.0
      CNUME=0.0
      DENI=0.0
      DENII=0.0
      DLDI=0.0
      DNUME=0.0
      FUNCT=0.0
      VC=0.0
      WR=0.0
      WT=0.0
      XL=0.0
      XLF=0.0
      REFF=0.0
C***** TIME STEP EQUALS TO 1 MILLISECOND ****
      DT=1.0
C***** TIME INTERVAL IN CALCULATION *****
      COMPT=500.0
C*****
C***** CETA MUST NOT BE GREATER THAN 180 ELEC DEG****
C***** CALCULATE TIMES FOR GATE TRIGGERING SIGNAL
C***** AND TIMES WHEN GATE SIGNAL IS REMOVED ***
      PERID=1000.0/F
      IF(GAMMA-CETA) 120,125,130
  120 TGAM(1)=0.0
      TGAM(2)=(180.0+GAMMA-CETA)*(PERID/360.0)
      GO TO 135
  125 TGAM(1)=0.0
      TGAM(2)=TGAM(1)+(PERID/2.0)
      GO TO 135
  130 TGAM(1)=(GAMMA-CETA)*(PERID/360.0)
      TGAM(2)=TGAM(1)+(PERID/2.0)
  135 THCYC(1)=(180.0-CETA)*(PERID/360.0)
      THCYC(2)=THCYC(1)+(PERID/2.0)


      JCYC=(COMPT*F)/1000.0
      JHCYC=2*JCYC
      JHG=JHCYC+2
      DO 136 JG=3,JHG
      THCYC(JG)=THCYC(JG-1)+(PERID/2.0)
  136 TGAM(JG)=TGAM(JG-1)+(PERID/2.0)
C***** CALCULATE SWITCH ON AND OFF TIME *****
      PEMECH=30000.0/RPM
      HPEME=PEMECH/2.0
      TALP(1)=HPEME*(1.0-(ALPHA/90.0))
      TBET(1)=HPEME*(2.0-(BETA/90.0))
      JLAS=COMPT/PEMECH
      JLASI=JLAS+2
      DO 140 JAB=2,JLASI
      TALP(JAB)=TALP(JAB-1)+PEMECH
  140 TBET(JAB)=TBET(JAB-1)+PEMECH
C***** CALCULATE TIME FOR MAX AND MIN INDUCTANCE ****
C***** AT  T=0.00 SEC XL=XLMAX *****
      TMAXL(1)=0.0
      TMINL(1)=HPEME
      JLASI=JLAS+2
      DO 150 JAB=2,JLASI
      TMINL(JAB)=TMINL(JAB-1)+PEMECH
  150 TMAXL(JAB)=TMAXL(JAB-1)+PEMECH
C***** SELECT GATE SIGNAL WHICH IS IN THE ON PERIOD *
      NQ=1
      JC=1
      JG=1
      JAB=1
      NT=1
C***** NUMBER OF STEPS FOR ONE CYCLE OF TORQUE ***
      NTT=300
C*****
  200 TM=TM+DT
      IF(TM.GT.COMPT) GO TO 990
  203 IF(TM.GE.TALP(JAB)) GO TO 215
  205 IF(JC.LE.1) GO TO 210
      NT=NT+1
      IF(NT.GT.NTT) GO TO 900
  210 NQ=NQ+1
      GO TO 200
  215 IF(TM.LE.TBET(JAB)) GO TO 220
      JAB=JAB+1
      GO TO 203
  220 IF(TM.GE.TGAM(JG)) GO TO 225
      GO TO 205
  225 IF(TM.LE.THCYC(JG)) GO TO 250
      JG=JG+1
      GO TO 220
  250 JX=1
      GO TO 252
  251 JX=2
```

```
C***** CALCULATE THE VALUE OF VOLTAGE AT THIS TIME STEP
  252 WT=(2.0*PI*F*TM)/1000.0
      CETR=CETA*PI/180.0
      FUNCT=SIN(WT+CETR)
      AMVS=1.4142135*VS
      VC=AMVS*FUNCT
C***** CALCULATE VALUE OF XL AT THIS STEP
      DLDT=(XLMAX-XLMIN)/HPEME
      IF(TM-TMINL(JAB)) 260,263,264
  260 XL=XLMAX-DLDT*(TM-TMAXL(JAB))
      DXLT=TM-TMAXL(JAB)
      IF(DXLT.GE.DT) GO TO 261
      DDDT=DT-DXLT
      XLF=XLMAX-(DDDT*DLDT)
      GO TO 280
  261 XLF=XL+(DLDT*DT)
      GO TO 280
  263 XL=XLMIN
      XLF=XL+(DLDT*DT)
      GO TO 280
C*****
  264 IF(TM-TMAXL(JAB+1)) 265,268,269
  265 XL=XLMIN+DLDT*(TM-TMINL(JAB))
      DXLT=TM-TMINL(JAB)
      IF(DXLT.GE.DT) GO TO 266
      DDDT=DT-DXLT
      XLF=XLMIN+(DLDT*DDDT)
      GO TO 280
  266 XLF=XL-(DLDT*DT)
      GO TO 280
  268 XL=XLMAX
      XLF=XL-(DLDT*DT)
      GO TO 280
C*****


  269 IF(TM-TMINL(JAB+1)) 270,273,274
  270 XL=XLMAX-DLDT*(TM-TMAXL(JAB+1))
      DXLT=TM-TMAXL(JAB+1)
      IF(DXLT.GE.DT) GO TO 271
      DDDT=DT-DXLT
      XLF=XLMAX-(DLDT*DDDT)
      GO TO 280
  271 XLF=XL+(DLDT*DT)
      GO TO 280
  273 XL=XLMIN
      XLF=XL+(DLDT*DT)
      GO TO 280
C*****
  274 IF(TM-TMAXL(JAB+2)) 275,277,278
  275 XL=XLMIN+DLDT*(TM-TMINL(JAB+1))
      DXLT=TM-TMINL(JAB+1)
      IF(DXLT.GE.DT) GO TO 276
      DDDT=DT-DXLT
      XLF=XLMIN+(DLDT*DDDT)
      GO TO 280
  276 XLF=XL-(DLDT*DT)
      GO TO 280
  277 XL=XLMAX
      XLF=XL-(DLDT*DT)
      GO TO 280
  278 XL=XLMAX-DLDT*(TM-TMAXL(JAB+2))
      DXLT=TM-TMAXL(JAB+2)
      IF(DXLT.GE.DT) GO TO 279
      DDDT=DT-DXLT
      XLF=XLMAX-(DLDT*DDDT)
      GO TO 280
  279 XLF=XL+(DLDT*DT)
C***** AT FIRING TIME CURRENT EQUALS TO ZERO ****
  280 IF(JX.EQ.1) GO TO 282
      GO TO 284
  282  CNEW=0.0
      TORQ=0.0
      GO TO 305
```

```
C***** AFTER FIRING TIME CALCULATE CURRENT
  284 ANUME=2.0*VC
      BNUME=COLD*(R-(2000.0*XLF)/DT)
      DENI=R+(2000.0*XL)/DT
      CNEW=(ANUME-BNUME)/DENI
C***** SIMULATION OF TRIAC ACTION *****
      IF(ABS(CNEW).GT.0.001) GO TO 285
      IF(ABS(CNEW)-ABS(COLD)) 287,290,290
  285 IF((CNEW*COLD).GE.(-0.000)) GO TO 290
  287 CNEW=0.000
      COLD=CNEW
      GO TO 205
C***** FIND MAXIMUM CURRENT
  290 ABCS=ABS(CNEW)
      IF(ABCS.GT.CMAX) CMAX=ABCS
C***** CALCULATE TORQUE *****
      CNUME=0.125*(COLD+CNEW)*(COLD+CNEW)
      DNUME=XL-XLF
      WR=(2.0*PI*RPM)/60.0
      DENII=(WR*DT)/1000.0
      TORQ=(CNUME*DNUME)/DENII
C***** FIND MAXIMUM TORQUE
      IF(TORQ.GE.TMAX) TMAX=TORQ
  305 CONTINUE
C***** CALAULATE SUM OF CURRENT AND TORQUE ***
      SUMC=SUMC+CNEW
      SUMT=SUMT+TORQ
C***** CALCYLATE INST POWER INPUT***
      PIN=PIN+(VC*CNEW)
C***** SUM OF CURRENT SQUARE ***
      CSQ=CSQ+(CNEW*CNEW)
      TM=TM+DT
      JC=JC+1
      COLD=CNEW
      NT=NT+1
      IF(NT.GT.NTT) GO TO 900
      IF(TM.GT.COMPT) GO TO 990
      GO TO 251
C****** CALCULATE MEAN AND RMS VALUE ****
  900 TOSTP=NTT
      AVC=SUMC/TOSTP
      AVT=SUMT/TOSTP
      AVCSQ=CSQ/TOSTP
      RMSC=SQRT(AVCSQ)
      OUTP=AVT*RPM*(2.0*PI/60.0)
      RLOSS=R*AVCSQ
      ATC=AVT/RMSC
      REFF=(OUTP/(OUTP+RLOSS))*100.0


C****** PRINT RESULTS *******
      WRITE(6,860) RPM,AVC,RMSC,AVT,OUTP,RLOSS,REFF,CMAX,
     1ALPHA,BETA
  800 FORMAT(10X,"SUPPLY VOLTAGE(RMS)=",F10.2,"V.")
  801 FORMAT(10X,"R=",F10.4,"OHMS",3X,
     1"MAXL=",F10.4,"H.",3X,"MINL=",F10.4,"H.")
  803 FORMAT(10X,"VOLTAGE PHASE ANGLE=",F10.2,"DEG(ELEC)")
  804 FORMAT(10X,"FIRING ANGLE =",F10.2,"DEG(ELEC)")
  850 FORMAT(//,10X,"RPM.",5X,"IAVE(A.)",5X,"I-RMS(A.)",
     15X,"T-AVE(NM)",5X,"OUTP(W.)",5X,"RLOSS(W.)",5X,
     2"EFF(%)",5X,"MAXA.",5X,"ALPHA",5X,"BETA")
  860 FORMAT(6X,F7.1,F13.5,F4.5,F15.5,F14.3,
     1F15.3,F12.3,F10.3,F10.2,F9.2)
      RPM=RPM-100.0
      IF(RPM.GE.100.0) GO TO 70
      CETA=CETA+18.0
      GO TO 60
  990 STOP
      END
```

APPENDIX B5

ROTOR MOMENT OF INERTIA

The axial moment of inertia of the salient-pole rotor can be calculated from the basic equation which defines the moment of inertia I of mass m with constant mass density ρ as

$$I = \rho \int r^2 dV \qquad \text{(B5.1)}$$

where dV is the element volume

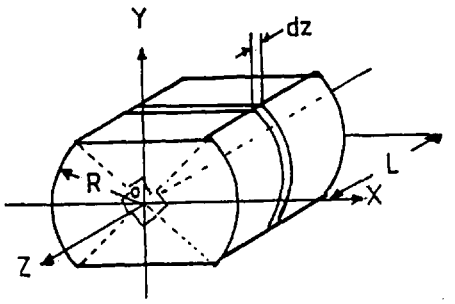

Fig. 5.1

With reference to Fig. B5.1, if the rotor is considered to be made of a series of thin disc dz, equation (B5.1) can be rewritten as

$$I_z = \rho \int_0^L \int r^2 dA \; dz \qquad \text{(B5.2)}$$

and due to the uniform cross-section along z axis (B5.2) becomes

$$I_z = \rho L \int r^2 dA \qquad \text{(B5.3)}$$

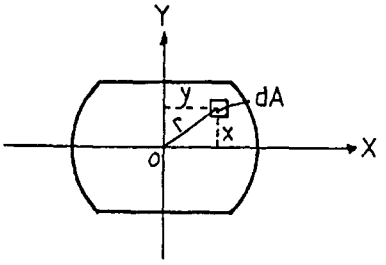

where dA is the element area and r is the distance from dA to z axis.

Since $r^2 = x^2 + y^2$,

$$I_z = \rho L \left[\int x^2 dA + \int y^2 dA \right] \qquad \text{(B5.4)}$$

or $$I_z = \rho L (I'_y + I'_x) \qquad \text{(B5.5)}$$

where $I'_y = \int x^2 dA$ is the area moment of inertia about y axis

and $I'_x = \int y^2 dA$ is the area moment of inertia about x axis

The area moment of inertia about x axis is

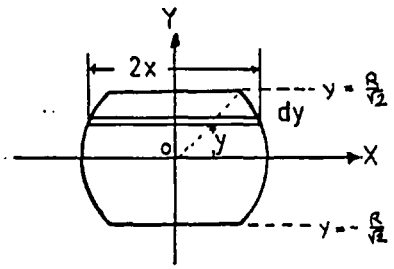

$$I'_x = \int_{\frac{-R}{\sqrt{2}}}^{\frac{R}{\sqrt{2}}} 2\, xy^2 dy$$

$$= \frac{\pi}{8} R^4 \qquad \text{(B5.6)}$$

The area moment of inertia about y axis may be considered as a composite area composed of Y_1 and Y_2. Hence

$$I'_y = I_{y1} + I_{y2}$$

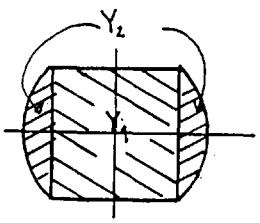

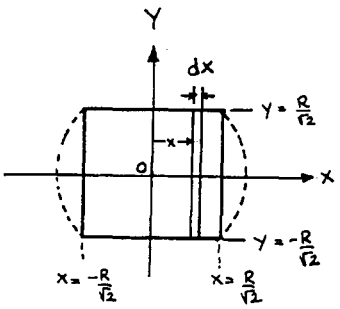

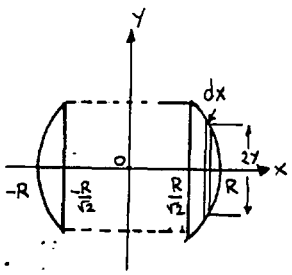

and $$I_{y1} = \int_{\frac{-R}{\sqrt{2}}}^{\frac{R}{\sqrt{2}}} x^2 \sqrt{2}\, R\, dx$$

$$= \frac{R^4}{3}$$

and $$I_{y2} = \int_{-R}^{\frac{-R}{\sqrt{2}}} 2yx^2\,dx + \int_{\frac{R}{\sqrt{2}}}^{R} 2yx^2\,dx$$

$$= \frac{\pi}{8} R^4$$

and so $$I'_y = R^4\left(\frac{1}{3} + \frac{\pi}{8}\right) \qquad \text{(B5.7)}$$

Substituting (B5.6) and (B5.7) into (B5.5), the moment of inertia of the salient pole rotor about z axis is

$$I_z = \rho L R^4\left(\frac{\pi}{4} + \frac{1}{3}\right)$$

For other components (i.e. shaft, disc, pulley, etc.) the moment of inertia was calculated from standard expressions.

REFERENCES

Part A

CHAPTER 1

1.1 Allen, C.L.C.:"Water turbine driven induction generators", Proc. IEE, Dec, 1959, 107A, pp. 529-550.

1.2 Smith, R.T. and Burton C.E.:"Effect of wind harmonics and gust torques on induction generators, Part 1", ASME paper 75-WA, Pet. 4, 1975.

1.3 Taylor, R.H.; Leicester, R.J.; Gardner, G.E. and Franklin, P.J.:"Integration of wind rotor power onto an electricity supply system", Proc. of 1st BWEA Wind Energy Workshop, April 1979, pp. 134-146.

1.4 Debontridder, J.; Vanderput, A.; Marcelis, R; Geysen, W.; De Keusler, C. and Fierens, E.: "The combination asynchronous generator vertical-axis wind turbine for small power applications", Proc. of Int. Conf. on Elec. Mach., Brussels, September, 1978.

1.5 Eastham, J.F.:"Principle and characteristics of induction generators", Electrical Review, Nov 1960, pp. 809-913.

1.6 Arrillaga, J.:"Static power conversion from self excited induction generators", Proc. IEE, Vol. 125, No. 8, Aug 1978, pp. 743-746.

1.7 Ooi, B.T. and David, R.A.:"Induction-generator/synchronous condenser system for wind turbine power", Proc. IEE, Vol. 126, 1979, pp. 69-74.

1.8 Watson, D.B.; Arrillaga, J. and Densem, T.:"Controllable d.c. power supply from wind-driven self-excited induction machines", Proc. IEE, Vol. 126, 1979, pp. 1245-1248.

1.9 Jones, C.V.:"The unified theory of electrical machines", Butterworths, London, 1957.

1.10 Fitzgerald, A.E.; Kingsley, C. and Kusko, A.: "Electric machinery", 3rd Ed., McGraw-Hill, 1971, p.543.

CHAPTER 2

2.1 Alger, D.L.:"Induction machines (thier behaviour and uses), 2nd Ed., Gordon & Breach, 1970, Ch. 7, p. 201.

2.2 Say, M.G.:"Alternating current machines", 4th Ed., Pitman, 1976, Ch. 2.

2.3 Bone, J.C.H.:"Influence of rotor diameter and length on the rating of induction motors", IEE Proc. Part B Elec. Pow. Appl., Vol. 1, No. 1, Feb 1978, pp. 2-6.

2.4 De Jong, H.C.J.:"A.C. motor design with conventional and converter supplies", IEE Monograph, Clarendon Press, 1976, Ch. 4.

2.5 Anscombe, L.D. and Ellison, A.J.:"Technical aspects of interchange with the grid", J. Inst. Fuel, June 1949, pp. 257-262.

2.6 Elliot, D.E.:"Economic wind power", Applied Energy, 1975, 1, pp.167-172.

2.7 Bolton, H.R. et al:"Double output generator scheme for wind energy conversion", Proc. of British Wind Energy Association Conference, Cranfield, 1980.

Part B

CHAPTER 1

1.1 Bowers, B.:"The early history of the electric motor", Philips Technical Review, 35, 1975, pp.77-95.

1.2 Nasar, S.A.:"D.C. switched reluctance motor", Proc. IEE, Vol. 116, No. 6, 1969, pp. 1048-1049.

1.3 Nasar, S.A.:"The goodness of a reluctance machine", Proc. IEE, Vol. 118, No. 6, 1971, p. 796.

1.4 Unnewehr, L.E. and Koch, W.H.:"An axial-airgap reluctance motor for variable-speed applications", IEEE Trans., 1974, PAS-93, pp. 367-376.

1.5 Byrne, J.V. and Lacy, J.G.:"Characteristics of saturable stepper and reluctance motors", Proc. of IEE Conf. on Small Electrical Machines, 136, 1976, pp. 93-96.

1.6 Koch, W.H.:"Thyristor-controlled pulsating-field reluctance motor system", Electric Machines and Electromechanics, Vol. 1, 1977, pp. 201-205.

1.7 Bausch, H. and Rieke, B.:"Performance of thyristor-fed electric car reluctance machines", Proc. of Int. Conf. on Electrical Machines, Brussels, 1978, paper E4/2.

1.8 Lawrenson, P.J.; Stephenson, J.M.; Blenkinsop, P.T.; Corda, J. and Fulton, N.N.:"Variable-speed switched reluctance motors", IEE Proc. B Elec. Power Appl., 1980, 127, (3), pp. 253-265.

1.9 Ray, W.F. and Davis, R.M.:"Inverter drive for doubly-salient reluctance motor: Its fundamental behaviour, linear analysis and cost implications", IEE Proc. B Elec. Power Appl., 1979, 2, (6), pp. 185-193.

1.10 Davis, R.M.; Ray, W.F. and Blake, R.J.:"Inverter drive for switched reluctance motor: Circuits and component rating", IEE Proc. B Elec. Power Appl., 1981, 128, (2), pp. 126-136.

1.11 Lawrenson, P.J.; Stephenson, J.M.; Fulton, N.N. and Corda, J.:"SRMs for traction drives", Proc. of Int. Conf. on Electrical Machines, Athens, 1980, Part 1, pp. 410-417.

1.12 Lawrenson, P.J.; Ray, W.F.; Davis, R.M.; Stephenson, J.M.; Fulton, N.N. and Blake, R.J.:"Controlled-speed SRMs-Present status and future potential", Proc. of Drives/motors/controls'82 Conf., Leeds, 1982, pp. 23-31.

1.13 Bolton, H.R.; Pedder, D.A.G. and Anderson, J.C.: "Development of a reluctance motor for fan drive application", Report to Relite Electric Ltd., July, 1975.

1.14 Bolton, H.R. and Pedder D.A.G.:"Low-cost reluctance drive system for low-power, low-speed applications", Proc. of IEE Conf. on Electrical Variable Speed Drives, November, 1979, pp. 88-92.

CHAPTER 2

2.1 Bolton, H.R. and Pedder, D.A.G.:" Low-cost reluctance drive system for low-power, low-speed applications", Proc. of IEE Conf. on Electrical Variable-Speed Drives, November, 1979, pp. 88-92.

2.2 Davis, R.M.:"Power diode and thyristor circuits", IEE Monograph Series 7, Peter Peregrinus Ltd., 1979.

2.3 Mullard:"Power engineering using thyristors", Vol. 1, Mullard ltd., 1970.

2.4 McNulty, T.C.:"A review of thyristors characteristics and applications", RCA application note, AN 4242, pp. 400-401.

2.5 Pelly, B.R.:"Power MOSFET application note", International Rectifier, No. AN 930/A, November, 1979.

2.6 Lander, C.W.:"Power electronics", Mc Graw-Hill, 1981, p. 5.

2.7 Ray, W.F. and Davis R.M.:"Inverter drive for doubly-salient reluctance motor: Its fundamental behaviour, linear analysis and cost implications", IEE Proc. B Elec. Power Appl., 1979, 2, (6), pp. 185-193.

2.8 Lujic. A.:"Controlling brushless d.c. motors", Machine Design, 41, (25), 1969, pp. 113-115.

2.9 Electrocraft Corp.:"DC motors, speed controls, servo systems", 3rd Ed., Pergamon Press, 1977, Ch. 3.

2.10 Lander, C.W.:"Power electronics", McGraw-Hill, 1981, Ch. 10.

2.11 Ramamoorty, M.:"An introduction to thyristors and their applications", McMillan Press Ltd., 1977, Ch. 11.

2.12 Hurley, N.V.:"Investigations into some novel switching mode converters and systems for d.c. supply smoothing", Ph.D.Thesis, Imperial College (London), 1977, pp. 216-218.

2.13 Peter, J.M.:"Limits of safe operation of power transistor in switching mode", Power transistors in the switching mode, Sescosem Pub., pp. 4-31.

2.14 Marshall, R.C.:"Earthing, shielding and filtering problems", Wireless World, 1976, August, pp. 68-69; September, pp. 85-86; November, pp. 73-75; December, pp. 65-66.

2.15 Datasheet:"Thyristors: Radio frequency interference", Electrical Review, 1975, p.433.

2.16 Kamerbeek, E.M.H.:"Scaling laws for electric motors", Philips Tech. Rev. 35, 1975, No. 4, pp. 116-123.

CHAPTER 3

3.1 Proceedings of the International Conference on Stepping motors and systems, University of Leeds, 1974, 1976, 1979.

3.2 Slemon, G.R. and Straughen, A.:"Electric machines", Addison Wesley, 1980.

3.3 Stephenson, J.M. and Čorda, J.:"Computation of torque and current in doubly-salient reluctance motors from nonlinear magnetisation data",Proc. IEE, Vol. 126, No. 5, May, 1979, pp.393-396.

3.4 Bolton, H.R. and Pedder D.A.G.:"Low-cost reluctance drive system for low-power, low-speed applications", Proc. IEE Conf. on Electrical Variable-Speed Drives, Nov 1979, pp.88-92.

3.5 Ray, W.F. and Davis, R.M.:"Inverter drive for doubly salient reluctance motor: Its fundamental behaviour, linear analysis and cost implications", IEE Proc. Elec. Power Appl., Vol 2, No. 6, Dec 1979, pp. 185-193.

3.6 Udeagwu, F.C.:"Computer aided prediction and experimental varification of a steady state performance of a novel reluctance motor, M.Sc. Thesis, Imperial College (London), Sept 1977.

3.7 Orr, E.R.:"A thyristor firing circuit for a.c. power application", Industrial Electronics, Nov 1964, pp. 509-513.

5.8 Hughes, A.; Lawrenson, P.J.; Steele, M.E. and Stephenson, J.M.:"Prediction of stepping motor

performance", Proc. of Int. Conf. on Stepping Motors and Systems, Leeds, 1974, pp. 67-76.

3.9 Carter, G.W.:"The electromagnetic field in its engineering aspects", 2nd Ed., Longmans, 1976, Ch. 11.

3.10 Cotton, H.:"Advanced electrical technology", Pitman and sons Ltd., pp. 1157-1164.

3.11 Ewing, J.S.:"Lumped circuit impedance representation for d.c machines", IEEE Trans., PAS-87, No. 4, 1968, pp. 1106-1110.

CHAPTER 4

4.1 Bolton, H.R.; Pedder, D.A.G. and Anderson, J.C.: "Development of a reluctance motor for fan drive application", Report to Relite Electric Ltd., July, 1975.

4.2 Say, M.G.:"Alternating current machines", 4th Ed., Pitman Publishing, 1977, pp. 54-55.

4.3 Ferranti Component Divisions:"ZN 1066 E/J switching regulator control and drive unit", Ferranti Electronics Ltd., Issue 2, May 1978.

4.4 Bolton, H.R. and Pedder, D.A.G.:"Low-cost reluctance drive system for low-power, low-speed applications", Proc. IEE Conf. on Electrical Variable Speed Drives, Nov 1979, pp.88-92.

4.5 Moulin, G.M.:"Single-phase reluctance motor", 2nd year report, I.U.T. CACHAN, 1976.

4.6 Ramamoorty, M.:"An introduction to thyristors and their applications", The McMillan Press Ltd., 1978, pp.48-50.

4.7 Kendall, P.G. and Johnson, P.A.:"Limits for harmonic distortion in the U.K. electricity supply systems", Proc. IEE Conf. Pub. on Power Electronics, Sept 1977, pp. 174-178.

4.8 Electricity Council:"Engineering recommendation", G5/3.

4.9 British Standard Institution:"B.S. 5406", 1976.

4.10 British Electricity Board:"ACE report No. 73", 1979.

4.11 Chatratana, S.; Bolton, H.R. and Pedder, D.A.G.: "Investigation into small single-phase switched reluctance motors", Proc. IEE 2nd Int. Conf. on Small and Special Elec. Mach., Sept 1981, pp. 99-102.

4.12 Monro, D.M.:"ALGORITHM: Fast Fourier Transform", Application Report, No. 5, Imperial College, London.

4.13 Bergland, G.D.:"A guide of fast Fourier transform", IEEE Spectrum 6, 7 (July 1969), pp. 41-52.

4.14 Benny, L.B.:"Mathematics for students of engineering and applied science", Oxford Uni. Press, 1958, pp. 517-541.

4.15 Williamson, S.:"Reduction of voltage and current harmonics introduced by a single phase triac AC controller by means of shunt resistance", IEEE Trans., IECI-28, No. 4, Nov 1981, pp. 266-272.

CHAPTER 5

5.1 Millman, J.:"Microelectronics: Digital and analog circuits and system", McGraw-Hill, 1979, Sec. 16-2, p.574.

5.2 R.S. Datasheet:"Voltage to frequency converter 307-070", R.S. Component Ltd., R/3201, Dec 1977.

5.3 Veinott, C.G.:"Fractional and subfractional horse - power electric motors", 3rd Ed., McGraw-Hill, 1970, Ch. 10.

5.4 SG 1524/SG 2524/SG 3524 Regulating pulse width modulator, Silicon General Inc., Sept 1976.

5.5 SG 1527/SG 3627 Dual high current output driver, Silicon General Inc., March 1978.

5.6 Say, M.G.:"Alternating current machines", 4th Ed., Pitman, 1976, p.64.

5.7 Roters, H.C.:"Electromagnetic Devices, 1st Ed., John Wiley & Sons Inc., 1941.

5.8 Binns, K.J. and Lawrenson, P.J.:"Analusis and computation of electric and magnetic field problems", Pergamon Press, 1963.

4.9 Ashen, R.A.:"Some aspects of high-torque, low speed brushless electric motors", Ph.D. Thesis, Imperial College (London), 1977, p. 20.

CHAPTER 6

6.1 Kellock, B.:"New-look pump part radiates cash savings..", Machinery and Production Engineering, 17 Sept 1980, Vol. 137, No. 3529.

6.2 Lawrenson, P.J.; Stephenson, J.M.;Blenkinsop, P.T.; Corda, J. and Fulton, N.N.:"Variable speed switched reluctance motors", IEE Proc. B Elec. Power Appl., 1980, 127, (3), pp. 253-265.

6.3 Mukherji, K.C. and Neville, S.:"Magnetic permeance of identical double slotting", Proc. IEE, Vol. 118, No. 9, 1971, pp. 1257-1268.

6.4 Harris, M.R.; Hughes, A. and Lawrenson, P.J.:"Static torque production in saturated doubly-salient machines", Proc. IEE, Vol. 122, 1975, pp. 1121-1127.

6.5 Ward, P.A. and Lawrenson, P.J.:"Magnetic permeance of doubly-salient airgap", Proc. IEE, Vol. 124 No. 6, 1977, pp. 542-544.

6.6 Horner, G.R. and Lacey, R.J.:"High performance brushless P.M, motors for robotics and actuator applications", Proc. on Electrical Drives/ Motors/Controls'82, U. of Leeds, 1982,pp.91-96.

6.7 "Switchgear; solid power devices", Electronics & power, Vol. 28, No. 5, May 1982, pp.379-393.

CHAPTER 7

7.1 Chatratana, S.; Bolton, H.R. and Pedder, D.A.G.: "Investigation into small single-phase switched reluctance motors", Proc. IEE 2nd Int. Conf. on Small and Special Elec. Mach., Sept 1981, pp. 99-102.

7.2 Nyudo, S.; Yakawa, M. and Higuchi, A.:"Control circuit of electromagnetic clutch and brake obtaining fast response with high efficiency", National Defence Academy, Yokosuka, Kanagawa, Japan.

INTERNATIONAL CONFERENCE ON ELECTRICAL MACHINES

SEPTEMBER 15, 16, 17, 1980 - ATHENS HILTON HOTEL - ATHENS - GREECE

AN ASSESSMENT OF THE PLAIN SINGLE PHASE, MAINS-CONNECTED INDUCTION MACHINE AS A GENERATOR

S. Chatratana and H.R. Bolton
Department of Electrical Engineering, Imperial College, London SW7 2BT.

ABSTRACT

An assessment is presented of the super-synchronous generating capabilities of the mains-connected single phase induction machine. Forward and backward rotating field analysis enables the influence of motor design parameters on performance criteria such as maximum efficiency, operating slip range, maximum power and slip for maximum power to be examined. It is found that reasonably good performance can be obtained with motors of suitable design, desirable features including low magnetising current, low rotor resistance (but an absence of deep bar effect to minimise backward field losses) and moderate specific output (as a motor) per D^2L. Possible applications include small scale generation - subject to supply authority regulations - from water, windpower, and waste-heat energy recovery schemes. A number of the theoretical results are verified by laboratory measurements on an induction machine.

INTRODUCTION

The economic viability of wind and water power conversion systems and certain waste-heat recovery schemes is improving as real energy costs rise and much research, development, assessment and resource-measurement work by individuals, commercial concerns and government agencies into various aspects of wind and small hydro systems is under way. A sizable body of opinion feels that in suitable circumstances, a good case can be made for further exploitation of these energy resources at the medium and small scale as well as at the large scale and a number of interesting system configurations suitable for small and medium scale use have been proposed. In many cases, an isolated electrical system is appropriate with battery, resistance heater or multi-machine loading. In countries where private, 'non-firm' generation into the main power system is allowable and where tariff structures are fairly generous towards this class of generation, mains connection is worth considering. The mains-connected three phase induction generator[1] has a good record both in hydro[2] and in wind[3] schemes and references 4 and 5 give prediction methods for wind turbine driven three phase induction generator systems.

Many consumers are connected via a single phase feeder only and the question often arises as to the feasibility of induction generation in this case. A number of electrical circuit configurations are possible. Probably the simplest one is where a single phase winding only is used on the generator since this avoids the slight reliability reductions and self-excitation risks associated with the 'capacitor-run' configuration. The performance of the plain single phase, mains-connected induction generator is examined in this paper.

ANALYSIS

The equivalent circuit for a single phase induction machine when it runs on main winding alone and iron loss is negligible is shown in fig. 1[4] where R_{11} and X_{11} are the resistance and leakage reactance of the winding, X_{m1} is the magnetising reactance, R_{21} and X_{21} are the rotor referred resistance and standstill leakage reactance (resumed constant) and s is the per unit slip respectively. If one phase of a three phase induction machine is used the values of the forward and backward equivalent circuit impedances of fig. 1: R_{11}, X_{11}, $X_{m1}/2$, $X_{21}/2$, $R_{21}/2s$ and $R_{21}/2(2-s)$ in terms of the per phase impedances R_1, X_1, X_m, R_2, X_2 for balanced three phase operation and the zero sequence per phase reactance X_o, obtained via the symmetrical components transformation method given in reference 7, are:

$$R_{11} = R_1 \qquad \frac{1}{2}X_{m1} = \frac{1}{3}X_m$$

$$X_{11} = \frac{2}{3}X_1 + \frac{1}{3}X_o \qquad \frac{1}{2}R_{21} = \frac{1}{3}R_2$$

$$\frac{1}{2}X_{21} = \frac{1}{3}X_2$$

Derivation of the machine's steady state performance relations is simplified if the following substitutions are made:

$$z_1 = R_1 + j\left(\frac{X_o}{3} + \frac{2X_1}{3}\right) \quad \text{or} \quad R_1 + X_{11}$$

$$z_f = j\frac{X_m}{3} \,/\!/\, \left(\frac{R_2}{3s} + j\frac{X_2}{3}\right) \quad \text{or} \quad j\frac{X_{m1}}{2} \,/\!/\, \left(\frac{R_{21}}{2s} + j\frac{X_{21}}{2}\right)$$

$$z_b = j\frac{X_m}{3} \,/\!/\, \left(\frac{R_2}{3(2-s)} + j\frac{X_2}{3}\right) \quad \text{or} \quad j\frac{X_{m1}}{2} \,/\!/\, \left(\frac{R_{21}}{2(2-s)} + j\frac{X_{21}}{2}\right)$$

and the rotor forward and backward resistances subdivided into I^2R loss and mechanical output portions:

$$\frac{R_{21}}{2s} = \frac{R_{21}}{2} + R_{21}(1-s)/2s \ ;$$

$$\frac{R_{21}}{2(2-s)} = \frac{R_{21}}{2} + R_{21}(s-1)/2(2-s)$$

The input current I_1 is hence $I_1 = V/(Z_1 + Z_f + Z_b)$ and the airgap e.m.f. $E = V - I_1 Z_1$. The forward and backward rotor currents I_{2f} and I_{2b} are $E_f/(R_{21}/2s + jX_{21}/2)$ and $E_b/(R_{21}/2(2-s) + j\frac{X_{21}}{2})$ respectively where $E_f = E.Z_f/(Z_f + Z_b)$ and $E_b = E - E_f$. The 'gross' mechanical power P_{mech} is thus:

$$P_{mech} = I_{2f}^2 R_{21}(1-s)/2s - I_{2b}^2 R_{21}(s-1)/2(2-s)$$

and the 'gross' torque T is:

$$T = \frac{1}{\omega_s}\left[I_{2f}^2 R_{21}/2s - I_{2b}^2 R_{21}/2(2-s)\right]$$

Note that for super-synchronous operation with s negative, both forward and backward fields contribute braking (negative) torques and that the total input shaft mechanical power and torque will be $(P_{mech} + P_{WF})$ and $(T_{mech} + T_{WF})$ respectively where P_{WF} and T_{WF} are the windage and friction power loss and torque. The output power to the mains is

$$P_e = -Re\left[V I_1^*\right]$$

$$\text{or} \quad P_{mech} - I_1^2 R_{11} - \frac{R_{21}}{2}\left[I_{2f}^2 + I_{2b}^2\right]$$

It has been found possible to obtain algebraic relations for a number of important performance parameters, viz:

i) range of slip over which generation takes place. With any induction machine at large negative slips, losses can exceed the converted mechanical power and the power fed to the mains becomes negative. The slip s_o at which P_e falls to zero can be found by setting $Re\left[V I_1^*\right]$ to zero, substituting for I_1 and solving for slip. If the assumption is made that $R_2 \ll (X_m + X_2)$, the relation for s_o is found to be:

$$s_o = 1 - \sqrt{1 + \frac{R_{21}}{R_{11}}\left(\frac{X_{m1}}{X_{m1} + X_{21}}\right)^2}$$

Since X_{m1} is usually much greater than X_{21}, the slip range depends almost entirely on the ratio of stator to rotor resistance.

ii) Maximum airgap power conditions. The slip s_{max} for maximum airgap power P_{amax} can be found by setting $\frac{d}{ds}\left[Re(E\,I_1^*)\right]$ to zero. If it is again assumed that $R_2 \ll (X_m + X_2)$, then s_{max} is given by:

$$s_{max} = 1 - \sqrt{1 + K} \quad \text{where} \quad K = \frac{R_{21}(2X_{21} + X_{m1})}{X_{21}(X_{21} + X_{m1})}$$

When this is substituted into the P_a relation, P_{amax} is found to be:

$$P_{amax} = -E^2 . \frac{\left(\frac{X_{3m1} X_{2m1}}{X_{21}}\right) - R_{21}}{(R_{21}^2 + 2R_{21} X_{3m1} + 2X_{3m1}^2)}$$

where $X_{3m1} = 2X_{21} + X_{m1}$ and $X_{2m1} = X_{21} + X_{m1}$

Assuming again that $R_{21} \ll (X_{21} + X_{m1})$ gives

$$P_{amax} = -\frac{E^2(X_{21} + X_{m1})}{2X_{21}(R_{21} + 2X_{21} + X_{m1})}$$

$$\text{or} \quad -\frac{3E^2(X_2 + X_m)}{4X_2(R_2 + 2X_2 + X_m)}$$

MEASUREMENTS

No-load and short and open circuit standstill tests on a three phase, four pole, 50 Hz, slip ring induction motor rated (under balanced three phase conditions) at 6·3 kW, 110 volts (Δ) gave the following results: R_1, X_1, X_2, X_m, R_2, X_o = 0·52, 1·49, 1·49, 49·1, 1·05, 3·21 Ω respectively. Fig. 2 shows current and power versus speed predictions for single phase operation using the relations of the analysis above, together with measured results. In making the predictions, iron losses were allowed for by the addition of 40 Ω 'iron loss resistors' to the equivalent circuit in parallel with the magnetising reactance branches and friction and windage losses were allowed

for by adding 420.(1 - s) watts to the predicted values of gross mechanical power (i.e. windage and friction loss assumed proportional to speed, and iron losses to airgap flux squared), both allowances being based on measured loss values. There are some discrepancies between the curves, probably due to changes in R_{21}, X_{m1}, X_0 and iron loss due to skin effect, saturation and so on, but the agreement is reasonably good. Predicted and measured values of s_o, s_{max} and P_{amax} were -0·51, -0·51; -0·31, -0·32; and 4·79, 4·75 kW respectively. P_{amax} calculated using the approximate expression was 4·89 kW.

EFFECT ON PERFORMANCE OF DESIGN PARAMETERS

Predictions of output power P_e versus speed for a set of machines having equal X_{m1} values but various combinations of R_{11}, R_{21}, X_{21} and X_{m1} were made. The value of X_{m1} chosen together with the base values of R_{11}, R_{21}, X_{21} (denoted by R_{10}, R_{20} and X_{20}), were those of the test machine. Iron, friction and losses were neglected. The results shown in table 1, as might be expected, indicate that: (i) a progressive decrease in slip range occurs as R_{11} increases (ii) the peak power depends on X_{21} (iii) the stiffness of the generator's characteristic depends on R_{21}. R_{21} does not affect P_{amax} but high R_{21} gives a larger slip range and a larger s_{max}. A typical set of P_e versus slip curves are shown in fig. 3. Fig. 4 shows corresponding efficiency curves. It can be seen that, even when iron windage and friction losses are neglected, efficiency levels are a little low. Clearly low R_{11}, R_{21}, X_{11}, X_{21} values, a high X_m value and low I.W.F. losses are desirable if reasonably efficient operation is to be obtained and this means that, where possible, machines with the following features should be chosen:

i) small airgap; unsaturated operation at specified voltage; small number of poles (to maximise X_{m1}).

ii) rotor bars of generous cross section, of copper if possible, but not too deep (to minimise R_2 but avoid deep bar effects which cause dangerous increases in R_2 as seen by the backward field). Minimum rotor slot bridges (to minimise X_2, subject to starting current constraints).

iii) machine wound specifically for plain single phase operation (to maximise useful copper volume and iron utilisation)

iv) low loss laminations and moderate rated current and flux density levels (to give generally low I^2R and iron losses), hence moderate rated output per D^2L.

v) low loss bearings, and high efficiency fan (to minimise P_{WF}).

CONCLUSIONS

An analysis method and results have been presented for the single phase operation of an induction generator. The generator's torque versus speed characteristics are very similar to those of standard three phase, mains-connected induction generators and the same considerations are relevant when the design of a complete turbine/gearbox/generator/feeder/protection and control system is undertaken[1-2]. The generator torque will obviously be modulated at twice mains frequency and some mechanical shaft damper may be desirable to avoid resonance phenomena. The results show that when single phase supplies only are available, the plain single phase induction generator is worth considering, though the fact that efficiency levels are only moderately good suggests that mains-connected, capacitor-run schemes could well be more economic. Since the choice of capacitor value would not usually need to be compromised to give good standstill torque (merely good running torque, as a generator) it is likely that phase balance would be reasonably good and efficiency hence improved throughout the relevant slip range.

ACKNOWLEDGEMENTS

The support of the SRC and, for one of the authors, the Thai Government, is gratefully acknowledged.

REFERENCES

1. Anscombe, L.D. and Ellivon, A.J.: 'Technical aspects of interchange with the grid', J.Inst.Fuel, June 1949, pp.257-262

2. Allen, C.L.C.: 'Water turbine driven induction generators', Proc. IEE, December 1959, 107A, pp.529-550

3. Elliot, D.E.: 'Economic wind power', Applied Energy, 1975, 1, pp.167-197

4. Debontridder, J. et al: 'The combination asynchronous generator-vertical axis wind turbine for small power applications', Proc. of Int. Conference on Electrical Machines, Brussels, 1978 (Paper: G5/5)

5. Bolton, H.R. et al: 'Double output generator scheme for wind energy conversion', Proc. of British Wind Energy Association Conference, Cranfield, 1980

6. Fitzgerald, A.E., Kingsley, C. and Kusko, A.: 'Electric Machinery', 3rd edition, McGraw-Hill, 1971, p.543

7. Jones, C.V.: 'The Unified Theory of Electrical Machines', Butterworths, London, 1967

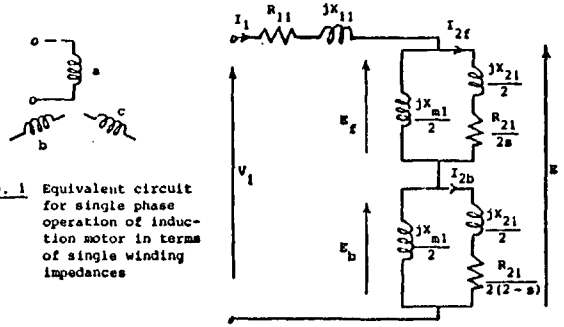

Fig. 1 Equivalent circuit for single phase operation of induction motor in terms of single winding impedances

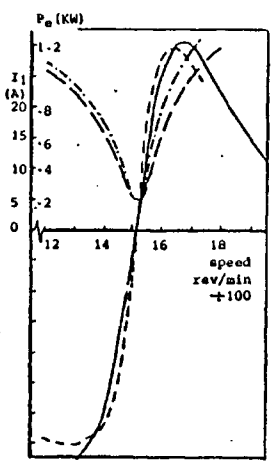

Fig.2 Single phase induction machine performance

Power to supply P_e :
predicted ——
measured - - - -

Supply current I_1 :
predicted —— ——
measured - · - · -

R_{21}/R_{20}	R_{11}/R_{10}	X_{21}/X_{20}	$-s_o$ (%)	$-s_{max}$ (%)	$P_{max} \pm 10$ (watts)	Ref. no.
½	½	½	51	7	148	
		1	49	6	125	
		2	42	4	910	
	1	½	28	6	145	
		1	27	5	122	
		2	25	4	87	
	2	½	16	6	137	
		1	15	5	112	
		2	14	4	76	
1	½	½	1	14	157	1
		1	95	13	134	2
		2	85	10	91	3
	1	½	52	13	148	4
		1	50	11	122	5
		2	45	9	85	6
	2	½	29	10	137	7
		1	28	9	111	8
		2	26	8	75	9
2	½	½	50	28	154	
		1	40	23	125	
		2	30	18	98	
	1	½	91	25	146	
		1	87	21	119	
		2	8	17	84	
	2	½	52	21	134	
		1	51	18	107	
		2	47	15	76	

Table 1 Performance data versus machine parameter values

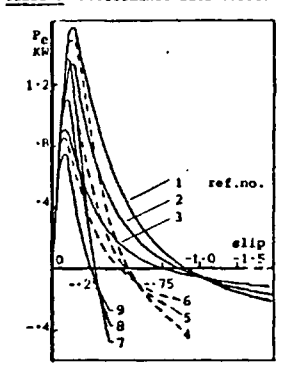

Fig.3 Effect of design changes on P_e - slip characteristic.

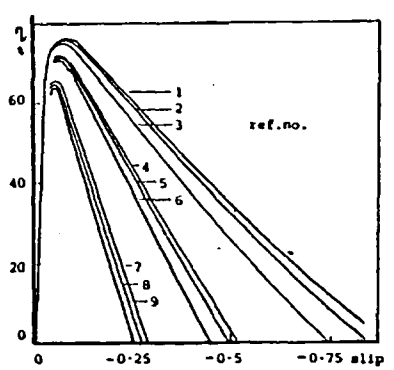

Fig.4 Effect of design changes on efficiency - slip characteristic.

INVESTIGATIONS INTO SMALL SINGLE-PHASE SWITCHED RELUCTANCE MOTORS

S. Chatratana*, H.R. Bolton* and D.A.G. Pedder**

*Imperial College, London **Kingston Polytechnic

INTRODUCTION

In a previous IEE conference paper (1) the historical background, extending back to the 1840s, of switched reluctance motor technology was summarised and results presented of an investigation into a single-phase SRM system. Since then a number of major papers (2)-(6) have appeared dealing with polyphase SRM system design, prediction and behaviour and reiterating the principal advantages of this form of drive (brushless, speed-controllable operation, robust and straightforward motor construction, relatively simple and low-cost, unipolar feed circuit).

The single-phase SRM is perhaps the most robust and straightforward of motor types and may be considered for drive applications where the inherently discontinuous nature of its torque output is allowable. The 'single channel', unipolar nature of its feed means that the cost and complexity of the feed are brought to an absolute minimum. One of the continuing objections to variable-frequency a.c. drives for rugged-environment applications is the need for a multi-channel feed (as opposed to the single channel feed sufficient for d.c. and a.c.commutator motors), even though total feed power ratings are similar. In applications where starting torque requirements are modest or where a centrifugal clutch can be incorporated between motor and load, the single-phase SRM system with its single channel feed may be considered as a reasonably strong contender.

This paper outlines the authors' work on SPSRM drives since 1978 and presents results for two categories of motor construction and two feed circuit configurations.

Motor Configurations and Design Aspects

Three principal categories of motor configuration can be defined, according to the orientation of the main flux paths: radial/circumferential, radial/axial and axial/circumferential. Fig. 1 shows a 1 pole, radial/axial motor with 6 saliencies per pole and a rotor-outside configuration. Fig. 2c shows another 1 pole radial/axial flux motor with 2 saliencies per pole and a rotor-inside configuration. In each case the winding consists of a single, circular coil. Figs. 2a and 2b show 2 pole, 1 saliency per pole radial/circumferential flux motors with conventional and U-core configurations respectively. Conventional stamped laminations can be used with radial/circumferential motors whereas the radial/axial motors are more difficult to laminate. However, as can be seen, very simple windings can be used on radial/axial motors. The stator configuration in the Fig. 2b motor is very similar to that used in some small clock motors and shaded-pole single-phase induction motors. (The bobbin coil is wound on the detachable, top core-portion and the coil and core-portion are then slid into position as a unit between the two side-arm portions of the pre-assembled core). Manufacturing cost is very low since the coil winding and assembly operations are very straightforward but stator leakage reactance is larger than in motors of the Fig. 2a type. For all motor configurations the usual factors must be considered when choosing design parameters such as numbers of poles, saliencies per pole and winding turns, stator pole arc, rotor pole arc, airgap length, stack length, etc and when choosing between standard and segmented rotor types. In each of the motors illustrated, the number of stator and rotor saliencies is identical and fairly low and this results of course in relatively large step angles and low switching frequencies.

The discontinuous nature of the torque poses special problems at starting. The starting method outlined in reference (1) which depends on a 'starting magnet' fixed to the stator is satisfactory when load torque and friction are small at low speeds. When this is not the case, the 'starting magnet' method can be used in conjunction with a viscous coupling-element orcentrifugal clutch in the shaft. Torsional vibration during motor operation can be filtered if desired, at least over most of the speed range, by means of suitable torsional compliances in the shaft and stator mounting.

Feed Configurations

System behaviour with two types of feed circuit has been investigated. The Fig. 3 circuit comprises a mains filter and diode-rectifier, a d.c. link with some smoothing together with a two-transistor unipolar-output bridge able to give full reverse voltage pulldown and energy recovery through the diodes. The transistors can be PWM driven to effect torque control with extended cut-off periods approximately corresponding to periods of reducing coil inductance. The triac in the extremely simple Fig. 4 circuit is burst-fired during periods which approximately correspond with periods of increasing coil inductance, firing angle variation being used for torque control. As explained in reference (1), the Fig. 4a circuit with its lack of freewheel path was found experimentally to give better system operation than alternative direct mains-fed circuits (some with thyristors) incorporating freewheel paths. The principal reason for this is the rapid pull-down caused by reverse supply polarity at the end of 'on' periods.

The extremely low cost of the Fig. 4 configuration has provided a strong incentive to continued investigations into its operation with each of the Fig. 4b triggering schemes in spite of the presence of some obvious shortcomings in terms of limited speed range and mains harmonics. Some of the results with both the Fig. 4 and the Fig. 3 configurations are presented below. Configurations incorporating bifilar-wound pull-down windings (2) and single-transistor switching circuits have not so far been examined.

Analysis

If iron windage and friction losses are neglected, the SPSRM may be represented as detailed in reference (1) by an equivalent R-L series circuit comprising the winding resistance R (fixed) and inductance L (variable). In the concentrated-coil motors investigated, saturation has not affected operation significantly and the inductance versus rotor angle characteristics have been modelled fairly accurately by simple triangular functions. The instantaneous winding current i is computed using a time-stepping method from the circuit relation: $v = iR + Ldi/dt + idL/dt$ where v is the instantaneous supply voltage. In the case of Fig. 3 supply configuration, $v = \pm V_{d.c.}$ with switching instants determined by the shaft angle sensor and control circuitry. With the Fig. 4 configuration, v just after triac firing is set equal to $V.\sin \omega t$ until i falls or is reduced to zero; i is then set equal to zero until the next firing instant. The computer program flow diagram is shown in summarised form in Fig. 5. Instantaneous torque is found using $T = \frac{1}{2}i^2 dL/d\theta$ and other quantities such as mean power input, efficiency and mean torque are calculated by standard means.

Results

(a) D.C. link feed. Tests were conducted with two motors of the Fig. 1 and Fig. 2a types respectively. The Fig. 1 motor, details of which are given in reference (1), was designed for low speed duties with low switching frequencies and employed a solid iron magnetic circuit to minimise cost. Test and predicted performance curves are compared on Fig. 6 for the case of a rail voltage of 50 V and switching angles α and β (electrical angles before q and d rotor positions respectively) of 24° and 24°. Significant iron losses are evident in the upper half of the speed range. The results of tests and predictions on a small shaded pole 50 Hz induction motor, modified to give a motor of the Fig. 2a type, are shown in Fig. 7. Motor details were: rotor diameter 31 mm; rotor axial length 38 mm; stator and rotor pole arcs 90° and 90°; air-gap length 0·43 mm; coil turns: 130; coil resistance (20°C) and inductance 0·51 Ω and 86 mH (min) to 203 mH (max) and a 50 V supply with α and β of 90° and 90° was used. The extremely high speed capability of small SPSRMs was demonstrated, though the lack of special lamination steel and bearings in the test motor led to significant iron loss and noise above 10,000 r.p.m. Power outputs at 6500 r.p.m. and 17,500 r.p.m. were 50 W (max. power point) and 6 W respectively. The quality of the drive in terms of efficiency and output power can be set in context by noting that the full load efficiency and output power of the original induction motor when supplied at 240 V, 50 Hz (sine) were 25% and 15W.

(b) Triac feed. Fig. 8 shows the performance of the small Fig. 2a motor when connected to a triac-controlled 50 Hz, mains feed of the Fig. 4 configuration. The speed range of zero to 3000 r.p.m. corresponds to a switching frequency range of zero to 100 Hz and the winding voltage and current waveforms are inevitably very different from the near-ideal ones that occur with d.c. link feeds. In addition to the current harmonics that occur in any mains-fed triac or thyristor circuit, beating effects occur between the mains and switching frequencies and give rise to current and torque sub-harmonics. As is usual with inductive loads the triac triggering mode (single pulse or repetitive or d.c. pulse) has a significant effect on the current waveform and the rapidly changing inductance can make the effect quite marked at certain switching frequencies. Curve a on Fig. 8 shows the mean measured torque versus speed. The zero mean torque evident over certain narrow speed bands means that the motor cannot of course be used to drive a load within these bands. The motor was however able to accelerate through these bands when unloaded and when connected to inertial loads of moderate value and it would seem that this ability is closely related to the synchronising ability of synchronous and reluctance motors on fixed frequency feeds whereby the rotor gains sufficient additional speed during a positive torque pulse to attain a speed where the mean torque is positive and sufficiently large to maintain continued operation. The performance prediction process was quite lengthy due to the fact that at each speed, the repeating sequence of torque and current generally took many mains cycles, and because the nature of the sequence and hence the values of the mean torque and current varied considerably according to the exact phase relationship at the time datum between the first switching instant and the mains supply zero crossing. The sequence repetition time and the range of mean torques and input currents was computed at each speed and the torque envelope is plotted on Fig. 8. Whereas an absolutely constant speed is assumed during the prediction process, in practice the motor speed and torque will follow limit cycles whose magnitudes will partly depend on the nature of the load. At quasi-synchronous speeds, the sequence repetition-time is a small, integral number of mains half-periods and the elevated torques and efficiencies available at these speeds can be observed.

Mains Harmonics with Fig. 4 type feed

An inevitable and important constraining factor in the use of the Fig. 4 feed configuration is caused by the regulations and recommendations (7)-(10) covering the allowable magnitudes of harmonic currents supplied to thyristorised and other equipment connected to the mains. The current drawn by a SPSRM scheme of the Fig. 4 type contains harmonics of a large range of orders from d.c. upwards and although this is nothing new to supply authorities who have to contend with half-wave, full-wave and phase-angle-controlled rectifiers, burst-fired and phase-controlled a.c. regulators and arc-furnace loads often of substantial power ratings, the relatively large harmonic amplitudes inevitable (at least at most speeds) with the Fig. 4 scheme and the fact that the load is a single-phase one means that harmonic effects must be considered at an early stage. Fig. 9, which shows a plot of the amplitudes of the current harmonics drawn by the experimental Fig. 1 motor when running at 550 r.p.m. and delivering 26 W, is typical of those for operation at non quasi-synchronous speeds and reasonably high switching frequencies. In assessing whether the amplitudes fall below the recommended limiting values, knowledge of the parameters of the particular mains feeder is required. The regulations and recommendations on 'harmonics' are consulted for current harmonics of frequencies greater than 50 and those on 'voltage fluctuations' for the sub-harmonic currents. Preliminary work suggests that for typical domestic and light industrial single-phase feeders, the Fig. 4 scheme will not cause problems for

motor ratings below about 200 W and 3 kW respectively.

Feed Circuit Costs

Estimated costs for quantity production of the feed circuits (including optical position sensor and assembly cost) were:

170 V, 1 A d.c.link circuit (Fig. 3) £8.40
240 V, 8 A triac circuit (Fig. 4) £5.10

The estimated cost of a thick film version of the d.c. link circuit is £5.40 and both this and the £8.40 includes mains filter and smoothing capacitor costs.

Conclusions

The low cost of the triac scheme provides an incentive for its use when application conditions allow. The d.c. link circuit, though somewhat more expensive, greatly extends the speed range, improves control flexibility and gives reduced mains harmonics. The likelihood of performance improvements with more developed versions of the motor is high, given the rudimentary nature of the experimental unit tested and, subject to starting requirements, one may perhaps expect to see this brushless, potentially quite drive system competing in the domestic and light industrial equipment fields with drives based on small, phase-controlled, a.c. commutator machine drives.

REFERENCES

1. Bolton, H.R. and Pedder, D.A.G., "Low-cost reluctance drive system for low power, low speed application", Proc. IEE Conference on Variable Speed Drives, September 1979.

2. Ray, W.F. and Davis, T.M., "Inverter drive for doubly salient reluctance motor: its fundamental behaviour, linear analysis and cost implications", Proc. IEE, 1979, 126, (Part B), (6), 185-193.

3. Lawrenson, P.J. et al, "Variable-speed SRMs", Proc. IEE, 1980, 127, (Part B), (3), 253-265.

4. Stephenson, J.M. and Corda, J., "Computation of torque and current in doubly salient reluctance motors from nonlinear magnetisation data", Proc. IEE, 1969, 126, (Part B), (5), 393-396.

5. Lawrenson, P.J. et al, "SRMs for traction drives", Proc. ICEM Conference, Athens, September 1980.

6. Davis, R.M. et al, "Inverter drive for SRM: circuits and component ratings", Proc. IEE, 1981, 128, (2), (Part B), 126-136.

7. Kendall, P.G. and Johnson, P.A., "Limits for harmonic distortion in the U.K. electricity supply system", Proc. IEE Conference on Power Electronics, September 1977.

8. Electricity Council, Engineering Recommendation G5/3.

9. British Standard 5406: 1976.

10. British Electricity Boards: ACE Report No.73 (1979).

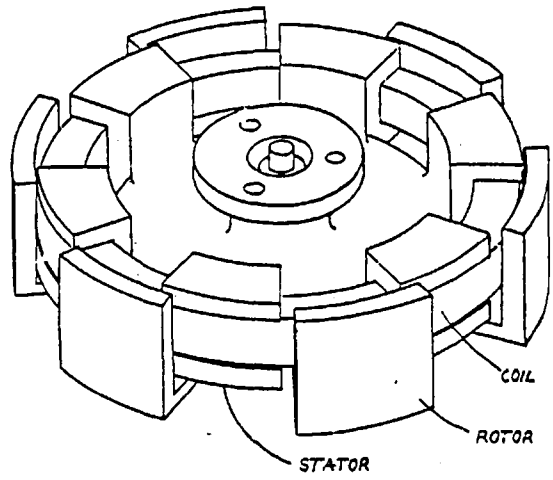

Fig.1 Single-coil, radial-axial flux motor with external rotor.

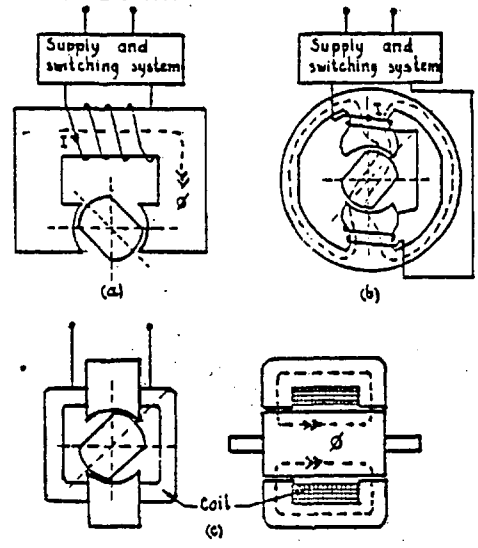

Fig.2 Motor configurations: (a) 'U-core' radial-circumferential flux motor (b) conventional radial-circumferential flux motor (c) radial-axial flux motor.

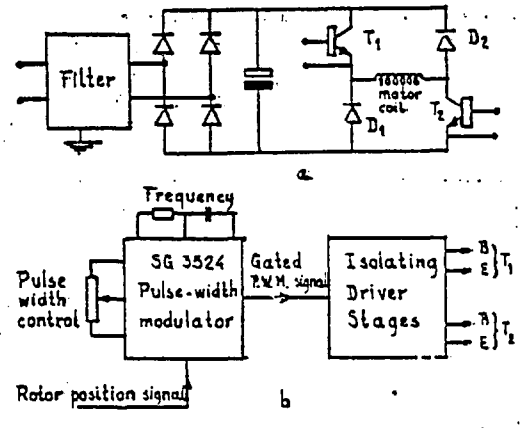

Fig.3 D.c. link feed: (a) power circuit (b) control circuit.

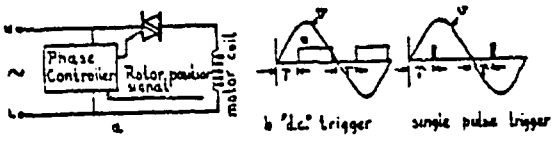

Fig.4 (a) Triac circuit (b) trigger waveforms

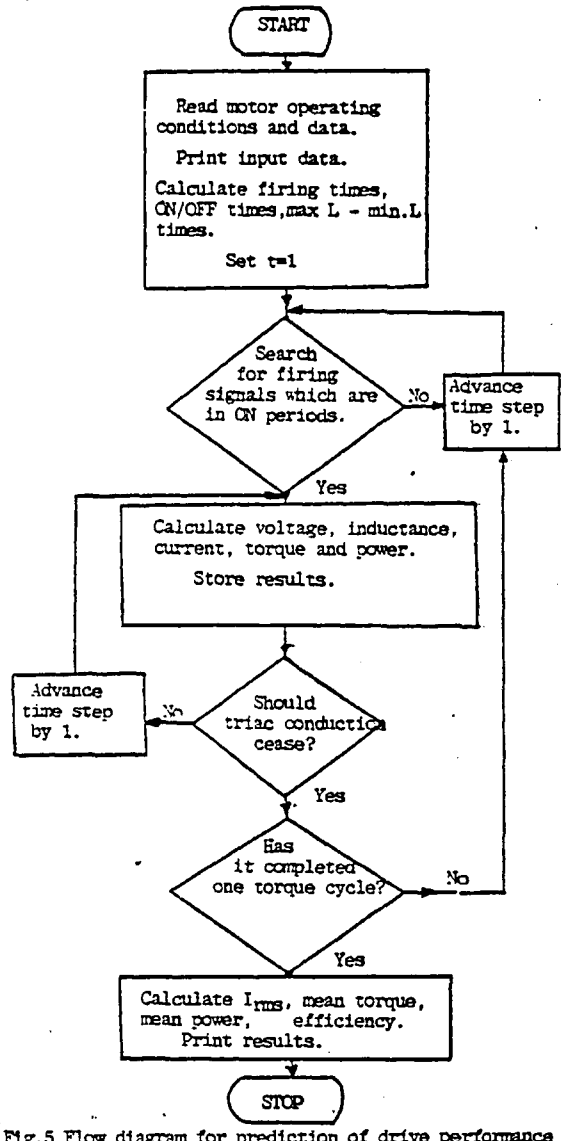

Fig.5 Flow diagram for prediction of drive performance with triac feed.

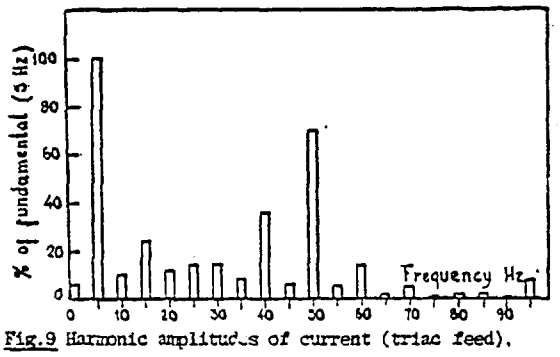

Fig.9 Harmonic amplitudes of current (triac feed).

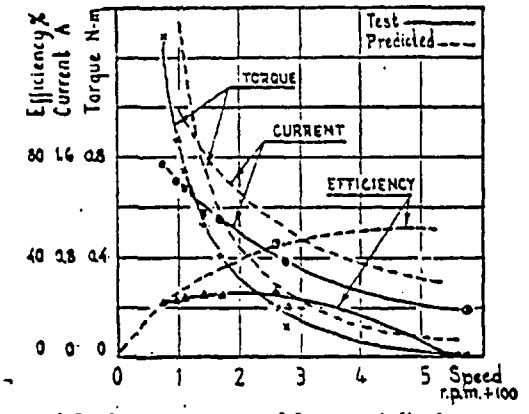

Fig.6 Performance curves of low speed fig.1 motor with d.c. link feed.(note:losses in solid iron excluded from predictions)

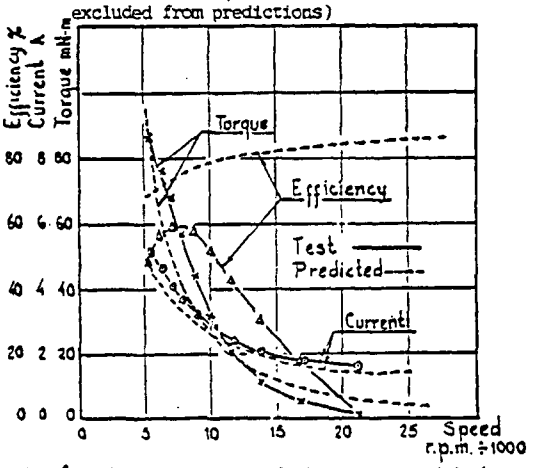

Fig.7 Performance curves of fig.2a motor with d.c. link feed.(I.W.F.losses excluded from prediction)

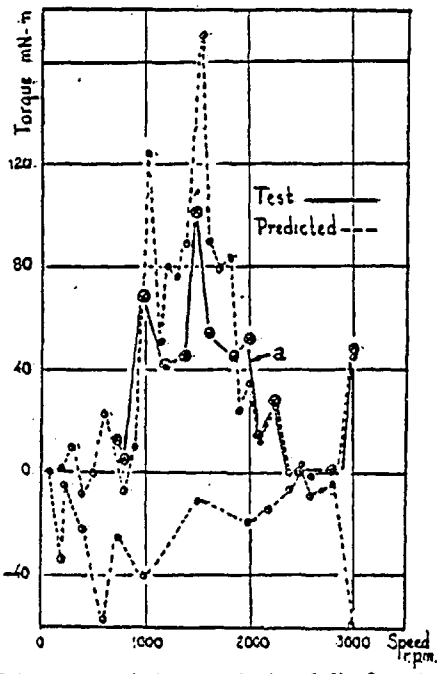

Fig.8 Torque-speed characteristic of fig.2a motor with triac circuit (25 volts rms)